UNIVERSITY OF ALBERTA

SKIMMING FLOW IN A LARGE MODEL OF A STEPPED SPILLWAY

by

MOHAMMAD REZA CHAMANI ©

A THESIS SUBMITTED TO THE FACULTY OF GRADUATE AND RESEARCH IN
PARTIAL FULFILLMENT OF THE REQUIREMENT FOR THE DEGREE OF
DOCTOR OF PHILOSOPHY

in

WATER RESOURCES ENGINEERING

DEPARTMENT OF CIVIL ENGINEERING

EDMONTON, ALBERTA
FALL 1997

National Library
of Canada

Acquisitions and
Bibliographic Services

395 Wellington Street
Ottawa ON K1A 0N4
Canada

Bibliothèque nationale
du Canada

Acquisitions et
services bibliographiques

395, rue Wellington
Ottawa ON K1A 0N4
Canada

Your file Votre référence

Our file Notre référence

The author has granted a non-exclusive licence allowing the National Library of Canada to reproduce, loan, distribute or sell copies of this thesis in microform, paper or electronic formats.

L'auteur a accordé une licence non exclusive permettant à la Bibliothèque nationale du Canada de reproduire, prêter, distribuer ou vendre des copies de cette thèse sous la forme de microfiche/film, de reproduction sur papier ou sur format électronique.

The author retains ownership of the copyright in this thesis. Neither the thesis nor substantial extracts from it may be printed or otherwise reproduced without the author's permission.

L'auteur conserve la propriété du droit d'auteur qui protège cette thèse. Ni la thèse ni des extraits substantiels de celle-ci ne doivent être imprimés ou autrement reproduits sans son autorisation.

0-612-22963-7

Canada

UNIVERSITY OF ALBERTA

Library Release Form

NAME OF AUTHOR: Mohammad Reza Chamani

TITLE OF THESIS: Skimming Flow in a Large Model of a Stepped Spillway

DEGREE: Doctor of Philosophy

YEAR THIS DEGREE GRANTED: FALL 1997

Permission is hereby granted to THE UNIVERSITY OF ALBERTA LIBRARY to reproduce single copies of this thesis and to lend or sell such copies for private, scholarly, or scientific research purposes only.

The author reserves all other publication rights in association with the copyright in the thesis, and expect as hereinbefore provided, neither the thesis nor any substantial portion thereof may be printed or otherwise reproduced in any material whatever without the author's prior written permission.

M.R.Chama

Mohammad Reza Chamani
191 Haghparasty Lane
Sadi St., Najafabad
Isfahan, IRAN 85137

Date: ...Aug 27, 1997..

UNIVERSITY OF ALBERTA

FACULTY OF GRADUATE STUDIES AND RESEARCH

The undersigned certify that they have read, and recommend to the Faculty of Graduate Studies and Research for acceptance, a thesis entitled **SKIMMING FLOW IN A LARGE MODEL OF A STEPPED SPILLWAY** submitted by **Mohammad R. Chamani** in partial fulfillment of the requirements for the degree of **Doctor of Philosophy** in Water Resources Engineering.

FE Hicks

Dr. F. E. Hicks (Chair)

Dr. N. Rajaratnam (Supervisor)

Dr. P. M. Steffler

Dr. J. Leonard

J. D. Scott

Dr. J. D. Scott

Dr. J. A. McCorquodale (External examiner, University of New Orleans, La., U.S.A.)

Date: 26 Aug 97

To my mother, Sekineh

ABSTRACT

The present investigation is the first major contribution to the study of skimming flow in large scale models to develop a better understanding of aerated flow in stepped spillways. Most observations were performed in the developed flow region. Detailed measurements of air concentration and velocity were made. Vortical structures were observed visually with the aid of a high speed video camera.

Air entrainment created a highly irregular and wavy surface in which returning water drops ejected from the surface continuously entrained air. Stable recirculating eddies were formed in the grooves of the steps which were maintained through the transmission of the shear stress of the main flow. Observations revealed that the inception of air entrainment was strongly influenced by the steps. The enhancement of the growth of the boundary layer and the deflection of the internal flow by steps caused early inception of air entrainment.

Photographic observations and air concentration profiles showed that two zones within the depth of self-aerated flow existed in the developed region. In the lower zone, air bubbles were kept in suspension by the turbulent transport. In the upper zone, water drops ejected from the transition zone, were traveling in a stream of air. Due to the similarity of flow over stepped spillways to the flow in steep channels, a basis for the analysis of air concentration distribution was established. It was found that stepped spillways entrain more air than chute spillways. This indicates that steps enhance turbulence in the flow.

The velocity distribution in the lower zone of the flow depth in the developed region was analyzed using Prandtl-Karman universal velocity equation. Skin friction coefficient was calculated based on the uniform flow expression for the developed region. An empirical equation was derived to estimate the skin friction coefficient for the skimming flow. It appeared that the recirculating eddies in the step grooves and vortical structures at step tips were the major causes for energy dissipation. Results of the energy

loss showed that the skimming flow dissipates less energy than the jet flow where significantly more energy dissipation occurs.

ACKNOWLEDGMENTS

The author wishes to acknowledge with gratitude the instruction, valuable advice and encouragement received from Dr. N. Rajaratnam. His strong knowledge in fluid mechanics has motivated me during my study. He has not only supervised the research and the writing of this thesis, but has fathered me like his son as well.

I have also enjoyed the instructions of the Water Resources staff, Dr. P. M. Steffler and Dr. F. Hicks, which have updated and improved my fluid mechanics knowledge. I would like to acknowledge these individuals and to thank them all.

The assistance of Mr. S. Lovell in the construction and maintenance of the models and instrumentations is greatly appreciated. The help of Mr. P. Fedun in the maintenance of the models is also appreciated. Mr. R. Haley from the Department of Electrical Engineering deserves particular recognition for his assistance in providing and operating the high-speed video camera. Special thanks to Miss. K. A. Mazurek for proof-reading this thesis with patience which improved its quality.

I would like to thank the Ministry of Culture and Higher Education (MCHE), Government of the Islamic Republic of Iran, for providing the financial support for my Ph.D. program. In particular, I would like to express my deepest gratitude to the people of the Islamic Republic of Iran for bearing the entire cost of my education from elementary school to the Ph.D. program. Finally, the author is indeed indebted to his family, specially his mother, Sekineh, for her spiritual encouragement and support even from a far distance away.

TABLE OF CONTENTS

1. INTRODUCTION 1

2. LITERATURE REVIEW 5
    - 2.1 Introduction 5
    - 2.2. Physical Model Studies 5
        - 2.2.1 Essery and Horner (1978) 6
        - 2.2.2 Sorensen (1985) 7
        - 2.2.3 Bayat (1991) 8
        - 2.2.4 Diez-Cascon, et al. (1991) 9
        - 2.2.5 Bindo et al. (1993) 11
        - 2.2.6 Christodoulou (1993) 12
        - 2.2.7 Tozzi (1994) 13
    - 2.3 Flow Characteristics - Analytical Studies 15
        - 2.3.1 Rajaratnam (1990) 15
        - 2.3.2 Chanson (1993, 1994) 16
    - 2.4 Flow in Steep Channels 18
        - 2.4.1 Straub et al. (1953 & 1958) 18
        - 2.4.2 Knight and Macdonald (1979) 22
    - 2.5 Inception Section of the Air Entrainment 24
    - 2.6 General Comments 27

3. EXPERIMENTAL PROGRAM 49
    - 3.1 Introduction 49
    - 3.2 Aim of the Experimental Program 49
    - 3.3 Instrumentation 50
        - 3.3.1 Air concentration Probe 50
            - 3.3.1.1 Introduction 50
            - 3.3.1.2 Theory 50
            - 3.3.1.3 Electrical Probe and Circuit Design 53
            - 3.3.1.4 Testing Procedure 54
        - 3.3.2 Velocity Meter 54
            - 3.3.2.1 Introduction 54

3.3.2.2 Theory 55
3.3.2.3 Velocity Meter 56
3.3.3 Flow Visualization 56
3.4. Experimental Setup and Procedure 57
3.4.1 General description of the Model 57
3.4.2 Measurements 58
3.5 Experimental Errors and Uncertainties 59
3.5.1 Definitions 59
3.5.2 Theory 60
3.5.2 Uncertainty Evaluation 61

4. EXPERIMENTAL RESULTS AND ANALYSIS 74
4.1 Introduction 74
4.2 Flow Patterns and Its Classification 74
4.2.1 Introduction 74
4.2.2 Types of Flow 74
4.2.3 State of Skimming Flow Regime 75
4.3 Results and Analysis 78
4.3.1 Introduction 78
4.3.2. Inception of Air Entrainment 79
4.3.3 Air Concentration and Characteristic Depths 81
4.3.3.1 Introduction 81
4.3.3.2 Data Processing 81
4.3.3.3 Characteristic Depth and Concentration Definitions 82
4.3.3.4 Analysis of Data 83
4.3.4 Air-Water Mixture Velocity 89
4.3.4.1 Introduction 89
4.3.4.2 Velocity Profile Distribution 90
4.3.4.3 Universal Velocity Profile 92
4.3.5 Skin Friction Coefficient 95
4.3.6 Energy Dissipation 98

5. CONCLUSIONS AND RECOMMENDATIONS 174
5.1 Summary 174

5.2 Conclusions 175
5.3 Recommendations 176

REFERENCES **178**

APPENDICES

A. AIR CONCENTRATION PROFILES FOR VARIOUS VALUES OF FLOW DISCHARGE, STEP HEIGHT AND CHANNEL SLOPE **182**

B. VELOCITY PROFILES FOR VARIOUS VALUES OF FLOW DISCHARGE, STEP HEIGHT AND CHANNEL SLOPE **229**

C. LOGARITHMIC VELOCITY PROFILES AT DIFFERENT ORIGINS FOR VARIOUS VALUES OF FLOW DISCHARGE, STEP HEIGHT AND CHANNEL SLOPE **276**

LIST OF TABLES

Table	Title	Page
2.1	Distance of the inception section of air entrainment from the crest (adapted from Lane, 1939)	30
2.2	Values of Parameters defined in Eq. (2.20)	31
3.1	RCC or Rehabilitated Concrete dams with stepped spillways (adapted from Frizell, 1992)	64
4.1	Dimensions of vortex tubes	103
4.2	The location of inception section in terms of step numbers	103
4.3	Values of the "rooster tail" height	103
4.4	Values of parameters of universal velocity distributions for a stepped spillway with l/h= 0.6	104
4.5	Values of parameters of universal velocity distributions for a stepped spillway with l/h= 0.8	105

LIST OF FIGURES

Figure	**Title**	**Page**
1.1	Cost comparison of RCC and mass concrete dams (adapted from Logie, 1985)	3
2.1	Velocity measurements at the toe of the chute spillway and the stepped spillway (adapted from Sorensen, 1985)	32
2.2	Comparison of the theoretical and experimental results (adapted from Diez-Cascon et al., 1991)	32
2.3	Schematic sketch for the flow state in the stepped spillways (adapted from Bindo et al., 1993)	33
2.4	A graph for the design of stepped spillways (adapted from Bindo et al., 1993)	34
2.5	Dimensionless plot of the energy dissipation for stepped spillways (adapted from Christodoulou, 1993)	35
2.6	Variation of the Darcy friction factor with roughness (adapted from Tozzi, 1994)	36
2.7	A schematic sketch for the flow in the developed region of a stepped spillway (adapted from Tozzi, 1994)	37
2.8	Variation of Darcy friction factor for skimming flow: (a) steep slopes; (b) flat slopes (adapted from Chanson, 1994)	38
2.9	Variation of the air concentration with channel slopes (adapted from Straub and Lamb, 1953)	39

2.10 Variation of the measured velocities with channel slopes (adapted from Straub and Lamb, 1953) 40

2.11 Variation of the mean air concentration with discharge at various channel slopes (adapted from Straub and Anderson, 1958) 41

2.12 Variation of the upper depth of flow with discharge at various channel slopes (adapted from Straub and Anderson, 1958) 42

2.13 Variation of the mean depth of the flow with discharge at various channel slopes (adapted from Straub and Anderson, 1958) 43

2.14 Classification of flow patterns for a channel with roughness elements (adapted from Knight and Macdonald, 1979) 44

2.15 Variation of the roughness ratio with the relative roughness (adapted from Knight and Macdonald, 1979) 45

2.16 Variation of the distance of air entrainment inception section from the crest with the discharge (adapted from Hickox, 1945) 46

2.17 Boundary layer and water surface profiles in non-aerated region in a stepped spillway model (adapted from Horner, 1969) 47

2.18 Definition sketch for parameters in Eq. (2.20) 48

3.1 The stepped spillway model 65

3.2 Variation of the relative velocity uncertainty with the air concentration 66

4.1 Variation of the distance of the inception section from the crest of stepped spillways with Froude number 106

4.2 Variation of the distance of the inception section from the crest of stepped spillway models with Froude number 107

4.3 Variation of the "rooster tail" height with discharge for l/h= 0.6 108

4.4 Mean range of concentration values in the developed region of a stepped spillway with l/h=0.8, h= 125. mm (yc/h=1.0) 109

4.5 Relative Discharge & Concentration Profiles in Developed Region of a Stepped Spillway (l/h= 0.6, h=12.5 cm) 110

4.6 Air Concentration profile at step tip #13 in a stepped spillway with l/h=0.6, h= 125. mm (yc/h=1.0) 111

4.7 Air concentration profile at different step numbers in a stepped spillway with l/h= 0.8 and h= 31.25 mm (yc/h= 4.0) 112

4.8 Estimation of air concentration distribution parameters in the lower zone of the developed region in a stepped spillway with l/h= 0.6 and h= 125 mm (yc/h= 1.0) 113

4.9 Variation of the mean air concentration with the discharge in stepped spillways for various values of slope and step height 114

4.10 Variation of the air concentration at the transition depth with discharge in stepped spillways for various values of slope and step height 115

4.11 Variation of the air concentration at half-way of the transition depth with discharge in stepped spillways for various values of slope and step height 116

4.12 Variation of power parameter in Eq. (4.6) with discharge in stepped spillways for various values of slope and step height 117

4.13 Relation of the mean air concentration to the shear velocity and transition depth in stepped spillways for various values of slope and step height 118

4.14 Relation of the mean air concentration to flow parameters in stepped spillways for various values of slope and step height 119

4.15 Relation of the mean air concentration to flow discharge and slope in stepped spillways for various values of slope and step height 120

4.16 Relation of the mean air concentration to flow discharge and slope in stepped spillways for various values of slope and step height 121

4.17 Relation of the upper depth of flow with discharge in stepped spillways for various values of slope and step height 122

4.18 Relation of the transition depth with discharge in stepped spillways for various values of slope and step height 123

4.19 Relation of the projection height with discharge in stepped spillways for various values of slope and step height 124

4.20 Relation of the characteristic depth ratio with discharge in stepped spillways for various values of slope and step height 125

4.21 Mean range of stagnation head in a stepped spillway with l/h= 0.6 and h= 62.5 mm (yc/h= 2.0) 126

4.22 Velocity profile at step tip #16 in a stepped spillway with l/h=0.6, h= 125 mm (yc/h=1.3) 127

4.23 Relation of the characteristic depth ratio with discharge in stepped spillways for various values of slope and step height 128

4.24 Velocity profiles taken by different methods in a stepped spillway with l/h= 0.6 and h= 62.5 mm (yc/h= 1.4) 129

4.25 Velocity profiles taken by different methods in a stepped spillway with l/h= 0.6 and h= 62.5 mm (yc/h= 2.0) 130

4.26 Velocity profiles taken by different methods in a stepped spillway with l/h= 0.6 and h= 31.25 mm (yc/h= 2.8) 131

4.27 Velocity profiles taken by different methods in a stepped spillway with l/h= 0.6 and h= 31.25 mm (yc/h= 4.0) 132

4.28 Logarithmic velocity profiles at different origins at step #13 in a stepped spillway with l/h=0.6, h= 125 mm, k= 76.6 mm (yc/h=1.0) 133

4.29 Variation of the relative roughness ratio with discharge for different step heights and spillway slope 134

4.30 Universal velocity profiles at step #13 of a stepped spillway with l/h=0.6 and h= 125 mm (k= 76.6 mm, ε= 64.0 mm) 135

4.31 Universal velocity profiles at step #26 of a stepped spillway with l/h=0.6 and h= 62.5 mm (k= 38.3 mm, ε= 33.0 mm) 136

4.32 Universal velocity profiles at step #64 of a stepped spillway with l/h=0.6 and h= 31.25 mm (k= 19.15 mm, ε= 17.0 mm) 137

4.33 Universal velocity profiles at step #16 of a stepped spillway with l/h=0.8 and h= 125 mm (k= 83.3 mm, ε= 64.0 mm) 138

4.34 Universal velocity profiles at step #64 of a stepped spillway with l/h=0.8 and h= 31.25 mm (k= 20.8 mm, ε= 20.8 mm) 139

4.35 Universal velocity profiles in stepped spillways for different spillway slopes and step heights 140

4.36 Universal velocity profiles in the lower region of the flow in a stepped spillway with l/h=0.6 and h= 125 mm (k= 76.6 mm) 141

4.37 Universal velocity profiles in the lower region of the flow in a stepped spillway with l/h=0.6 and h= 62.5 mm (k= 38.3 mm) 142

4.38 Universal velocity profiles in the lower region of the flow in a stepped spillway with l/h=0.6 and h= 31.25 mm (k= 19.15 mm) 143

4.39 Universal velocity profiles in the low region of the flow in a stepped spillway with l/h=0.8 and h= 125 mm (k= 83.3 mm) 144

4.40 Universal velocity profiles in the lower region of the flow in a stepped spillway with l/h=0.8 and h= 31.25 mm (k= 20.8 mm) 145

4.41 Universal velocity profiles in the lower region of the flow in stepped spillways for various values of slope and step height 146

4.42 Schematic sketch showing the control volume for the developed region in the skimming flow 147

4.43 Variation of the skin friction coefficient for the skimming flow in stepped spillways and fishways and pipe flow 148

4.44 Variation of the average skin friction coefficient for the skimming flow in stepped spillways and fishways and pipe flow 149

4.45 A schematic sketch of the flow in the developed region with a varying density and velocity 150

4.46 Variation of energy loss with discharge in stepped spillways for various value of step height and slope 151

A.1 Concentration profile at step tip #13 in a stepped spillway with l/h=0.6, h= 125. mm (yc/h=0.7) 183

A.2 Concentration profile at step tip #13 in a stepped spillway with l/h=0.6, h= 125. mm (yc/h=0.8) 184

A.3 Concentration profile at step tip #13 in a stepped spillway with l/h=0.6, h= 125. mm (yc/h=1.0) 185

A.4 Concentration profile at step tip #13 in a stepped spillway with l/h=0.6, h= 125. mm (yc/h=1.1) 186

A.5 Concentration profile at step tip #16 in a stepped spillway with l/h=0.6, h= 125. mm (yc/h=1.2) 187

A.6 Concentration profile at step tip #16 in a stepped spillway with l/h=0.6, h= 125. mm (yc/h=1.3) 188

A.7 Concentration profile at step tip #26 in a stepped spillway with l/h=0.6, h= 62.5 mm (yc/h=1.3) 189

A.8 Concentration profile at step tip #26 in a stepped spillway with l/h=0.6, h= 62.5 mm (yc/h=1.4) 190

A.9 Concentration profile at step tip #26 in a stepped spillway with l/h=0.6, h= 62.5 mm (yc/h=1.5) 191

A.10 Concentration profile at step tip #26 in a stepped spillway with l/h=0.6, h= 62.5 mm (yc/h=1.6) 192

A.11 Concentration profile at step tip #26 in a stepped spillway with l/h=0.6, h= 62.5 mm (yc/h=1.7) 193

A.12 Concentration profile at step tip #26 in a stepped spillway with l/h=0.6, h= 62.5 mm (yc/h=1.8) 194

A.13 Concentration profile at step tip #32 in a stepped spillway with l/h=0.6, h= 62.5 mm (yc/h=2.0) 195

A.14 Concentration profile at step tip #26 in a stepped spillway with l/h=0.6, h= 62.5 mm (yc/h=2.1) 196

A.15 Concentration profile at step tip #32 in a stepped spillway with l/h=0.6, h= 62.5 mm (yc/h=2.2) 197

A.16 Concentration profile at step tip #32 in a stepped spillway with l/h=0.6, h= 62.5 mm (yc/h=2.3) 198

A.17 Concentration profile at step tip #32 in a stepped spillway with l/h=0.6, h= 62.5 mm (yc/h=2.4) 199

A.18 Concentration profile at step tip #32 in a stepped spillway with l/h=0.6, h= 62.5 mm (yc/h=2.5) 200

A.19 Concentration profile at step tip #32 in a stepped spillway with l/h=0.6, h= 62.5 mm (yc/h=2.6) 201

A.20 Concentration profile at step tip #32 in a stepped spillway with l/h=0.6, h= 62.5 mm (yc/h=2.6) 202

A.21 Concentration profile at step tip #64 in a stepped spillway with l/h=0.6, h= 31.25 mm (yc/h=2.8) 203

A.22 Concentration profile at step tip #64 in a stepped spillway with l/h=0.6, h= 31.25 mm (yc/h=3.0) 204

A.23 Concentration profile at step tip #64 in a stepped spillway with l/h=0.6, h= 31.25 mm (yc/h=3.2) 205

A.24 Concentration profile at step tip #64 in a stepped spillway with l/h=0.6, h= 31.25 mm (yc/h=3.4) 206

A.25 Concentration profile at step tip #64 in a stepped spillway with l/h=0.6, h= 31.25 mm (yc/h=3.6) 207

A.26 Concentration profile at step tip #64 in a stepped spillway with l/h=0.6, h= 31.25 mm (yc/h=3.8) 208

A.27 Concentration profile at step tip #64 in a stepped spillway with l/h=0.6, h= 31.25 mm (yc/h=4.0) 209

A.28 Concentration profile at step tip #64 in a stepped spillway with l/h=0.6, h= 31.25 mm (yc/h=4.2) 210

A.29 Concentration profile at step tip #64 in a stepped spillway with l/h=0.6, h= 31.25 mm (yc/h=4.4) 211

A.30 Concentration profile at step tip #15 in a stepped spillway with l/h=0.8, h= 125. mm (yc/h=0.7) 212

A.31 Concentration profile at step tip #15 in a stepped spillway with l/h=0.8, h= 125. mm (yc/h=0.8) 213

A.32 Concentration profile at step tip #15 in a stepped spillway with l/h=0.8, h= 125. mm (yc/h=0.9) 214

A.33 Concentration profile at step tip #15 in a stepped spillway with l/h=0.8, h= 125. mm (yc/h=1.0) 215

A.34 Concentration profile at step tip #15 in a stepped spillway with l/h=0.8, h= 125. mm (yc/h=1.1) 216

A.35 Concentration profile at step tip #15 in a stepped spillway with l/h=0.8, h= 125. mm (yc/h=1.2) 217

A.36 Concentration profile at step tip #15 in a stepped spillway with l/h=0.8, h= 125. mm (yc/h=1.3) 218

A.37 Concentration profile at step tip #60 in a stepped spillway with l/h=0.8, h= 31.25 mm (yc/h=2.6) 219

A.38 Concentration profile at step tip #60 in a stepped spillway with l/h=0.8, h= 31.25 mm (yc/h=2.8) 220

A.39 Concentration profile at step tip #60 in a stepped spillway with l/h=0.8, h= 31.25 mm (yc/h=3.0) 221

A.40 Concentration profile at step tip #60 in a stepped spillway with l/h=0.8, h= 31.25 mm (yc/h=3.2) 222

A.41 Concentration profile at step tip #60 in a stepped spillway with l/h=0.8, h= 31.25 mm (yc/h=3.4) 223

A.42 Concentration profile at step tip #60 in a stepped spillway with l/h=0.8, h= 31.25 mm (yc/h=3.6) 224

A.43 Concentration profile at step tip #60 in a stepped spillway with l/h=0.8, h= 31.25 mm (yc/h=3.8) 225

A.44 Concentration profile at step tip #60 in a stepped spillway with l/h=0.8, h= 31.25 mm (yc/h=4.0) 226

A.45 Concentration profile at step tip #60 in a stepped spillway with l/h=0.8, h= 31.25 mm (yc/h=4.2) 227

A.46 Concentration profile at step tip #60 in a stepped spillway with l/h=0.8, h= 31.25 mm (yc/h=4.4) 228

B.1 Velocity profile at step tip #13 in a stepped spillway with l/h=0.6, h= 125. mm (yc/h=0.7) 230

B.2 Velocity profile at step tip #13 in a stepped spillway with l/h=0.6, h= 125. mm (yc/h=0.8) 231

B.3 Velocity profile at step tip #13 in a stepped spillway with l/h=0.6, h= 125. mm (yc/h=1.0) 232

B.4 Velocity profile at step tip #13 in a stepped spillway with l/h=0.6, h= 125. mm (yc/h=1.1) 233

B.5 Velocity profile at step tip #16 in a stepped spillway with l/h=0.6, h= 125. mm (yc/h=1.2) 234

B.6 Velocity profile at step tip #16 in a stepped spillway with l/h=0.6, h= 125. mm (yc/h=1.3) 235

B.7 Velocity profile at step tip #26 in a stepped spillway with l/h=0.6, h= 62.5 mm (yc/h=1.3) 236

B.8 Velocity profile at step tip #26 in a stepped spillway with l/h=0.6, h= 62.5 mm (yc/h=1.4) 237

B.9 Velocity profile at step tip #26 in a stepped spillway with l/h=0.6, h= 62.5 mm (yc/h=1.5) 238

B.10 Velocity profile at step tip #26 in a stepped spillway with l/h=0.6, h= 62.5 mm (yc/h=1.6) 239

B.11 Velocity profile at step tip #26 in a stepped spillway with l/h=0.6, h= 62.5 mm (yc/h=1.7) 240

B.12 Velocity profile at step tip #26 in a stepped spillway with l/h=0.6, h= 62.5 mm (yc/h=1.8) 241

B.13 Velocity profile at step tip #32 in a stepped spillway with l/h=0.6, h= 62.5 mm (yc/h=2.0) 242

B.14 Velocity profile at step tip #32 in a stepped spillway with l/h=0.6, h= 62.5 mm (yc/h=2.1) 243

B.15 Velocity profile at step tip #32 in a stepped spillway with l/h=0.6, h= 62.5 mm (yc/h=2.2) 244

B.16 Velocity profile at step tip #32 in a stepped spillway with l/h=0.6, h= 62.5 mm (yc/h=2.3) 245

B.17 Velocity profile at step tip #32 in a stepped spillway with l/h=0.6, h= 62.5 mm (yc/h=2.4) 246

B.18 Velocity profile at step tip #32 in a stepped spillway with l/h=0.6, h= 62.5 mm (yc/h=2.5) 247

B.19 Velocity profile at step tip #32 in a stepped spillway with l/h=0.6, h= 62.5 mm (yc/h=2.6) 248

B.21 Velocity profile at step tip #64 in a stepped spillway with l/h=0.6, h= 31.25 mm (yc/h=2.8) 249

B.22 Velocity profile at step tip #64 in a stepped spillway with l/h=0.6, h= 31.25 mm (yc/h=3.0) 250

B.23 Velocity profile at step tip #64 in a stepped spillway with l/h=0.6, h= 31.25 mm (yc/h=3.2) 251

B.24 Velocity profile at step tip #64 in a stepped spillway with l/h=0.6, h= 31.25 mm (yc/h=3.4) 252

B.25 Velocity profile at step tip #64 in a stepped spillway with l/h=0.6, h= 31.25 mm (yc/h=3.6) 253

B.26 Velocity profile at step tip #64 in a stepped spillway with l/h=0.6, h= 31.25 mm (yc/h=3.8) 254

B.27 Velocity profile at step tip #64 in a stepped spillway with l/h=0.6, h= 31.25 mm (yc/h=4.0) 255

B.28 Velocity profile at step tip #64 in a stepped spillway with l/h=0.6, h= 31.25 mm (yc/h=4.2) 256

B.29 Velocity profile at step tip #64 in a stepped spillway with l/h=0.6, h= 31.25 mm (yc/h=4.4) 257

B.20 Velocity profile at step tip #64 in a stepped spillway with l/h=0.6, h= 31.25 mm (yc/h=2.6) 258

B.30 Velocity profile at step tip #15 in a stepped spillway with l/h=0.8, h= 125. mm (yc/h=0.7) 259

B.31 Velocity profile at step tip #15 in a stepped spillway with l/h=0.8, h= 125. mm (yc/h=0.8) 260

B.32 Velocity profile at step tip #15 in a stepped spillway with l/h=0.8, h= 125. mm (yc/h=0.9) 261

B.33 Velocity profile at step tip #15 in a stepped spillway with l/h=0.8, h= 125. mm (yc/h=1.0) 262

B.34 Velocity profile at step tip #15 in a stepped spillway with l/h=0.8, h= 125. mm (yc/h=1.1) 263

B.35 Velocity profile at step tip #15 in a stepped spillway with l/h=0.8, h= 125. mm (yc/h=1.2) 264

B.36 Velocity profile at step tip #15 in a stepped spillway with l/h=0.8, h= 125. mm (yc/h=1.3) 265

B.37 Velocity profile at step tip #60 in a stepped spillway with l/h=0.8, h= 31.25 mm (yc/h=2.6) 266

B.38 Velocity profile at step tip #60 in a stepped spillway with l/h=0.8, h= 31.25 mm (yc/h=2.8) 267

B.39 Velocity profile at step tip #60 in a stepped spillway with l/h=0.8, h= 31.25 mm (yc/h=3.0) 268

B.40 Velocity profile at step tip #60 in a stepped spillway with l/h=0.8, h= 31.25 mm (yc/h=3.2) 269

B.41 Velocity profile at step tip #60 in a stepped spillway with l/h=0.8, h= 31.25 mm (yc/h=3.4) 270

B.42 Velocity profile at step tip #60 in a stepped spillway with l/h=0.8, h= 31.25 mm (yc/h=3.6) 271

B.43 Velocity profile at step tip #60 in a stepped spillway with l/h=0.8, h= 31.25 mm (yc/h=3.8) 272

B.44 Velocity profile at step tip #60 in a stepped spillway with l/h=0.8, h= 31.25 mm (yc/h=4.0) 273

B.45 Velocity profile at step tip #60 in a stepped spillway with l/h=0.8, h= 31.25 mm (yc/h=4.2) 274

B.46 Velocity profile at step tip #60 in a stepped spillway with l/h=0.8, h= 31.25 mm (yc/h=4.4) 275

C.1 Logarithmic velocity profiles at different origins at step #13 in a stepped spillway with l/h=0.6, h= 125. mm, k= 76.6 mm (yc/h=0.7) 277

C.2 Logarithmic velocity profiles at different origins at step #13 in a stepped spillway with l/h=0.6, h= 125. mm, k= 76.6 mm (yc/h=0.8) 278

C.3 Logarithmic velocity profiles at different origins at step #13 in a stepped spillway with l/h=0.6, h= 125. mm, k= 76.6 mm (yc/h=1.0) 279

C.4 Logarithmic velocity profiles at different origins at step #13 in a stepped spillway with l/h=0.6, h= 125. mm, k= 76.6 mm (yc/h=1.1) 280

C.5 Logarithmic velocity profiles at different origins at step #13 in a stepped spillway with l/h=0.6, h= 125. mm, k= 76.6 mm (yc/h=1.2) 281

C.6 Logarithmic velocity profiles at different origins at step #13 in a stepped spillway with l/h=0.6, h= 125. mm, k= 76.6 mm (yc/h=1.3) 282

C.7 Logarithmic velocity profiles at different origins at step #26 in a stepped spillway with l/h=0.6, h= 62.5 mm, k= 38.3 mm (yc/h=1.3) 283

C.8 Logarithmic velocity profiles at different origins at step #26 in a stepped spillway with l/h=0.6, h= 62.5 mm, k= 38.3 mm (yc/h=1.4) 284

C.9 Logarithmic velocity profiles at different origins at step #26 in a stepped spillway with l/h=0.6, h= 62.5 mm, k= 38.3 mm (yc/h=1.5) 285

C.10 Logarithmic velocity profiles at different origins at step #26 in a stepped spillway with l/h=0.6, h= 62.5 mm, k= 38.3 mm (yc/h=1.6) 286

C.11 Logarithmic velocity profiles at different origins at step #26 in a stepped spillway with l/h=0.6, h= 62.5 mm, k= 38.3 mm (yc/h=1.7) 287

C.12 Logarithmic velocity profiles at different origins at step #26 in a stepped spillway with l/h=0.6, h= 62.5 mm, k= 38.3 mm (yc/h=1.8) 288

C.13 Logarithmic velocity profiles at different origins at step #26 in a stepped spillway with l/h=0.6, h= 62.5 mm, k= 38.3 mm (yc/h=2.0) 289

C.14 Logarithmic velocity profiles at different origins at step #26 in a stepped spillway with l/h=0.6, h= 62.5 mm, k= 38.3 mm (yc/h=2.1) 290

C.15 Logarithmic velocity profiles at different origins at step #26 in a stepped spillway with l/h=0.6, h= 62.5 mm, k= 38.3 mm (yc/h=2.2) 291

C.16 Logarithmic velocity profiles at different origins at step #26 in a stepped spillway with l/h=0.6, h= 62.5 mm, k= 38.3 mm (yc/h=2.3) 292

C.17 Logarithmic velocity profiles at different origins at step #26 in a stepped spillway with l/h=0.6, h= 62.5 mm, k= 38.3 mm (yc/h=2.4) 293

C.18 Logarithmic velocity profiles at different origins at step #26 in a stepped spillway with l/h=0.6, h= 62.5 mm, k= 38.3 mm (yc/h=2.5) 294

C.19 Logarithmic velocity profiles at different origins at step #26 in a stepped spillway with l/h=0.6, h= 62.5 mm, k= 38.3 mm (yc/h=2.6) 295

C.20 Logarithmic velocity profiles at different origins at step #64 in a stepped spillway with l/h=0.6, h= 31.25 mm, k= 19.14 mm (yc/h=2.6) 296

C.21 Logarithmic velocity profiles at different origins at step #64 in a stepped spillway with l/h=0.6, h= 31.25 mm, k= 19.14 mm (yc/h=2.8) 297

C.22 Logarithmic velocity profiles at different origins at step #64 in a stepped spillway with l/h=0.6, h= 31.25 mm, k= 19.14 mm (yc/h=3.0) 298

C.23 Logarithmic velocity profiles at different origins at step #64 in a stepped spillway with l/h=0.6, h= 31.25 mm, k= 19.14 mm (yc/h=3.2) 299

C.24 Logarithmic velocity profiles at different origins at step #64 in a stepped spillway with l/h=0.6, h= 31.25 mm, k= 19.14 mm (yc/h=3.4) 300

C.25 Logarithmic velocity profiles at different origins at step #64 in a stepped spillway with l/h=0.6, h= 31.25 mm, k= 19.14 mm (yc/h=3.6) 301

C.26 Logarithmic velocity profiles at different origins at step #64 in a stepped spillway with l/h=0.6, h= 31.25 mm, k= 19.14 mm (yc/h=3.8) 302

C.27 Logarithmic velocity profiles at different origins at step #64 in a stepped spillway with l/h=0.6, h= 31.25 mm, k= 19.14 mm (yc/h=4.0) 303

C.28 Logarithmic velocity profiles at different origins at step #64 in a stepped spillway with l/h=0.6, h= 31.25 mm, k= 19.14 mm (yc/h=4.2) 304

C.29 Logarithmic velocity profiles at different origins at step #64 in a stepped spillway with l/h=0.6, h= 31.25 mm, k= 19.14 mm (yc/h=4.4) 305

C.30 Logarithmic velocity profiles at different origins at step #15 in a stepped spillway with l/h=0.8, h= 125. mm, k= 83.3 mm (yc/h=0.7) 306

C.31 Logarithmic velocity profiles at different origins at step #15 in a stepped spillway with l/h=0.8, h= 125. mm, k= 83.3 mm (yc/h=0.8) 307

C.32 Logarithmic velocity profiles at different origins at step #15 in a stepped spillway with l/h=0.8, h= 125. mm, k= 83.3 mm (yc/h=0.9) 308

C.33 Logarithmic velocity profiles at different origins at step #15 in a stepped spillway with l/h=0.8, h= 125. mm, k= 83.3 mm (yc/h=1.0) 309

C.34 Logarithmic velocity profiles at different origins at step #15 in a stepped spillway with l/h=0.8, h= 125. mm, k= 83.3 mm (yc/h=1.1) 310

C.35 Logarithmic velocity profiles at different origins at step #15 in a stepped spillway with l/h=0.8, h= 125. mm, k= 83.3 mm (yc/h=1.2) 311

C.36 Logarithmic velocity profiles at different origins at step #15 in a stepped spillway with l/h=0.8, h= 125. mm, k= 83.3 mm (yc/h=1.3) 312

C.37 Logarithmic velocity profiles at different origins at step #60 in a stepped spillway with l/h=0.8, h= 31.25 mm, k= 20.8 mm (yc/h=2.6) 313

C.38 Logarithmic velocity profiles at different origins at step #60 in a stepped spillway with l/h=0.8, h= 31.25 mm, k= 20.8 mm (yc/h=2.8) 314

C.39 Logarithmic velocity profiles at different origins at step #60 in a stepped spillway with l/h=0.8, h= 31.25 mm, k= 20.8 mm (yc/h=3.0) 315

C.40 Logarithmic velocity profiles at different origins at step #60 in a stepped spillway with l/h=0.8, h= 31.25 mm, k= 20.8 mm (yc/h=3.2) 316

C.41 Logarithmic velocity profiles at different origins at step #60 in a stepped spillway with l/h=0.8, h= 31.25 mm, k= 20.8 mm (yc/h=3.4) 317

C.42 Logarithmic velocity profiles at different origins at step #60 in a stepped spillway with l/h=0.8, h= 31.25 mm, k= 20.8 mm (yc/h=3.6) 318

C.43 Logarithmic velocity profiles at different origins at step #60 in a stepped spillway with l/h=0.8, h= 31.25 mm, k= 20.8 mm (yc/h=3.8) 319

C.44 Logarithmic velocity profiles at different origins at step #60 in a stepped spillway with l/h=0.8, h= 31.25 mm, k= 20.8 mm (yc/h=4.0) 320

C.45 Logarithmic velocity profiles at different origins at step #60 in a stepped spillway with l/h=0.8, h= 31.25 mm, k= 20.8 mm (yc/h=4.2) 321

C.46 Logarithmic velocity profiles at different origins at step #60 in a stepped spillway with l/h=0.8, h= 31.25 mm, k= 20.8 mm (yc/h=4.4) 322

LIST OF PLATES

Plate	Title	Page
3.1	A close-up view of the air bubbles trapped in the recirculating flow on a step	67
3.2	The electrical air concentration probe	68
3.3 (a-b)	The electrical circuit for the air concentration probe	
	(a) the circuit	69
	(b) the wave generator	70
3.4	The experimental setup for the velocity measurements	71
3.5	The flushing system designed to evacuate the air bubbles from the Prandtl tube	72
3.6	The stepped spillway model	73
4.1	Side view of a stepped spillway model featuring the non-aerated region	152
4.2	Front view of the stepped spillway model showing that the air entrainment starts earlier at side walls than the central part	153
4.3	The developing region of the skimming flow over a stepped spillway model	154
4.4	A close-up view of the flow in the developing region	155
4.5	Side view of the developed region in the skimming flow	156
4.6	A close-up view of the flow in the developed region showing two different zones	157

4.7(a-d) The evolution and termination of the vortex tube generated at a step tip in the developed region of a skimming flow (l/h= 0.6, h=125 mm)
(a) frame # 4622 158
(b) frame # 4661 159
(c) frame # 4728 160
(d) frame # 4742 161

4.8(a-b) The varying flow surface in the developed region (l/h= 0.6, h= 125 mm)
(a) frame # 607 162
(b) frame # 915 163

4.9(a-d) Process of the "rooster tail" formation (l/h= 0.6, h= 125 mm)
(a) frame # 502 164
(b) frame # 599 165
(c) frame # 705 166
(d) frame # 810 167

4.10(a-b) The existence of dark and white cloudlets in the air-water mixture (l/h= 0.6, h= 62.5 mm)
(a) frame # 273 168
(b) frame # 373 169

4.11(a-d) The passage of a dark cloudlet, marked as A, between two consecutive step tips on a streamline (l/h= 0.6, h= 62.5 mm)
(a) frame # 166 170
(b) frame # 176 171
(c) frame # 185 172
(d) frame # 196 173

LIST OF SYMBOLS

A	constant in the velocity equation
a	constant in the inception section equation
B, B', B''	constants in the velocity equation
B_w	channel width
b	constant in the inception section equation
C	air concentration
$\overline{C}$	mean air concentration
C_1	air concentration at $y_T/2$
C_T	air concentration at y_T
c	constant in the inception section equation
c_f	skin friction coefficient
cl	confidence level of w
D	data
D_1, D_n	n independent data
D_H	hydraulics diameter
D_m	mean value of D
d	constant in the inception section equation
dQ	integrated water discharge
E	specific energy
E_b	specific energy at the base of a stepped spillway
E_u	specific energy at the upstream of a stepped spillway
E'	specific energy at the toe of a chute spillway
$\overline{E_b}$	mean specific energy at the base of a stepped spillway
$\overline{E_u}$	mean specific energy at the upstream of a stepped spillway
e	constant in the inception section equation
F	$= q/\sqrt{g y_0^3}$ = Froude number
F_i	$= q/\sqrt{g(h/l)k^3}$ = Froude number of the inception section of air entrainment
F^*	$= q/\sqrt{g \sin\theta\, k^3}$ = Froude number defined in terms of the roughness k

f	Darcy friction factor
g	gravity acceleration
H	height of a stepped spillway
h	step height
h_e	discharge head
h_{stag}	stagnation pressure head
h_{stat}	static pressure head.
k	height of a roughness projection normal to the bed
L	distance from the crest
L_i	distance of the inception section of air entrainment from the spillway crest
m	mass of a body
N	number of steps
p_{stag}	stagnation pressure
p_{stat}	static pressure
Q	flow discharge
q	specific discharge
p_r	wetted perimeter
R	electrical resistance of a liquid
R	result
R_1	electrical resistance of a suspension
R_p	electrical resistance of the air concentration probe
R_s	arbitrary series electrical resistance
r	specific resistivity of a fluid
r_1	specific resistivity of a suspended sphere
r_2	specific resistivity of a suspension
s	$= \sin \theta =$ slope of a stepped spillway
u	velocity
u_*	bed shear velocity
u_m	air-water mixture velocity
V	Mean velocity
V_m	mean velocity of the air-water mixture
V_b	rising velocity of air bubbles
v_0	supply voltage

v_p	voltage across the R_p
v_s	voltage across the R_s
v_{0i}	initial supply voltage when the air concentration probe is placed in pure water
v_{si}	initial voltage across the arbitrary resistance when the air concentration probe is placed in pure water.
W	weight of a body
$W_1,\ldots,\ W_n$	uncertainty intervals of n independent data
W_C	uncertainty interval of the air concentration
W_R	uncertainty interval of the result
W_{V_m}	uncertainty intervals of the velocity
$W_{\Delta h}$	uncertainty interval of the pressure head
w	uncertainty interval
x	factor described in Eq.(3.6)
y	depth of flow with respect to the tip of a step
y_1	flow depth at the toe of a stepped spillway
y_2	sequence depth of the hydraulic jump
$y_{.9}$	depth of the aerated flow where air concentration is 90%
y_0	normal depth
y_*	thickness of viscous sub-layer
y_c	$= \sqrt[3]{q^2/g}$ = critical depth
$\bar{y}$	sum of water column in an aerated flow
y_m	projection height
y_s	elevation of the flow surface
y_T	transition depth
y_u	upper depth of the aerated flow where air concentration reaches a specific value
y_ε	$= y+k-\varepsilon$ = depth of flow with respect to the displaced origion
y_{um}	depth of flow at which velocity profile starts to decline
y_{rt}	height of the rooster tail
y^+	$= y/k_s$ = a dimensionless distance
$\overline{y_*}$	measure of the flow depth above the streamline y defined in Eq. (4.25)

$y^{'}$	height above the transition depth
$y^{''}$	$= y_T - y$ = distance below the transition depth
$\bar{y}$	sum of water column in an aerated flow
Z_0	elevation of the upstream channel bed above the base of a stepped spillway
z	constant in the velocity equation
τ	shear stress
$\bar{\tau}$	bed shear stress
γ_m	specific weight of the air-water mixture
α	kinetic energy correction factor for a non-aerated flow
α_e	kinetic energy correction factor for the aerated flow
β	proportionality factor
δ	boundary layer height
ΔE	energy loss
Δh	$= h_{stag} - h_{stat}$ = pressure head
Δx, Δy, Δz	dimensions of a fluid element
ε	origin displacement
ε_b	mixing parameter
κ	von Karman universal constant
λ	roughness spacing
θ	inclination of a stepped spillway
ρ	mass density
ρ_m	mass density of the air-water mixture
ρ_w	mass density of water
$\overline{\rho_m}$	average mass density of the air-water mixture

Chapter 1
INTRODUCTION

The search for effective spillway designs has been ongoing since the very beginning of the building of dams. Stepped spillways have been used for over 2,500 years (Chanson, 1994). The recent technological advance of Roller Compacted Concrete (RCC) dams has increased the interest in stepped spillways (Hansen, 1986; Dunstan, 1990). Over a short period, the use of RCC dams and the associated use of stepped spillways for the gravity dams, have gained widespread acceptance. This is partly due to the intrinsic low-cost and speed of construction (Parker, 1992, Logie, 1985). Figure 1.1 shows basic cost comparison for conventionally constructed gravity dams and RCC gravity dams. The RCC technique is also adopted increasingly for the rehabilitation of earth and concrete dams. Steps have been added with the RCC technique to dam embankments to allow safe passage of overtopping floods. Thus, the capacity of the spillways can be increased to accommodate extreme hydrological events such as the Probable Maximum Flood (PMF) at little cost (Frizell, 1992).

A stepped spillway consists of an open channel with a series of steps that are built into the face of the spillway. The rough or stepped face of the spillway can dissipate a significant portion of the energy of the flow over its surface. The dissipation of kinetic energy reduces the scour in the natural channel below the structure and hence the cost of the stilling basin. It also eliminates the problem of cavitation on the spillway. Preliminary investigation on stepped spillway models revealed that two types of flow exist that depend on the discharge:

i) Jet Flow: At relatively low discharges, the flow strikes the tread of the step immediately below. The energy dissipation is mainly due to the jet mixing in the recirculating pool formed on each step and sometimes by a partial hydraulic jump.

ii) Skimming Flow: At higher discharges, the steps become completely submerged. The flow skims over the steps and is retarded by the recirculating fluid trapped on each step. One predominant feature of the flow is the creation of large air concentrations in the flow. Self-aeration is the natural phenomenon whereby atmospheric air is drawn into and mixed with the water to create a white and spray-like appearance. This creates a violently agitated and ill-defined free surface. This condition is prevalent in high speed open channel flows and is frequently observed in stepped spillways. Flow causing steps to be "drowned" will be described as Skimming Flow.

These basic flow types are shown in Plates 1.1 and 1.2.

At the present time, little information is available on the flow characteristics of stepped spillways. Previous investigations focused mainly on physical models used to evaluate the energy dissipation resulting from specific stepped spillway designs. Unfortunately, these investigations have considered the flow only as one-phase flow and the effect of air entrainment was generally neglected. The basic objective of the present investigation is to find a solution of this complex problem of flow behavior on stepped spillways through the use of a relatively large physical model and the provision of fundamental information for the analytical design of such structures. This study has been limited to the Skimming Flow regime. The primary objectives of the study are therefore :

i) The observation, analysis and classification of the flow behavior.

ii) The quantitative analysis of the influence of discharge intensity, overall spillway slope and step size on the characteristics of the flow over the spillway.

iii) The presentation of the experimental data in a concise, dimensionless form that readily yields the flow characteristics important in the design of prototype structures.

iv) An examination of the validity of applying empirical and theoretical relationships developed for water flow in relatively rough open channel flow, thus allowing the stepped spillway to be described as a steep open channel with large artificial roughness.

Chapter two presents a review of earlier investigations on the hydraulics of flow over stepped spillways. This chapter focuses mainly on the experimental studies. A major part of the project involved the construction of the physical model and instrumentation to measure various spillway flow parameters. Part of the instrumentation included the construction of a probe for measuring air concentration in the skimming flow. The physical model and instrumentation are described in detail in chapter three. An error analysis is also included in chapter three. Typical results from the experimental program are presented in chapter four. In chapter four, the analysis of the experimental data is also presented. On the basis of the analysis, a design method is proposed whereby the air concentration and velocity profiles within the fully developed region may be predicted. Chapter five completes the thesis by presenting the conclusions based on the results of the experimental study. This chapter also incorporates suggestions for further work.

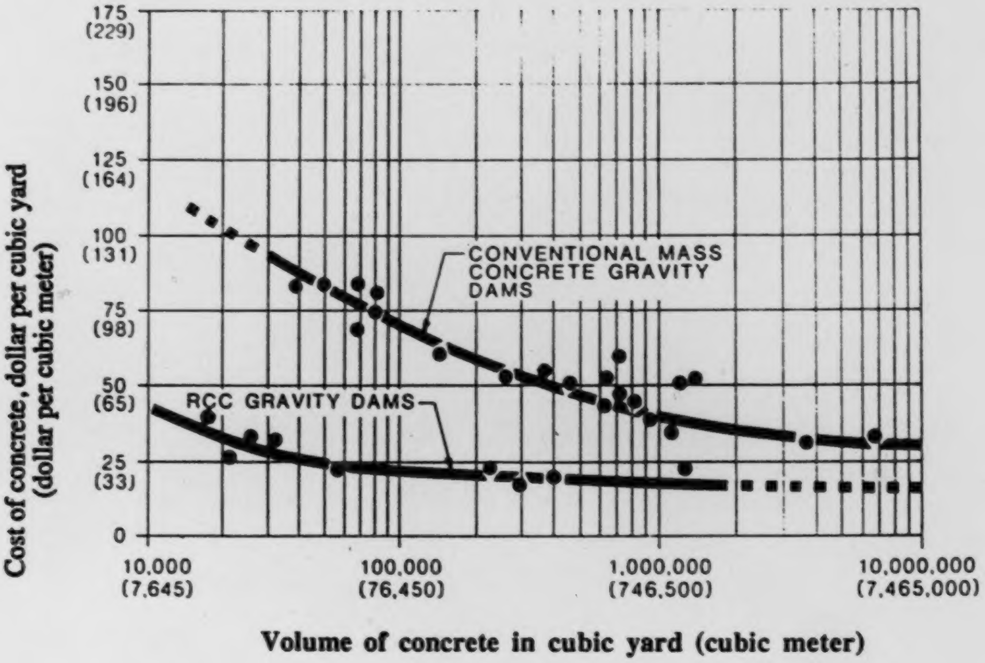

Figure 1.1 Cost comparison of RCC and mass concrete dams (adapted from Logie, 1985)

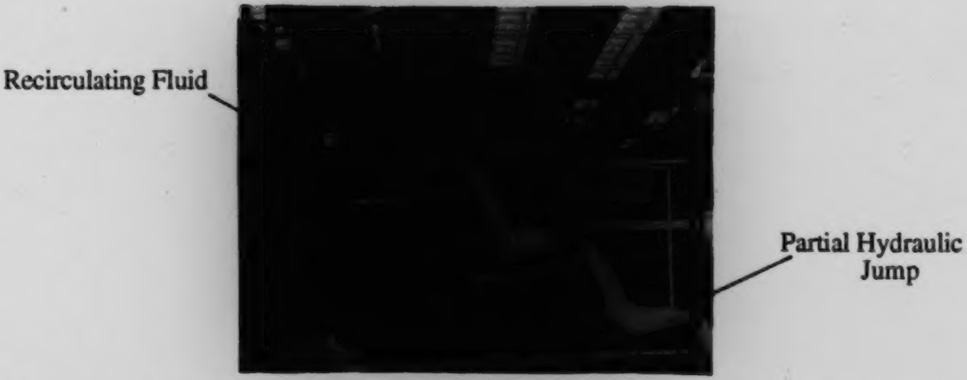
Recirculating Fluid
Partial Hydraulic Jump

Plate 1.1 Jet flow on a stepped spillway model (adapted from Essery and Horner, 1978)

Plate 1.2 Skimming flow over a stepped spillway model

Chapter 2
LITERATURE REVIEW

2.1 Introduction

The published literature indicates an awareness that the design of the self-aerated flows on stepped spillways is poorly understood. During the last decade, the demand for a more comprehensive understanding of self-aerated flows has intensified. Although numerous physical model studies of projects incorporating stepped spillways have been undertaken, the effect of self-aeration has been neglected in the flow parameters. Self-aeration is an unavoidable feature of flow on stepped spillways as the high velocity flow, disturbed by the steps, entrains air. Problems associated with the analysis of two-phase flows have slowed progress in this area.

Most investigations of stepped spillways have focused on an estimation of the energy loss on the spillway. Efforts have also been made to understand the mechanism for energy loss, mostly through the use of photographic observations. Attempts to study the flow parameters which are responsible for the dissipation of energy, however, have been limited.

Other researchers have studied self-aerated flow in chute spillways, mostly in the last half century. These works were notable for their clarification of the detailed structures of fully developed, self-aerated flow (a flow where terminal air and velocity profiles have been reached). Analytical solutions were developed to explain the air concentration distributions.

Results from both subjects of investigation can be combined to gain an understanding of self-aerated flows on stepped spillways. The volume of published material is considerable, so that the following survey covers mainly those publications which have made significant contributions to the subject. Due to the nature of the present investigation, a preference is also given to those publications that experimentally studied the phenomenon of skimming flow on stepped spillways. The objective is to allow for a better appreciation of the mechanisms of the flow and therefore the present investigation.

2.2. Physical Model Studies

Most investigations, presented in this section, were based upon experiments and models studies in laboratories. The objectives of these studies were typically to evaluate the shape of the spillway crest and/or the step geometry, and to quantify the energy dissipation.

2.2.1 Essery and Horner (1978)

In this extensive experimental study, the flow behavior on stepped spillway models was analyzed. A basis for predicting prototype performance from model studies was established by determining the factors which influence flow characteristics. A wide range of step geometry and flow conditions were studied. The results of this study were presented in the form of dimensionless plots which were used for the design of stilling basins.

Five models featuring thirty, twenty, ten, eight, and three steps were built. In each model, the height, length, and inclination of steps to the horizontal were varied to ensure a wide range of step configurations. The height of each step ranged from 1067 mm for the three step model to 29 mm for thirty step model. The step length was varied from 1067 mm for three step model to 69 mm for thirty step model. These ranges covered the spillway slope from 1.2H:1V to 2.4H:1V.

The experimental results for jet flow included the measurements of velocity and flow depth. The results showed the influence of discharge, slope, step size, and step inclination on the specific force and specific energy. A graph was presented that shows the onset of skimming flow on thirty step model. Essery and Horner found that skimming flow is initiated when y_c/h is about 0.8, where y_c is the critical depth of the flume and h is the step height. Other observations of skimming flow on thirty step model revealed that three zones exist as following:

i) A "clear water" zone at the upstream end of the spillway where the velocity increases and hence the depth decreases.

ii) A "white water" zone which forms some distance below the clear water zone, where water drops are ejected upward into the air. The flow in this zone is a mixture of air and water.

iii) A zone of equilibrium where the flow becomes uniform. This occurs after a short length in the white water zone.

Other observations of skimming flow were not presented as there were problems associated with the measurement of air concentration. Essery and Horner believed that scale effect of the models could not be estimated since skimming flow in the larger models used in the study of jet flow could not be created because the large discharges required could not be provided.

2.2.2 Sorensen (1985)

The performance of a stepped spillway for the new Monksville Dam in the United States was examined in a physical model study in the Hydraulics Laboratory of Lehigh University. The objectives were to design the proper spillway crest and to determine the energy dissipation as well as the height of the training wall along the stepped spillway face. The Waterways Experiment Station (WES) standard Ogee spillway profile was modified to ensure the effectiveness of flow transition below the crest.

The stepped spillway measured 120 ft heigh and had a 0.78H:1V slope below the point of tangency of the spillway profile. Three models were studied, one with a scale of 1/10, another two with a 1/25 scale. The 1/10 model of the upper part of the spillway was built to investigate the performance of the crest and the geometry of the first few steps. The first model of 1/25 scale of the chute spillway was built to provide comparison data for the second model of scale 1/25, a full stepped spillway profile. All models tested had a clear Plexiglas front wall and a width of 1 ft. The first few steps had heights equivalent to 1 and 1.5 ft in the prototype and the remaining step heights were 2 ft in prototype scale. The step height of 2 ft was chosen because of the construction techniques used for building the concrete dam.

Measurements included the upstream depth, which was measured with a precision point gage. Discharges ranged from 0.056 to 2.53 cfs/ft (model values). Flow depths were measured vertically on different step tips with a scale. Due to the air entrainment, "a conservative" depth was recorded that includes bulking of the flow. Across the toe of the spillway, at least six depth measurements were made at equally spaced intervals and the averages were used.

For the 1/10 scale model, the results showed that for discharges more than 0.38 cfs/ft, there was a smooth transition of flow onto the steps. For discharges smaller than 0.38 cfs/ft, the flow deflected outward, impinging on the spillway face several steps down the spillway. Observations showed that the deflected jet could be eliminated by adding few smaller steps on the curved section of the WES Ogee profile. Three steps of 0.75 ft height and one step of 0.5 ft height were added upstream of the first step. Dye injection in the second model of 1/25 scale revealed that the flow entered the recirculating flow developed in the steps, rotated for a short time and then returned to the main flow. In the aerated region, the air bubbles entered the recirculating flow and they were rotating with the flow. The section of air inception moved downstream as the discharge increased. The author presented a table that gives the step number at which the air entrainment commenced for different discharges. Using the discharge and the depth of flow, the continuity principle was used to calculate the velocity at the spillway toe. To check the accuracy of this velocity calculation, a stagnation tube was used to measure the velocity head. These measurements were within 10-15% of the values of the calculated velocities.

A plot of the velocities at the toe versus discharge for both chute and stepped spillways was presented (Figure 2.1). It showed that the toe velocity increased with increasing discharge. The reduction of toe velocity in the stepped spillway from the chute spillway was clearly indicated. For example, the toe velocity in the model was reduced from 18 fps for the chute spillway to 6.5 fps for the stepped spillway for the probable maximum flood discharge. Overall, the reduction of the kinetic energy at the toe of the stepped spillway varied from 94% to 88% compared to that of the chute spillway. As the flow progressed downstream from the crest, the depth of flow decreased up to the section of air inception. Due to the bulking of flow by the air entrainment, the depth continually increased toward the spillway toe. The variation of the depths along the spillway face showed that after a certain distance from the crest of the spillway, the depth of the flow is almost constant. An exception is the increase of the depth at the toe of the spillway. However, this increase was less than 15% compared to the constant depth and due to the difficulty in measuring the flow depth, it can be considered that a fully developed region developed over the spillway.

Results from testing on the model of the chute spillway showed that no air entrainment occurred. It was argued that there was scale effect as air entrainment in the prototype is expected. Sorensen deduced that the scale effect for the stepped spillway was small since the steps, which are the main roughness, are scaled down. He classified the skimming flow as a "quasi-smooth" flow based on the work of Morris (1955 & 1961). In this type of flow, the energy dissipation is due to the generation of tip vortices and the maintenance of the stable recirculating flow trapped on the steps.

In this investigation, "conservative depths" that included the bulking of the flow were measured in the aerated zone. The term "conservative depths" is not clearly defined as there is no definite upper boundary to the air-entrained flow. Measurement of velocities with stagnation tube without the associated air concentrations is of questionable value. As will be shown in the chapter 3 of this thesis, the error of ignoring the air concentration in the calculation of the velocity can be significant.

2.2.3 Bayat (1991)

A model study was conducted to evaluate the energy loss in the stepped spillway of a dam to be erected on the Karun River in Iran. The spillway height is 180 m and the overall spillway slope was 0.8H:1V. Using the recommendation of USBR, the scale of the model was set as 1/25. The standard Ogee profile was modified so that the tips of the steps followed the standard profile down to the spillway toe. Tests were carried out in a flume of 30 cm width. The transitional steps, located at the upstream end of the profile, had smaller and variable heights. The unstepped part of the crest and the transitional steps were kept unchanged and only the stepped part had different geometry in the different models. Three models with step heights of 20, 24, and 30 mm were chosen. The vertical flow depth at the spillway toe was measured by means of scale strips. No direct velocity measurement were made due to the aerated flow conditions.

Observations included the discharge, the elevation of water surface upstream of the crest, and the depth of flow at the toe of the spillway. The residual energy at the toe of the spillway, based on the flow depths, showed energy dissipation to be 86% to 97%. A relationship between the specific energy at the spillway toe and discharge was established. It was found that the model with a step height of 20 mm was more effective in dissipating energy.

Although the scale of the model was set to 1/25, the experimental set up showed that the model height was only 1.05 m. Considering the dimension of the prototype, this height should be 7.2 m. The results of energy loss calculation based entirely on average flow depths are not reliable as the criteria used for measuring depths of the aerated flow were not clearly defined. The effect of air entrainment was not taken into consideration.

2.2.4 Diez-Cascon, et al. (1991)

The energy dissipation characteristics of a stepped spillway was studied by a model in the Hydraulic Laboratory of Iberduero SA and the Water Environment Sciences and Technology Department in Spain. The prototype spillway height was 38.0 m from the crest to the toe. The spillway crest was of the Ogee type. The control section at the end of the stilling basin assured that the hydraulic jump occurred immediately after the spillway toe.

The model study was carried out on a scale of 1/10 with step heights of 3 cm in the first series of tests and 6 cm in the following series. The Ogee curve reached the downstream stepped zone with 0.75H:1V slope. At the bottom of the spillway, a curved flip bucket with the radius of 46 cm was installed. The residual energy was to be dissipated in the horizontal basin located immediately after the spillway toe. Twelve piezometric taps were placed at tips and threads of steps to measure pressures. The discharge ranged from 0.68 to 8.85 $m^3/s/m$ (prototype values).

Two regimes of jet and skimming flows were observed with a transition state that was gradual and continuous. In jet flow, which occurred for discharges less than 1.25 $m^3/s/m$, the flow was characterized by continuous fall, with or without the partial hydraulic jump on each step. On each step, a vortex formed that occupied part of the zone between the falling jet and the step. The deflection of the flow by the first step could have been corrected by adding more and smaller steps. For discharges more than 1.25 $m^3/s/m$, the flow skimmed over the steps and vortices occupied the zone between the main flow and the steps. After the few first steps, air entrainment was initiated and there was bulking of the flow. At a certain distance from the crest, a developed region, which was referred to as a "constant depth regime" was formed for each discharge. This distance increased with increasing discharge.

Tests revealed that the classical hydraulic jump theory for alternate depth did not match the results for the stepped spillway. For step heights 30 and 60 cm (prototype), the sequence depth of the hydraulic jump, y_2, were measured. The depths of the flow at the toe of the stepped spillway, y_1, were measured for the 60 cm step height. The free surface of the aerated flow was badly defined and oscillated around the mean value of the flow depth. It was mentioned that the mean values were necessarily imprecise. It was also found that values of y_1 were much higher than would be expected in a chute spillway. It was argued that the difference could have resulted from the fact that air entrainment was not taken into consideration in the formulation.

The air concentration was estimated by the ASCE (1961) formula as follows:

$$\overline{C} = 0.743 \, \boldsymbol{log(sin}\theta/q^{1/5}\boldsymbol{)} + 0.876 \qquad (2.1)$$

where $\overline{C}$= mean air concentration, θ= inclination of a spillway to the horizontal and q= specific discharge (cfs/ft). This formula was originally derived for chute spillways. Using the experimental values of y_2, the ASCE formula for air concentration, continuity and momentum principles, an approach to estimate y_1 was presented. The experimental values of y_1 appeared to be higher than the predicted values (Fig 2.2). The energy dissipation was calculated based on the theoretical results ranged from 88% to 92% for discharges from 1.8 to 5.4 $m^3/s/m$ for prototype values.

The flow depth, y_1, was later referred to as the depth of flow in the developed region. Although the energy of the flow in the developed region can be assumed to be equal to the energy at the toe, it can not be concluded that the flow depth would be equal. The method of calculating y_1 by using Eq. (2.1) for the air concentration in stepped spillways is questionable since this formula was derived for chute spillways. There was no measurement of air concentration to confirm the validity of applying Eq. (2.1) for the stepped spillway. The calculated energy loss, based on the predicted values of y_1, was over estimated.

2.2.5 Bindo et al. (1993)

A summary of a model study of the stepped spillway of the M'Bali dam was presented in this report. The dam was constructed on the M'Bali river, about 85 km northwest of the town M'Bali in the Central African Republic. This dam allowed for regulation of the river for hydroelectric plants (total capacity 18.8 MW) downstream of the dam. The M'Bali dam was a composite structure with central concrete gravity section and two lateral earthfill and rockfill sections on each side. The stepped spillway measured 24.5 m in height from the crest to the toe and was 60 m long. The initial steps, located from 1 to 3.5 m below the crest elevation, had variable heights. The remaining step heights were 0.8 m and the overall slope of the spillway was 0.8H:1V. The model test was carried out on a 1/20 scale in the Laboratoire d'Hydraulique et de Construction Navales, at the University of Liege, Belgium. A 1/40 scale model was also prepared with the provision of half-size steps.

The flow over the spillway was assumed to dissipate more energy by the provision of the steps. The macro-turbulence in the flow produced by the steps aided the growth of the boundary layer, with a thickness that increased much faster than for a chute spillway. The flow was divided into three zones (Figure 2.3):

1) A non-aerated zone at the upstream end of the spillway where the boundary layer was growing. Here the flow was supercritical and the depth decreased with distance.

2) A second zone starting where the boundary layer reached the surface, with air entering into the flow from the free surface. In this zone, the depth gradually increased due to the bulking effect of air entrainment.

3) A zone of developed aerated flow in which the flow characteristics such as depth, velocity, and air concentration were constant. It was

concluded that these characteristics could be a function of slope of the spillway.

Tests showed that the height of the initial steps should be increased near the crest to avoid overshooting of the flow for low discharges. The energy dissipation varied from 50 percent (design discharge) to 90 percent (low discharge). Figure 2.4 shows the relationship between the apparent velocity in the uniform zone (*V*) and height of the spillway (*H*) for various discharges in dimensionless form. The apparent velocity, *V*, does not consider the air concentration in the aerated zone. This graph was established for the stepped spillway design for heights of up to 80 *m*, and various unit discharges from 0 to 20 $m^3/s/m$. It was recommended that the height of the steps be chosen so that, for the maximum discharge, the air entered the flow 5 to 10 *m* higher than the toe elevation. Some observations of flow characteristics on the prototype such as the section of air inception and downstream hydraulic jump, showed good agreement with those of the model. No deterioration of the concrete surface was observed during the inspection of the steps and the stilling basin in March 1991.

The apparent velocities were calculated from depth measurement in the developed region. Bindo et al. mentioned that the air entrainment effect was neglected and may result in an underestimation of the velocity (up to 60%). There was no information about the definition of the characteristic depth that was measured; depth at specific air concentration. There was also no report of the characteristics of the aerated and non-aerated region, defined in Figure 2.4. Figure 2.4 shows that for a specific spillway height (*H*) and discharge, the regime will change from aerated to non-aerated (probably jet flow) if the step height increases. The authors also did not present information about the energy loss, an important design criteria. Finally, the experimental data were not included in the report, therefore the accuracy of data interpolation in Figure 2.4 is undetermined.

2.2.6 Christodoulou (1993)

Experimental studies was carried out to find a solution for the energy loss in a stepped spillway in the Applied Hydraulics Laboratory of the National Technical University of Athens. The standard WES profile was used to envelope the tip of the seven steps with variable step height to width ratio in the curved part of the spillway. The remaining eight steps with height equal to 2.5 cm were located on the straight part of the spillway with a slope 0.7H:1V (55°). The spillway was placed in a 0.5 m wide laboratory flume which was connected to the supply reservoir through an elliptical transition.

The discharge, model values, ranged from 10 L/s to 45 L/s. A total of eight runs were conducted with the incremental rate of 5 L/s. The discharge was measured by a differential manometer and the vertical depth of the flow was measured at the tips of step numbers 10 and 13 by a point gage. The average of three depth readings across the width of the spillway was used as the flow depth.

Based on the depth measurements, mean velocities were calculated and the values of energy dissipation and friction factor were presented. The coefficient of skin friction, c_f, was calculated using the assumption of uniform flow, as (similar to Eq. (2.5)):

$$c_f = \frac{2 y_0^3 g \sin\theta}{\left(\frac{Q}{B_w}\right)^2} \tag{2.2}$$

where y_0 = (uniform) normal depth, Q = discharge and B_w = the width of the flume. The relative energy loss for step number 13, close to the spillway toe, was higher. The results of energy dissipation were compared with those of Sorensen (1985). It was seen that the values of energy dissipation were considerably less than those of Sorensen.

Christodoulou proposed an approximate but practical method of estimating the energy loss. He suggested that the number of the steps has an apparent effect on the energy loss. Evidence for this hypothesis was provided from the observation that for increasing the number of the steps, the energy loss was higher for the Sorensen experiment. Figure 2.5 shows a plot of non-dimensional parameters based on Christodoulou's experimental data along with the Sorensen's observations. A mean curve drawn through the experimental data was introduced as a relatively good measure, for design practice, for a preliminary estimate of the energy loss.

Due to the small height of the model (36.0 cm), it is doubtful that developed flow occurred and therefore air entrainment may not even have been initiated in the model. The measurements may represent the region in which the flow accelerated, known as the non-aerated region. Figure 2.5 suggests that for certain discharges, the energy dissipation decreases with increasing the total height of the spillway. This conclusion is contradictory to the previous observations which showed that the formation of the developed region, in which the flow characteristics remain steady, would result in more energy dissipation with increasing the spillway height.

2.2.7 Tozzi (1994)

To evaluate the performance of a stepped spillway, an experimental study was carried out at CEHPAR's Hydraulic Laboratory, University of Parana, Brazil. The results on the energy dissipation on a stepped spillway with 0.75H:1V slope with different step heights were compared to those of a chute spillway with the same slope. An expression for the growth of the turbulent boundary layer thickness was introduced to define the section of the air entrainment inception. Tests were carried out on a 1/15 scale model of the 35 m high spillway. The discharge ranged from 86.1 to 201.4 L/s/m (model values). For each run, five step heights of 5, 10, 20, 30, and 60 mm as well as unstepped model were tested to cover a wide range of flow roughness.

The friction factor was investigated in a closed conduit model instead over the stepped spillway to by-pass the problem associated with the measurement of flow depth in the highly aerated flow. Based on the experimental data, a general expression for the Darcy friction factor, f, was established as follows:

$$\frac{1}{\sqrt{f}}=2.16+1.24\,log\left(\frac{y}{k}\right) \tag{2.3}$$

where y = flow depth and k = height of the step. The expression is valid for $h/k>$ 1.80 and for lower values, f becomes constant and equal to 0.163. Figure 2.6 shows similar relations established for the 2H:1V and 6.69H:1V slopes as well as experimental data.

The depth of the flow in the non-aerated region was measured and then compared to the theoretical values. Using the friction factor and the assumption of gradually varied flow, the non-aerated depth of the flow was computed through the application of the Standard Step Method. The difference between the experimental and theoretical depth of the flow was 7% for all step heights. The velocity profile was measured in the aerated zone of the flow. The representative depth of the flow associated to the maximum velocity point above which the velocity was found to be essentially constant (Figure 2.7). However, it is not clear that how the velocity profile was measured.

The residual specific energy values were calculated using three methods:

i) Use of analytically computed non-aerated flow depth at the toe of the spillway and a kinetic energy factor equal to 1.10

ii) Integrate the velocity profile measured at the end of the spillway

iii) Measure the sequent depth of the hydraulic jump established downstream of the spillway toe

The calculated results of residual energy showed a maximum difference of 15% which corresponds to the 7% difference in the flow depth. The energy loss for the stepped spillway ranged from 47% to 74% while for the chute spillway the values of energy loss ranged from 13% to 24%. This showed that stepped spillways could dissipate three to four times more energy than chute spillways.

No justification was given for extending the friction factor analysis for a closed conduit to a stepped spillway. The assumption of constant velocity profile in the upper region of the flow is contradictory to the findings of the present investigation. It is also not clear if the measured velocity corresponded to the air-water mixture or the water velocity.

2.3 Flow Characteristics - Analytical Studies

Investigations which present methods to predict flow patterns in stepped spillways are presented in this section. Reviews of recent developments in stepped spillway design are also presented. Model and prototype data were used to evaluate the validity of established relationships or to drive empirical equations to estimate flow characteristics.

2.3.1 Rajaratnam (1990)

This investigation presents a method to predict the shear stress coefficient and the energy loss in stepped spillways. Rajaratnam was the first to present the idea of a fully developed region in the skimming flow. He assumed that in a spillway with a large number of steps, the flow becomes fully developed after the first few steps. The shear stress between the slowing stream and the recirculating fluid on the step, τ, was defined by the relation

$$\tau = c_f \frac{\rho V^2}{2} \tag{2.4}$$

where ρ = mass density of the flow and V= the mean velocity. He then applied the momentum equation for uniform flow to derive the following equation:

$$c_f = \frac{2 y_0^3 g \sin\theta}{q^2} \tag{2.5}$$

The observations of Sorensen (1985) were used to evaluate c_f for skimming flow. The values of c_f for relatively larger discharges were found to vary from 0.11 to 0.2 while for the last two smaller discharges c_f was found to be 0.25 and 0.28. Rajaratnam argued that the larger values of c_f might result from the transition state of flow between jet and skimming regimes. The average value of 0.18 was chosen for c_f. Rajaratnam further proposed a method to estimate the energy loss using the analysis of c_f. The residual energy at the toe of the stepped spillway, E_b, was given by the following equation:

$$E_b = \left(\frac{c_f q^2}{2 g sin\theta} \right)^{1/3} + \left(\frac{q sin\theta}{c_f \sqrt{2g}} \right)^{2/3} \tag{2.6}$$

A similar equation was written for the residual energy at the toe of a chute spillway, E_u, with the assumption of no energy loss. Finally, an equation was derived for the energy loss, ΔE:

$$\frac{\Delta E}{E_u} = \frac{(1-C_D) + \frac{F^2}{2} \frac{\left(C_D^2 - 1\right)}{C_D^2}}{1 + \frac{F^2}{2}} \tag{2.7}$$

where $C_D = \left(c_f / c_f'\right)^{1/3}$, c'_f= skin friction coefficient for the smooth spillway, and F= the Froude number at the toe of the chute spillway. He further used a value of 0.0065 for c_f'. For a relatively large value of F, it was found that $\Delta E/E_u$ is equal to 8/9. This large amount of energy loss would be normally expected in the skimming flow regime.

Eq. (2.7) was derived with the assumption that the flow at the toe of the stepped spillway is not aerated. Observations of the present investigation, which will be presented in chapter 4, show that the flow is highly aerated. Although Rajaratnam's investigation presented a simple solution for estimating the energy loss, the derived equations are of limited design use because, at the present state of the art, the terms c_f and c_f' can be predicted only from experimental observations. Experimental studies have shown a wide range for the variation of c_f with the flow roughness (Figure 2.8). This makes it difficult to find an average value for c_f.

2.3.2 Chanson (1993, 1994)

In these investigations, the hydraulic characteristics of stepped spillways were reviewed. It was reported that the oldest stepped spillways were built on the Khosr River around 694 B.C. in Iraq. A table was presented that contained a list of the old dams which used the stepped spillways.

Chanson assumed that the onset of skimming flow is a function of the discharge and the slope. The experimental data of Essery and Horner (1978), Peyras et al. (1992), and Beitz and Lawless (1992) were used to establish the following equations for the occurrence of skimming flow:

$$\left(\frac{y_c}{h}\right)_{onset}=1.01-0.37\frac{h}{l} \tag{2.8a}$$

$$\left(\frac{y_c}{h}\right)_{onset}=1.057-0.465\frac{h}{l} \tag{2.8b}$$

where y_c= the critical depth l = the length of the step tread.

He further assumed that vortices developed on the steps were maintained through the transfer of turbulent shear stress between the main flow and the recirculating flow. A balance between the shear force and the gravity force in the developed region was used as the uniform flow condition was expected. The Darcy friction factor, f, was found from the force balance (similar to Eq. (2.5)):

$$f=\frac{8g\ y_0^2\sin\theta}{q_w^2}\left(\frac{D_H}{4}\right) \tag{2.9}$$

where q_w= the water unit discharge and D_H= the hydraulic diameter. In his dimensional analysis, he showed that f can be a function of the Reynolds number, roughness height and the spillway slope. His analysis of the model and prototype data using Eq. (2.9) showed that f is independent of the Reynolds number. For steep slope ($\theta > 25°$), the results showed a considerable scatter that covered two logarithmic cycles (Figure 2.8-a). He also showed that f for flatter slopes ($\theta < 12°$) was independent of the channel slope and could be described by the equation (Figure 2.8-b):

$$\frac{1}{\sqrt{f}}=1.42\ln\left(\frac{D_H}{k}\right)-1.25 \tag{2.10}$$

where k is the step height normal to the bed. The effect of air entrainment was neglected as no information was available on the air concentration values. The author believed that the values of the friction factor could be overestimated because of potential errors in the flow depth measurements.

Chanson further derived an expression for the energy loss, ΔE, based on the condition that uniform flow was reached at the end of the spillway:

$$\frac{\Delta E}{E_u}=1-\frac{\left(\frac{f}{8 sin\theta}\right)^{1/3} cos\theta+\frac{\alpha}{2}\left(\frac{f}{8 sin\theta}\right)^{-2/3}}{\frac{H_{dam}}{y_c}+1.5} \qquad (2.11)$$

where $E_u=H_{dam}+1.5y_c=$ the upstream energy and $\alpha=$ the kinetic energy correction factor. He later corrected the above expression by replacing the friction factor by the friction factor for the air-water mixture.

The most notable value of these investigations was the derivation of empirical expressions based on model and prototype data. However, some data were extracted from the experiments on gabions and rockfill dams and could not be representative of stepped spillways as, in gabions and rockfill dams, part of the flow moves through the structures as well. Expressions for the friction factor were based on using the flow depth without the effect of air entrainment. Although Chanson further corrected this problem by considering the air-water friction factor, the empirical expression was derived using the data of chute and rockfill spillways. The large scatter of data in Figure 2.8-a showed the inaccuracy of measurement and lacking of a proper definition of flow depth in the case of air entrainment flow.

2.4 Flow in Steep Channels

As mentioned earlier, comprehensive studies of flow in steep channels have been carried out. The flow in a steep channels is, in many aspects, similar to skimming flow on stepped spillways. This section reviews the results of steep channel investigations which pertain to the analysis of stepped spillways.

2.4.1 Straub et al. (1953 & 1958)

This classical experimental study of flow in steep channels was carried out at the St. Anthony Falls Hydraulic Laboratory. These investigations were notable for the clarification of the detailed structure of fully developed, self-aerated flow. The experiments were undertaken in a 50 ft long channel that was 1.5 ft wide with a slope ranging from 7.5° to 75°. By installing an artificial roughness on the channel bed, the air entrainment process was intensified to lessen the scale effect. The non-slip fabric coating had granular particles with a mean size of 0.028 in. and a mean spacing of 0.039 in. Discharge varied from 2.2 to 15 cfs. The measurements of air concentrations and velocities were taken in the developed region where the air concentration profiles were the same at two sections 10 ft apart along the channel. The air concentration was measured by an electrical probe which will be fully described in chapter 3 of this thesis. The results of the air concentration were compared with the results obtained by means of a mechanical sampler. The velocities were also measured in some of the experimental runs by a device which timed the travel of salt-water cloudlets between two electrodes placed 3 in. apart in the air-water flow. Timing accuracy in the neighborhood of 1/100,000 second as well as appropriate pickup and amplifying stages were incorporated into a unit electronic circuit. This direct measurement of mixture velocity doesn't depend on the knowledge of the fluid density or the condition of fluid homogeneity.

Since there is no definite upper boundary for air-water flow, a number of definitions for depths and concentrations were presented, each having particular application. The mean air concentration, $\overline{C}$, was defined as

$$\overline{C}=\frac{1}{y_u}\int_0^{y_u} C\,dy \tag{2.12}$$

where y_u = the upper depth of flow, and y = the normal distance from the bed. The upper depth of the flow was arbitrarily defined as that value of y where air concentration has some prescribed value. Straub et al. chose two prescribed air concentration values for the definition of y_u . In the 1958 work, for some purposes and because of the asymptotic nature of the air concentration profile, an air concentration of 99% was chosen. In the 1953 work, a prescribed value of $C= 95\%$ was also chosen, because at the corresponding depth, C could be reliably measured and the accumulated discharge was about 98% to 99%. A mean depth, $\bar{y}$, was used to represent the depth of flow equal to the total column of water in the air-water mixture and was defined as

$$\bar{y}=\int_{0}^{\infty}(1-C)dy \tag{2.13}$$

Plots of the variation of C and velocity, u, with the depth and $\overline{C}$, y_u, and $\bar{y}$ with discharge and slope were presented. Typical plots for the variation of these flow characteristics are shown in Figures. 2.9 to 2.13. These results showed that a for a given discharge, y_u decreased at first and increased as the slope increased. The upper depth of the flow was basically the same over considerable range of slopes (15 to 30 degrees) and depended only on the discharge. The mean depth, $\bar{y}$, increased with the discharge and decreased with the slope. It was interesting to note the increment of the mean air concentration for a wide range of discharges was not considerable. However, $\overline{C}$ increased considerably with the slope. The velocity profile in Figure 2.10 shows a sharp reduction in the velocity in the upper portion of the flow.

The authors assumed that aeration started in a region where the boundary layer reached the water surface and it depended on the turbulence intensity of the flow. Apparently, aeration occurred when the turbulence of the transverse velocities were sufficient to cause water droplets to break through the surface into the air and fall back into the streaming flow. Observations indicated that the flow can be divided into two distinct regions:

i) a lower region in which air bubbles are suspended in the flow by turbulent fluctuations; and

ii) an upper region consisting of droplets and larger agglomerations of water ejected from the flowing stream into the atmosphere.

The boundary which separates these two regions was referred to as the transition depth.

In the upper region, it was assumed that the turbulent velocity fluctuations normal to the bed were randomly distributed with a mean value of zero. Therefore, for fluctuations that ejected water upwards above the transition depth, the water drops followed one-half of a Gaussian probability distribution. The height of the projection distance may be considered proportional to the square of the transverse velocities fluctuations, so that this height also is randomly distributed about zero and can be represented by one-half of a Gaussian distribution. The projected particles therefore travel a distance y' above the transition depth with a distribution frequency that can be described as

$$f(y') = \frac{2}{y_m\sqrt{\pi}} e^{-\left(\frac{y'}{y_m}\right)^2} \tag{2.14}$$

where y_m is a measure of the mean distance of y'. The proportion of all particles at a distance y' that left the flow at the transition depth can then be expressed by the probability of such a distribution:

$$P_{y'} = \frac{2}{y_m\sqrt{\pi}} \int_{y'}^{\infty} e^{-\left(\frac{y'}{y_m}\right)^2} dy' \tag{2.15}$$

Straub and Anderson (1958) argued that the concentration of water particles at any distance y' may be assumed to be proportional to the probability as:

$$\frac{1-C}{1-C_T} = \frac{2}{y_m\sqrt{\pi}} \int_{y'}^{\infty} e^{-\left(\frac{y'}{y_m}\right)^2} dy' \tag{2.16}$$

where C_T is the air concentration at the transition depth.

The air bubble distribution in the lower region was analyzed by a theory that is commonly used to describe the distribution of suspended sediment in streamflow. The two phenomenon are similar, although air bubbles tend to rise and sediments tend to fall. The equilibrium between the buoyancy of air bubbles and the concentration gradient was described by

$$-CV_b + \varepsilon_b \frac{dC}{dy} = 0 \tag{2.17}$$

where V_b= the rising velocity of air bubbles, and ε_b= a mixing parameter of the air bubble transfer. Straub and Anderson stated that the value of ε_b is not known in aerated flow, but assumed that it is proportional to the momentum mixing parameter in a non-aerated flow. Therefore, ε_b was taken to have a parabolic distribution in the lower region. Substituting the value of ε_b in Eq. (2.17) and integrating results in the following expression for air concentration in the lower region:

$$C=C_1\left(\frac{y}{y_T-y}\right)^z \tag{2.18}$$

in which

$$z=\frac{V_b}{\beta\kappa u_*} \tag{2.19}$$

where β= a proportionality factor, κ= the von Karman universal constant, u_*= the bed shear velocity, y_T= the transition depth, and C_1= the air concentration at a depth equal to $y_T/2$. The constants in the derived equations for both regions depend on the intensity of turbulent fluctuations and could not be evaluated analytically, but were estimated from experimental data.

The authors later developed empirical equations that gave the variation of air concentration and depth parameters with the channel slope and discharge. To compare the results of aerated flow with non-aerated flow, they performed experiments on flatter slopes to create the non-aerated flows. They then showed that the Chezy formula can be used for the aerated flow and that the Chezy resistance coefficient is essentially the same as that for non-aerated flow. The results also indicated that the mean velocity of an aerated flow is greater than that of a corresponding non-aerated flow.

Questions arise on the validity of Eq.(2.16) since a proportionality factor is missing in this equation. The result of $\overline{C}$ published in the Straub and Lamb (1953) investigation does not match with those of the 1958 work by Straub and Anderson. For a slope of 37.5° and discharge of 6.4 cfs, in 1953 study $\overline{C}$ was 0.445 while in the 1958 work (Figure 2.11), $\overline{C}$ was reported about 0.63. Although the upper flow depth for the calculation of $\overline{C}$ in Eq. (2.12) were different, this slight difference cannot be the cause for such a considerable difference in the mean air concentration calculation.

2.4.2 Knight and Macdonald (1979)

This particular investigation describes an experimental study in a channel with artificial roughness elements fixed at regular intervals across a laboratory flume. The different flow patterns over the roughness elements and the variation of the bed resistance factor were observed. The experiments were carried out in a channel 15.25 m long and 0.46 m wide. The flow rate ranged from 0 to 180 L/s. The slope of the channel was 0.958×10^{-3}. The artificial roughness elements were perspex strips with a square cross section of 3.0 mm by 3.0 mm and occupied the whole width of the channel. These were placed at a spacing that ranged from 10.4 mm to 1,000 mm to provide eleven roughness. The variation of the ratio λ/k ranged from 3.57 to 333, where λ is the roughness spacing and k is the roughness height. The aspect ratio, B_w/y, varied from 1.5 to 15, where B_w is the channel width and y is the flow depth. This provided a relative roughness ratio that varied from 10.25 to 102.5. At the beginning of each test, the water surface slope was checked to ensure that the flow was uniform.

Based on the nature of flow at the boundary, six flow patterns for flow over roughness elements were observed by dye injection techniques (Figure 2.14). Morris (1959) had already recognized four flow patterns within this classification. The six types of flow patterns were classified as follows:

i) Smooth turbulent flow ($\lambda/k=\infty$): The roughness elements are completely submerged in the viscous sublayer.

ii) Semi-smooth turbulent flow (λ/k = 333 to 13.9): In this case, which is also classified as "isolated roughness", the form drag on the roughness elements makes up only a part of the overall friction factor. The wake produced by the roughness elements extended about 30 mm downstream.

iii) Non-uniform hyperturbulent flow ($\lambda/k = 10.4$): In this type of flow, the wake from one roughness element just reaches the upstream edge of the next downstream element.

iv) Uniform hyperturbulent flow (λ/k = 6.95): Here the roughness elements are sufficiently close to one another so that the wake from one element joins with that from the next element to produce a uniform layer of turbulence above the bed. In this case, which is also referred to as "wake-interference" flow, there is no part of the bed over which the viscous sublayer exists.

v) Semi-quasi smooth flow ($\lambda/k = 5.21$): For this flow, the recirculating flow trapped in the groove between roughness elements does not quite fill the entire groove. The recirculating flow is not stable and is able to separate and combine with the main stream.

vi) Quasi-smooth flow (λ/k= 3.47): In this type of flow, which is referred to as "skimming flow", the roughness elements are spaced so closely as to form a smooth "pseudo-wall". Stable recirculating flows are

> maintained through transmission of shear stress from the main stream past the tips of the roughness elements. In addition, small-scale vorticity will be generated continuously along the pseudo wall. Energy is expended to generate these vortices and to maintain the stable recirculating flow.

Knight and Macdonald further concluded that the maximum bed resistance occurred at about $\lambda/k = 8$, the wake interference flow, and was equal to about f=0.028. In a series of plots, Knight and Macdonald presented the variation of Darcy friction factor with Reynolds Number and λ/k. They also showed that the ratio of Nikuradse roughness to the element roughness could reach as high as 10 for lower values of discharge and λ/k (Figure 2.15).

The ratio λ/k provides a good basis for recognizing skimming flow. However, skimming flow occurs in stepped spillways that possess steep slopes. The writer believes that the dominant gravity force and roughness projection in stepped spillway flows may result in different flow patterns.

2.5 Inception Section of the Air Entrainment

Self-aeration is a typical characteristic of flow in steep open channels. In a high velocity flow, the section of inception of air entrainment is one of the most important characteristics. Knowledge of the physics governing air inception is of great importance to the design of stepped spillways. If the section of inception is located near the upstream end of the spillway, the uniform region length is longer, thereby resulting in greater energy dissipation. This results in a reduced cost for the stilling basin below the spillway. This section provides a summary of investigations on chute and stepped spillways that discuss the air entrainment phenomenon and the inception section of the air entrainment.

Michels and Lovely (1953) classified the various types of air entrainment in terms of the associated characteristics of the turbulent flow:

> i) Rippled flow: a smooth undulating water surface. This occurs in the upper non-aerated region of the spillway.
>
> ii) Choppy flow: an agitated water surface where small portions of water envelop and then release air upon subsiding. This occurs in a channel of medium slope.

iii) Scarified flow: a thin layer of an air-water mixture forms near the water surface. This occurs for a flow in long chutes of narrow width and/or with wall surface having an uneven shape.

iv) Emulsified flow: a continuous even concentration of air through the flow depth. This flow has an uneven surface and is found in steep, wide chutes.

v) Ebullient flow: a boiling air-water mixture that extends irregularly through a portion of the flow. This occurs when a high-velocity jet discharges into an energy dissipator.

vi) Spraying flow: a water jet that discharges into the atmosphere. An example is flow from a needle outlet discharging into the air.

vii) Separation flow: a high-velocity flow which separates from a solid boundary. This can occur in high-velocity flow around baffles in an energy dissipator.

Michels and Lovely then discussed three necessary conditions that are prerequisites for the occurrence and continuation of air entrainment. First, the momentum associated with the turbulent velocity component normal to the surface must be greater than the surface tension forces to allow the water particle to leave the surface. Second, the particle speed relative to the surrounding atmosphere must exceed some value for air to be enveloped by fluid particles. Third, the turbulent velocities must remain constant or increase to allow the continuation of air entrainment downstream of the inception section. The authors designated the flow on steep channels as emulsified flow and discussed the conditions for air entrainment in this type of flow. They concluded that the turbulent boundary layer must extend to the surface for air entrainment to commence. Moreover, the slope of the energy gradient could define a lower limit of turbulence necessary to cause air entrainment.

The section at which the air entrainment starts is called the "section of inception". Early observations on chute spillways by Lane (1939), Hickox (1945), Halbronn (1954), Rao Govinda and Rajaratnam (1961), Hino (1961), Campbell et al. (1965), Gangadharaiah and Nagar (1970), and Wood (1991) revealed that a turbulent free surface is a prerequisite for the inception of air entrainment. The boundary layer thickness should equal the flow depth to meet this requirement. In addition, the energy of the turbulent component of the velocity normal to the bed should exceed the energy of the surface tension to entrain air into the flow.

Lane (1939) argued that the inception section on prototype spillways depends on at least four factors: 1) the turbulence setup on the spillway crest or upstream of it 2) the roughness of the spillway surface 3) the flow depth and 4) the height of the spillway. He then used observations of prototype spillways to show the effect of above factors on the location of the inception section. Lane further compiled observations of the velocity and distance at sections where appreciable entrainment appeared to begin in prototype chute spillways (Table 2.1). The velocities were calculated using the free fall theory.

Hickox (1945) used prototype observations to show that the section of inception moves downstream of the crest as the discharge increases. For this reason, he argued that at the inception section the turbulence of the flow should reach the surface. Based on observations, Hickox developed a plot that shows the distance at which air entrainment begins on chute spillways (Figure 2.16). He also showed that the ratio of this distance to water depth is almost constant for all discharges and equal to about 100/1.

Rao Govinda and Rajaratnam (1961) and Hino (1961) concluded that the section of inception for a smooth spillway occurred at a section where the bed boundary layer reaches the free surface where the turbulent intensities of the flow are sufficiently high. They argued that masses of fluid or eddies project into the atmosphere if their kinetic energy exceeds the surface tension energy, causing air entrainment to occur. Rao Govinda and Rajaratnam and Hino have computed the kinetic energies of eddies and surface tension and showed that the inception number should have a critical value for inception to occur. Gangadharaiah and Nagar (1970) calculated the inception number based on the results of several investigations on chute spillways and argued that it should be more than 56. It is not clear how they chose this value as the inception number varied from 24 to 40,000. The higher values represent the inception number for prototype spillways. However, Wood (1991) argued that once the boundary layer turbulence reached the surface on a prototype spillway, the energy of the turbulent eddies is sufficient for air entrainment.

Horner (1969) confirmed that the section of inception occurred at the location where the boundary layer intersects the surface for skimming flow on a stepped spillway model by determining the velocity profiles at the step tips in the non-aerated region. He observed the growth of the boundary layer in the non-aerated region and determined its proximity to the surface at the section of inception (Figure 2.17). Horner (1969) argued that the ejection of the water slugs at the section of inception occurred when the turbulent component of velocity normal to the bed are strong enough to cause slugs of water to break through the surface. He also argued that the piercing of the surface by turbulence cells and the subsequent splash on return to the main flow caused air pockets to become engulfed near the surface of the stream.

A general expression for the growth of boundary layer is presented in the following form:

$$\delta = a K^b L^c s^d F^{*e} \tag{2.20}$$

where K= some kind of roughness, L= distance from the crest, $s = \sin \theta$= the slope of the spillway, $F^* = q_w / \sqrt{g K^3 s}$= the Froude number defined in terms of the roughness height, and a, b, c, d, e are coefficients. Table 2.2 presents the empirical values of these parameters developed for chute and stepped spillways by several investigators. Parameters used in these equations are defined in Figure 2.18. Gangadharaiah and Nagar (1970) also presented a graph that showed the distance, L_i, at which the boundary layer thickness equals the depth of the flow for limited range of an average roughness, K, and design discharge head, h_d.

Although the idea of turbulent boundary layer has appeared for a long time in the literature, the lack of an analytical solution for the inception section is evident. The empirical relations for the growth of the boundary layer are mostly based on observations on chute spillways. The extension of these relations to stepped spillways is questionable, since the dominant projections (steps) certainly influence the flow characteristics in the non-aerated region. As it will be seen in chapter four, provision of steps enhances the boundary layer growth and the flow patterns are considerably different from those in chute spillways.

2.6 General Comments

Most investigators have experienced difficulty in fitting their experimental data to a generally acceptable relationship. The empirical approach used in most of the studies reported rendered varying relationships among slope, flow depth, velocity, and air concentration which appear to define the data from that particular study, but do not always agree well with results of other investigations. Consequently, even in the most comprehensive investigations, qualifying limits have been placed on the proposed relationships.

It is also known that the high velocity flows in stepped spillways were not well presented in most investigations, mainly due to the size of the model. In some investigations, the model size was too small to allow the flow to attain the developed flow regime. In some cases, aeration was not initiated due to an inadequacy of the length of the spillway face. Thus, the application of the research to practical design problems depends on detailed corroborative information from large scale models. Despite this dependence, such information has not yet been obtained.

The initiation of air entrainment was also not studied systematically to find the flow characteristics that influence this phenomenon. It was reported that aeration commenced when the boundary layer thickness equals flow depth and the turbulent components of velocity normal to the surface are sufficiently strong to cause slugs of water to break through the surface. However, no observations were made to validate these assumptions. The section of inception of air entrainment was estimated empirically using the formulation of smooth spillways. The coefficients in the formulae were later corrected for stepped spillways using limited experimental data.

Questions of the measurement of flow depths arise as there is no definite surface in the air-water flow. Most studies reported measurements of a "conservative " or a "mean value" flow depth. These definitions of flow depth, based on the judgment of the observers, will influence the accuracy of these measurements and thus the resulting characteristics derived from the flow depth. It is necessary to assess the flow depth by arbitrarily defining the surface as that position in the flow at which air concentration has a prescribed value. However, this task was impossible as no air concentration profiles were previously available.

The analysis for the shear stress friction factor was limited to the uniform region where the balance of force between gravity and the shear exists. The Darcy friction factor, f, or the coefficient of skin friction, c_f, was estimated using Eq. (2.9) or Eq. (2.5) and evaluated using the depth of flow measurements. Figure 2.8 is a typical plot of such a calculation which shows a considerable scatter for some discharges. Here again, the inaccuracy of the depth measurement could be the main reason for the discrepancy of these results. An exception was the results of Tozzi (1994), who studied the friction factor in a stepped closed conduit to avoid the problem with the measurement of flow depth. However, extending the results to the stepped spillways was not at all justified.

Although stepped spillways have become popular for their significant energy loss, observations of flow characteristics that affect the mechanism of energy dissipation have been limited. Skimming flow was classified as a quasi-smooth flow in which the roughness elements are spaced so close that the flow skims over the vortices which form on the steps. Small scale vortices are also developed at the tips of the steps. Some investigators calculated the energy loss based on the depth measurements in the developed region or at the toe of spillways. Others presented formulations that depended on the value of the friction factors. Considering the error in the depth measurement or the friction factor estimation, the calculated energy loss is of questionable value. Again an exception is the work of Tozzi (1994), in which the measured velocity profile was integrated and compared with two other methods. However, it is not clear whether the density of the mixture was considered in Tozzi's work.

Although the flow over stepped spillways is a mixture of air and water flow, no measurements of air concentration have been made. After a certain distance from the crest, the air entrainment starts and the bulking of the flow commences. Further downstream, a developed region forms where the flow characteristics such as flow depth, velocity, and air concentration become constant. In large spillways, the developed region includes most of the spillway face. Knowledge of the air concentration is essential to analyze the flow characteristics such as depth, velocity, and friction factor.

The above paragraphs show the complexity of the flow over stepped spillways and the problems that investigators have faced to analyze the flow parameters. It also gives us a clear picture of the progress of the works that have been carried out. It is necessary to conduct more studies to investigate the mechanism of air entrainment and its effect on flow parameters. More fruitful researches should also be done to develop and optimize design procedures for the construction of stepped spillways.

Dam	Distance of Inception Section from the crest (ft)	Corresponding Velocity of Free Fall (ft/s)
Norris	120	88
Madden	145	96
Gatun	65+	65
Triunfo Creek	40+	51
Schuylerville	25+	40
Dnieprostroy	100+	80
Bassano	40+	51
Grand Lake	50+	57
Chute a Caron	140+	95

Table 2.1 Distance of the inception section of air entrainment from the crest (adapted from Lane, 1939)

	Parameters						
Investigator	*K*	*L*	*a*	*b*	*c*	*d*	*e*
Halbronn (1954) (smooth)	-----	x	0.0104	0	0.8515	-0.0485	0
Halbronn (1954) (rough)	Nikuradse equivalent sand roughness	x	0.0447	0.154	0.846	0	0
Campbell et al. (1965)	absolute roughness	L_i	0.80	0.233	0.767	0	0
Gangadharaiah et al. (1970)	average roughness	L_i	70	-0.79	1.79	0	0
Wood (1991)	Nikuradse equivalent sand roughness	L_i	0.223	1.0	0	-0.04	0.643
Chanson (1994) (stepped spillways)	h*cos θ	L_i	0.40	1.0	0	-0.04	0.64

Table 2.2 Values of Parameters defined in Eq. (2.20)

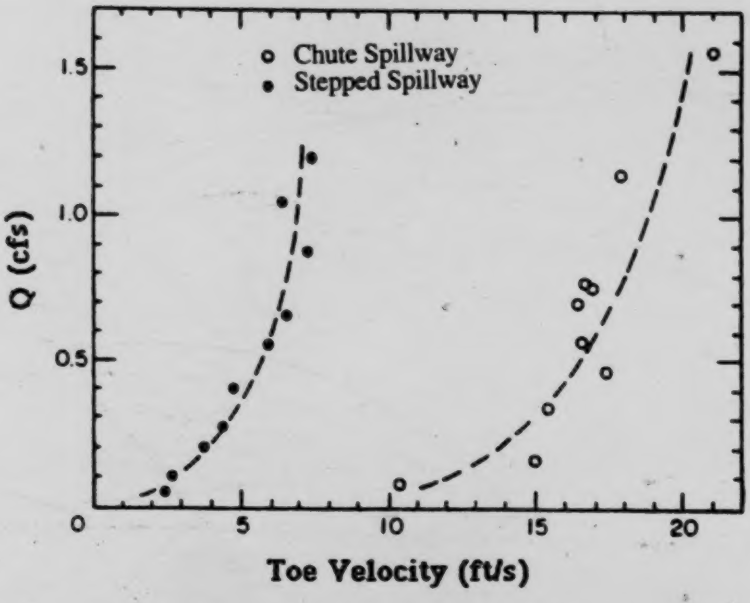

Figure 2.1 Velocity measurements at the toe of the chute spillway and the stepped spillway (adapted from Sorensen, 1985)

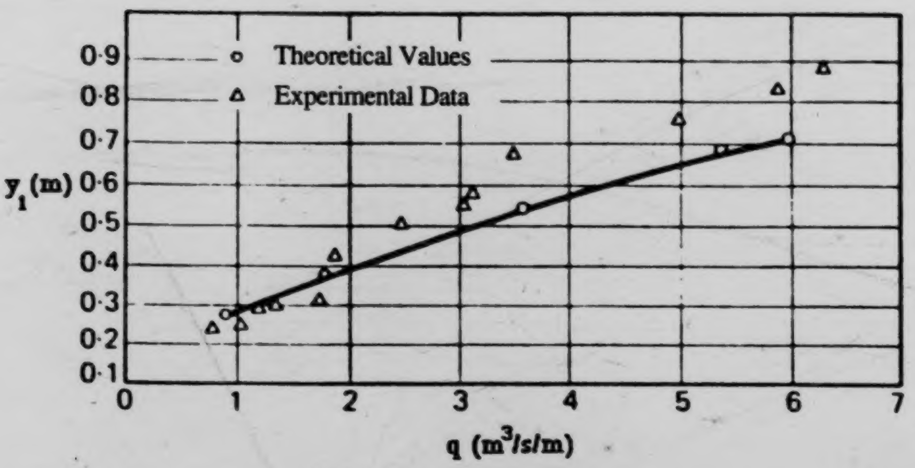

Figure 2.2 Comparison of the theoretical and experimental results (adapted from Diez-Cascon et al., 1991)

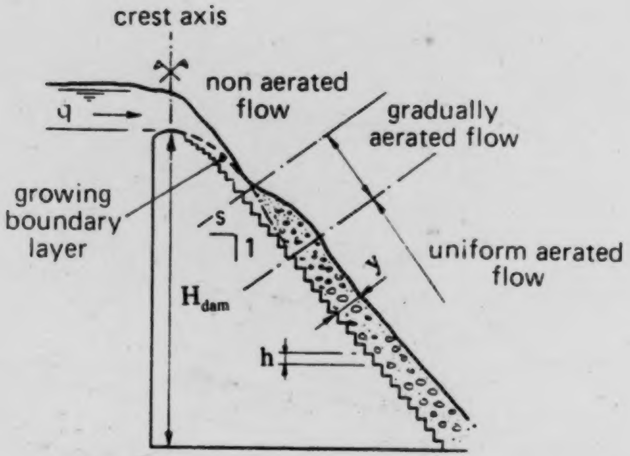
crest axis
q
non aerated flow
gradually aerated flow
growing boundary layer
s
1
uniform aerated flow
y
H_dam
h

Figure 2.3 A schematic sketch for the flow state in the stepped spillways (adapted from Bindo et al., 1993)

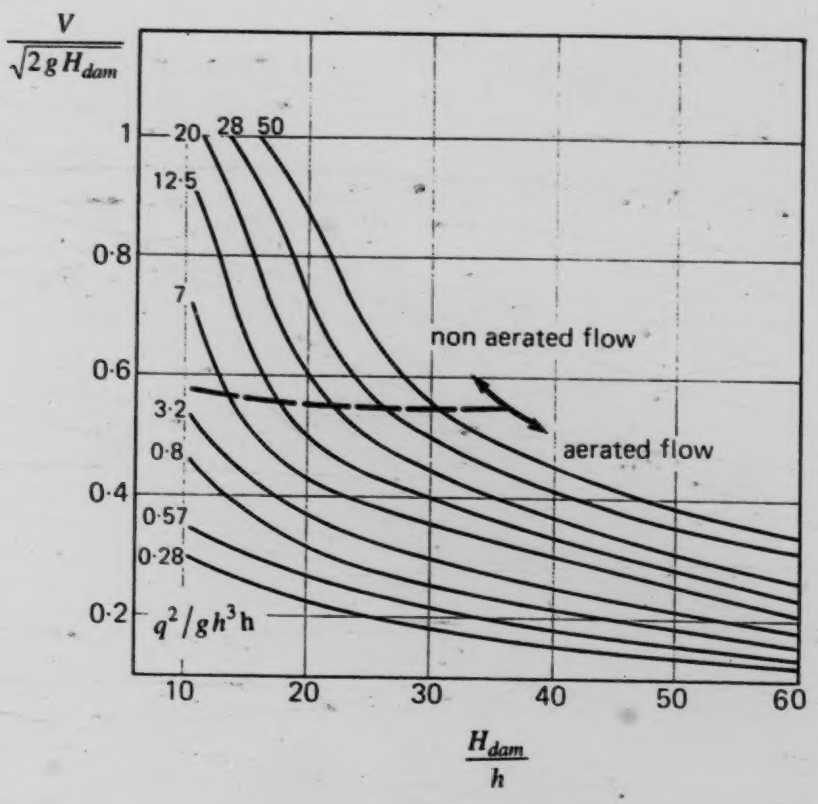

Figure 2.4 A graph for the design of stepped spillways (adapted from Bindo et al., 1993)

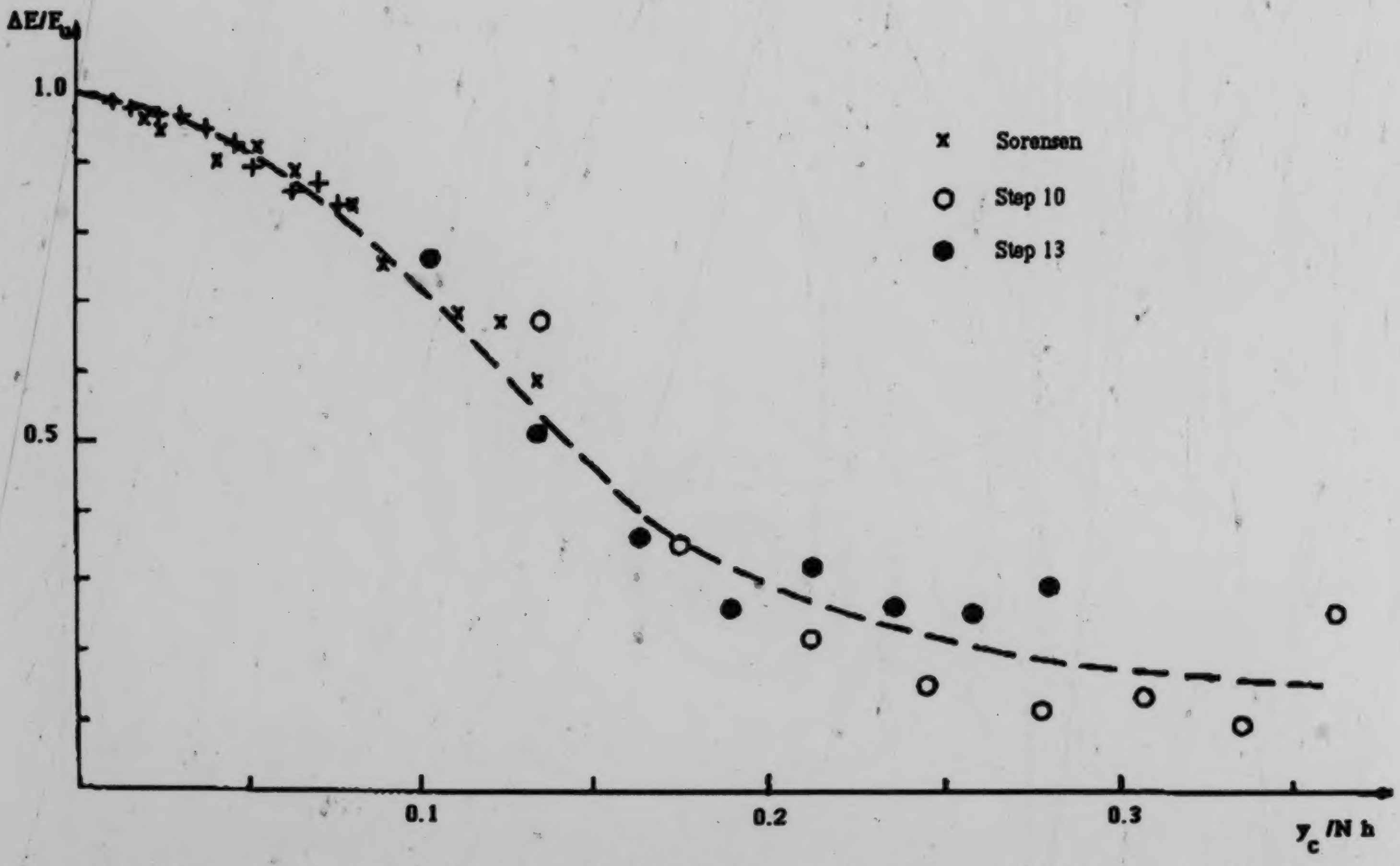

Figure 2.5 Dimensionless plot of the energy dissipation for stepped spillways (adapted from Christodoulou, 1993)

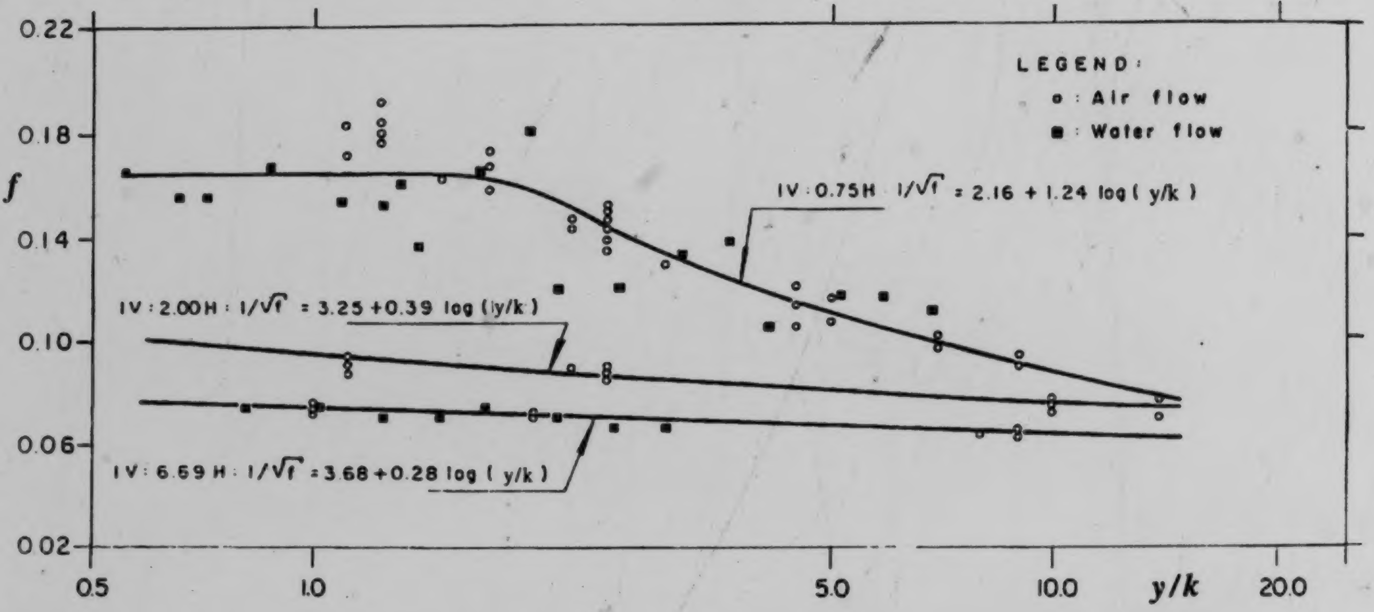

Figure 2.6 Variation of the Darcy friction factor with roughness (adapted from Tozzi, 1994)

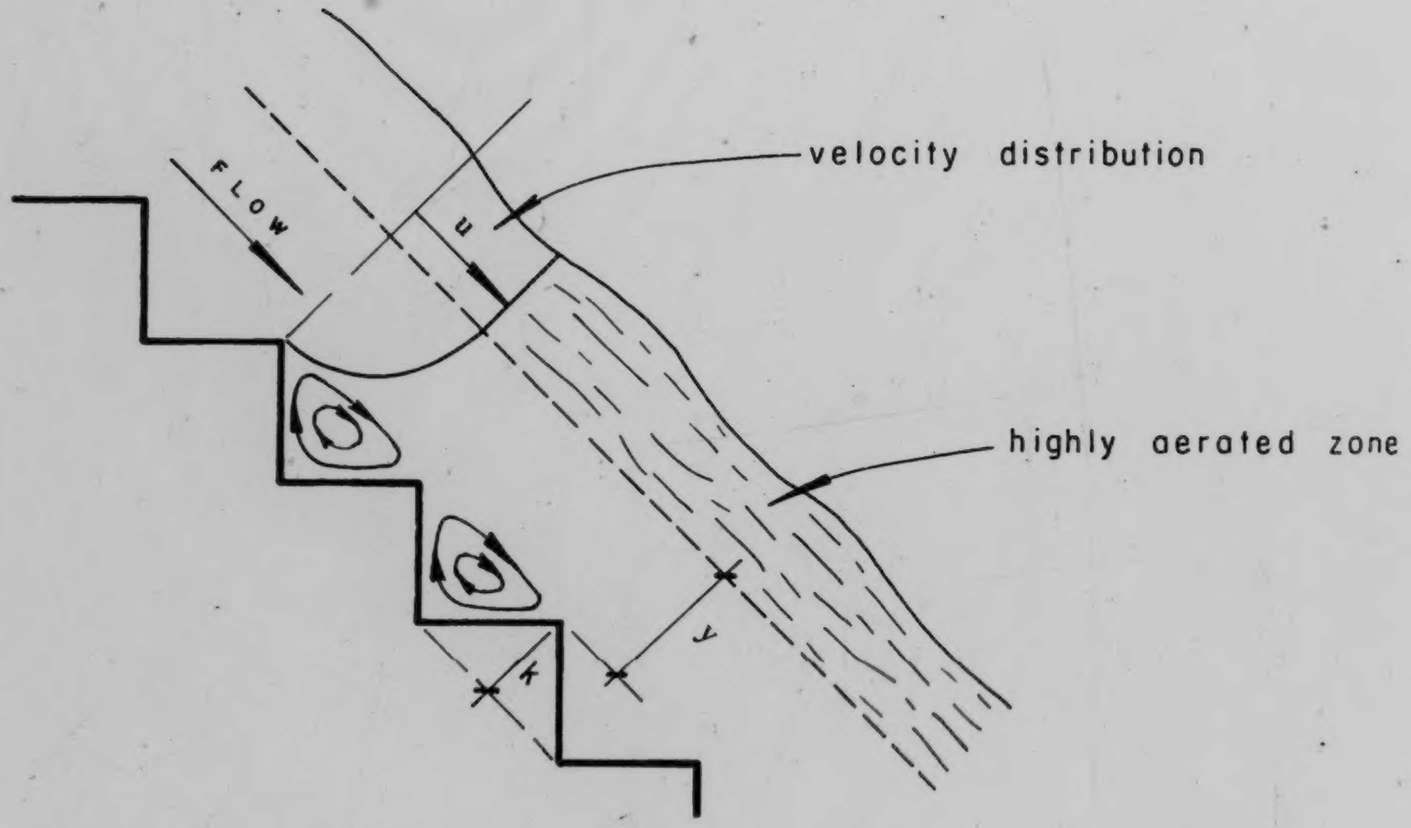
velocity distribution
highly aerated zone
FLOW
u
y
k

Figure 2.7 A schematic sketch for the flow in the developed region of a stepped spillway (adapted from Tozzi, 1994)

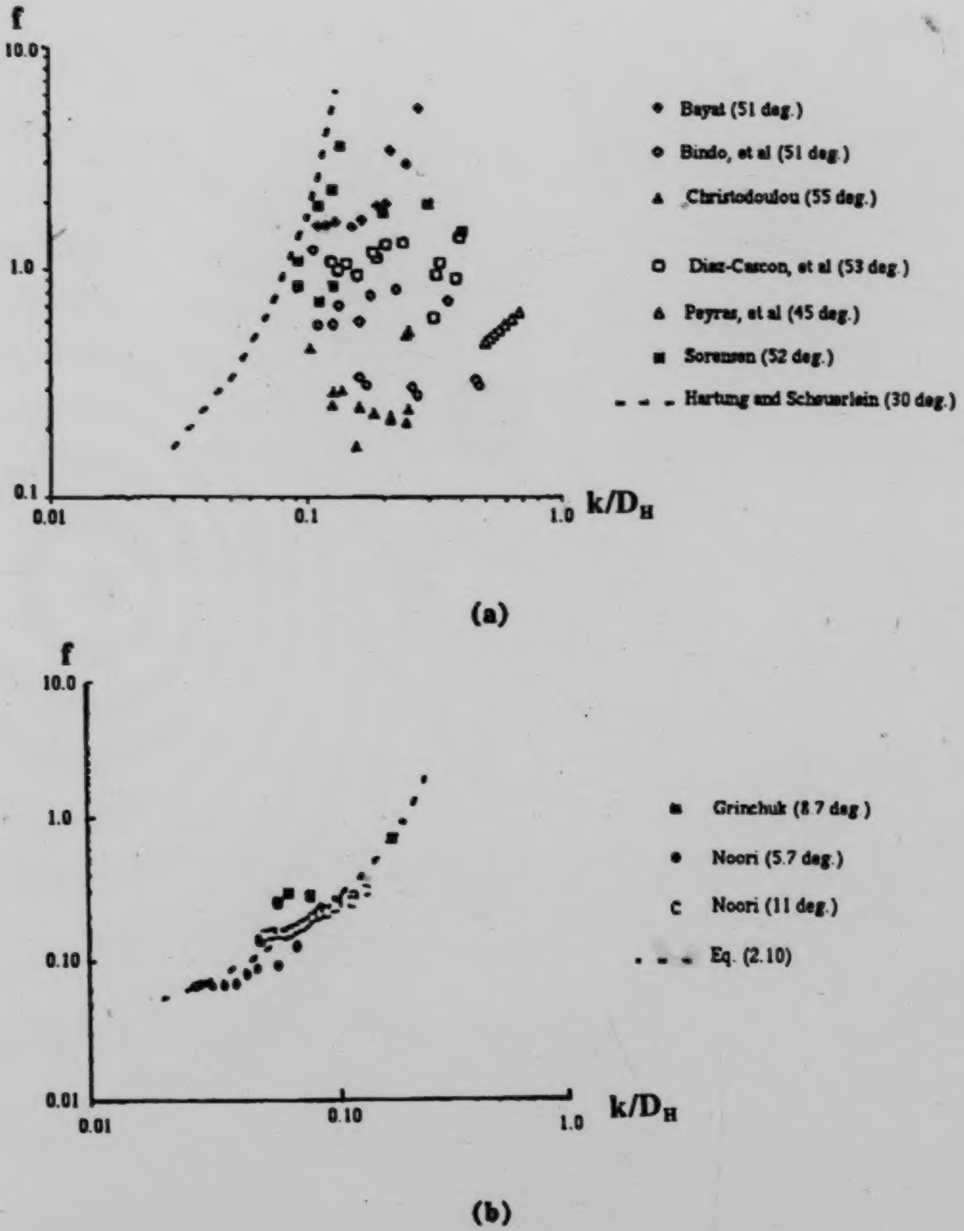

Figure 2.8 Variation of Darcy friction factor for skimming flow: (a) steep slopes; (b) flat slopes (adapted from Chanson, 1994)

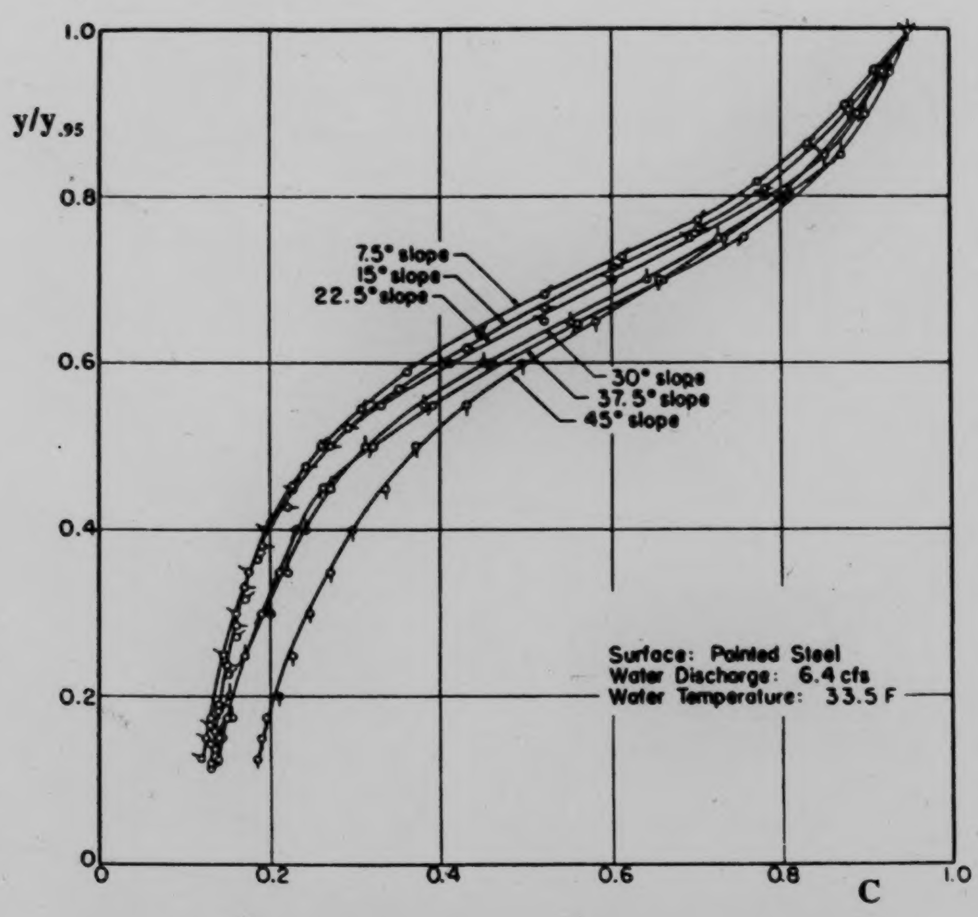

Figure 2.9 Variation of the air concentration with channel slopes (adapted from Straub and Lamb, 1953)

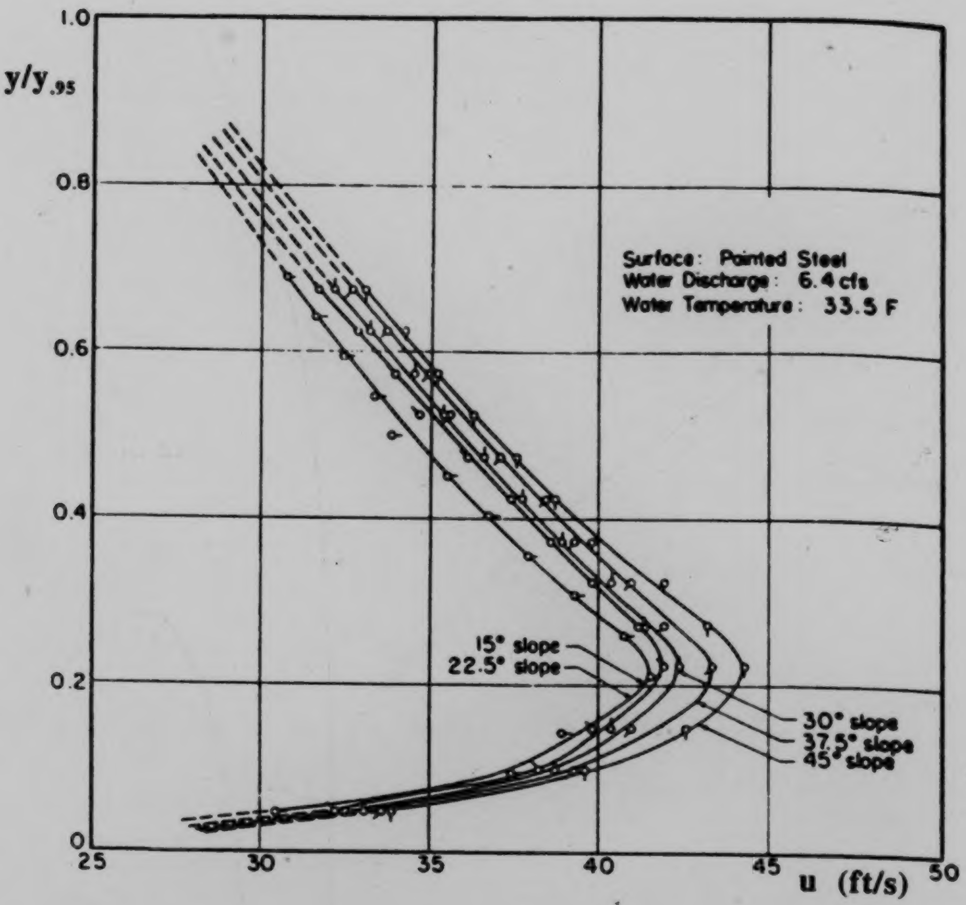

Figure 2.10 Variation of the measured velocities with channel slopes (adapted from Straub and Lamb, 1953)

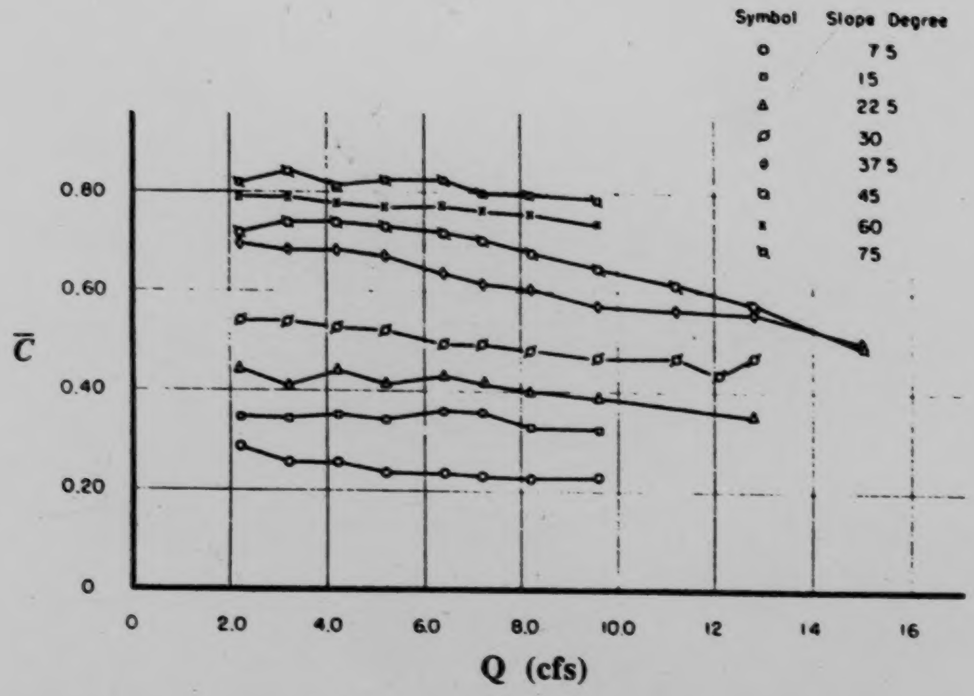

Figure 2.11 Variation of the mean air concentration with discharge at various channel slopes (adapted from Straub and Anderson, 1958)

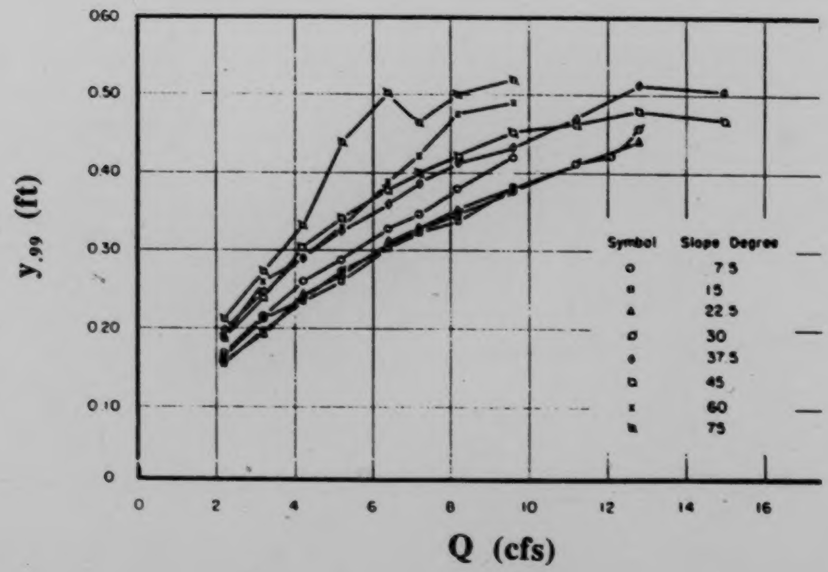

Figure 2.12 Variation of the upper depth of flow with discharge at various channel slopes (adapted from Straub and Anderson, 1958)

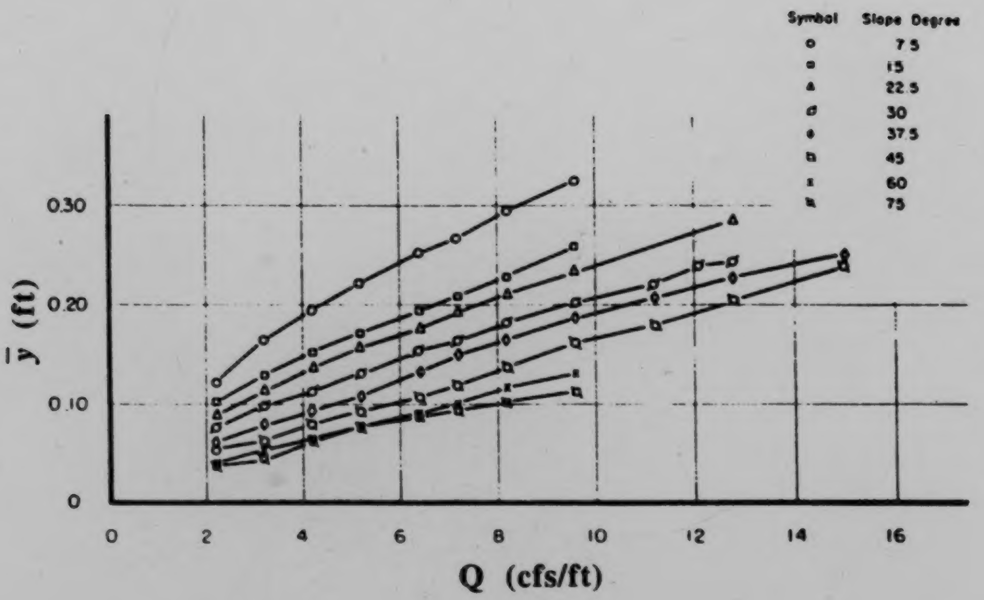

Figure 2.13 Variation of the mean depth of the flow with discharge at various channel slopes (adapted from Straub and Anderson, 1958)

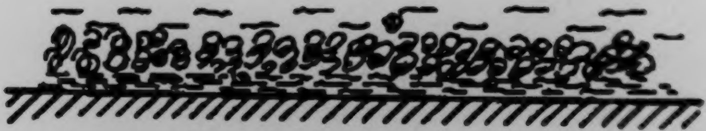

i) smooth turbulent flow

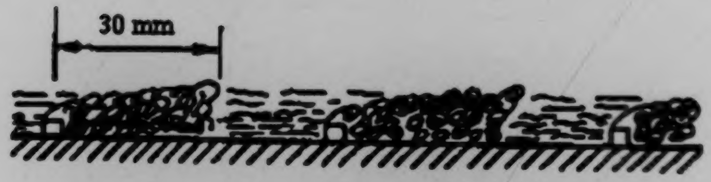

ii) semi-smooth turbulent flow

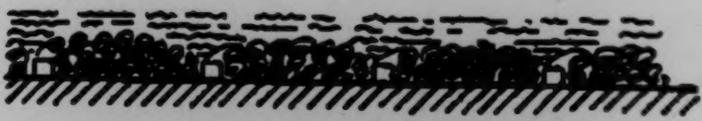

iii) non-uniform hyperturbulent flow

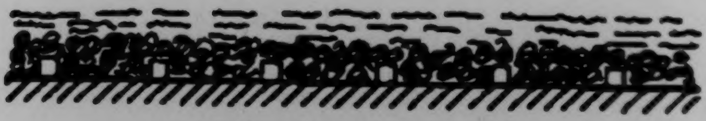

iv) uniform hyperturbulent flow

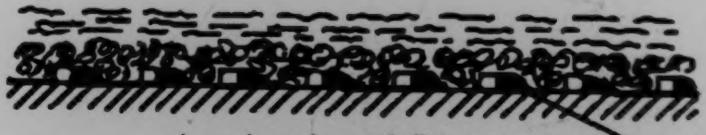

v) semi-quasi smooth flow

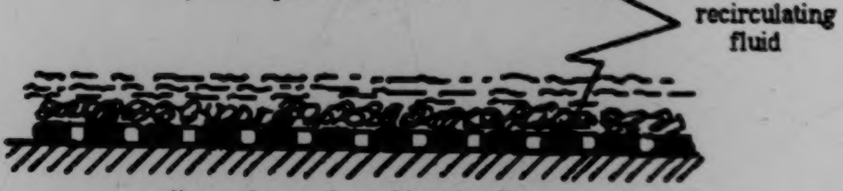

vi) quasi-smooth or skimming flow

Figure 2.14 Classification of flow patterns for a channel with roughness elements (adapted from Knight and Macdonald, 1979)

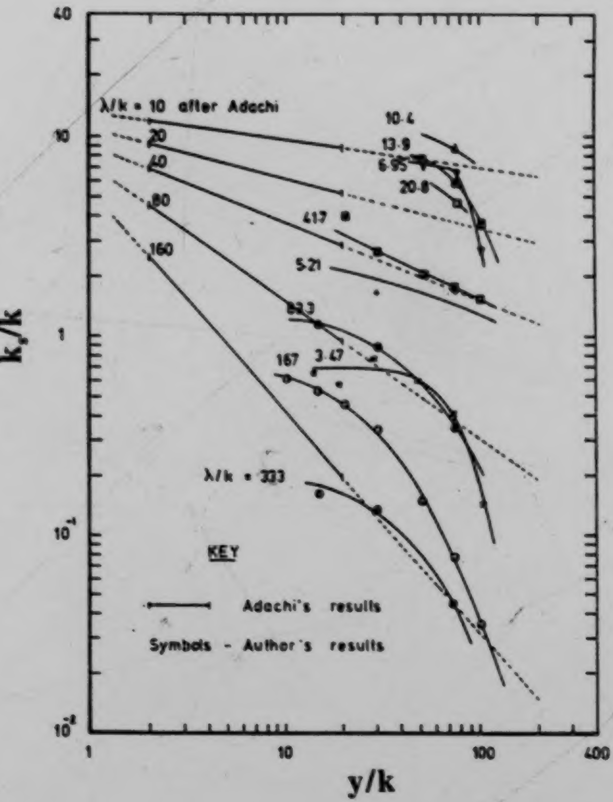

Figure 2.15 Variation of the roughness ratio with the relative roughness (adapted from Knight and Macdonald, 1979)

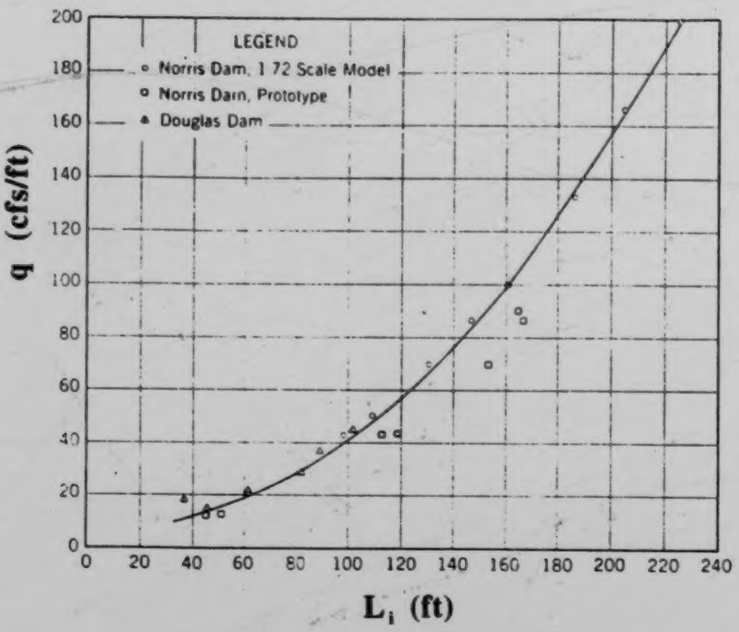

Figure 2.16 Variation of the distance of air entrainment inception section from the crest with the discharge (adapted from Hickox, 1945)

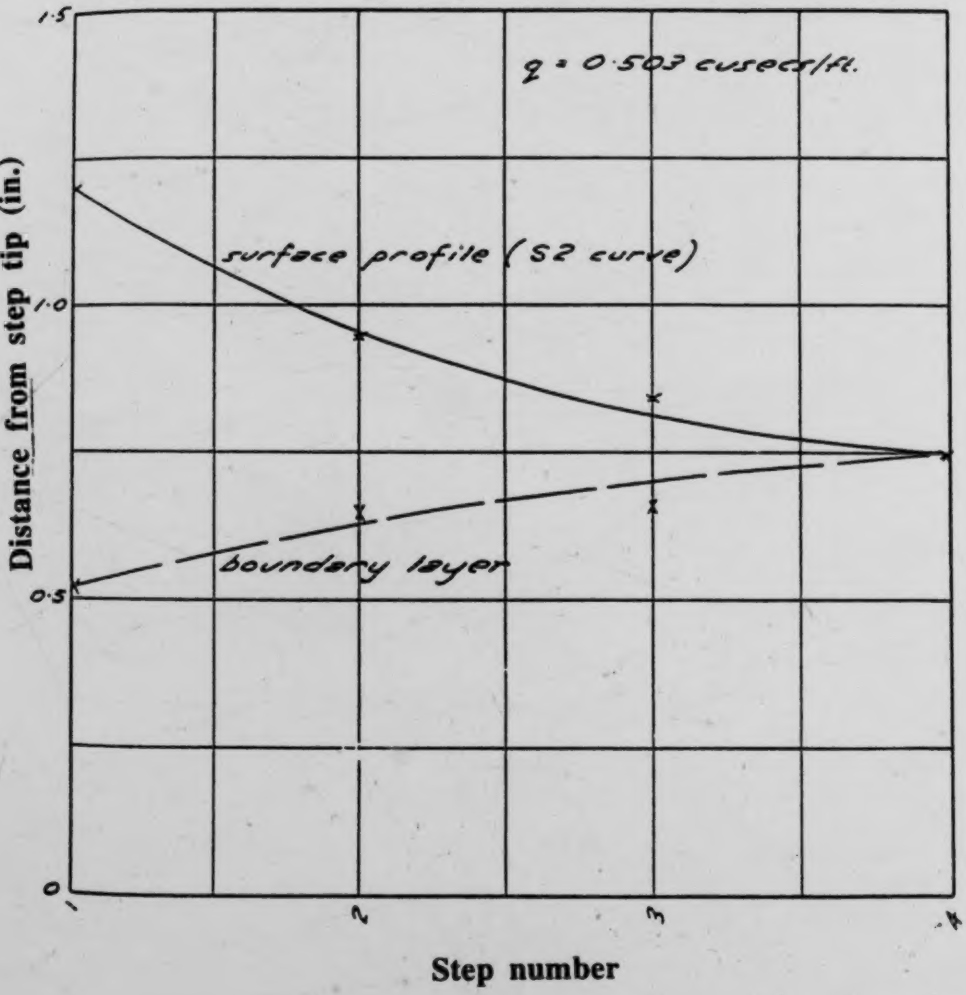

Figure 2.17 Boundary layer and water surface profiles in non-aerated region in a stepped spillway model (adapted from Horner, 1969)

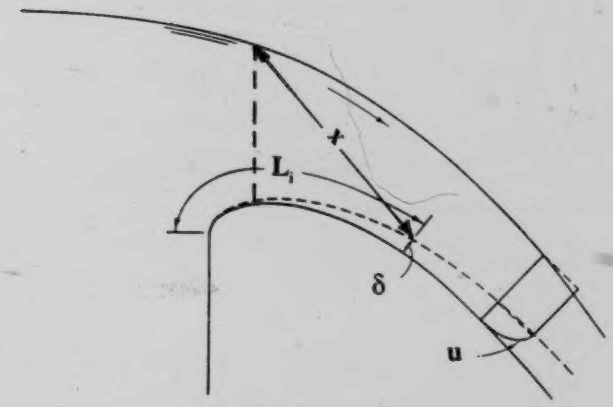

Figure 2.18 Definition sketch for parameters in Eq. (2.20)

Chapter 3
EXPERIMENTAL PROGRAM

3.1 Introduction

This chapter describes the experimental arrangement used for this study that was built in the T. Blench Hydraulics Laboratory at University of Alberta. The chapter is divided into four sections which describes:

i) the aim of the experimental program
ii) the instrumentation used
iii) the experimental setup and procedure used
iv) experimental errors and uncertainties in measurement.

It was necessary to build a device to measure the air concentration in the flow of the air-water mixture. The observations were limited to the skimming flow regime. Although most observations are carried out in the developed region, observations were also made in the non-aerated and the developing region of the flow.

3.2. Aim of the Experimental Program

As discussed in the previous chapter, there are several aspects of the design of stepped spillways that are in need of clarification. Skimming flow over stepped spillways is not displayed well in small scale models. A full understanding of the phenomenon of the self-aerated flow requires a series of tests on large scale models of stepped spillways. As well, former experimental works made no provision for defining the distribution of the air in the flow. The experiments reported herein were initiated to measure flow characteristics, including air concentrations, and represents the first known attempt to obtain detailed information from large scale models.

The aims of the experimental program were:

1) to construct large scale models with various step heights and slopes;
2) to obtain air concentration and velocity profiles along the length of the models; and
3) to observe the flow profiles to obtain information regarding the complex flow structures.

The results from the experimental program are presented in the next chapter.

3.3 Instrumentation

The experimental program necessitated the development and use of some specialized equipment. This included the development and construction of a device that could easily measure the air concentration at any point in the flow. The Prandtl tube was used to measure pressure heads in the flow and in combination with the air concentration profile, velocities could be determined. Flow visualization was achieved with the aid of both normal and high speed videos. The following provides a detailed explanation of each part of the equipment.

3.3.1 Air concentration Probe

3.3.1.1 Introduction

The measurement of the air concentration requires that portion of the cross section included in a single measurement must be small in relation to the entire cross section. However, the volume of the individual measurement must also be large enough to accommodate several air bubbles of various sizes. It is also important that the instrument has only a small dependence on external calibration to reduce the work load. Unfortunately, there are no absolute standards for comparison that may be used as a control on the experimental work.

The air concentration probe should be sturdy to withstand the force of the high velocity flow in the self-aerated region. The shape of the probe element should disturb the stream as little as possible. Any disturbance may cause the air bubbles to separate from the water because of the density difference. Simplicity of operation, a potential for less observational errors, and time conservation are desirable assets to any method of measurement. An electrical method appeared to offer the best choice of fulfilling these requirements.

3.3.1.2 Theory

The electrical method of measuring air concentration in an air-water mixture relies on the measurement of the electrical conductivity of the air-water mixture. The electrical conductivity of a fluid with suspended particles varies with the volume of the particles in a fluid. An expression for the conductivity of suspended homogeneous, nonpolarizable spheres was expressed by Maxwell (1873) as

$$\frac{r-r_1}{2r+r_1}=C\frac{r_2-r_1}{2r_2+r_1} \qquad (3.1)$$

where C is the volume concentration of the suspended spheres and r_1, r_2, and r are the specific resistivities of the fluid, suspended spheres, and suspension, respectively. If the spheres are considered to be nonconducting, then $r_2 \rightarrow \infty$ and Eq. (3.1) is the solution for the volume concentration of the suspended spheres:

$$C=\frac{r-r_1}{2r+r_1} \tag{3.2}$$

If the specific resistivities are taken over the same volume, electrical resistance may be substituted in for the resistivity values, therefore:

$$C=\frac{R_l-R_1}{2R_l+R_1} \tag{3.3}$$

where R_l and R_1 are respectively the electrical resistances of the suspension and the liquid.

Next it is assumed that air bubbles in the air-water flow are spherical and nonconducting. The validity of this assumption was discussed by Lamb and Killen (1950). To apply Eq.(3.3) as a function of the concentration and the resistance, consider the following equivalent electrical circuit:

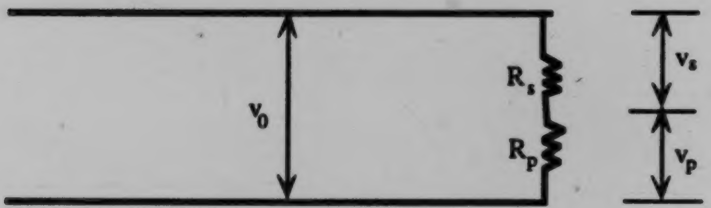

where v_0= the supply voltage, R_p= the resistance of the probe, R_s= an arbitrary series resistance, v_s= the voltage across the R_s, and v_p= the voltage across the probe. If I is the current in the circuit and C is the volumetric concentration of the air, Eq. (3.3) can be written as follows:

$$C=\frac{\frac{v_p}{I}-R_1}{2\frac{v_p}{I}+R_1}=\frac{v_p-IR_1}{v_p+\frac{IR_1}{2}} \tag{3.4}$$

or

$$C=\frac{v_0-I(R_s+R_1)}{v_0-I\left(R_s-\frac{R_1}{2}\right)} \tag{3.5}$$

It must be noted that R_1 is the resistance of the water with no air present. In the pure water condition, C has a zero value:

$$v_{0i}=I(R_s+R_1)\xrightarrow{v_{si}=I_i R_s}\frac{v_{0i}}{v_{si}}=1+\frac{R_1}{R_s}=x \tag{3.6}$$

where x= the factor described above, v_{0i}= the initial supply voltage, and v_{si}= the initial voltage across the arbitrary resistance when the probe is placed in pure water. Substitution of Eq. (3.6) into Eq. (3.5) will give:

$$C=\frac{\frac{v_0}{v_s}-x}{\frac{v_0}{v_s}-\frac{3-x}{2}} \tag{3.7}$$

If we set $x=3$ when the probe is calibrated in the pure water, Eq. (3.7) is converted into

$$C=1-\frac{3v_s}{v_0} \tag{3.8}$$

It is seen from Eq. (3.6) if the ratio of v_{0i} to v_{si} is equal to 3 at the initial condition, the relation between v_s and C is linear.

Lamb and Killen (1950) suggested the upper limit of 60 or 70 percent of air concentration for the application of the electrical probe. However, a comparison of the results of the air concentration above 60 percent obtained with an electrical probe with those of a mechanical sampler showed good agreement. They devised a simple test to obtain a picture of the flow structure and found that the flow near the surface is composed of alternate slugs of nonconducting air and conducting air-water mixture. If the electrical probe follows the rapid change of concentration, its mean reading over a period of time would yield the true value of the mean concentration. In their experiments, the electrical probe was used to evaluate the air concentration as high as 90 per cent with good accuracy. Above this, measurements were not expected to be reliable. For details, the reader is referred to Lamb and Killen (1950).

3.3.1.3 Electrical Probe and Circuit Design

A cell having electrodes in the wall envelops the air-water mixture being tested and leads are furnished to connect the electrodes to the bridge. Shunt capacity, polarization, and the ability to maintain the system at a constant temperature are the main factors to obtain accurate results. Two plates were attached to the end of a strut, projecting forward from the strut into the flow. Requirements are that the plates must cause minimum disturbance to the flow and possess sufficient rigidity to prevent excessive vibration. The plates must also be insulated except at the end on the inner surface where the electrodes are located. The plates have waterproof leads to them from the electrical circuit. Although a baked-on enamel might be excellent for this purpose, the use of conformal coating was satisfactory for the insulation of the plate.

The next step was to determine the spacing and the size of the electrodes. The size and the spacing between the two electrodes must satisfy the following requirements:

i) the space must be small enough to maintain the vertical resolution of the measurements and to avoid the shunt capacity; and

ii) The space has to be large enough to include several bubbles and to reduce the polarization effect.

Lamb and Killen (1950) suggested that the shunt and polarization effects could be reduced by choosing frequencies of 3500 to 4000 Hz. It was also proposed that the effects of polarization could be reduced by using platinized electrodes, although stainless steel also proved satisfactory. Lamb and Killen (1950) chose an electrode spacing of 6.33 mm. There was no information regarding the order of the bubble sizes in their experiments. Observations of the present experiments by high speed video did not produce a clear picture for the bubble size. However, the photographic pictures from the recirculating flow trapped on the steps showed that a wide range of bubble size exists, varying from 1 to 5 mm (Plate 3.1). Considering this and the above factors, the plates were set 10 mm apart and the size of the electrode was chosen as 10 mm by 10 mm.

The final design is shown in Plate 3.2. A stainless steel plate of 1.0 mm thickness was used to give the structural strength and to minimize the disturbance to the flow. The plates and the leads were supported by a Teflon rod which was made of a nonconductive material. This measure was taken to insure that any leak between the plates and their respective electrical leads is prevented.

The circuit consists of a wave generator, two voltmeters, and a variable resistance box (Plate 3.3(a-b)). A sine wave generator was used to give a frequency of 5,000 cycles and an output of 3 volts. One of the voltmeters showed the voltage across the probe and the other read the input voltage. The resistance box was only used for the initial calibration.

3.3.1.4 Testing Procedure

The procedure basically involved obtaining a mean concentration across the electrodes. The mean air concentration was measured with the electrical probe as follows:

> i) The probe was calibrated by placing it into a sample of water taken from the flow. The variable resistance was adjusted until the value of the factor x (defined in Eq. (3.6)) was equal to 3.
>
> ii) The probe was lowered to the desired position in the air-water mixture; the mean values of v_s and v_0 were noted and the air concentration was calculated from Eq. (3.8). The probe could be moved across a section of the flow to obtain the air concentration profile.

The time between the initial and final reading must be limited to a period which does not include a temperature change large enough to affect the ratio of the resistance.

A series of experiments showed that the calibration could be improved by placing the probe in the flowing stream. After calibrating in a sample of water (setting $x = 3$), the probe was placed in the non-aerated region of the flow. The new reading showed a maximum difference of 20% in the lower region of the air-water flow compared to the reading of x when the probe was placed in a sample of still water. There is no clear explanation for such difference, although there could be a dynamic effect when the probe was inserted into the flow. Despite this discrepancy, it was decided to calibrate the probe in the non-aerated region of the flow.

3.3.2 Velocity Meter

3.3.2.1 Introduction

A satisfactory method of measuring point velocities in high speed air-water flow has proved particularly elusive in the past. Viparelli (1953) used a form of Prandtl tube incorporating a three way tapping where the high velocity flow was passed through the tube until the time a reading was taken. In this way, air bubbles were kept out of the manometer lines. Straub et al (1954) developed a "salt-water" velocity meter to measure the velocities in model studies. The instrumentation consisted basically of a device that recorded the travel time of a salt-water slug injected into the air-water mixture. The passage of the ionized slug was detected by electrodes at distance fixed 76.2 mm apart in the flow stream. The speed of injection was about 20 slugs per second with individual slugs of about 0.03 cm^3 of 6% saline solution injected in about 1/600 second. Absolute control of the size of the salt slug and the frequency of the injection was of critical importance.

The writer chose a method whereby velocities were obtained by measuring stagnation pressures with a Prandtl tube. Observations of Straub et al (1954) and the present investigation revealed that the flow stream in the developed region of the air-water mixture was parallel to the slope of the spillway. Therefore, the tip of Prandtl tube was set parallel to the slope to measure the streamwise velocity. Details of the device will be described in the remainder of this section.

3.3.2.2 Theory

The basic relation linking stagnation pressure and velocity may be expressed in the form

$$p_{stag} = p_{stat} + \frac{1}{2}\rho_m u_m^2 \tag{3.9}$$

where p_{stag}= the stagnation pressure, p_{stat}= the static pressure, ρ_m= the density of the mixture, and u_m= the time average velocity of the mixture. The above equation is generally applied to homogeneous fluids. Viparelli (1953) suggested that the above formula as applied for air-water mixtures in the development of his Prandtl tube technique. His checks on the meter accuracy validated the assumption.

The mixture density may be expressed in terms of the air concentration by the relation (neglecting the density of the air)

$$\rho_m = \rho_w (1 - C) \tag{3.10}$$

where ρ_w is the water density. Substitution of Eq. (3.10) into Eq. (3.9) yields

$$p_{stag} = p_{stat} + \frac{1}{2}\rho_w (1 - C) u_m^2 \quad \rightarrow \quad u_m = \sqrt{\frac{2\left(p_{stag} - p_{stat}\right)}{\rho_w (1 - C)}} \tag{3.11}$$

In the present investigation, manometer lines were used to read the pressure heads. Therefore, Eq. (3.11) in terms of pressure head, i.e. $p = \gamma h$, is converted to:

$$u_m = \sqrt{\frac{2g\left(h_{stag} - h_{stat}\right)}{(1-C)}} \tag{3.12}$$

where h_{stag} = the stagnation pressure head and h_{stat} = the static pressure head.

3.3.2.3 Velocity Meter

The apparatus for measuring velocity consisted of a Prandtl tube, a manometer, and a flushing system (Plate 3.4). The Prandtl tube had an external diameter of 3.2 mm and internal diameter of 1.1 mm. The internal and the external tubes show the stagnation and static pressure head, respectively. The manometer consisted of two glass tubes mounted on a vertical wooden plate. The wooden plate was scaled to show the reading of the pressure heads.

Early experiments showed that the high velocity air-water mixture pushes air bubbles into the Prandtl tube. Because of the small internal diameter of the tube, the air bubbles obstructed flow into the tube, thus making the manometer readings inaccurate. To avoid this problem, a flushing system was designed to evacuate the air bubbles that entered the system (Plate 3.5). The flushing system consists of a small reservoir of water installed at high elevation. When obstruction of the tube by air bubbles was noted, the flushing tank was connected to the manometer tube and a reverse flow moved the trapped air out of the system.

3.3.3 Flow Visualization

Flow visualization is very useful for developing an understanding of the flow patterns. Some flow characteristics in the air-water mixture cannot be measured by currently available instrumentation. However, the macroscopic structures of the flow, which include the organized and non-organized large-scale vortical structures, play an important role in the dynamics of the flow. The purpose of flow visualization was to characterize these large scale eddy features of the flow. It was also attempted to use these observations to obtain some velocity measurements to compare with the results of Prandtl tube measurements.

The photographic work involved the use of a Kodak-Spin Physics (SP2000) high-speed video camera system. The pictures were taken from the side of the channel at a rate of 2000 frames per second. The camera was focused on a plane very close to the Plexiglas wall, so that the pictures show only the flow near the side wall. The camera was focused on a different length of the channel depending on the size of the roughness. The time interval for each run was from one to six seconds. The footage was recorded on a normal video tape at different speeds and could be viewed one frame at a time. The frames were studied to observe the vortical flow structures in the recirculating flow on steps or at the tips of the steps. The entrained air in the flow is the reflecting medium for the light focused on the flow and made the vortices traceable. The videos are also useful to investigate the manner in which the air is entrained and mixed with the flow. A normal video recorder and a 35 mm camera were also used to obtain information regarding the point of air inception and bubble diameter in the recirculating area. A more detailed explanation of this photographic analysis is presented in the next chapter.

3.4. Experimental Setup and Procedure

3.4.1 General description of the Model

The model was built in the T. Blench Hydraulics Laboratory at University of Alberta. This apparatus included a supply reservoir, a water supply line, a magnetic flow meter, a stilling tank, a short upstream channel, a stepped channel, and a downstream horizontal channel. A diagrammatic sketch of the model is shown in Figure 3.1.

The water flowed from the supply reservoir through a 0.20 m diameter circular pipe. The pipe contained a magnetic flow meter near the supply reservoir to measure the discharge. A butterfly valve was located near the inlet of the stilling tank to control the flow. The stilling tank was installed to calm the high velocity flow from the supply line so that a steady low velocity flow approached the upstream channel. The operation of the stilling tank was improved by installing a hogs hair screen at the inlet. The upstream channel was 0.30 m wide and the channel sides were constructed of Plexiglas. The elevation of the upstream channel bed was 2.50 m above the downstream channel bed. The upstream channel was connected to the stepped channel with a WES Ogee standard spillway profile. The unstepped profile zone reached tangency with the downstream face at a constant slope. Two different slopes of the stepped channel were used for testing. The width of the channel was chosen so that side wall effects due to the growth of the side wall boundary layer and air entrainment along the sides could be avoided in the central portion of the cross section. That the width was adequate to make the flow two-dimensional in the center portion was demonstrated by earlier measurements of air concentration and velocity in a transverse section by Straub et al (1953). The stepped channel was 0.30 m wide. The criteria for choosing the slopes of the channel was prototype stepped spillways. Frizell (1992) listed the recent dams that used stepped spillways either for regular or emergency overflow (Table 3.1). The best range of the slopes in most dams due to economic, constructability, and stability criteria was chosen as from 0.6H:1V to 0.8H:1V. For the first set of experiments, the channel slope was set to $l/h = 0.6$, where l is the length of the step tread and h is the height of the step. In the first series of tests, the step height was fixed at 125 mm in the stepped face of the channel. For the following series, the step height was changed with the interposition of half-size steps to obtain 62.5 and 31.25 mm height. For the second set, the slope was set at 0.8 and two different step height of 125 and 31.25 mm were chosen. The bottom of the last step joined the bed of the horizontal downstream channel which directed the water to the supply reservoir. Plate 3.6 shows part of the experimental setup.

3.4.2 Measurements

The measurements included the discharge, the point of air inception and vortical structures, air concentration and velocity profiles, and depth. A magnetic flow meter, photographs, an electrical probe, a Prandtl tube, and a point gauge were respectively used to obtain these measurements. Most measurements were made in a vertical centerline plane in the developed region, unless otherwise noted.

The flow in the model was measured by means of a magnetic flow meter installed in the supply line. The principle of the magnetic meter is that when a moving conductor crosses the lines of a magnetic field, a voltage is induced. If the dimensions of the conductor are constant, the voltage is proportional to the velocity. The flowing liquid itself is the moving conductor, therefore, the voltage varies directly with the variation in the velocity or discharge of the flowing flow. The range of the discharge varied from 21 *L/s* to 62 *L/s*, the maximum limit of the stilling tank.

The normal video camera was used to study the point of air inception. From the frames of the high-speed video camera, it was possible to study the mechanism of the air entrainment. The high-speed pictures were also used to obtain information regarding the initiation, termination, and size of the vortex tubes formed on the steps. By measuring the time travel of two fixed points in the flow, the 1/2000 second frame enabled the measurement of approximate velocities of the air-water mixture.

The air concentration was measured by the electrical probe described in section 3.2.1. Velocities were measured using the Prandtl tube described in section 3.3.2. The carriage holding the probe or the tube was designed so that it was possible to traverse the flow section both vertically and horizontally. Readings were taken at 3 mm intervals on a line normal to the channel slope with the lowest point 6 mm from the tip of the steps. The uppermost reading was taken where the probe was almost out of the flow and the meter registered about 96 percent air concentration. The air concentration and velocity profiles were obtained for each slope and each water discharge. The depth of the flow at the upstream channel was measured with a point gauge that could be moved over the frame at the top of the channel.

3.5 Experimental Errors and Uncertainties

3.5.1 Definitions

Bendat and Piersol (1971) discussed that any observation can be classified as deterministic or nondeterministic data. Deterministic data are those that can be determined by an explicit mathematical relationship. For example, consider the second law of Newton, $W=mg$, where W is the weight of a body, m is the mass of a body, and g is the acceleration. This relationship defines the exact weight of a body at any time. Hence the physical data representing the weight of the body are deterministic. However, there are certain physical phenomena that produce data which are not deterministic because each observation of the phenomenon will be unique. For example, the electrical output of a noise generator cannot be described by an explicit mathematical relationship. These data are nondeterministic (random) in nature and can be described in terms of probability statements and statistical averages.

There are always debates over the classification of various physical data as being either deterministic or random. It might be argued that no physical data are deterministic, as there is always a possibility that some unforeseen factors that might influence the phenomenon are not considered in the mathematical expression. On the other hand, it might be argued that no data are random as mathematical expression might be developed if sufficient knowledge of the mechanism producing the data was available. In practical terms, if experimental data can be repeated many times with identical results (within the limits of experimental error), then the data can be considered deterministic. Otherwise, the data are random in nature.

From the analysis viewpoint, deterministic phenomena can be categorized as being either periodic or nonperiodic. Periodic data can be classified as being sinusoidal or complex periodic. Nonperiodic data can categorized as being either "almost-periodic" or transient. Of course, any combination of these forms may occur. A random phenomenon is represented by a single time history which is called a "sample function". A collection of all possible sample functions is called a random process. Random processes can be categorized as being either stationary or nonstationary. Stationary random processes can be further classified as being either ergodic or nonergodic.

From the reliability viewpoint, Kline and McClintock (1953) classified experiments as being either single-sample or multi-sample experiments. If the experiments are repeated using different observers and instruments so that the reliability of the results can be analyzed through the use of statistics, the experiments are called multi-sample. In most engineering experiments, it is not practical to evaluate the reliability of the results by repetition. The type of experiments where the reliability of the results not analyzed by repetition are called single-sample. A practical way to estimate the reliability of the results in a single-sample experiment was presented by Kline and McClintock (1953) and will be described briefly in this section.

The difference between the true and measured values is called an "error", but the "uncertainty", which may vary with each observation, is what the observer thinks the error may be. A "data point" is the recorded value of a variable which is the quantity observed directly in an experiment. A "result" is produced by calculations or making corrections to the data. Errors can be classified as accidental, fixed, and mistakes. For details, the reader is referred to Kline and McClintock (1953).

3.5.2 Theory

Kline and McClintock (1953) suggested that a satisfactory way to analyze uncertainties in a single-sample experiment is to describe a distribution for the uncertainties. A data point will then be presented by a mean value and an uncertainty interval based on a certain confidence. If D_m represents the mean value and w represents the uncertainty interval with a confidence level of cl, then the data, D, can be expressed as

$$D=D_m \pm w(cl\%) \tag{3.13}$$

For example, suppose that the stagnation pressure head, h_{stag}, is given by

$$h_{stag}=970 \pm 10\ mm(95\%) \tag{3.14}$$

This means that the observer believes that under the circumstances of the experimental procedure, 95% of the h_{stag} measurements fall within ±10 mm of the mean value 970 mm.

The observer should determine the uncertainty interval on a given confidence for each data. Some of these intervals are based on an estimates rather than experiment and the confidence level may not be better than 50%. Of course, such estimates are not guesses but are based on factors such as sensitivity, fluctuation, and the accuracy of instruments.

Assume that a result, R, is a function of n independent data (or variables), $D_1, D_2, \ldots\ldots\ldots D_n$, $R = R(D_1, D_2, \ldots\ldots\ldots D_n)$. The data have the uncertainty intervals $W_1, W_2, \ldots\ldots\ldots W_n$ with the same confidence levels. The uncertainty interval, W_R, for the result with the same confidence level can be expressed by

$$W_R = \left[\left(\frac{\partial R}{\partial D_1} W_1\right)^2 + \left(\frac{\partial R}{\partial D_2} W_2\right)^2 + \ldots\ldots + \left(\frac{\partial R}{\partial D_n} W_n\right)^2\right]^{1/2} \tag{3.15}$$

3.5.3 Uncertainty Evaluation

Because of the nature of the experiment, it was difficult to collect enough data to construct a distribution to find the uncertainty confidence. Uncertainties were estimated with a confidence level of 50%. Kline and McClintock (1953) suggested that 50% confidence levels might be satisfactory if the uncertainty is of the order of a few percent or less of the original data.

The depth at the upstream channel was measured with a point gauge that could be read to the nearest thousandth of a meter. Because of the fluctuation of the water surface, the uncertainty interval was estimated as ±2 mm. The position of the Prandtl tube and the air concentration probe in the flow were measured by a scale calibrated to the 0.5 mm, so the uncertainty level was set at ±0.25 mm. The manometer board was scaled to 2 mm. The agitated nature of the flow in the air-water region caused fluctuations in the pressure heads readings. Considering the complexity of the flow, it is reasonable to make an estimate of the accuracy. The interval uncertainty for the pressure heads was set at ±15 mm.

The accuracy of the air concentration depends on both the initial calibration and the variability in measurements because of the turbulent structure of the air entrainment phenomenon. The insertion of the air concentration probe in the non-aerated region for the initial calibration showed a little fluctuation in the voltmeter readings. The voltmeter was accurate to an uncertainty interval of ±0.01 volt. However, when the probe was inserted in the aerated region, completely different situation arise. Due to the nature of the air-water mixture, the readings had considerable variability, especially in the mid-lower region of the flow. Because of the tedious nature of the experimental work in measuring the air concentration, it was not practical to obtain a large number of the air concentration readings. Considering the discussion that will be presented in section 4.3.3.2, the uncertainty interval for the air concentration was set at 2%.

The uncertainty in velocity measurements was estimated based on Eq. (3.15) since velocity is classified as a "result" calculated from Eq. (3.12). Applying Eq. (3.12) to Eq. (3.15) yields

$$W_{V_m}=\left[\left(\frac{\partial V_m}{\partial \Delta h}W_{\Delta h}\right)^2+\left(\frac{\partial V_m}{\partial C}W_C\right)^2\right]^{1/2} \tag{3.16}$$

where $\Delta h = h_{stag} - h_{stat}$, and W_{V_m}, $W_{\Delta h}$, W_C, are the uncertainty intervals for velocity, pressure head, and air concentration, respectively. The partial derivatives in Eq. (3.16) are

$$\begin{cases} \dfrac{\partial V_m}{\partial \Delta h}W_{\Delta h}=\dfrac{1}{2}\sqrt{\dfrac{2g}{\Delta h(1-C)}}W_{\Delta h} \\ \dfrac{\partial V_m}{\partial C}W_C=-\dfrac{1}{2(1-C)}\sqrt{\dfrac{2g\Delta h}{(1-C)}}W_C \end{cases} \tag{3.17}$$

It is more useful to express the velocity uncertainty in term of the relative from, W_{V_m}/V_m. Thus, Eq. (3.17) is converted in

$$\begin{cases} \dfrac{\partial V_m}{V_m\partial \Delta h}W_{\Delta h}=\dfrac{1}{2}\dfrac{W_{\Delta h}}{\Delta h} \\ \dfrac{\partial V_m}{V_m\partial C}W_C=-\dfrac{1}{2}\dfrac{W_C}{(1-C)} \end{cases} \longrightarrow \frac{W_{V_m}}{V_m}=\left[\left(\frac{1}{2}\frac{W_{\Delta h}}{\Delta h}\right)^2+\left(-\frac{1}{2}\frac{W_C}{(1-C)}\right)^2\right]^{1/2} \tag{3.18}$$

Eq. (3.18) shows that the relative uncertainty of velocity not only depends on the uncertainties of the air concentration and pressure head but on the air concentration value as well. The pressure head readings varies from about 200 mm for lowest point in the section to about 1100 mm for the maximum velocity. Figure (3.2) shows the variation of the relative velocity uncertainty with the air concentration based on the average estimation of the relative uncertainties of pressure head of 2% and air concentration of 2%. Figure 3.2 shows that the relative velocity uncertainty increases with increasing air concentration. For example, at *C*=90% and 95%, the relative velocity uncertainty are 9% and 19%, respectively. The writer believes that beyond *C*=90%, the results are not reliable considering the high uncertainty and limitations of the air concentration probe.

Dam and location (Reference, date)	Design unit discharge ($m^3/s/m$)	Hydraulic Height (m)	Downstream Slope (H:V)
Upper Stillwater, U.S.A (Houston, 1987)	11.5	61.6	0.32:1 top 0.60:1 toe
Monksville, U.S.A (Sorensen, 1985)	9.3	36.6	0.78:1
Stagecoach, U.S.A (Stevens)	3.6	42.7	0.80:1
De Mist Kraal, South Africa (Jordaan, 1986)	10.2	18	0.60:1
Zaaihoek, South Africa	5.1	36.6	0.62:1
Lower Chase Creek, U.S.A	3.3	18	0.70:1
Milltown Hill, U.S.A (Frizell, 1990)	14.3	54.9	0.75:1
Middle Fork, U.S.A	overtops for events >500 yrs.	37.8	0.80:1
Knellport, South Africa	8.4	43.1	0.60:1
Santa Cruz, U.S.A	4	36.6	0.65:1
Bucca Weir, Australia	55.6	11.9	0.50:1
Jequitai, Brazil	9.2	36.2	0.80:1
Junction Falls Dam, U.S.A	11.4	9	0.875:1
Les Olivettes, France	7.2	31.5	0.75:1
Cedar Falls, U.S.A	2.8	7.6	0.80:1

Table 3.1 RCC or Rehabilitated Concrete dams with stepped spillways (adapted from Frizell, 1992)

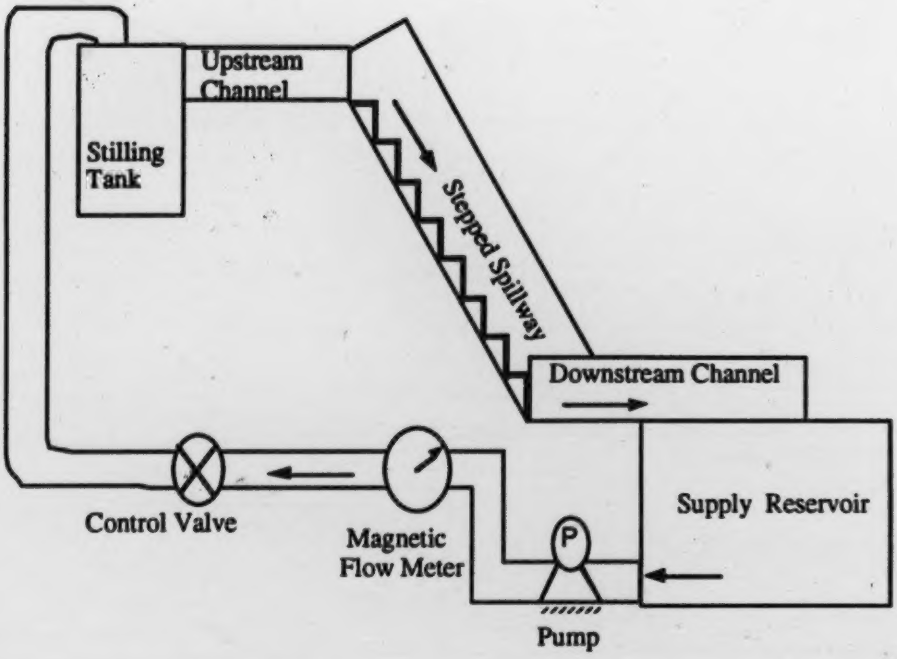
Upstream Channel
Stilling Tank
Stepped Spillway
Downstream Channel
Supply Reservoir
Control Valve
Magnetic Flow Meter
P
Pump

Figure 3.1 The stepped spillway model

Figure 3.2 Variation of the relative velocity uncertainty with the air concentration

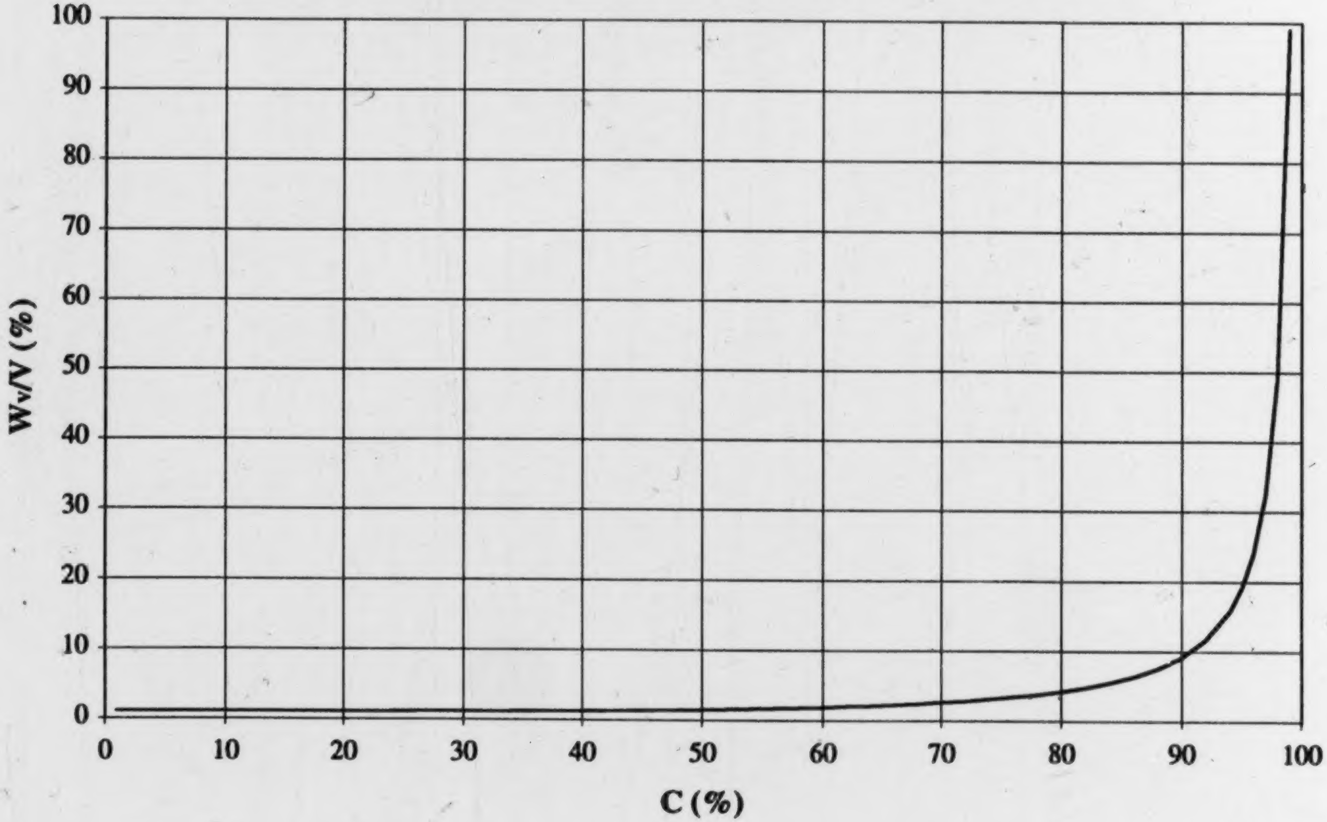

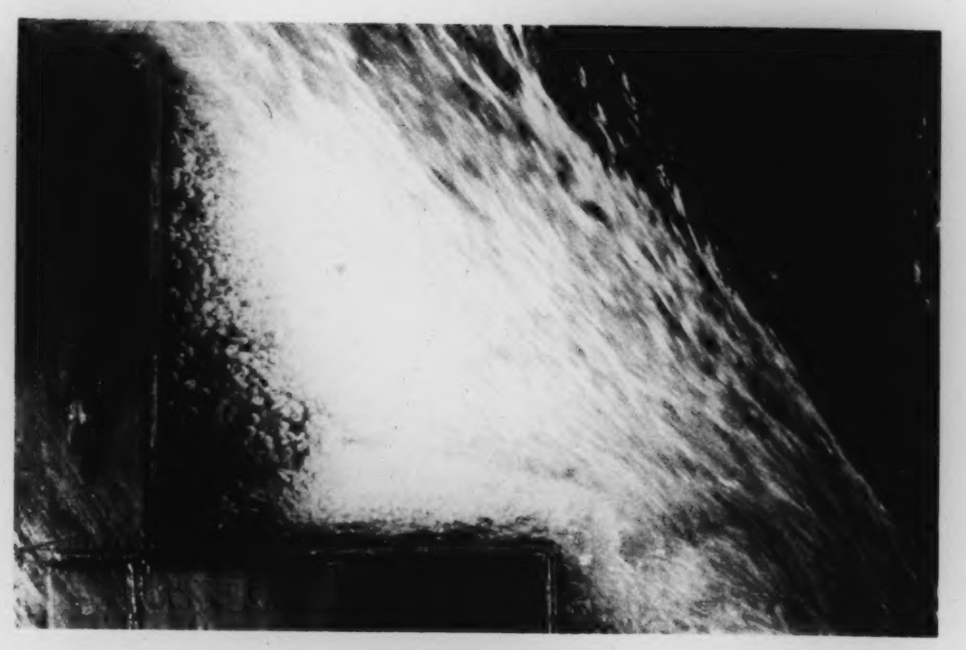

Plate 3.1 A close-up view of the air bubbles trapped in the recirculating flow on a step

Plate 3.2 The electrical air concentration probe

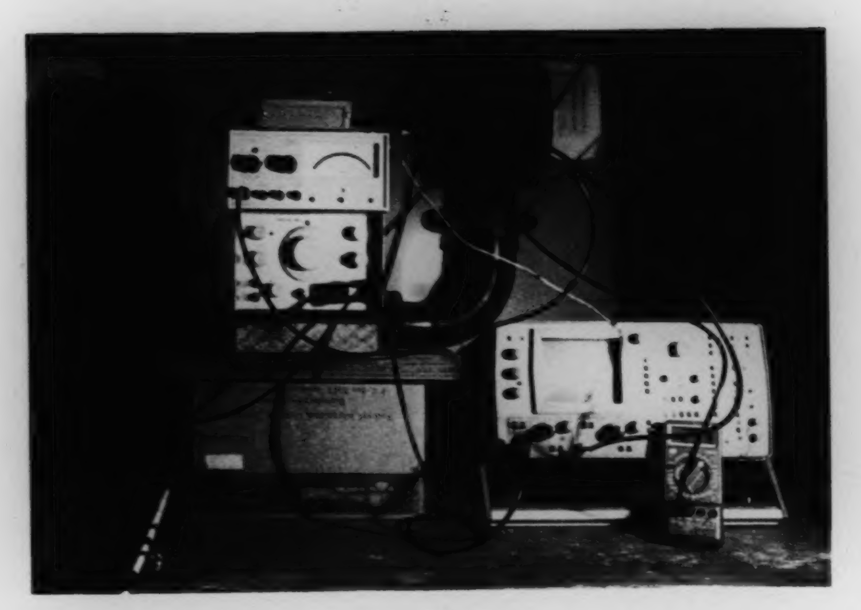

(a)

Plate 3.3 (a-b) The electrical circuit for the air concentration probe
(a) the circuit
(b) the wave generator

WAVETEK
off
freq Hz
cal
gated
cont
trig
man
trig
mode

(b)

Plate 3.3 (a-b) The electrical circuit for the air concentration probe

(a) the circuit

(b) the wave generator

Plate 3.4 The experimental setup for the velocity measurements

Plate 3.5 The flushing system designed to evacuate the air bubbles from the Prandtl tube

Plate 3.6 The stepped spillway model

Chapter 4
EXPERIMENTAL RESULTS AND ANALYSIS

4.1 Introduction

In this chapter, the main objectives of this study are realized, that is to provide a detailed description of skimming flow and to investigate the validity of applying the theoretical relationships developed for flows in open channels with a roughness less severe than that of a stepped spillway. Although most observations had been made in the uniform region of the flow, detailed photographic observations show some flow patterns in the non-aerated region. The flow behavior and classification are first described. Results and analysis are then separately presented for each region of the flow.

4.2 Flow Patterns and Their Classification

4.2.1 Introduction

The behavior of flow over a stepped spillway is both complex and varied. To describe flow conditions concisely, it is convenient to classify flow patterns by a visual comparison of the flow and step geometry. This procedure enables two basic types of flow to be distinguished: jet flow, where the flow hits the tread of the step immediately below; and skimming flow, where a coherent stream proceeds down the spillway. The flow in the skimming regime is evaluated based on the variation of flow characteristics from one step to the next. Three flow regions were observed: (1) a non-aerated region in which the flow patterns differ on every step, (2) a developing region where bulking of the flow due to air entrainment is initiated, and (3) an aerated, developed (or uniform) region in which the flow characteristics remain approximately constant from section to section. This classification is similar to that used for chute spillways to recognize different flow regions. Using the above method of classification, the flow behavior observed on the experimental models will be described in this section and analyzed in subsequent sections.

4.2.2 Types of Flow

A preliminary investigation using the stepped spillway models confirmed that, depending on the discharge, two main types of the flow can exist on stepped spillways. At smaller discharges, the flow impinges on the tread of the lower step. This type of flow has been distinguished as jet flow. In this regime, two main features contribute to the flow energy loss: the recirculating flow formed in the pool beneath the main flow and a partial hydraulic jump that may be formed downstream of the point of jet impact. As the discharge increases, the impact point of the jet flow moves towards the end of the step. At higher discharges, the steps become completely submerged and a relatively smooth flow skims them. For this case, the spillway can be described as a steep open channel with large roughness elements. Flows causing steps to be drowned are referred to as skimming flows. Between these two regimes, a transition state exists where the upper portion of the flow overshoots the tips of the steps and disperses with considerable turbulence. Since this investigation is primarily concerned with skimming flow, a detailed description of this phenomenon will be presented next.

4.2.3 State of Skimming Flow Regime

As discussed earlier, when the discharge intensity becomes sufficiently high, the steps become completely submerged and skimming flow sets in. An added feature of this type of flow is the occurrence of air entrainment. It is a common characteristic of high velocity flows in spillways. Self-aeration is the entrainment by the flow of air from above the stream and the diffusion of this air through the depth of the flow to create a violently agitated stream with an ill-defined free surface. The formation and characteristics of the air-water mixture in the models tested agreed with the patterns observed in chutes spillways by Straub and Anderson (1958).

Flow characteristics were observed at various sections along the length of the spillway length for several skimming flows in the model. A non-aerated region was formed at the upstream end of the spillway, where the flow contained little or no entrained air (Plate 4.1). This type of flow can be classified as "rippled flow" as described by Michels and Lovely (1953). Any air entrainment in this region is due to disturbances caused by surface longitudinal surface vortices or side wall generated turbulence. As the flow begins to accelerate down the spillway, the velocity increases with an associated reduction in flow depth. Early investigators showed that the boundary layer on the bed develops in the initial reach in smooth spillways. In the present investigation, the boundary layer was generated by both the bed and the walls of the channel. The large bed roughness projections (steps) resulted in a dominant bed generated boundary layer. Photographs of the flow showed that the air entrainment was initiated along the side walls sooner than in the central part of the spillway (Plate 4.2). Air at the sides was entrained by the turbulence from the side wall boundary layer near the water surface. For entrainment resulting from the wall generated boundary layer, the location where self-aeration begins was a function of the distance from the wall. Outside the boundary layer, potential flow exists. The boundary layer which grows from the spillway floor has important effects on the entire behavior of the flow. The most important point is that when the boundary layer thickness equals the depth of the flow, the free surface would be turbulent. Since a turbulent free surface is a prerequisite for air entrainment and the boundary layer is the primary source of that turbulence, the significance of the development of the boundary layer lies in its connection with the air entrainment process.

High-speed photographs of the flow in the model revealed that the roughness elements (steps) that projected into the flow influenced the position of the inception of the air entrainment in two ways. Since the size of the roughness relative to the flow depth in a stepped spillway is much greater than that of a chute spillway, the growth of the boundary layer is enhanced by the wakes and eddies formed on the steps. The second factor is the deflection of the internal jet caused by the steps. As the flow approaches the steps, part of the internal flow diverts towards the tread of the steps and is then deflected towards the surface where air entrainment is initiated. In general, observations confirmed that for a specific discharge, the inception sections for two models with different step sizes could occur at different locations. The greater the relative size of the step, the earlier the inception of the air entrainment occurred along the flow.

Below the inception section, an aerated reach extends to the base of the model. A layer containing a mixture of air and water gradually extended through the depth of flow. The air concentration increases continuously from the bed. For this section of the spillway where there is bulking of the flow caused by air entrainment, the flow characteristics vary with distance along the channel and is referred to as the developing region (Plate 4.3). Observations showed that the air-water mixture in this region had a highly irregular, wavy surface in which the returning water droplets ejected from the surface continuously entrained air (Plate 4.4). This air formed bubbles which were diffused through the stream by the turbulent motion normal to the direction of flow. The ejected water traveled through the air in a curved path, returning to the main stream some distance downstream.

After an initial length of flow in the developing region where the concentration of air is obviously increasing, the flow collects more and more air until a condition of equilibrium is reached. In this region, the amount of air escaping from the water equals the amount being mixed into it. Air concentration, along with the other flow properties, does not vary with distance in this region. This section of the aerated zone where the reach appeared to be uniform is referred to as the developed (uniform) region (Plate 4.5). The penetration of air into the flow depends on the turbulence intensity. Transport of air bubbles into the flow by turbulence is counteracted by the buoyant force on each bubble. This process is similar to suspended load in rivers, with the difference being that the air bubbles are lighter than water. A balance is reached wherein as much air is expelled from the flow as is being entrained into it. This balance can be compared to the suspended load balance on a reach of a sediment carrying river where neither degradation or aggradation occurs. When the flow envelops as much air as it can retain and the surface topography becomes similar at every section, the flow reaches a condition of uniform flow for the given slope, roughness, and discharge. The concentration of air increases from the bed to the surface, contrary to the suspended load which is heavier than water.

Photographs revealed that two zones within the depth of self-aerated flow exist (Plate 4.6). First, there is a lower zone in the air-water mixture where air bubbles are kept in suspensions by the turbulent transport through the section. The turbulent fluctuations are responsible for the diffusion and suspension of air bubbles. The second zone is in the upper part of the depth in which water drops, ejected from the lower zone, are projected upwards. Water drops are detached from the main stream and thrown upwards due to their momentum. The ejected drops follow a path that reaches a maximum height and, since there is no mechanism to keep them in the air, then fall back into the flow. The trajectory of the water droplets is long and flat because of the dominant longitudinal flow velocity. The boundary which separates the two zones is referred to as the transition depth. The air concentration in the developed region increases continuously from the bed toward the surface. In the lower zone, the velocity increases continuously up to the transition depth. The rough surface and the high flow velocity of air-water mixture tend to drag a considerable volume of air into motion above the flow. A velocity deficiency can be expected in the air-water mixture in the upper zone because of the drag necessary to sustain the air motion.

As discussed, in a quasi-smooth or skimming flow, small-scale vorticities are generated continuously along the pseudo wall. In the present investigation, photographic works revealed that macro-scale vorticities are generated at the tips of steps. These vortical structures appear in the form of vortex tubes. Plates 4.7(a-d) show the high-speed images of the evolution and termination of such structures in the developed region. A segment of the vortex tube is located on the tread of the step while the remaining part penetrates into the main flow (Plate 4.7(b)). Table 4.1 shows the dimensions of vortex tubes extracted from high-speed images. Plate 4.7(c) shows that the high velocity flow pinches the vortex tube at the tip of the step and the vortex tube is divided into two parts. The upper part of the vortex tube is carried out by the main flow to downstream. The lower part is then elongated and circulate with the recirculating flow into the step groove until it is terminated (Plate 4.7(d)). This vortex tube possibly contributes to the energy loss.

4.3 Results and Analysis

4.3.1 Introduction

Experimental results described herein are largely restricted to the velocity and air concentration measurements traversing the depth of flow where normal aeration had been attained in the developed region. Observations showed that the flow surface was highly turbulent and unstable in relation to the surface aeration pattern. Plates 4.8(a-b) show two pictures taken by a high-speed video camera. The unstable nature of flow at the surface implies that the assumption of one-dimensional flow (parallel to the channel slope) is not justifiable in the upper zone of the developed region. Thus, considerable care has to be exercised in the interpretation of results near the flow surface.

Another factor that is to be considered in the interpretation of the results is the limitation of the instrumentation. The air concentration probe described in section 3.3.1 can measure air concentration up to 90% with good accuracy. Above this concentration, measurement was not expected to be reliable. The accuracy of velocity measurements was limited to, rather than independent of, the accuracy of the air concentration probe. Figure 3.2 provides a good basis for the accuracy of velocity measurements. The error of velocity values increase with air concentration value or depth. Thus, the results of velocity measurements in the upper zone of the flow in the developed region is not as reliable as those in the lower zone.

In the following sections, the results of photographic works involving the inception section phenomenon are presented first. The air concentration and velocity profiles in the developed region are then presented. Analysis of the universal velocity profile and coefficient of skin friction concludes this chapter. In each section, presentation of experimental observations is accompanied by appropriate analysis.

4.3.2. Inception of Air Entrainment

As discussed earlier, the point at which the air entrainment begins is the inception section. The location of inception section is measured by taking the mean distance from the crest of the spillway. Identification of factors that influence this distance is important in hydraulic design. The shorter this distance, the sooner the developed region is established, which contributes to increased dissipation of flow energy, thus reducing the cost of the stilling basins built downstream of spillways. A theoretical basis for this phenomenon is not discussed as some flow patterns around the inception section are not easy to predict analytically. A brief description of early findings by other investigations was presented in chapter two.

Results were obtained by flow visualization using either a high-speed video camera or normal video camera. Table 4.2 lists the step number at which air entrainment commenced for different step heights and discharges. For each step height, the section of inception moves downstream as the discharge increases. This is because the flow depth increases with increasing discharge and the boundary layer reaches the free surface further downstream. For any given discharge, the section of inception is closer to the crest for larger step heights. This is due to the contribution of the internal jet that is deflected by the steps. This particular phenomenon which happens in stepped spillways can be described in detail with the aid of high-speed photographs.

Measurements of the distance of the inception section from the crest, L_i, are shown in Figure 4.1. The definition for L_i is shown in Figure 2.18 and $F^* = q \Big/ \sqrt{g \sin\theta k^3}$ is a Froude number where q is the discharge per unit width, θ is the spillway angle and k is the roughness height normal to the bed. Wood (1983) used dimensional analysis to show that L_i can be approximated by a simple power formula. This is illustrated in Figure 4.1. Wood used observations of laboratory model studies and prototypes of chute spillways to establish this formula. The value of k_s, the Nikuradse equivalent sand roughness, was replaced by k. Later, Chanson (1994) developed a similar relation by using observations of some model studies on stepped spillways. These observations were obtained from models with spillway slopes ranging from 27° to 52°. For a given F^*, Figure 4.1 shows that L_i for a stepped spillway is smaller than that for a standard spillway. This indicates the flow roughness in stepped spillways enhance the flow turbulence and early air entrainment is expected. Figure 4.1 shows that Chanson's relation agrees well with the writer's experimental observations.

The writer modified Chanson's relation by introducing the section of inception Froude number, $F_i = q/\sqrt{g(h/l)k^3}$, as follows:

$$\frac{L_i}{k} = 8.0\, F_i^{0.858} \tag{4.1}$$

Figure 4.2 shows the relationship between L_i/k and F_i, as well as the experimental observations. The proposed relation agrees well with the experimental observations for a wide range of F_i.

After viewing video images at slower speeds, it was possible to observe the flow structures at the inception section. Results for step height, h = 125 mm and discharge, Q = 41.53 L/s are shown in Plate 4.9(a-d) at different time frames. These images were constructed after repeatedly watching the video images. The arrows in these figures show the direction of the flow. In Plate 4.9(a), the 2-D flow over the crest length approaches the first step. In this region, the velocity increases while the flow depth decreases. As the flow leaves the solid boundary of the crest, part of the flow close to the bottom is diverted into the groove of the step (Plate 4.9(b)). This part of the flow is referred to as the "internal jet". The upper part of the flow, which is referred to as the "outer jet", continues accelerating downstream. As it is shown in Plate 4.9(c), the internal jet hits the tread of the step and is deflected. Then, the internal jet curves upward and collides with the outer jet. The collision of these two jets provides for the formation of vortices and consequently enhances the turbulence intensities. After the collision, part of the jet ejects out of the flow and air entrainment starts (Plate 4.9(d)). The air is entrained into the flow in a curved path and the entrained air is carried into the recirculating area. This phenomenon, which was more visible in tests with large step sizes, is defined as a "rooster tail" (Plate 4.3). The rooster tail may extend a considerable height above the main flow. The maximum height of the rooster tail depended on the step size and the discharge.

The phenomenon of the rooster tail, as described earlier, is the result of the deflection of the internal jet. Table 4.3 presents the height of the rooster tail, y_{rt}, extracted from the high-speed and normal video images. y_{rt} is measured as the maximum height above the water surface at the inception section. For each step height, y_{rt} increases as the discharge increases. This may be due to the fact that the flow has higher velocity. For any given discharge, y_{rt} increases with increasing height of the step. The results show that the ratio y_{rt}/h can be determined by a mean line passing through the data (Figure 4.3). This ratio is a factor in determining the height of the training required for the spillways.

4.3.3 Air Concentration and Characteristic Depths

4.3.3.1 Introduction

Observations from testing of air concentration consisted of a large number of voltage readings which subsequently required translation into air concentrations. Air concentration was measured by using an electrical probe, calibrated at the beginning of each run as described in section 3.3.1.4. The air concentration is defined as the volume of air per unit volume of air-water mixture. It was assumed that the measured concentration represented the average value of the concentration in the probe area which measures 10 mm by 10 mm and that this measurement was applicable at the midpoint of this area. For each run, measurements of air concentration were taken along a section normal to the bed. Readings were taken at 3 mm intervals with the lowest point 6 mm from the tip of a step. The lowest point of measurement in a region between two steps was chosen as an imaginary line connecting the tips of the steps.

4.3.3.2 Data Processing

For each reading, the air concentration was obtained by:

$$C=1-\frac{3v_s}{v_0} \tag{3.8}$$

Readings of air concentration at any point varied considerably in the lower zone of the flow. Figure 4.4 shows the mean range of air concentration profile in the developed region. The amplitude of the air concentration range in the lower part of the flow is larger than that for the upper part of the flow. For each point, the maximum and minimum readings were recorded. Since there was no computerized data processing available, two methods of averaging were used. First, readings were sampled at consecutive time intervals of 2 seconds for a period of 20 seconds and an average was calculated. To evaluate the accuracy of this type of averaging, an alternative method was used with the aid of photographic work for a few points. For each point, a video camera recorded the readings for 20 seconds. Then, the video frames were viewed at a time interval of 1/30 second and a total of 600 readings were averaged for each point. The results showed a maximum 2% difference between the two types of averaging. The first method of averaging was chosen for its simplicity.

At the beginning of testing, it was thought that the considerable variation of air concentration at each point resulted from the flow disturbance due to the air concentration probe or by the vibration of the probe itself. However, photographic works showed that this variation was not induced by the presence of the air concentration probe, but is part of the self-aeration phenomenon. Plates 4.10(a-b) show typical high-speed images of the flow in the developed region at different times. The reflection of the camera lights on the air-water mixture helps to distinguish the variation in air concentration. The images show the existence of dark and white cloudlets in the air-water mixture. Normally, a darker cloudlet possesses less air concentration than a lighter one. In this set of high-speed pictures of the flow, the passage of dark and white cloudlets can be observed at any point in the flow. This shows that the air concentration at any point in the flow varies with time.

4.3.3.3 Characteristic Depth and Concentration Definitions

Since no definite free surface exists, definitions for depth and concentration are required to describe the aerated condition. The mean air concentration, $\overline{C}$, in the vertical plane is defined as (similar to Eq. 2.12):

$$\overline{C}=\frac{1}{y_u}\int_0^{y_u} C\,dy \tag{4.2}$$

The upper depth of flow, y_u, is a characteristic depth for the self-aerated flow and defined as a depth where air concentration reaches a specific value. Straub and Lamb (1953) used a value of y_u where the air concentration is 0.95. Straub and Anderson (1958) used the depth at a point where the concentration is 0.99. Recently, Wood (1991) used of a value of 0.90. The determination of this characteristic depth, however, depends on the particular application where y_u is used. For different purposes, y_u may be defined by different air concentrations. The following guidelines were used in determining y_u:

i) A considerable percentage of accumulated water discharge can be obtained at y_u.

ii) A reliable air concentration can be measured at y_u.

A typical plot of the relative total water discharge ratio, dQ/Q, and the corresponding air concentration for l/h= 0.6 and h= 125 mm is presented in Figure 4.5, where dQ is the integrated water discharge. For any given value of C, dQ/Q is larger for higher discharges. For C= 0.20, dQ/Q decreases from a value of 0.49 for y_c/h = 1.3 to about 0.18 for $y_c/h = 0.7$, where y_c is the critical depth. This indicates that air penetration in the air-water mixture is less for higher discharges. This difference in dQ/Q for different discharges is reduced for higher values of air concentrations. A close inspection of Figure 4.5 shows that for C= 0.90, dQ/Q is in the range of 0.96 to 0.98 for different discharges. As mentioned in section 3.3.1.2, the measurement of air concentration is not reliable beyond C=0.90. In addition, the resulting error in the velocity calculation is considerable (section 3.5.2). Therefore, it seems reasonable to define y_u as y_9 where air concentration equals to 0.90. Eq. (4.2) can be then rearranged as follows:

$$\overline{C}=\frac{1}{y_9}\int_0^{y_9} C\,dy \tag{4.3}$$

The total water column in each section can be represented by a mean depth, $\overline{y}$, as (similar to Eq. (2.13)):

$$\overline{y}=\int_0^{y_9}(1-C)\,dy \tag{4.4}$$

Again the upper limit for the above integration is chosen as y_9. Using the definition of mean air concentration (Eq. 4.3) and substituting it into Eq. (4.4), a relationship between $\overline{C}$ and $\overline{y}$ can be determined:

$$\overline{y}=y_9\left(1-\overline{C}\right) \tag{4.5}$$

Another characteristic depth is the transition depth, y_T, which is equal to the depth of the transition level. This level is the boundary between the two zones in the developed region as described in section 4.2.3.

4.3.3.4 Analysis of Data

As discussed, the output reading from the air concentration probe represents the mean air concentration over the area of the probe. For each experiment, a continuous air concentration curve, with respect to distance normal to the bed, was obtained. Figure 4.6 shows a typical air concentration profile in the developed region, taken in the center of the width of the flow. The air concentration increases gradually from the bed and more rapidly in the central region. It can be seen that, except very near the bed, the profile gradient, dC/dy, increases from the bed until a maximum is reached. Beyond this point, dC/dy decreases towards the surface. It appears that the air concentration profile is comprised of two parts which possess basically different characteristics. Although there is no sharp boundary between the two parts, this curve tends to support the idea of lower and upper zones. Straub and Anderson (1958) noted the same observations in their experimental profiles. Air concentration profiles for each slope and discharge for the present experiments are given in Appendix A.

Air concentration profiles at various distances form the crest were used to determine the uniformity of the flow for each slope and step height. Figure 4.7 shows such profiles taken at 4 step intervals for $l/h= 0.8$ and $h= 31.25$ mm. The profiles at steps 64 and 56 exhibit small differences in the figure and they are definitely closely grouped. On the other hand, the profiles at step 48 or earlier are definitely different from the other two to a degree which is a typical profile of section where normal aeration has not been established. For the data reported here, a condition of normal aeration was reached at step 64 or 56 but not at step 48. For this set of flow conditions, the concentration profiles were taken at step 64 where fully developed flow was established.

Also as discussed, the flow of the air-water mixture in the developed region can be divided into distinct zones: a lower zone which consists of air bubbles suspended in the water, and an upper zone where water drops are ejected from the stream into the atmosphere. Because of the similarity of flow on stepped spillways to the flow in steep channels, the method described by Straub and Anderson (1958) is used as a basis for analysis. This leads to the development of a procedure whereby the air concentration profile within the region of developed flow may be derived.

The air concentration distribution in the lower region is obtained on the basis of the equilibrium between the air bubble buoyancy and the turbulent transport. The resulting air concentration can be described by (similar to Eq. 2.18):

$$C=C_1\left(\frac{y}{y^*}\right)^z \tag{4.6}$$

where $y^*=y_T-y$, with the other parameters described in section 2.4.1 and C_1 is a constant is equal to the air concentration at $y= y_T/2$.

In the upper region, turbulent fluctuations of the air-water mixture eject water drops into the air. The analysis is based on the assumption of a random distribution of turbulent fluctuations of the velocity normal to the bed. The resultant air concentration can be described by (section 2.4.1):

$$\frac{1-C}{1-C_T}=\frac{2}{y_m\sqrt{\pi}}\int_{y'}^{\infty} e^{-\left(\frac{y'}{y_m}\right)^2} dy' \tag{4.7}$$

where all parameters were described earlier in section 2.4.1. The gradient of the concentration is then equal to:

$$\frac{dC}{dy}=\frac{2\left(1-C_T\right)}{y_m\sqrt{\pi}}e^{-\left(\frac{y'}{y_m}\right)^2} \tag{4.8}$$

When $y'=0$ (transition level), dC/dy reaches its maximum value which is equal to:

$$\left(\frac{dC}{dy}\right)_{\max}=\frac{2\left(1-C_T\right)}{y_m\sqrt{\pi}} \tag{4.9}$$

At this location, the air concentration is C_T and the depth is y_T.

The applicability of Eqs. (4.6) and (4.7) to describe air concentration in the developed region obviously depends on the degree to which they can fit the experimental observations. The constants in these equations depend on the turbulence characteristics of the air-water mixture. At the present time, it is not possible to determine these constants analytically. These coefficients must be evaluated empirically from experimental observations. This can be achieved by examining the derived equations for the upper zone. Eq. (4.7), which represents the air concentration distribution in the upper zone, has two unknown parameters C_T and y_m. The transition concentration, C_T, and the mean value of the projection height, y_m, can be determined graphically and by the aid of Eq. (4.9). Using a plot of air concentration versus the normal distance from the bed, the point where the air concentration gradient, dC/dy, reaches its maximum was located graphically. This is shown in Figure 4.6. The air concentration and depth at the point of maximum concentration are the transition concentration, C_T, and depth, y_T. The value of y_m can be determined by inserting the value of C_T and $\left(dC/dy\right)_{\max}$ into Eq. (4.9).

For the lower zone, Eq. (4.6) indicates that the air concentration distribution is a function of $y/\left(y_T-y\right)$. Knowing the value of y_T, air concentration can thus be plotted as a function of $y/(y_T - y)$ (Figure 4.8 shows a typical plot of experimental observations). The coefficient C_l is the value of air concentration at $y/(y_T - y) = 1$. The exponent z is equal to the slope of a line fitting to the data if Figure 4.8 is plotted in a logarithmic graph. Alternately, the coefficient C_l and exponent z can be determined directly from the data by fitting a power law curve to the data, as shown in Figure 4.8. Eqs. (4.6) and (4.7) are plotted in Figure 4.6 and show the fit to the experimental observations. These equations are also plotted along with the observations for various values of discharge, step height and spillway slope in Appendix A.

In the lower zone, Eq. (4.6) departs from the experimental observations in the vicinity of y_T. As y approaches y_T, air concentration approaches infinity and the experimental observations depart from the curve for larger values of $y/(y_T - y)$. In most cases, the experimental observations agree well with the fitted curve up to $y/y_T = 0.9$. Eq. (4.7), which represents the air concentration distribution in the upper zone, departs from the experimental observations as $y' = y - y_T$ increases. The difference of predicted air concentration with experimental observations is less than 4%. It appears from the plot that air concentration can be represented by a cumulative Gaussian distribution.

The variation of the mean air concentration with discharge for various values of spillway slope and step height is presented in Figure 4.9. For any given value of discharge, the mean air concentration does not vary considerably with step height for the range of spillway slopes, *l/h*, equal to 0.6-0.8 . This suggests that the bulking of flows is not particularly sensitive to slope or step height changes. Observations of Straub and Lamb (1953) in steep channels showed the same tendency. They showed that the variation of the air concentration with channel slope is quite small. Except for *l/h*= 0.8 and *h*= 125 mm, the mean air concentration decreases gradually as the discharge increases. For *l/h*= 0.8 and *h*= 125 mm , the mean air concentration shows a tendency to first increase and then to decrease gradually with increasing discharge. Figure 4.10 shows the concentration at the transition depth, C_T. For most cases, C_T increases first with increasing discharge and then decreases as discharge increases. For *l/h*= 0.6 and *h*= 62.5 mm, the plot of C_T has the opposite trend, decreasing first and then increasing as discharge increases. The air concentration at $y_T/2$, C_l, is presented in Figure 4.11. For all values of spillway slope and step height, C_l decreases regularly with the discharge. An opposite trend exists in regard to the exponent z, as shown in Figure 4.12 for various values of discharge, step height and slope.

A number of characteristic depths and air concentration were developed based on the analysis of the self-aeration phenomenon. These flow characteristics vary with the flow conditions which influence the strength and scale of the generated turbulence. The turbulence is generated by the vortical structures formed over the roughness elements which are then diffused upward into the stream. Unfortunately, there is no information available in regard to the intensity and scale of this turbulence. However, the intensity of turbulence is related to the shear stress at the bed. As an approximation, the total shear stress or the shear velocity may be used as a measure of turbulence intensity. Straub and Anderson (1958) tested this hypothesis by plotting the mean concentration versus $u_*/y_T^{2/3}$ where u_* is defined as $u_* = \sqrt{g\, y_T \sin\theta}$. The expression $u_*/y_T^{2/3}$ was chosen empirically to correlate the data. Figure 4.13 shows the variation of the mean air concentration with $u_*/y_T^{2/3}$. However, the term $u_*/y_T^{2/3}$ is not a good parameter because:

i) The characteristic depth y_T represents only the lower zone of the developed region and thus is not an appropriate characteristic depth for the mean air concentration of the entire depth.

ii) The effect of the slope and step height is not taken into account.

The term $(l/h)^{0.11} h^{0.07} \big/ \left(y_{.9}^{0.44}\, u_*^{0.15}\right)$ is therefore chosen empirically to correlate the mean air concentration data (Figure 4.14). The results show a better correlation with the term $(l/h)^{0.11} h^{0.07} \big/ \left(y_{.9}^{0.44}\, u_*^{0.15}\right)$. It should be noted that the air concentration is averaged over the whole depth of flow which consists of two zones of different characteristics. A single curve passing through the data is a representation of mean air concentration for various values of discharge, slope and step height.

The term $(l/h)^{0.11} h^{0.07} \big/ \left(y_{.9}^{0.44}\, u_*^{0.15}\right)$ includes the depth $y_{.9}$ which is a function of air concentration distribution and is difficult to determine explicitly. However, it is related to the flow conditions such as the discharge and slope. Straub and Anderson used the term $\sin\theta/q^{0.2}$ to correlate the air concentration data. This relationship is shown in Figure 4.15, where the mean air concentration is plotted as a function of $\sin\theta/q^{0.2}$ for the present experimental results. For each spillway slope, the results for different step heights fall reasonably well on a single curve. The plot also shows the mean air concentration predicted by ASCE formula for chute spillways as given by (section 2.2.4):

$$\overline{C}=0.743\,log\left(sin\,\theta/q^{0.2}\right)+0.721 \tag{4.10}$$

Eq. (4.10) is in metric units. Figure 4.15 shows that the mean air concentration for stepped spillways is more than that for standard spillways for a given value of $sin\ \theta/q^{0.2}$. This shows that the roughness elements in stepped spillways allow for more air entrainment into the flow. This indicates that steps enhance the turbulence intensity of the air-water mixture.

The term $sin\ \theta/q^{0.2}$ is not a good expression for a dimensional plot. However, no parameter consisting of terms that describe the flow characteristics can be determined explicitly to normalize $sin\ \theta/q^{0.2}$. For a stepped spillway, this term does not include the effect of flow roughness as it was developed for smooth spillways. The present experimental observations are correlated by adding the step height as a parameter to the term $sin\theta/q^{0.2}$. Such calculation, however, shows a negligible correlation in regards to step height. The best correlation is found as the mean air concentration is plotted in terms of $(sin\,\theta)^{0.1}/q^{0.3}$ (Figure 4.16). A single curve passing through the experimental observations can be described by the expression

$$\overline{C}=0.93\ log\left(\frac{(sin\,\theta)^{0.1}}{q^{0.3}}\right)+1.05 \tag{4.11}$$

It appears that for stepped spillways, the mean air concentration is less sensitive to changes in spillway slope. The above relationship provides a means of estimating the mean air concentration to be expected in a stepped spillway flow. However, this relation is deduced from data with a limited range of flow conditions. Great care thus must be taken when using this equation for flow conditions outside this range.

Characteristic depths $y_{.9}$, y_T and y_m for various values of discharge, slope and step height are presented in Figures 4.17 to 4.19. In Figure 4.17, the upper depth, $y_{.9}$, varies in the same manner as in chute spillways, $y_{.9}$ increases regularly with discharge for given values of slope and step height. The value of $y_{.9}$ is less sensitive to the spillway slope. For lower discharges, all observations fall in a narrow band for all values of slope and step height. As discharge increases, the results for higher values of step height depart from other data.

Figure 4.18 shows that the transition depth, y_T, increases regularly with increasing discharge and decreases with decreasing slope. For any given slope, variation of y_T is relatively little over the entire range of discharge. For l/h = 0.6, the results fall together on a single curve, independent of the variation in step height. However, for l/h= 0.8, the data for a higher step height (h= 125 mm) depart considerably from those for h= 31.25 mm and joins the data of l/h= 0.6.

Figure 4.19 shows the mean projection height, y_m. Observations of this characteristic depth which depend on the turbulence intensity at the transition depth do not show a regular trend (Figure 4.18). The data are scattered over a considerable range of depth. In most cases, for a given discharge, y_m is larger for larger step heights than that for smaller steps. The data of y_m are not sensitive to spillway slope.

All of these characteristic depths are representative of different zones of the flow. The transition depth, y_T, is a characteristic depth which separates the lower zone from the upper zone of flow. This transition depth represents the depth of flow of the lower zone and it is related to the gradient of the air concentration gradient. The projection height, y_m, is a measure of the distance that water particles can travel above the transition depth. It is a representative of upper zone of the flow and depends on the intensity of turbulence fluctuations at the transition depth. The upper depth of flow, $y_{.9}$, is a measure of the whole flow depth and is related to the air concentration profile. Therefore, it seems reasonable to assume that the value of $y_{.9}$ can be related to the sum of y_T and y_m. Such relation is tested by plotting the experimental observations in the form of $(y_T + y_m)/y_{.9}$ as a function of discharge in Figure 4.20. The data cluster in a narrow band about $(y_T + y_m)/y_{.9} = 1$. Although $y_{.9}$ is an arbitrary depth obtained from the air concentration distribution, its correlation with other characteristic depths shows that $y_{.9}$ is a good representation of the flow depth in stepped spillways.

4.3.4 Air-Water Mixture Velocity

4.3.4.1 Introduction

There was no information available about the velocity distribution of the air-water flow on stepped spillways that could be used in a detailed analysis of shear stress or energy loss. Since the air concentration distribution was measured directly by independent means, it was decided to use a Prandtl tube to obtain applicable velocity measurements in conjunction with the data on air content. It was assumed that the air-water mixture at any point can be replaced by a homogeneous fluid with a density equal to the bulk density of the mixture. The use of the Prandtl tube involves the concept of a point or region of stagnation in the flow. There is a possible difference between the behavior of homogeneous and mixed flows in the vicinity of this stagnation point. If the air content in the flow is small, the curvature at the nose of a Prandtl tube separates the air from the water. At higher value of air concentration, a succession of impingement occurs against the nose of the Prandtl tube. This dynamic effect may increase the rise of the water column in the manometer lines and velocity readings may be overestimated. However, other methods of velocity measurements have showed little success in obtaining velocity distributions. An attempt by the writer to use a Laser Doppler Anemometer failed because air bubbles refract the laser beams and therefore data acquisition was not possible. The salt-velocity method developed by Straub and Killen (1953) requires precise control of the size of the salt slug and the frequency of the injection. The stagnation method was therefore chosen for its availability and simplicity. All measurements were obtained in the developed region of flow. It is assumed that the flow stream in the developed region is parallel to the slope and the Prandtl tube thus was set parallel to the streamline direction.

4.3.4.2 Velocity Profile Distribution

The velocity measurements of the air-water mixture involved observing the stagnation head, h_{stag}, and static head, h_{stat}. Manometer readings of the stagnation head varied little. Figure 4.21 shows a typical plot of the range of the stagnation head in the developed region. For each point, the maximum and minimum readings were recorded. The average between the maximum and minimum was used for the stagnation head. The relative amplitude of the stagnation head was almost constant. The maximum relative range was about 3%. Due to high velocities and small depths of flow, values of h_{stat} were very much smaller than h_{stag}.

The velocity of air-water mixture, u_m, at any point was obtained by:

$$u_m = \sqrt{\frac{2g\left(h_{stag} - h_{stat}\right)}{(1-C)}} \tag{3.12}$$

Because of the dependency of velocity calculation on air concentration, the manometer readings were taken at the same points along the depth of flow where air concentration was measured. Figure 4.22 shows a typical velocity profile in the developed region, taken in the center of the channel. The velocity profile is comprised of three sections. In the first section, the velocity increases gradually from the bed. It can be seen that the profile gradient decreases from the bed until it reaches a value of zero. At this point, the velocity reaches its maximum value. Beyond this point, the second section exists where the velocity and velocity gradient remain almost constant for a some depth. The extent of this section is larger for higher discharges. In the third section, a sharp velocity decrease occurs towards the surface. This velocity deficiency is expected in the air-water mixture in the upper portion of the stream because of the drag necessary to sustain the air motion above the flow. In addition, the water content of the flow decreases with depth in this section because of increasing air concentration. Since the momentum of water is large as compared to air, the momentum of the air-water mixture decreases. Observations of Straub and Lamb in steep channels noted the same tendency. The velocity gradient normally increases towards the surface in this section. As discussed, the error of velocity estimation increases sharply in this section (Figure 3.2). Because of the dependency of velocity results on the air concentration measurements, velocity profiles corresponding to air concentrations greater than 0.90 are not reliable in this section. The results of experiments in the form of velocity profiles for each slope and discharge are presented in Appendix B.

The sharp decrease of the velocity at the upper section of the profile indicates that flow characteristics in this zone are different from the lower part. As discussed, the flow depth consists of lower and upper zones which are separated by the transition depth. In the upper zone, the concentration of water drops which are ejected from the transition depth decreasing towards the surface. As a result, the momentum of the flow decreases towards the surface. It is, therefore, deduced that the velocity may decrease in the upper zone of the flow. To test this hypothesis, the variation of y_{um}/y_T against the discharge is plotted in Figure 4.23, where y_{um} is the depth at which velocity profile starts to decline. The depth ratio y_{um}/y_T varies from 1 to 1.7 for various values of the discharge, slope and step height. The range of y_{um}/y_T for various values of slope and step heights decreases for higher values of discharge. Figure 4.23 shows that the velocity decline happens in the upper zone of the flow depth.

An alternative method was used with the aid of photographic work to obtain approximate velocity profile to compare with those of the Prandtl tube measurements. As discussed, dark cloudlets in high-speed video images possess less air concentration than the surrounding mixture. These cloudlets can easily be tracked for a certain distance in the air-water mixture. The basic concept of velocity, which is the distance divided by time, provides the direct measurement for determining velocities for this method. It consists of timing the travel of dark cloudlets into the air-water mixture. The operating principle consists basically of marking a dark cloudlet and then recording the time interval required for this marked element to traverse a fixed distance. Plate 4.11(a-d) show typical high-speed images of the flow in the developed region at different times. The passage of a dark cloudlet, marked as A, is detected between two consecutive step tips on each streamline. The velocity is then calculated by dividing the distance between two consecutive steps by the travel time. This measurement was repeated four times for each set of flow condition and the average was recorded. The photographic measurements for four sets of flow conditions are presented in Figures 4.24 to 4.27 along with the results of Prandtl tube measurements. In the region near the bed, velocities of photographic measurements are larger than those obtained by the Prandtl tube. In the rest of the flow depth, the opposite trend exists. This apparent difference is due to the fact that the photographic measurement is done near the side wall. At the side wall, the velocity is less than that of the central region where the Prandtl tube was used. On the other hand, the photographic measurement consists of an average mixture velocity between two consecutive step tips. The velocity of the flow on the streamline connecting step tips is larger than that on the step tip because of the existence of no-slip condition at step tips. For streamlines near the boundary, therefore, velocities obtained by photographic observations are higher than those obtained by Prandtl tube measurements. An examination of Figures 4.24 to 4.27 shows a reasonable agreement between the photographic and Prandtl tube measurements. This shows that the Prandtl tube measurements provide reliable velocity profiles.

4.3.4.3 Universal Velocity Profile

Numerous experimental and theoretical open channel investigations have been devoted to the establishment of a relationship between the velocity, the hydraulic radius of the flow and the size of the roughness projections on the bed. Basically, such relationships have been obtained by deriving uniform flow expressions from boundary layer theory and then comparing these expressions with empirical uniform flow equations. To the writer's knowledge, all the above mentioned studies have been concerned with water flows having little or no entrained air. However, if the air-water mixture is assumed to behave as a homogeneous fluid with equivalent and constant properties, relationships similar in form to those established for flow of water alone might be expected.

The development of the Prandtl-Karman universal velocity distribution law was the first proposal towards a theoretical uniform flow expression. Briefly, the law relates the shear stress to the gradients of velocity distribution. To prove the law, it is necessary to develop a theory describing the interchange of fluid particles between the various velocity layers making up the flow. Prandtl developed the momentum transport theory to establish the law and von Karman established the similarity hypothesis. The velocity distribution was shown to be logarithmic. The resulting equation for velocity distribution can be described as follows:

$$\frac{u}{u_*}=\frac{1}{\kappa}\ln\frac{y}{y_*} \tag{4.12}$$

where κ is a constant found from experimental observations to be equal to 0.4, $y_* \propto (\nu/u_*)$ for a smooth boundary and $y_* \propto k$ for a rough boundary. This expression is commonly known as the Prandtl-Karman universal velocity distribution law. For rough turbulent flow in a circular pipe, Nikuradse found that y_* depends solely on the roughness height; that is $y_* = m k_s$, where m is approximately 1/30 for a completely rough boundary and k_s is the so-called Nikuradse equivalent sand roughness (roughness measured as the diameter of the equivalent sand particle used by Nikuradse). Therefore, Eq. (4.12) for a rough boundary can be simplified as

$$\frac{u}{u_*}=A\log\frac{y}{k_s}+B \tag{4.13}$$

where A= 5.75 and B is equal to 8.5 for fully rough boundary. Eq. (4.13) gives the velocity distribution in a turbulent flow over rough boundaries. It should be noted that constants used in Eq. (4.13) were derived from data on pipes. It is assumed, however, that it is allowed to use this equation for other cases such as in open channel turbulent flow.

The coefficients in Eq. (4.13) were derived based on Nikuradse experimental observations where circular pipes were covered on the inside as tightly as possible with sands of definite grain sizes glued on to the walls. The Nikuradse's roughness can be said of maximum density because the sand grains were as closely to each other as possible. For other forms of roughness, the roughness density is considerably smaller and such roughness cannot be defined by their heights. It is necessary to correlate any given roughness with its equivalent sand roughness and define the coefficient of resistance when inserted in Eq. (4.13). The correlation between such roughness and

Nikuradse sand roughness can simply be done by modifying Eq. (4.13) into the general form for any given roughness as:

$$\frac{u}{u_*}=5.75\log\frac{y}{k}+B' \tag{4.14}$$

Comparing Eq. (4.13) with Eq. (4.14), k_s can be obtained from the relationship

$$\frac{k_s}{k}=10^{\left(\frac{8.5-B'}{5.75}\right)} \tag{4.15}$$

In a fully turbulent flow with Nikuradse sand roughness, $B'=8.5$ and $k_s=k$.

To determine k_s, it is necessary to estimate the coefficient B' from the experimental observations by using Eq. (4.14). Observations should be plotted in form of the velocity versus the flow depth on a semi-log sheet. The shear stress velocity at the wall, u_*, and coefficient B' can be found by fitting a semi-logarithmic line to the data. To plot the velocity distribution, it is necessary to determine the origin of the plot. Perry et al. (1969) showed that, for a skimming flow, a boundary layer on a rough boundary behaves as if its origin is located some distance below the crest of the elements. This distance, which is referred to as the displacement in origin, defines an origin for the profile that gives the logarithmic distribution of velocity near the wall (Figure 4.28). The displacement in origin, ε, can be interpreted as an indication of the effect of the roughness on the mean flow. Perry et al. showed that ε depends on the shedding of vortical structures into the main flow. In a quasi-smooth flow, where roughness elements are more closely spaced and stable vortices are present in the grooves, ε is small.

A typical velocity distribution, plotted in the logarithmic scale as a function of $y_\varepsilon = y+k-\varepsilon$, is shown in Figure 4.28 for different values of ε. Logarithmic velocity profiles for each slope, step height and discharge for the present experiments are given in Appendix C. It can be seen that the experimental observations fall almost on a straight line up to a certain depth. The value of ε is crucial since small changes in ε results in a considerable variation in values of B' and consequently k_s. It is difficult to decide about the value of ε since there is no predicted values of ε available at the present state of knowledge. However, since u_* can be predicted from the plot of the velocity distribution, the writer compared this value with the value of u_* for the wall shear stress predicted by the uniform flow equilibrium, as described in section 4.3.5. The comparison enabled the determination of suitable ε for the velocity distribution. Once the value of ε is decided, if the velocity distribution in Figure 4.28 is defined as $u = A''\ln y_\varepsilon + B''$, values of u_* and B' can be found as

$$u_* = 0.4A'' \tag{4.16-a}$$

$$B' = \frac{B''}{u_*} + 2.5\ln k \tag{4.16-b}$$

Values of u_*, B' and k_s are shown in Figure 4.28 for h = 125 mm and l/h= 0.6. Tables 4.4 and 4.5 present estimations for these parameters for various values of slope and step height.

Variation of the ratio k_s/k is plotted against the discharge in Figure 4.29 for the experimental observations. k_s/k varies in the range of 1 to 3.5 for various values of slope and step height. Values of k_s/k for l/h= 0.8 is larger than those of l/h= 0.6. For any given slope, the value of k_s/k increases with decreasing step height. Eq. (4.15) shows that the increment in the ratio k_s/k results in the reduction of the coefficient B'. Therefore, it can be deduced that a reduction in step height or slope decreases the value of coefficient B' and increases the ratio k_s/k.

To investigate the similarity in the logarithmic velocity profile, experimental observations are plotted for each step height and slope in Figures 4.30 to 4.34. Consolidated results for the entire experimental observations are also shown in Figure 4.35 for comparison. For any given slope and step height, observations fall on a single line up to a certain value of y_ε/k_s. This dimensionless distance, which is referred to as $y^+ = y_\varepsilon/k_s$, is normally larger for higher discharges. It is feasible to plot the logarithmic velocity profile for each slope and step height up to y^+. Figures 4.36 to 4.40 shows such plots which logarithmic functions are fitted to the data and Eq.(4.13) for fully turbulent flow is also shown. Figure 4.41 shows the consolidated results for the entire experimental observations, plotted up to y^+.

4.3.5 Skin Friction Coefficient

Quasi-smooth or skimming flows occur over boundaries of recirculating water depressions. The roughness elements should be so close that their recirculating water remain in the grooves separating the elements. These depressions are maintained through the transmission of shear stress from the main flow.

As discussed, skimming flow over a stepped spillway becomes a fully developed flow after the initial steps. This means that forces acting on a fluid element are in balance. For such flow, the shear stress will be in equilibrium with the fluid weight. The momentum principle therefore results in (Figure 4.42)

$$\left(\tau+\frac{d\tau}{dy}\Delta y\right)dp_r-\tau\,dp_r-\gamma_m\,\Delta x\,\Delta y\,\Delta z\sin\theta=0 \tag{4.17}$$

where τ = the shear stress, p_r = the wetted perimeter, γ_m = the specific weight of the air-water mixture and θ is the angle of the spillway channel with the horizontal line. The shear stress at the side is negligible because the resistance at the side wall is much smaller than that of the recirculating fluid at the bottom. Replacing $\gamma_m=\rho_m g$ and $dp_r = \Delta z\ \Delta x$ and integrating, Eq. (4.18) can be written as

$$\bar{\tau}=\sin\theta\, g\int_0^{y_{.9}}\rho_m\,dy=\sin\theta\, g\,\overline{\rho_m}\,y_{.9} \tag{4.18}$$

where $\bar{\tau}$ = the bed shear stress that exists between the main flow and the recirculating fluid in the step groove and $\overline{\rho_m}$ = the average density of the air-water mixture. The bed shear stress can be also expressed in terms of the skin friction coefficient, c_f, as

$$\bar{\tau}=c_f\,\frac{\overline{\rho_m}\,V_m^2}{2} \tag{4.19}$$

Substituting Eq. (4.19) into Eq. (4.18) and summarizing, the skin friction coefficient can be expressed as

$$c_f=\frac{2g\,y_{.9}\sin\theta}{V_m^2} \tag{4.20}$$

The model observations of the present investigation are analyzed as well as observations from previous investigations on stepped spillways, pipe and fishway studies. The results are shown in Figure 4.43, where the skin friction coefficient is plotted as a function of *k/y* or *k/r*, where *r* is the radius of a pipe. Observations of the pipe flow extracted from Nikuradse's experiment. These pipes were artificially roughened by gluing sand of various sizes and in varying degrees of spacing on the pipe walls. The Sikora's (1997) work performed on a Denil fishway channel with flat slopes where l/h ranged from 3.33 to 20. There was little or negligible air entrainment in the fishway study.

The results shows a considerable scatter that covered two logarithmic cycles at higher values of the relative roughness. The reason for such considerable scatter may be:

i) The depth of the flow was used to calculate c_f for all previous works except Tozzi's and Nikuradse's works. As discussed, the air-water mixture in the spillway is highly agitated and the air concentration increases continuously towards the surface of the flow. The ejection of the water at the transition depth affects the flow surface, make it hard to define the free surface depth. In an aerated skimming flow, the average depth measurements will be judgmental and can't be accurate. One should define a characteristic depth at which the air concentration reaches a specific value.

ii) In all previous research, except Tozzi's and Nikuradse's works, the apparent velocity is also calculated from the depth measurement. This leads to more errors since the error from depth measurements contributes to values of velocities.

iii) It was seen that flows over stepped spillways in some models were not fully developed because of the size of the models. There are three distinct regions for the flow over the stepped spillway and the last stage is called the developed region. In this aerated region, flow patterns reach an equilibrium and most flow characteristics like velocity and air concentration become invariant. In some investigations, the total height of models were small so that the development of the flow were never reached. Since air entrainment is an important feature of the developed regime, it is necessary that the velocity and depth be measured in this region.

In the present investigation, the depth of flow at 90% air concentration is chosen as the characteristic depth. The average velocity of the mixture is obtained by integrating the velocity profile up to this characteristic depth.

Figure 4.44 shows the average skin friction coefficient, $\overline{c_f}$, where for each data set, the skin friction coefficient is averaged for a specific roughness height. As discussed, observations of some investigations are not accurate enough to rely upon them. It is deduced that a single line passing through the data of Nikuradse's, Tozzi's and the present results represents well the average skin friction coefficient. Such a line can be used to evaluate the shear stress for the skimming flow. The fitted line can be expressed in the general form as:

$$\frac{1}{\sqrt{c_f}} = 3.85\log\left(\frac{y}{k}\right) + 3.53 \tag{4.21}$$

The correlation factor, R^2, is 0.955 for the above equation. In Figure 4.44, Eq. (2.3) of Tozzi's work is also presented. Tozzi established his formula based on the experimental observations obtained in a closed stepped conduit model with $l/h = 0.75$. Eq. (4.21) can be used for a wide range of y/k since it was derived from the data of the pipe flow as well as the skimming flow in stepped spillways.

4.3.6 Energy Dissipation

In quasi-smooth or skimming flow, two main features of the flow contribute to the energy loss. Firstly, the recirculating fluids in the groove of steps retard the main flow. These stable depressions are maintained through the transmission of shear stress from the main flow which skims over the steps. The recirculating fluid is unable to separate and mix with the main flow because the roughness elements are spaced so close. Secondly, macro-scale vortical structures, described in section 4.2.3, are continuously generated at the tips of steps. In general, the energy of the flow is expended partially to generate these vortical structures and partly to maintain the stable recirculating fluid.

Because of the complexity of flow over stepped spillways, no general solution has been developed for predicting the energy loss. The solution presented by Rajaratnam (1990) requires the estimation of the friction factor for both standard and stepped spillways. In addition, the air entrainment is neglected in his calculation. A similar solution by Chanson (1993) depends on the estimation of friction factor for the aerated flow. The effect of air entrainment at the base of the spillway is neglected in Chanson's solution. Since no information is available regarding the turbulent components of the flow, a general solution for the energy loss is not possible at the present time. It is then decided to estimate the energy loss for the skimming flow using the experimental observations.

As discussed, the flow over a stepped spillway becomes uniform after certain length. This region extends to the base of the spillway and all flow characteristics do not change in this region. If the channel bed is chosen as the datum, the specific energy, which is the energy of flow per unit weight of the air-water mixture, is constant along the channel length in the developed region. The specific energy at the base is therefore equal to that at a section along the channel length in the developed region. The specific energy, E_b, for a streamline at y elevation can be written as (Figure 4.45):

$$E_b(y) = y\cos\theta + \frac{p(y)}{g\rho_m(y)} + \frac{[u_m(y)]^2}{2g} \tag{4.22}$$

where $p(y)$ is the pressure stress at y. The pressure distribution can be presented with a hydrostatic distribution. Considering that the density of flow varies with y, $p(y)$ can be described as:

$$p(y) = g\cos\theta \int_y^{y_s} \rho_m(y)\,dy \tag{4.23}$$

where y_s is the elevation of a defined water surface. Substituting Eq. (4.23) in Eq. (4.22) and summarizing, the following relation can be deduced:

$$E_b(y) = \cos\theta\left(y + \overline{y_*}\right) + \frac{[u_m(y)]^2}{2g} \tag{4.24}$$

where

$$\overline{y_*} = \frac{\int_y^{y_s} \rho_m(y)\,dy}{\rho_m(y)} \tag{4.25}$$

$\overline{y_*}$ is a measure of the flow depth above the streamline y if it is replaced by a flow with a density equal to $\rho_m(y)$ and a depth of $\overline{y_*}$. Eq. (4.24) represents the specific energy at a streamline y above the bed. The mean specific energy at the base of the spillway, $\overline{E_b}$, can be described as:

$$\overline{E_b} = \frac{\int_0^{y_s} \rho_m(y)\, u_m(y)\, E_b(y)\,dy}{\int_0^{y_s} \rho_m(y)\, u_m(y)\, dy} \tag{4.26}$$

Substituting Eq. (4.24) in Eq. (4.26) and summarizing, the following equation can be sought:

$$\overline{E_b}=\cos\theta\,\frac{\int_0^{y_s}\rho_m(y)\,u_m(y)\left(y+\overline{y_*}\right)dy}{\int_0^{y_s}\rho_m(y)\,u_m(y)\,dy}+\alpha_e\frac{{V_m}^2}{2g} \tag{4.27}$$

where

$$\alpha_e=\frac{1}{V_m^2}\,\frac{\int_0^{y_s}\rho_m(y)\left[u_m(y)\right]^3\,dy}{\int_0^{y_s}\rho_m(y)\,u_m(y)\,dy} \tag{4.28}$$

is the kinetic energy correction factor for the aerated flow and V_m is the average air-water mixture velocity over the entire section. The elevation of water surface, y_s, is chosen as that value of y where the air concentration is equal to 90% ($y_{.9}$). The density of the air-water mixture for a streamline y , $\rho_m(y)$, can be expressed in terms of the air concentration by the relation (neglecting the density of air)

$$\rho_m(y)=\rho_w\left(1-C(y)\right) \tag{4.29}$$

The first term in Eq. (4.27) represents the pressure head plus the datum head (potential energy head) while the second term represents the kinetic energy head. The assumption of the hydrostatic pressure distribution in the upper zone of the flow is clearly not realistic. Preliminary calculations show that the potential term in Eq. (4.27) ranges from 1% to 3% of the mean specific energy. An acceptable approximation for Eq. (4.27) is therefore can be described by

$$\overline{E_b}=\alpha_e\frac{V_m^2}{2g} \tag{4.30}$$

At the upstream channel, the flow is not aerated and the density of the flow is constant over the flow depth. For such flow, the specific energy can be described as

$$E_u(y)=Z_0+y+\frac{p(y)}{g\rho}+\frac{\left[u_w(y)\right]^2}{2g} \tag{4.31}$$

where u_w is the water velocity and Z_0 is the elevation of the channel bed above the base of the spillway and is equal to 2.50 m for the present investigation. If the hydrostatic pressure is defined for the upstream flow, i.e. $p(y)=g\rho(y_s-y)$, Eq. (4.31) can be summarized as

$$E_u(y)=Z_0+y_s+\frac{[u_w(y)]^2}{2g} \tag{4.32}$$

Using the definition of the mean specific energy from Eq. (4.26), the mean specific energy at the upstream can be described by the following equation:

$$\overline{E_u}=Z_0+y_s+\alpha\frac{V_w^2}{2g} \tag{4.33}$$

where

$$\alpha=\frac{\int_0^{y_s}[u_w(y)]^3\,dy}{V_w^3\,y_s} \tag{4.34}$$

is the kinetic energy correction factor for a non-aerated flow. The first, second and the third terms in Eq. (4.33) represents the datum, pressure and kinetic energy heads, respectively. Preliminary calculations show that the kinetic energy head ranges from 0.3% to 0.6% of the mean specific energy and it can be neglected. Eq. (4.33) is then can be approximated as

$$\overline{E_u}=Z_0+y_s \tag{4.35}$$

The total head loss along the spillway, ΔE, equals to the difference between the maximum head available, $\overline{E_u}$, and the residual energy at the base of the spillway, $\overline{E_b}$. If the relative energy loss is defined as $\Delta E/\overline{E_u}$, it can be shown that

$$\frac{\Delta E}{\overline{E_u}}=1-\frac{\overline{E_b}}{\overline{E_u}} \tag{4.36}$$

Substituting Eqs. (4.30) and (4.35) in Eq. (4.36), a general relation for the energy loss can be described as

$$\frac{\Delta E}{\overline{E_u}}=1-\frac{\alpha_e\frac{V_m^2}{2g}}{Z_0+y_s} \tag{4.37}$$

Figure 4.46 shows the variation of the energy loss with the discharge for various values of slope and step height for the present experimental observations. The energy loss ranges from 47% for l/h= 0.6 and h= 31.25 mm to 63% for l/h= 0.8 and h= 125 mm. Value of α_e ranges from 1.02 to 1.15. Figure 4.46 shows that the energy loss is less sensitive to the discharge. For a given slope, the energy loss decreases with decreasing step height. This is confirmed by the analysis of the friction factor which shows that the skin friction factor decreases as the roughness height reduces. The results of Tozzi's (1994) work are also plotted in Figure 4.46. His results were based on a model study where the step height varied from 5 mm to 60 mm and the spillway slope was 1V:0.75H.

Table 4.1 Dimensions of vortex tubes

h (mm)	Q (L/s)	24.32	41.53
125	Penertation Depth (mm)	22	30
	Thickness (mm)	18	15
62.5	Penertation Depth (mm)	20	15
	Thickness (mm)	12	7

Table 4.2 The location of inception section in terms of step numbers

Q (l/s)	h= 31.25 mm l/h= 0.6 (step #)	h= 125 mm l/h= 0.8 (step #)	h= 31.25 mm l/h= 0.8 (step #)
19.30	6_7		
21.76	10		9
24.32	12_13	1_2	12
26.97	15		14
29.71	16_17	2	17
32.54	18		19
35.46	20	2_3	21
38.45	22		23
41.53	23	3	25
44.68	26		28
47.91	28	3_4	31
51.21	30		33
54.59		4	
61.55		4_5	

Table 4.3 Values of the "rooster tail" height

Q (l/s)	h= 31.25 mm l/h= 0.6 (mm)	h= 62.5 mm l/h= 0.6 (mm)	h= 125 mm l/h= 0.6 (mm)
24.32	32	65	125
41.53	43	84	175

Table 4.4 Values of parameters of universal velocity distributions for a stepped spillway with l/h= 0.6

h (mm)	Q (L/s)	y_c/h	u_* (m/s)	k_s (mm)	C	y^+
125	24.32	0.7	1.02	157	6.7	0.3
	29.71	0.8	0.85	123	7.31	0.45
	41.53	1	0.97	175	6.43	0.4
	47.91	1.1	0.9	169	6.52	0.45
	54.59	1.2	0.82	138	7.02	0.5
	61.55	1.3	0.80	143	6.94	0.55
62.5	21.76	1.3	0.64	41	8.32	1.
	24.32	1.4	0.65	46	8.03	0.95
	26.97	1.5	0.63	45	8.07	1.1
	29.71	1.6	0.7	64	7.23	0.7
	32.54	1.7	0.75	73	6.89	0.65
	35.46	1.8	0.76	77	6.76	0.65
	41.53	2	0.71	63	7.24	0.95
	44.68	2.1	0.79	89	6.39	0.65
	47.91	2.2	0.72	72	6.93	0.85
	51.21	2.3	0.74	75	6.82	0.9
	54.59	2.4	0.75	78	6.74	0.8
	58.03	2.5	0.73	74	6.84	0.85
	61.55	2.6	0.73	83	6.57	0.8
31.25	21.76	2.6	0.73	43	6.48	0.85
	24.32	2.8	0.68	40	6.67	0.95
	26.97	3.0	0.67	40	6.65	1.15
	29.71	3.2	0.68	41	6.60	1.1
	32.54	3.4	0.67	41	6.61	0.95
	35.46	3.6	0.67	41	6.62	1.2
	38.45	3.8	0.69	45	6.39	0.95
	41.53	4.0	0.68	45	6.39	1.1
	44.68	4.2	0.66	42	6.56	1.05
	47.91	4.4	0.65	42	6.51	1.05

Table 4.5 Values of parameters of universal velocity distributions for a stepped spillway with l/h= 0.8

h (mm)	Q (L/s)	y_c/h	u_* (m/s)	k_s (mm)	C	y^+
125	24.32	0.7	0.95	150	7.03	0.3
	29.71	0.8	0.95	202	6.29	0.3
	35.46	0.9	0.91	191	6.42	0.3
	41.53	1.0	0.93	213	6.16	0.3
	47.91	1.1	0.88	203	6.27	0.35
	54.59	1.2	0.90	215	6.13	0.35
	61.55	1.3	0.95	218	6.10	0.5
31.25	21.76	2.6	0.87	66	5.62	0.55
	24.32	2.8	0.83	61	5.81	0.65
	26.97	3.0	0.82	61	5.82	0.70
	29.71	3.2	0.82	61	5.82	0.75
	32.54	3.4	0.80	61	5.83	0.75
	35.46	3.6	0.78	61	5.83	0.75
	38.45	3.8	0.80	61	5.79	0.8
	41.53	4.0	0.82	66	5.63	0.8
	44.68	4.2	0.82	65	5.64	0.85
	47.91	4.4	0.77	60	5.84	0.9

Figure 4.1 Variation of the distance of the inception section from the crest of stepped spillways with Froude number

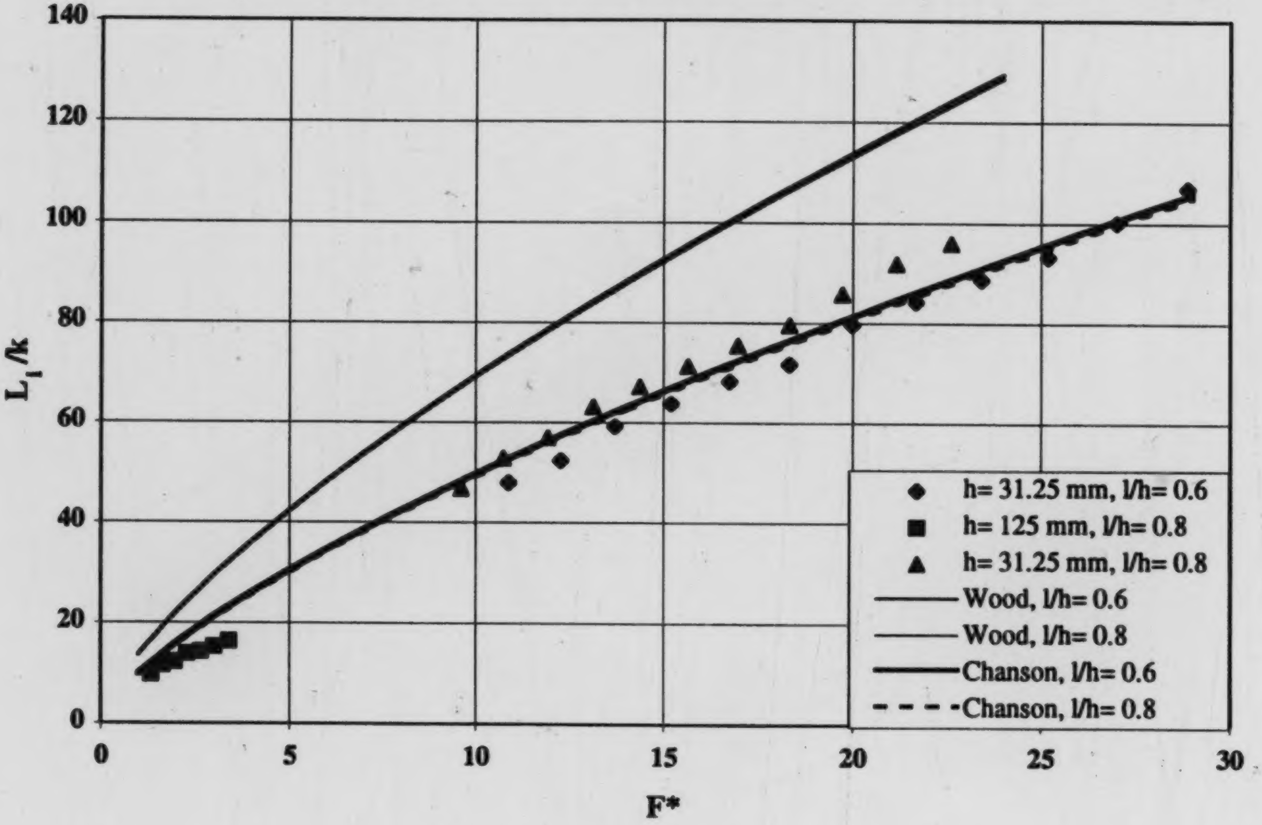

Figure 4.2 Variation of the distance of the inception section from the crest of stepped spillway models with Froude number

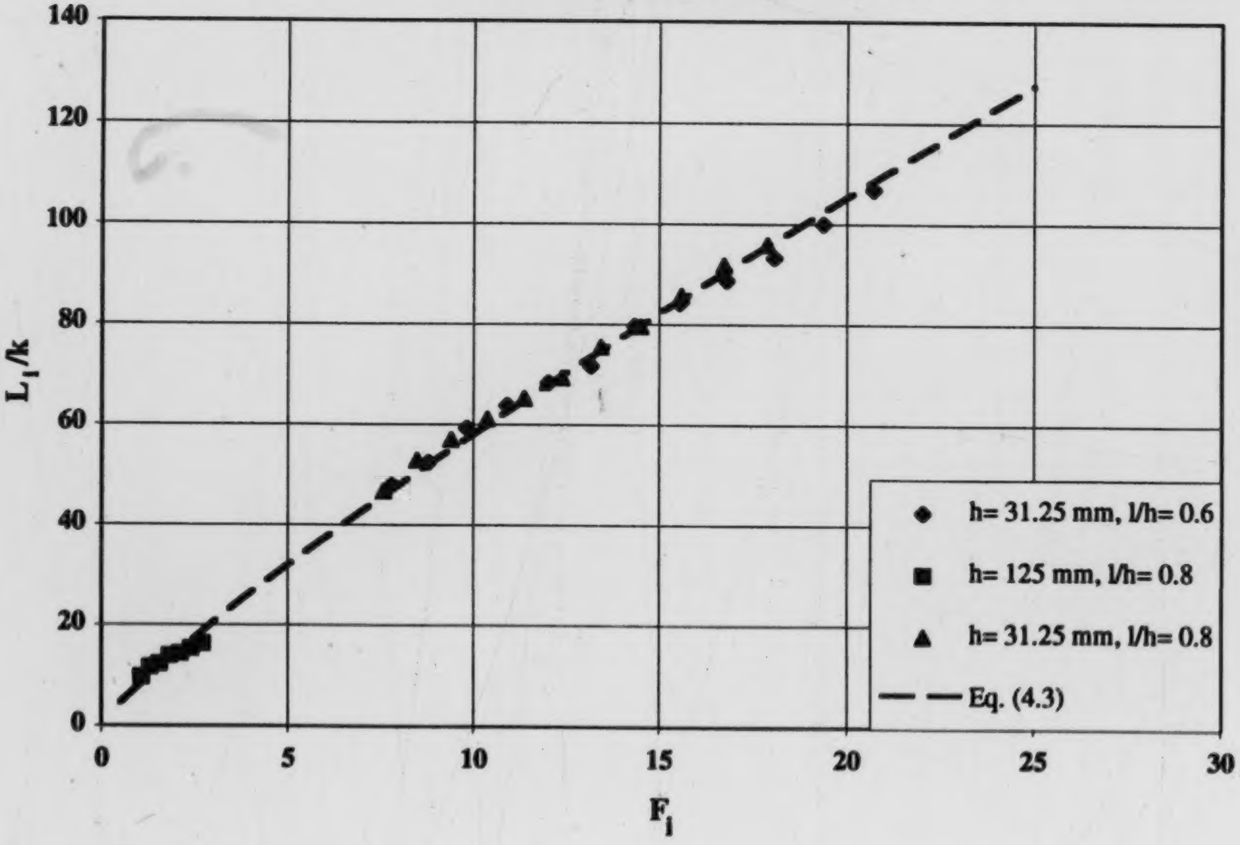

Figure 4.3 Variation of the "rooster tail" height with discharge for l/h= 0.6

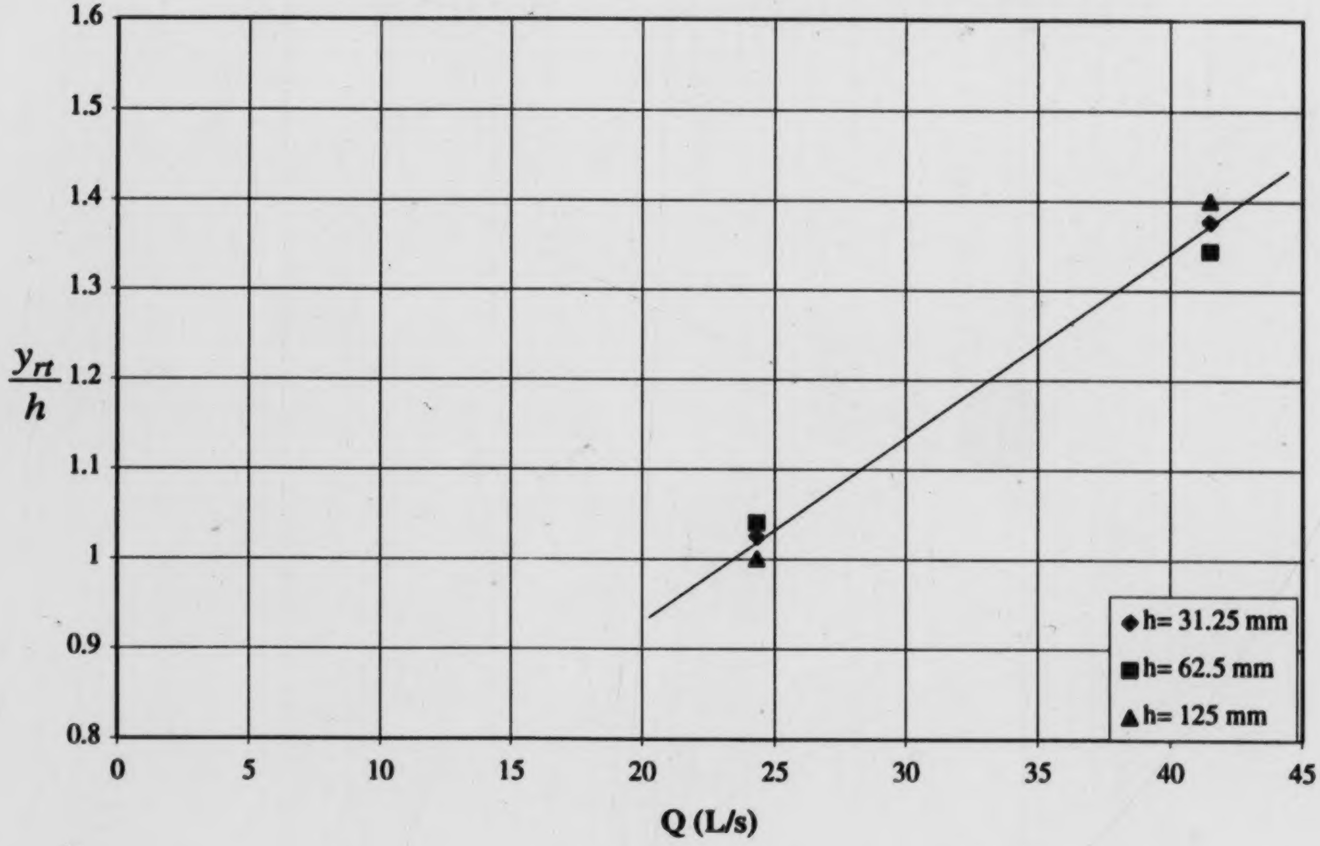

Figure 4.4 Mean range of concentration values in the developed region of a stepped spillway with l/h=0.8, h= 125. mm (yc/h=1.0)

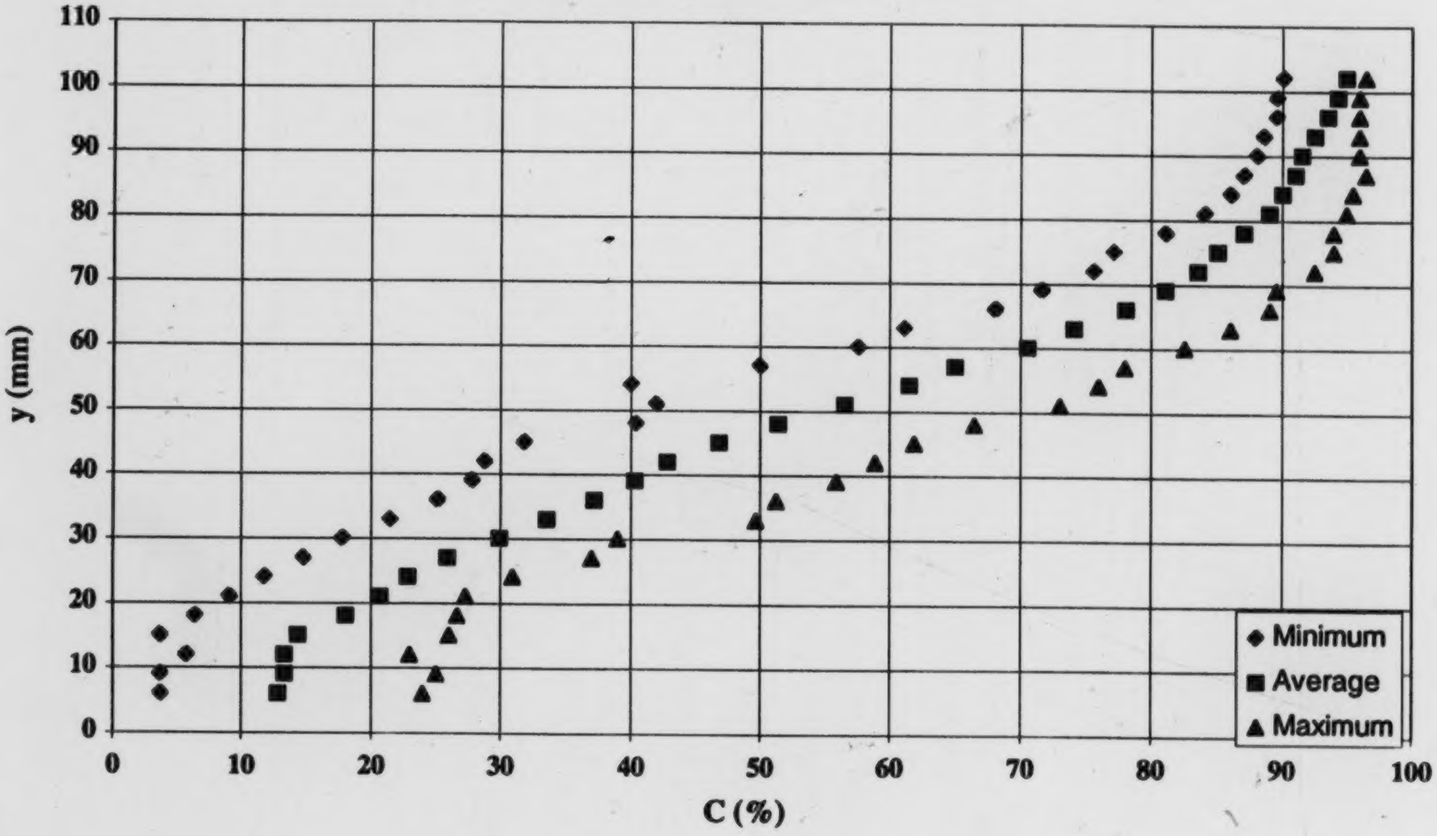

Figure 4.5 Relative Discharge & Concentration Profiles in Developed Region of a Stepped Spillway (l/h= 0.6, h=12.5 cm)

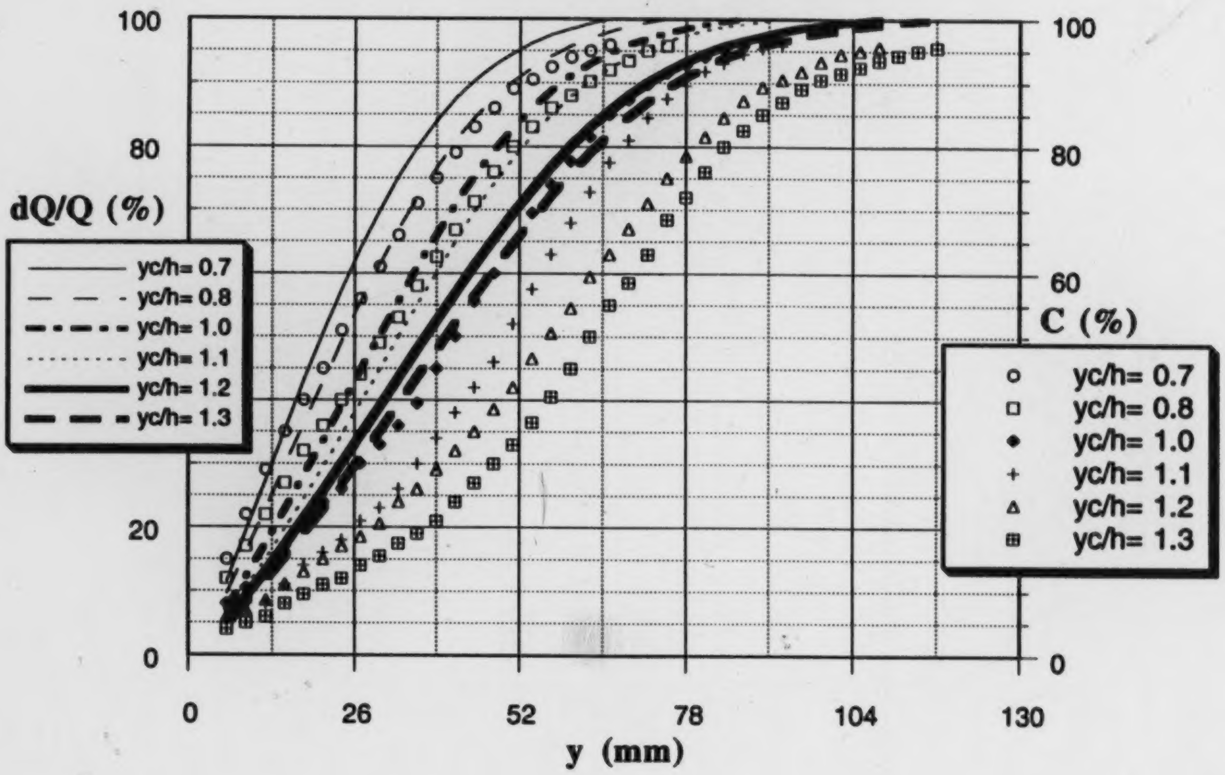

Figure 4.6 Air Concentration profile at step tip #13 in a stepped spillway with l/h=0.6, h= 125. mm (yc/h=1.0)

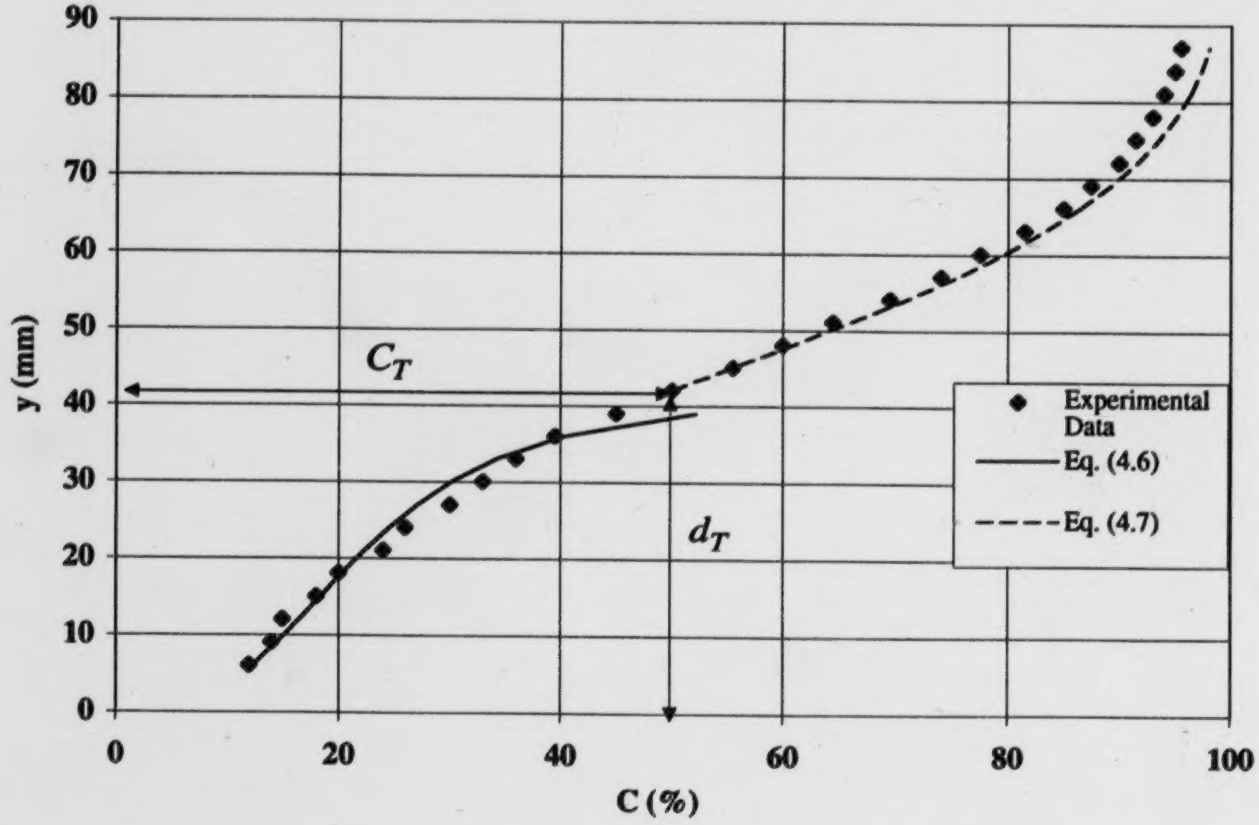

Figure 4.7 Air concentration profile at different step numbers in a stepped spillway with l/h= 0.8 and h= 31.25 mm (yc/h= 4.0)

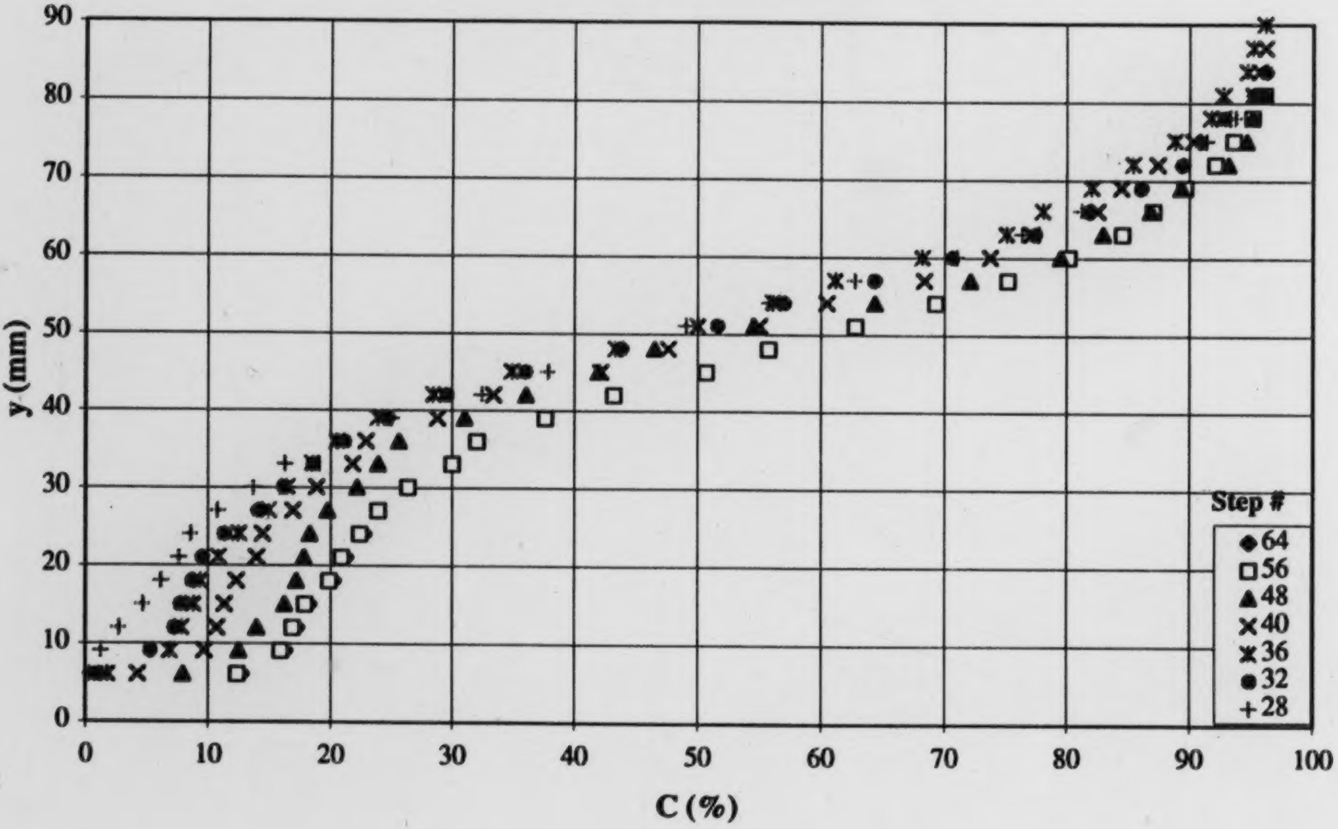

Figure 4.8 Estimation of air concentration distribution parameters in the lower zone of the developed region in a stepped spillway with l/h= 0.6 and h= 125 mm (yc/h= 1.0)

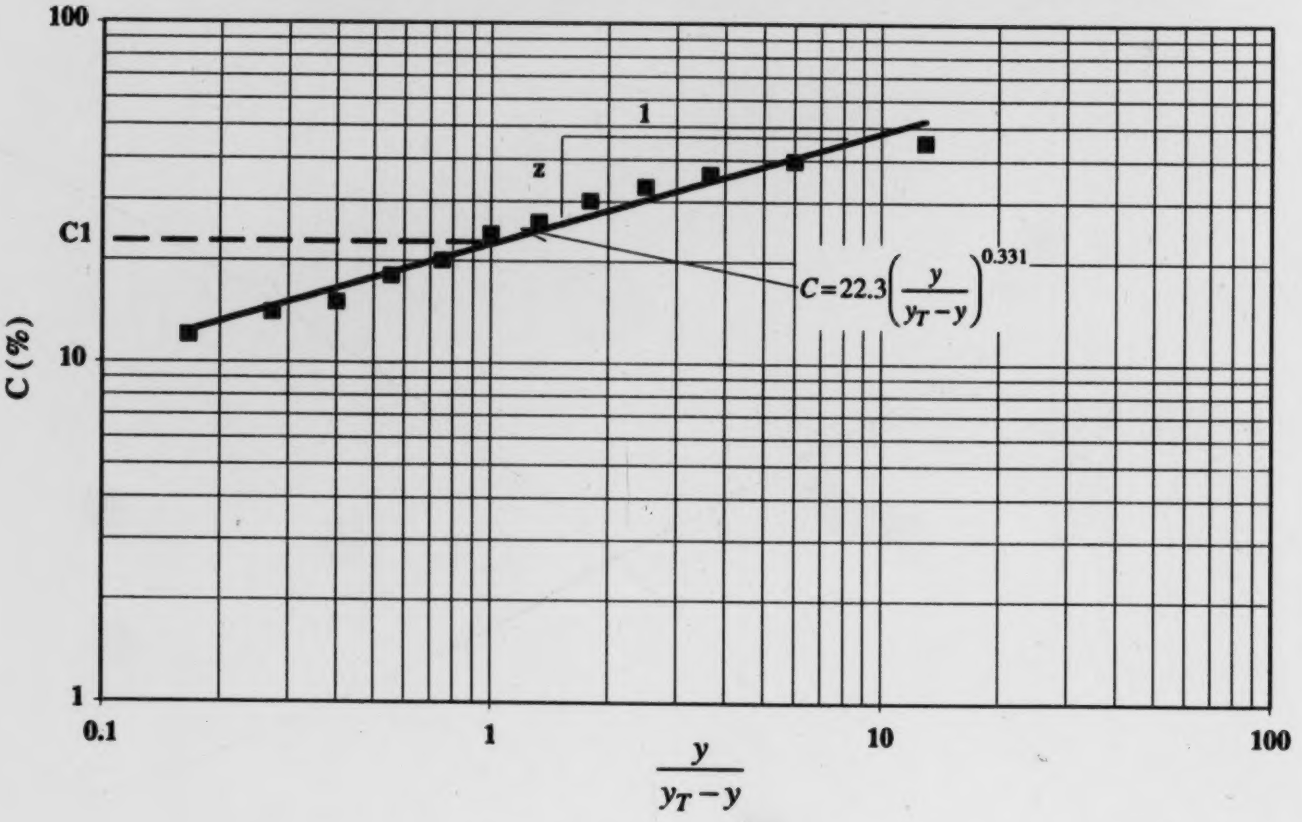

Figure 4.9 Variation of the mean air concentration with the discharge in stepped spillways for various values of slope and step height

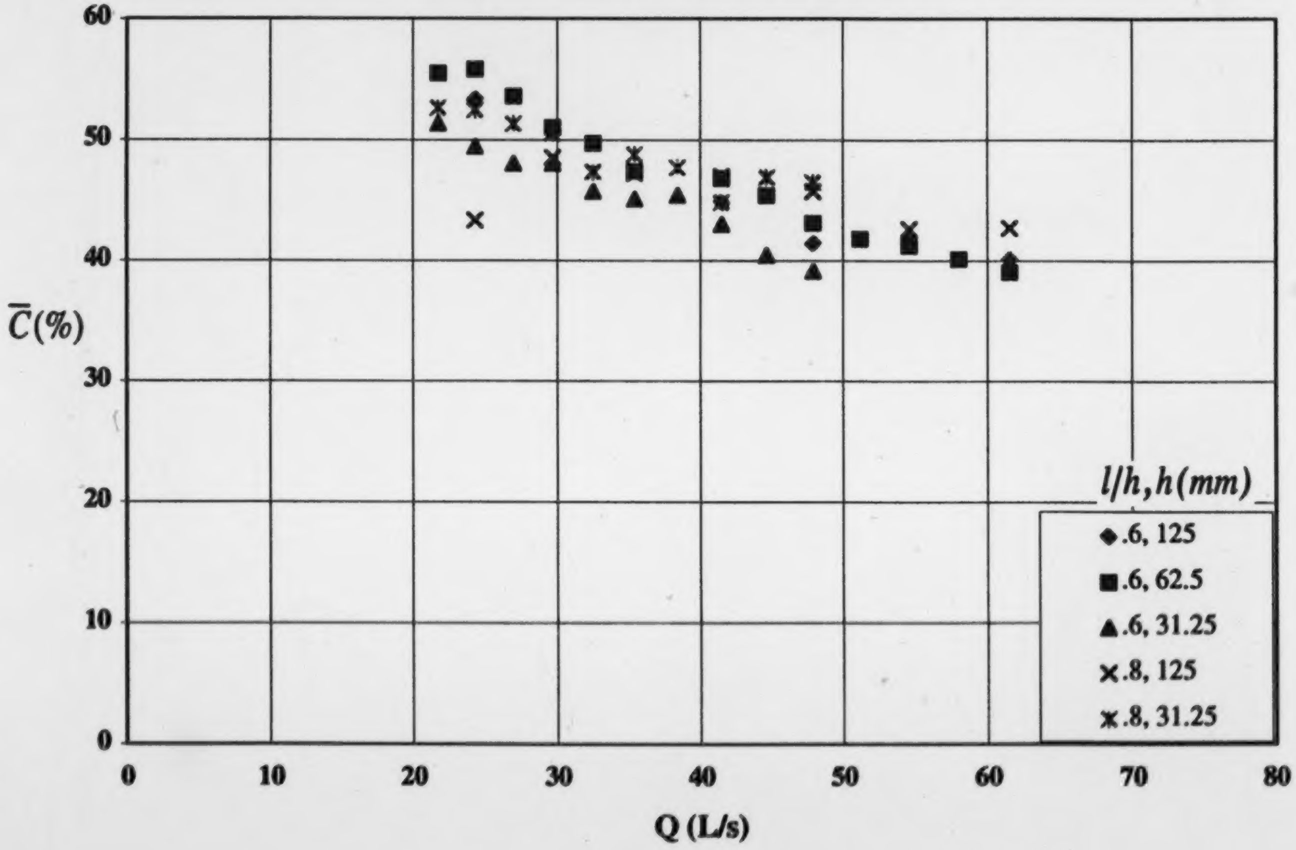

Figure 4.10 Variation of the air concentration at the transition depth with discharge in stepped spillways for various values of slope and step height

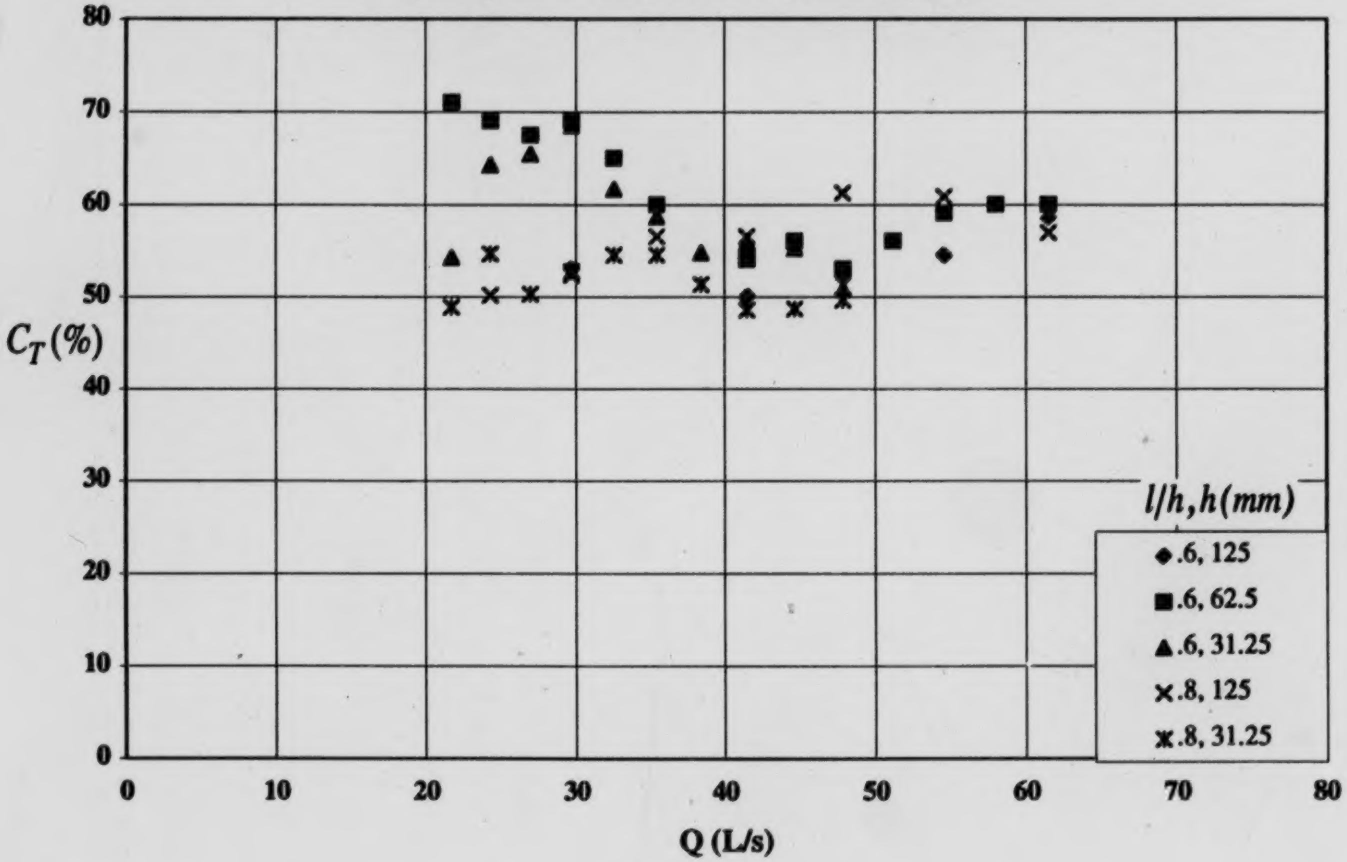

Figure 4.11 Variation of the air concentration at half-way of the transition depth with discharge in stepped spillways for various values of slope and step height

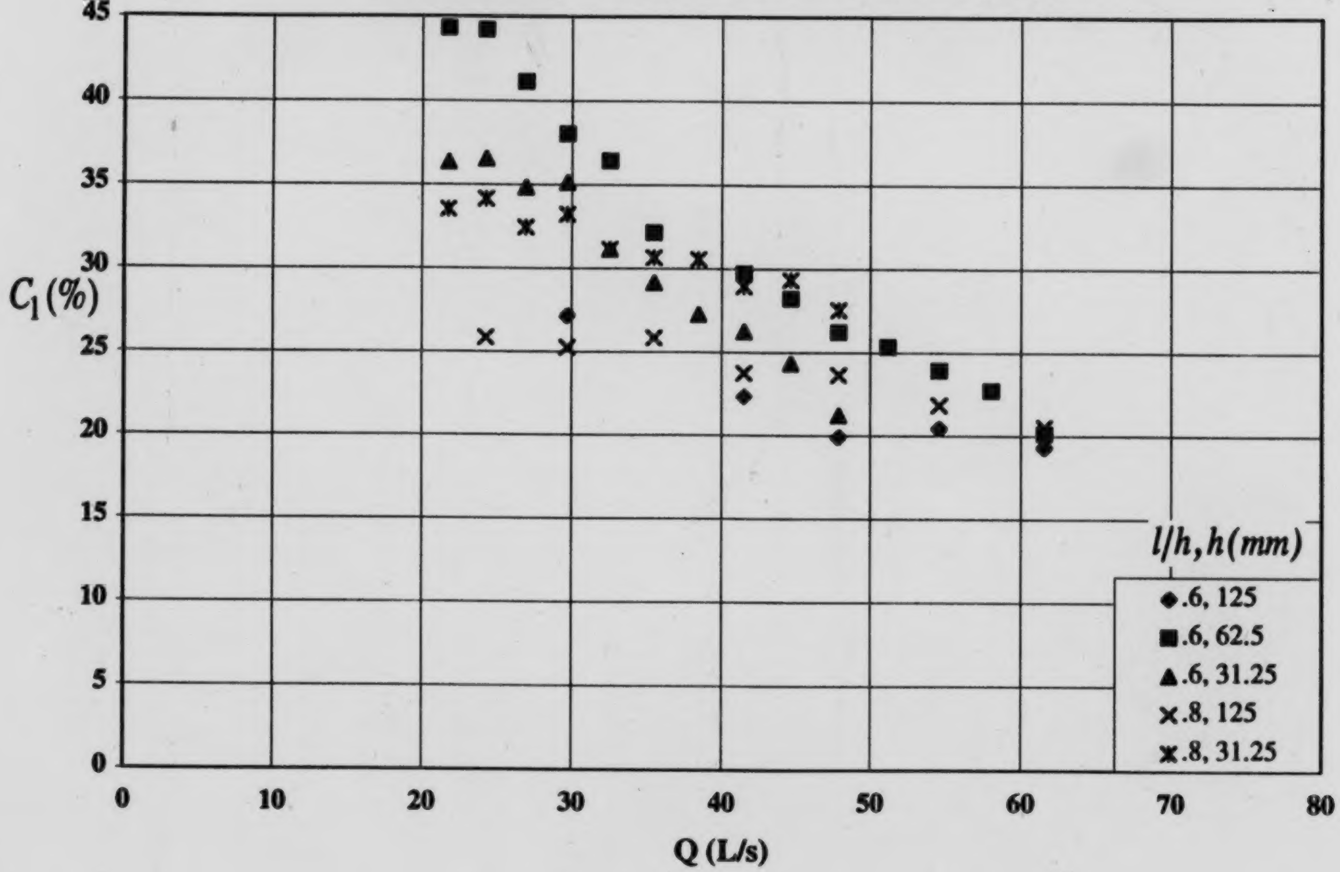

Figure 4.12 Variation of power parameter in Eq. (4.6) with discharge in stepped spillways for various values of slope and step height

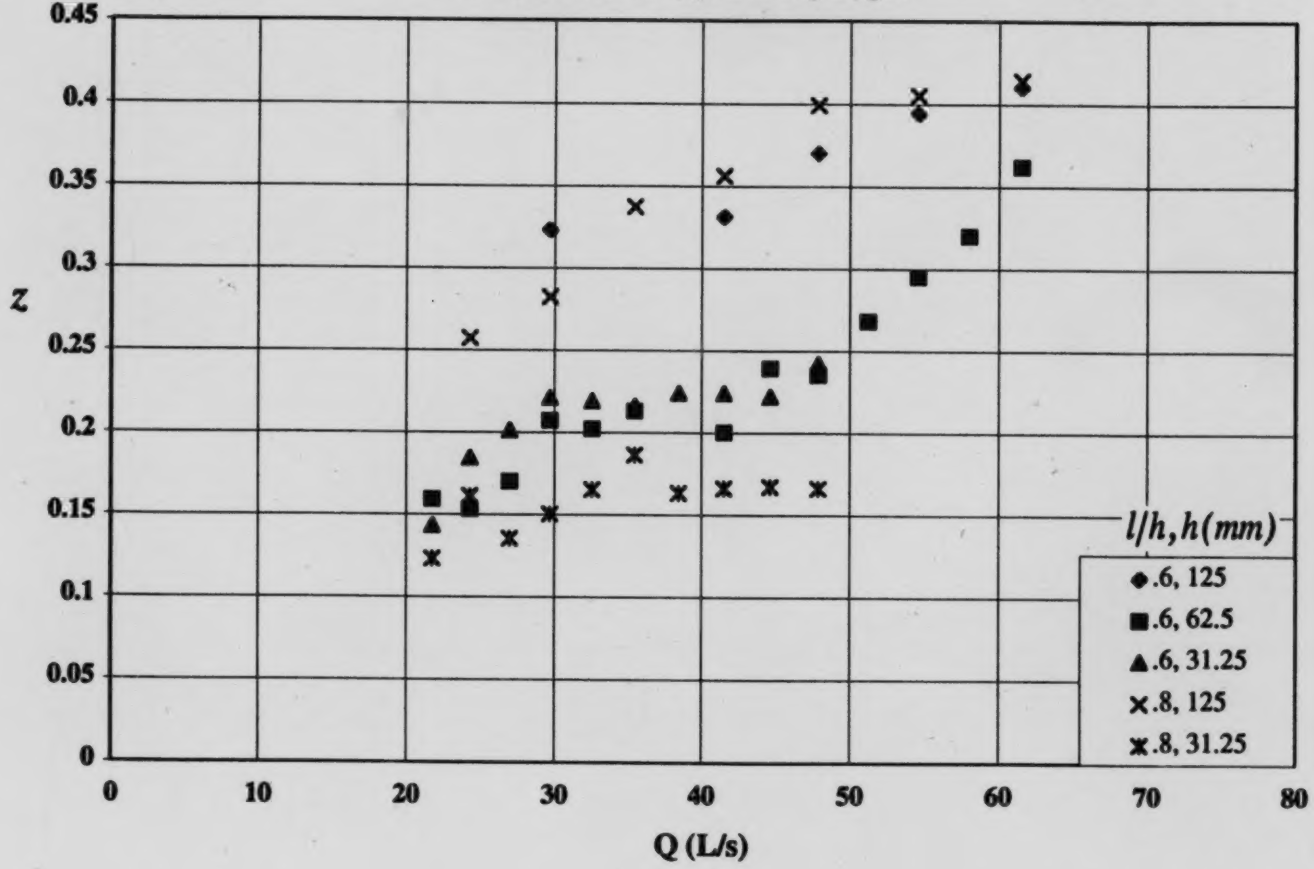

Figure 4.13 Relation of the mean air concentration to the shear velocity and transition depth in stepped spillways for various values of slope and step height

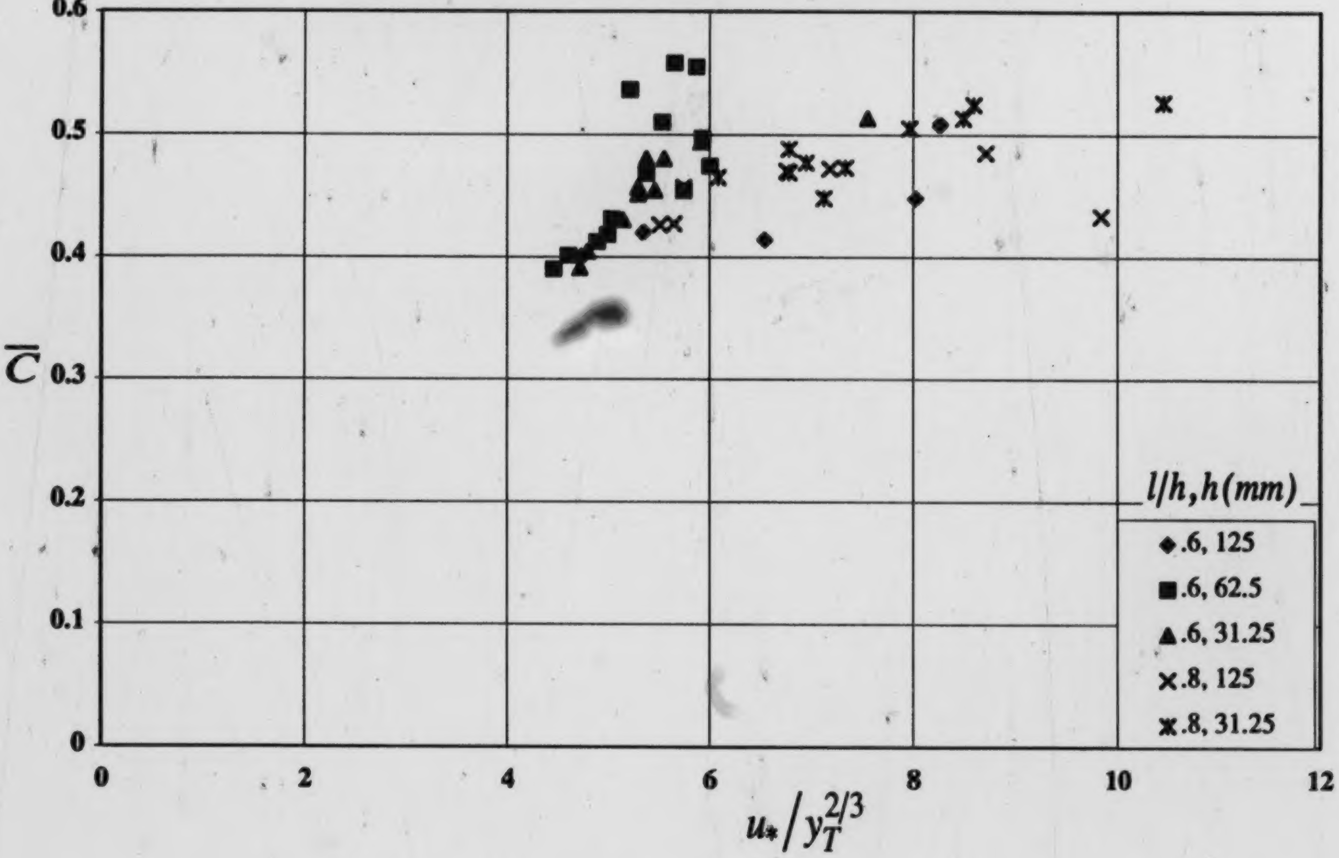

Figure 4.14 Relation of the mean air concentration to flow parameters in stepped spillways for various values of slope and step height

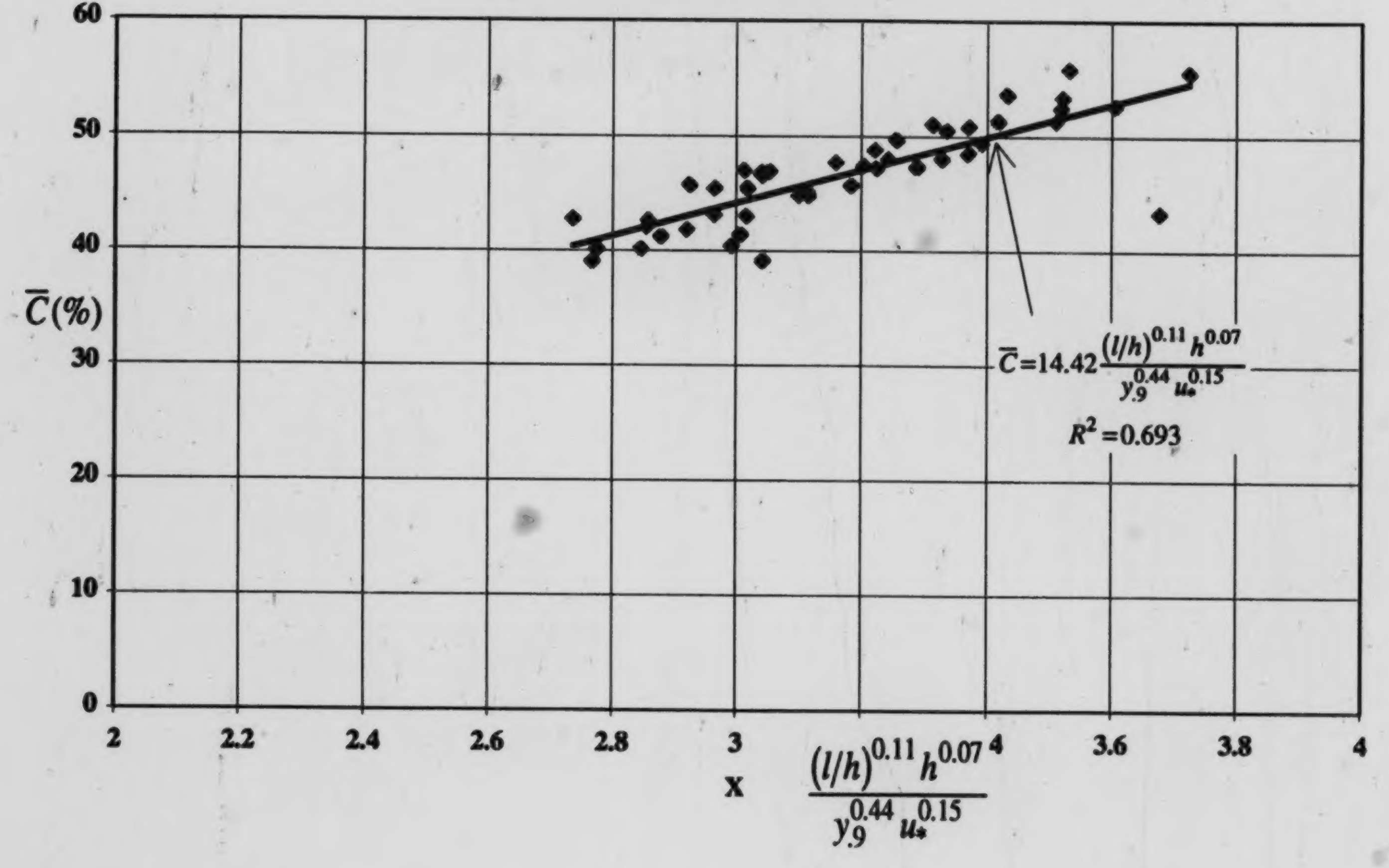

Figure 4.15 Relation of the mean air concentration to flow discharge and slope in stepped spillways for various values of slope and step height

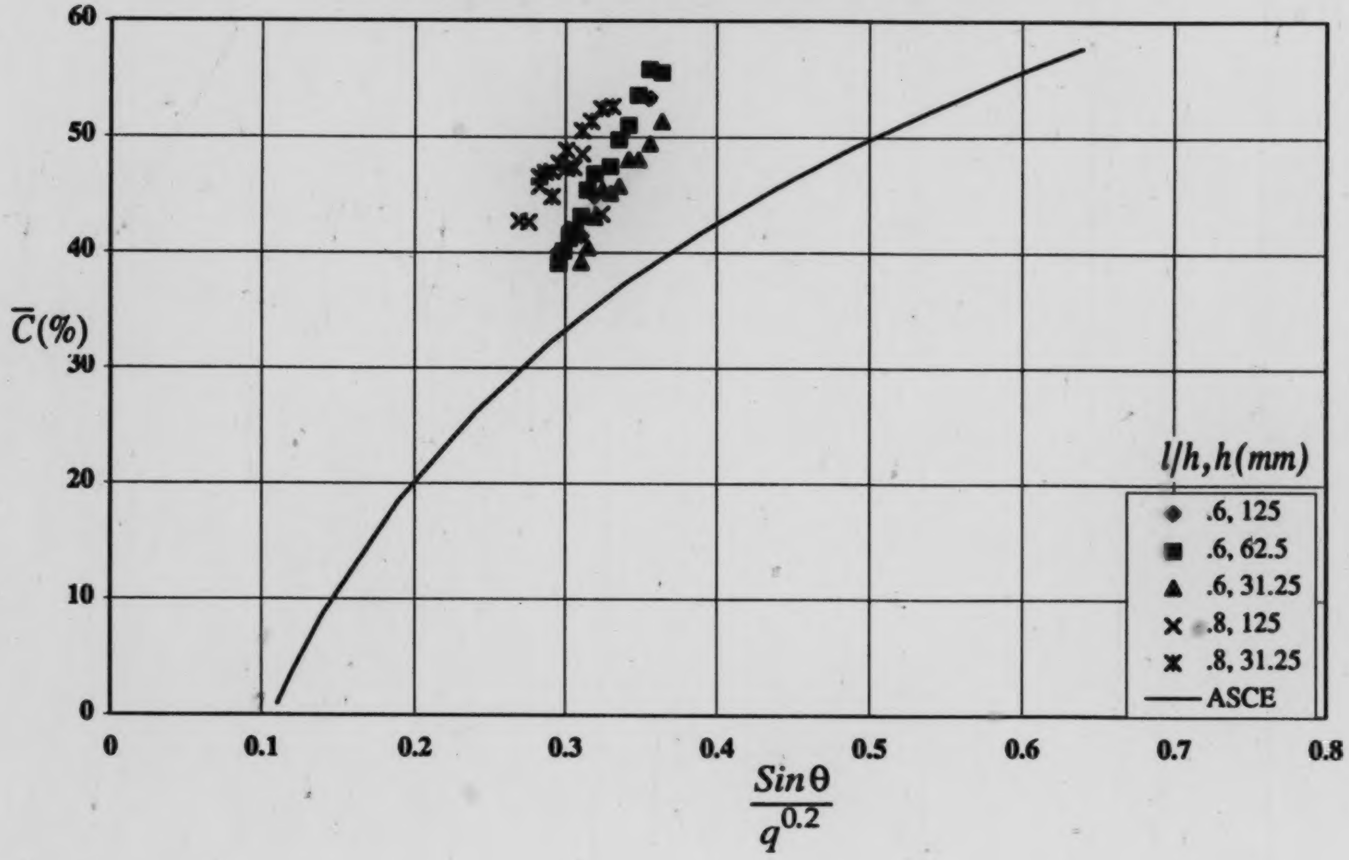

Figure 4.16 Relation of the mean air concentration to flow discharge and slope in stepped spillways for various values of slope and step height

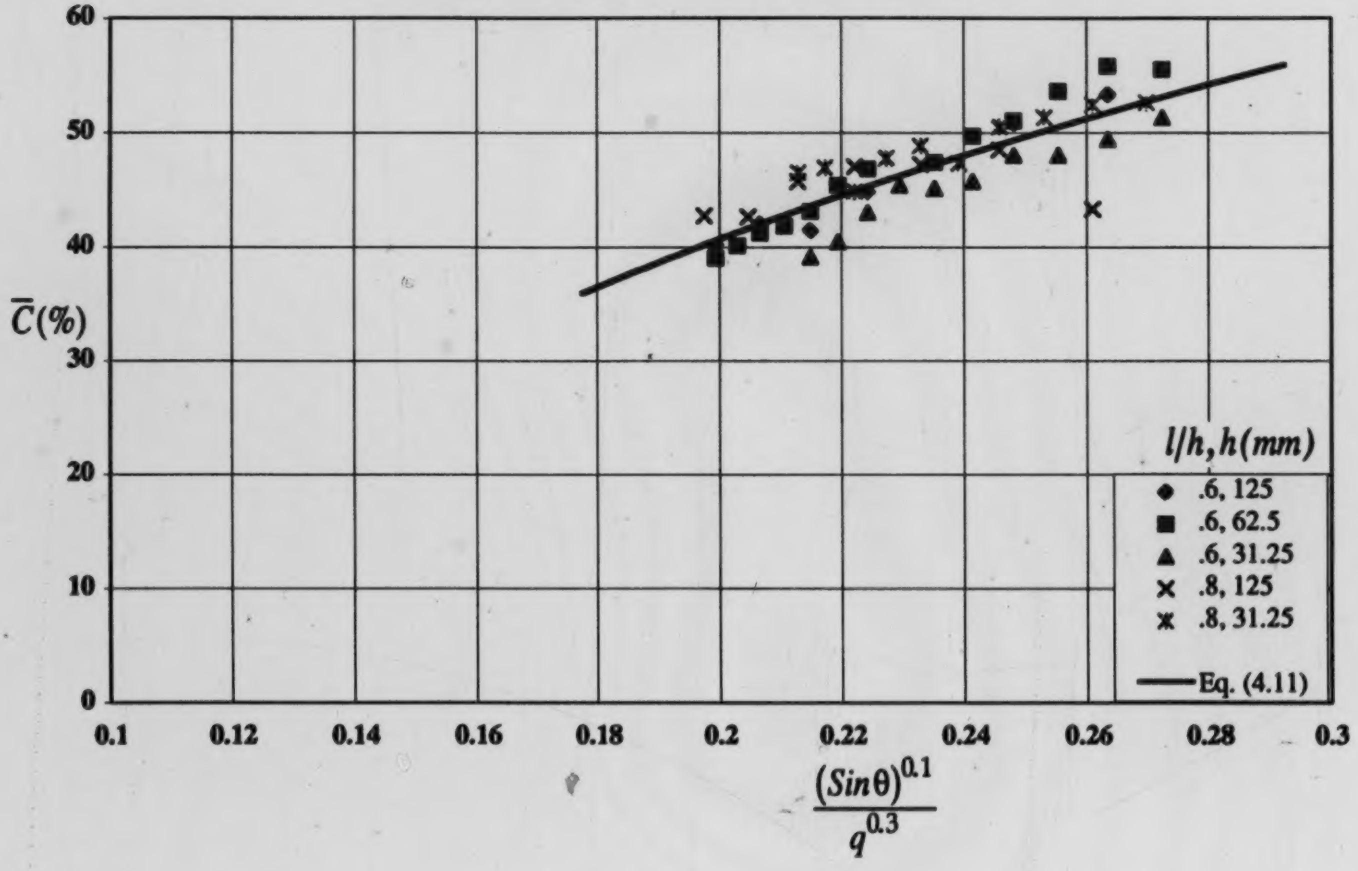

Figure 4.17 Relation of the upper depth of flow with discharge in stepped spillways for various values of slope and step height

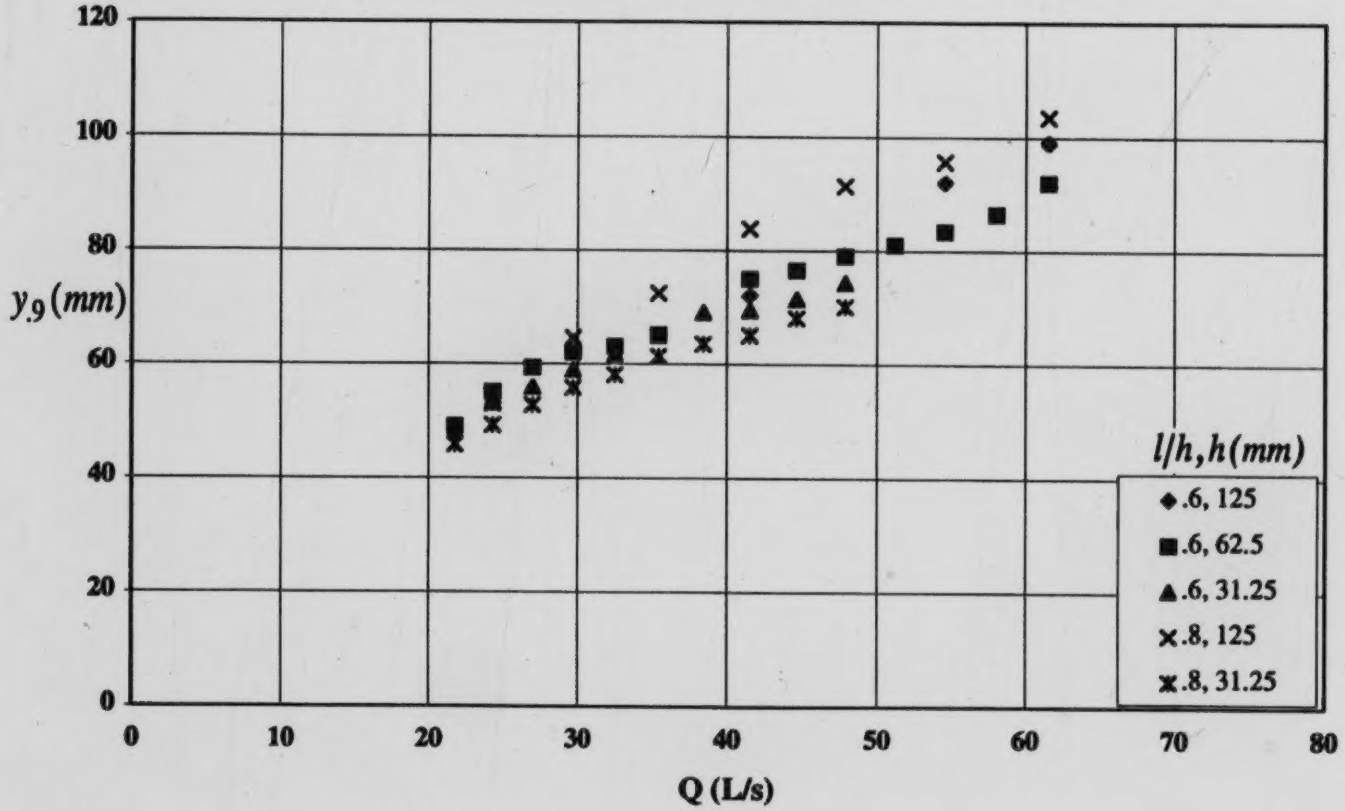

Figure 4.18 Relation of the transition depth with discharge in stepped spillways for various values of slope and step height

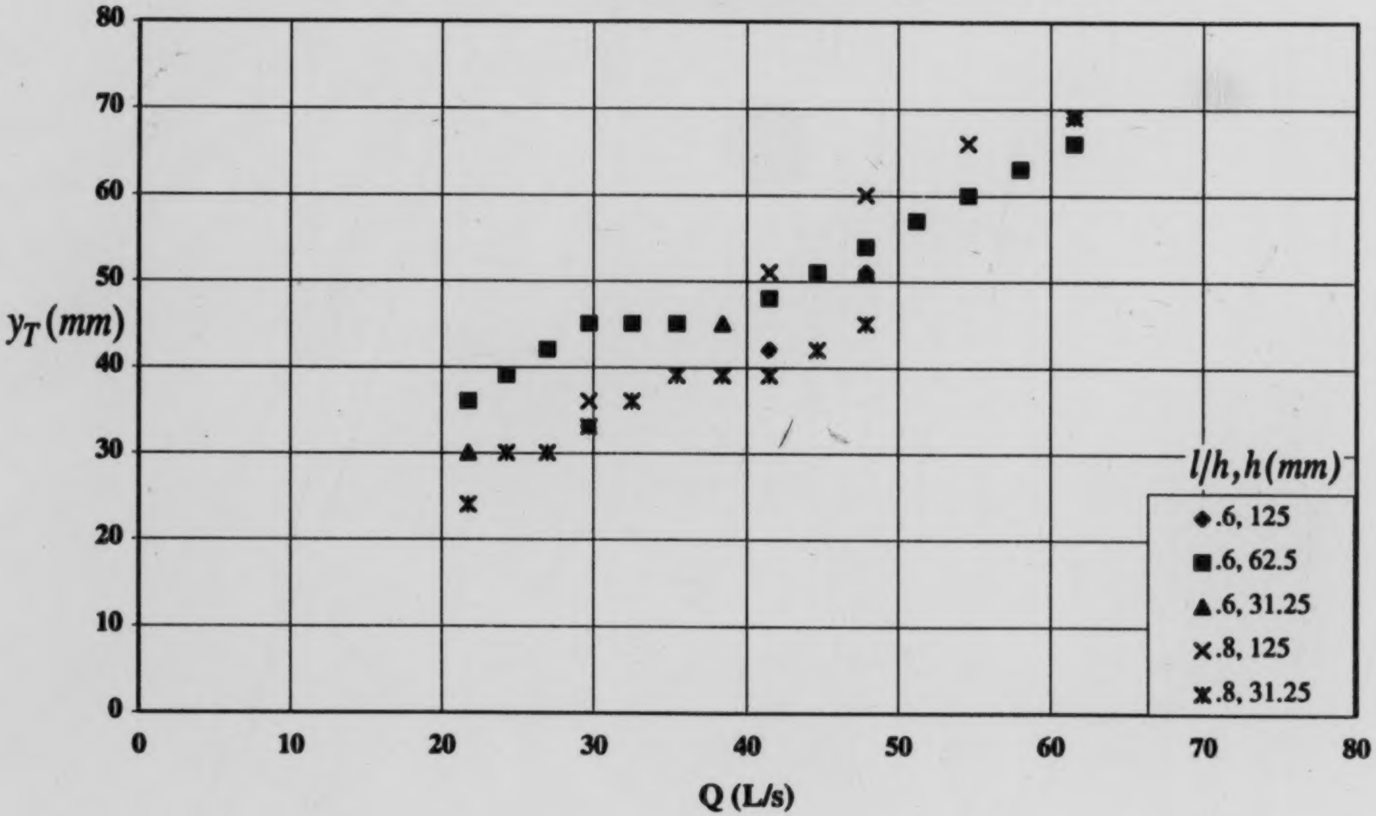

Figure 4.19 Relation of the projection height with discharge in stepped spillways for various values of slope and step height

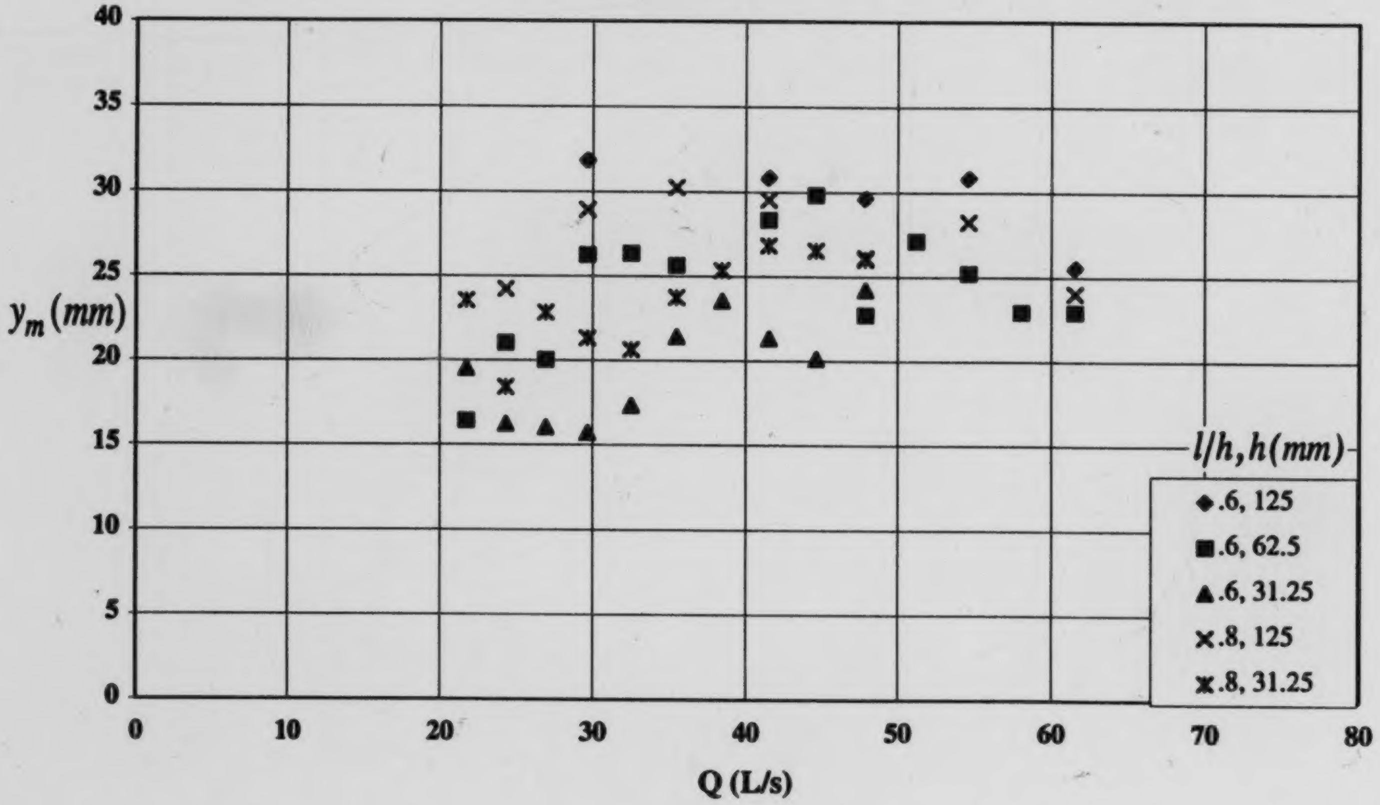

Figure 4.20 Relation of the characteristic depth ratio with discharge in stepped spillways for various values of slope and step height

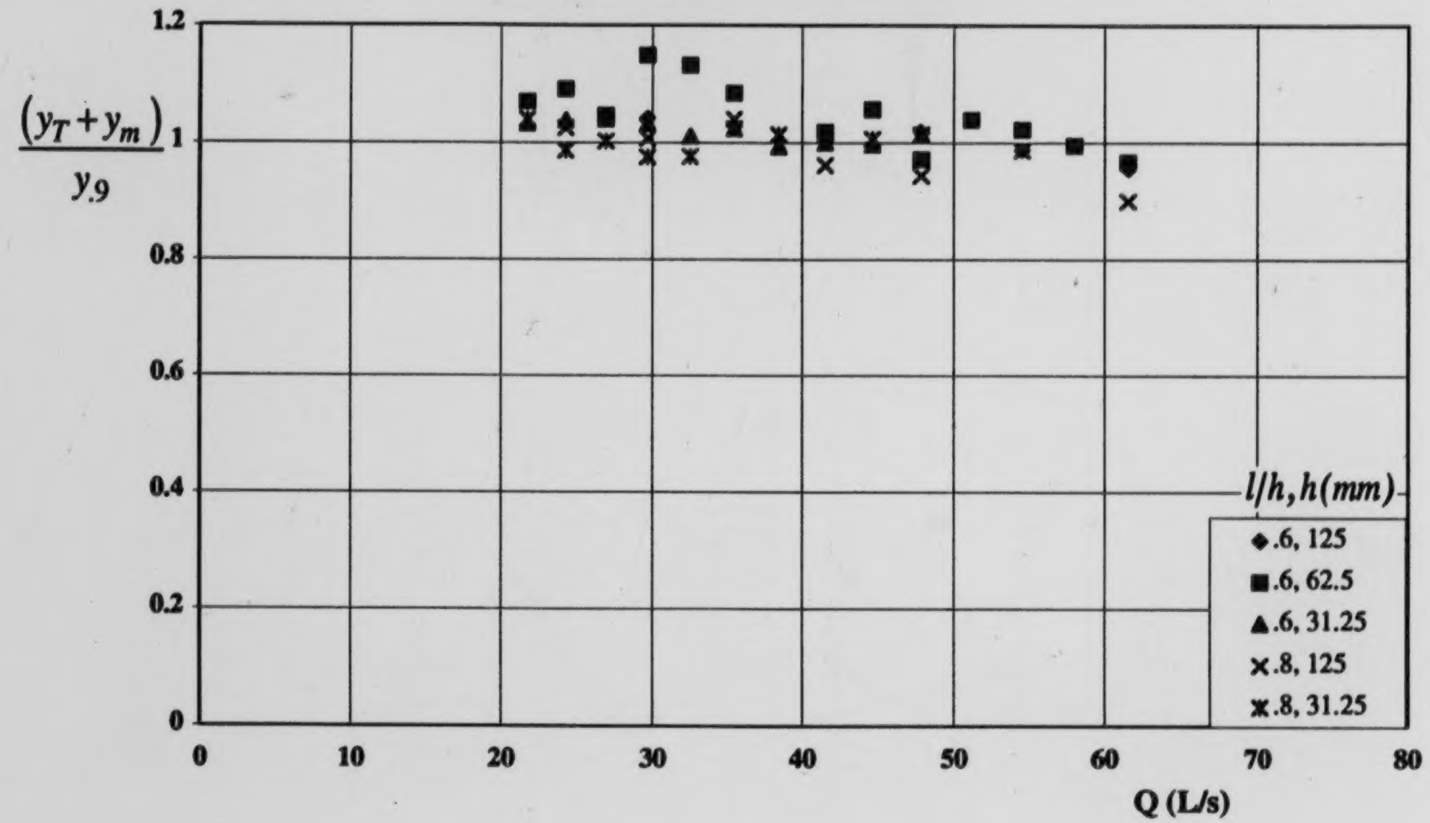

Figure 4.21 Mean range of stagnation head in a stepped spillway with l/h= 0.6 and h= 62.5 mm (yc/h= 2.0)

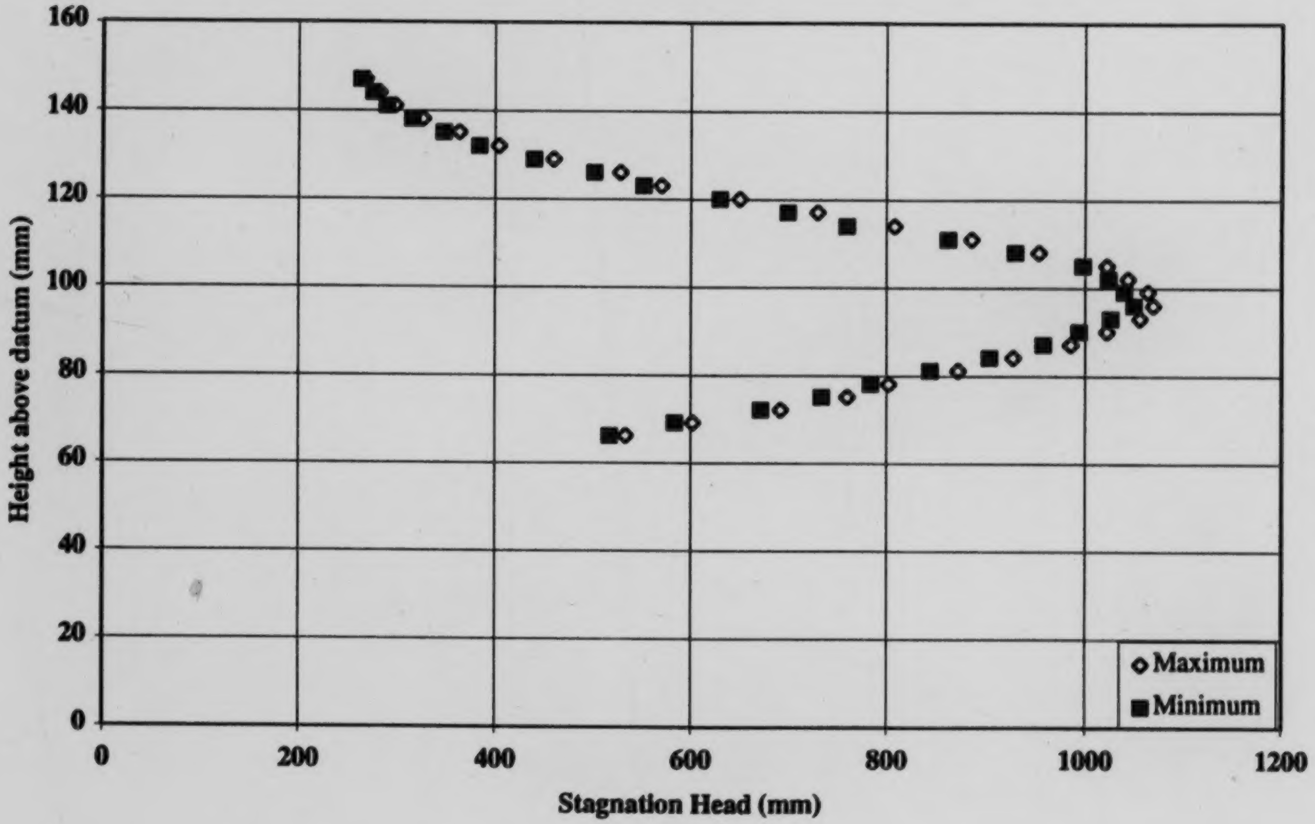

Figure 4.22 Velocity profile at step tip #16 in a stepped spillway with l/h=0.6, h= 125 mm (yc/h=1.3)

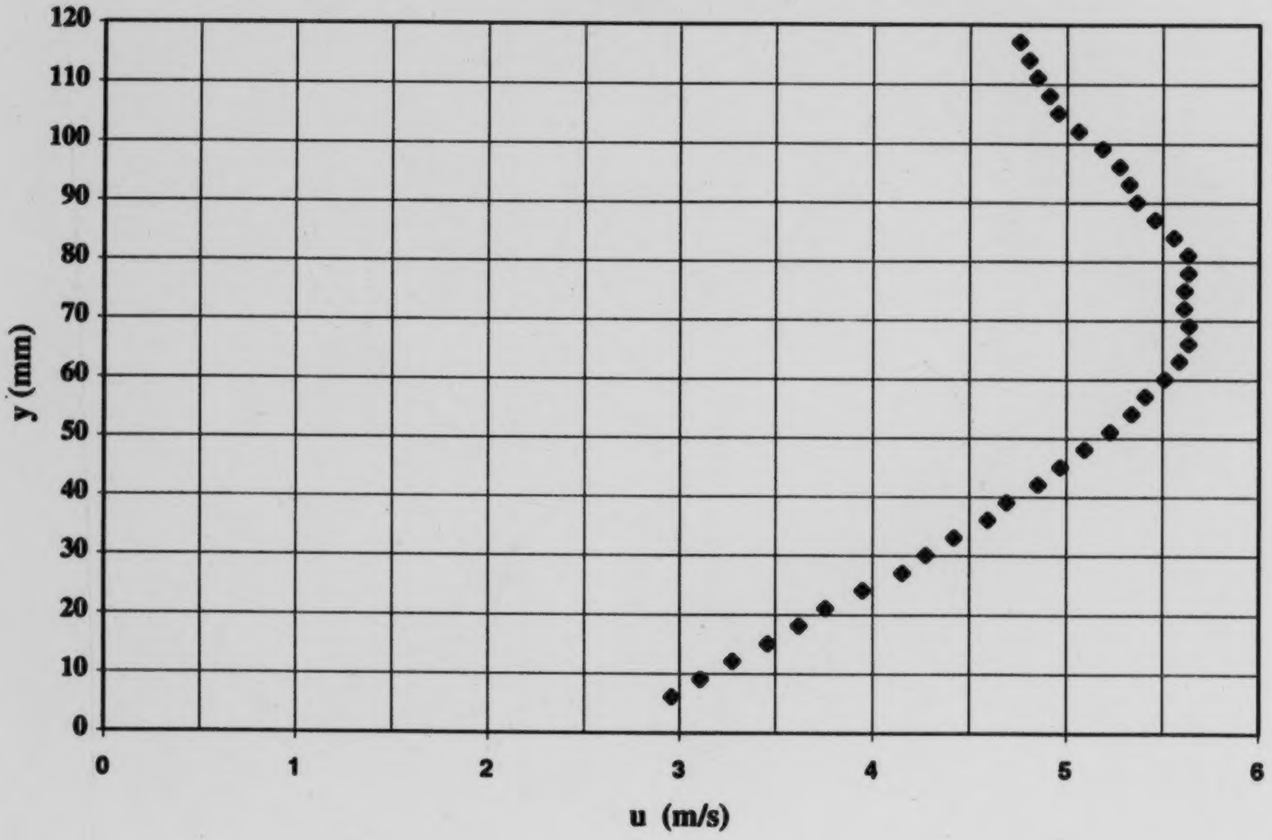

Figure 4.23 Relation of the characteristic depth ratio with discharge in stepped spillways for various values of slope and step height

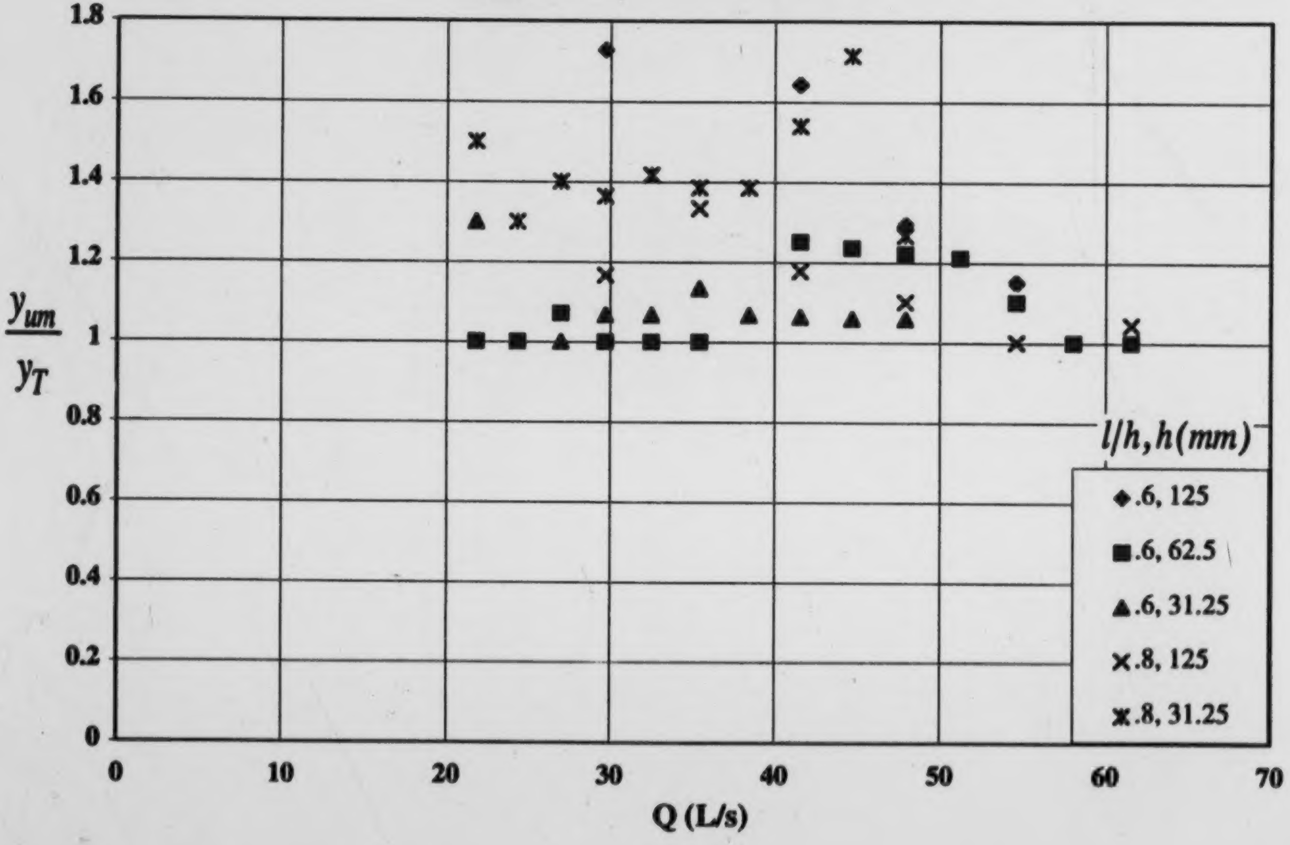

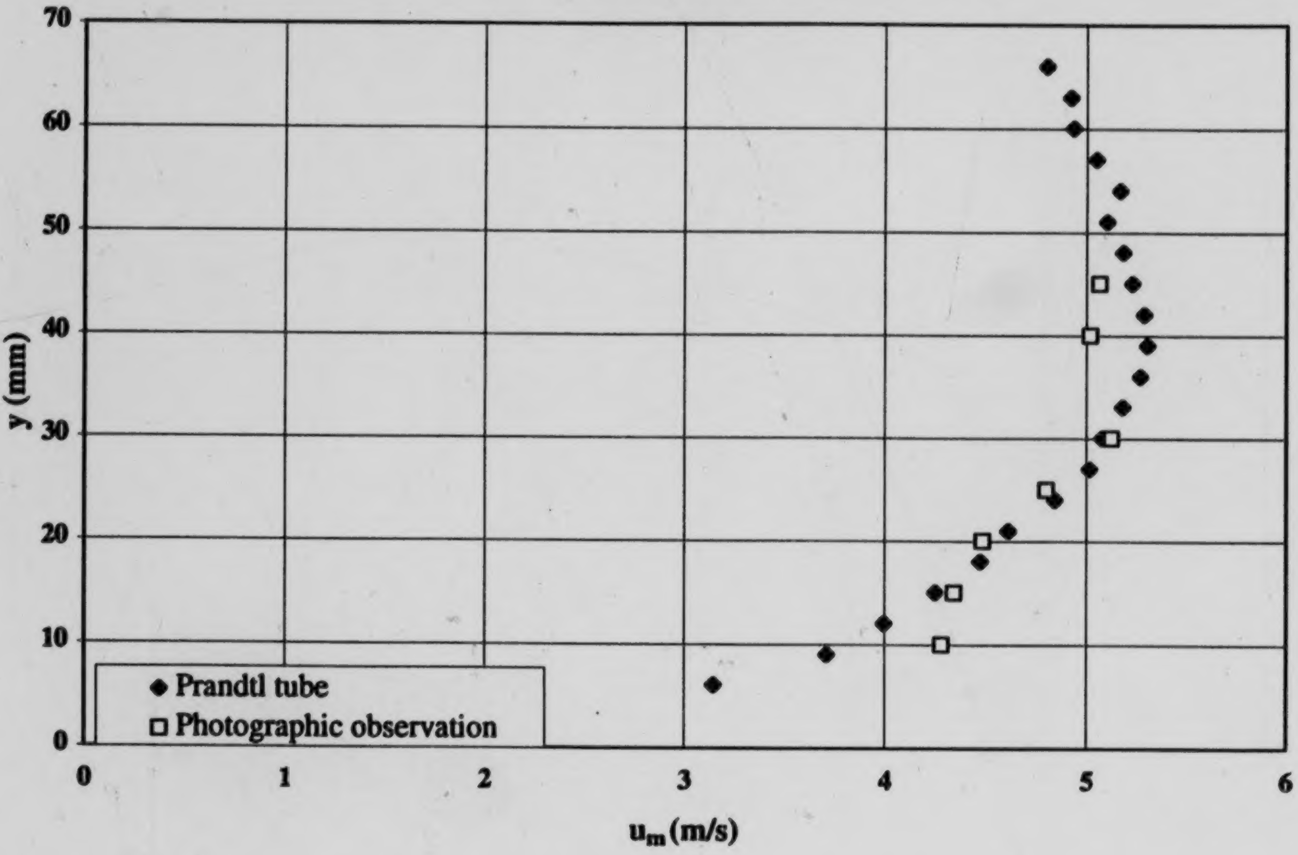

Figure 4.24 Velocity profiles taken by different methods in a stepped spillway with l/h= 0.6 and h= 62.5 mm (yc/h= 1.4)

Figure 4.25 Velocity profiles taken by different methods in a stepped spillway with l/h= 0.6 and h= 62.5 mm (yc/h) 2.0)

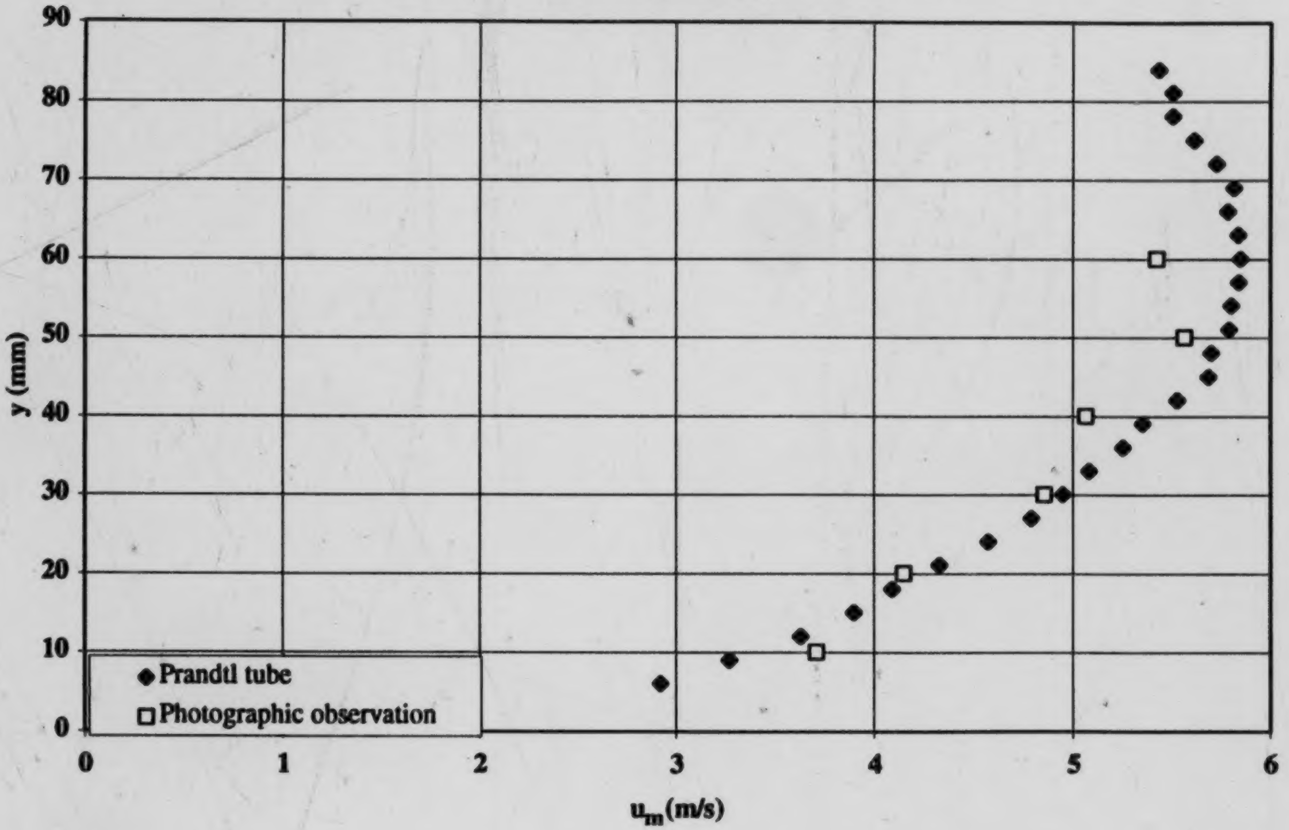

Figure 4.26 Velocity profiles taken by different methods in a stepped spillway with l/h= 0.6 and h= 31.25 mm (yc/h= 2.8)

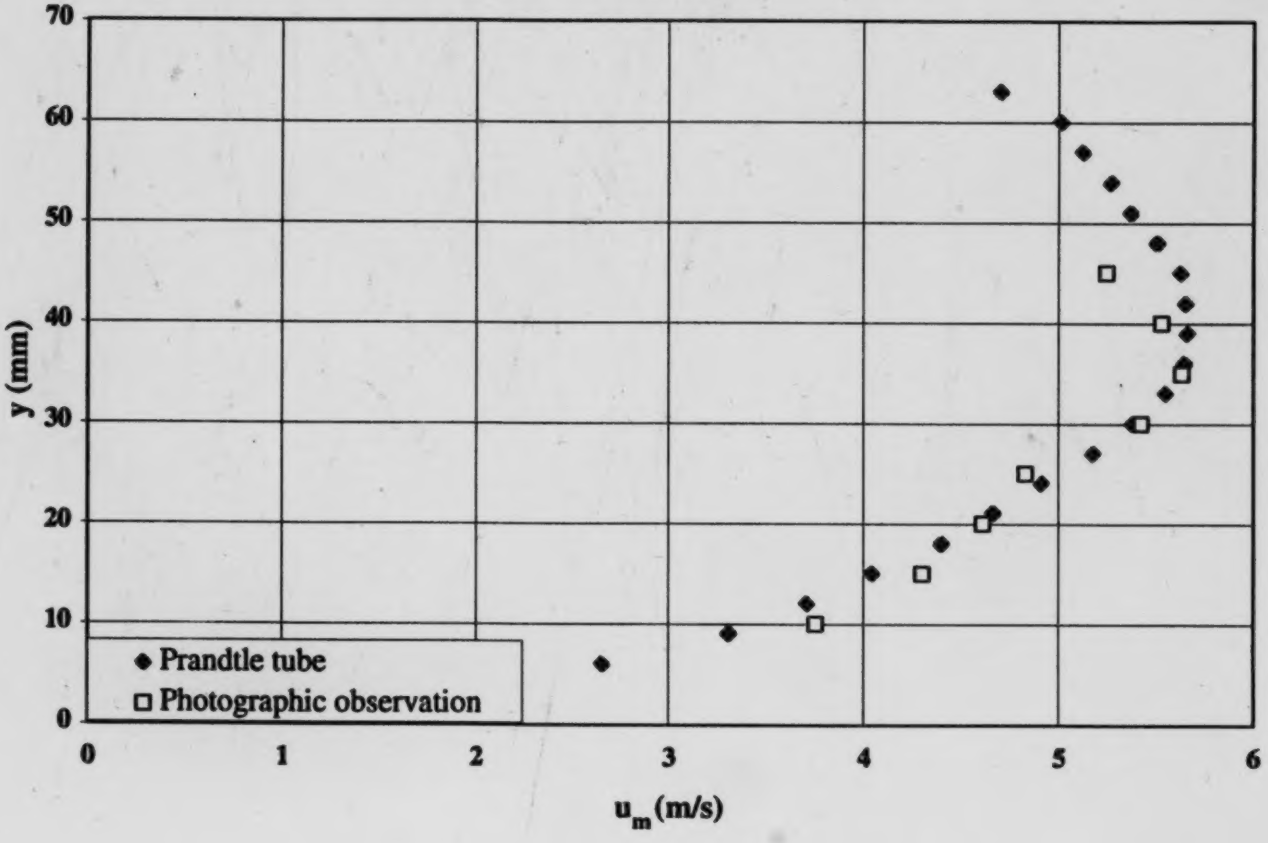

Figure 4.27 Velocity profiles taken by different methods in a stepped spillway with l/h= 0.6 and h= 31.25 mm (yc/h= 4.0)

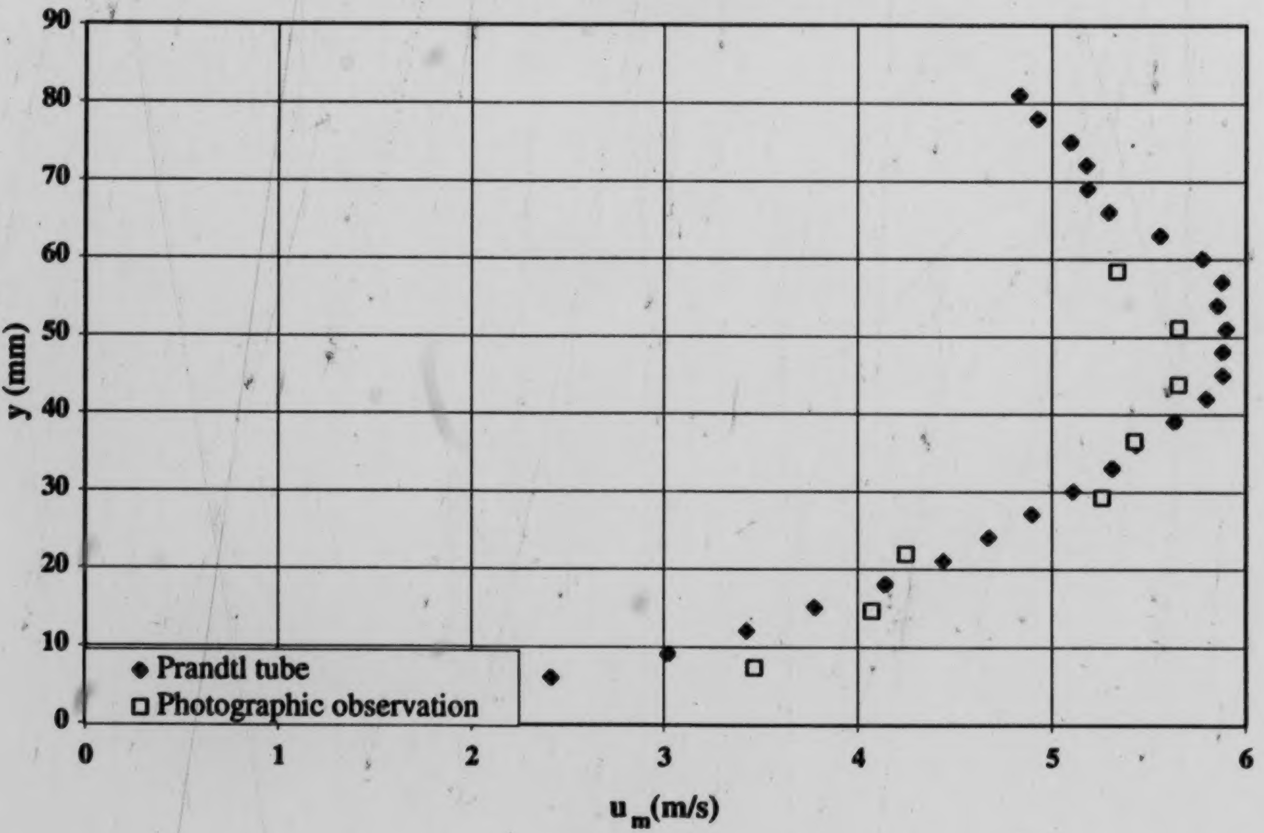

Figure 4.28 Logarithmic velocity profiles at different origins at step #13 in a stepped spillway with l/h=0.6, h= 125 mm, k= 76.6 mm (yc/h=1.0)

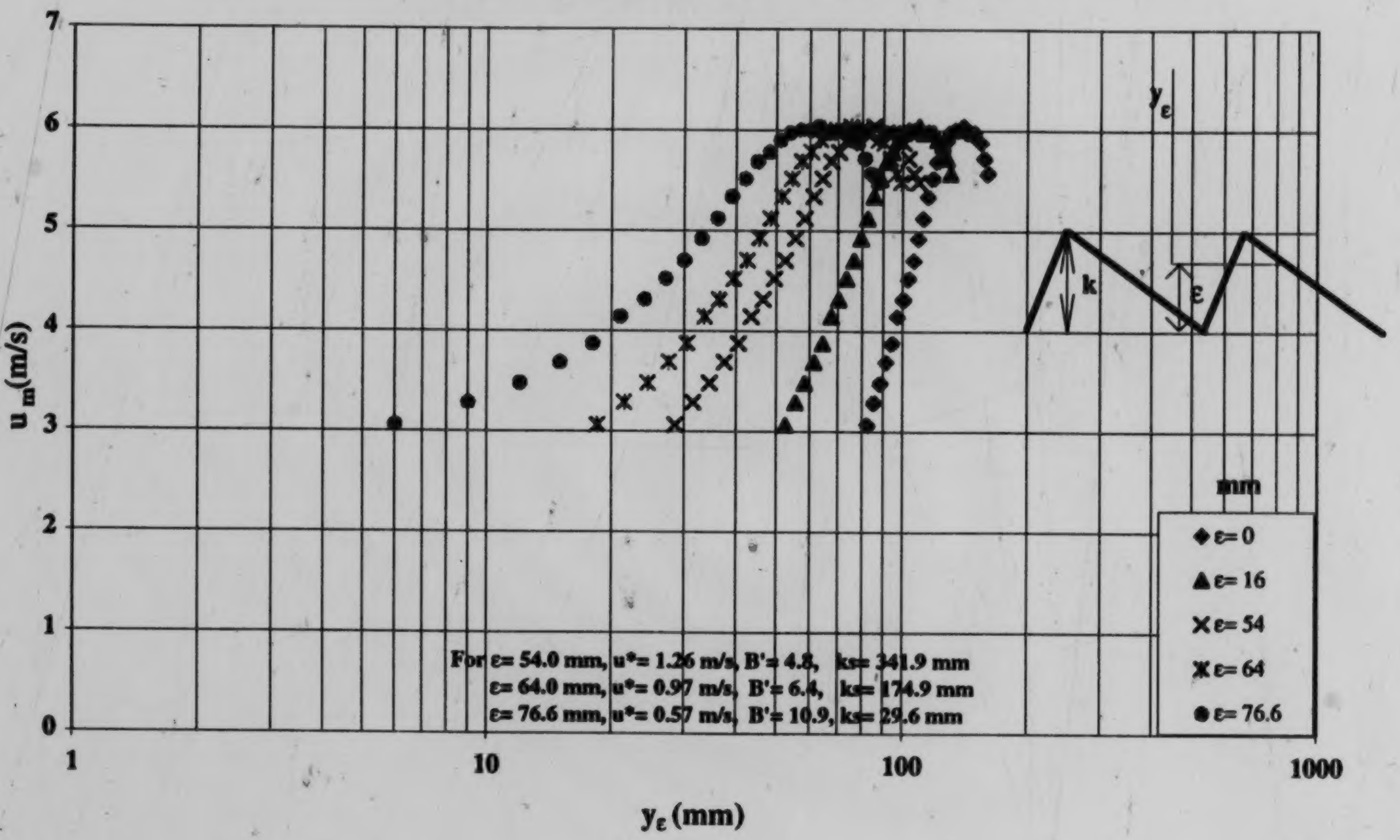

Figure 4.29 Variation of the relative roughness ratio with discharge for different step heights and spillway slope

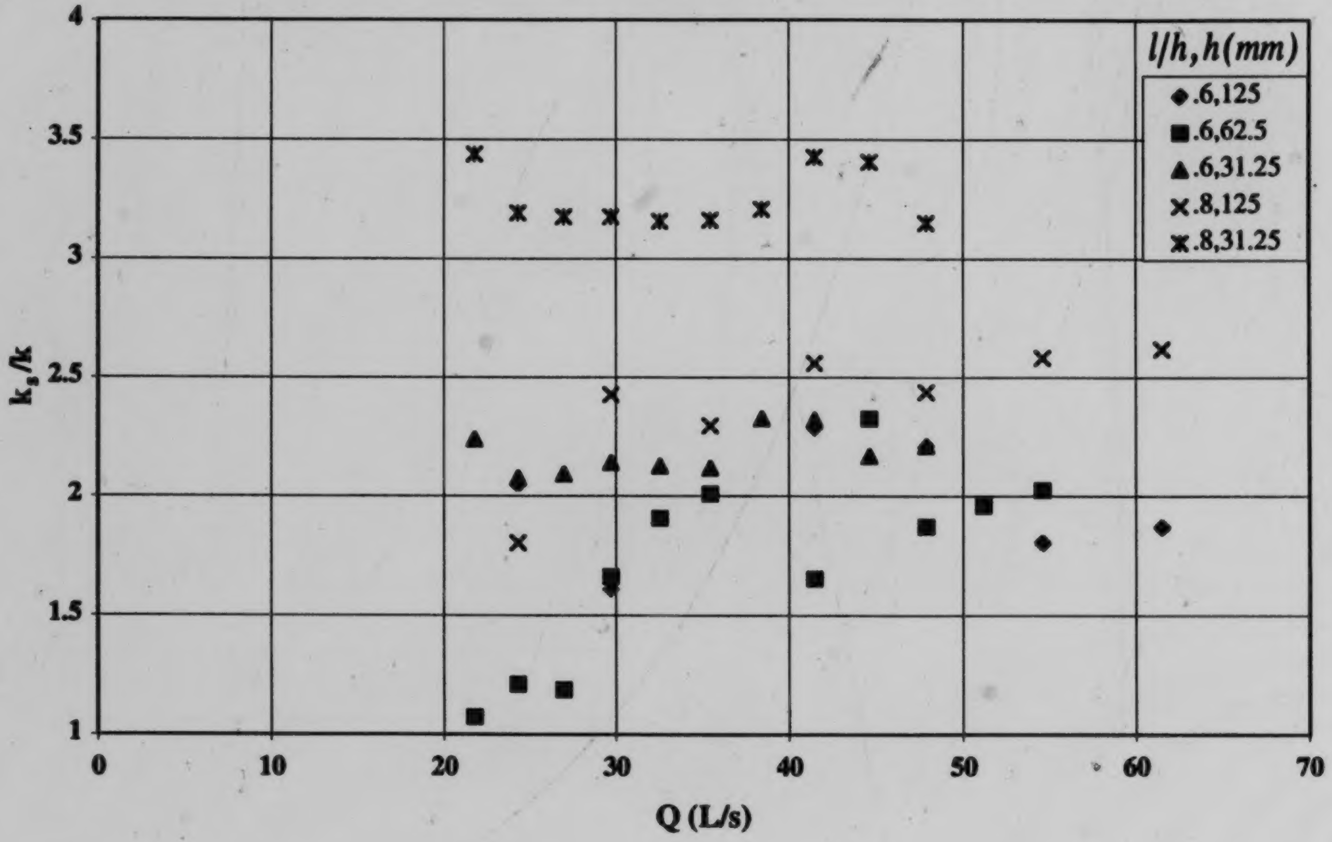

Figure 4.30 Universal velocity profiles at step #13 of a stepped spillway with l/h=0.6 and h= 125 mm (k= 76.6 mm, ε= 64.0 mm)

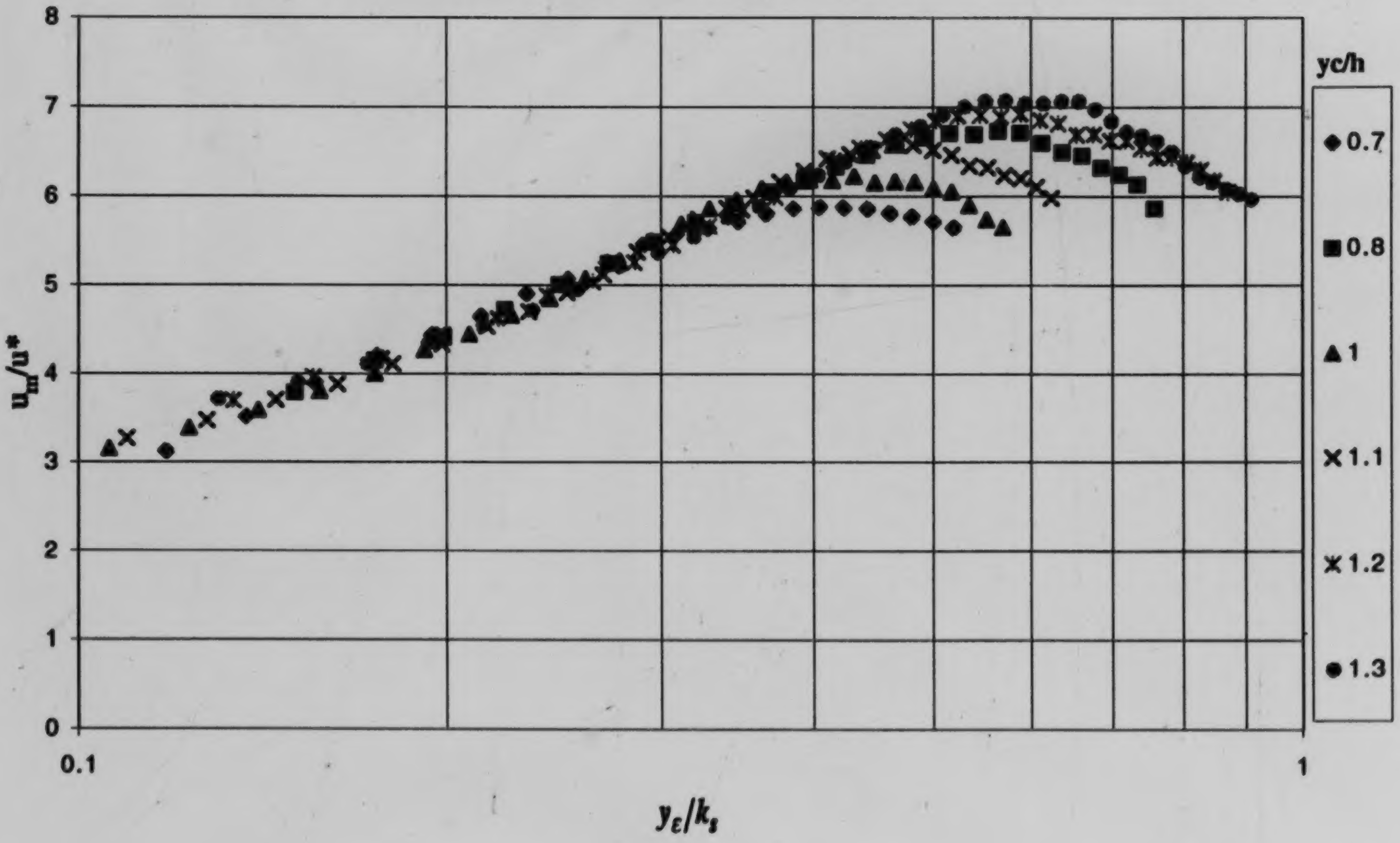

Figure 4.31 Universal velocity profiles at step #26 of a stepped spillway with l/h=0.6 and h= 62.5 mm (k= 38.3 mm, ε= 33.0 mm)

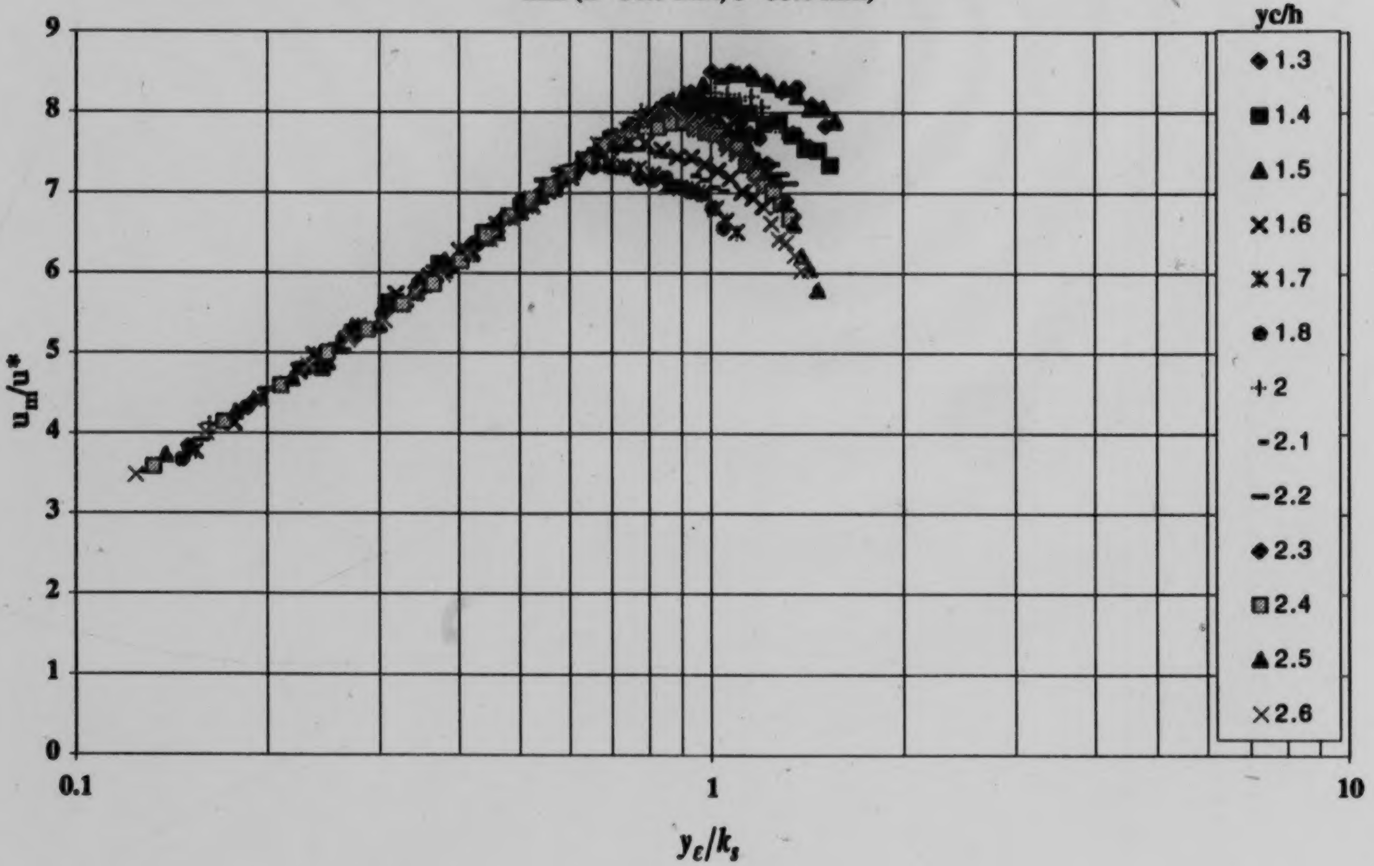

Figure 4.32 Universal velocity profiles at step #64 of a stepped spillway with l/h=0.6 and h= 31.25 mm (k= 19.14 mm, ε= 17.0 mm)

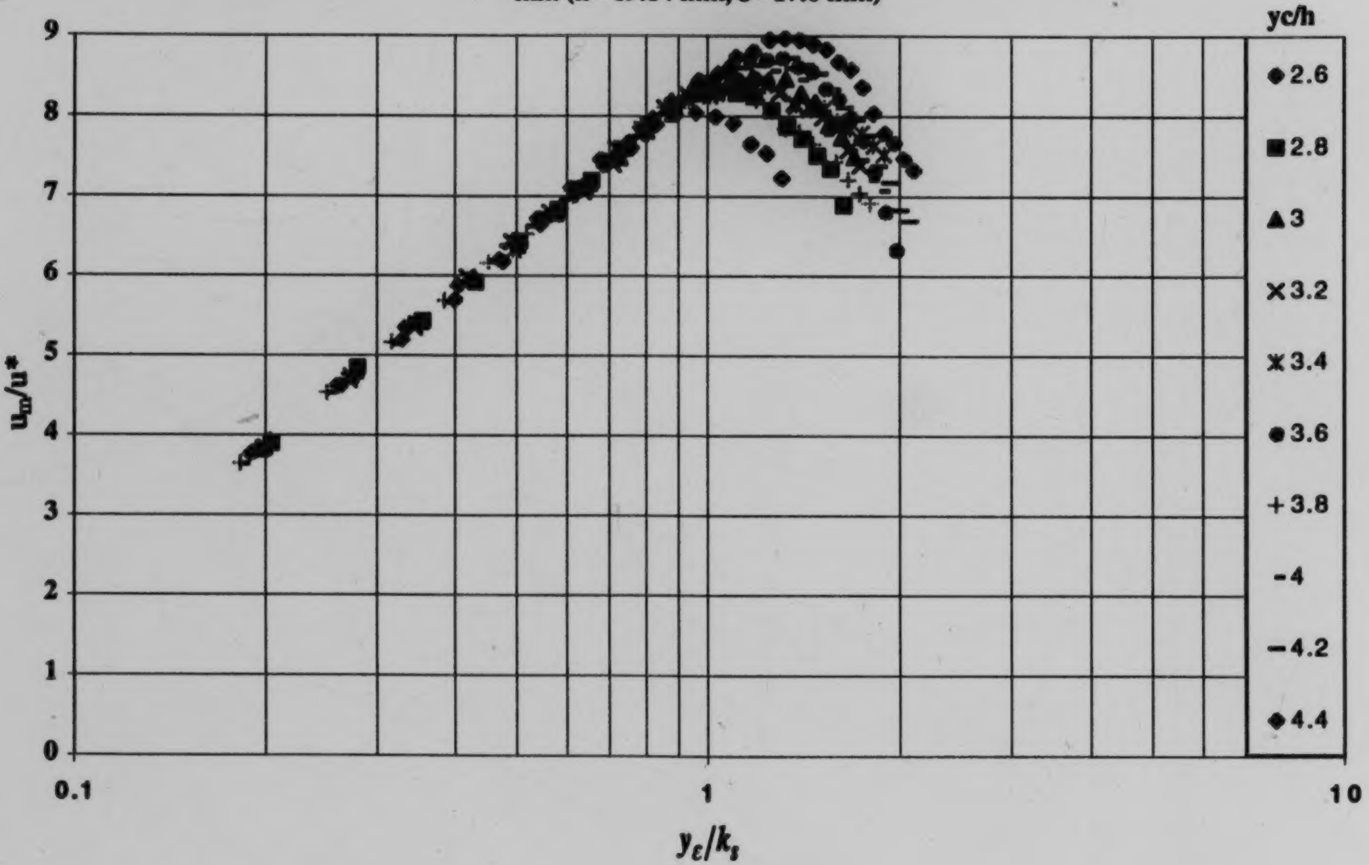

Figure 4.33 Universal velocity profiles at step #16 of a stepped spillway with l/h=0.8 and h= 125 mm (k= 83.3 mm, ε= 64.0 mm)

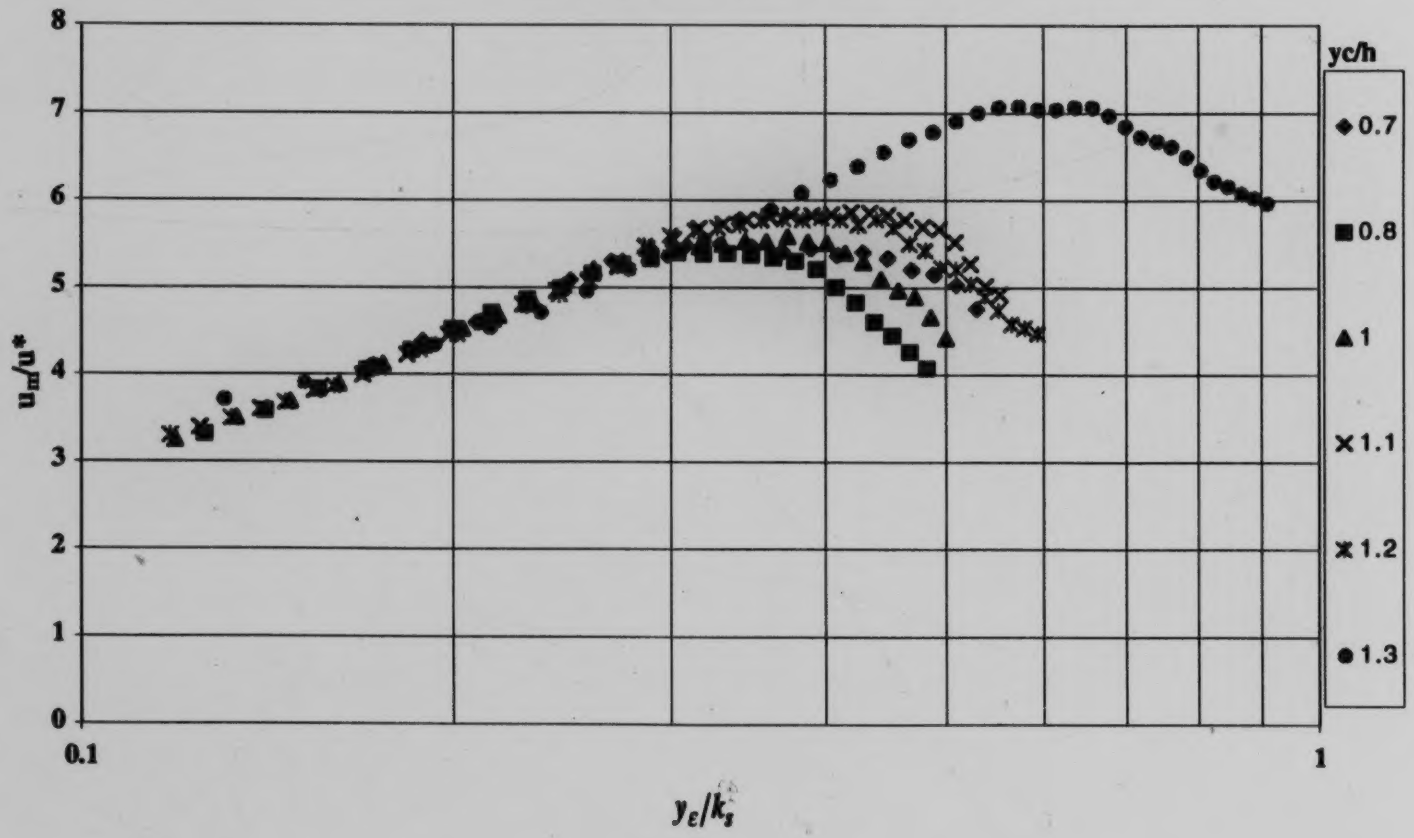

Figure 4.34 Universal velocity profiles at step #64 of a stepped spillway with l/h=0.8 and h= 31.25 mm (k= 20.8 mm, ε= 20.8 mm)

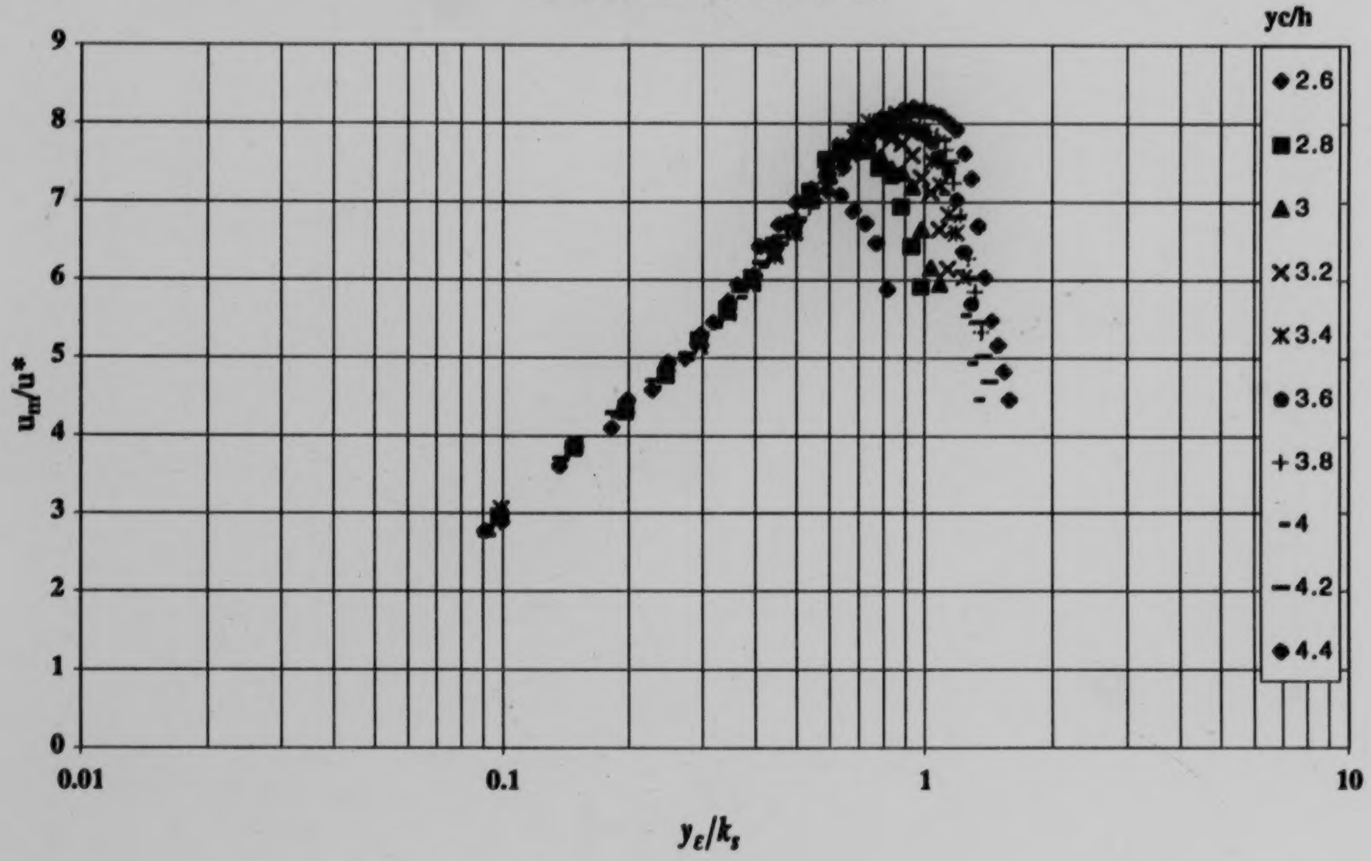

Figure 4.35 Universal velocity profiles in stepped spillways with different spillway slopes and step heights

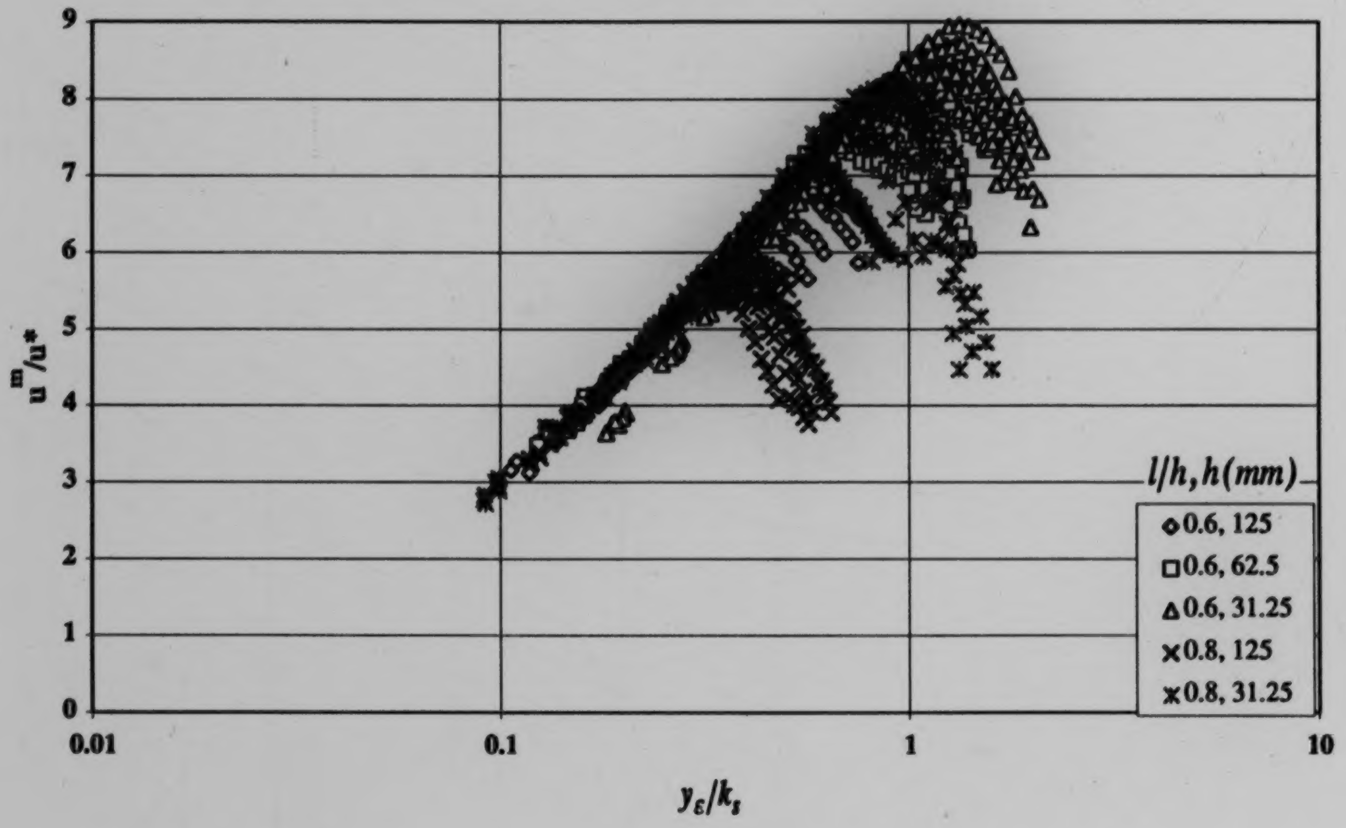

Figure 4.36 Universal velocity profiles in the lower region of the flow in a stepped spillway with l/h=0.6 and h= 125 mm (k= 76.6 mm)

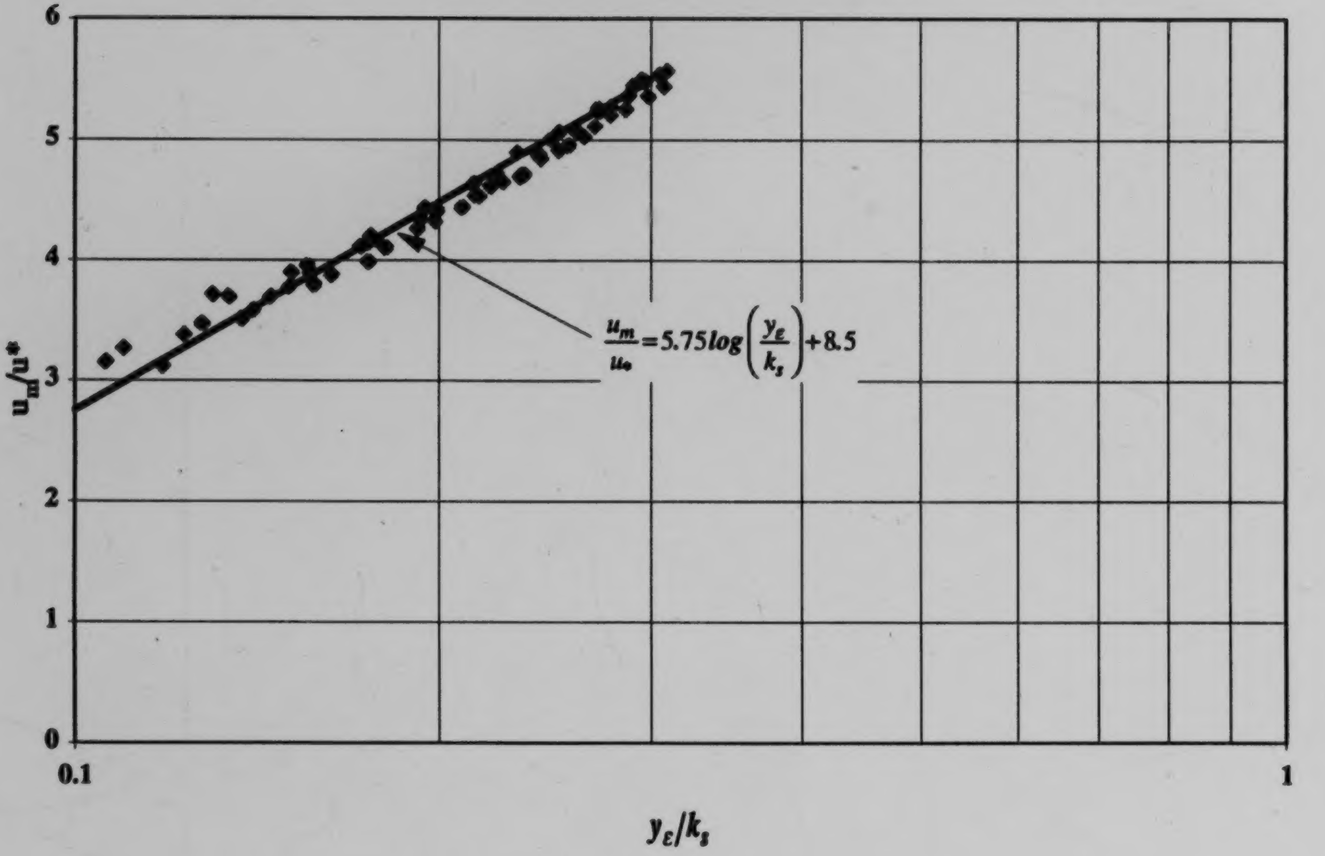

Figure 4.37 Universal velocity profiles in the lower region of the flow in a stepped spillway with l/h=0.6 and h= 62.5 mm (k= 38.3 mm)

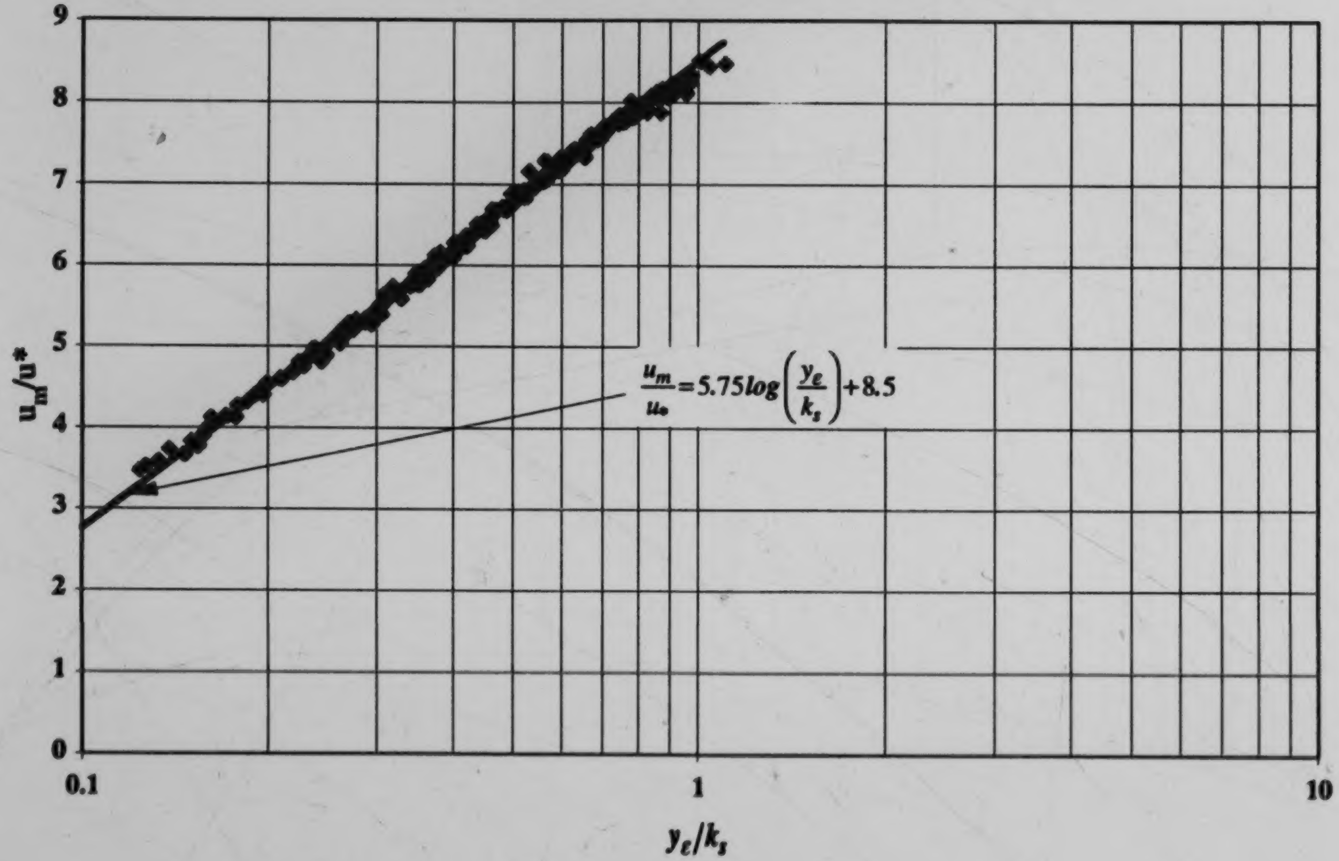

Figure 4.38 Universal velocity profiles in the lower region of the flow in a stepped spillway with l/h=0.6 and h= 31.25 mm (k= 19.15 mm)

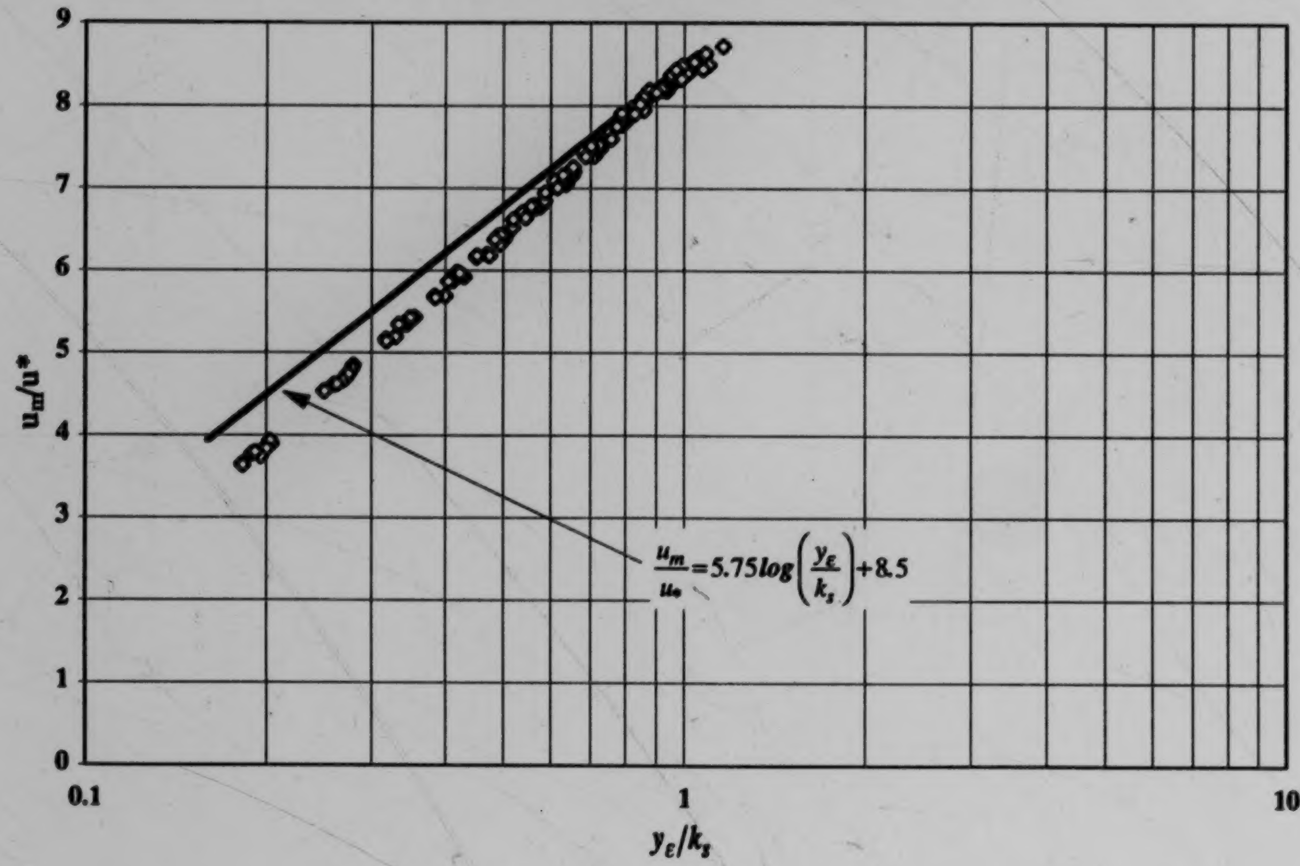

Figure 4.39 Universal velocity profiles in the low region of the flow in a stepped spillway with l/h=0.8 and h= 125 mm (k= 83.3 mm)

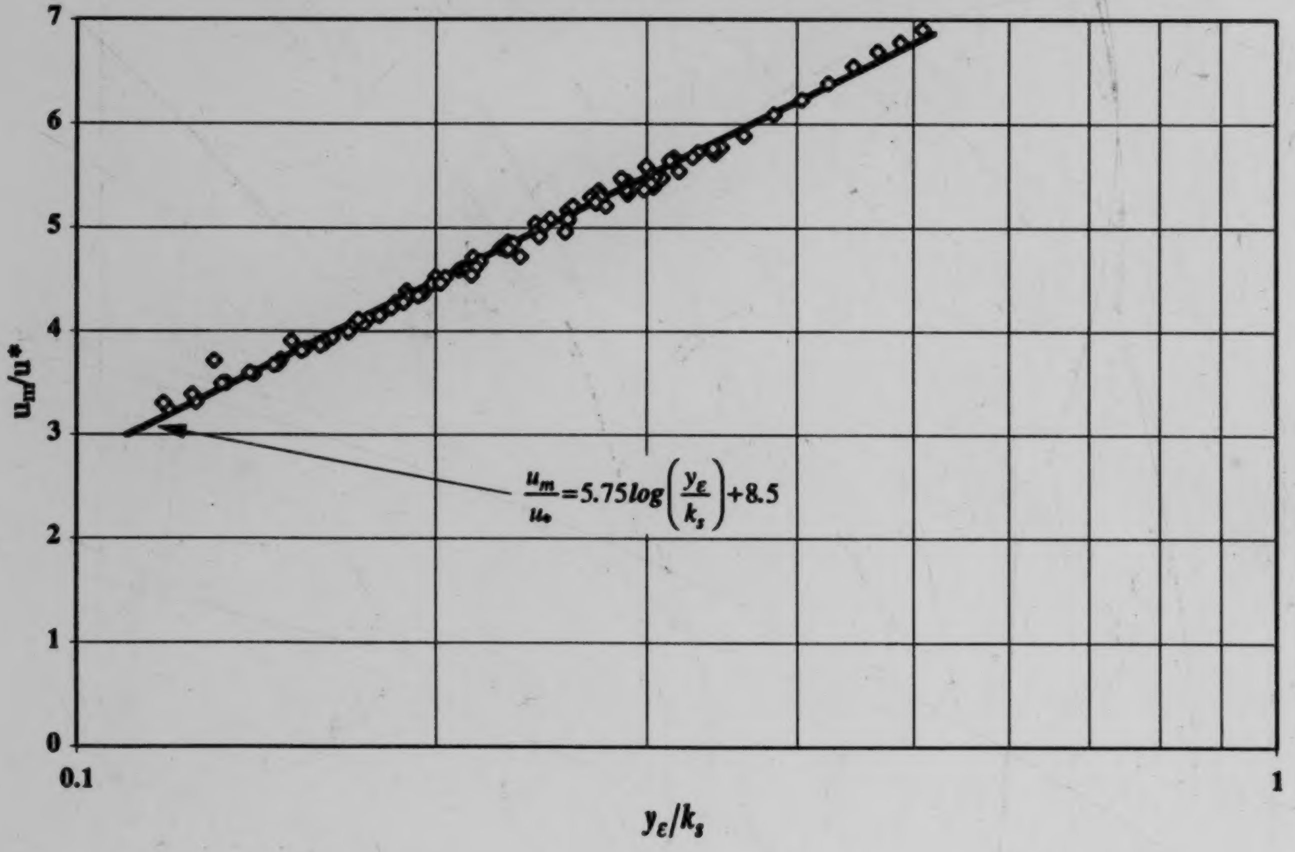

Figure 4.40 Universal velocity profiles in the lower region of the flow in a stepped spillway with l/h=0.8 and h= 31.25 mm (k= 20.8 mm)

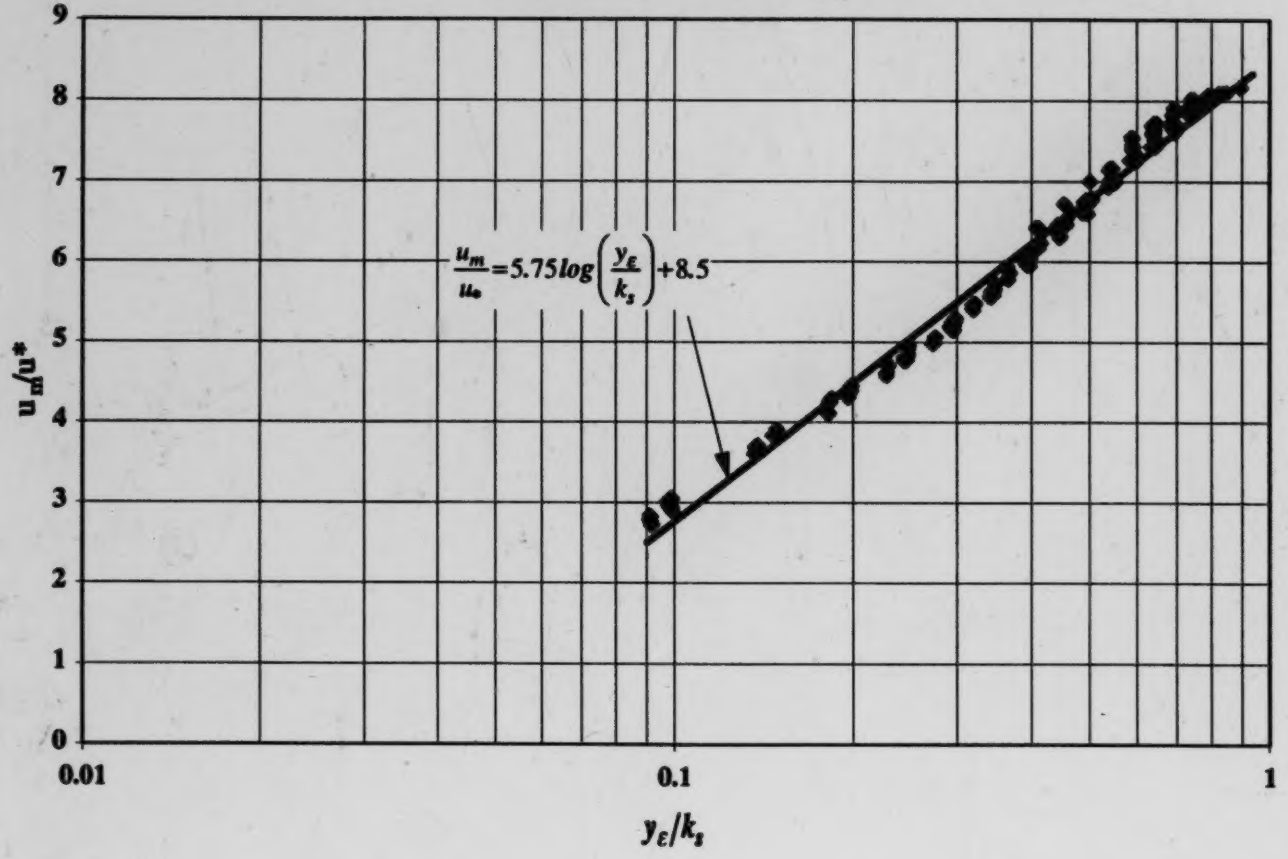

Figure 4.41 Universal velocity profiles in the lower region of the flow in stepped spillways with various values of slope and step height

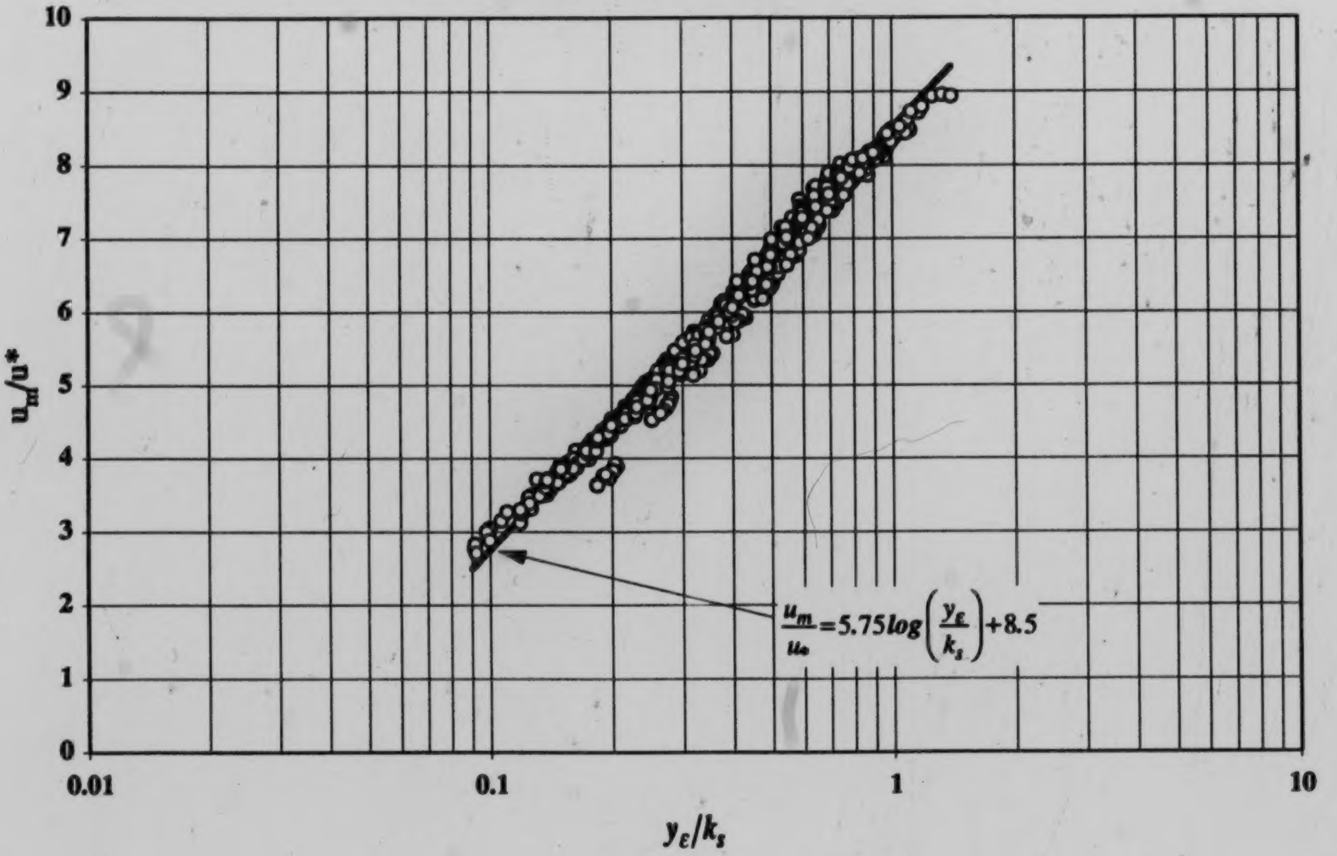

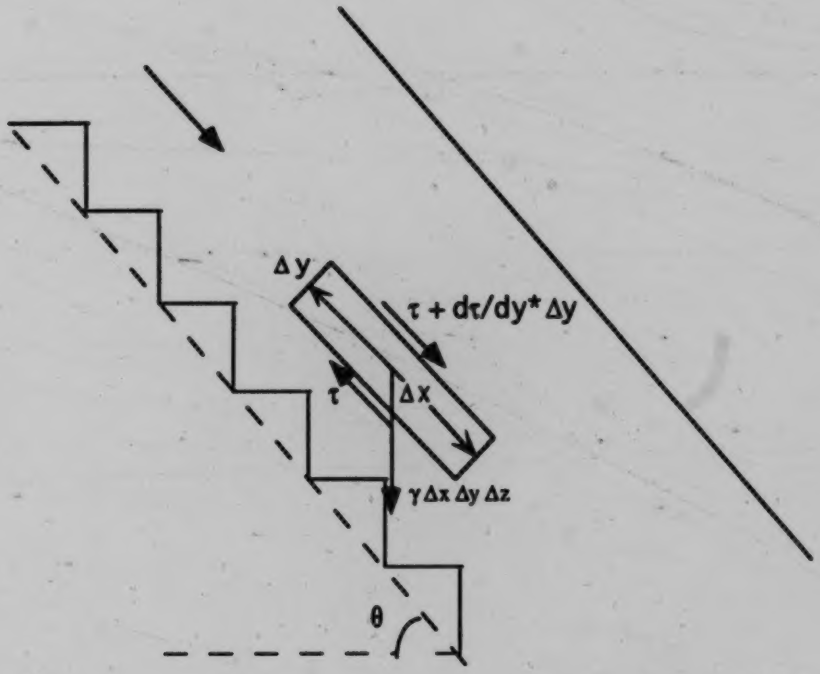
Δy
τ + dτ/dy* Δy
τ
Δx
γ Δx Δy Δz
θ

Figure 4.42 A schematic sketch showing the control volume for the developed region in the skimming flow

Figure 4.43 Variation of the skin friction coefficient for the skimming flow in stepped spillways and fishways and pipe flow

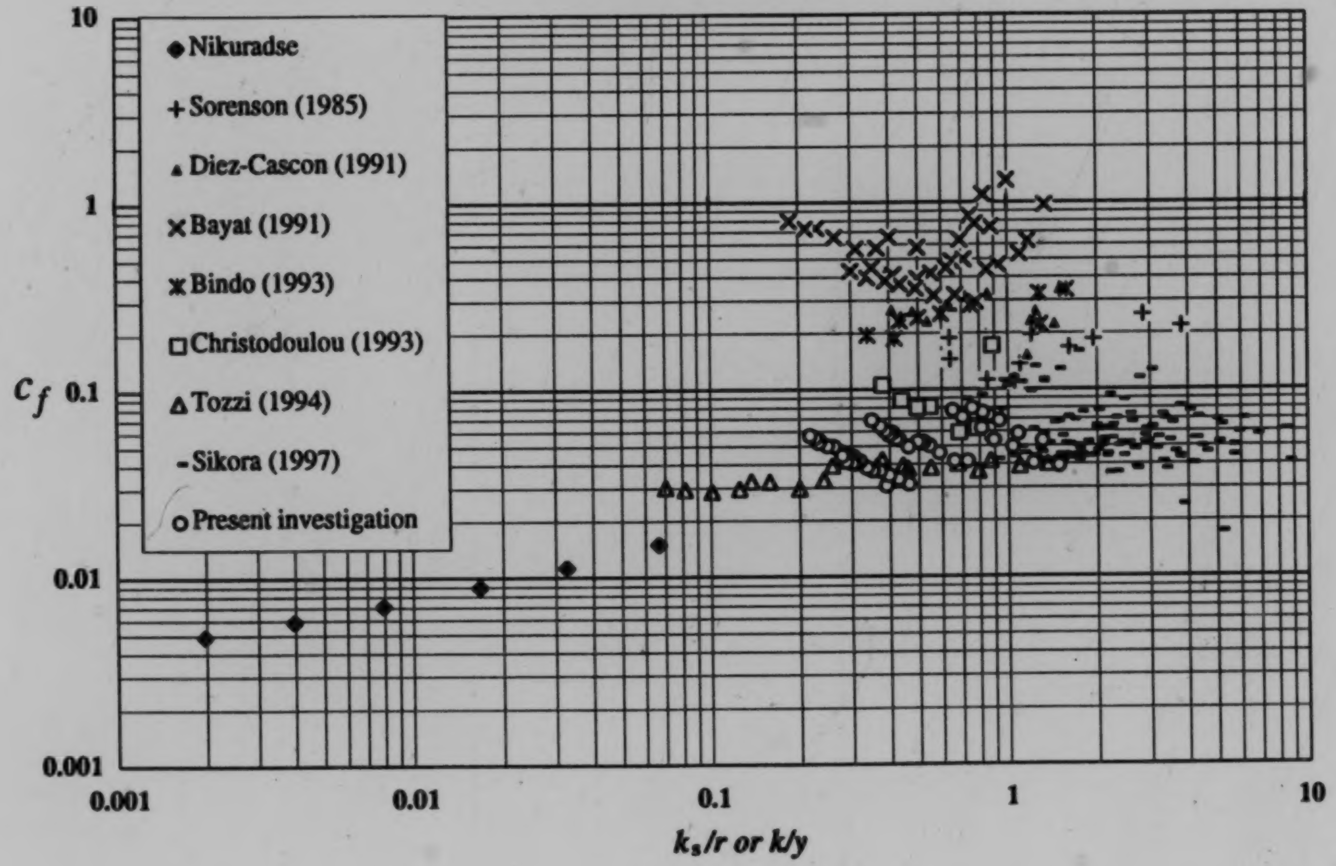

Figure 4.44 Variation of the average skin friction coefficient for the skimming flow in stepped spillways and fishways and pipe flow

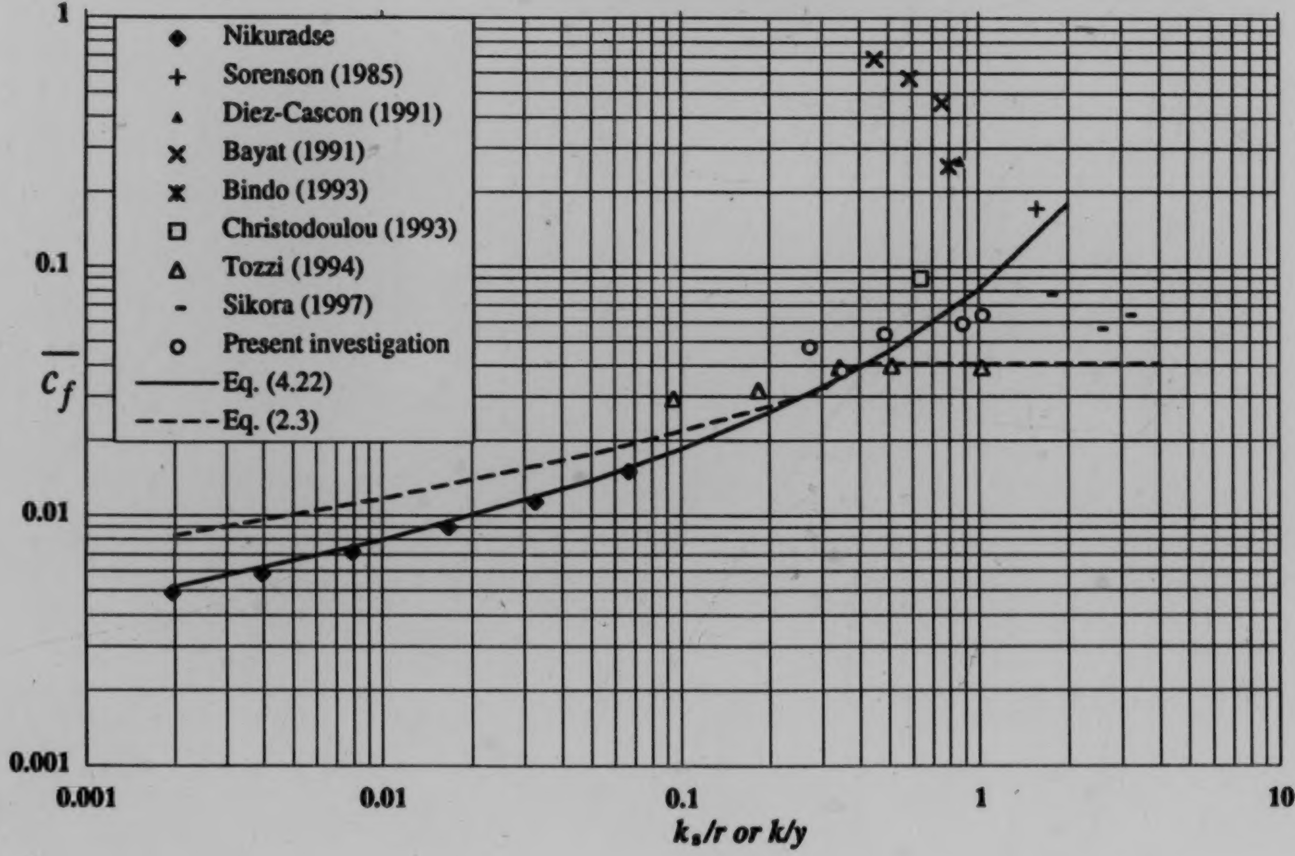

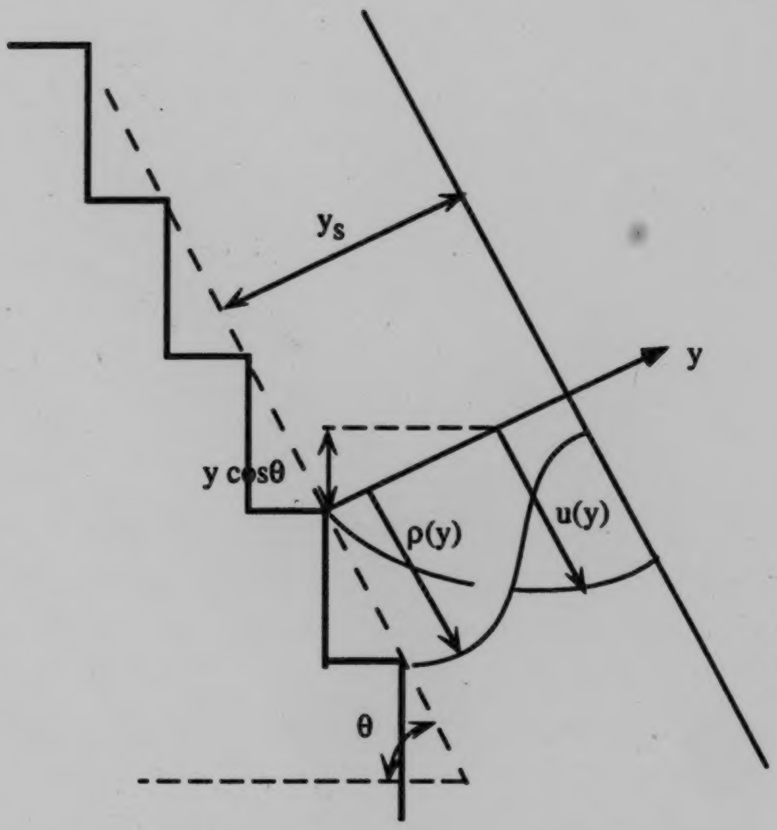
y_s
y
y cosθ
ρ(y)
u(y)
θ

Figure 4.45 A schematic sketch of the flow in the developed region with a varying density and velocity

Figure 4.46 Variation of energy loss with discharge in stepped spillways for various value of step height and slope

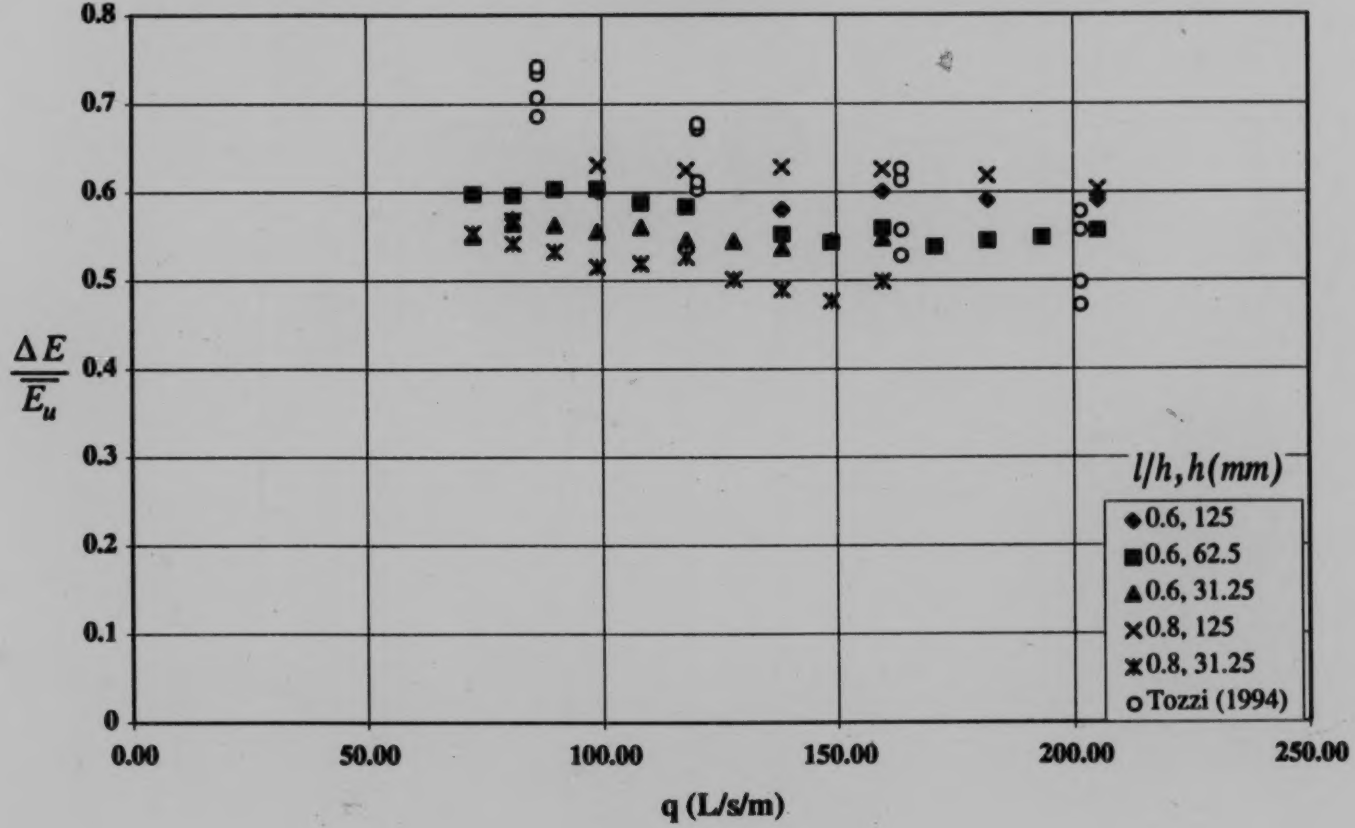

Plate 4.1 Side view of a stepped spillway model featuring the non-aerated region

Plate 4.2 Front view of the stepped spillway model showing that the air entrainment starts earlier at side walls than the central part

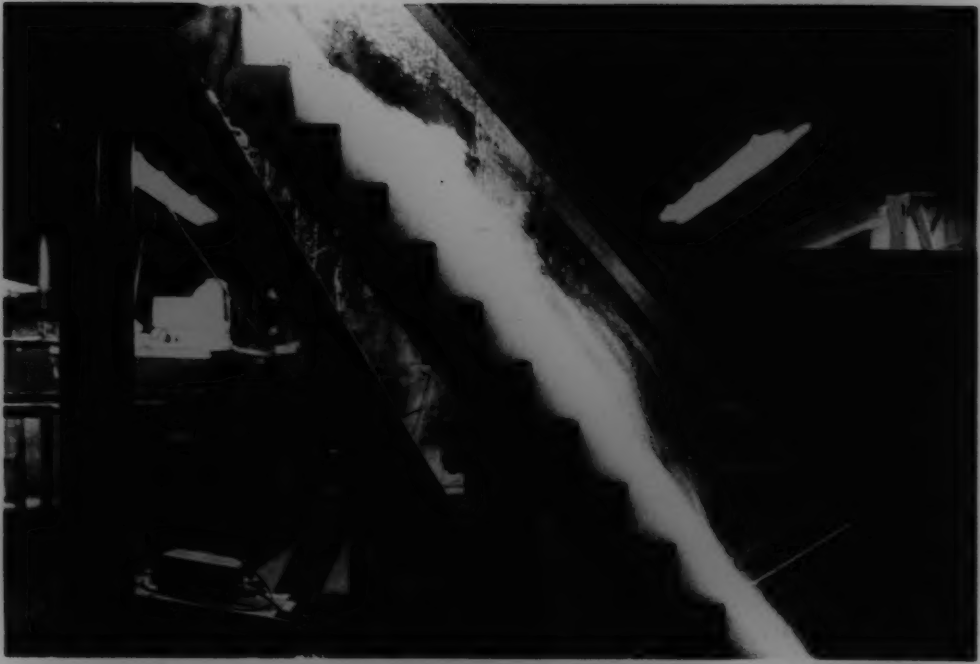

Plate 4.3 The developing region of the skimming flow over a stepped spillway model

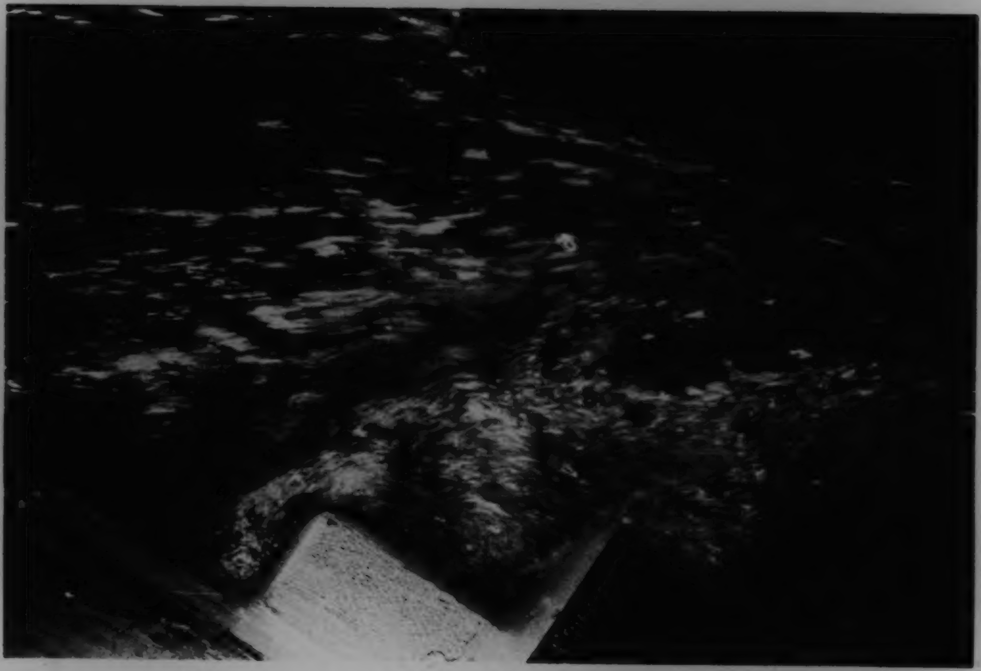

Plate 4.4 A close-up view of the flow in the developing region

Plate 4.5 Side view of the developed region in the skimming flow

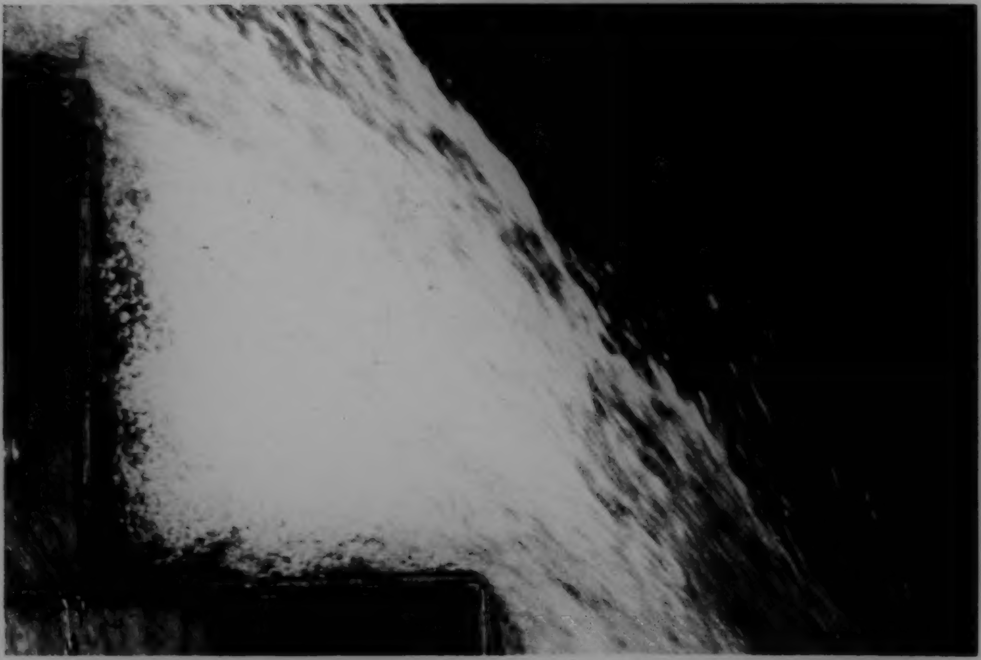

Plate 4.6 A close-up view of the flow in the developed region showing two different zones

(a) frame # 4622

Plate 4.7(a-d) The evolution and termination of the vortex tube at a step tip in the developed region of a skimming flow (l/h= 0.6, h= 125 mm)

Vortex tube base

(b) frame # 4661

(c) frame # 4728

(d) frame # 4742

(a) frame # 607

Plate 4.8(a-b) The varying flow surface in the developed region of the skimming flow (l/h= 0.6, h= 125 mm)

(b) frame # 915

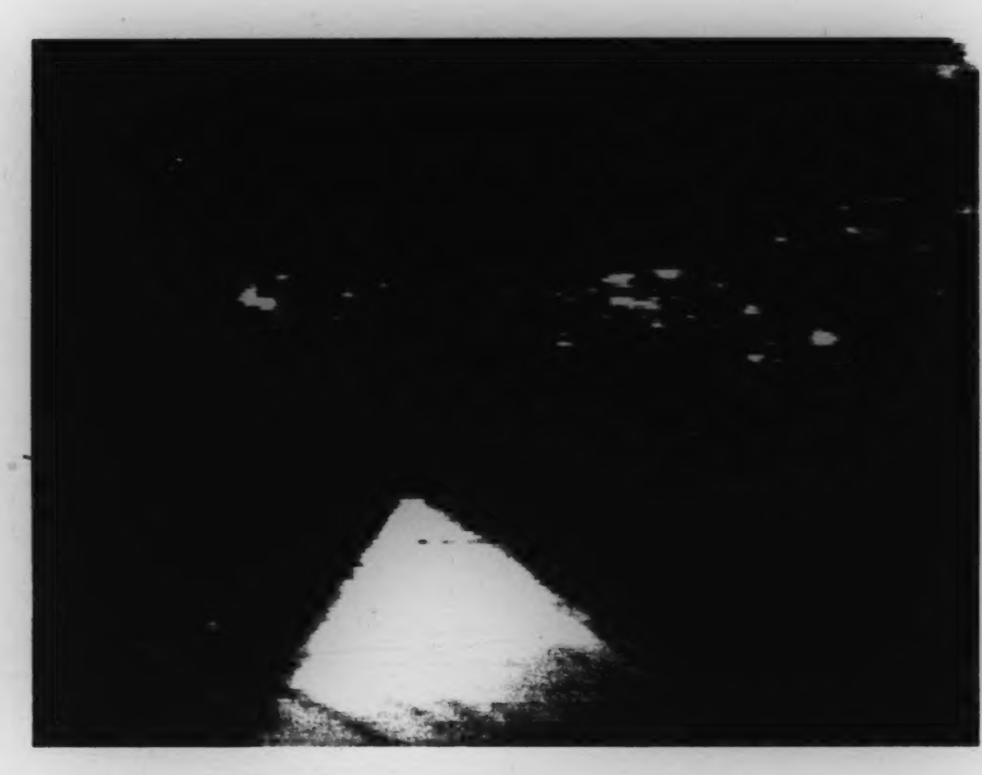

(a) frame # 502

Plate 4.9(a-d) The process of the "rooster tail" formation (l/h= 0.6, h= 125 mm)

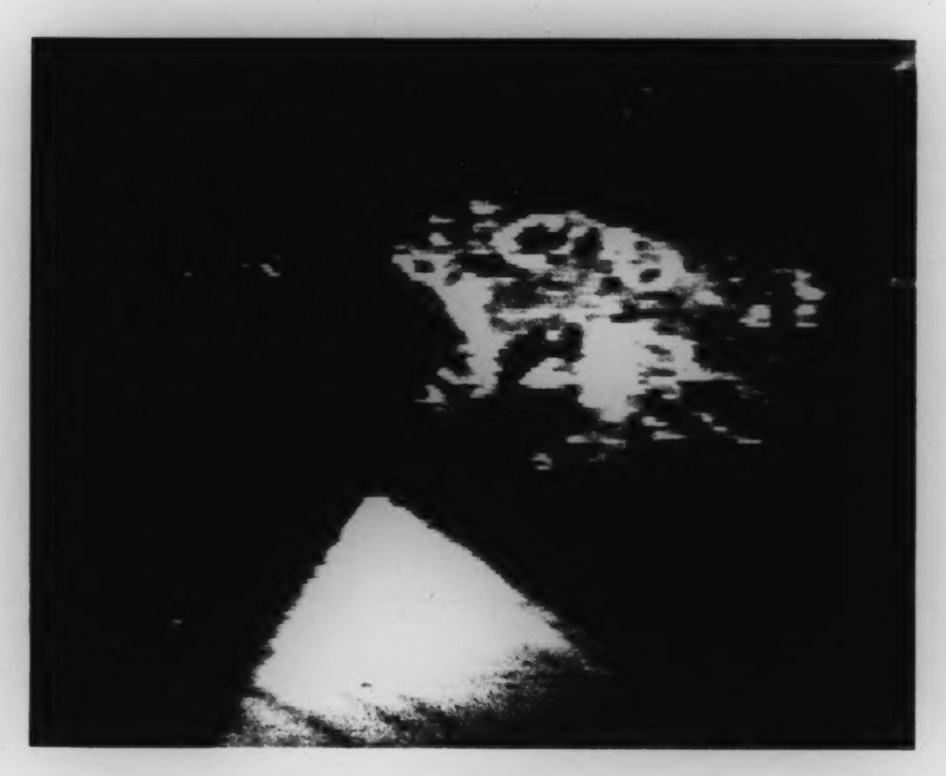

(b) frame # 599

(c) frame # 705

(d) frame # 810

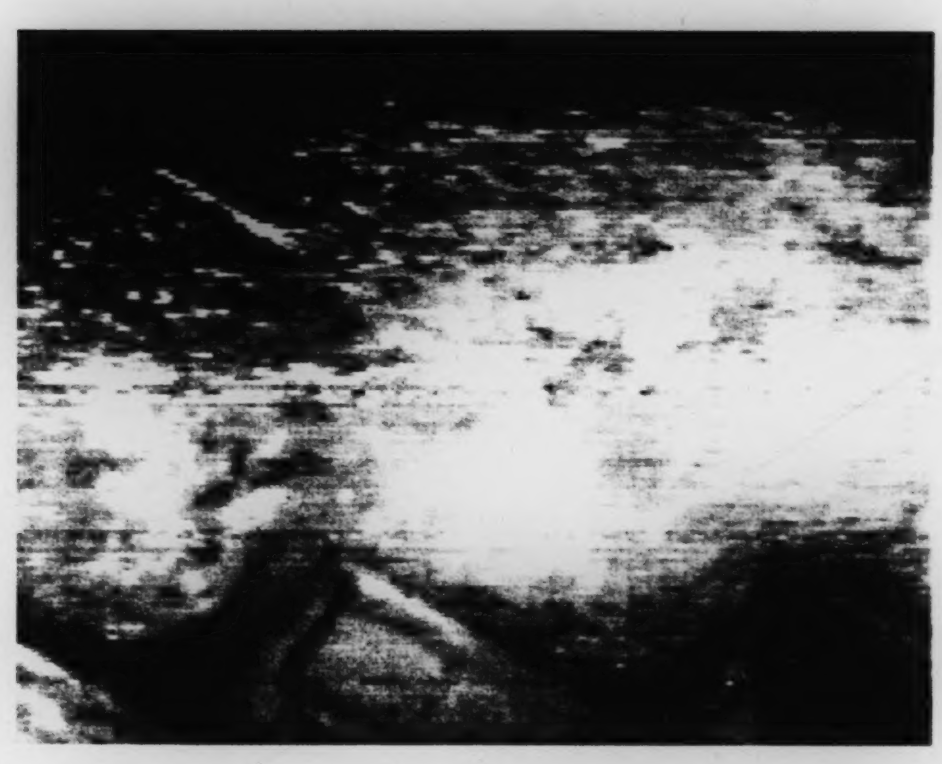

(a) frame # 273

Plate 4.10(a-b) The existence of dark and white cloudlets in the air-water mixture (l/h= 0.6, h= 62.5 mm)

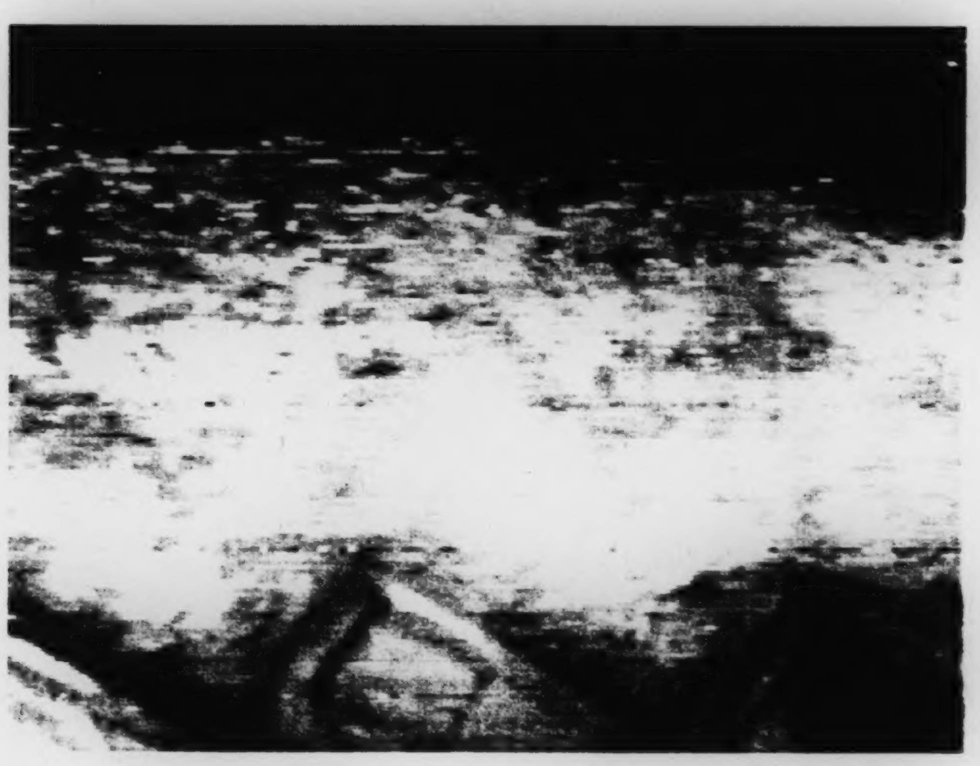

(b) frame # 373

(a) frame # 166

Plate 4.11(a-d) The passage of a dark cloudlet, marked as A, between two consecutive step tips on a streamline (l/h= 0.6, h= 62.5 mm)

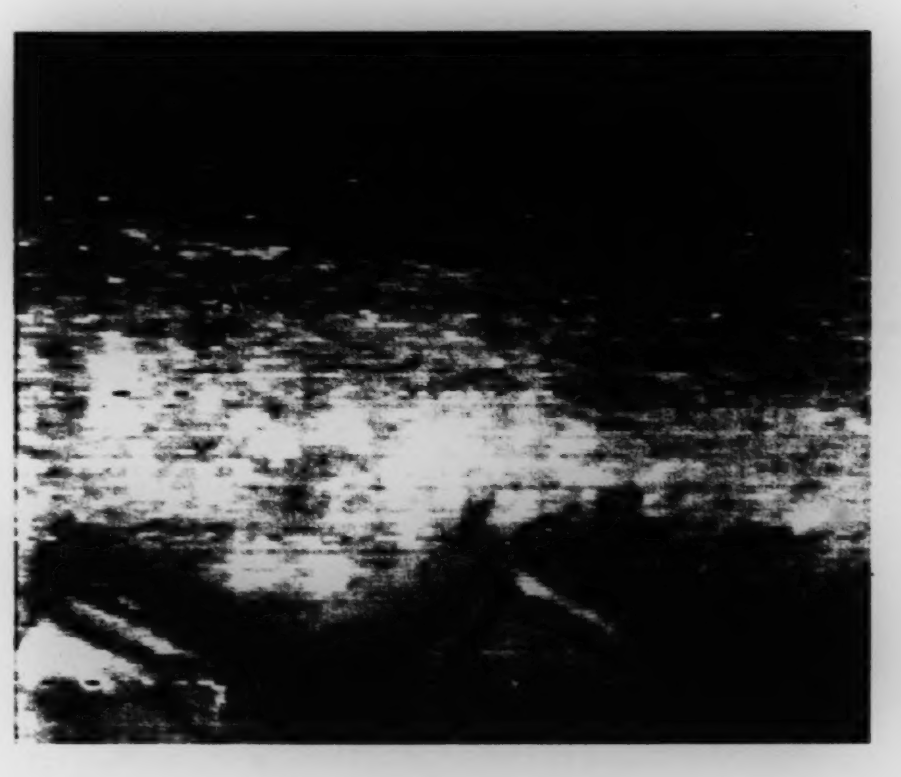

(b) frame # 176

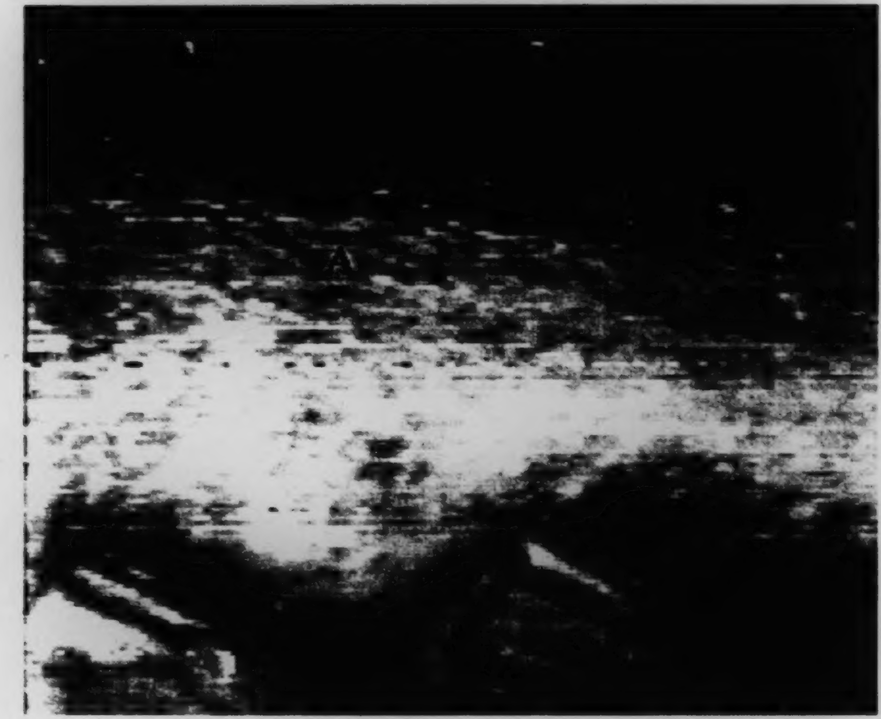

(c) frame # 185

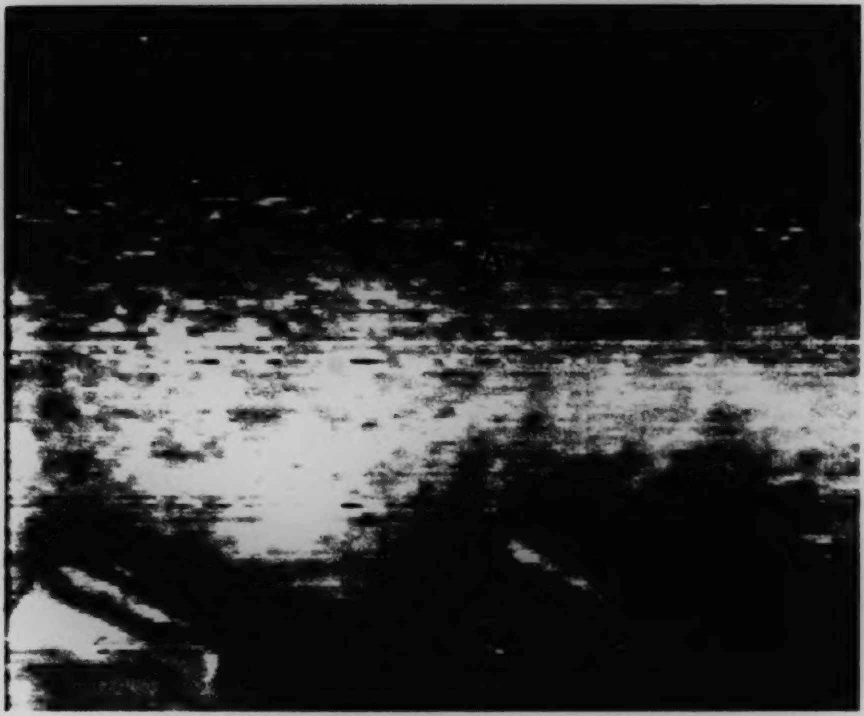

(d) frame # 196

Chapter 5
CONCLUSIONS AND RECOMMENDATIONS

5.1 Summary

A systematic approach to the skimming flow over a stepped spillway is presented in this thesis. A large scale model was constructed to avoid the significant scale effects in the modeling of a stepped spillway. An extensive experimental program was designed to measure the flow characteristics. Most observations were made in the developed region of the skimming flow. The air concentration was measured by an electrical probe constructed for this study and the velocity was measured by the Prandtl tube. Flow visualization was performed with the aid of a high-speed video camera to provide detailed information regarding the vortex structures. The air concentration data was analyzed based on a method developed for the analysis of flow in steep channels.

The skimming flow over a stepped spillway is both complex and varied. The flow is strongly influenced by the roughness elements. The self-aeration phenomenon, which is the entrainment of the air from the atmosphere and the diffusion of this air through the flow, creates a violently agitated stream with an ill-defined free surface. The bulking of the flow and the ejection of water drops are the common features in this type of flow. In the groove of each step, a stable recirculating eddy is formed which is maintained through the transmission of the shear stress of the main flow. Macro-scale vortex structures are also formed at the tips of steps.

A non-aerated region is formed at the upstream end of the spillway where the flow depth decreases. The large bed roughness projections result in a dominant bed generated boundary layer. Due to the experimental limitations, the growth of the boundary layer could not be studied. However, the inception of air entrainment was studied visually. Downstream of the inception point, a developing region is formed where the bulking of flow is caused by air entrainment. The flow characteristics vary with distance along the channel in this region. The air-water mixture in this region has a highly irregular, wavy surface in which the returning water drops ejected from the surface continuously entrained air. After a certain length in the developing region, a condition of equilibrium is reached where flow characteristics do not vary with distance in this region. This region is referred to as the developed region. Two zones within the depth of flow exist in the developed region. In the lower zone of the air-water region, air bubbles are suspended in the water. In the upper zone, water drops are ejected from the stream into the atmosphere.

The point of air inception was studied visually by the aid of a high-speed video camera. The enhancement of the growth of the boundary layer and the deflection of the internal flow by steps causes an early inception of air entrainment. The distance of the inception point from the crest is estimated empirically.

Air concentration profiles in the developed region were established based on the output readings from the electrical air concentration probe. Because of the similarity of flow over stepped spillways to flow in steep channels, the method described by Straub and Anderson is used as a basis for air concentration analysis. The results of the analysis showed a satisfactory agreement with the experimental data. The variation of some characteristic depths were also studied.

An indirect method of obtaining mixture velocity was introduced with the aid of the Prandtl tube measurement and air concentration values. An alternative method was used with the aid of photographic work to check the former method. A reasonable agreement between these two measurement methods was found. The Prandtl-Karman universal velocity distribution was examined for the experimental data. Parameters of the universal velocity distribution were evaluated.

Since the flow in the developed region is uniform, a method was introduced to estimate the skin friction coefficient in this region. The estimated values of the skin friction factor were compared to those obtained by other investigations on stepped spillways, pipe and fishways.

It was deduced that two main features contribute to the energy loss in stepped spillways. These include the recirculating fluids in the grooves of steps and vortex structures at the tips of steps. Values of energy loss for the present study as well as other investigations show a considerable energy loss.

5.2 Conclusions

The present study is the first major attempt to provide detailed information regarding flow characteristics of skimming flow over stepped spillways. A large model was constructed to avoid scale effects and to simulate prototype condition where significant air entrainment is expected. Such detailed observations had not been produced before.

Parameters that influence the air inception have been identified. The distance of the inception section of air entrainment from the crest for a stepped spillway was found to be smaller than that for a standard spillway. This indicates that steps enhance the flow turbulence. An empirical equation was derived to estimate the distance of the air inception section from the crest.

Air concentration profiles were obtained in the developed region. A method used to analyze the air concentration distribution showed a satisfactory agreement with the experimental data. It was found that stepped spillways entrains more air than chute spillways. This could reduce cavitation and associated erosion.

Velocity profiles were obtained in the developed region. The results of velocity measurements by two methods showed a reasonable agreement between these method findings. The Prandtl-Karman universal velocity profile was examined for the experimental data. It was shown that the logarithmic velocity profile exists for the entire experimental data in the lower zone of the flow depth in the developed region.

A reliable correlation was established to estimate the skin friction coefficient for the skimming flow based on the present study and results from other investigations. This relation can be used for a wide range of flow roughnesses.

The flow characteristics that influence the energy loss in stepped spillways have been identified. Estimations of energy loss for the present investigation showed that the skimming flow dissipates less energy than the jet flow.

5.3 Recommendations

- The growth of the turbulent boundary layer in the non-aerated region and the effect of roughness elements on the enhancement of this growth needs to be studied.
- The flow structures around the point of air inception should be studied more closely to identify the mechanism of air entrainment. A high-speed video camera that can provide images of 1/5000 second is most suited for this purpose.
- The mechanism of the self-aerated flow in the developed region should be investigated to understand the entrainment of the air and the diffusion process through the flow depth.
- A larger range of flow conditions should be examined to investigate a wider variation of flow characteristics.

- The turbulence components of velocities need to be measured. Non-intrusive methods such as LDA are most suitable for this purpose and will provide valuable insight into the flow characteristics.
- The velocity profile in the upper zone of the flow depth in the developed region needs to be analyzed.

REFERENCES

ASCE Task Committee on Air Entrainment in Open Channels Committee on Hydromechanics, "Aerated Flow in Open Channels". Journal of the Hydraulic Division, ASCE, Vol. 87, No. HY3, 1961, pp 73-82.

Beitz, E., and Lawless, M., "Hydraulic Model Study for Dam on GHFL 3791 Isaac River at Burton Gorge". Water resources Commission Report, Reference No. REP.24.1, 1992, Brisbane, Australia.

Bendat, J. S., and Piersol, A G., "Random Data: Analysis and Measurement Procedures". John Wiley & Sons Inc., 1971.

Bindo, M., Gautier, J., and Lacroix, F., "The Stepped Spillway of M'Bali Dam". Journal of International Water Power and Dam Construction, Vol. 45, 1993, pp 35-36.

Campbell, F. B., Cox, R. G., and Boyd, M. B., "Boundary Layer development and Spillway Energy Losses". Journal of the Hydraulic Division, ASCE, Vol. 91, No. HY3, 1965, pp 149-163.

Chamani, M., and Rajaratnam, N., "Jet Flow on Stepped Spillways". Journal of Hydraulic Engineering, ASCE, Vol. 120, No.2, 1994, pp 254-259.

Chanson, H., "Stepped Spillway Flows and Air Entrainment". Canadian Journal of Engineers, Vol. 20, 1993, pp 422-435.

Chanson, H., "Hydraulics of Skimming Flows Over Stepped Channels and Spillways". Journal of Hydraulic research, Vol. 32, No. 3, 1994, pp 445-460.

Chanson, H. , "Hydraulic Design of Stepped Cascades, Channels, Weirs and Spillways". Elsevier Science Ltd., Oxford, England, 1994.

Christodoulou, G. C., "Energy Dissipation on Stepped Spillways". Journal of Hydraulic Engineering, ASCE, Vol. 119, No. 5, 1993, pp 644-649.

Diez-Cascon, J., Blanco, J. L., Revilla, J., and Garcia, R., "Studies on the Hydraulic Behavior of Stepped Spillways". Journal of International Water Power and Dam Construction, Vol. 43, 1991, pp 22-26.

Dunstan, M. R. H., "A Review of Roller Compacted Concrete Dams in the 1980s". Journal of International Water Power and Dam Construction, Vol. 42, 1990, pp 43-45.

Ehrenberger, R., "Wasserbewegung inSteilen Rinnen (Schuss Tennen) mit besonderer Beruksichtigung der Selbstbeluftung". Zeitschrift des Oesterreichischer Ingenieur-und Architekten-Vereins, Nos. 15, 16, 17, and 18, 1926.

Essery, I. T. S., and Horner, M. W., "The hydraulic Design of Stepped Spillways". CIRIA Report No. 33, 1978, London, UK.

Frizell, K. H., "Hydraulics of Stepped Spillways for RCC Dams and Dam Rehabilitations". Proceedings, Roller Compacted Concrete III, 1992, pp 423-439.

Gangadharaiah, T., and Nagar, S. L. R, "Inception and Entrainment in Self-Aerated Flows". Journal of the Hydraulics Division, ASCE, Vol. 96, No.HY7, 1970, pp 1549-1565.

Halbronn, G., Discussion of Bauer (1954). Transactions, ASCE, Vol. 119, Paper 2719, 1954, pp 1234-1242.

Hansen, K. D., "Built in the USA - RCC Dams of the 1990's". Journal of International Water Power and Dam Construction, Vol. 46, 1994, pp 24-32.

Hickox, G. H., "Air Entrainment on Spillway Faces". Civil Engineering, Vol. 15, No. 12, 1945, pp .

Hino, M., "A theory on the Mechanism of Self-aerated flow on Steep Slope Channels. Applications of the Statistical Theory of Turbulence". Technical Report C-6101, Central Research Institute of Electric Power Industry, Tokyo, 1961.

Horner, M. W., "An Analysis of Flow on Cascades of Steps". Ph.D. thesis submitted to the University of Birmingham, England, 1969.

Kline, S. J., and McClintock, F. A., "Describing Uncertainties in Single-Sample Experiments". Mechanical engineering, Vol. 75, 1953, pp 3-8.

Knight, D. W., and Macdonald, J. A., "Hydraulic resistance of Artificial Strip Roughness". Journal of the Hydraulics Division, ASCE, Vol. 105, No.HY6, 1979, pp 675-690.

Lamb, O. P., and Killen, J. M., "An Electrical Method for Measuring Air Concentration in Flowing Air-Water Mixtures". Technical Paper No. 2, Series B, St. Anthony Falls hydraulics laboratory, University of Minnesota, Minnesota, U. S., 1950.

Lane, E. W., "Entrainment of air in swiftly flowing water". Civil Engineering, Vol. 9, No. 2, 1939, pp .

Logie, C. V., "Economic Considerations in Selection of a Roller Compacted Concrete Dam". Proceedings of the Symposium sponsored by the Colorado Section and Construction Division of the ASCE in Denver, Colorado, 1985, pp 111-122.

Maxwell, J. C., " A Treatise on Electricity and Magnetism". Oxford, Clarendon Press, UK, 1873.

Michels, V., and Lovely, M., "Some Observations of Air Entrained Flow". Proceedings, Minnesota International Hydraulics Convention, Minneapolis, Minnesota, 1953, pp. 403- 414.

Morris, H. M., "A new Concept of Flow in Rough Conduits". Transactions, ASCE, Vol. 120, 1955, pp 373-410.

Morris, H. M., "Design Methods for Flow in Rough Conduits". Journal of the Hydraulics Division, ASCE, Vol. 85, No. HY7, Paper 2081, 1959, pp. 454-473.

Morris, H. M., "Design Methods for Flow in Rough Conduits". Transactions, ASCE, Vol. 126, Part 1, 1961, pp 454-490.

Parker, J. W., "Economic Factors in Roller Compacted Concrete Dam Construction". Proceedings, Roller Compacted Concrete III, 1992, pp 227-241.

Perry, A. E., Schofield, W. H., and Joubert, P. N., "Rough Wall Turbulent Boundary Layers". Journal of Fluid Mechanics, Vol. 37, Part 2, 1969, pp 383-413.

Peyras, L., Royet, P., and Degoutte, G., "Flow and Energy Dissipation Over Stepped Gabion Weirs". Journal of Hydraulic Engineering, ASCE, Vol. 118, No. 5, 1992, pp 707-717.

Rajaratnam, N., "Skimming Flow in Stepped Spillways". Journal of Hydraulic Engineering, ASCE, Vol. 116, No. 4, 1990, pp 587-591.

Rao Govinda, N. S., and Rajaratnam, N., "On the Inception of Air Entrainment in Open Channel Flows". IAHR, 9th Convention, Dubrovnik, Yugoslavia, 1961, pp 9-12.

Sikora, G. J., "An Experimental Study of the Flow Regimes in Pool and Weir Fishways". Thesis submitted to the University of Alberta, Canada, in partial fulfillment of the requirement for the degree of Ph.D., 1997.

Sorensen, R. M., "Stepped Spillway Hydraulic Model Investigation". Journal of Hydraulic Engineering, ASCE, Vol. 111, No. 12, 1985, pp 1461-1472.

Straub, L. G., and Anderson, A. G., "Experiments on Self-Aerated Flow in Open Channels". Proceedings, ASCE, Vol. 84, No. HY 7, 1958, pp 1890-1 to 1890-35.

Straub, L. G., and Lamb, O. P., "Experimental Studies of Air Entrainment in Open Channel Flow". Proceedings, Minnesota International Hydraulics Convention, Minneapolis, Minnesota, 1953, pp. 425- 437.

Straub, L. G., Killen, J. M., and Lamb, O. P., "Velocity measurement of Air-Water Mixture:. Transaction, ASCE, Vol. 119, 1954, pp 207-220.

Tozzi, M. J., "Residual Energy in Stepped Spillways". Journal of International Water Power and Dam Construction, Vol. 46, 1994, pp 32-34.

Viparelli, M., "The Flow in Flume with 1:1 Slope". Proceedings, Minnesota International Hydraulics Convention, Minneapolis, Minnesota, 1953, pp. 415-423.

Wood, I. R., "Air Entrainment in Free-Surface Flows". IAHR, Hydraulic Structures Design Manual, A. A. Balkema Publishers, Rotterdam, The Netherlands, 1991.

APPENDIX A

AIR CONCENTRATION PROFILES FOR VARIOUS VALUES OF FLOW DISCHARGE, STEP HEIGHT, AND CHANNEL SLOPE

Figure A.1 Concentration profile at step tip #13 in a stepped spillway with l/h=0.6, h= 125. mm (yc/h=0.7)

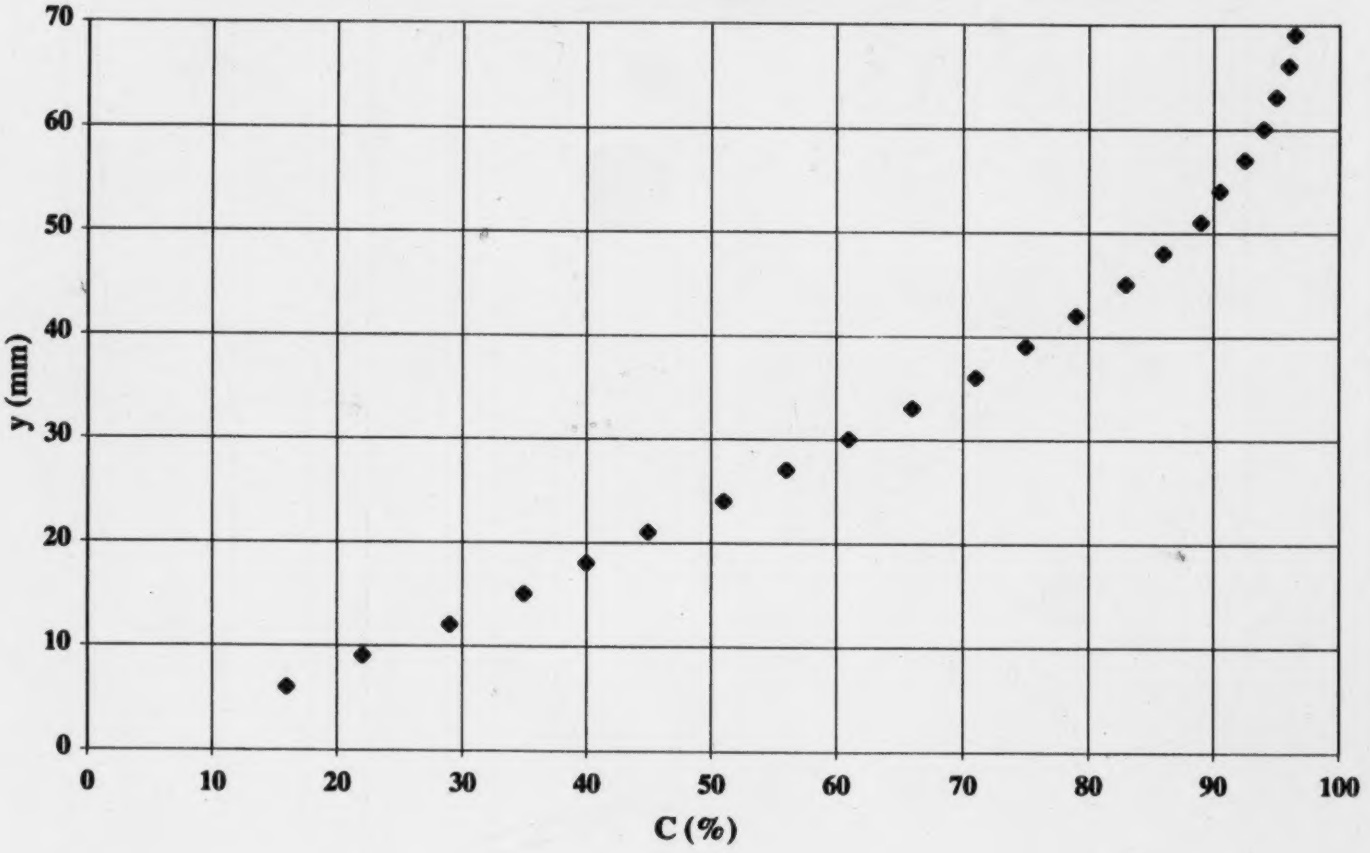

Figure A.2 Concentration profile at step tip #13 in a stepped spillway with l/h=0.6, h= 125. mm (yc/h=0.8)

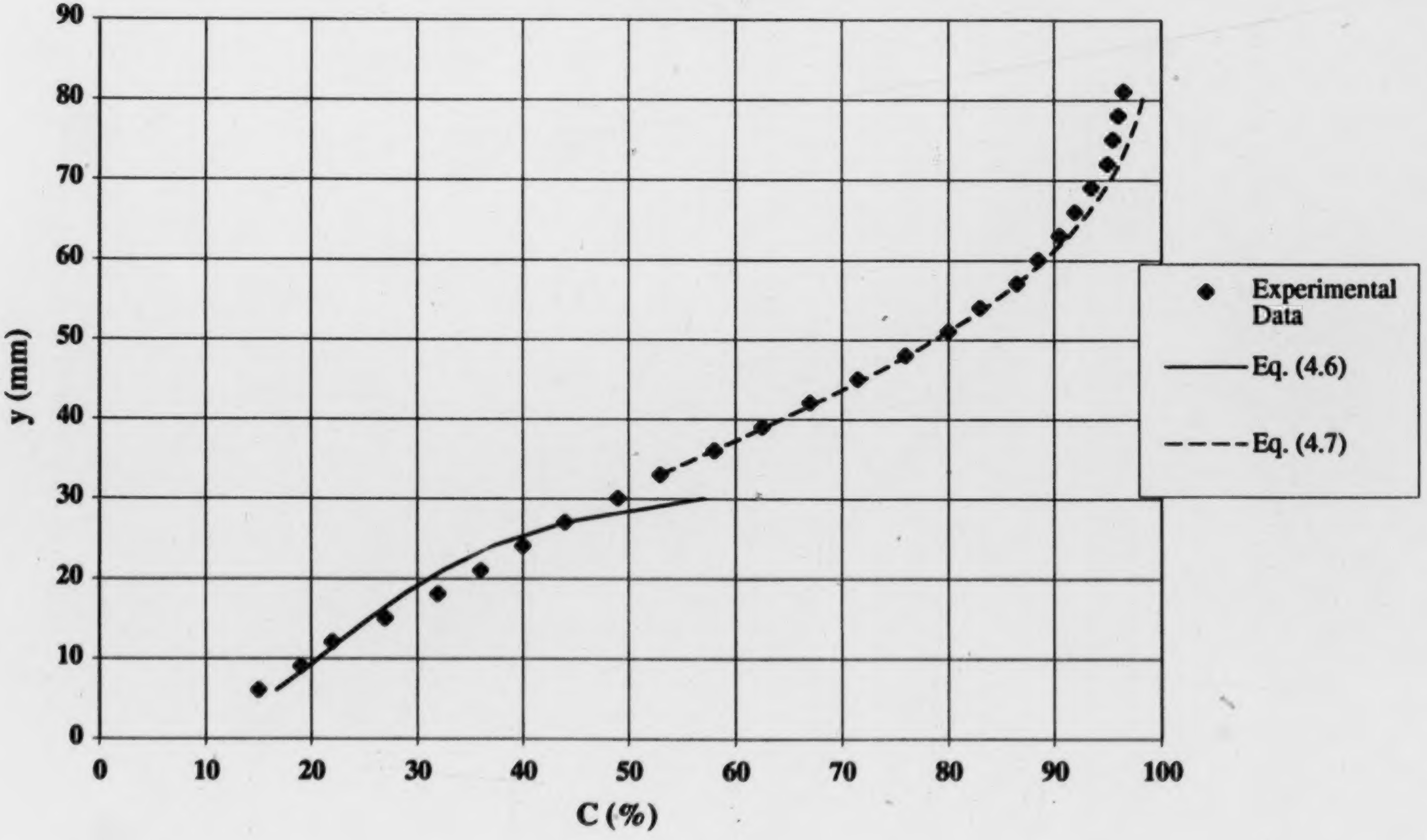

Figure A.3 Concentration profile at step tip #13 in a stepped spillway with l/h=0.6, h= 125. mm (yc/h=1.0)

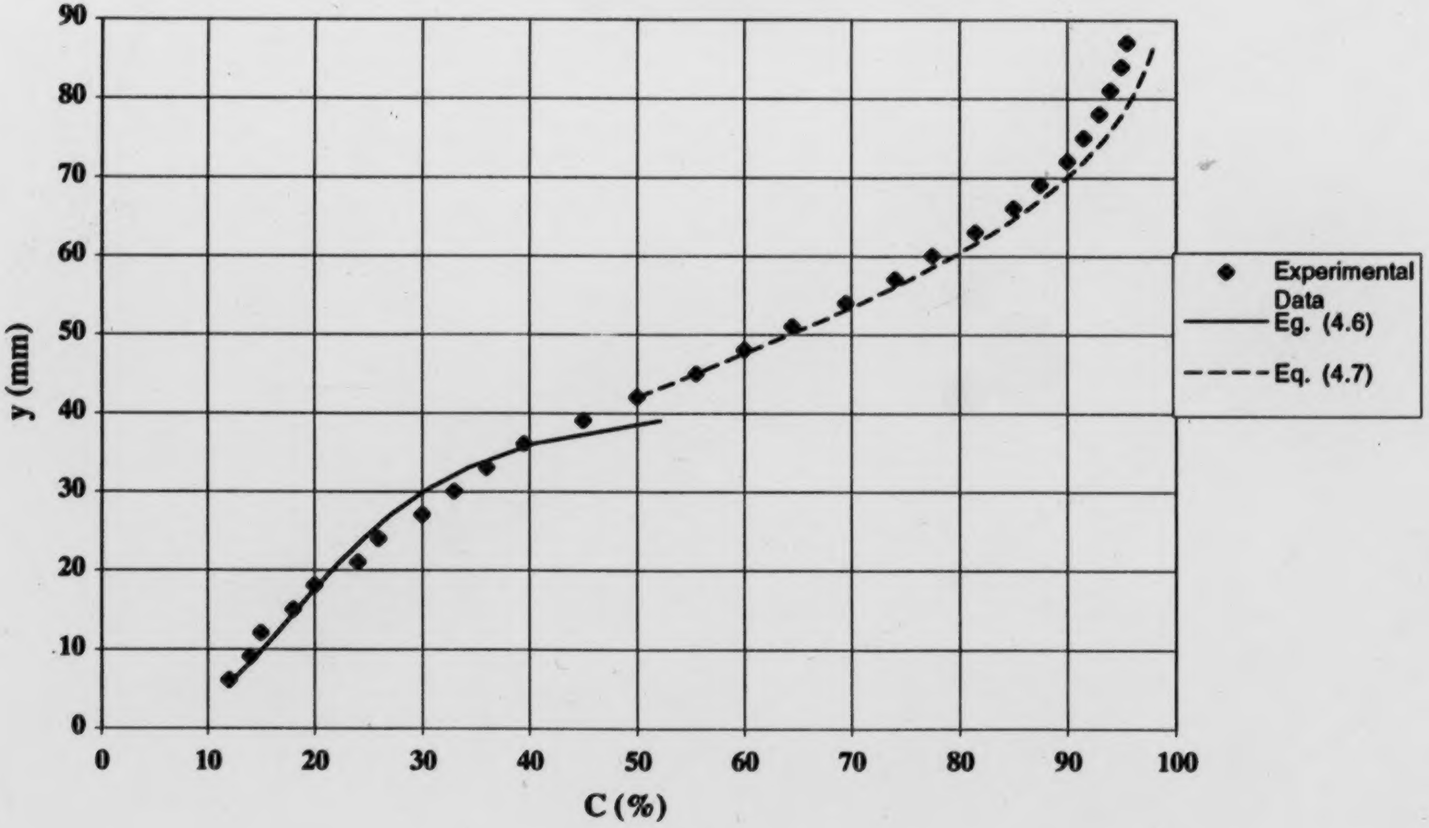

Figure A.4 Concentration profile at step tip #13 in a stepped spillway with l/h=0.6, h= 125. mm (yc/h=1.1)

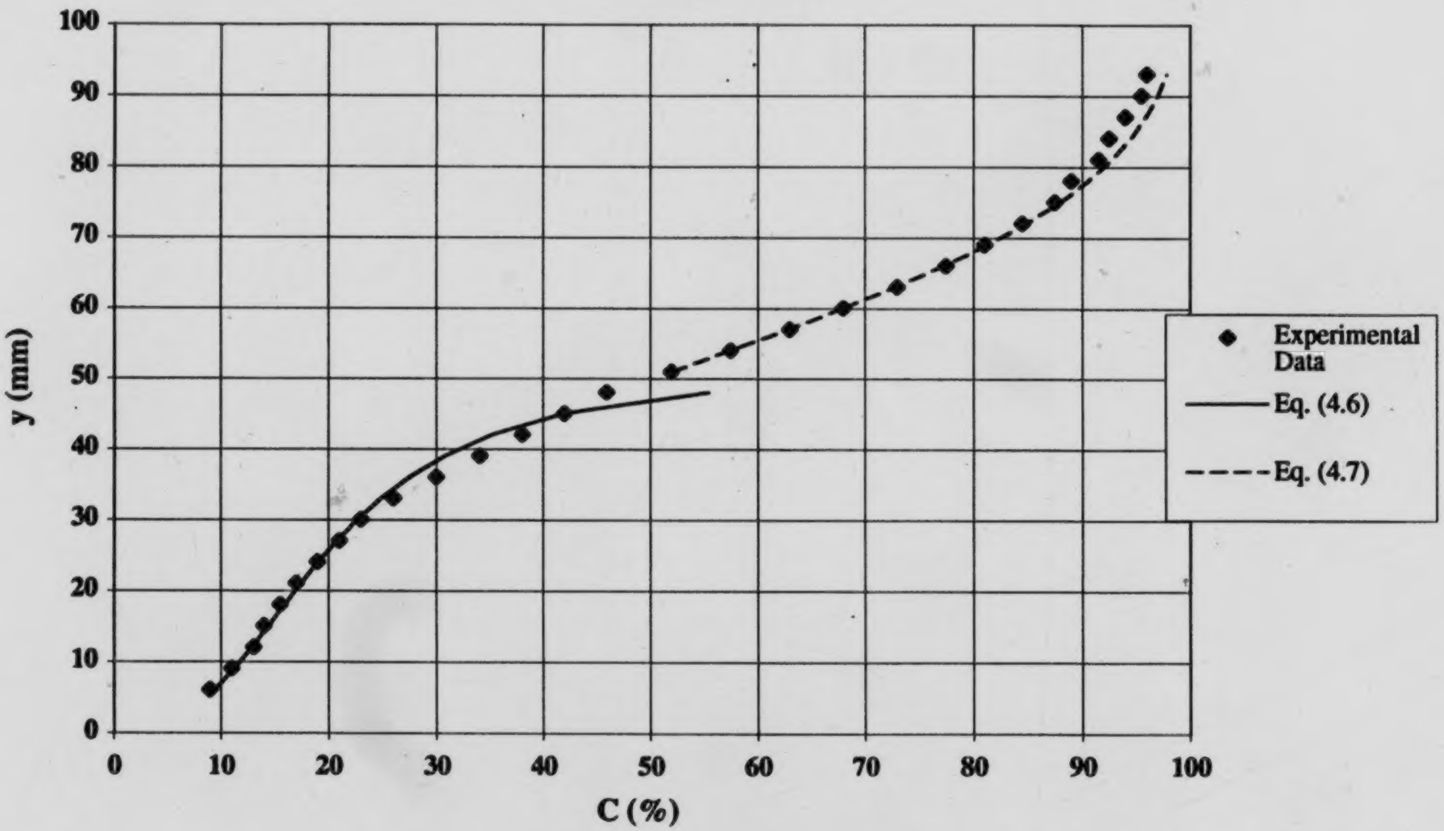

Figure A.5 Concentration profile at step tip #16 in a stepped spillway with l/h=0.6, h= 125. mm (yc/h=1.2)

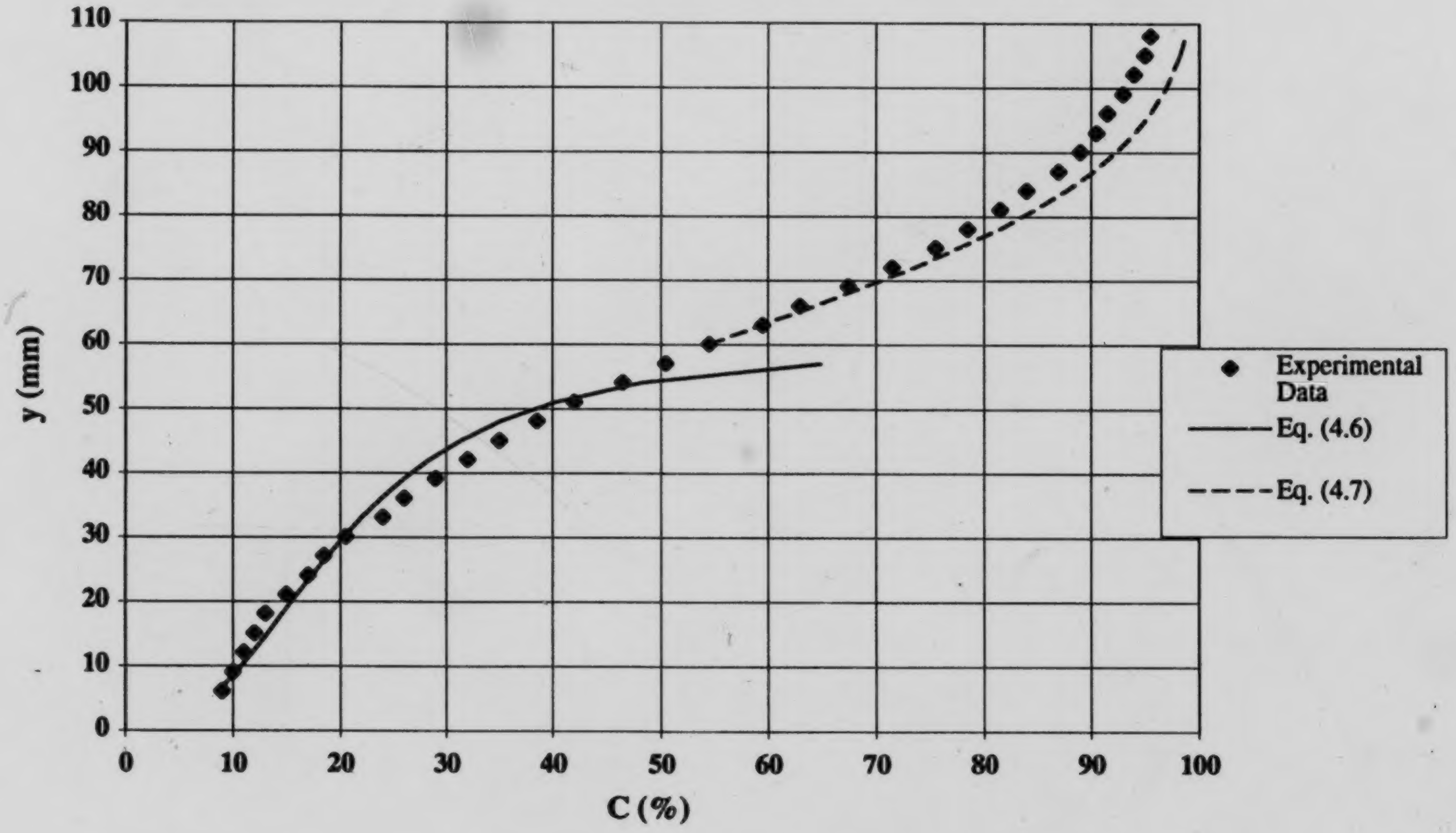

Figure A.6 Concentration profile at step tip #16 in a stepped spillway with l/h=0.6, h= 125. mm (yc/h=1.3)

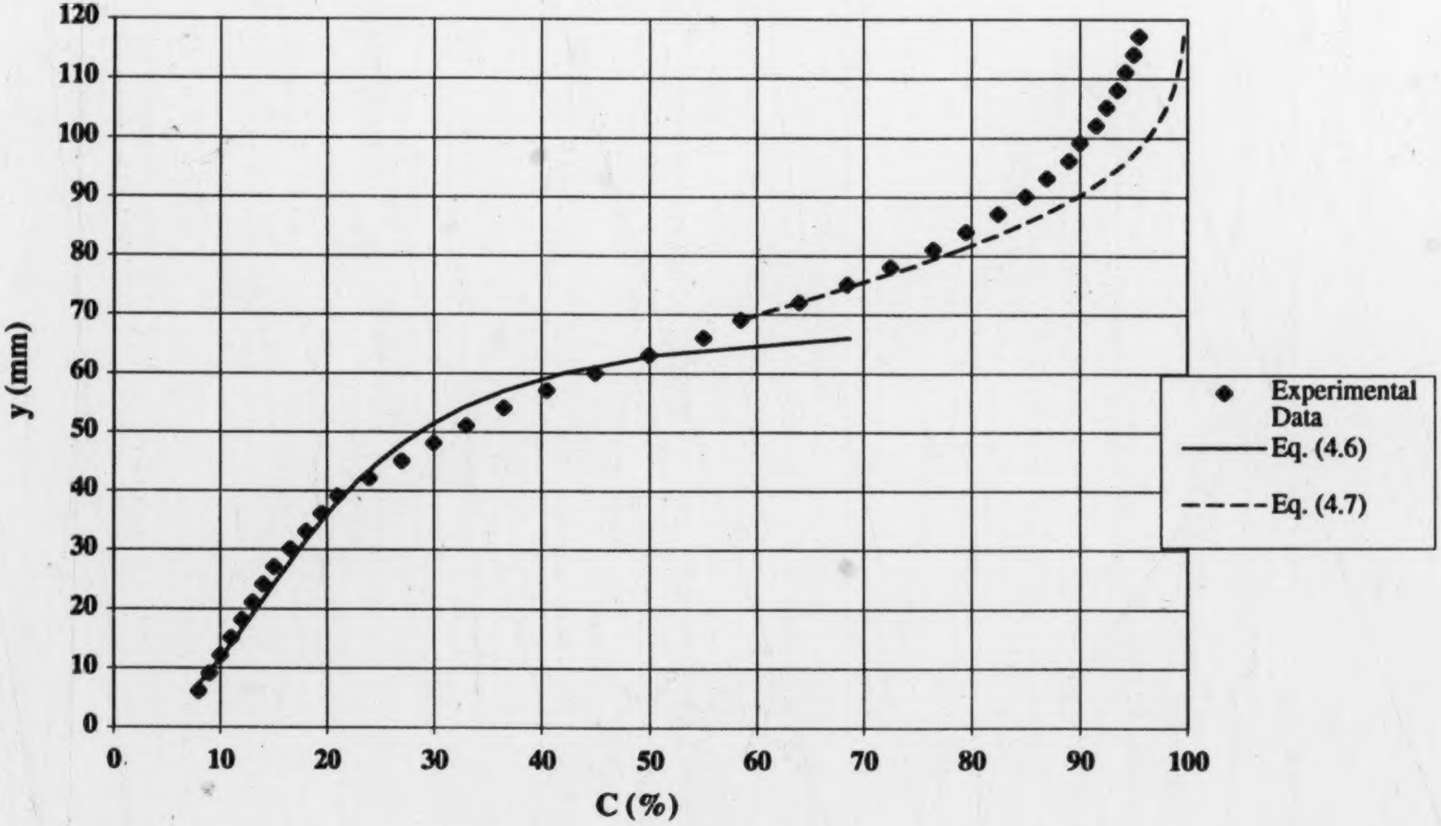

Figure A.7 Concentration profile at step tip #26 in a stepped spillway with l/h=0.6, h= 62.5 mm (yc/h=1.3)

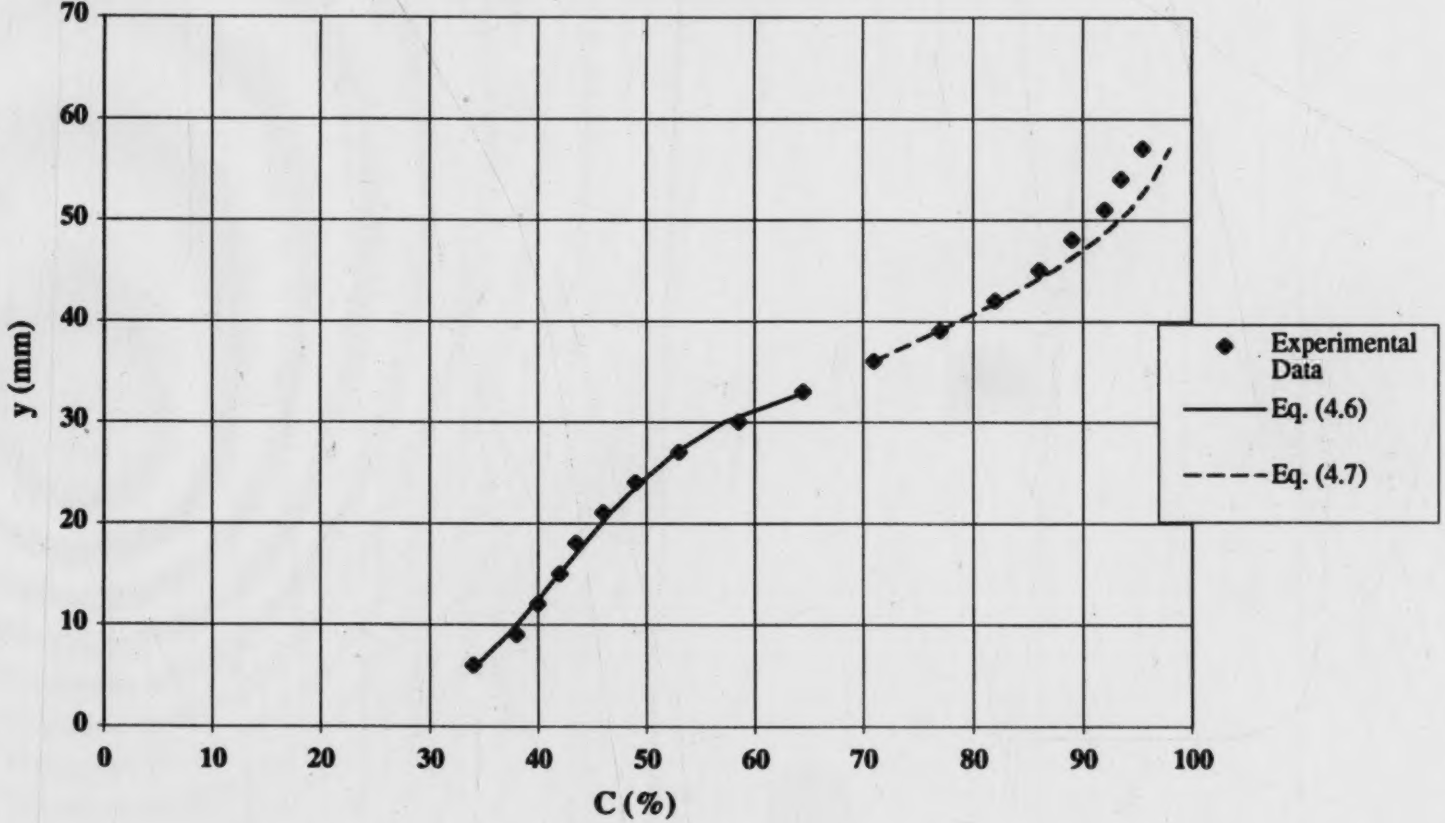

Figure A.8 Concentration profile at step tip #26 in a stepped spillway with l/h=0.6, h= 62.5 mm (yc/h=1.4)

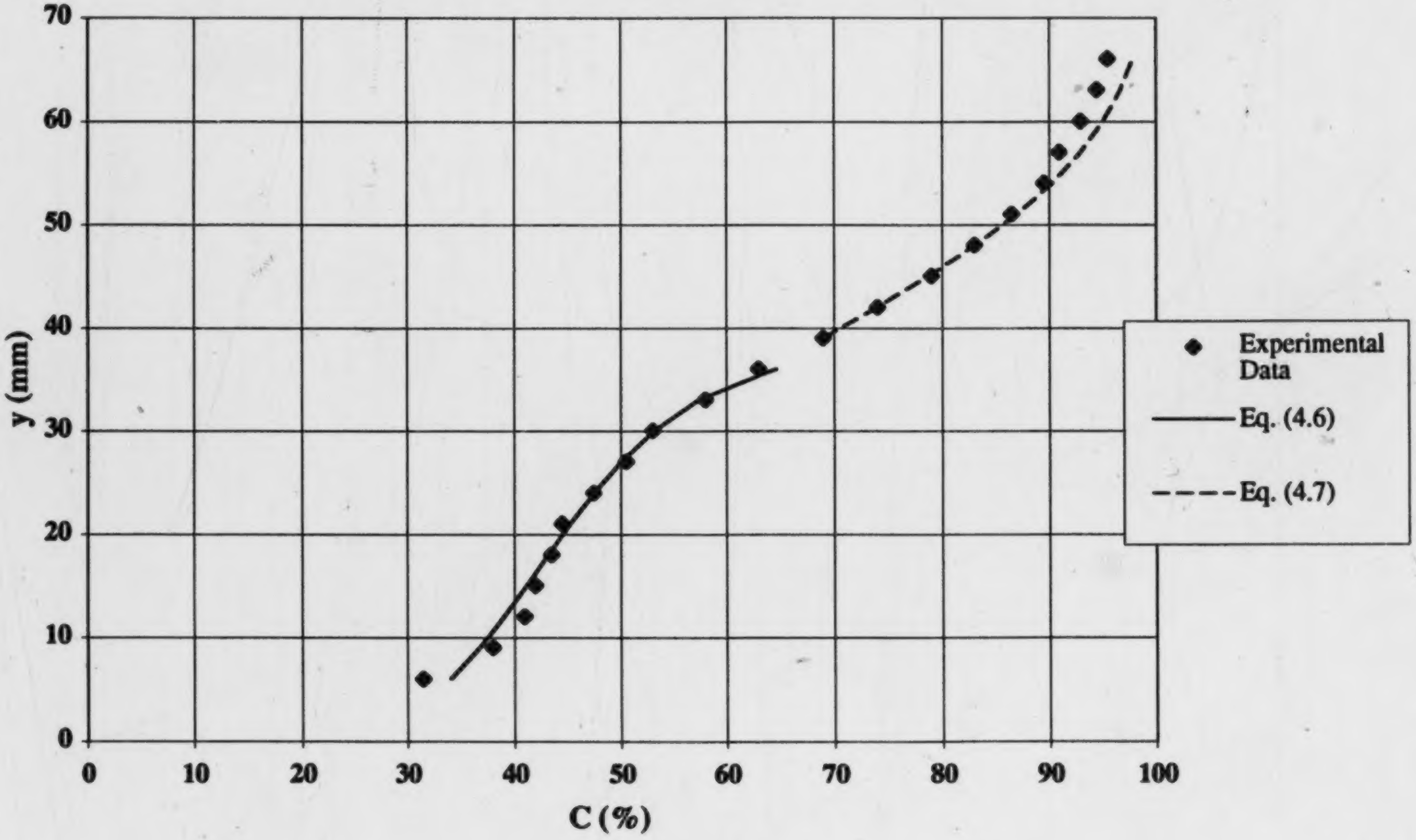

Figure A.9 Concentration profile at step tip #26 in a stepped spillway with l/h=0.6, h= 62.5 mm (yc/h=1.5)

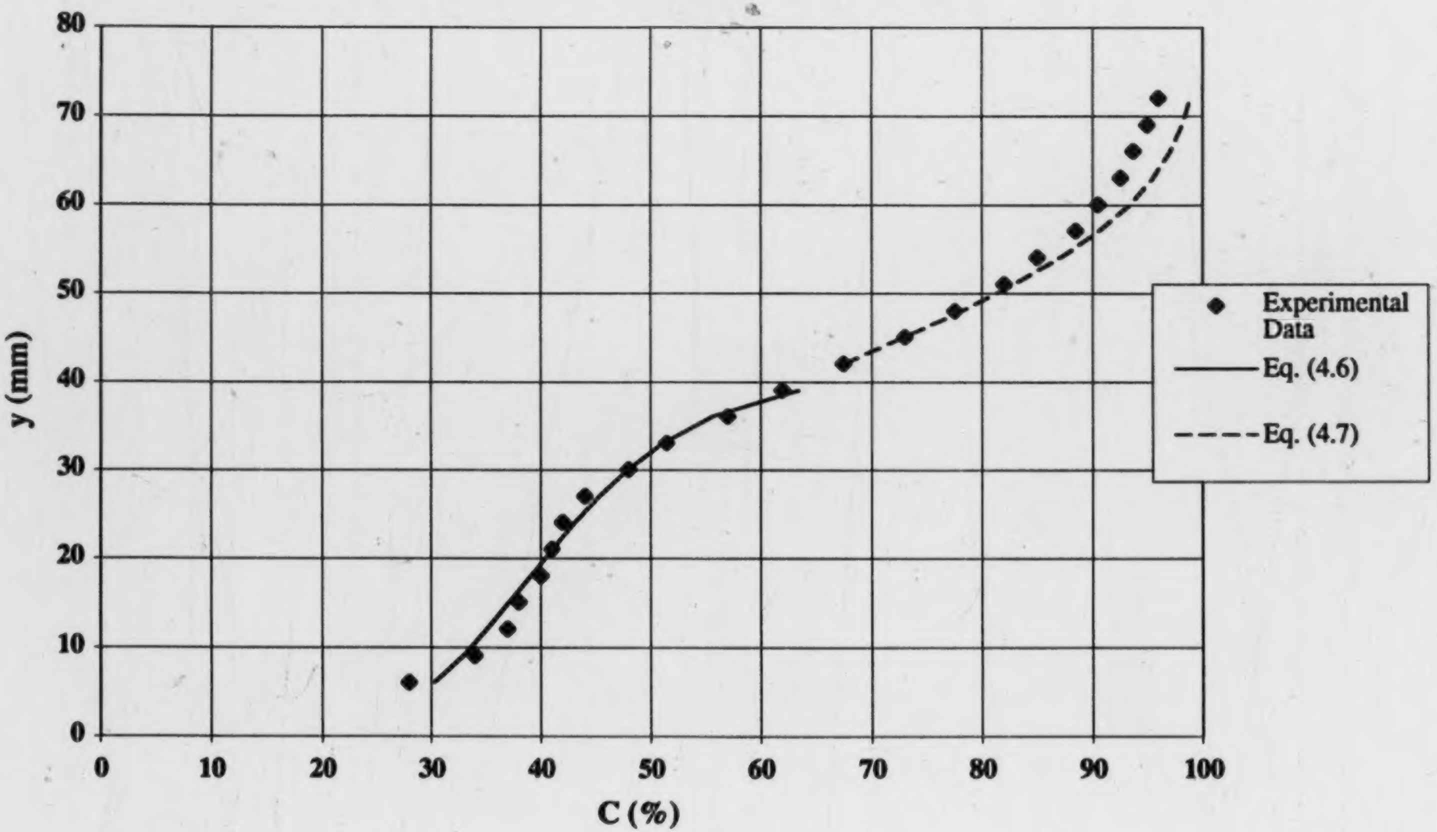

Figure A.10 Concentration profile at step tip #26 in a stepped spillway with l/h=0.6, h= 62.5 mm (yc/h=1.6)

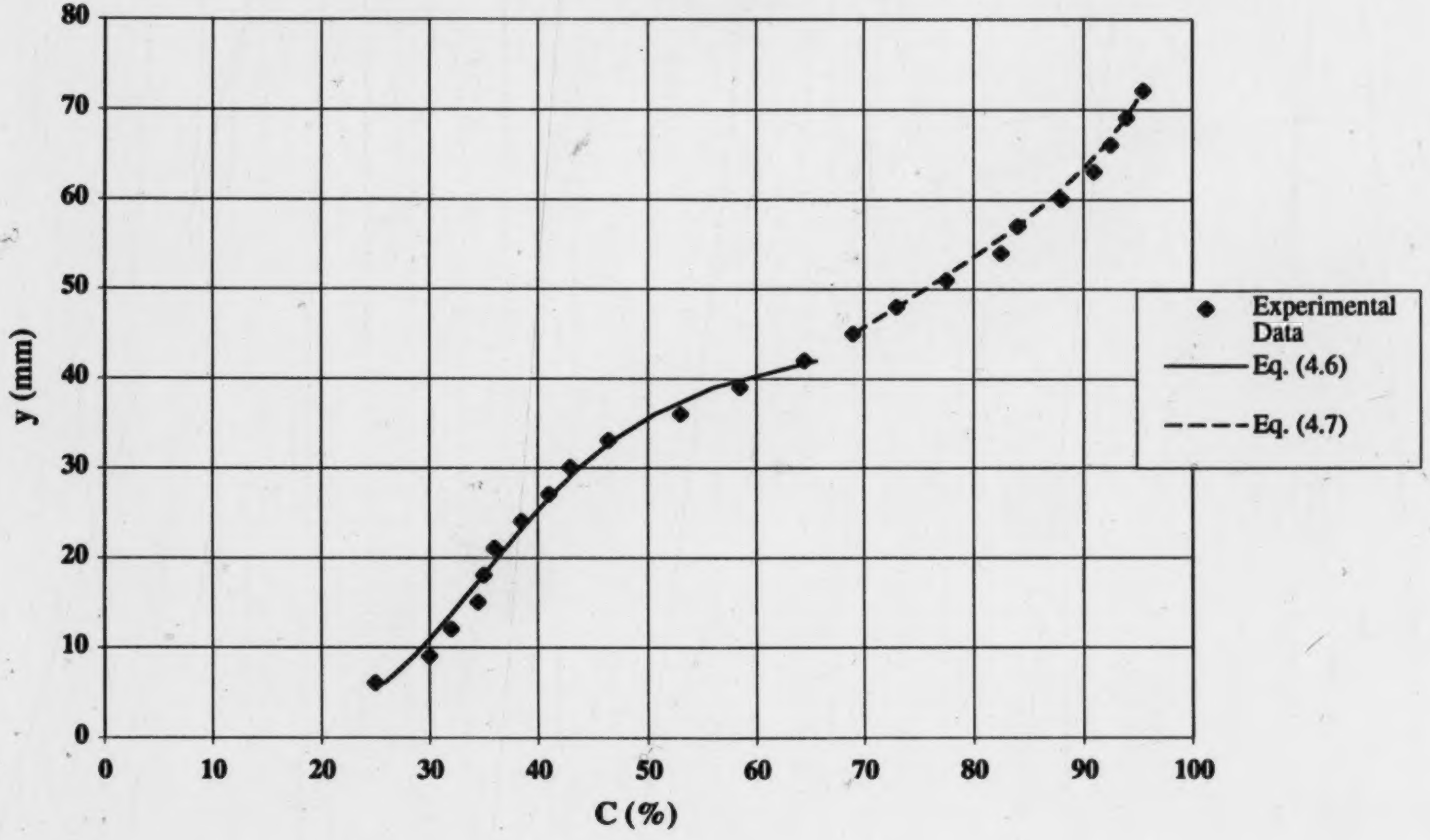

Figure A.11 Concentration profile at step tip #26 in a stepped spillway with l/h=0.6, h= 62.5 mm (yc/h=1.7)

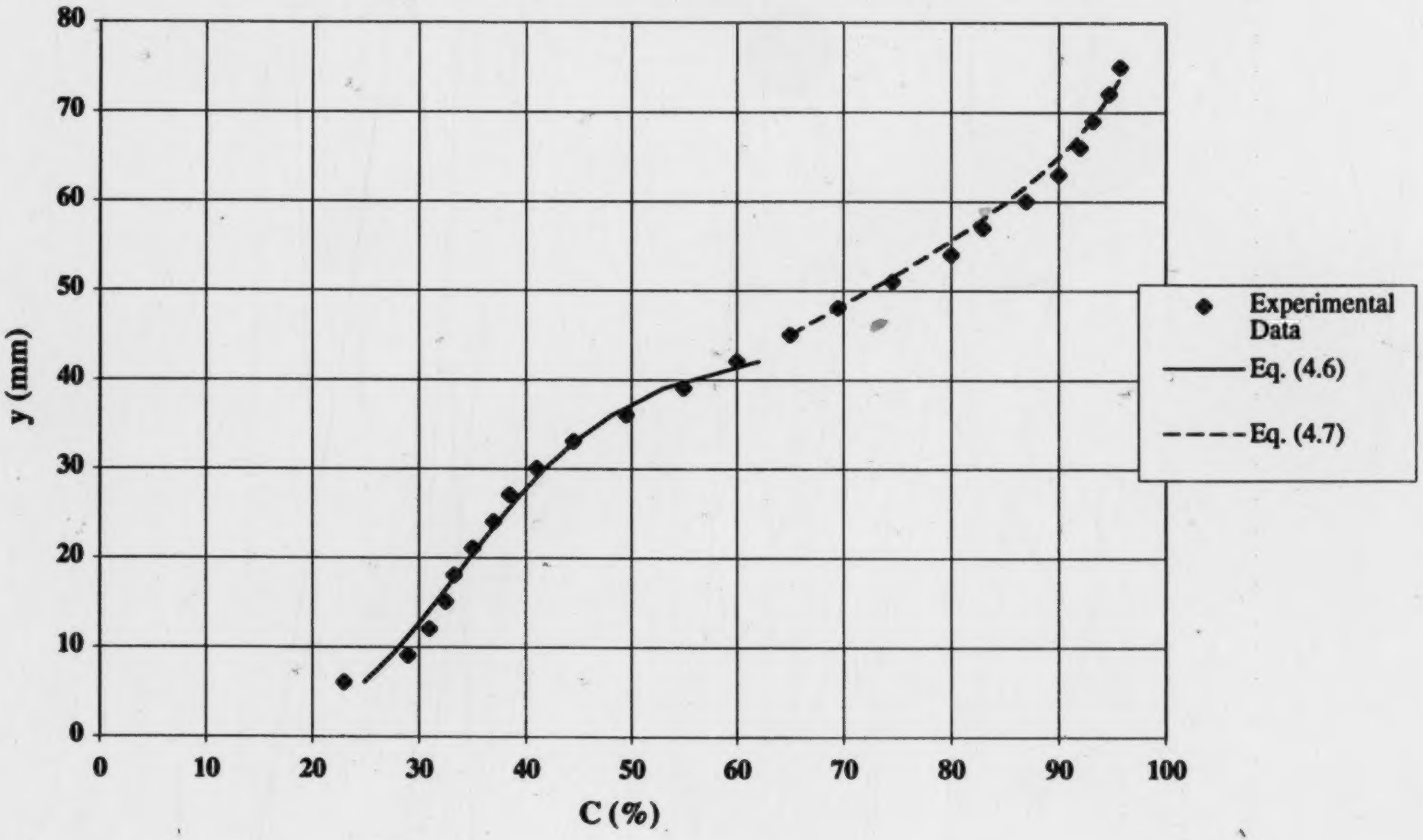

Figure A.12 Concentration profile at step tip #26 in a stepped spillway with l/h=0.6, h= 62.5 mm (yc/h=1.8)

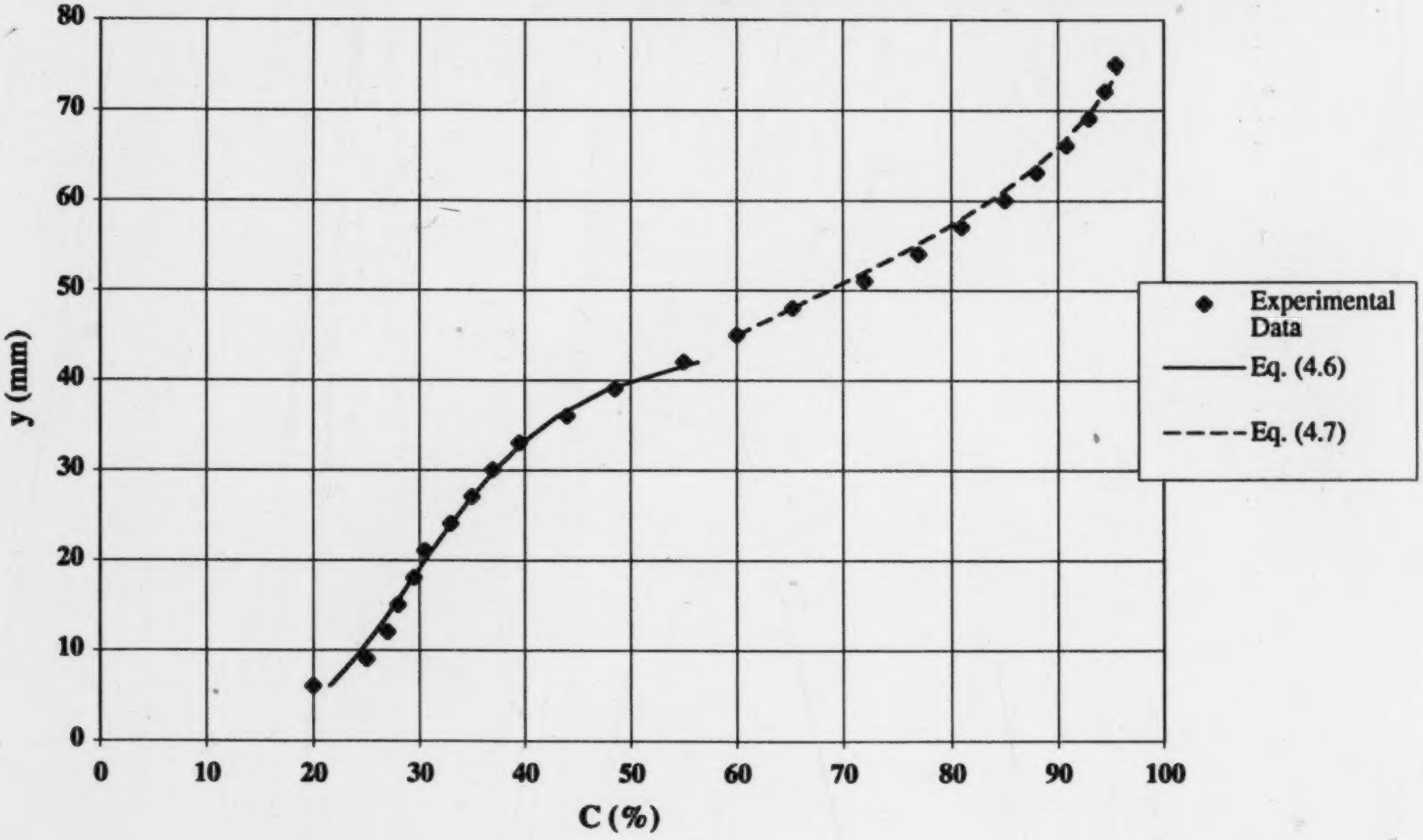

Figure A.13 Concentration profile at step tip #32 in a stepped spillway with l/h=0.6, h= 62.5 mm (yc/h=2.0)

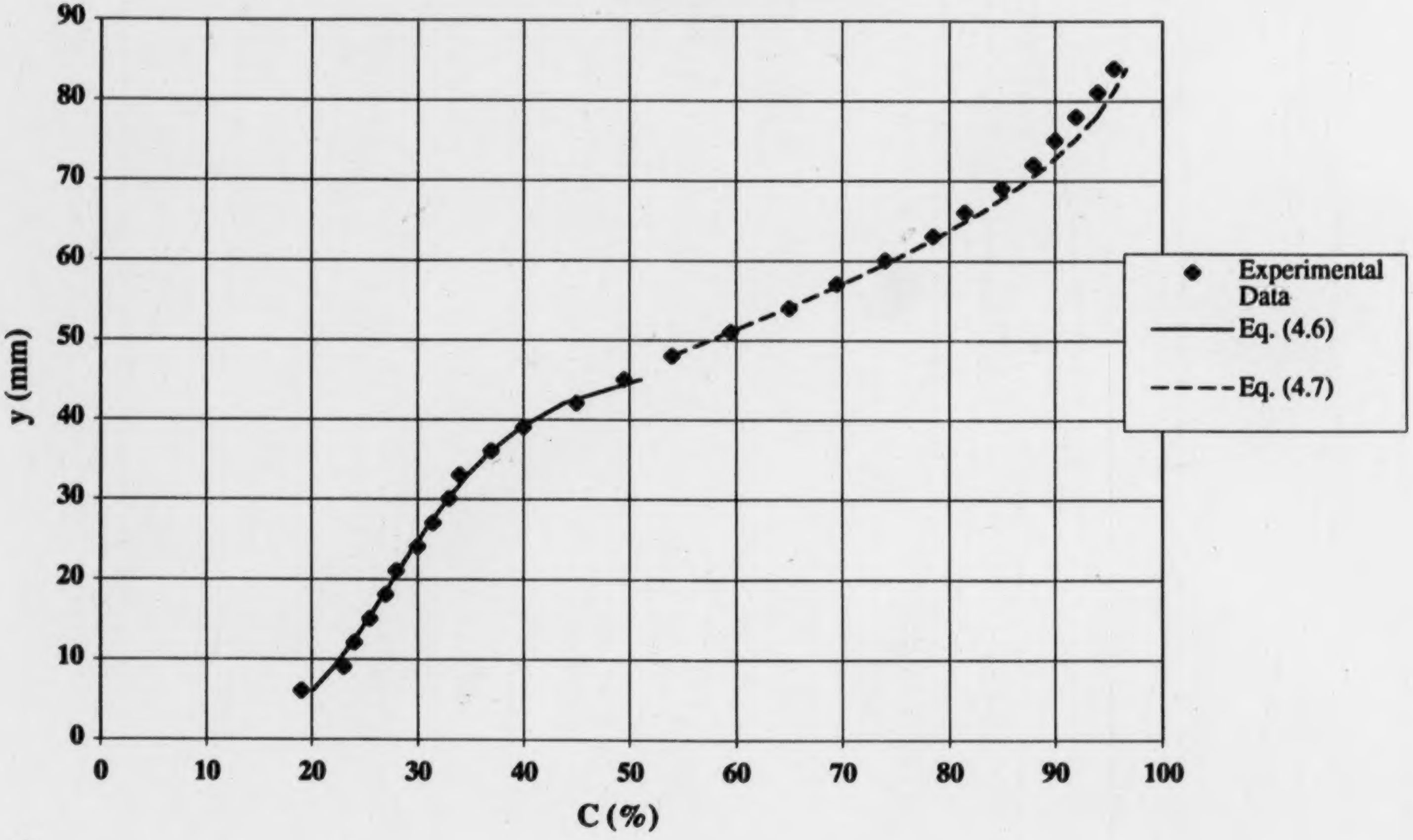

Figure A.14 Concentration profile at step tip #26 in a stepped spillway with l/h=0.6, h= 62.5 mm (yc/h=2.1)

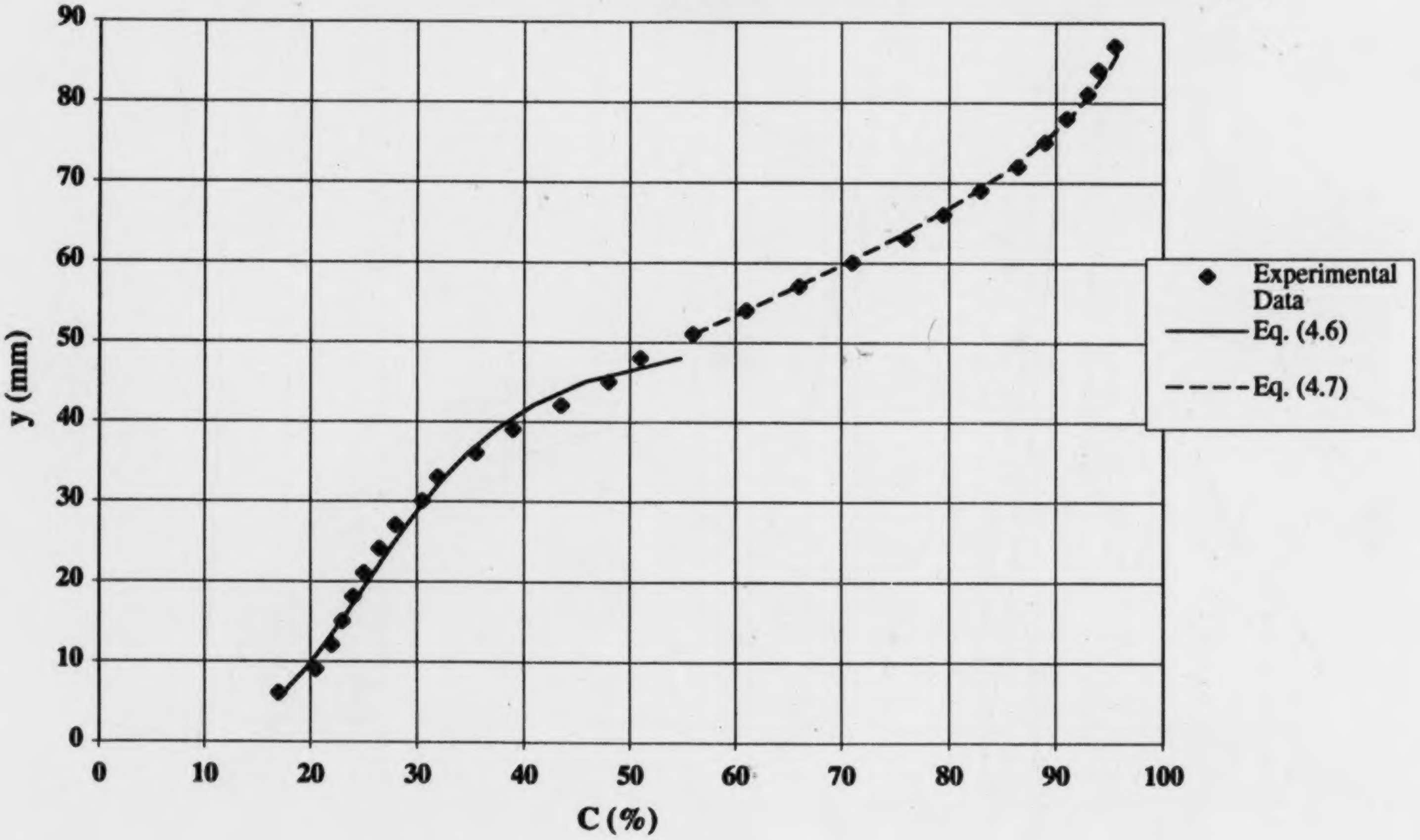

Fig. A.15 Concentration profile at step tip #32 in a stepped spillway with l/h=0.6, h= 62.5 mm (yc/h=2.2)

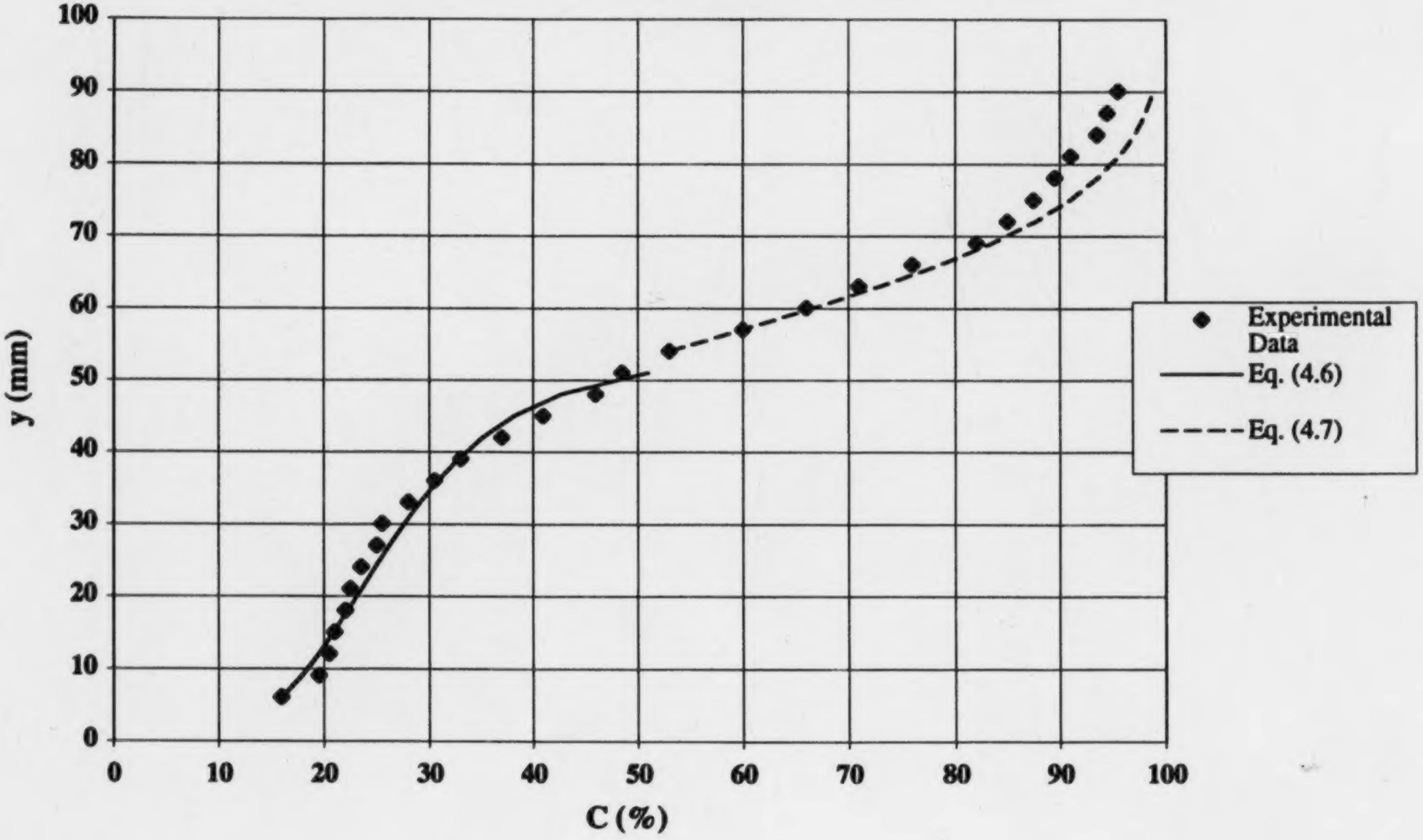

Figure A.16 Concentration profile at step tip #32 in a stepped spillway with l/h=0.6, h= 62.5 mm (yc/h=2.3)

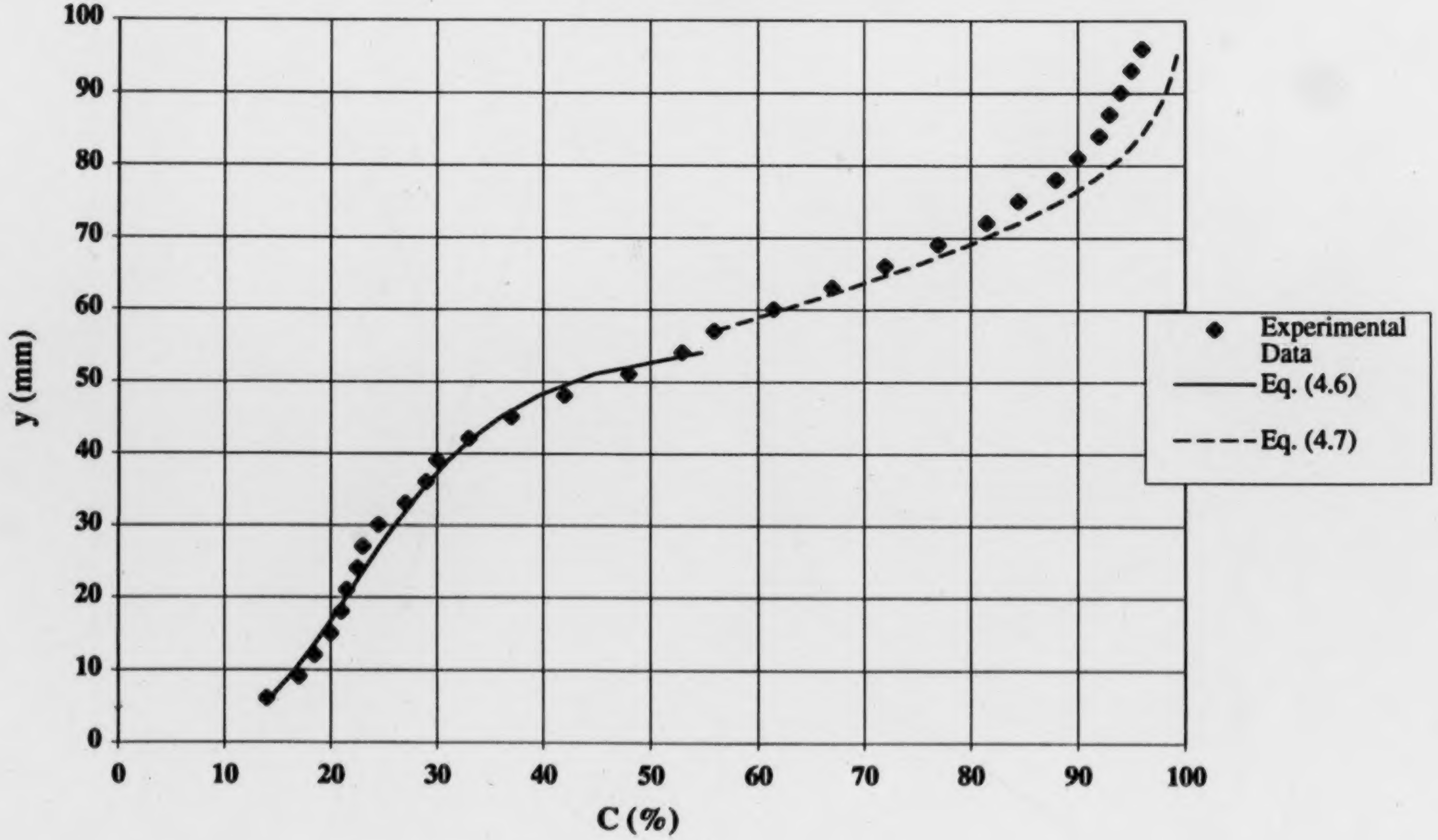

Figure A.17 Concentration profile at step tip #32 in a stepped spillway with l/h=0.6, h= 62.5 mm (yc/h=2.4)

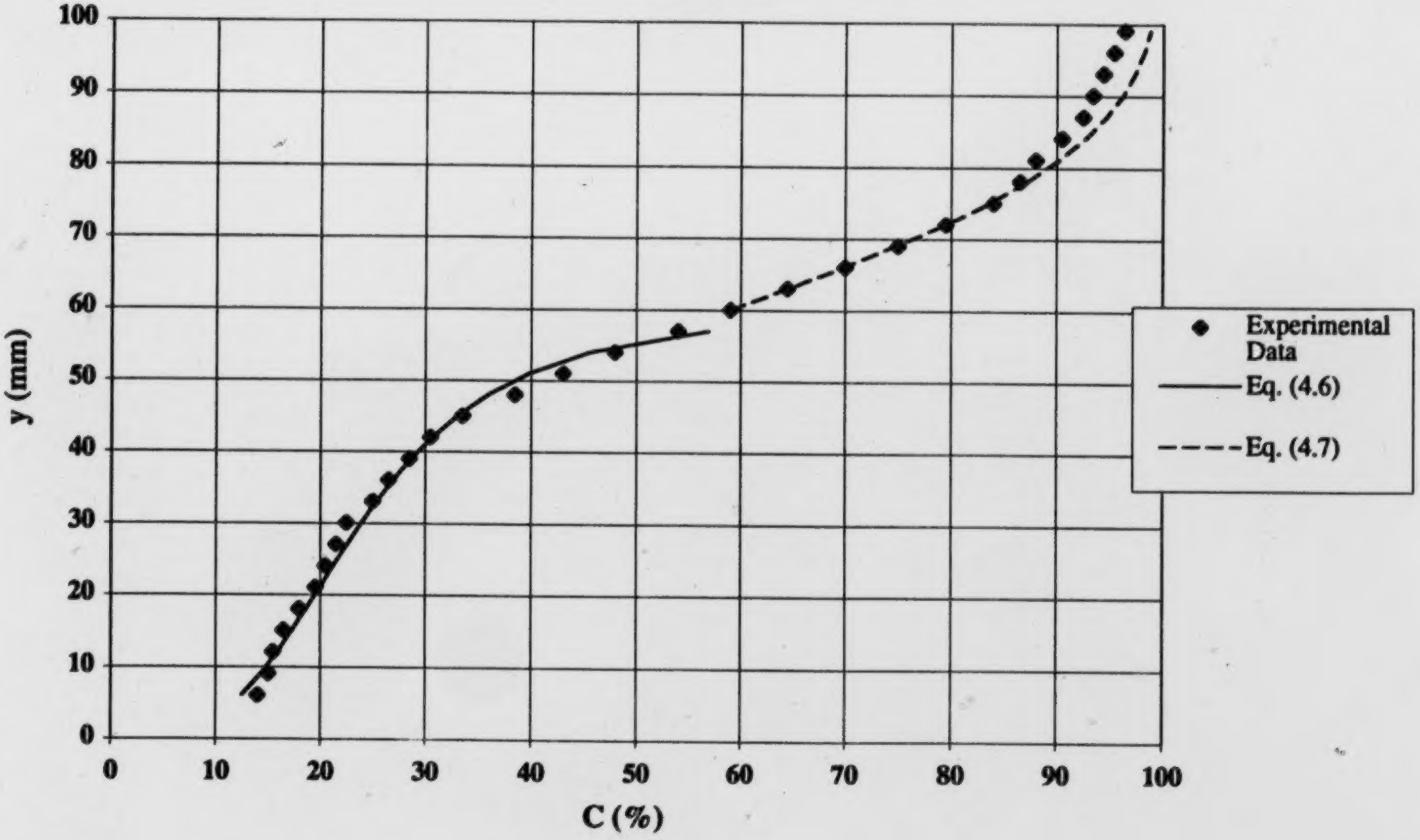

Figure A.18 Concentration profile at step tip #32 in a stepped spillway with l/h=0.6, h= 62.5 mm (yc/h=2.5)

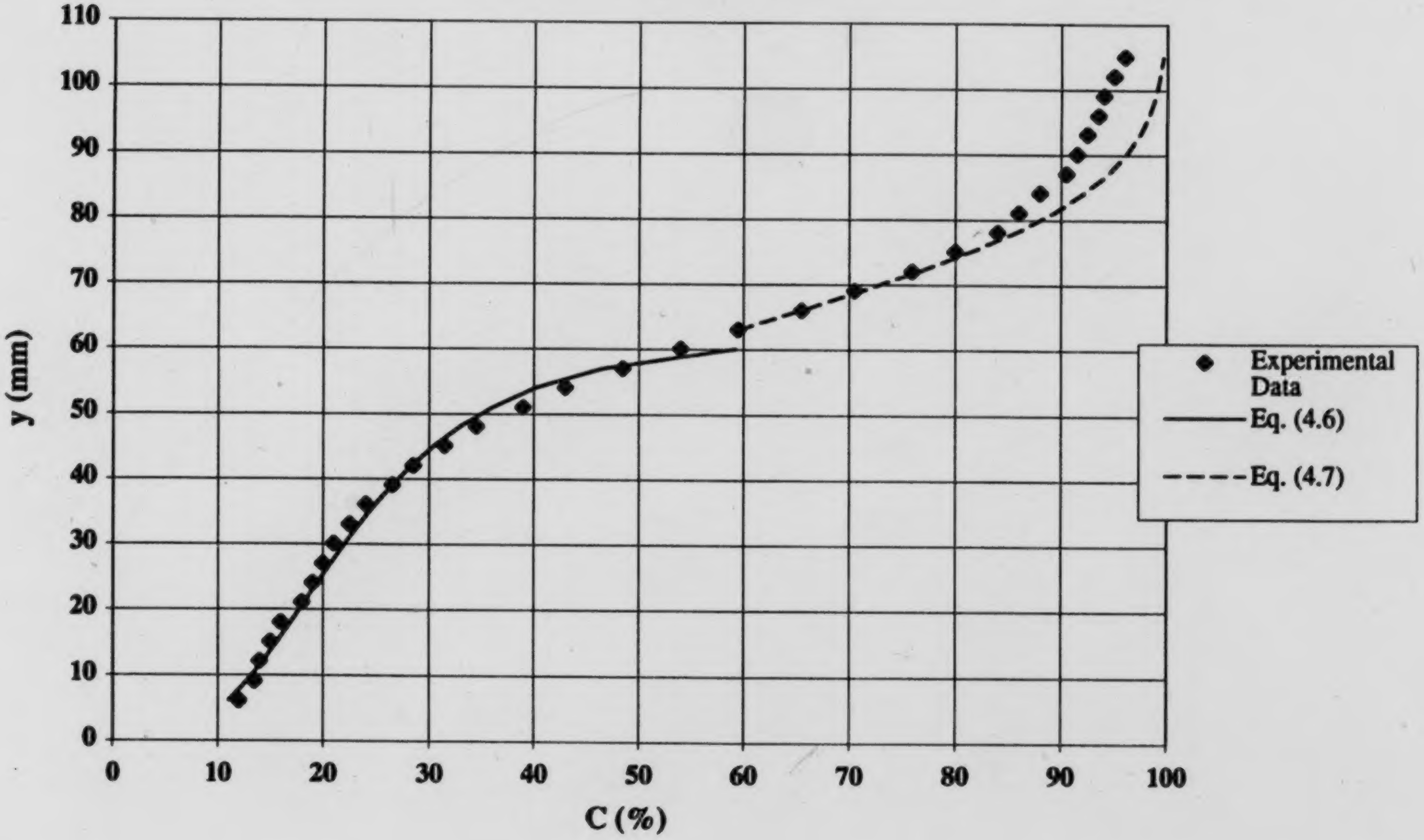

Figure A.19 Concentration profile at step tip #32 in a stepped spillway with l/h=0.6, h= 62.5 mm (yc/h=2.6)

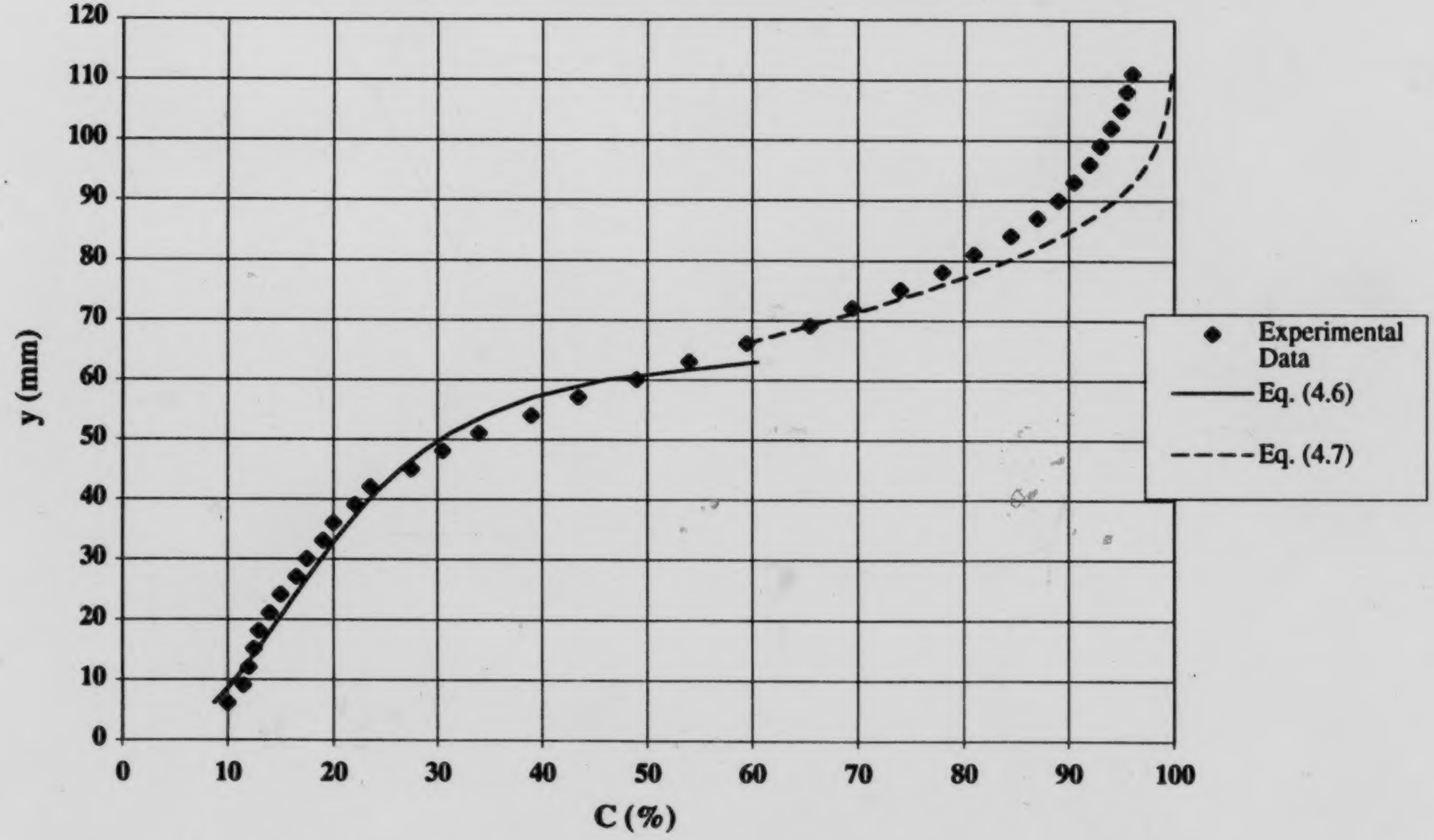

Figure A.20 Concentration profile at step tip #64 in a stepped spillway with l/h=0.6, h= 31.25 mm (yc/h=2.6)

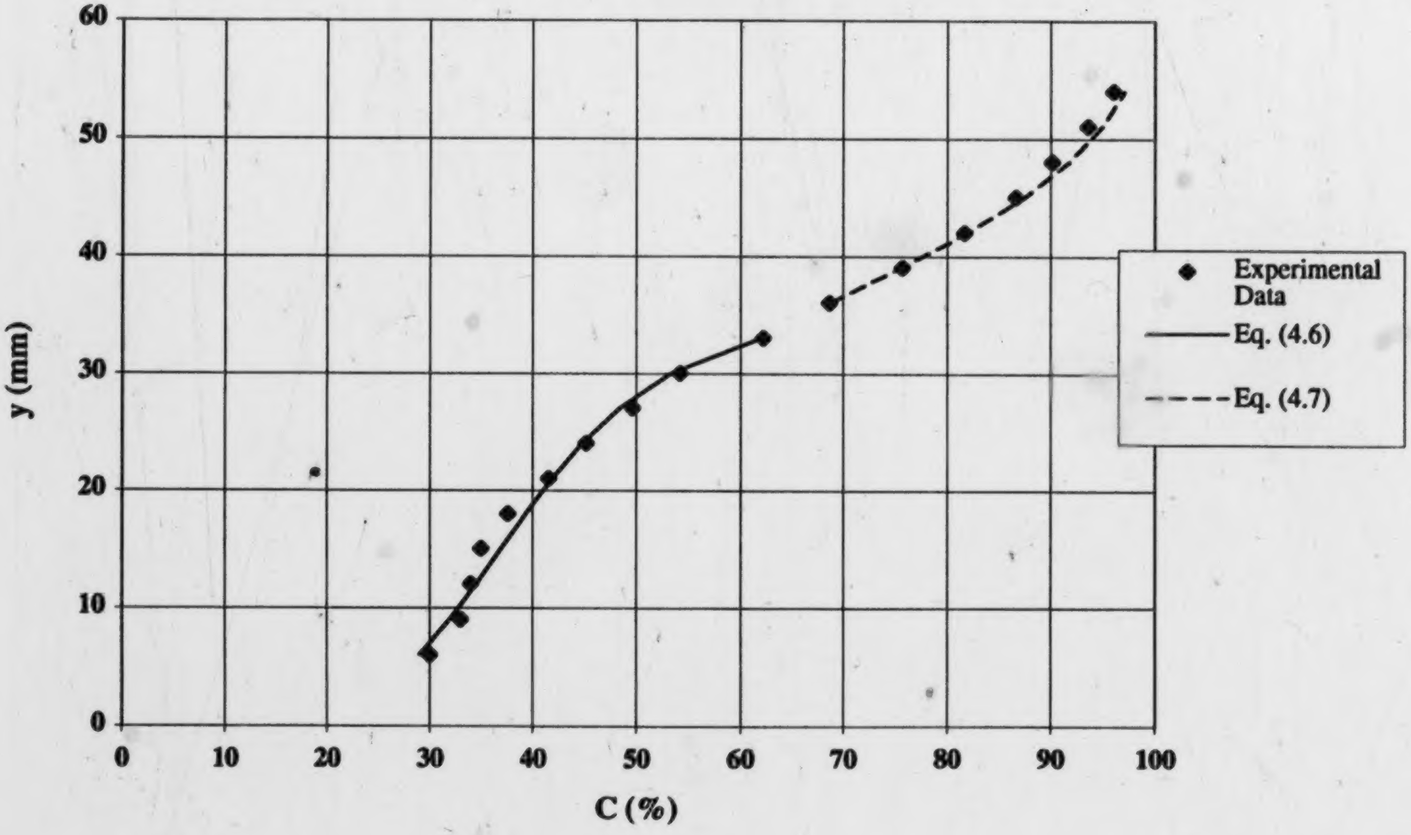

Figure A.21 Concentration profile at step tip #64 in a stepped spillway with l/h=0.6, h= 31.25 mm (yc/h=2.8)

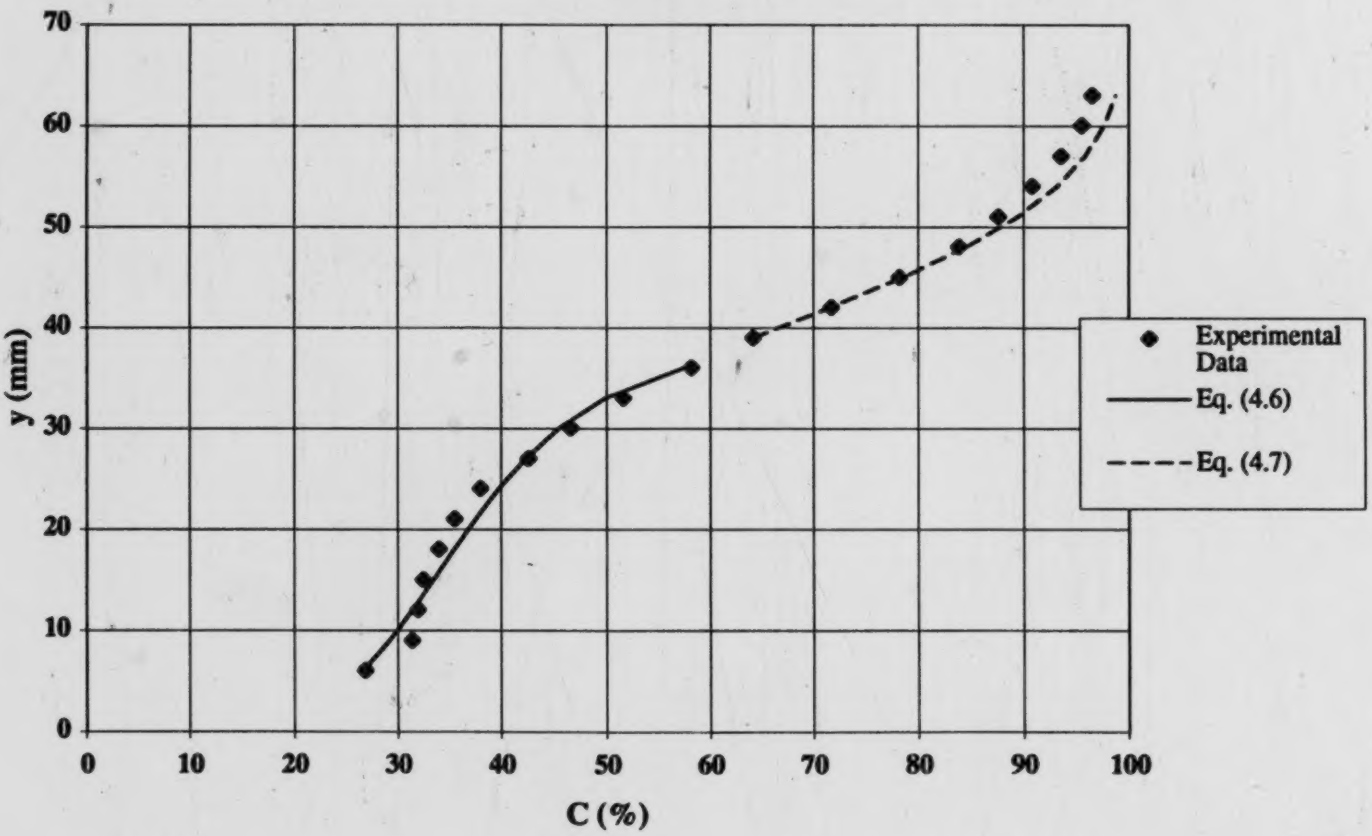

Figure A.22 Concentration profile at step tip #64 in a stepped spillway with l/h=0.6, h= 31.25 mm (yc/h=3.0)

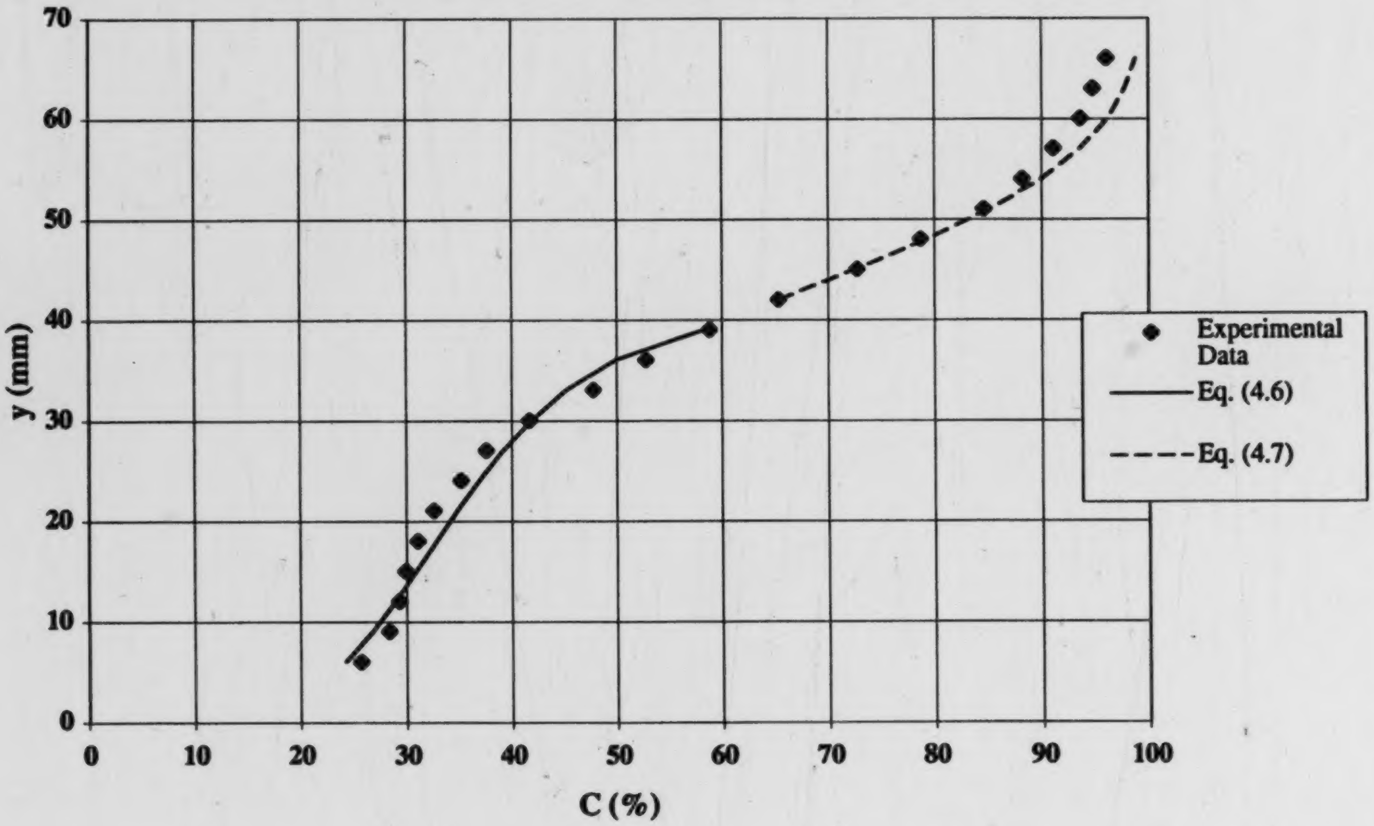

Figure A.23 Concentration profile at step tip #64 in a stepped spillway with l/h=0.6, h= 31.25 mm (yc/h=3.2)

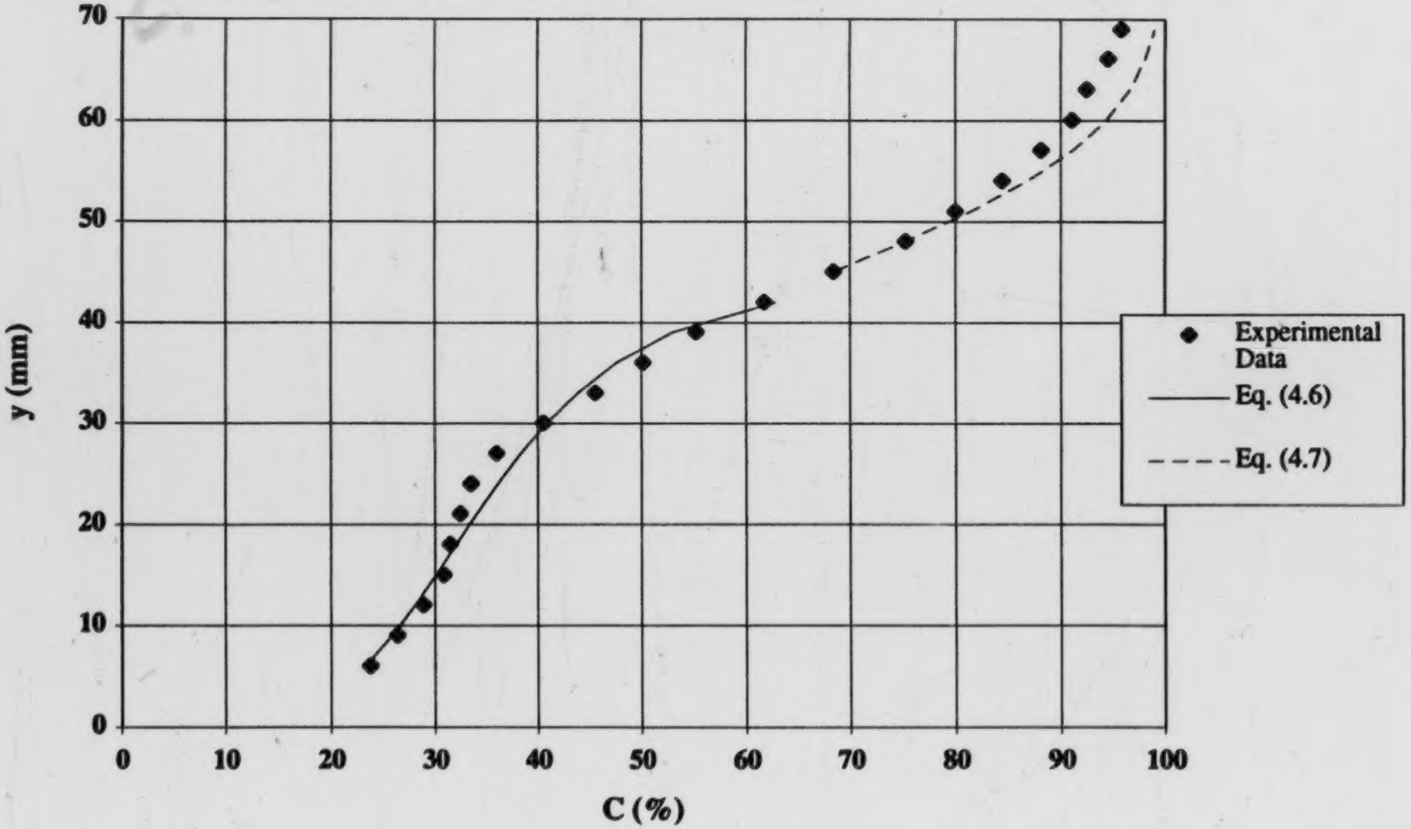

Figure A.24 Concentration profile at step tip #64 in a stepped spillway with l/h=0.6, h= 31.25 mm (yc/h=3.4)

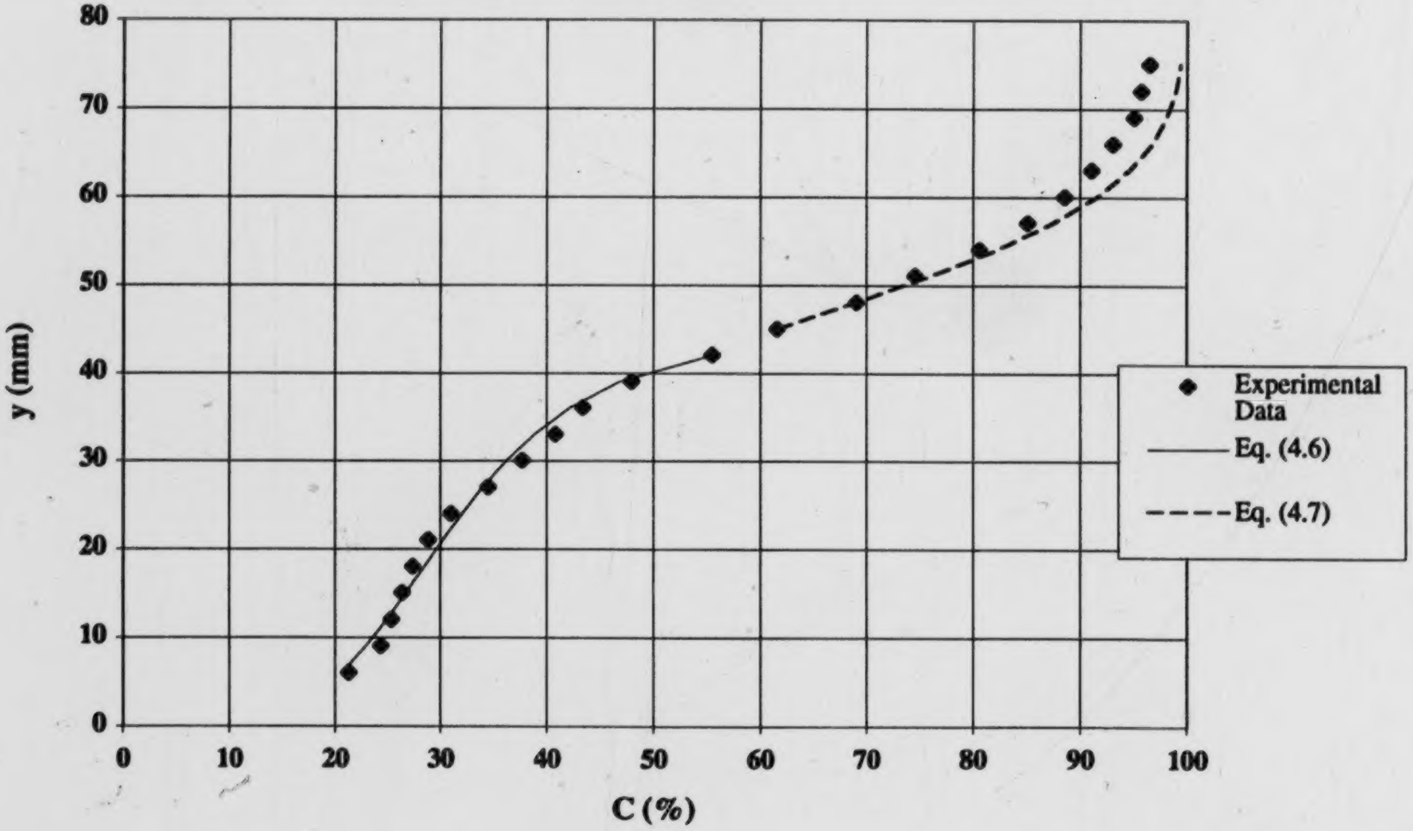

Figure A.25 Concentration profile at step tip #64 in a stepped spillway with l/h=0.6, h= 31.25 mm (yc/h=3.6)

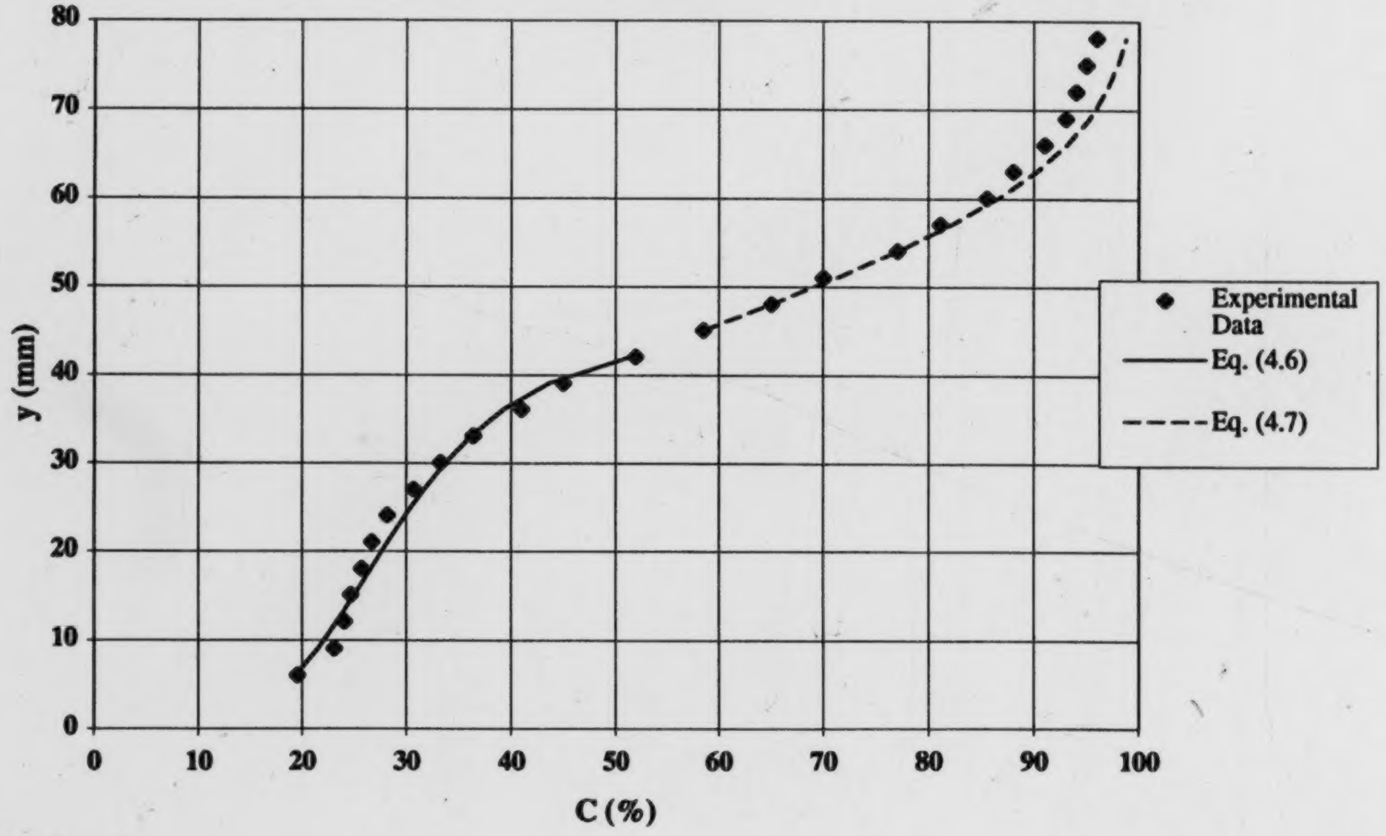

Figure A.26 Concentration profile at step tip #64 in a stepped spillway with l/h=0.6, h= 31.25 mm (yc/h=3.8)

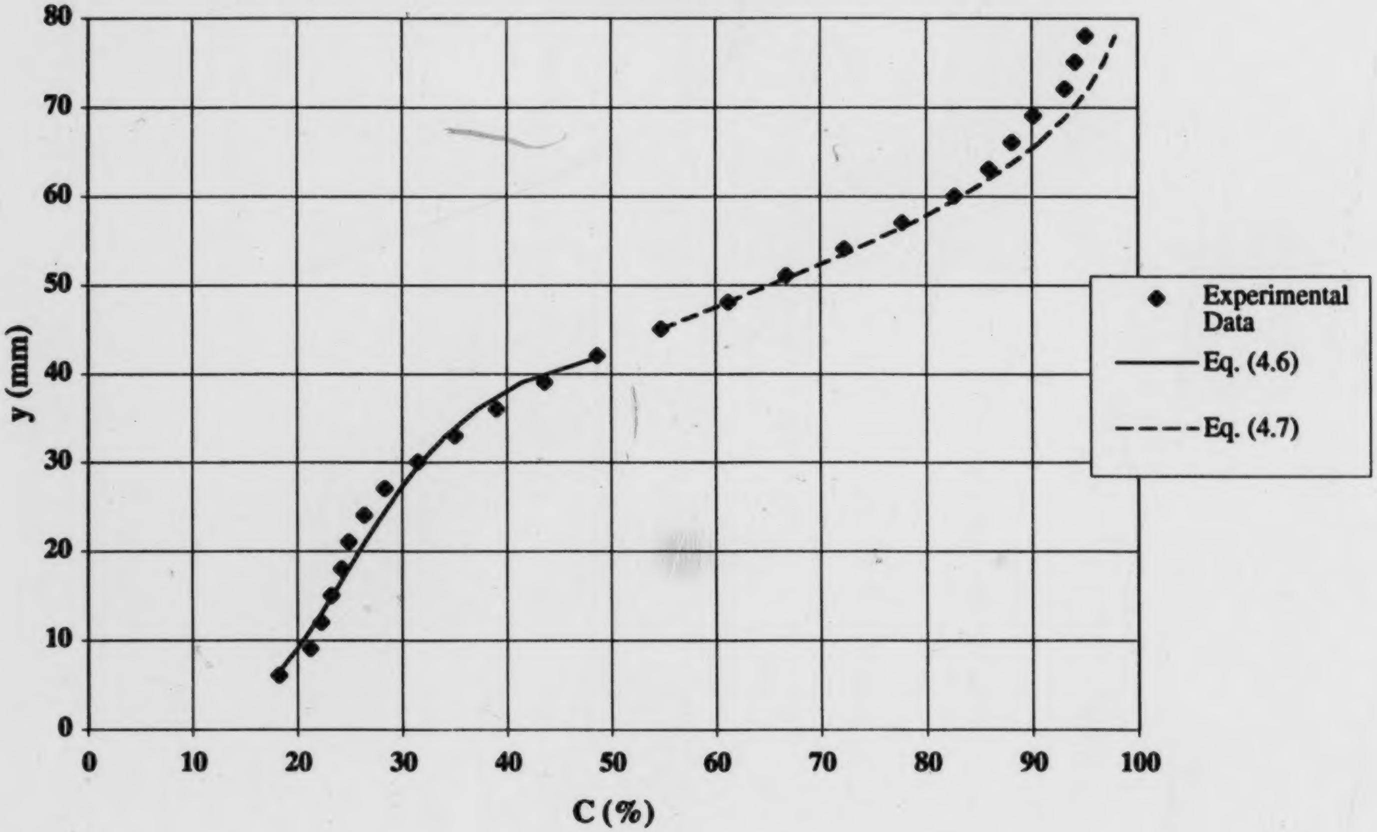

Figure A.27 Concentration profile at step tip #64 in a stepped spillway with l/h=0.6, h= 31.25 mm (yc/h=4.0)

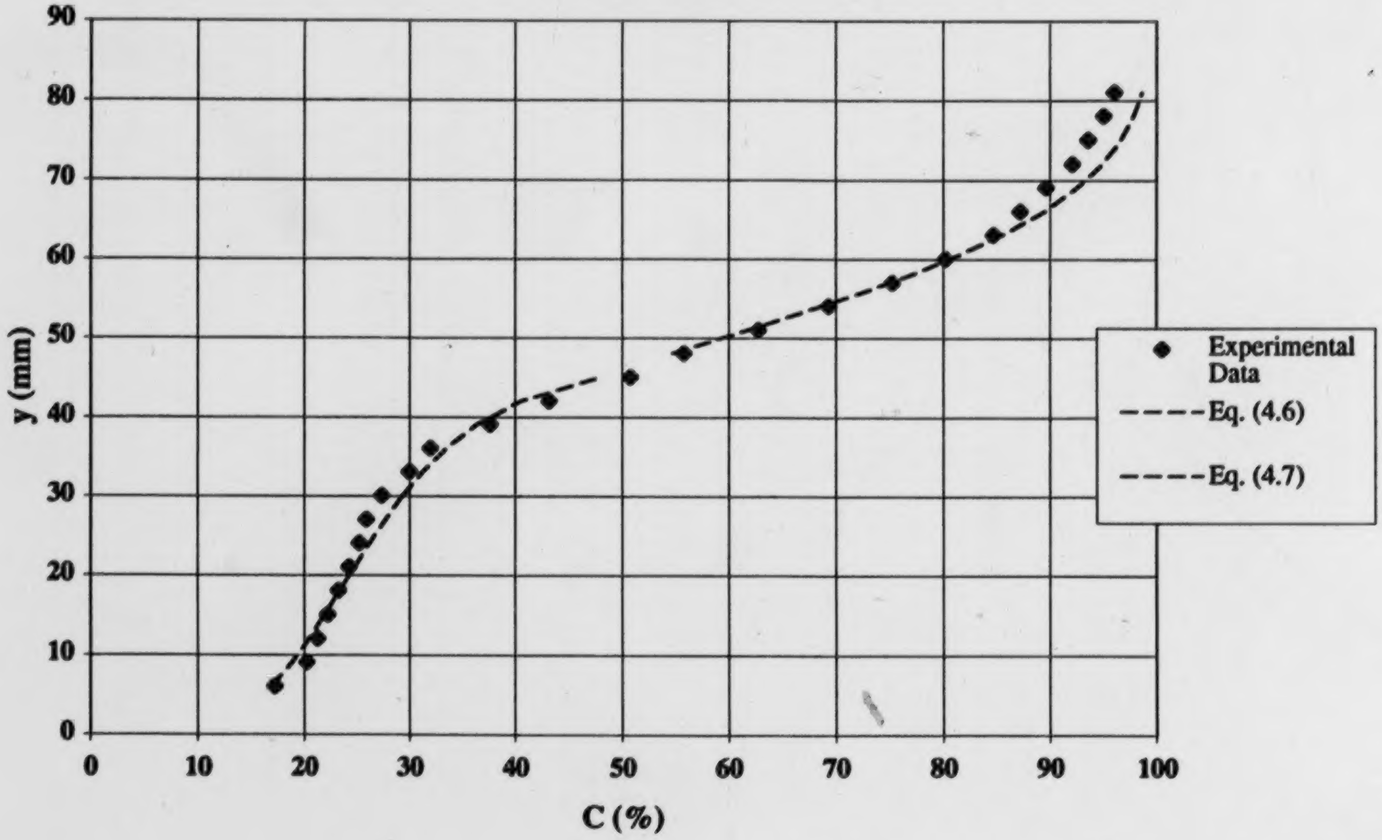

Figure A.28 Concentration profile at step tip #64 in a stepped spillway with l/h=0.6, h= 31.25 mm (yc/h=4.2)

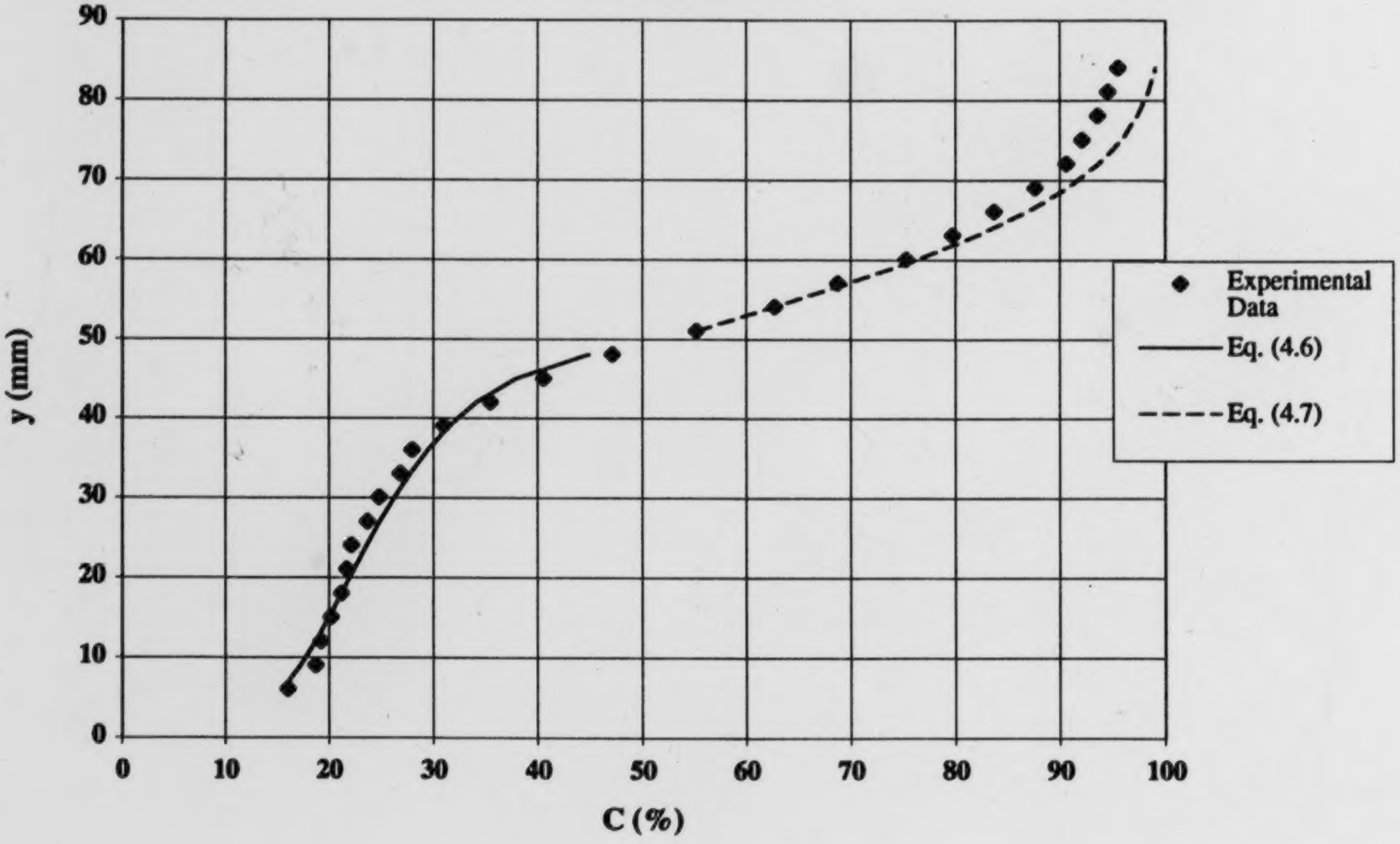

Figure A.29 Concentration profile at step tip #64 in a stepped spillway with l/h=0.6, h= 31.25 mm (yc/h=4.4)

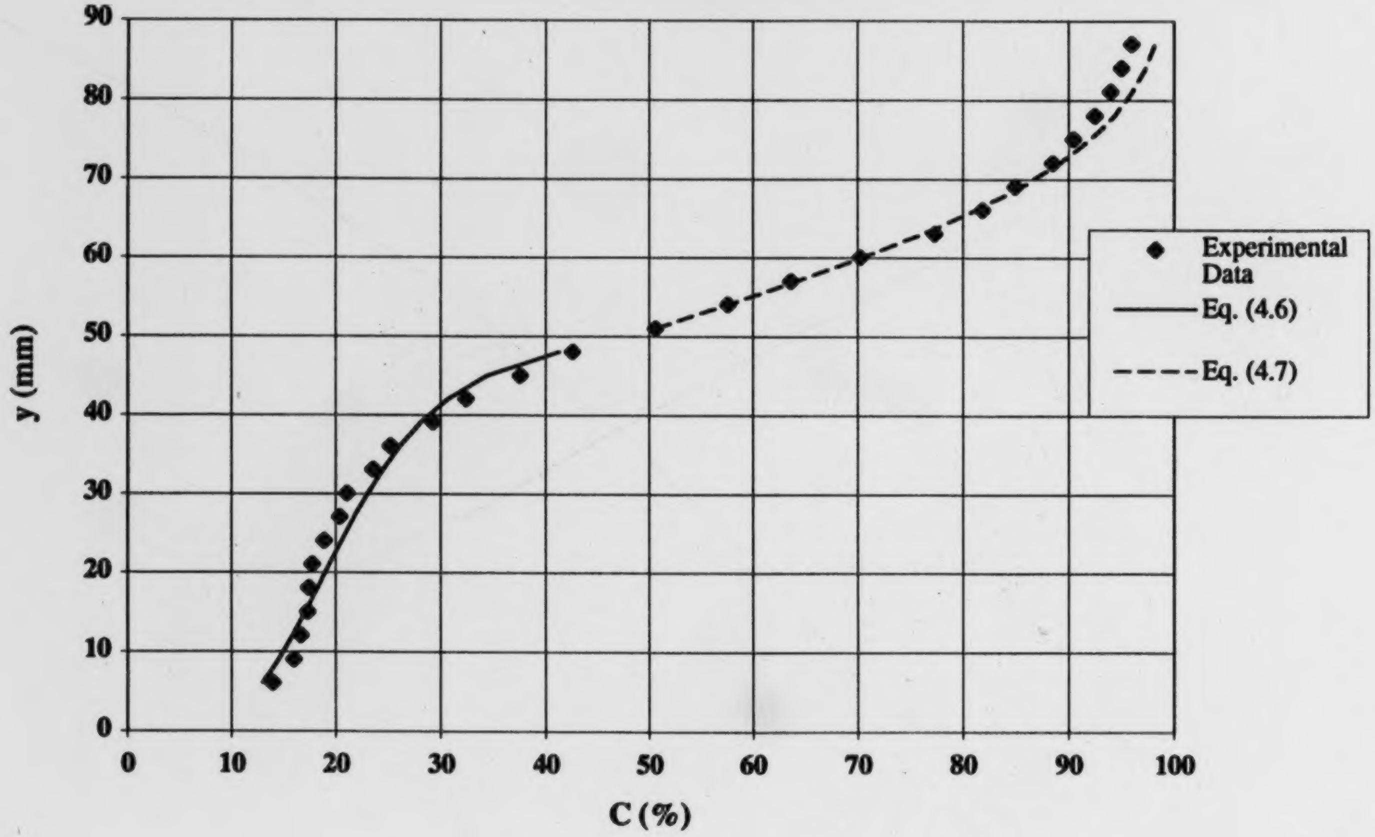

Figure A.30 Concentration profile at step tip #15 in a stepped spillway with l/h=0.8, h= 125. mm (yc/h=0.7)

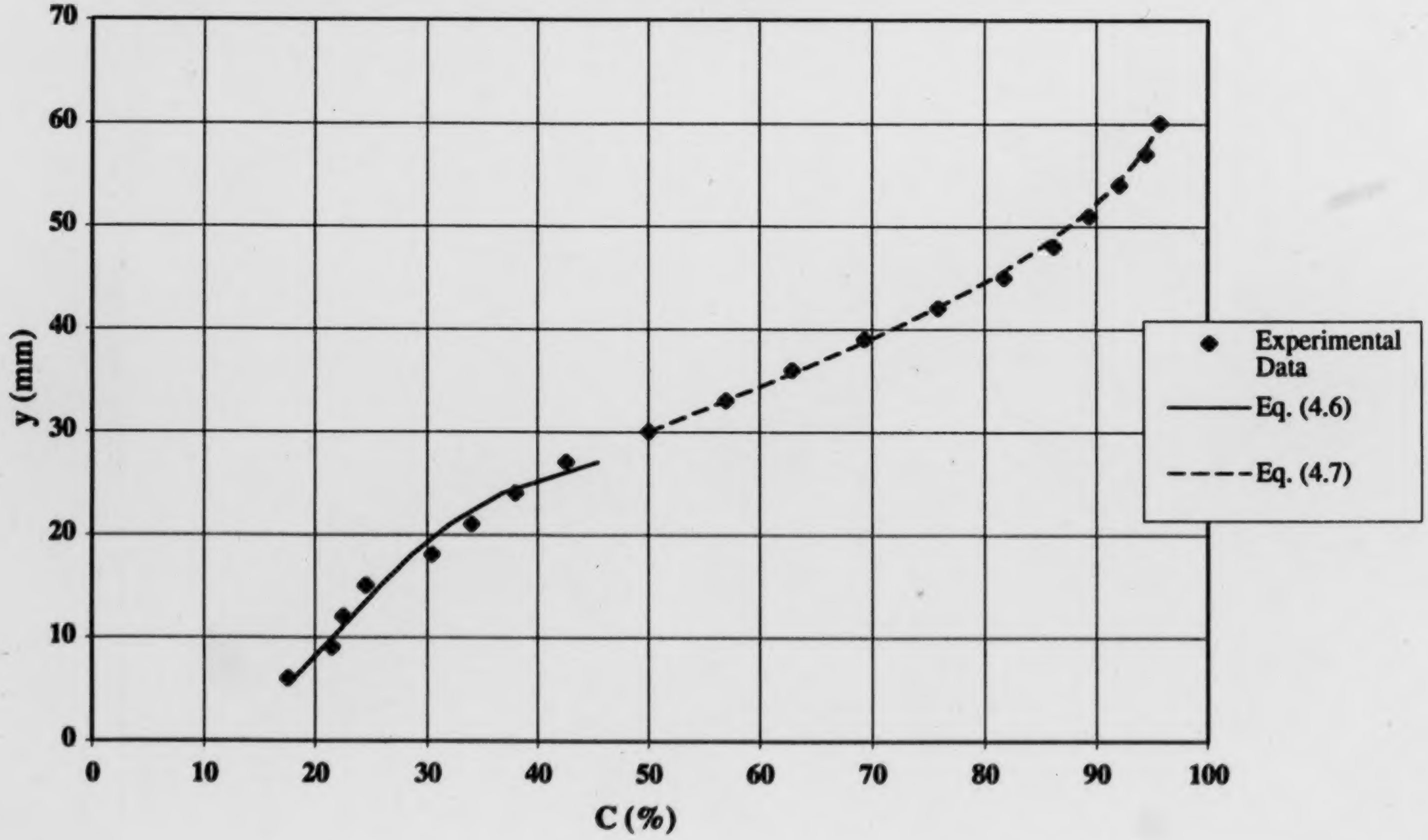

Figure A.31 Concentration profile at step tip #15 in a stepped spillway with l/h=0.8, h= 125. mm (yc/h=0.8)

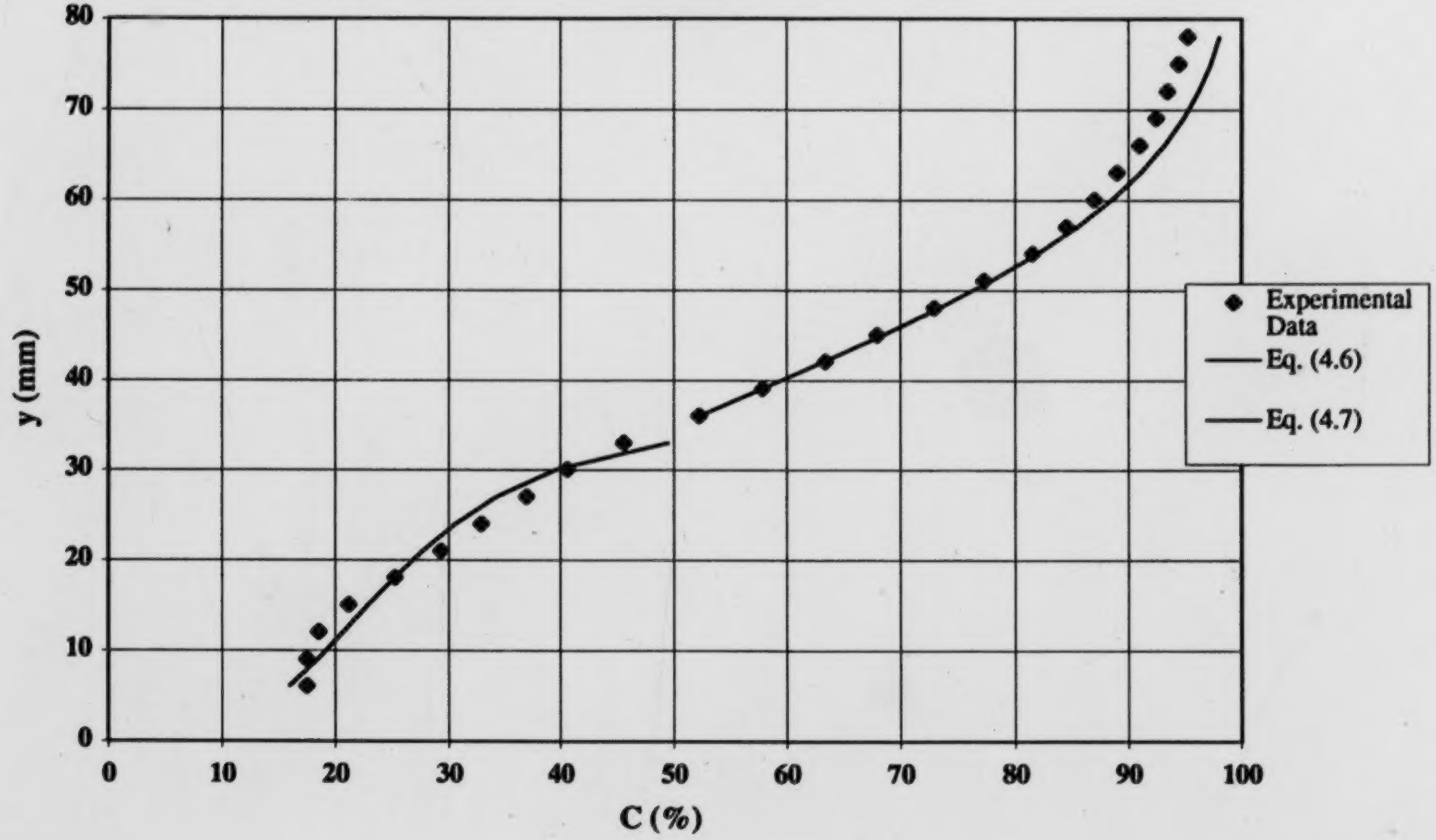

Figure A.32 Concentration profile at step tip #15 in a stepped spillway with l/h=0.8, h= 125. mm (yc/h=0.9)

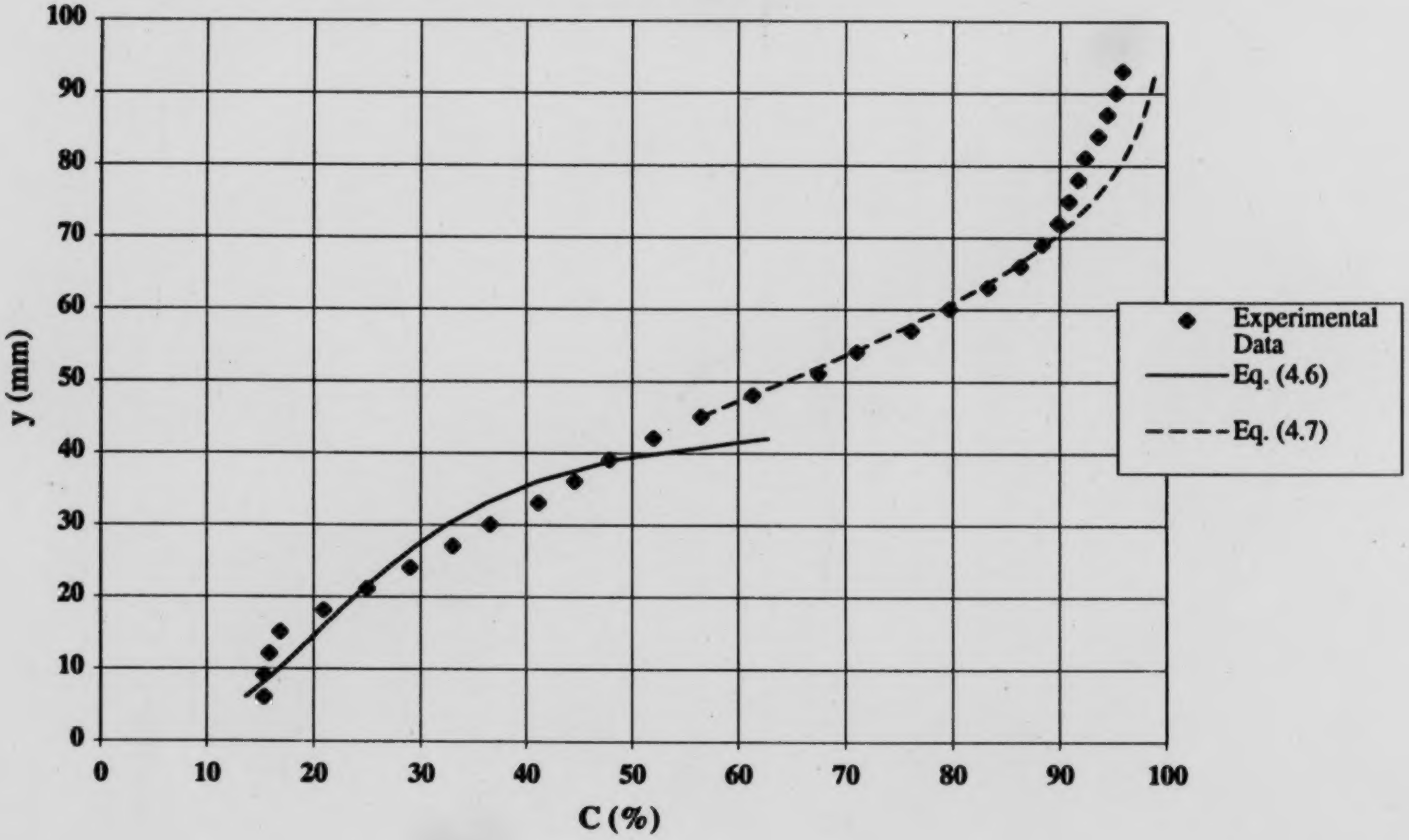

Figure A.33 Concentration profile at step tip #15 in a stepped spillway with l/h=0.8, h= 125. mm (yc/h=1.0)

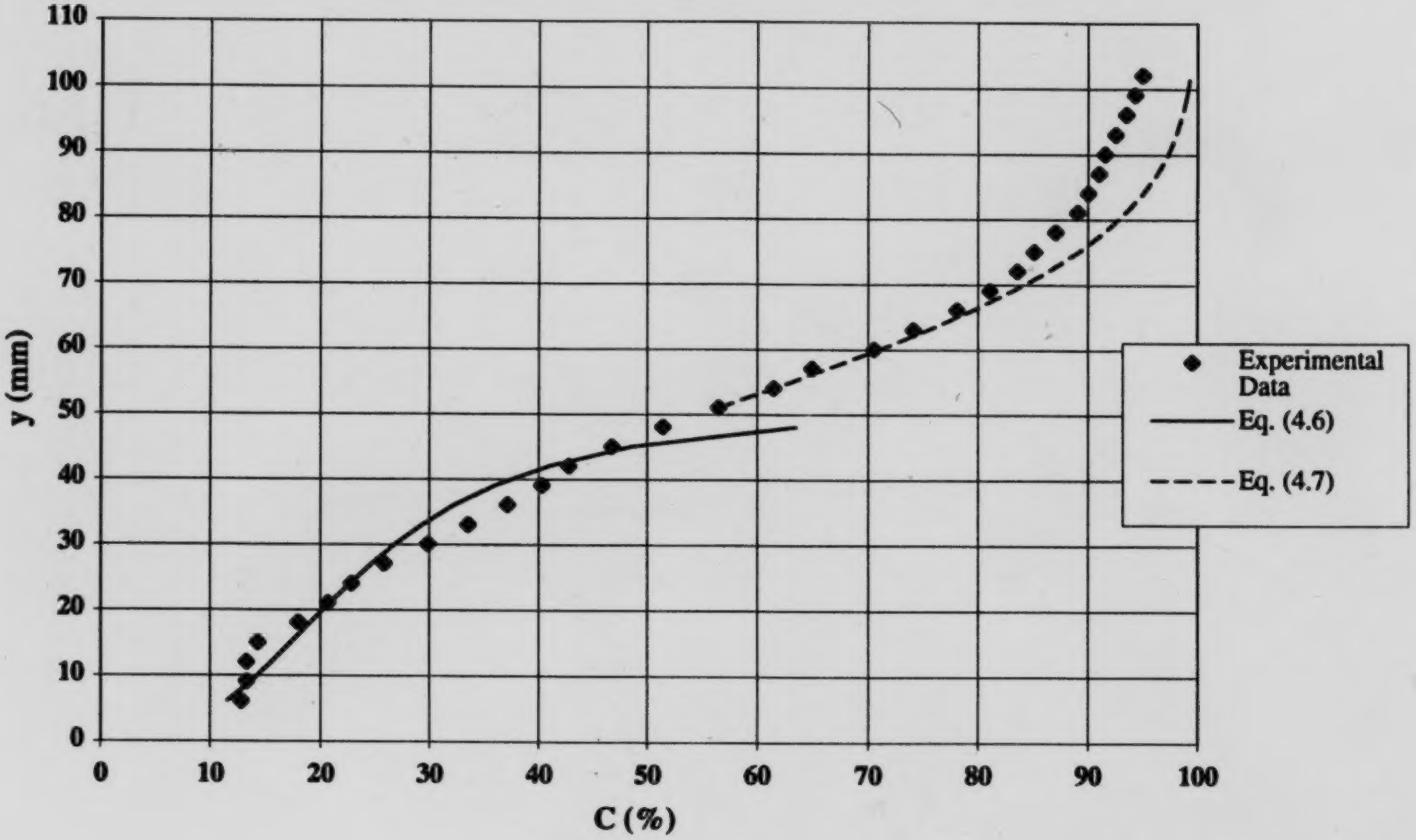

Figure A.34 Concentration profile at step tip #15 in a stepped spillway with l/h=0.8, h= 125. mm (yc/h=1.1)

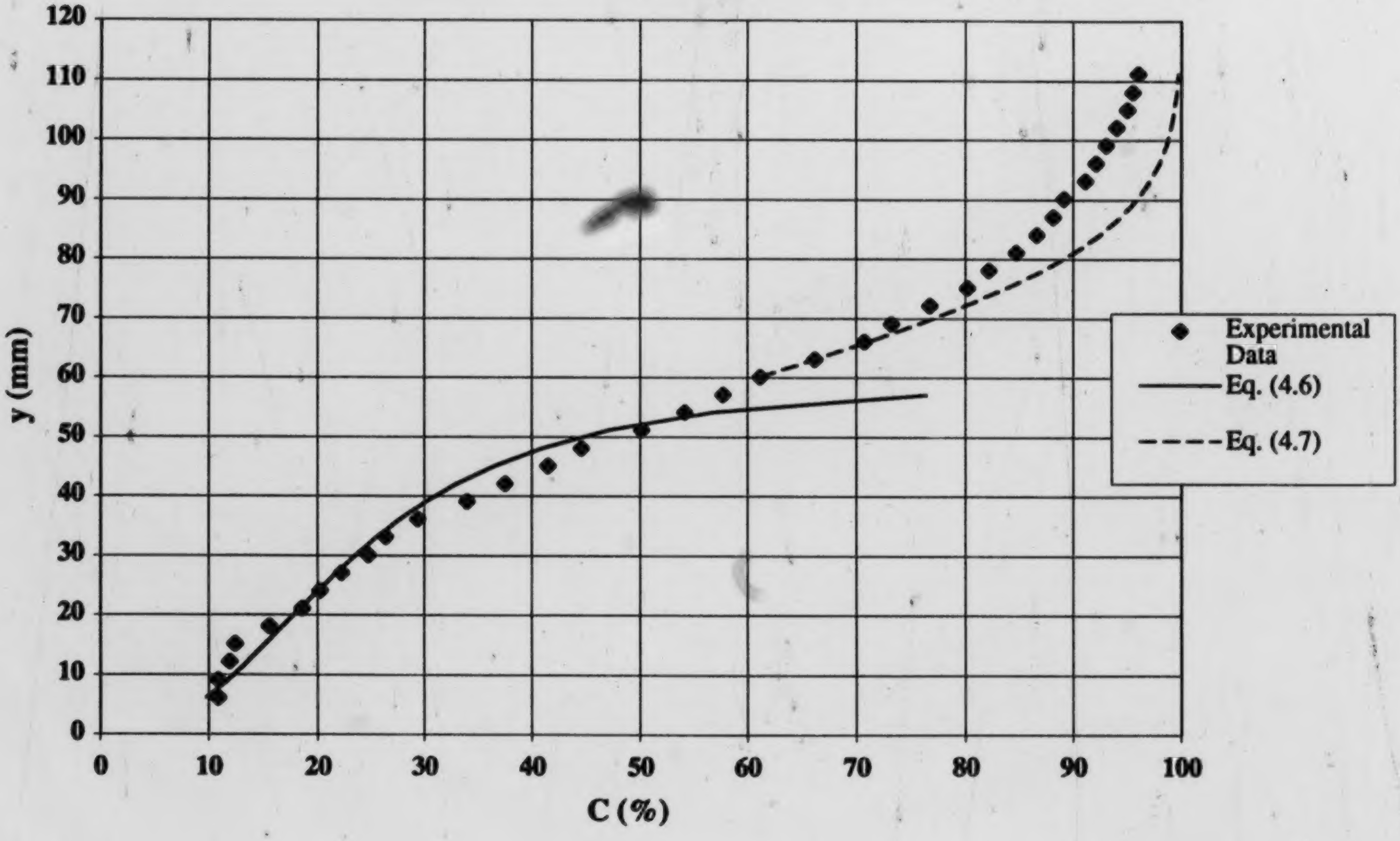

Figure A.35 Concentration profile at step tip #15 in a stepped spillway with l/h=0.8, h= 125. mm (yc/h=1.2)

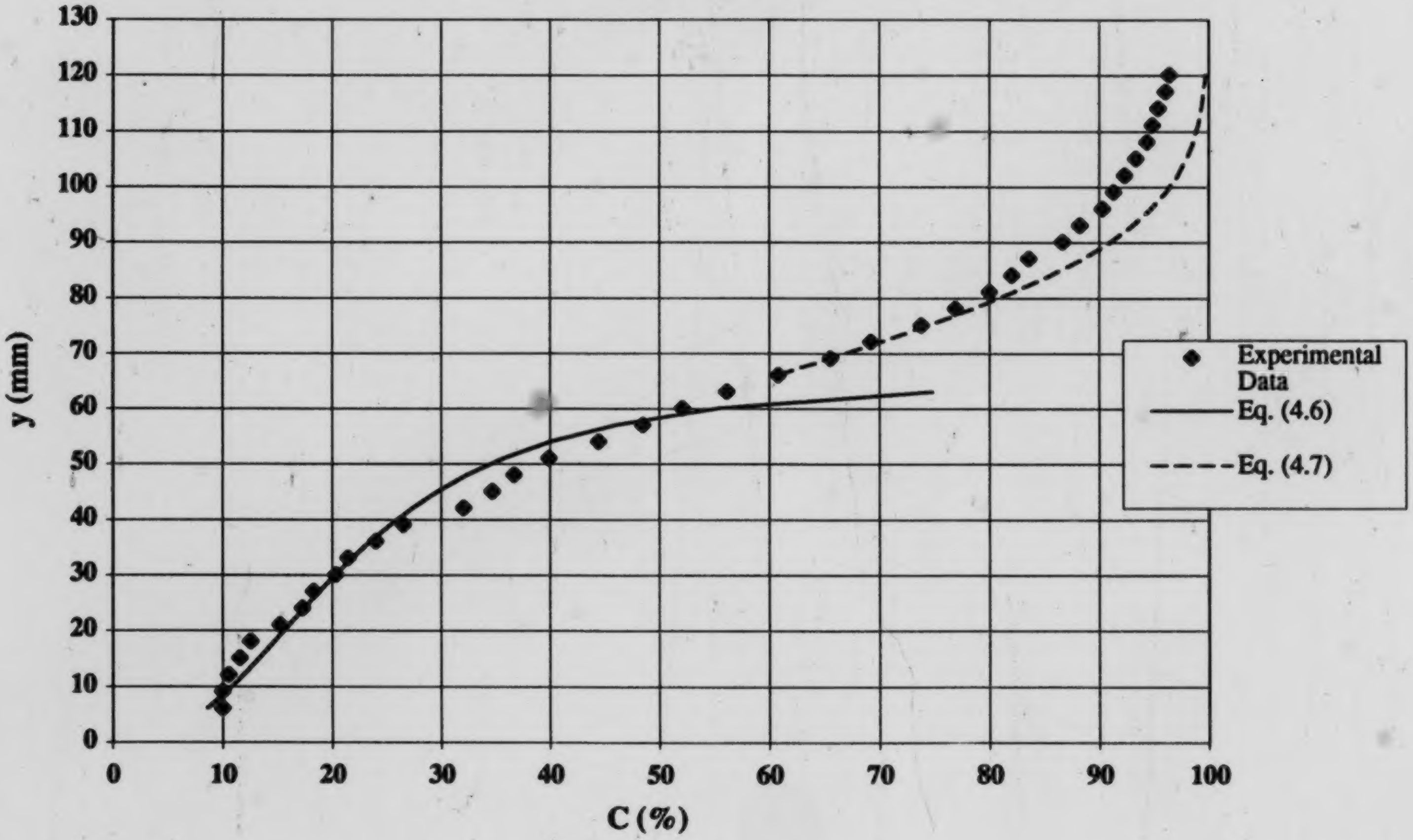

Figure A.36 Concentration profile at step tip #15 in a stepped spillway with l/h=0.8, h= 125. mm (yc/h=1.3)

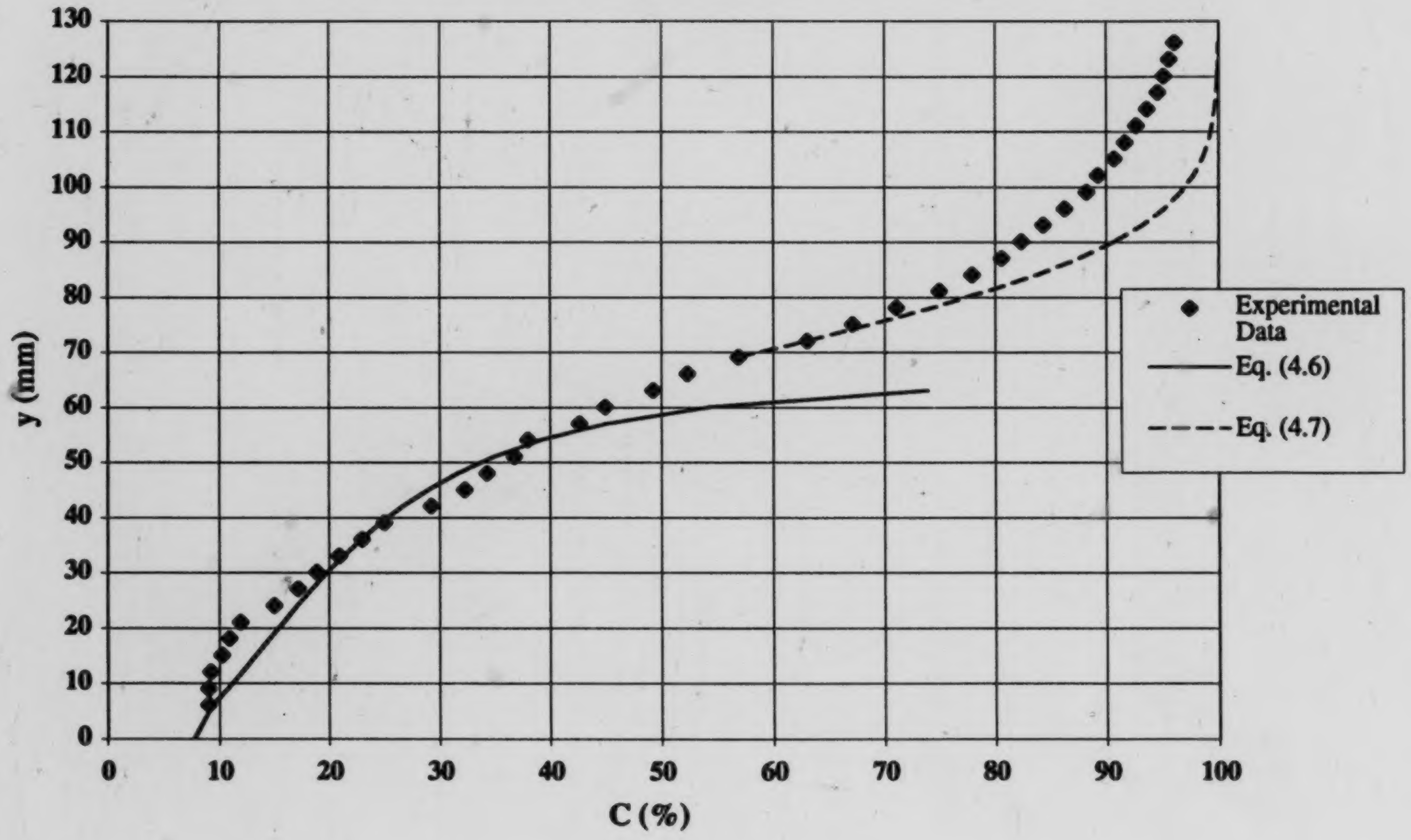

Figure A.37 Concentration profile at step tip #60 in a stepped spillway with l/h=0.8, h= 31.25 mm (yc/h=2.6)

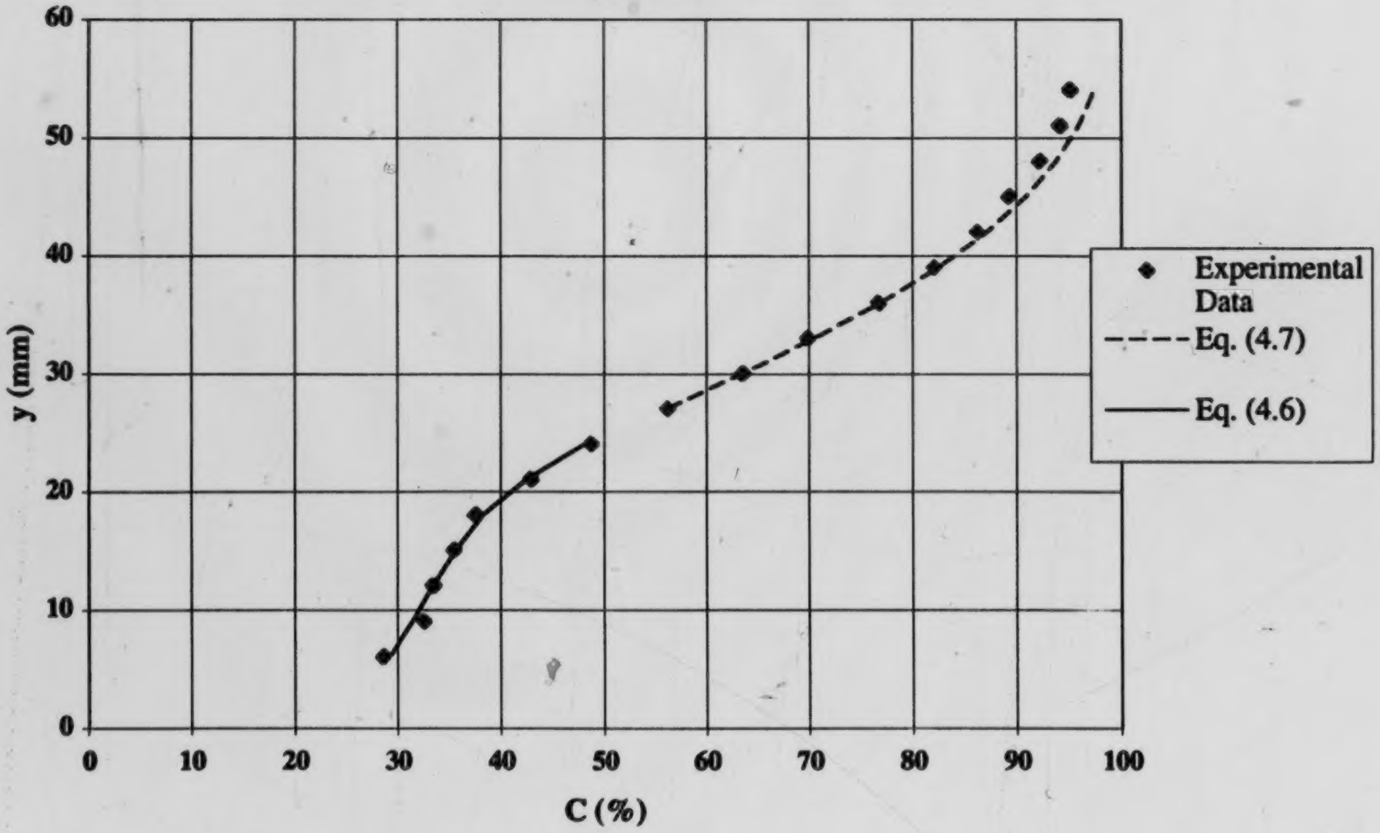

Figure A.38 Concentration profile at step tip #60 in a stepped spillway with l/h=0.8, h= 31.25 mm (yc/h=2.8)

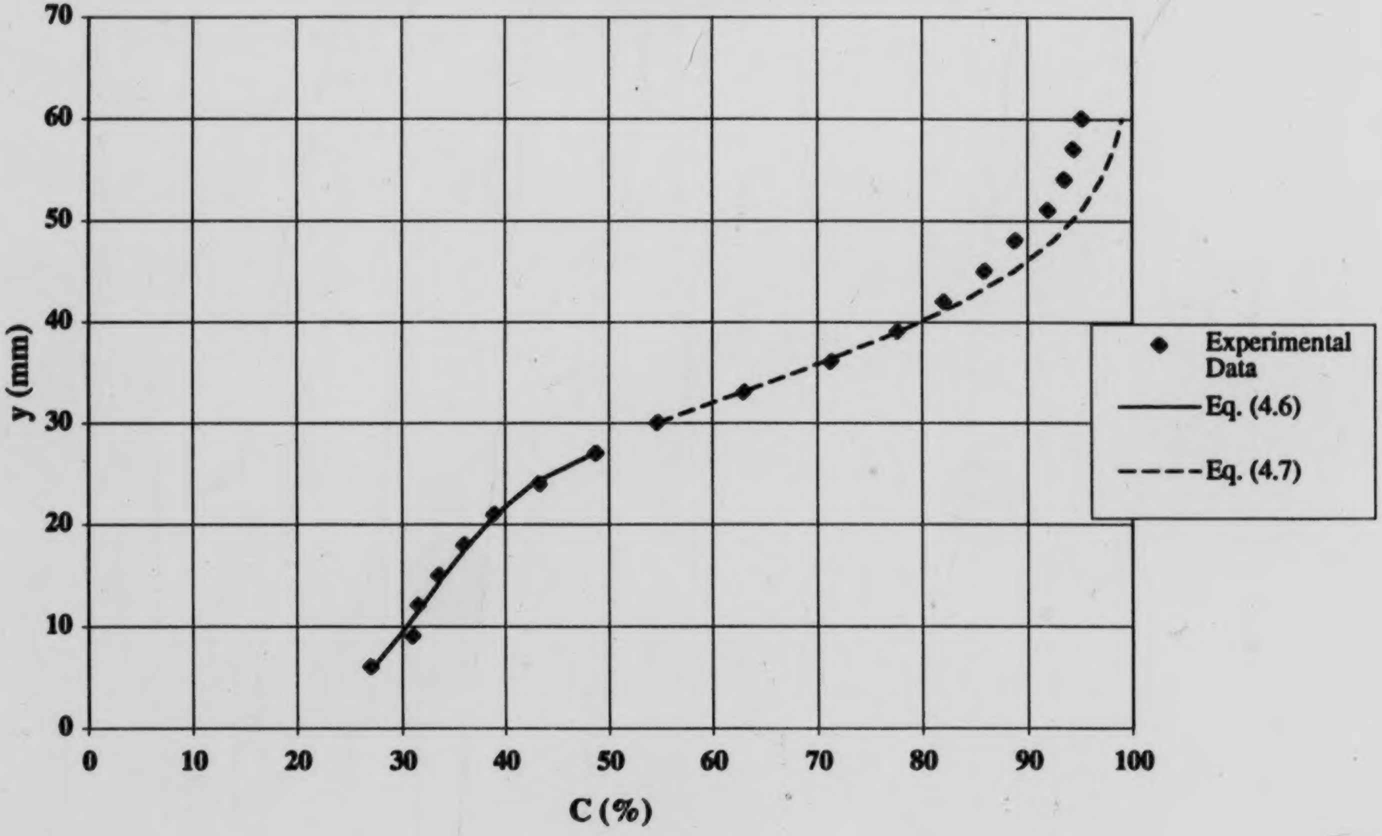

Figure A.39 Concentration profile at step tip #60 in a stepped spillway with l/h=0.8, h= 31.25 mm (yc/h=3.0)

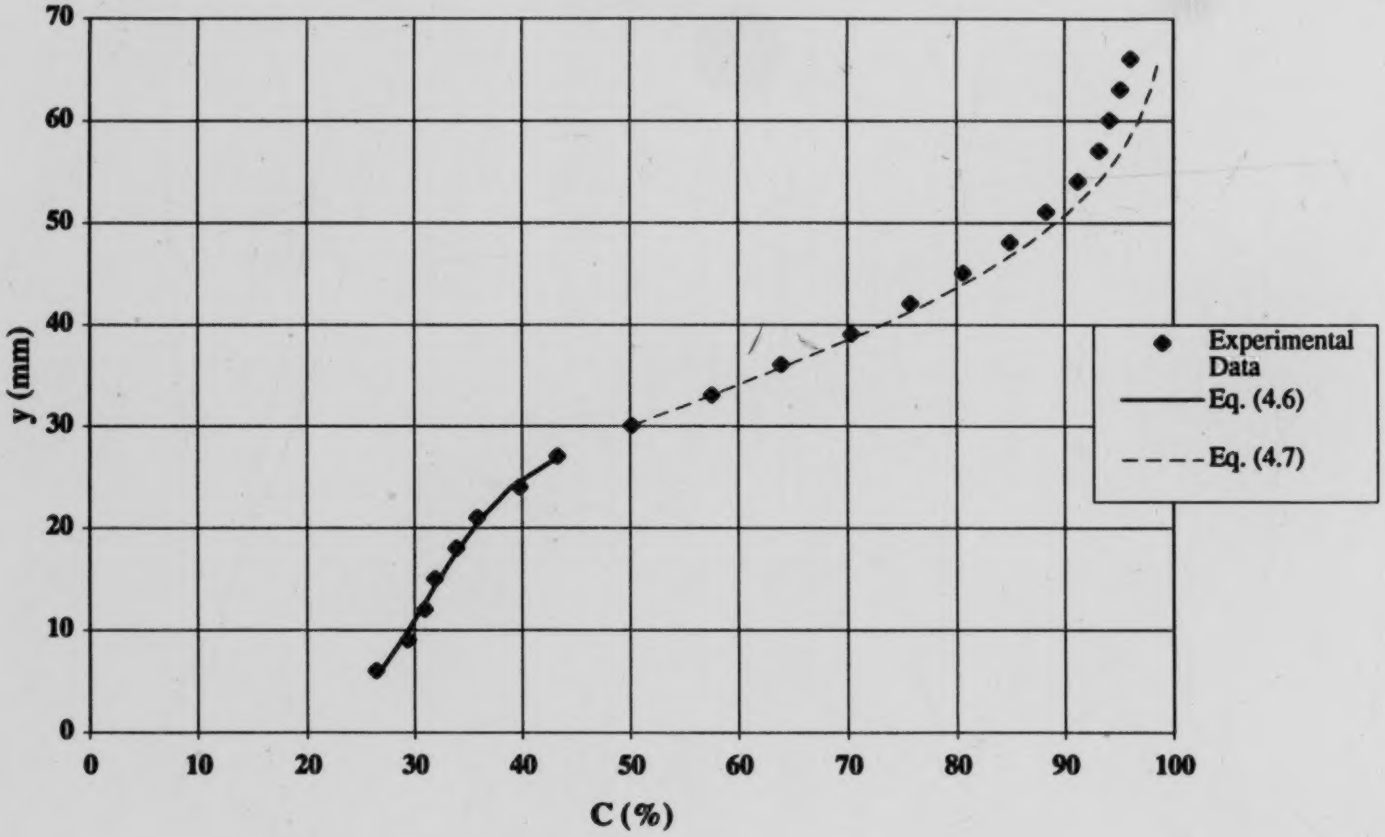

Figure A.40 Concentration profile at step tip #60 in a stepped spillway with l/h=0.8, h= 31.25 mm (yc/h=3.2)

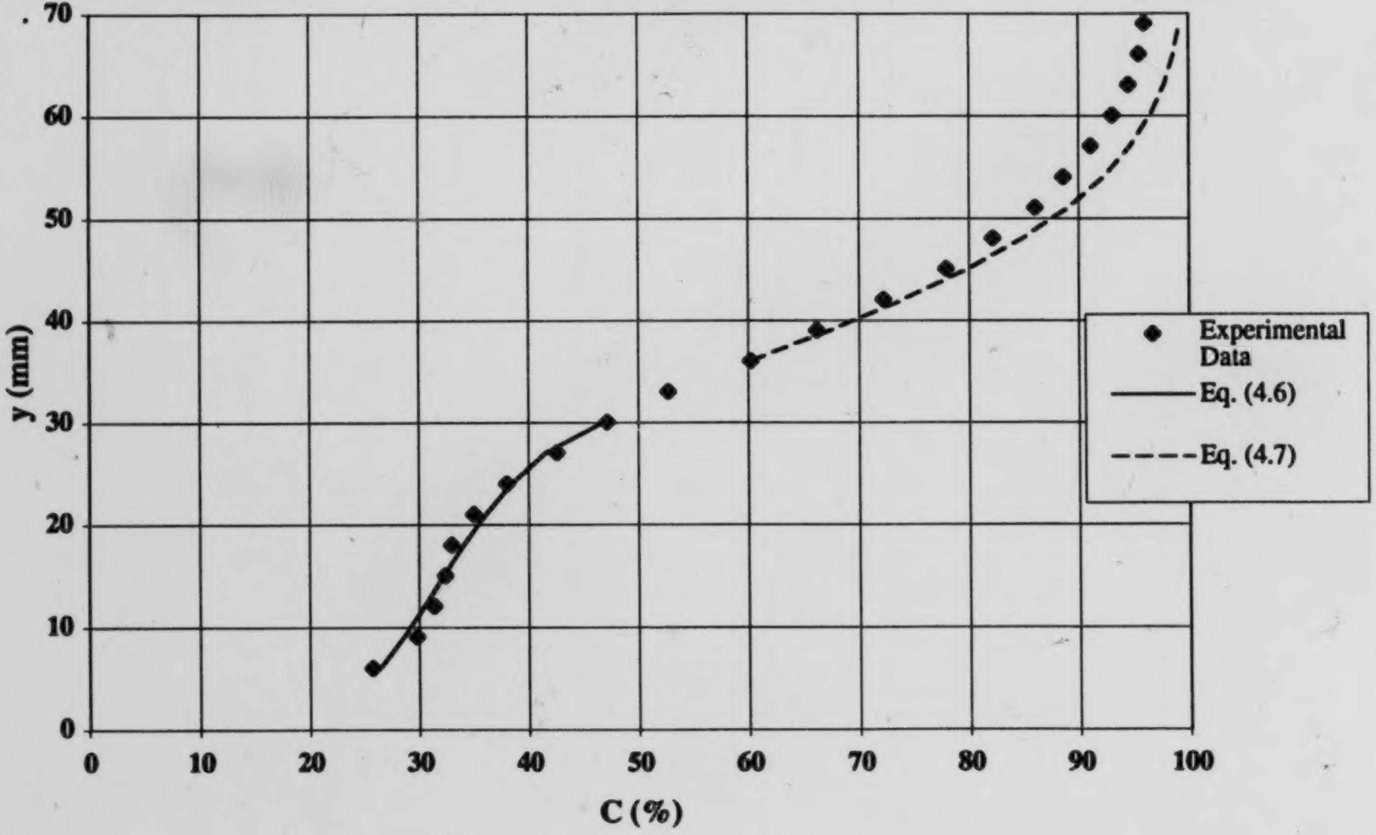

Figure A.41 Concentration profile at step tip #60 in a stepped spillway with l/h=0.8, h= 31.25 mm (yc/h=3.4)

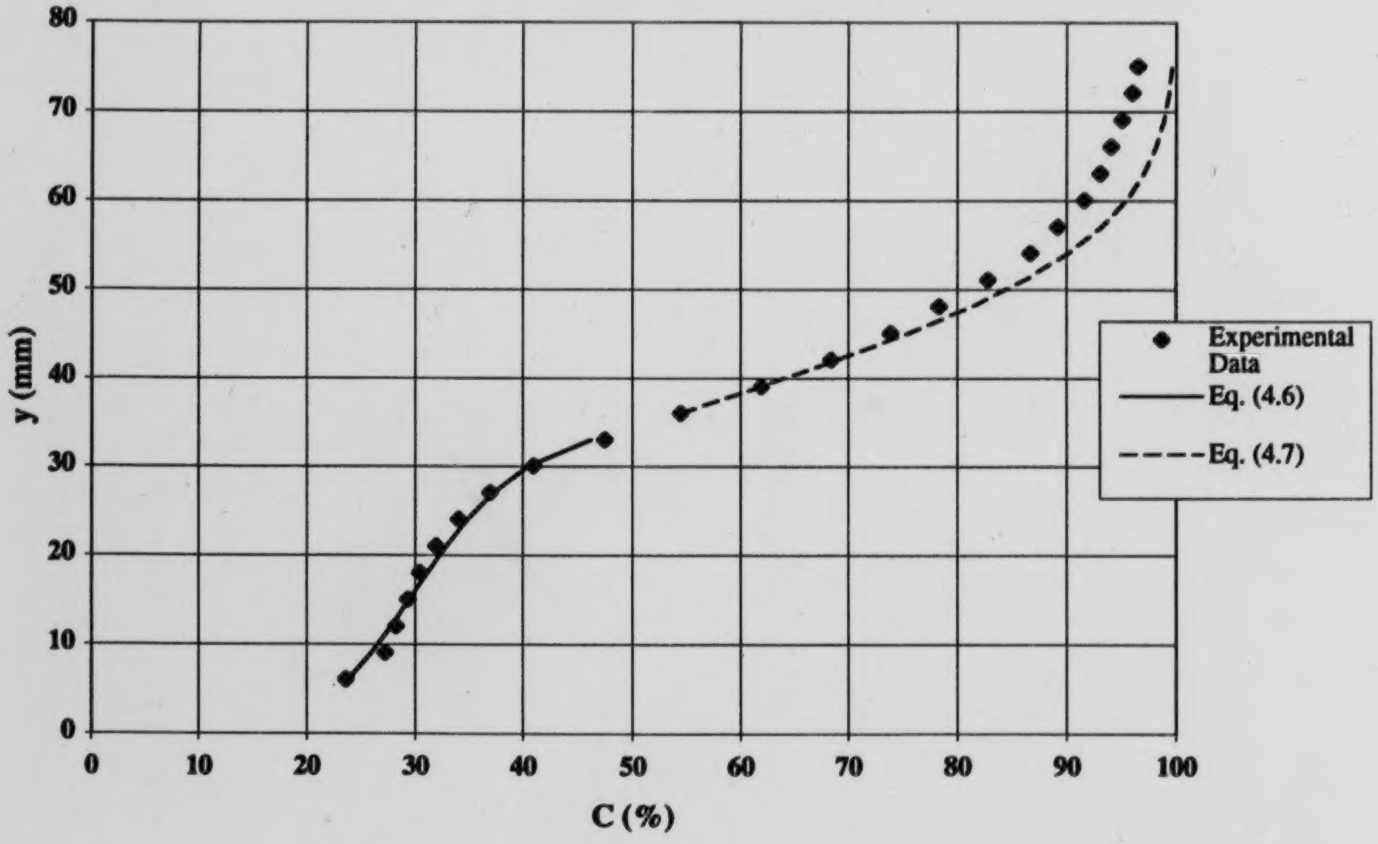

Figure A.42 Concentration profile at step tip #60 in a stepped spillway with l/h=0.8, h= 31.25 mm (yc/h=3.6)

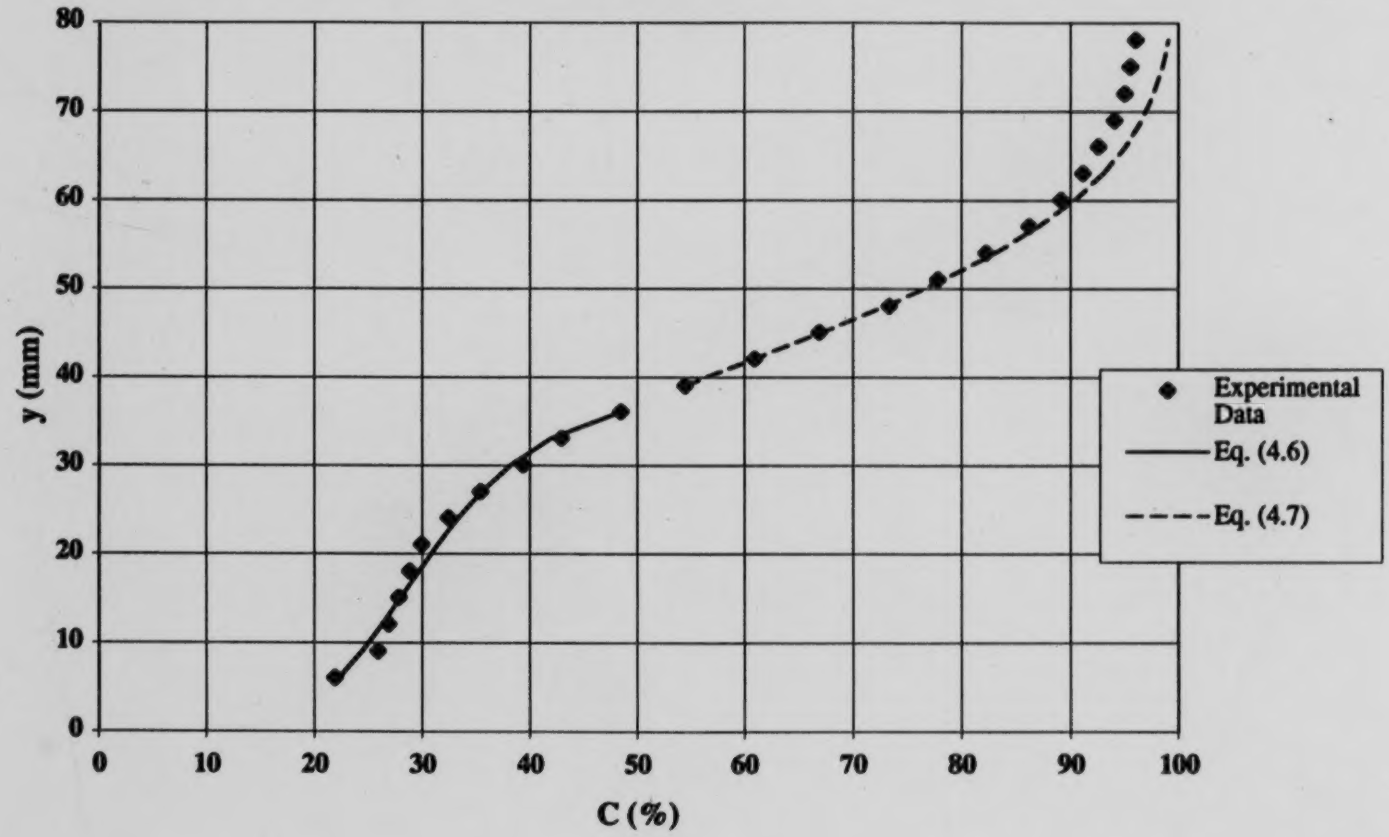

Figure A.43 Concentration profile at step tip #60 in a stepped spillway with l/h=0.8, h= 31.25 mm (yc/h=3.8)

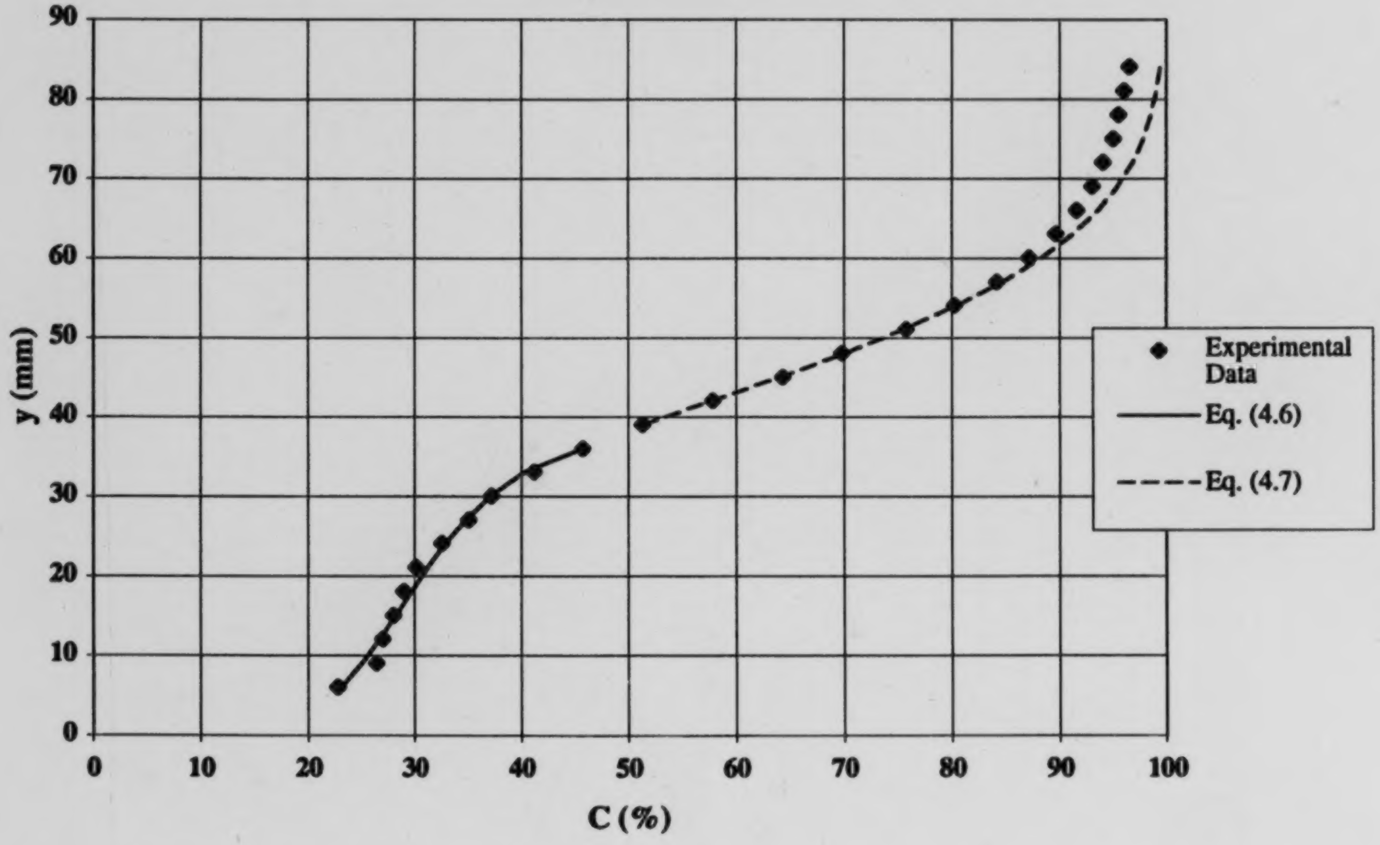

Figure A.44 Concentration profile at step tip #60 in a stepped spillway with l/h=0.8, h= 31.25 mm (yc/h=4.0)

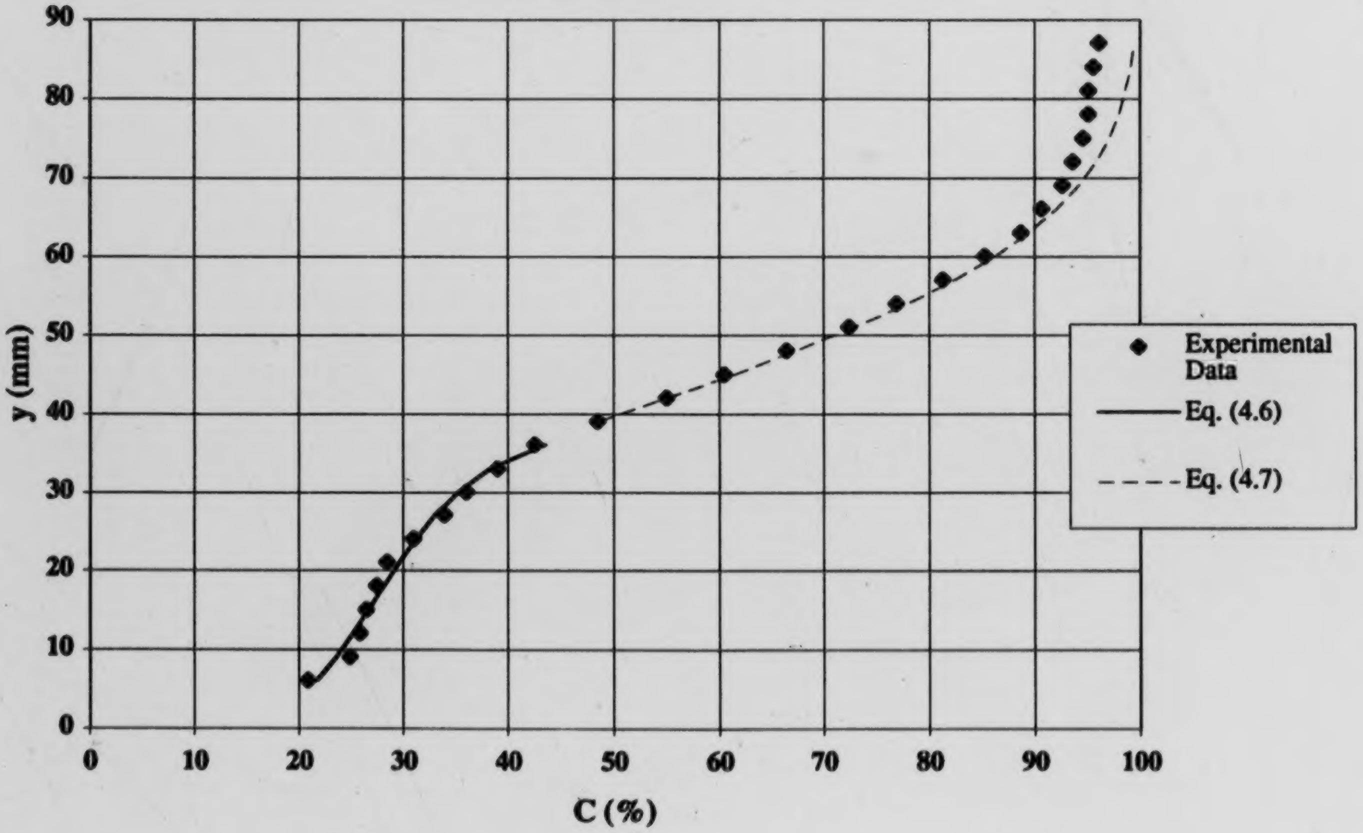

Figure A.45 Concentration profile at step tip #60 in a stepped spillway with l/h=0.8, h= 31.25 mm (yc/h=4.2)

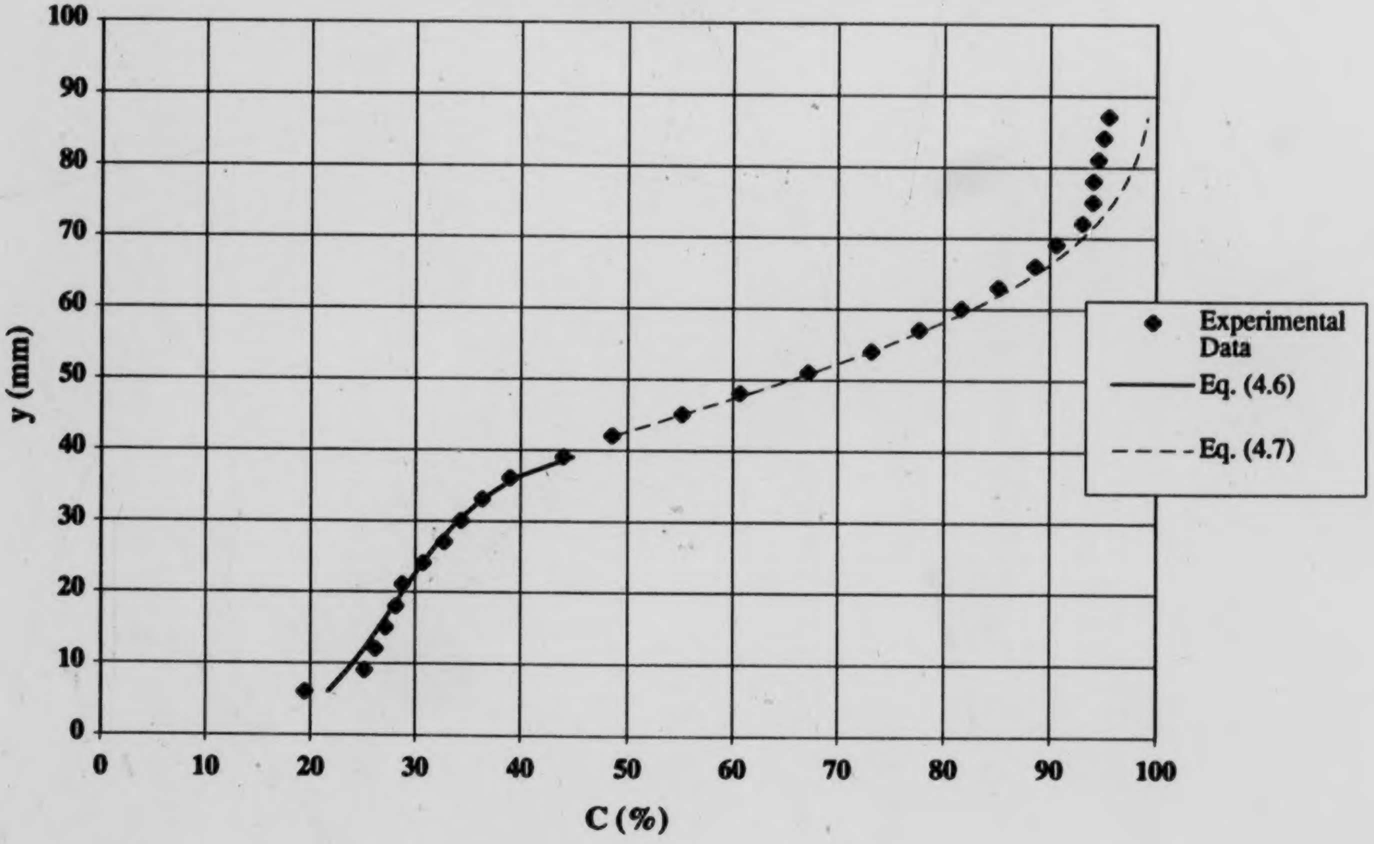

Figure A.46 Concentration profile at step tip #60 in a stepped spillway with l/h=0.8, h= 31.25 mm (yc/h=4.4)

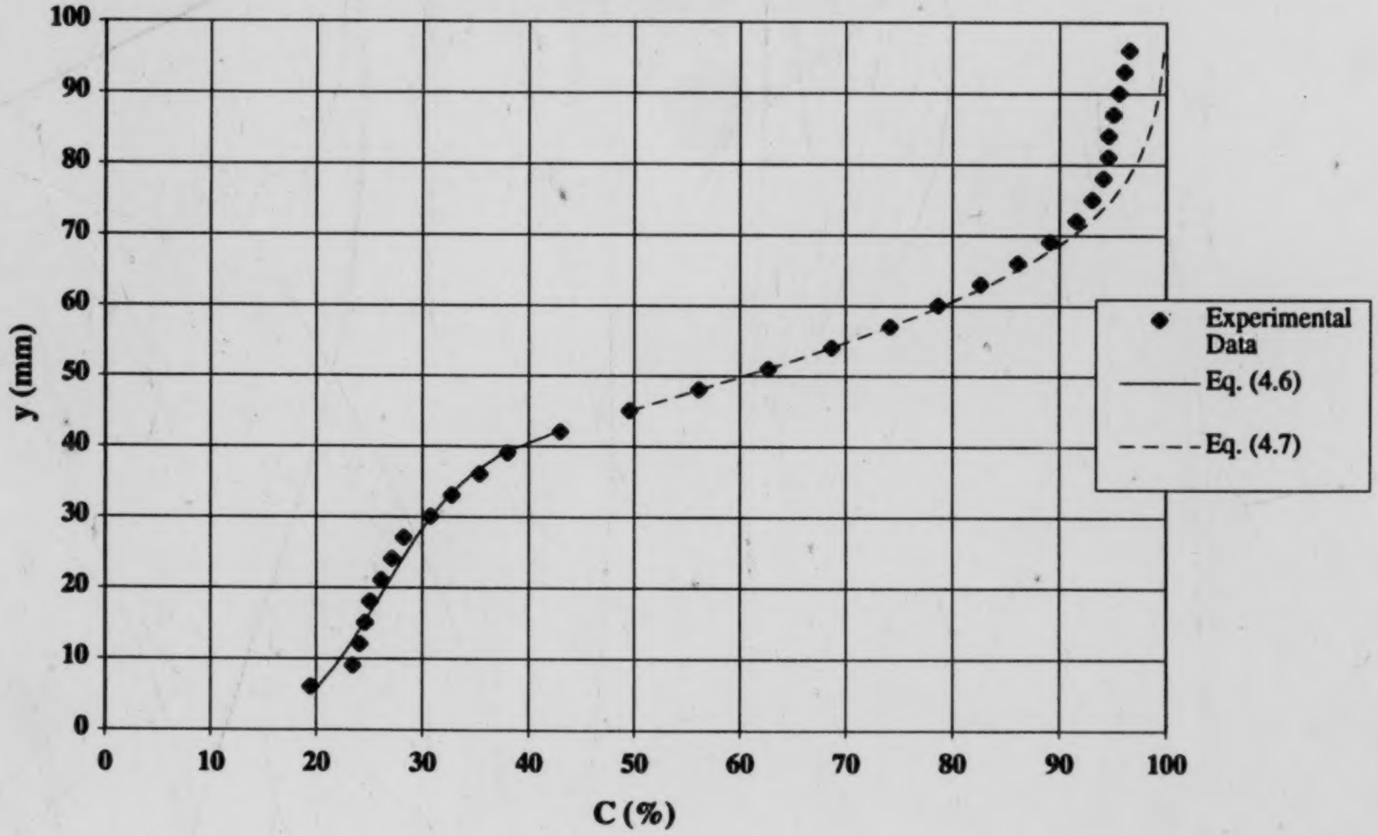

APPENDIX B

VELOCITY PROFILES FOR VARIOUS VALUES OF FLOW DISCHARGE, STEP HEIGHT, AND CHANNEL SLOPE

Figure B.1 Velocity profile at step tip #13 in a stepped spillway with l/h=0.6, h= 125. mm (yc/h=0.7)

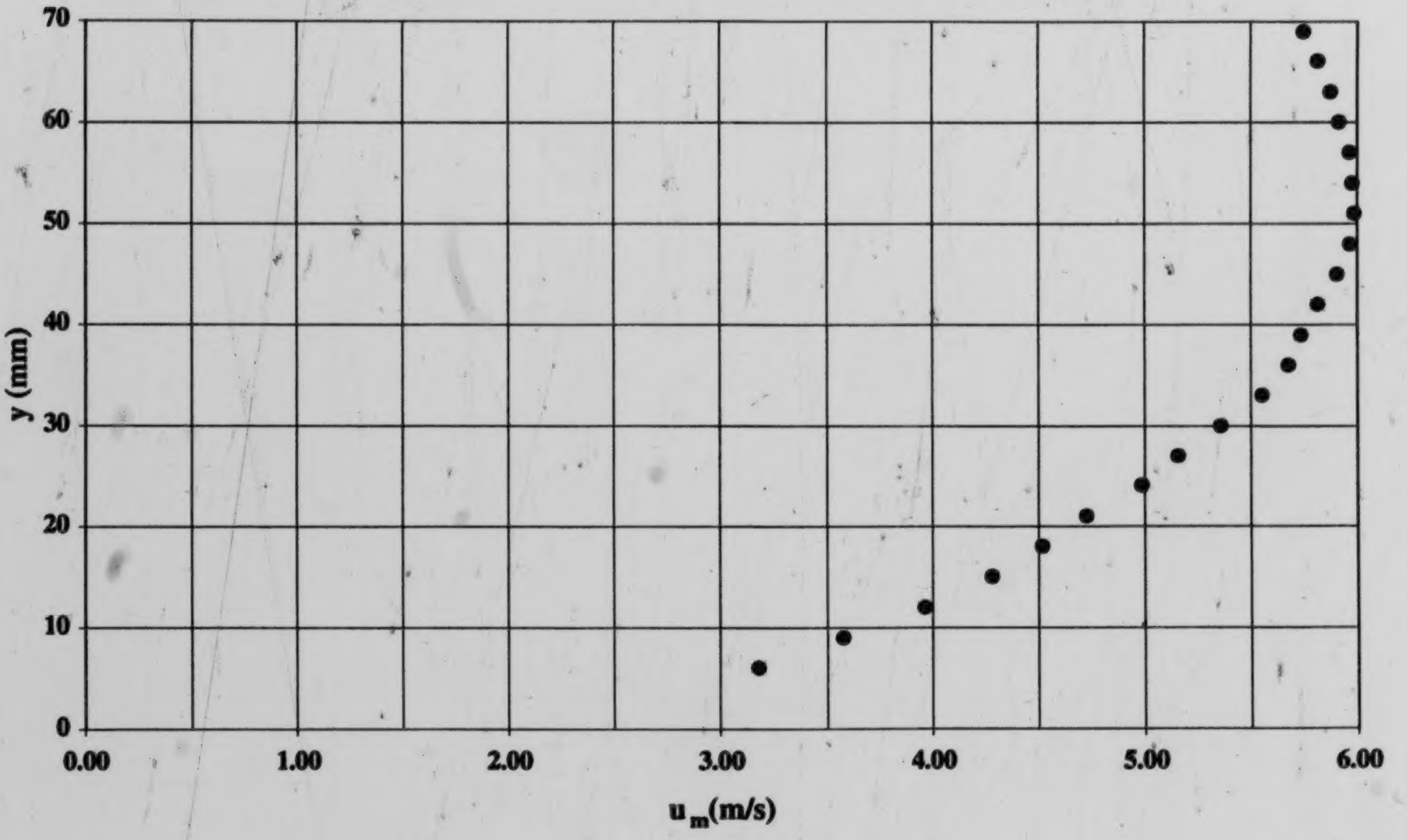

Figure B.2 Velocity profile at step tip #13 in a stepped spillway with l/h=0.6, h= 125. mm (yc/h=0.8)

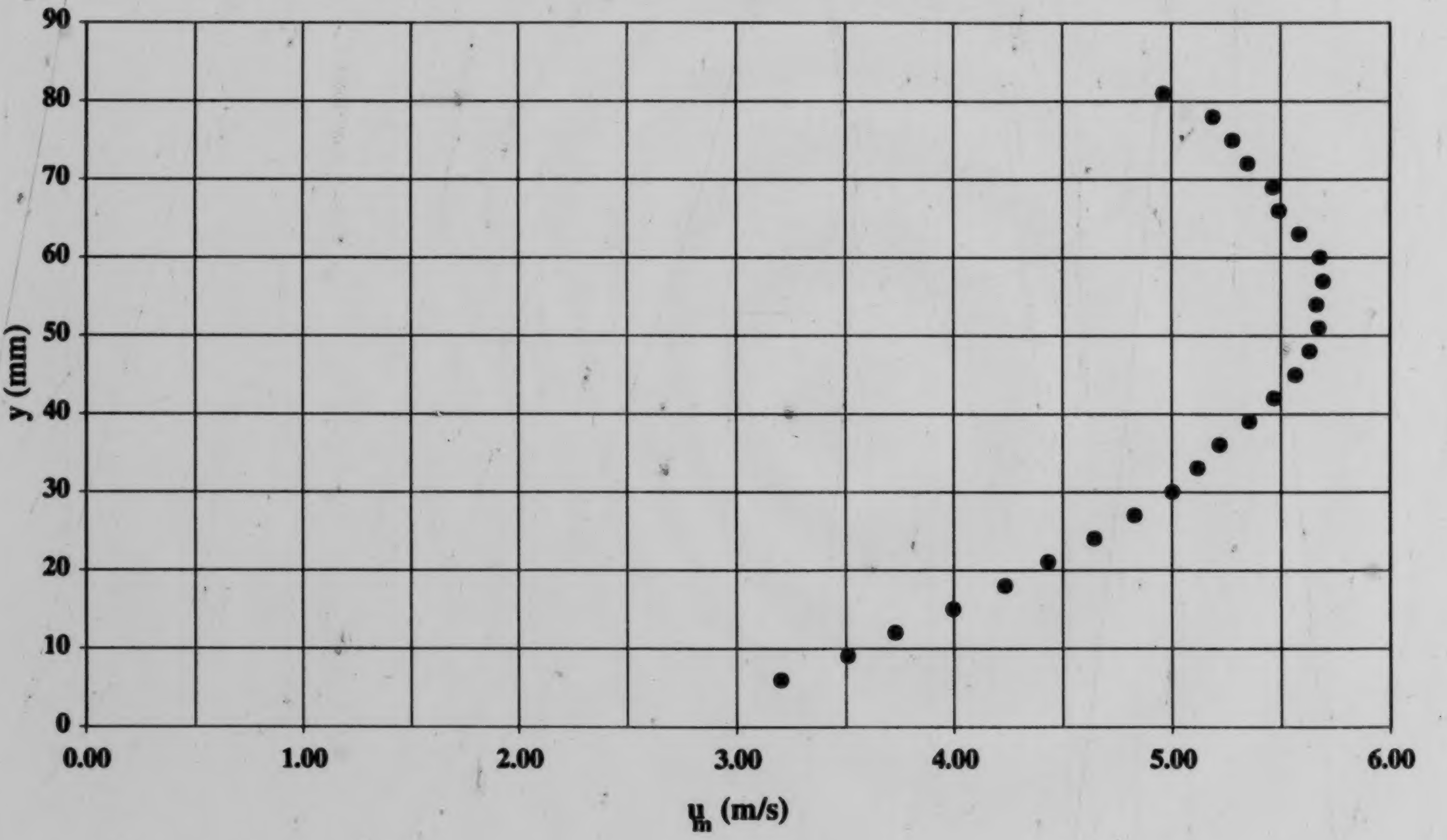

Figure B.3 Velocity profile at step tip #13 in a stepped spillway with l/h=0.6, h= 125. mm (yc/h=1.0)

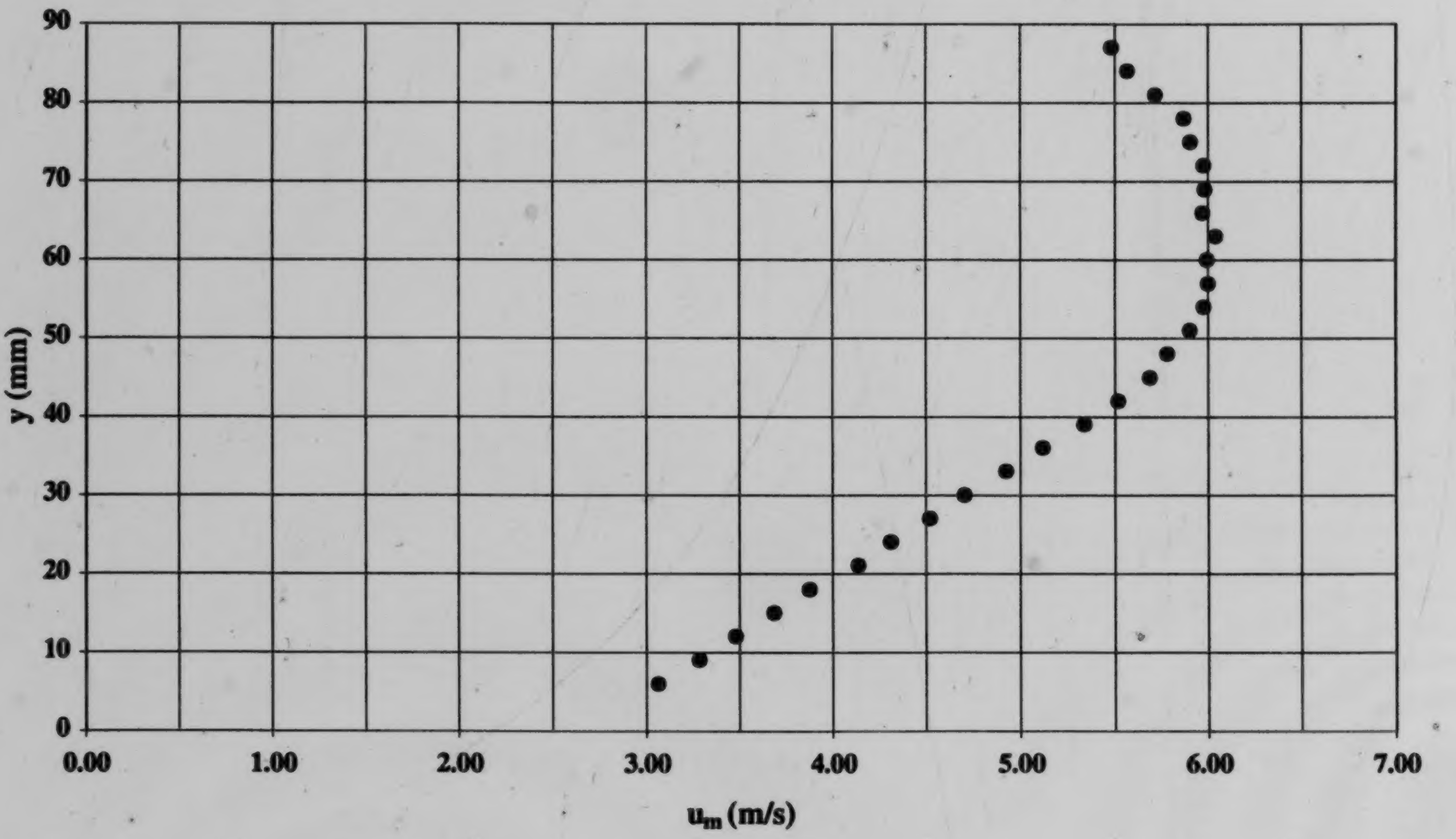

Figure B.4 Velocity profile at step tip #13 in a stepped spillway with l/h=0.6, h= 125. mm (yc/h=1.1)

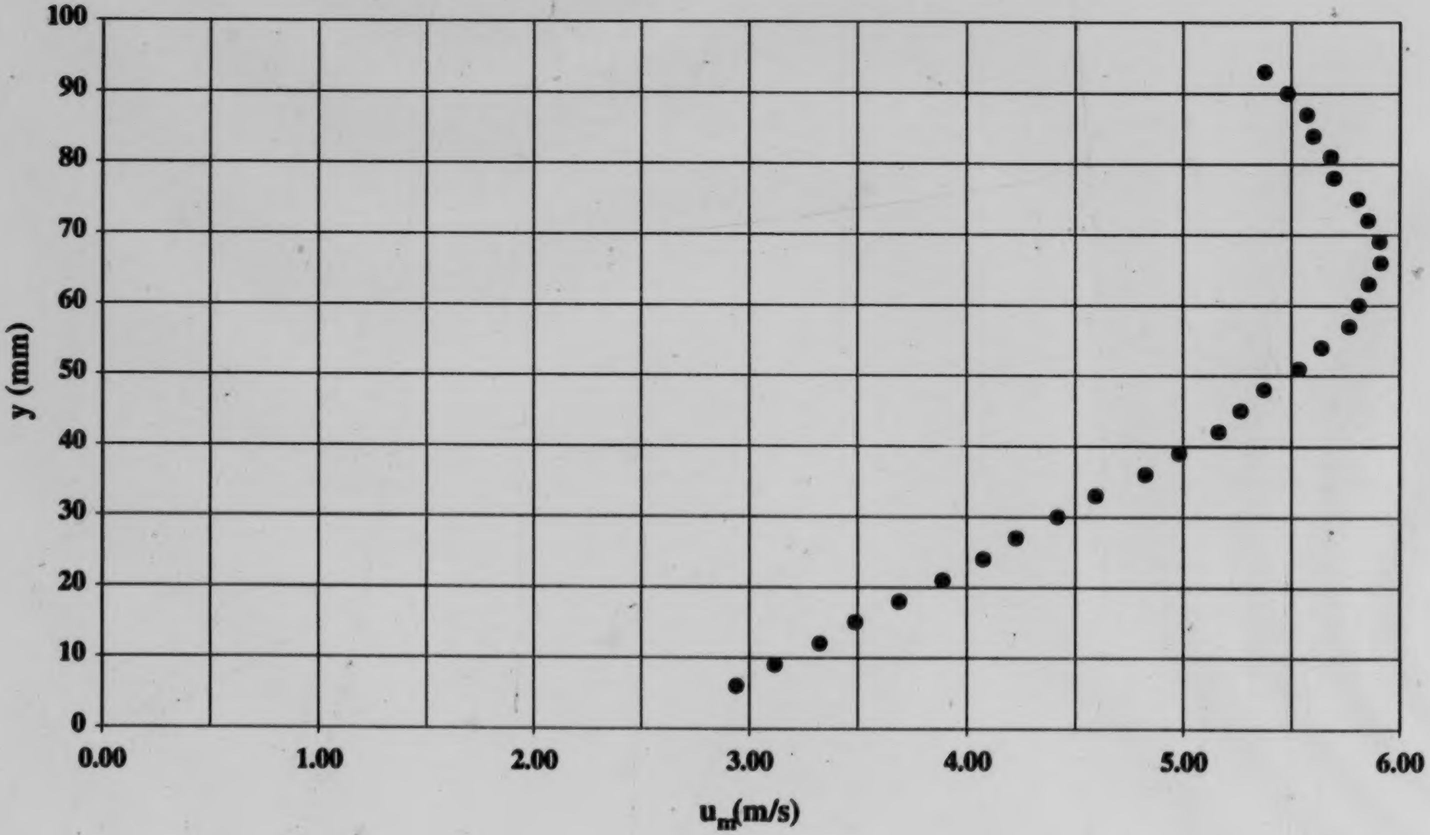

Fig. B.5 Velocity profile at step tip #16 in a stepped spillway with l/h=0.6, h= 125. mm (yc/h=1.2)

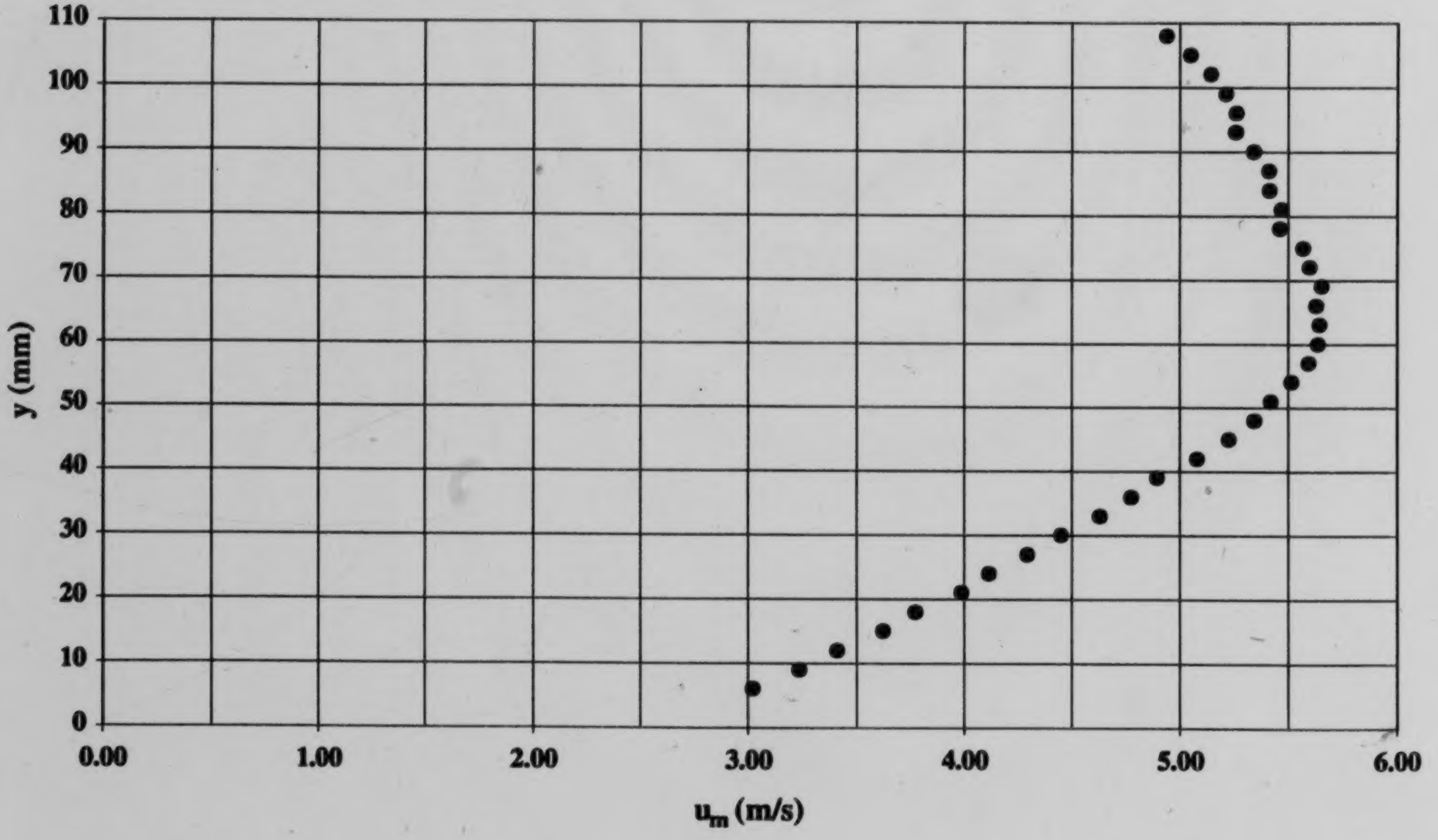

Figure B.6 Velocity profile at step tip #16 in a stepped spillway with l/h=0.6, h= 125. mm (yc/h=1.3)

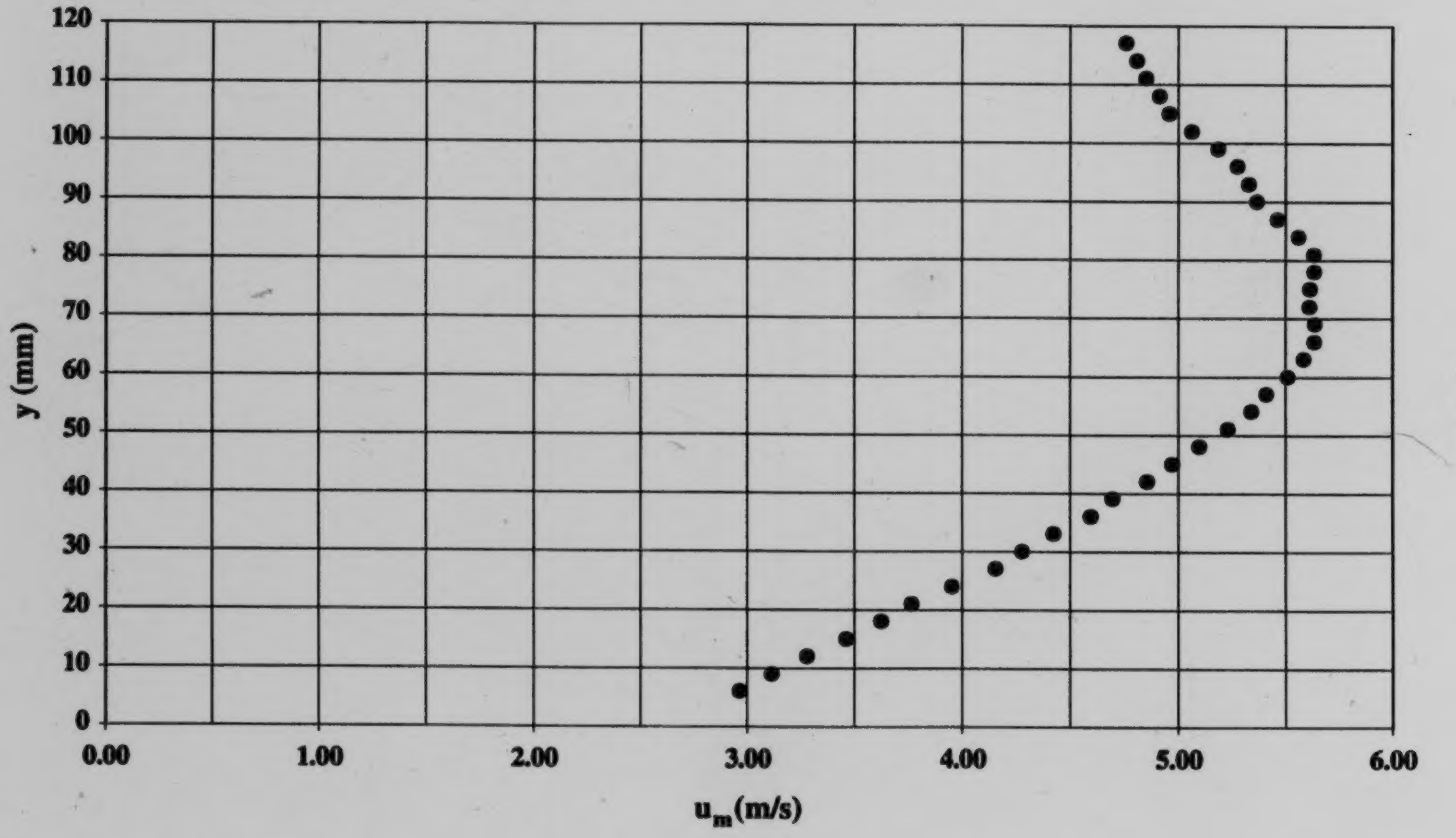

Figure B.7 Velocity profile at step tip #26 in a stepped spillway with l/h=0.6, h= 62.5 mm (yc/h=1.3)

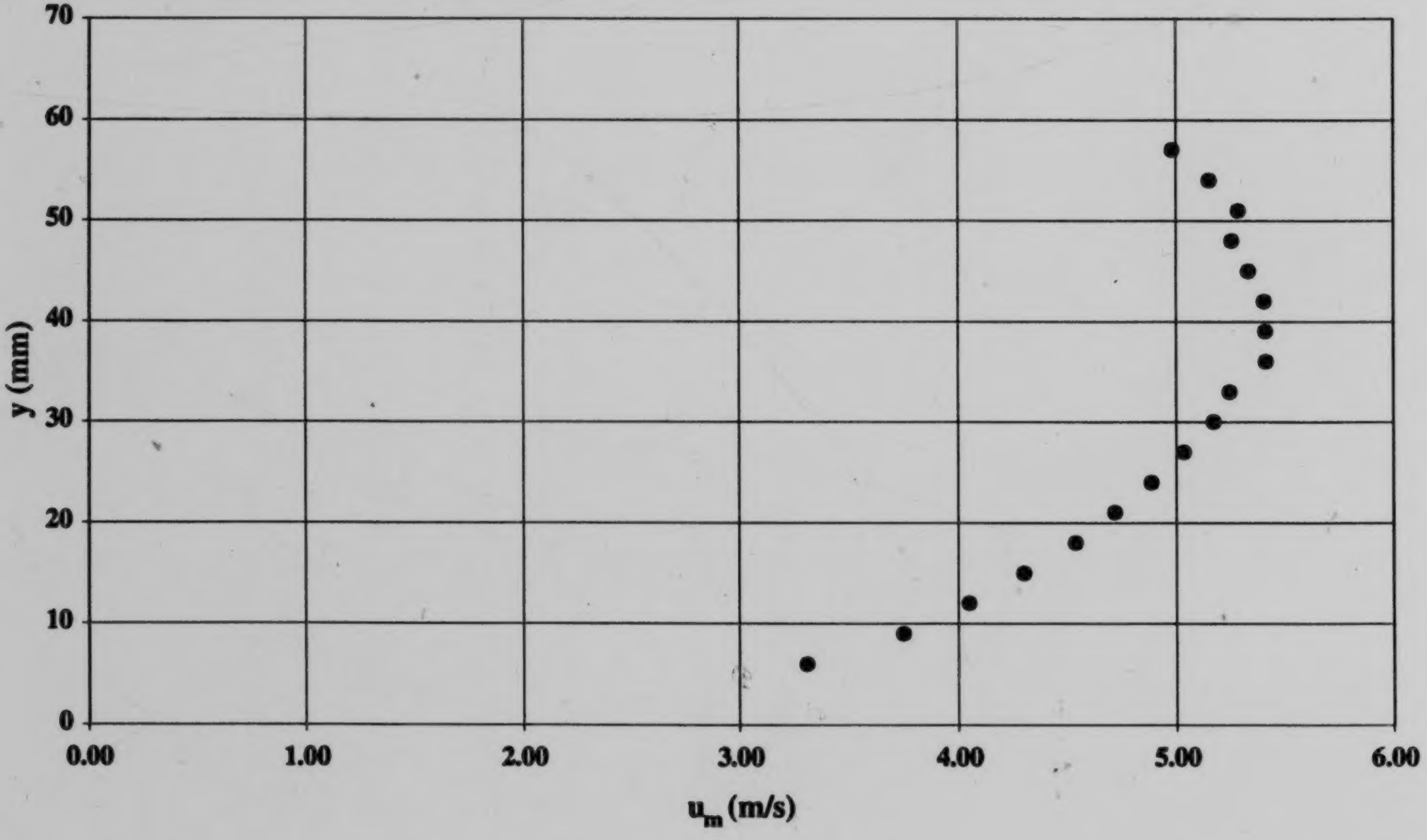

Figure B.8 Velocity profile at step tip #26 in a stepped spillway with l/h=0.6, h= 62.5 mm (yc/h=1.4)

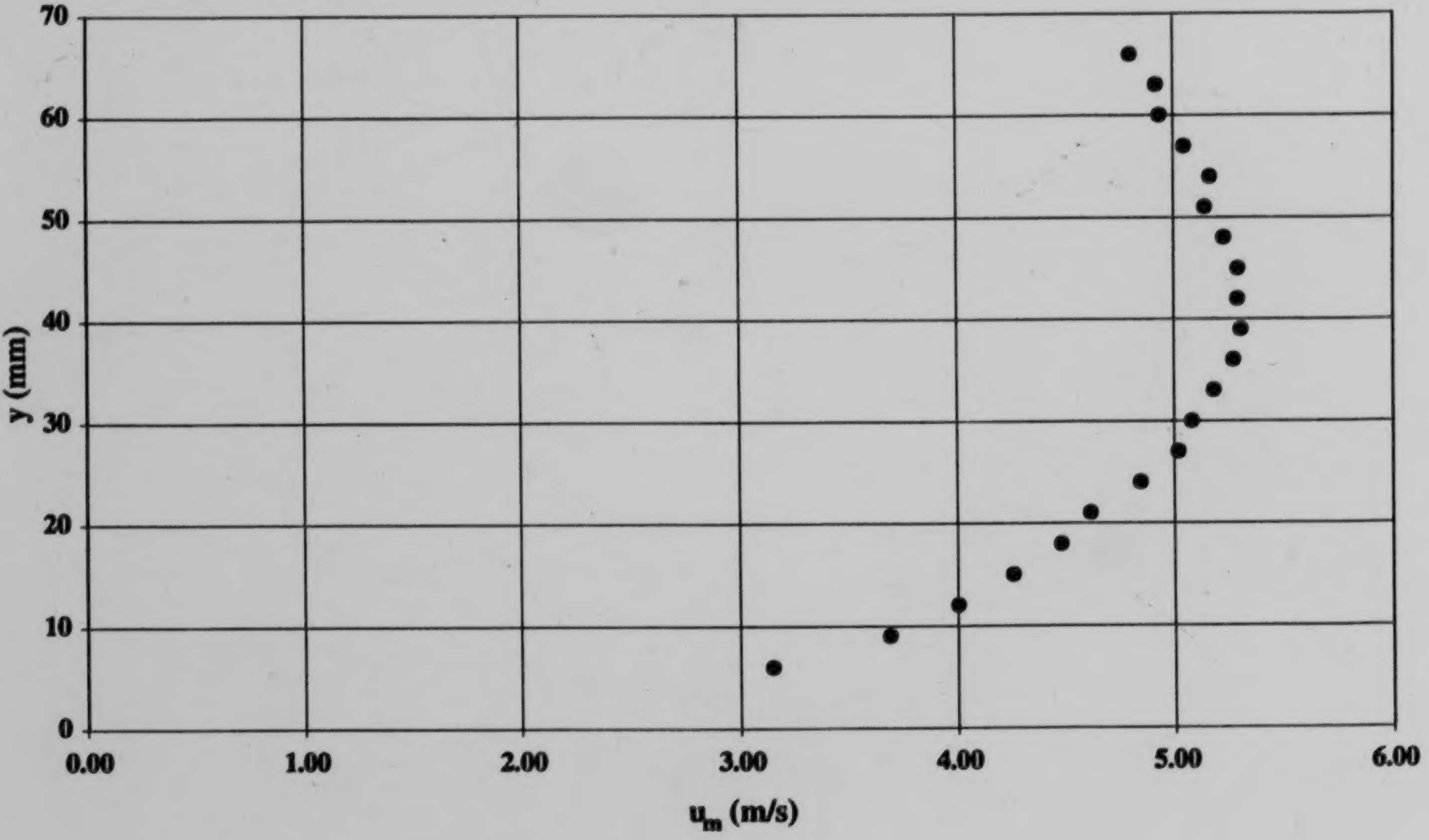

Figure B.9 Velocity profile at step tip #26 in a stepped spillway with l/h=0.6, h= 62.5 mm (yc/h=1.5)

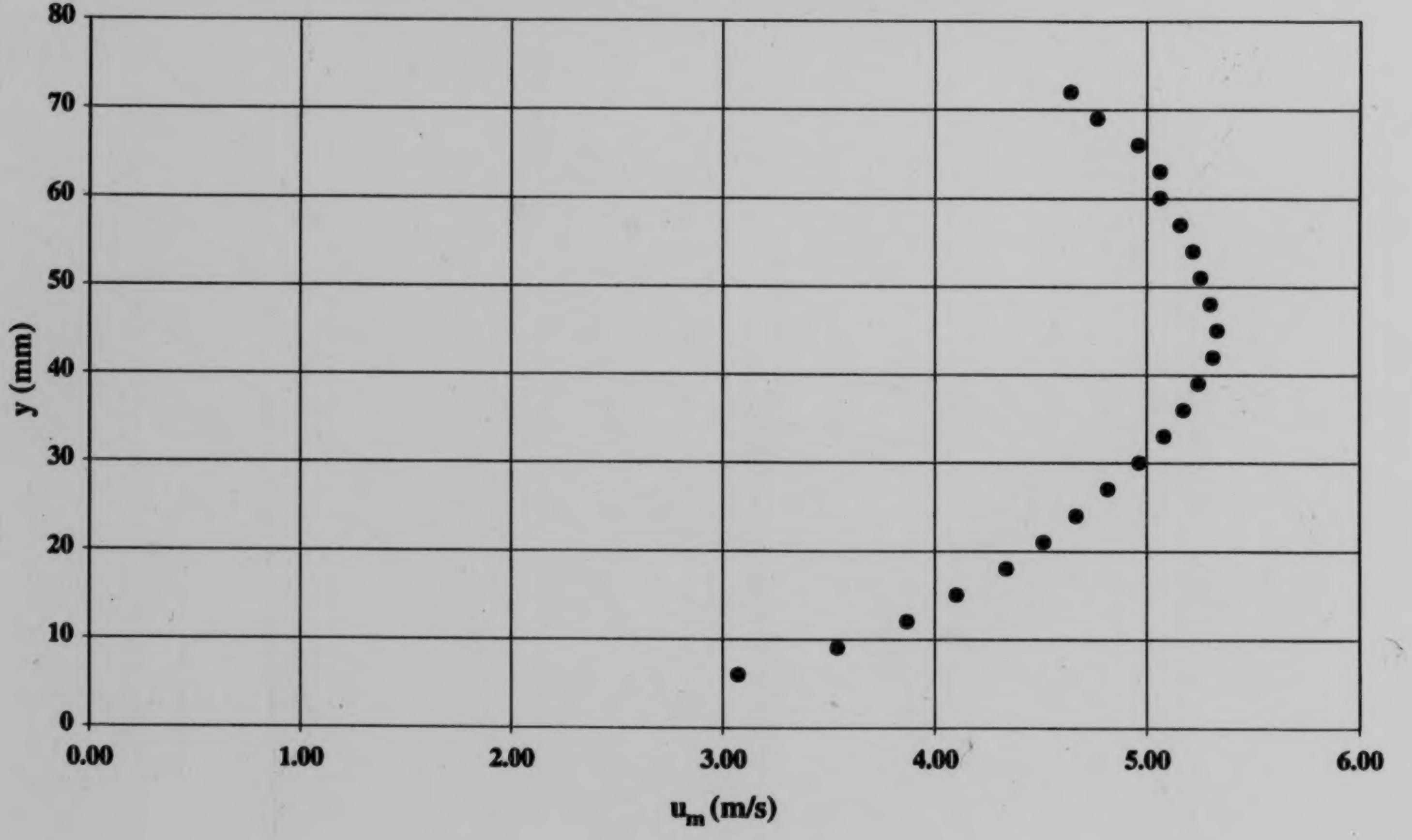

Figure B.10 Velocity profile at step tip #26 in a stepped spillway with l/h=0.6, h= 62.5 mm (yc/h=1.6)

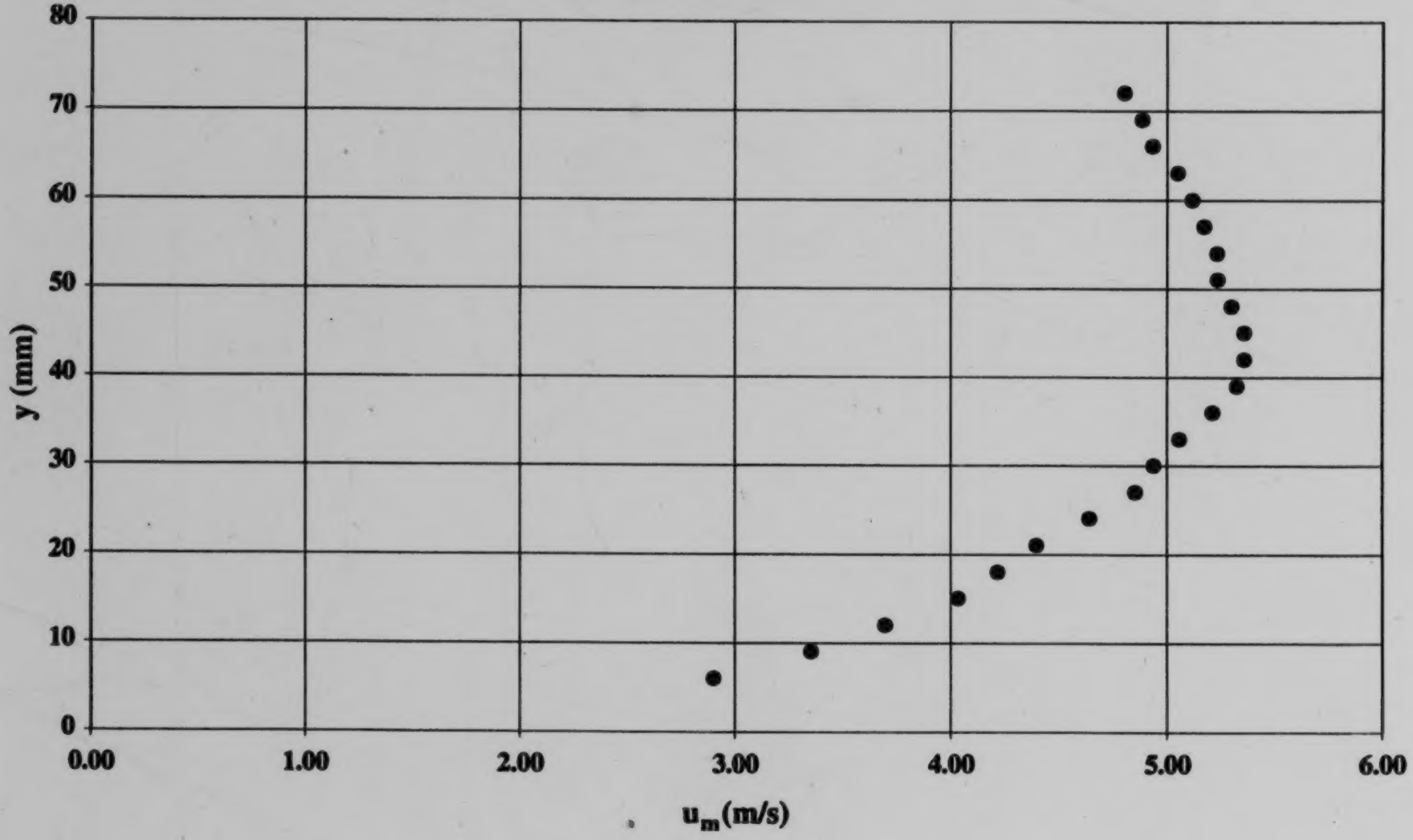

Figure B.11 Velocity profile at step tip #26 in a stepped spillway with l/h=0.6, h= 62.5 mm
(yc/h=1.7)

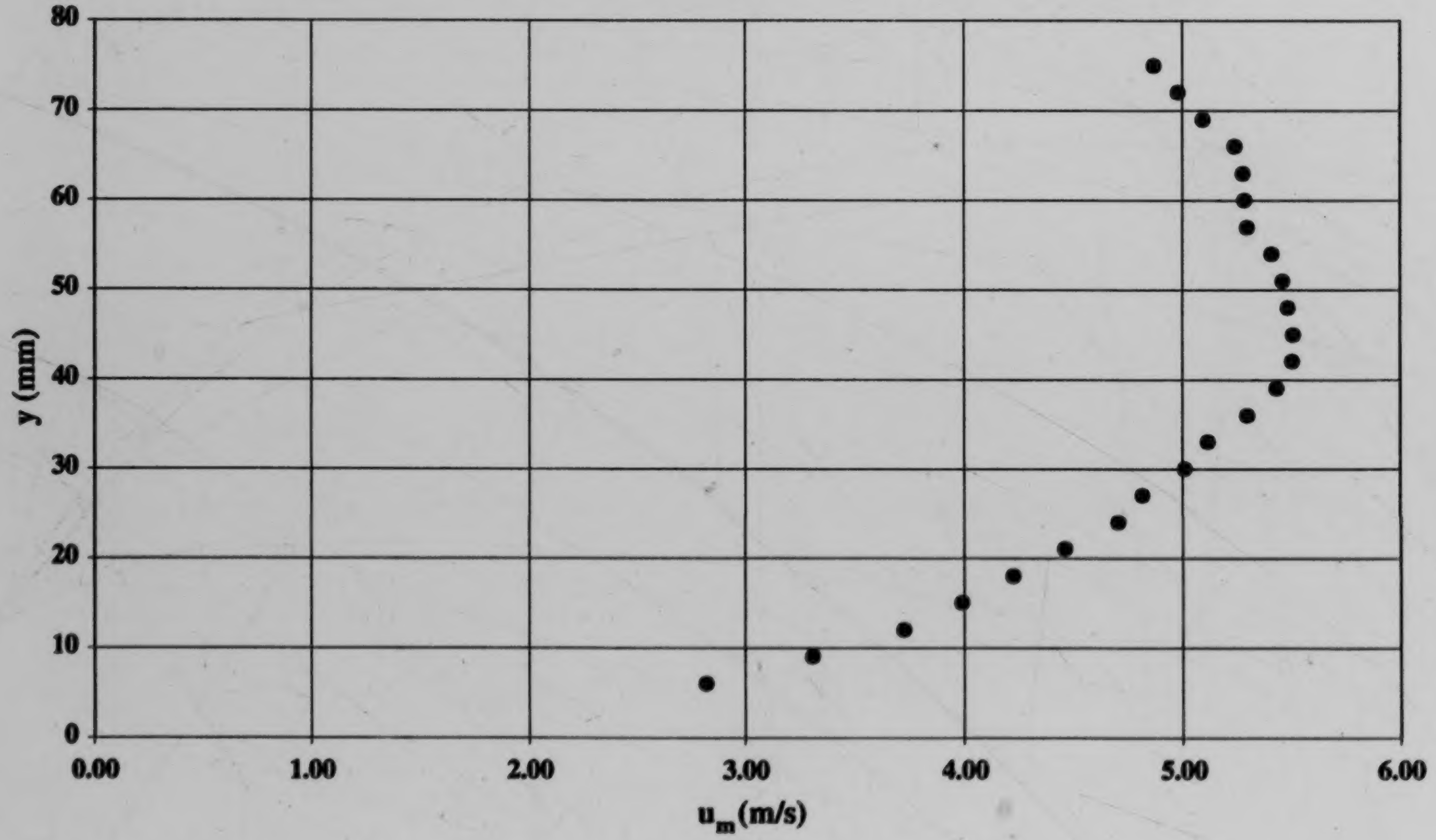

Figure B.12 Velocity profile at step tip #26 in a stepped spillway with l/h=0.6, h= 62.5 mm (yc/h=1.8)

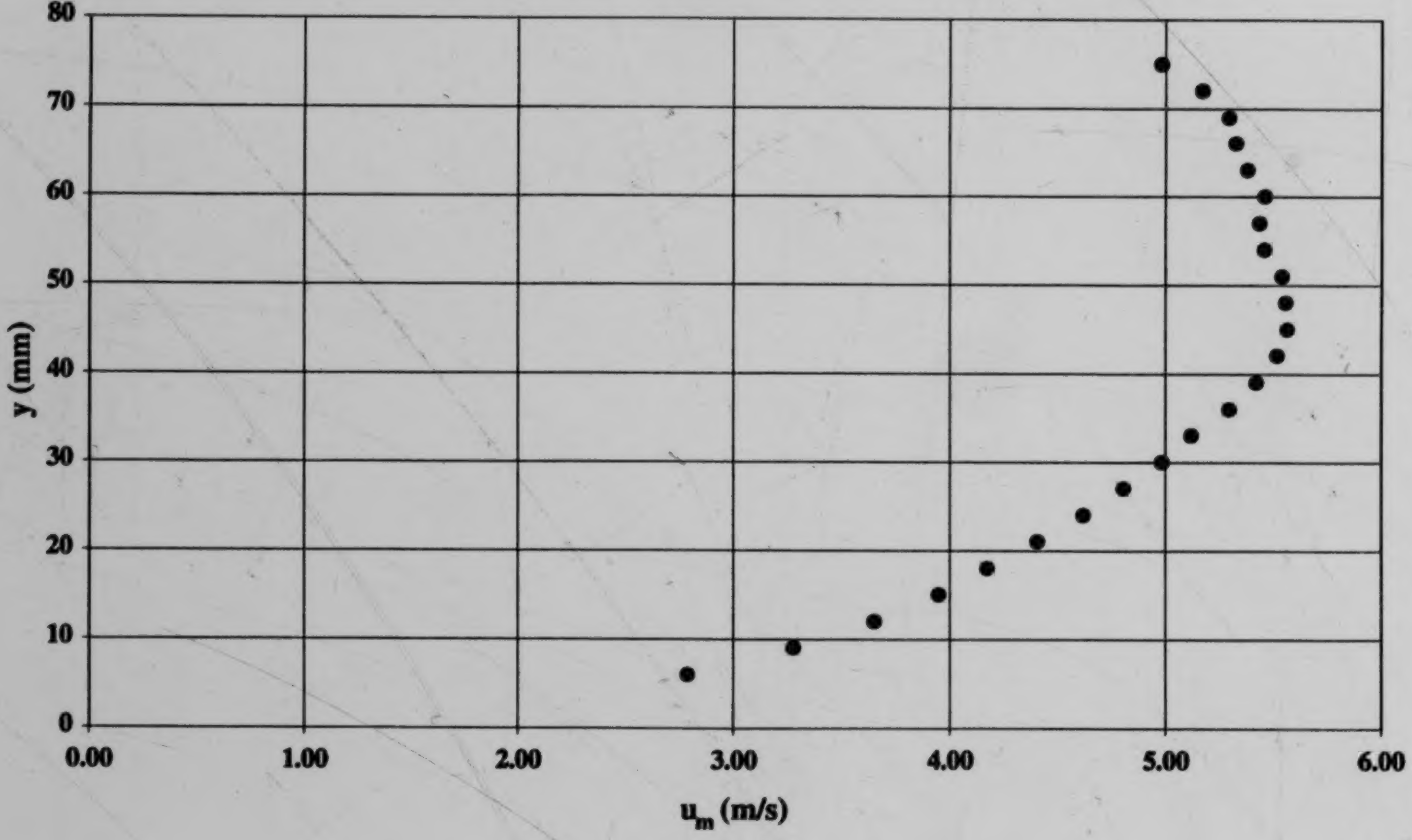

Figure B.13 Velocity profile at step tip #32 in a stepped spillway with l/h=0.6, h= 62.5 mm (yc/h=2.0)

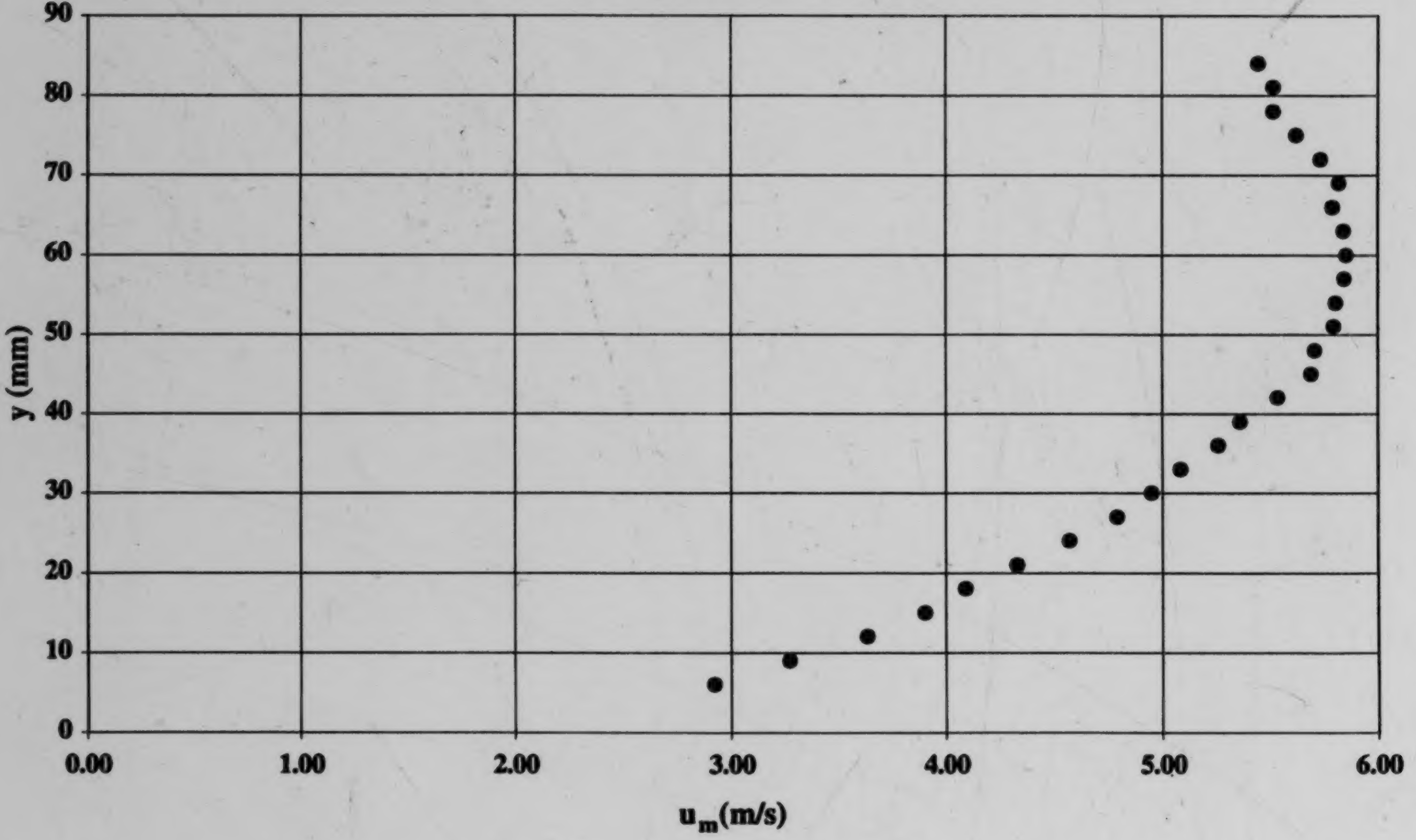

Figure B.14 Velocity profile at step tip #32 in a stepped spillway with l/h=0.6, h= 62.5 mm (yc/h=2.1)

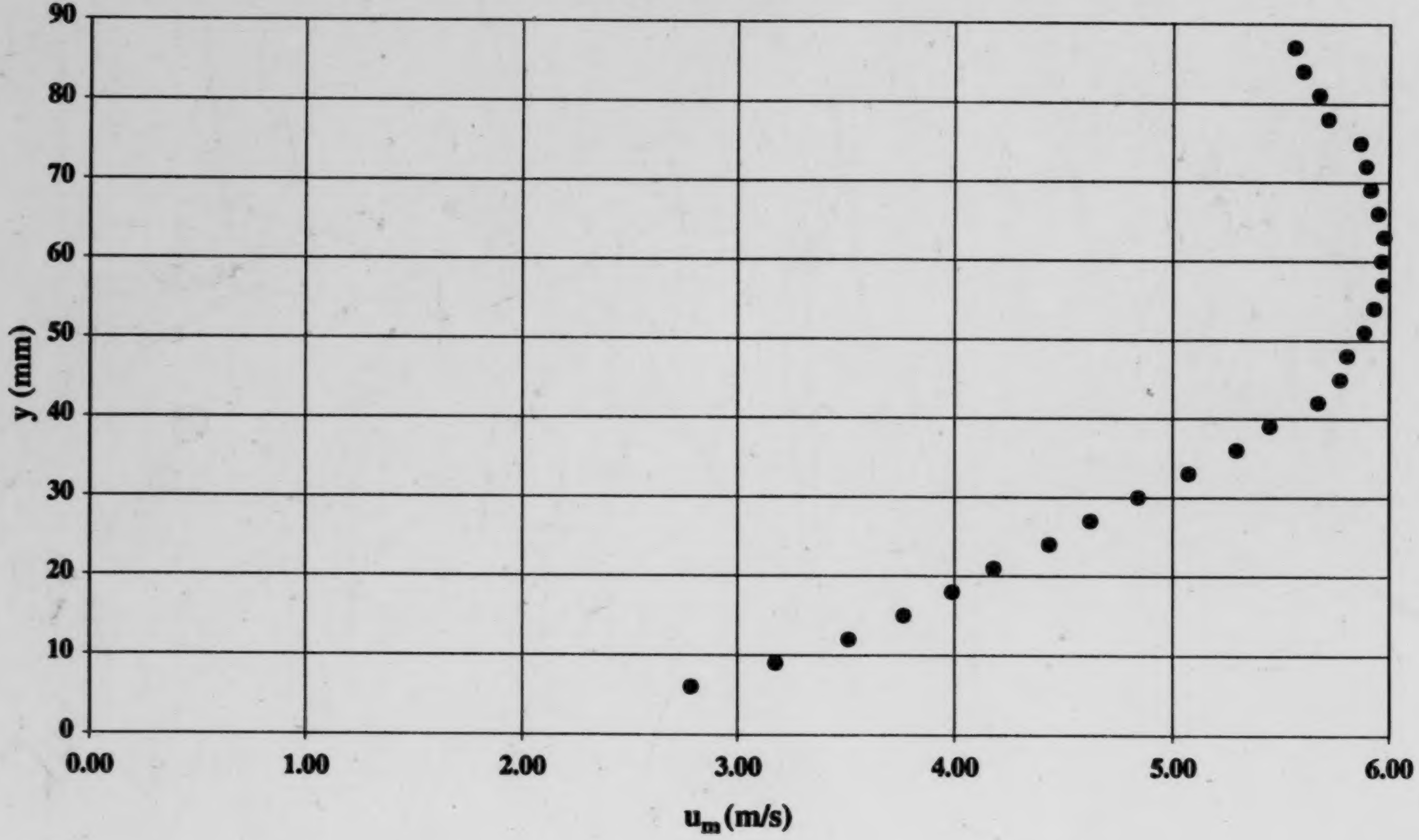

Figure B.15 Velocity profile at step tip #32 in a stepped spillway with l/h=0.6, h= 62.5 mm (yc/h=2.2)

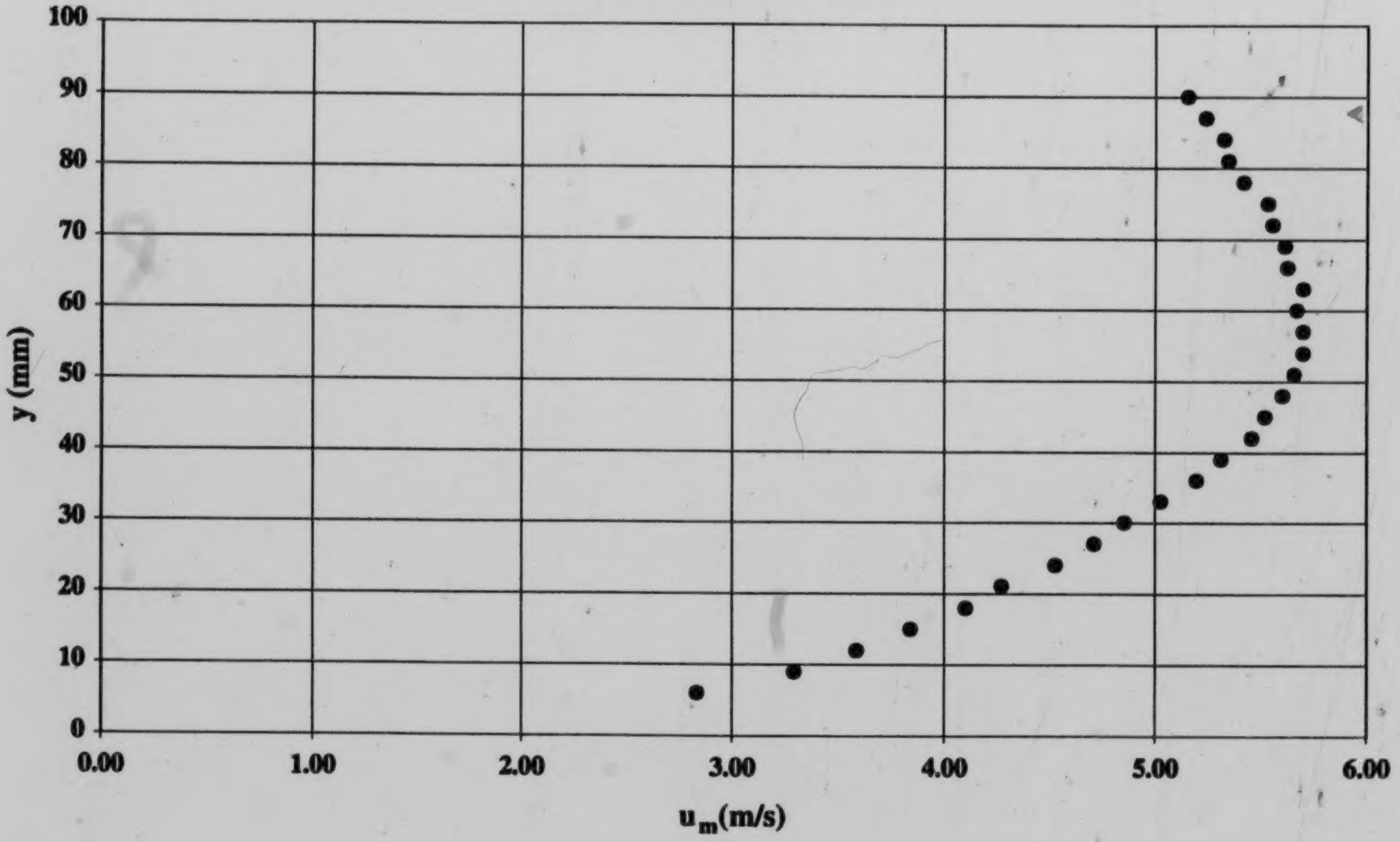

Figure B.16 Velocity profile at step tip #32 in a stepped spillway with l/h=0.6, h= 62.5 mm (yc/h=2.3)

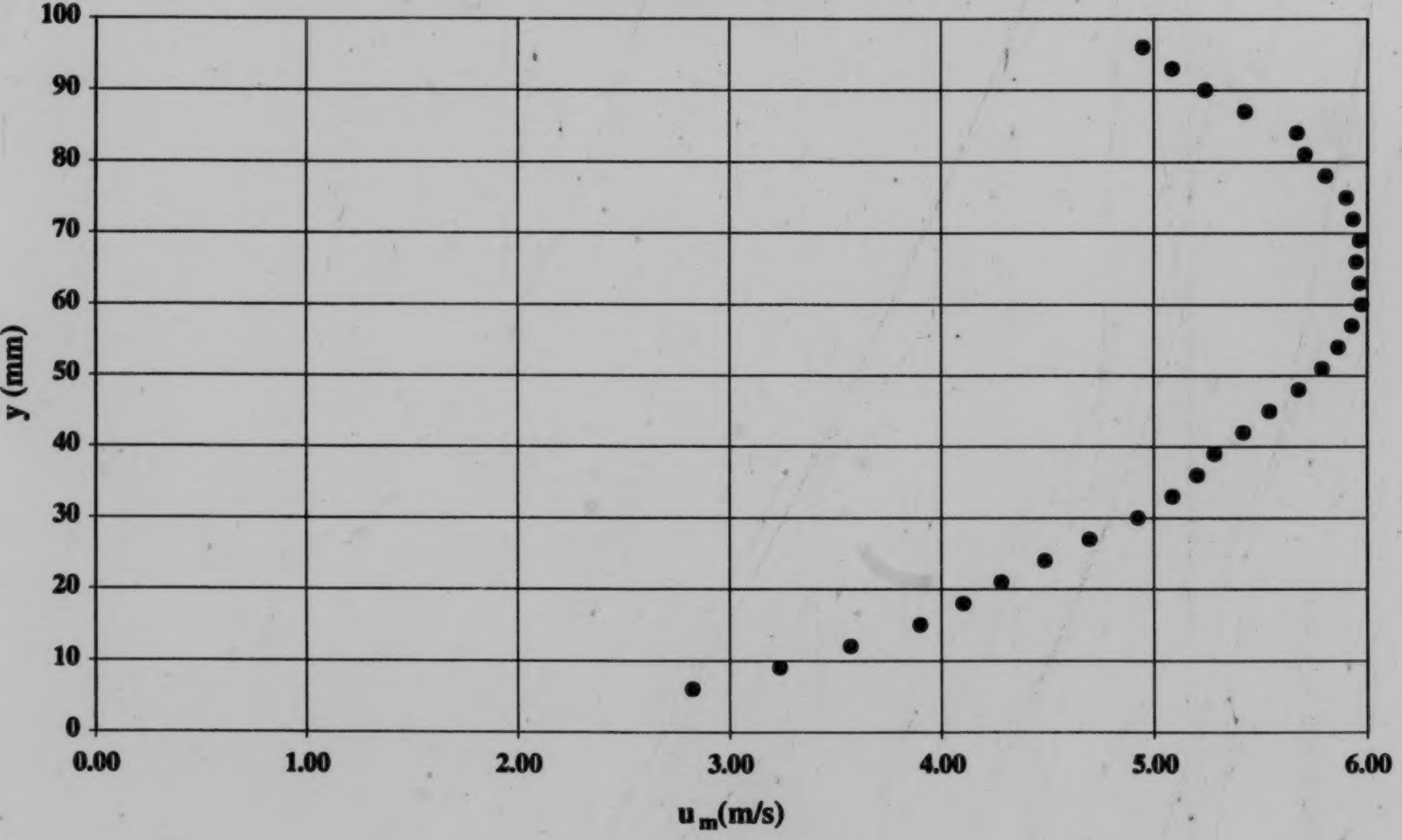

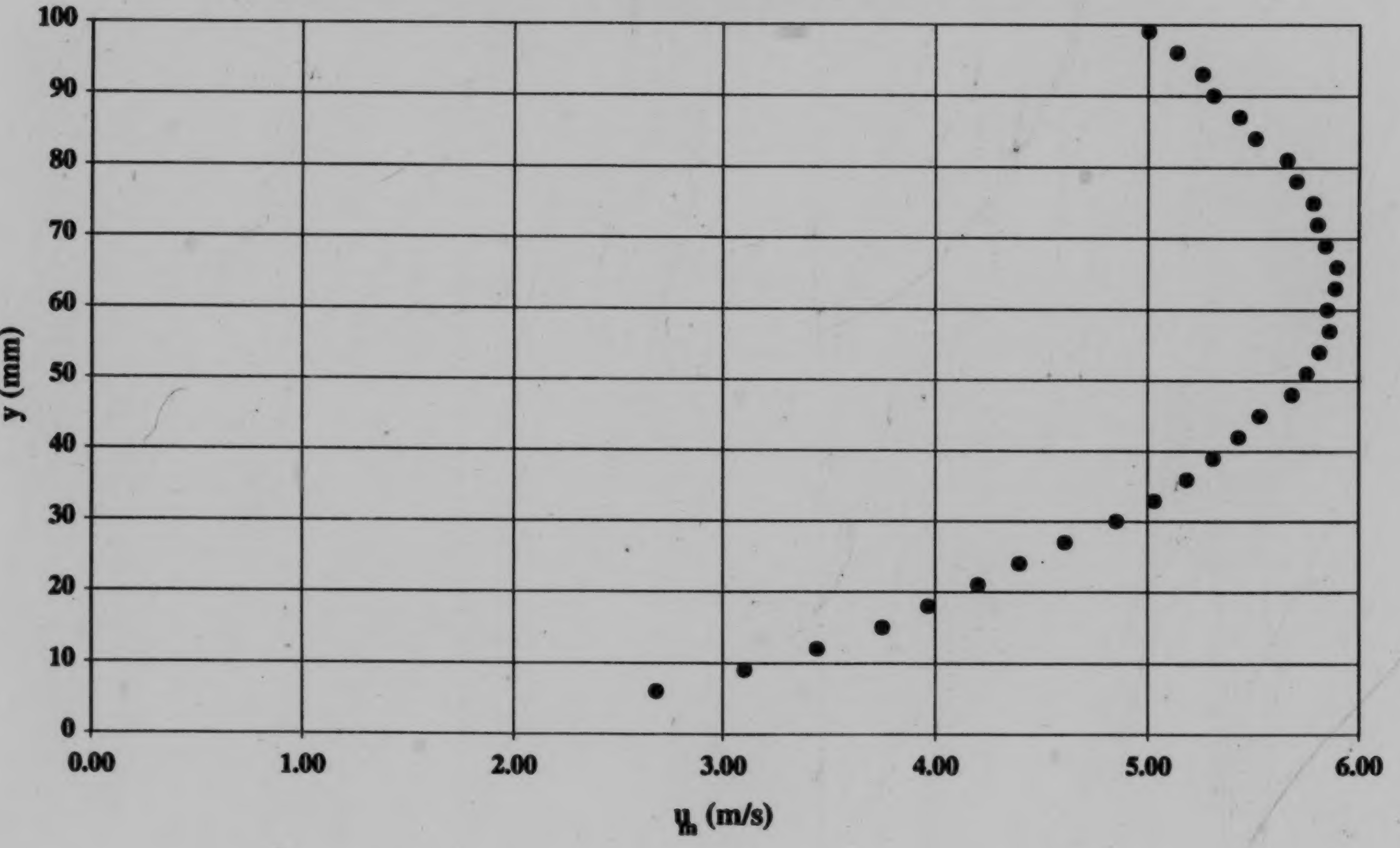

Figure B.17 Velocity profile at step tip #32 in a stepped spillway with l/h=0.6, h= 62.5 mm (yc/h=2.4)

Figure B.18 Velocity profile at step tip #32 in a stepped spillway with l/h=0.6, h= 62.5 mm (yc/h=2.5)

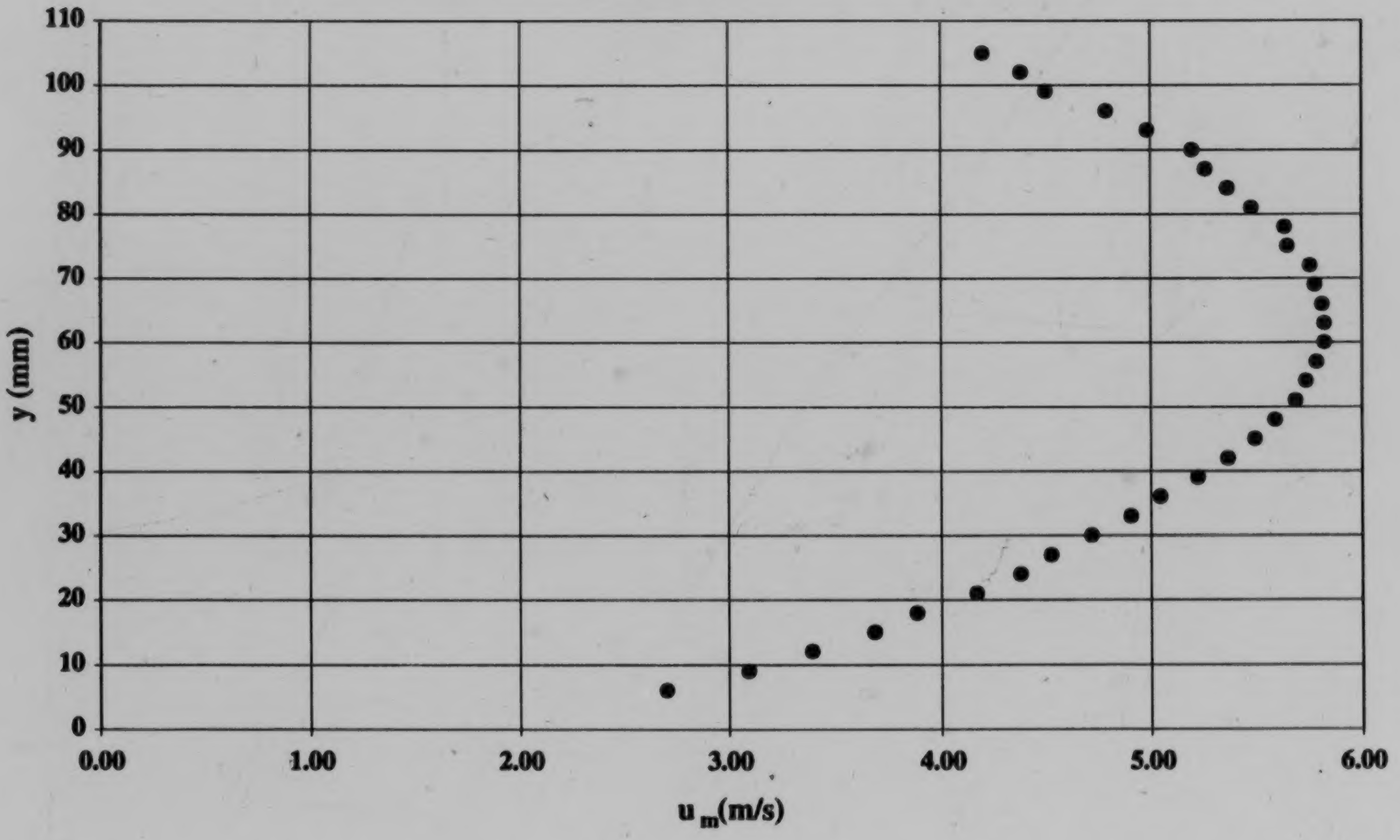

Figure B.19 Velocity profile at step tip #32 in a stepped spillway with l/h=0.6, h= 62.5 mm
(yc/h=2.6)

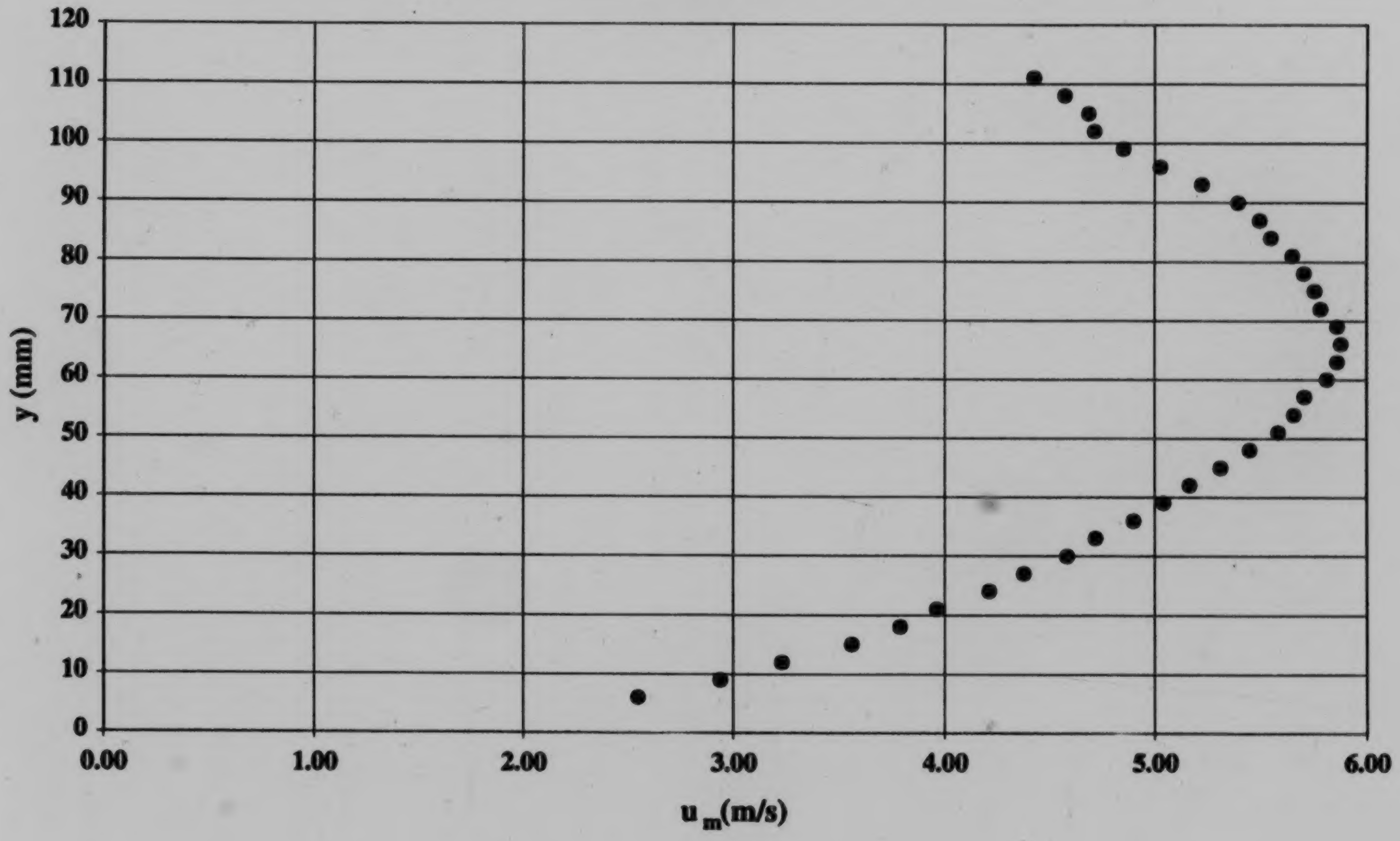

Figure B.20 Velocity profile at step tip #64 in a stepped spillway with l/h=0.6, h= 31.25 mm (yc/h=2.6)

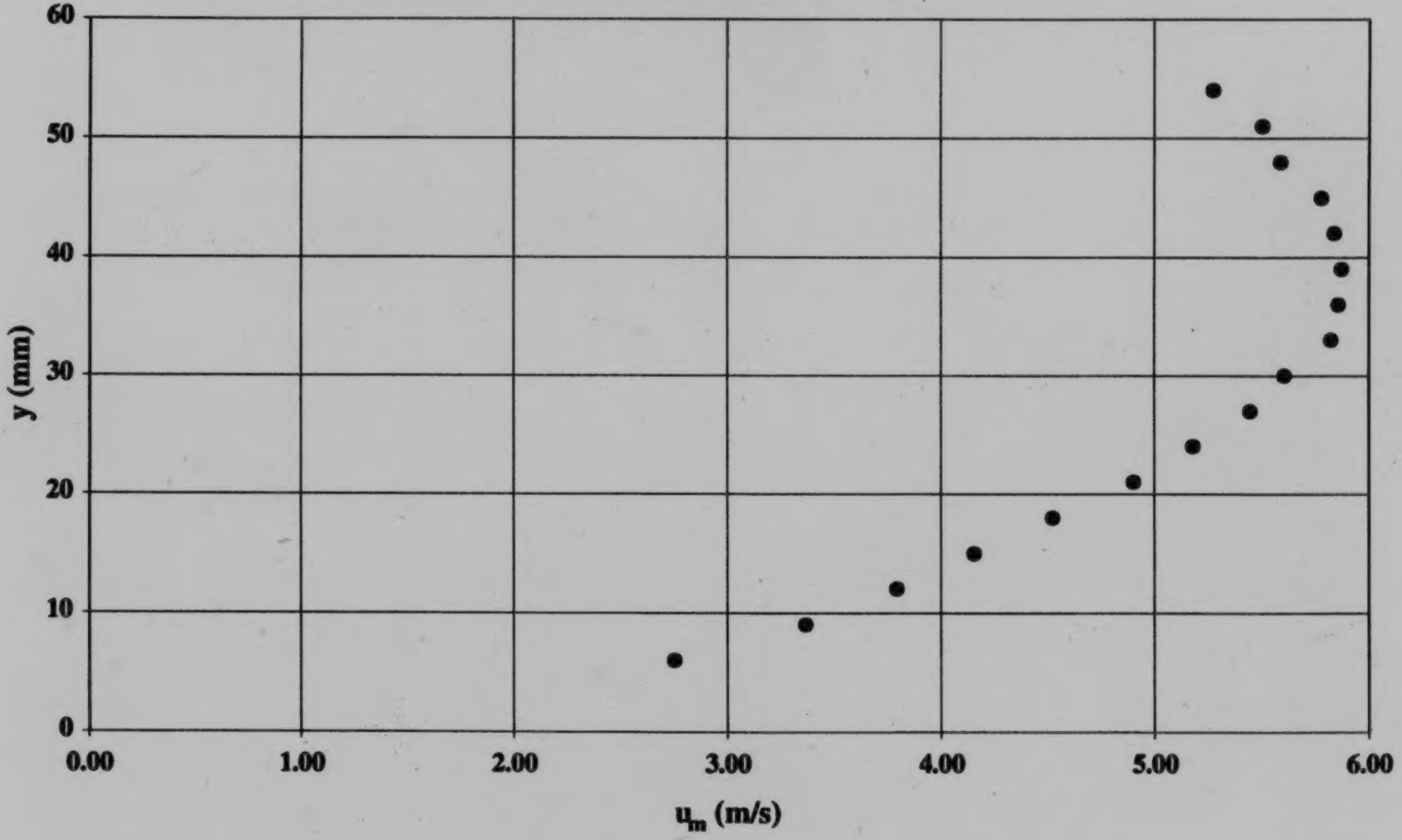

Figure B.21 Velocity profile at step tip #64 in a stepped spillway with l/h=0.6, h= 31.25 mm (yc/h=2.8)

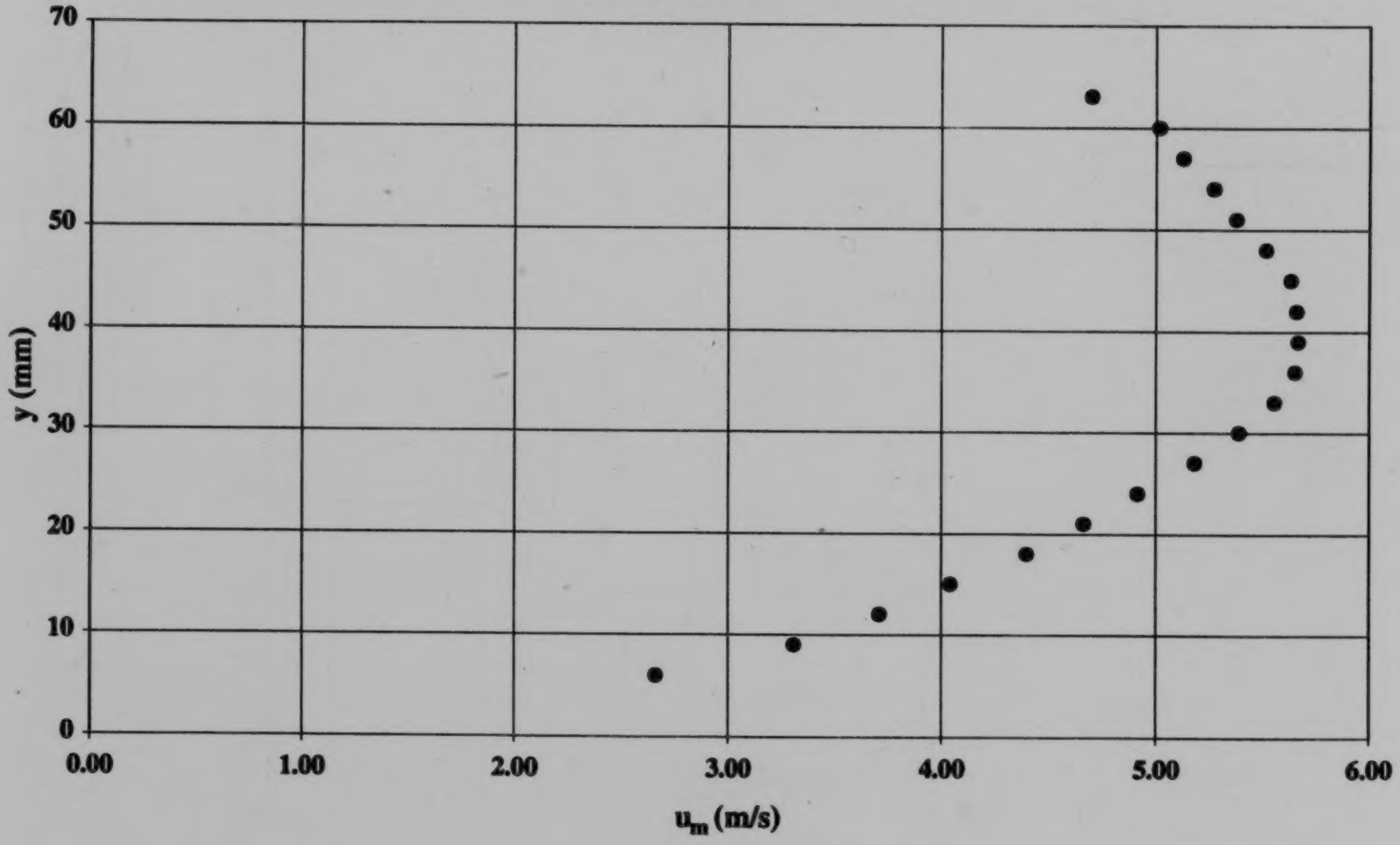

Figure B.22 Velocity profile at step tip #64 in a stepped spillway with l/h=0.6, h= 31.25 mm (yc/h=3.0)

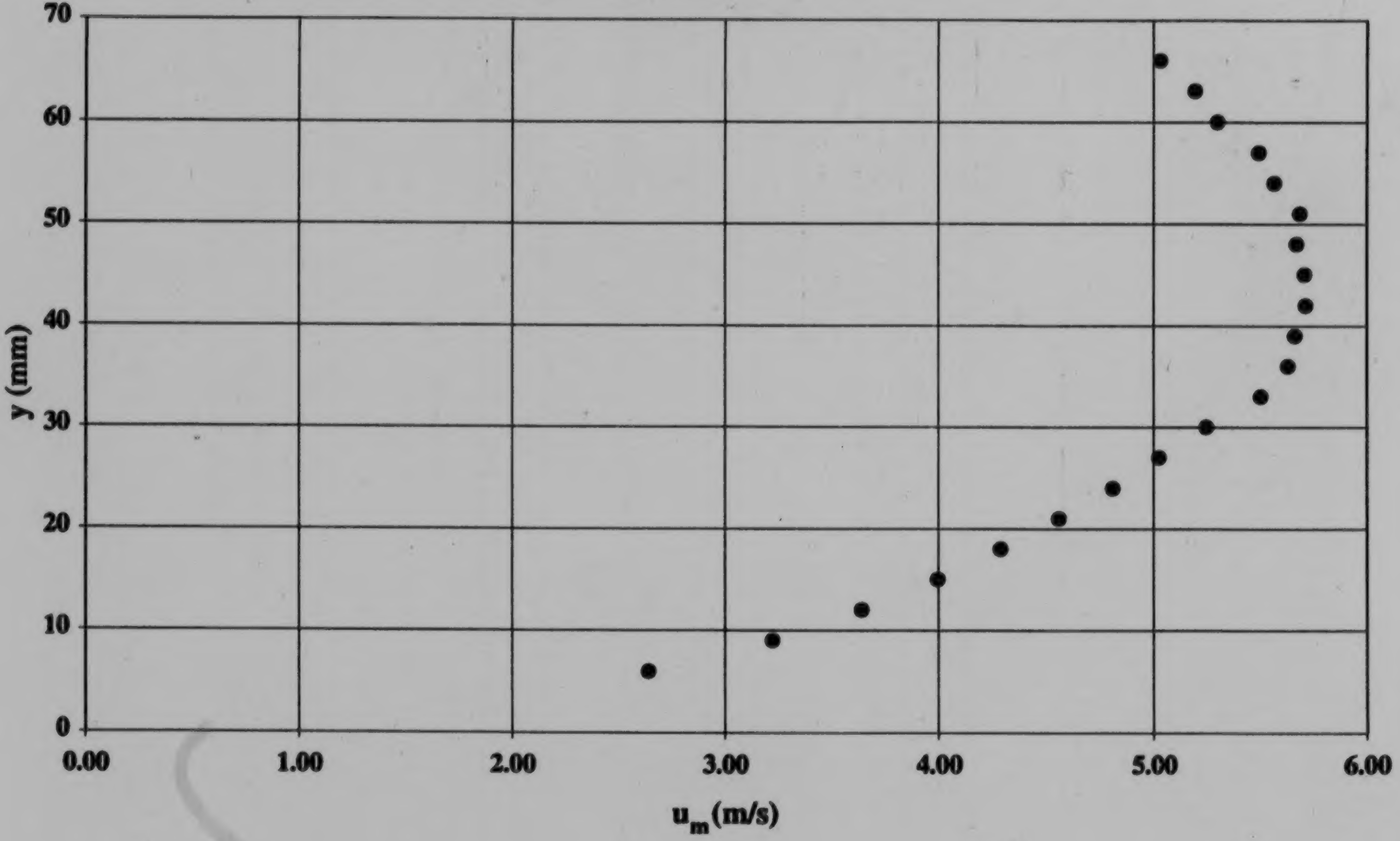

Figure B.23 Velocity profile at step tip #64 in a stepped spillway with l/h=0.6, h= 31.25 mm (yc/h=3.2)

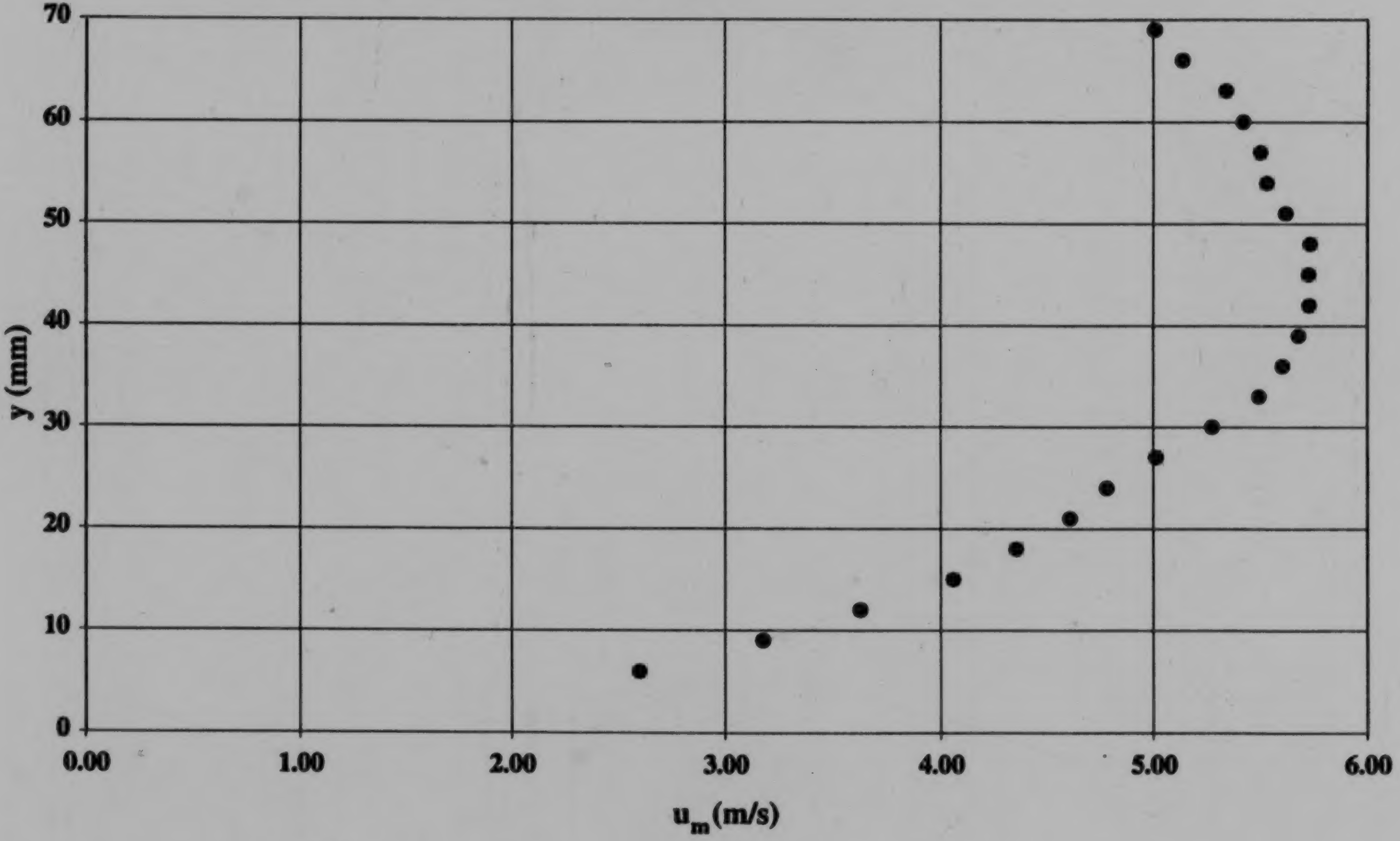

Figure B.24 Velocity profile at step tip #64 in a stepped spillway with l/h=0.6, h= 31.25 mm (yc/h=3.4)

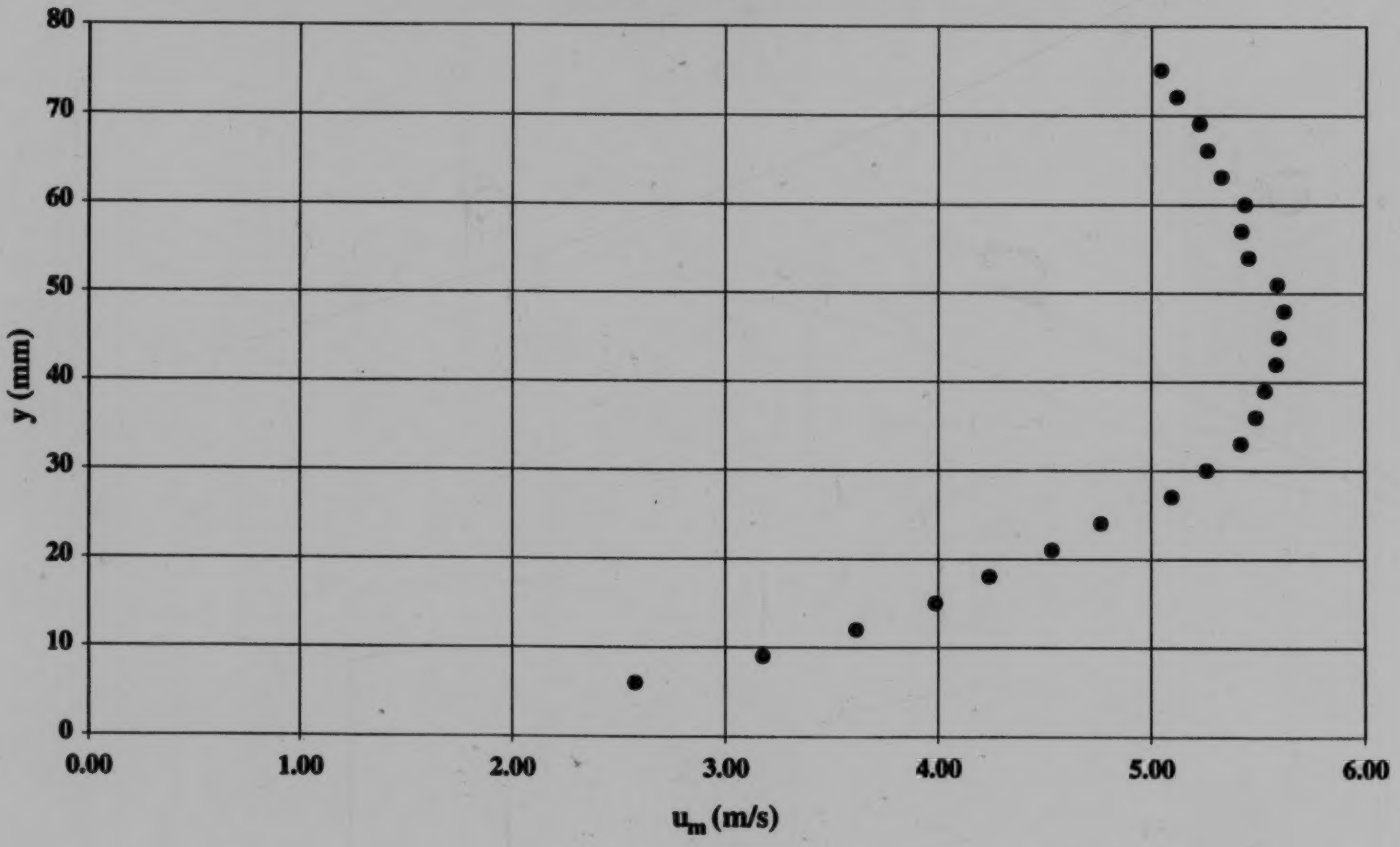

Figure B.25 Velocity profile at step tip #64 in a stepped spillway with l/h=0.6, h= 31.25 mm (yc/h=3.6)

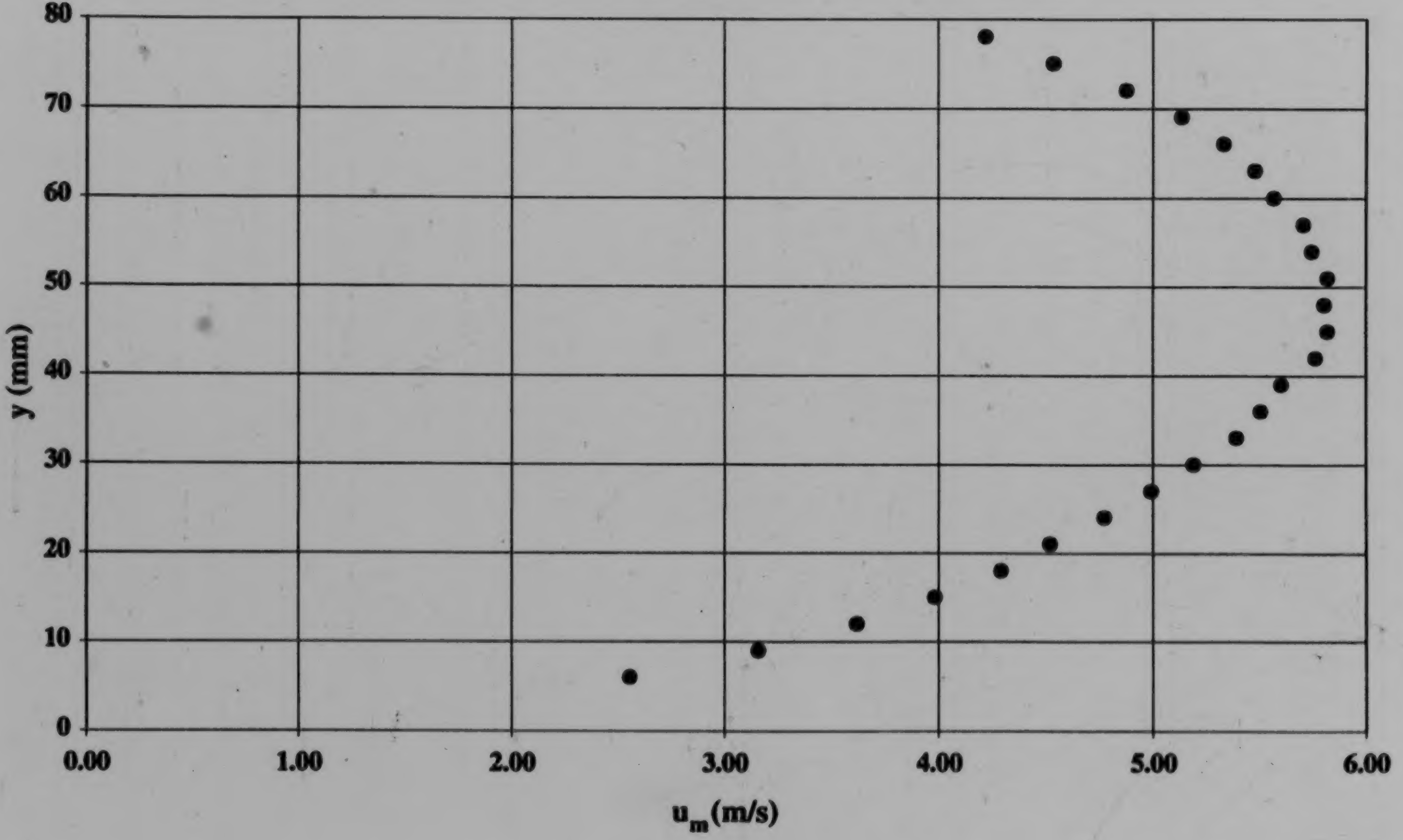

Figure B.26 Velocity profile at step tip #64 in a stepped spillway with l/h=0.6, h= 31.25 mm
(yc/h=3.8)

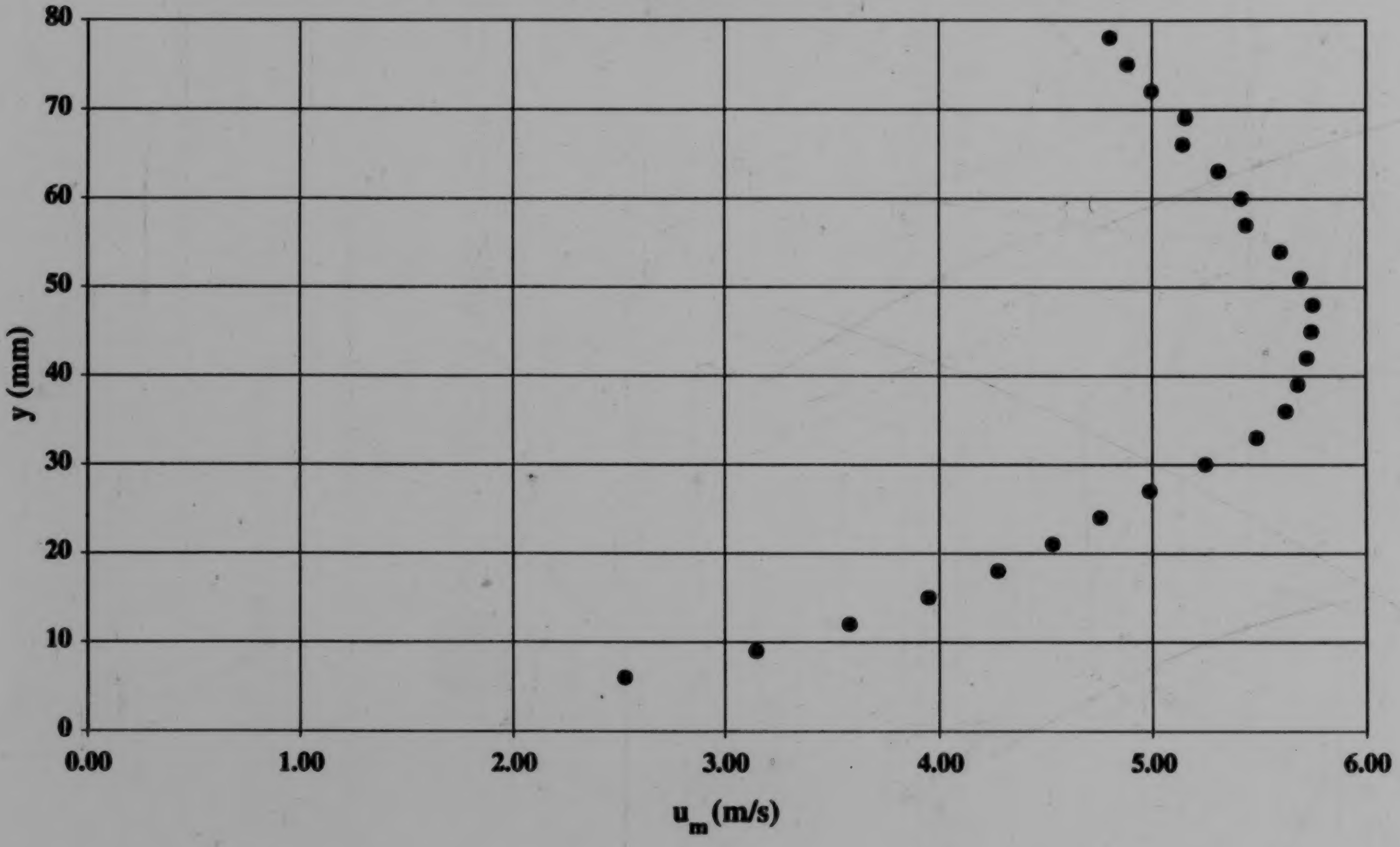

Figure B.27 Velocity profile at step tip #64 in a stepped spillway with l/h=0.6, h= 31.25 mm (yc/h=4.0)

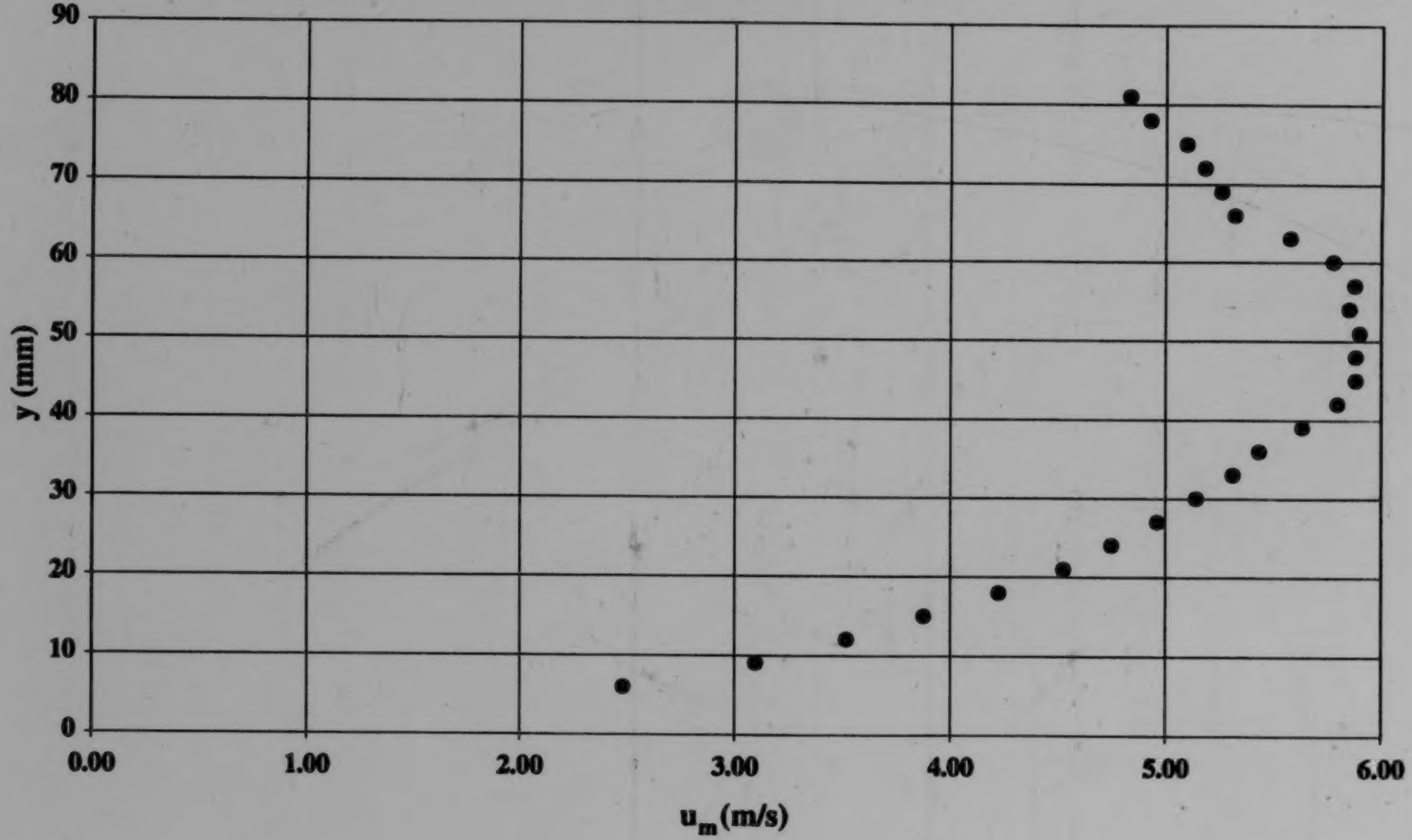

Figure B.28 Velocity profile at step tip #64 in a stepped spillway with l/h=0.6, h= 31.25 mm
(yc/h=4.2)

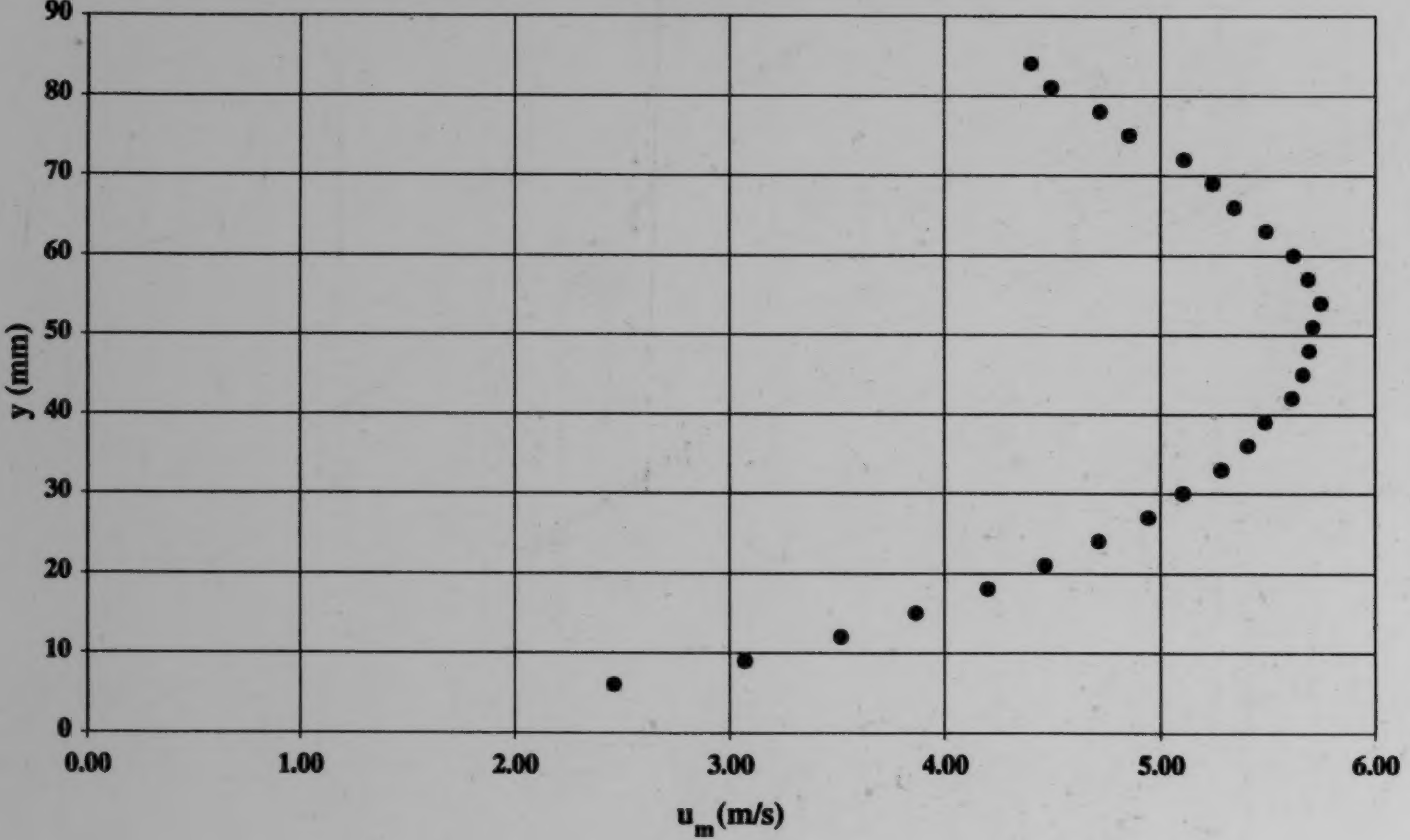

Figure B.29 Velocity profile at step tip #64 in a stepped spillway with l/h=0.6, h= 31.25 mm (yc/h=4.4)

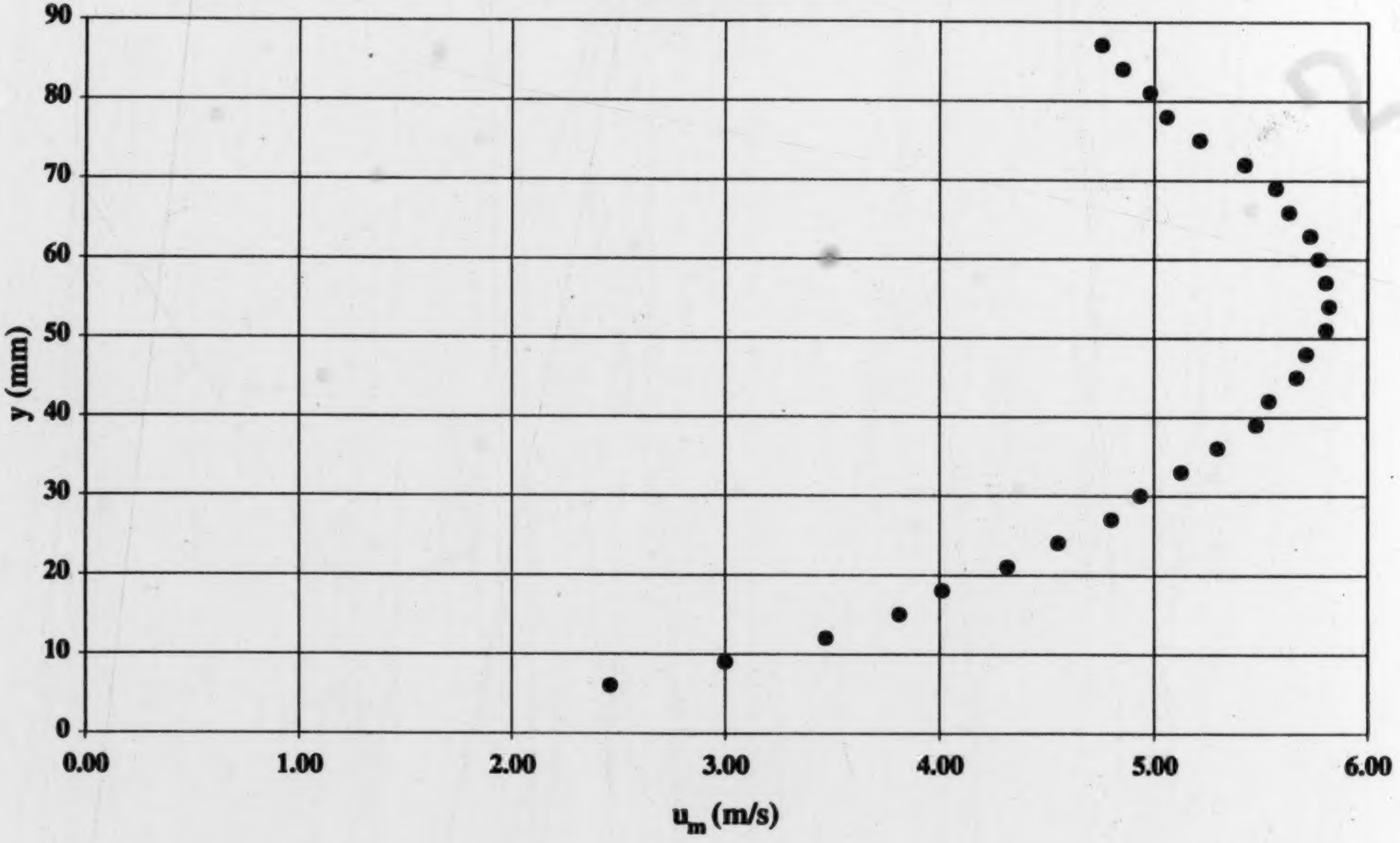

Figure B.30 Velocity profile at step tip #15 in a stepped spillway with l/h=0.8, h= 125. mm (yc/h=0.7)

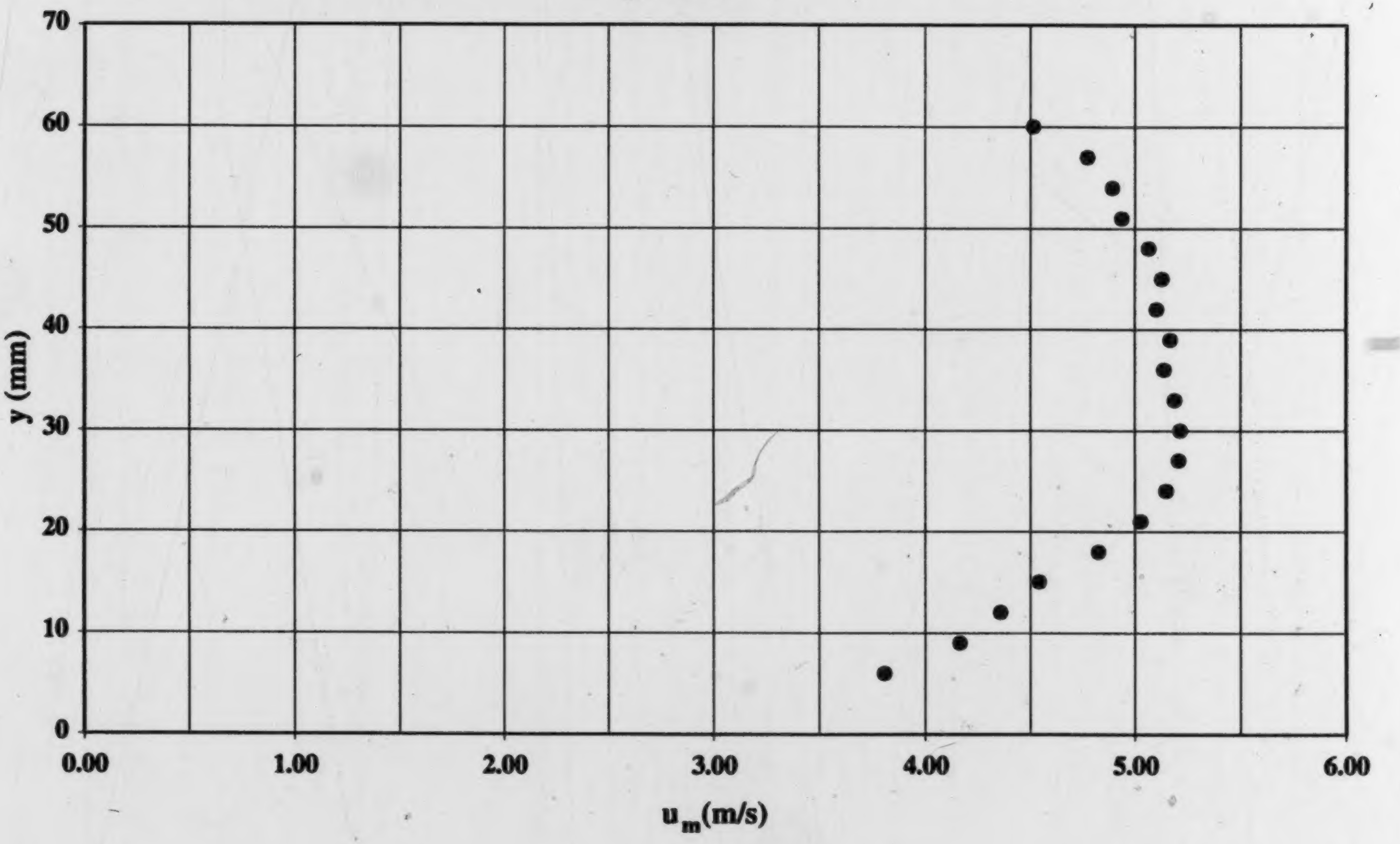

Figure B.31 Velocity profile at step tip #15 in a stepped spillway with l/h=0.8, h= 125. mm (yc/h=0.8)

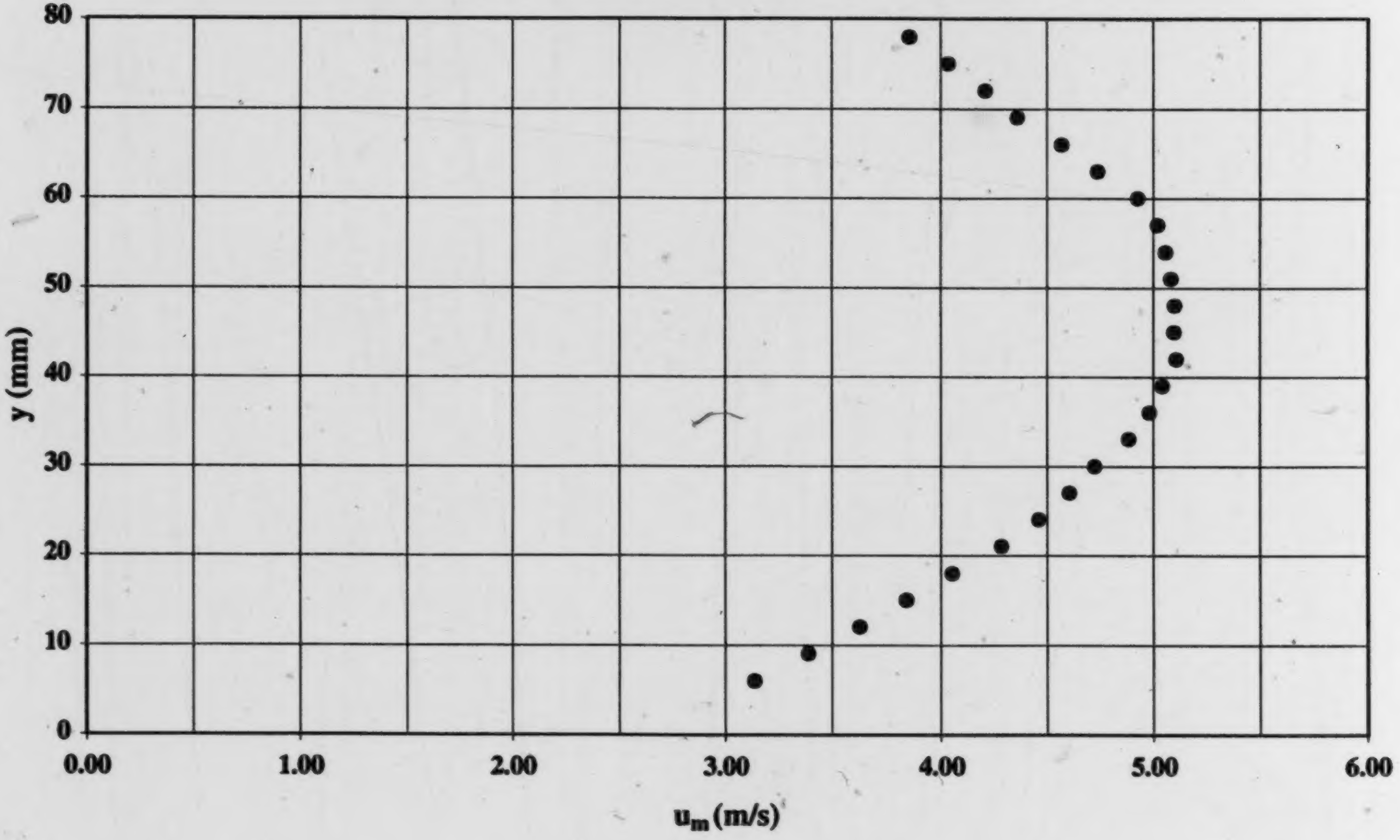

Figure B.32 Velocity profile at step tip #15 in a stepped spillway with l/h=0.8, h= 125. mm (yc/h=0.9)

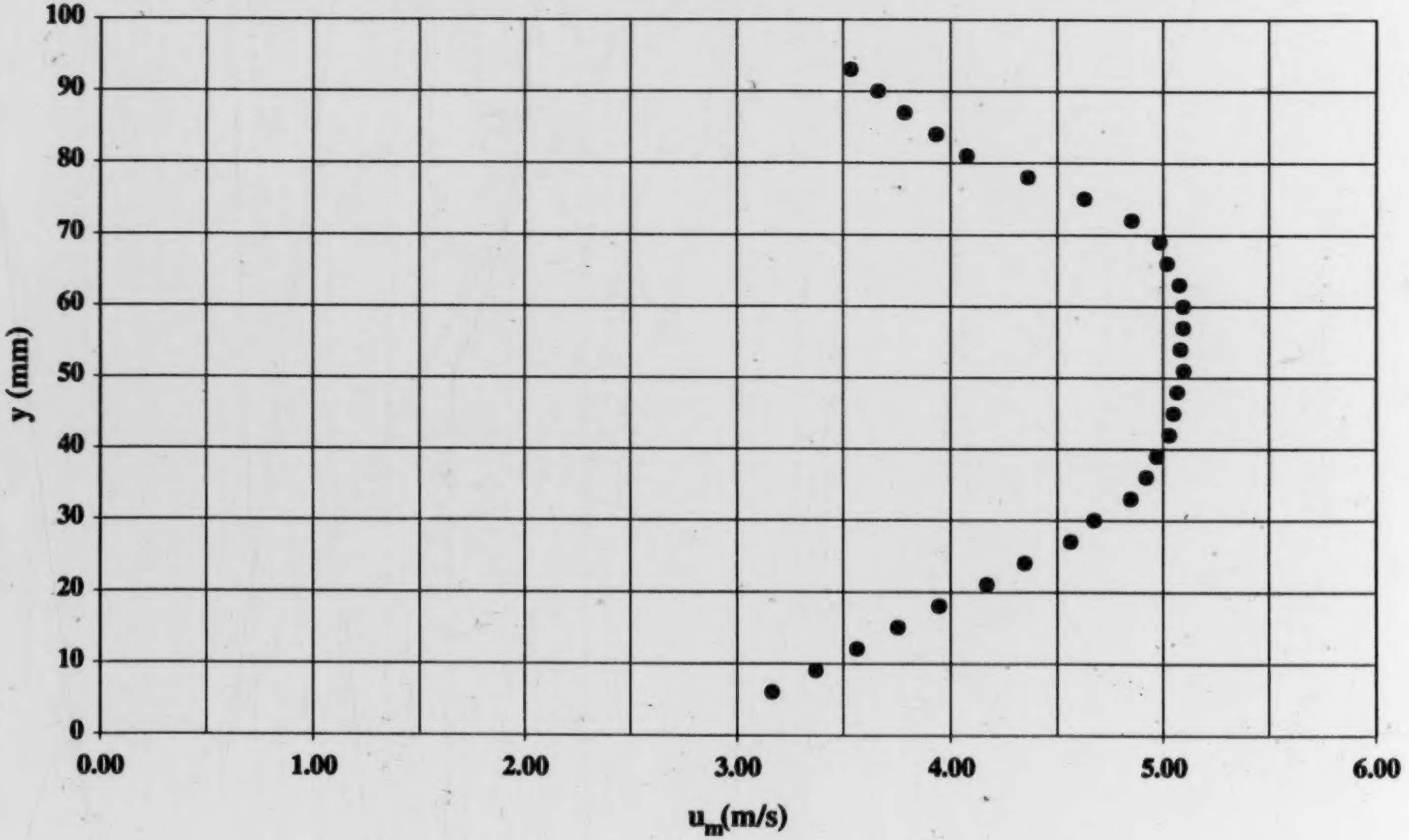

Figure B.33 Velocity profile at step tip #15 in a stepped spillway with l/h=0.8, h= 125. mm (yc/h=1.0)

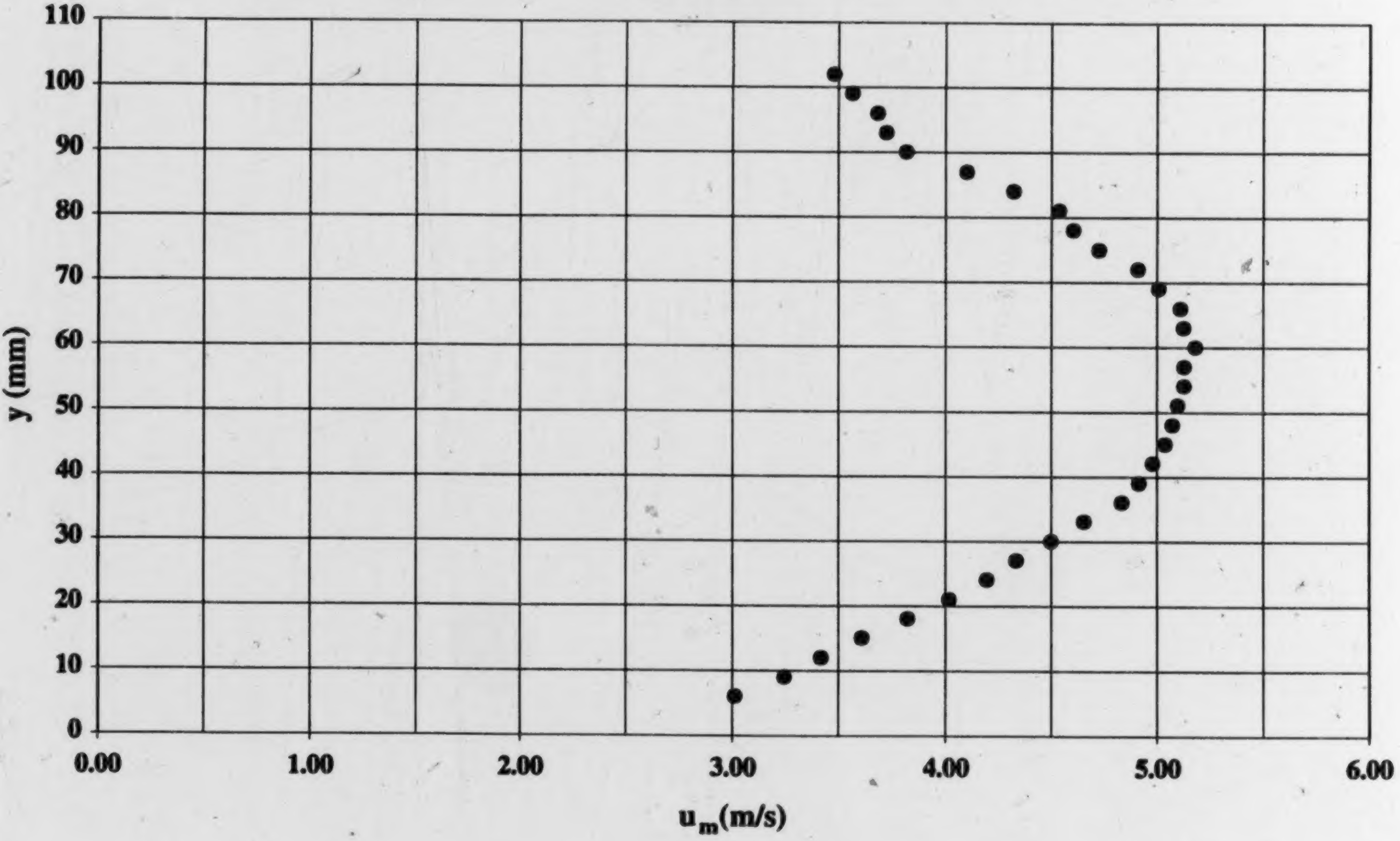

Figure B.34 Velocity profile at step tip #15 in a stepped spillway with l/h=0.8, h= 125. mm (yc/h=1.1)

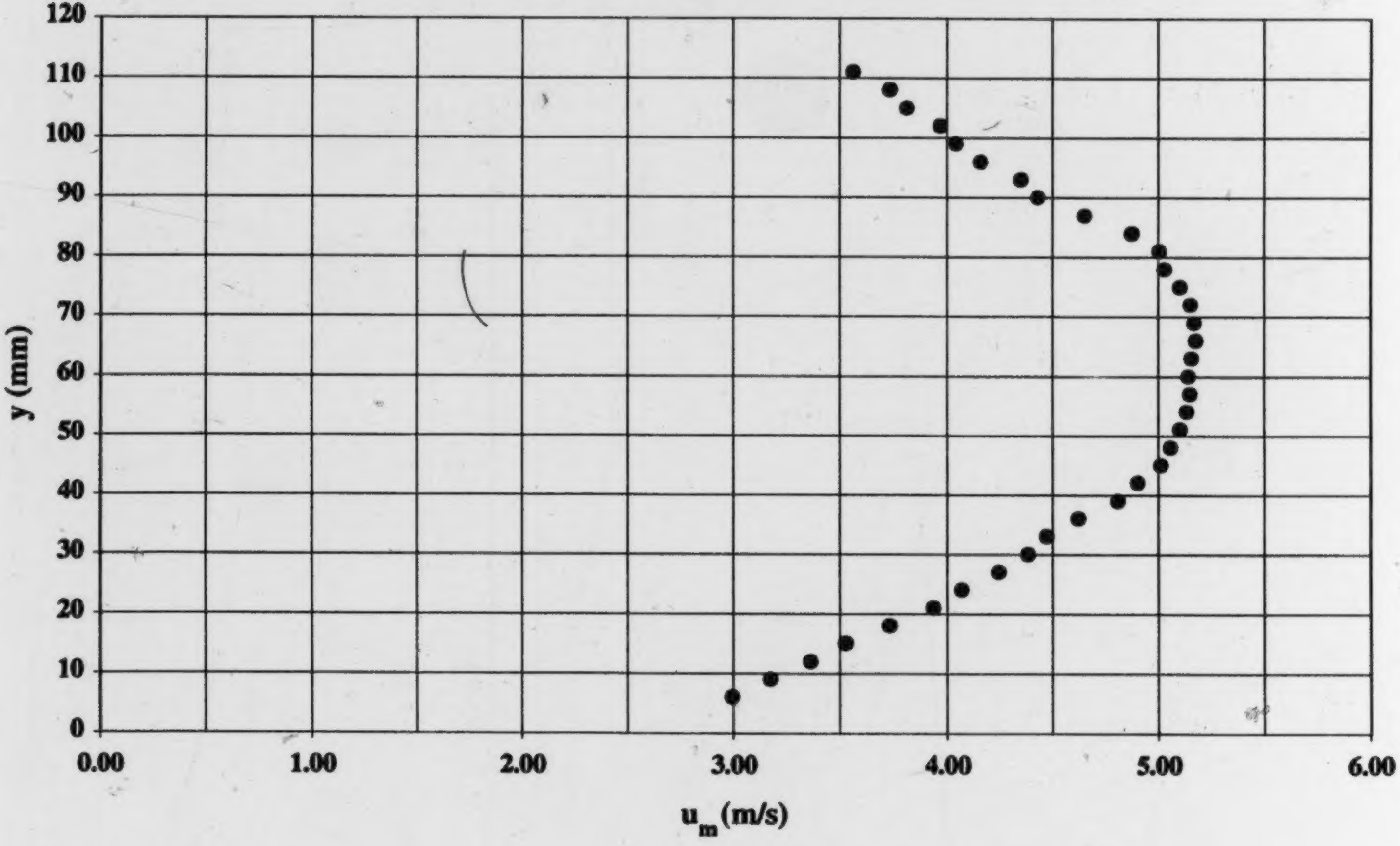

Figure B.35 Velocity profile at step tip #15 in a stepped spillway with l/h=0.8, h= 125. mm (yc/h=1.2)

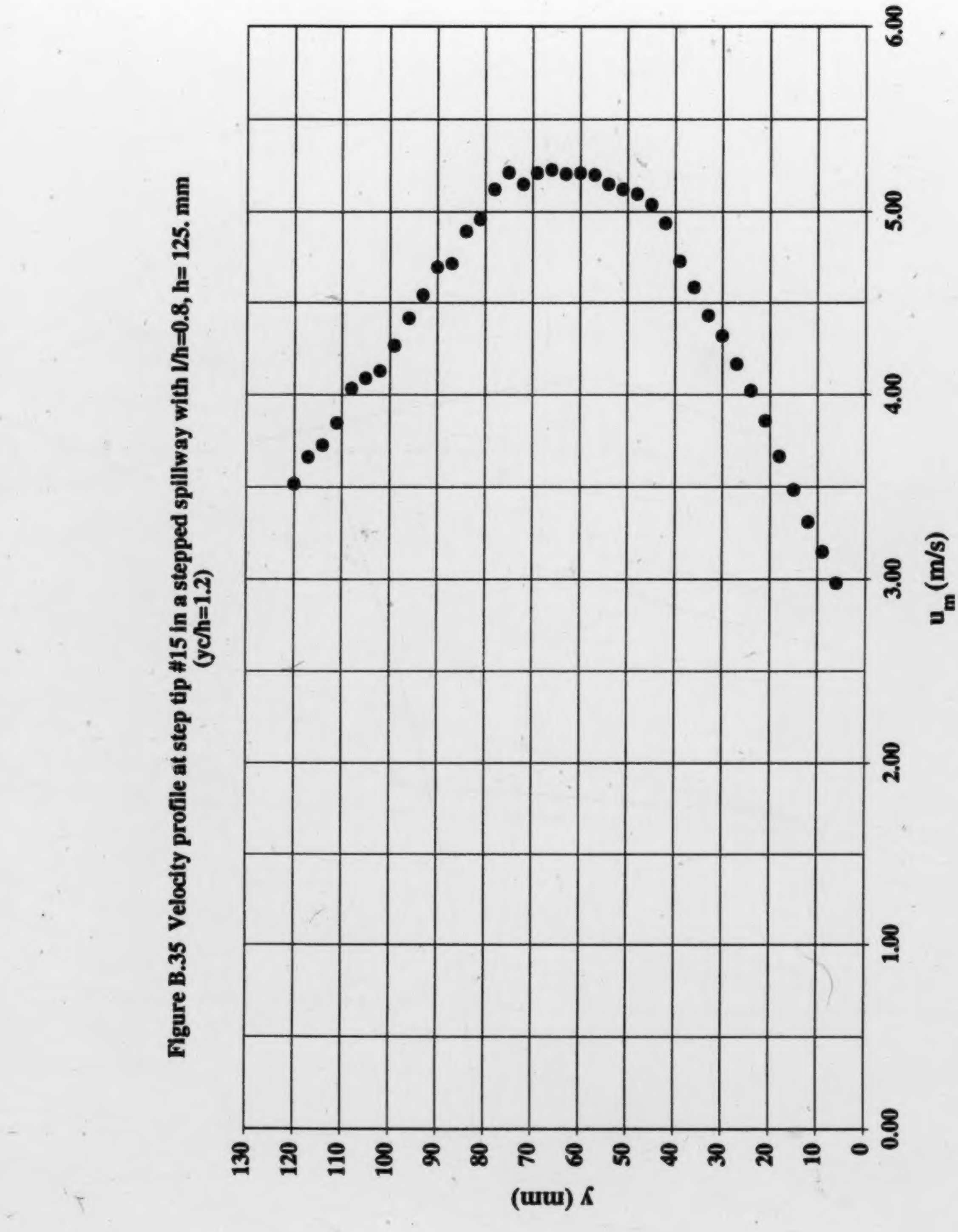

Figure B.36 Velocity profile at step tip #15 in a stepped spillway with l/h=0.8, h= 125. mm (yc/h=1.3)

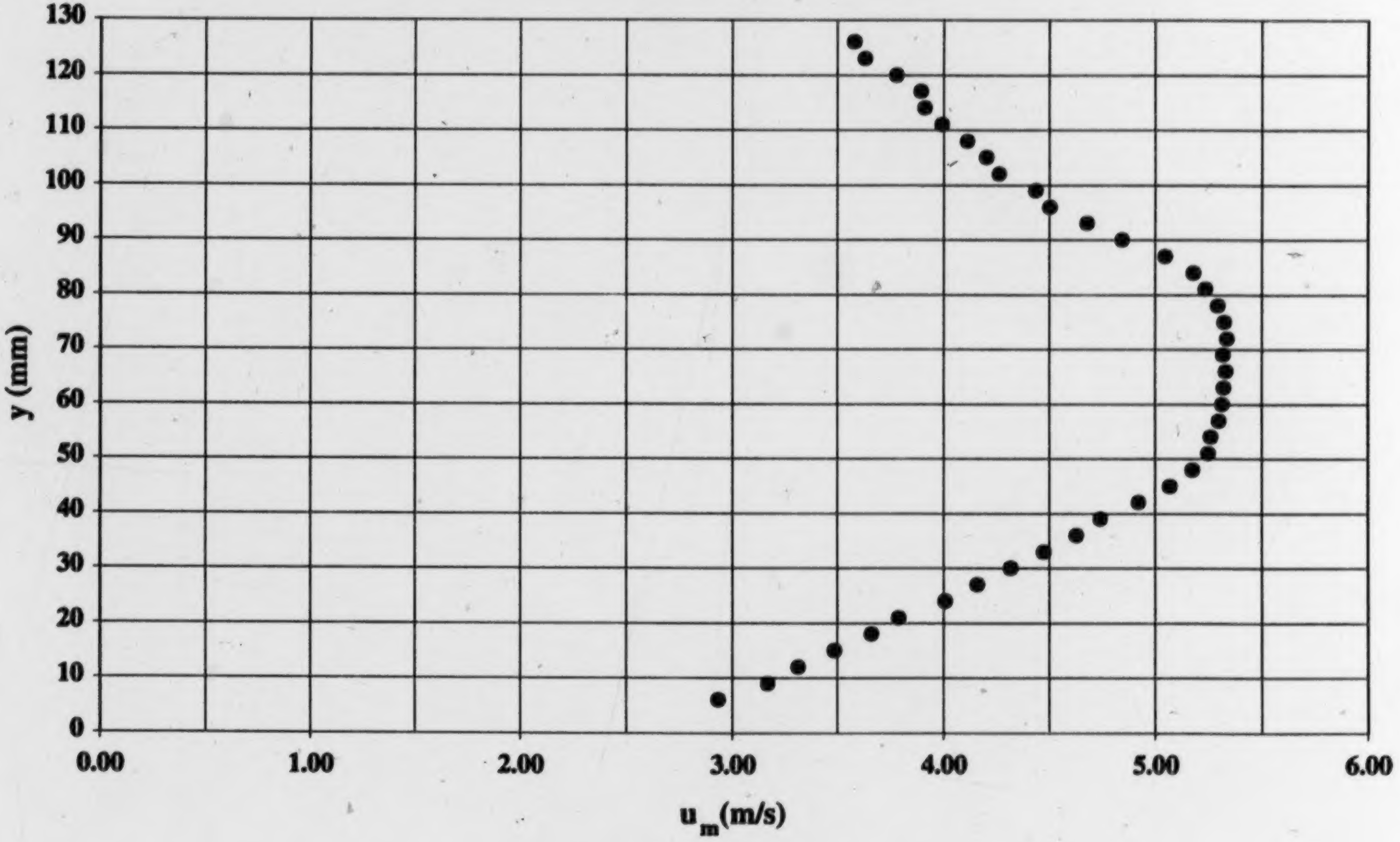

Figure B.37 Velocity profile at step tip #60 in a stepped spillway with l/h=0.8, h= 31.25 mm (yc/h=2.6)

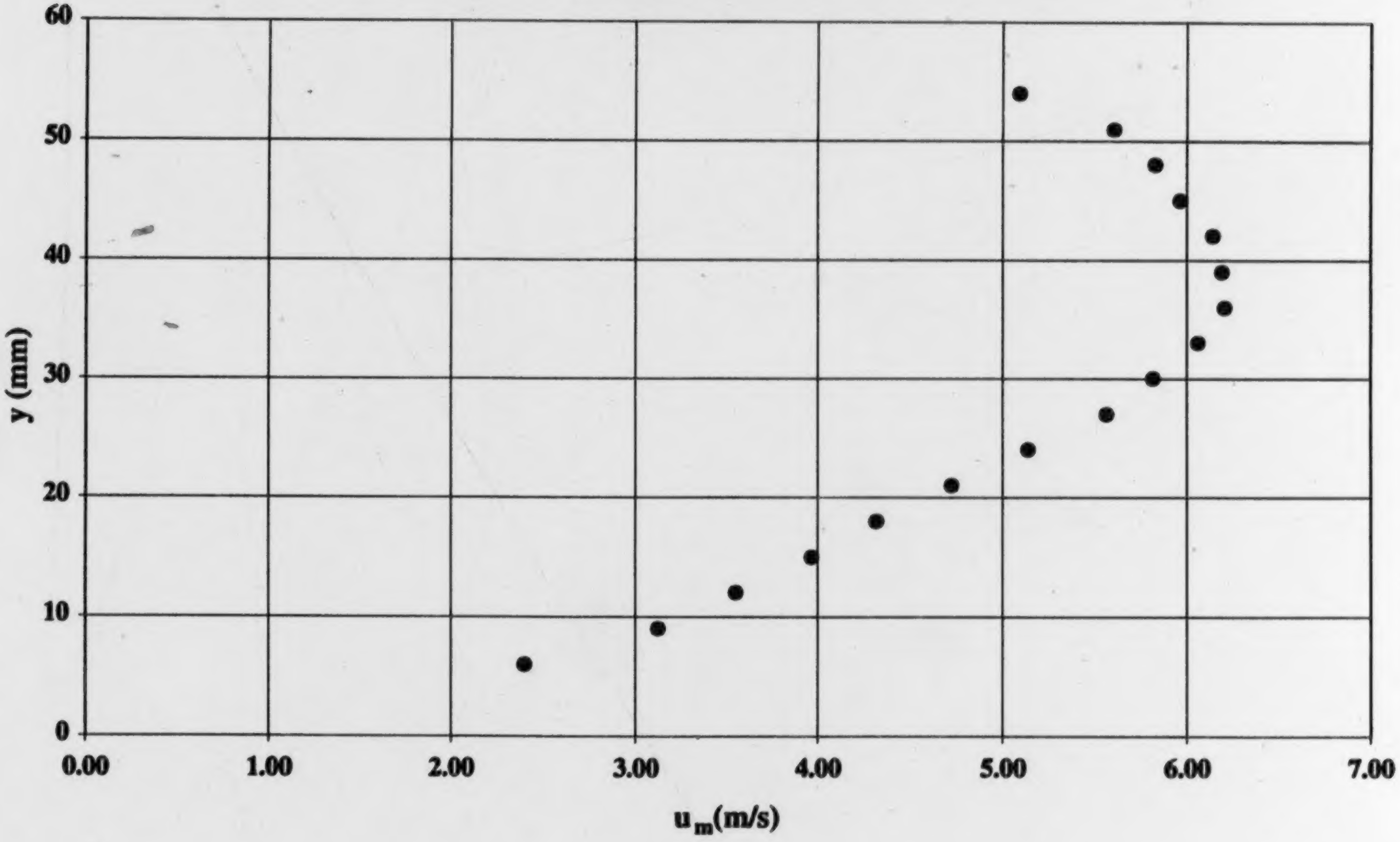

Figure B.38 Velocity profile at step tip #60 in a stepped spillway with l/h=0.8, h= 31.25 mm (yc/h=2.8)

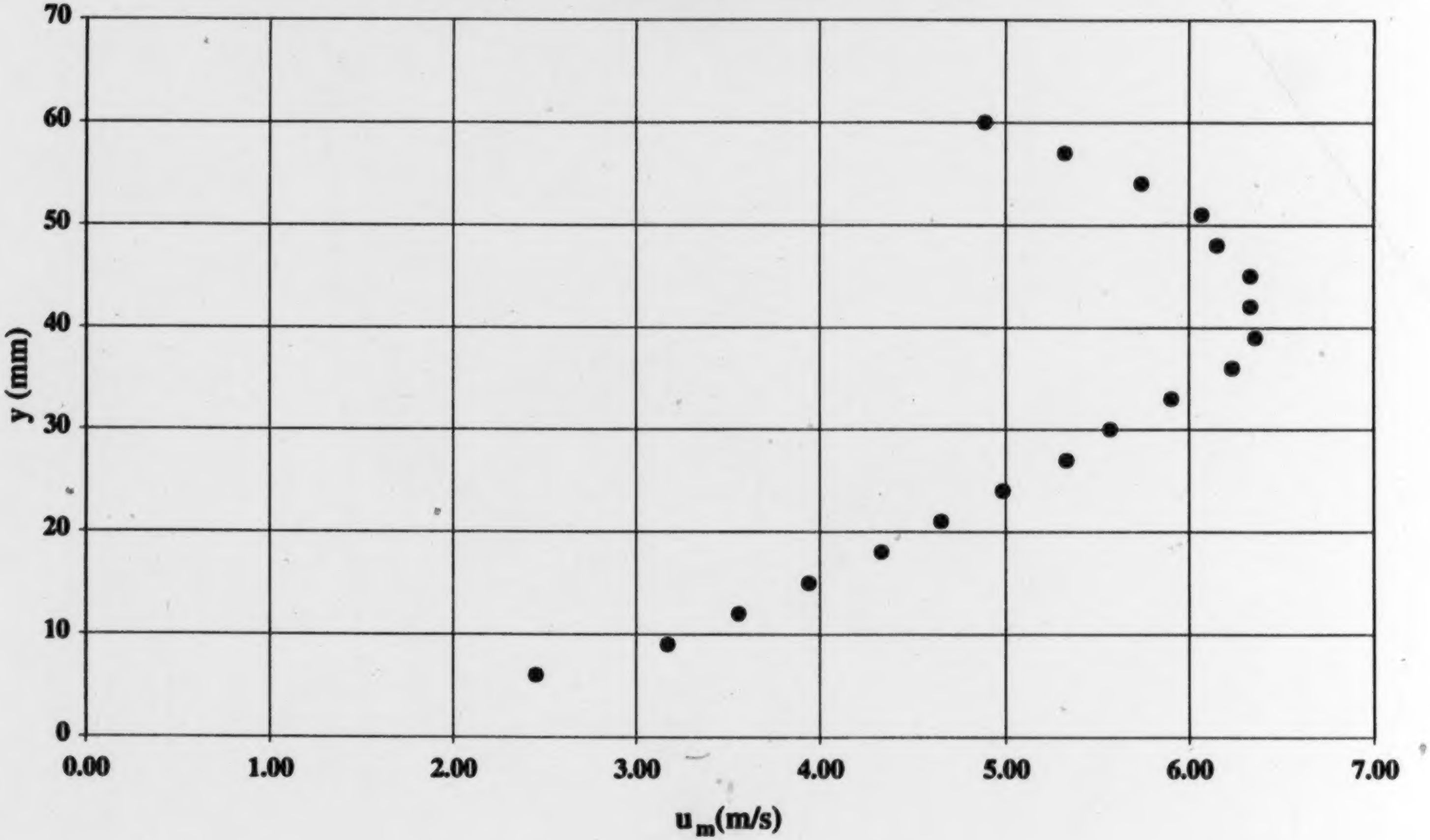

Figure B.39 Velocity profile at step tip #60 in a stepped spillway with l/h=0.8, h= 31.25 mm
(yc/h=3.0)

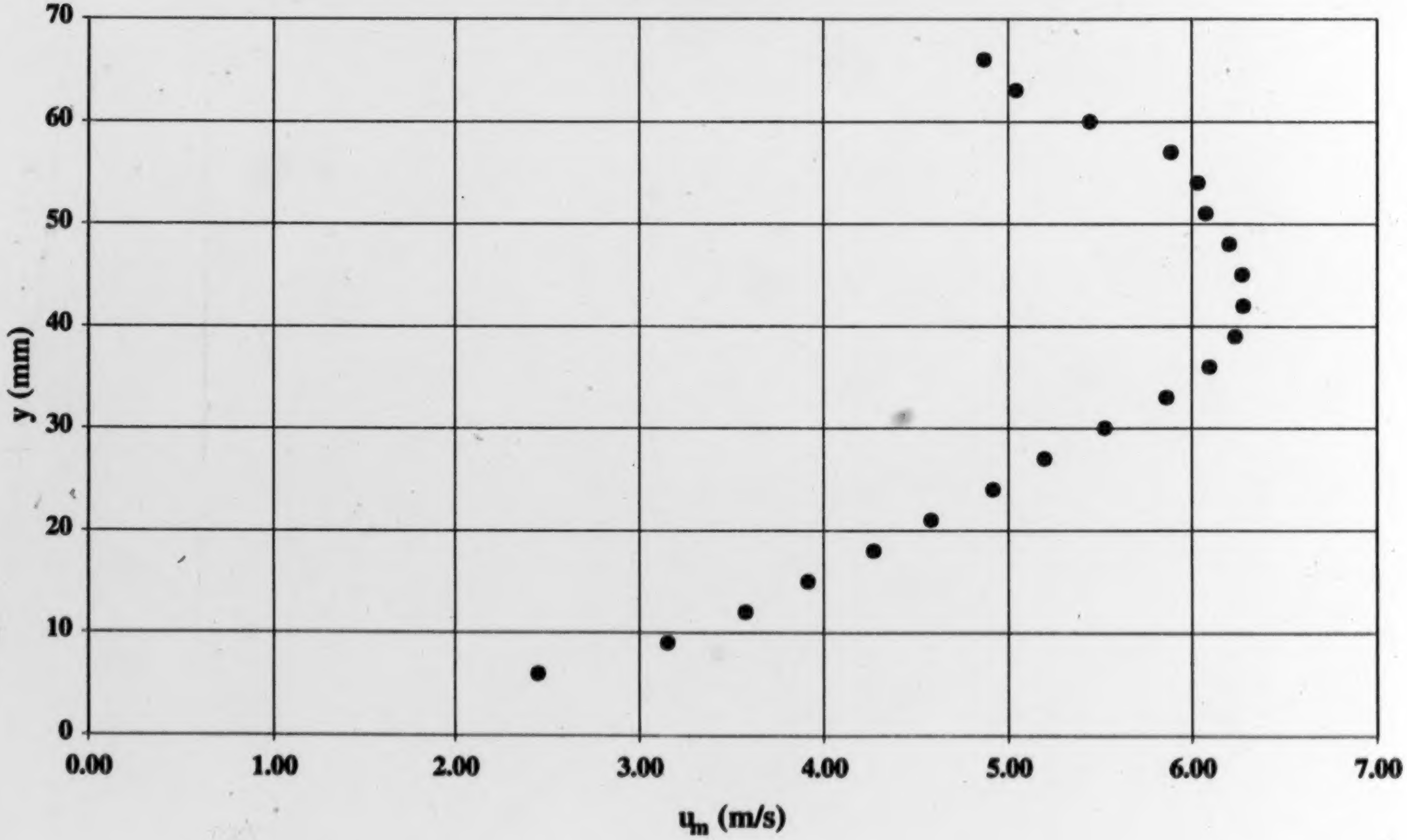

Figure B.40 Velocity profile at step tip #60 in a stepped spillway with l/h=0.8, h= 31.25 mm (yc/h=3.2)

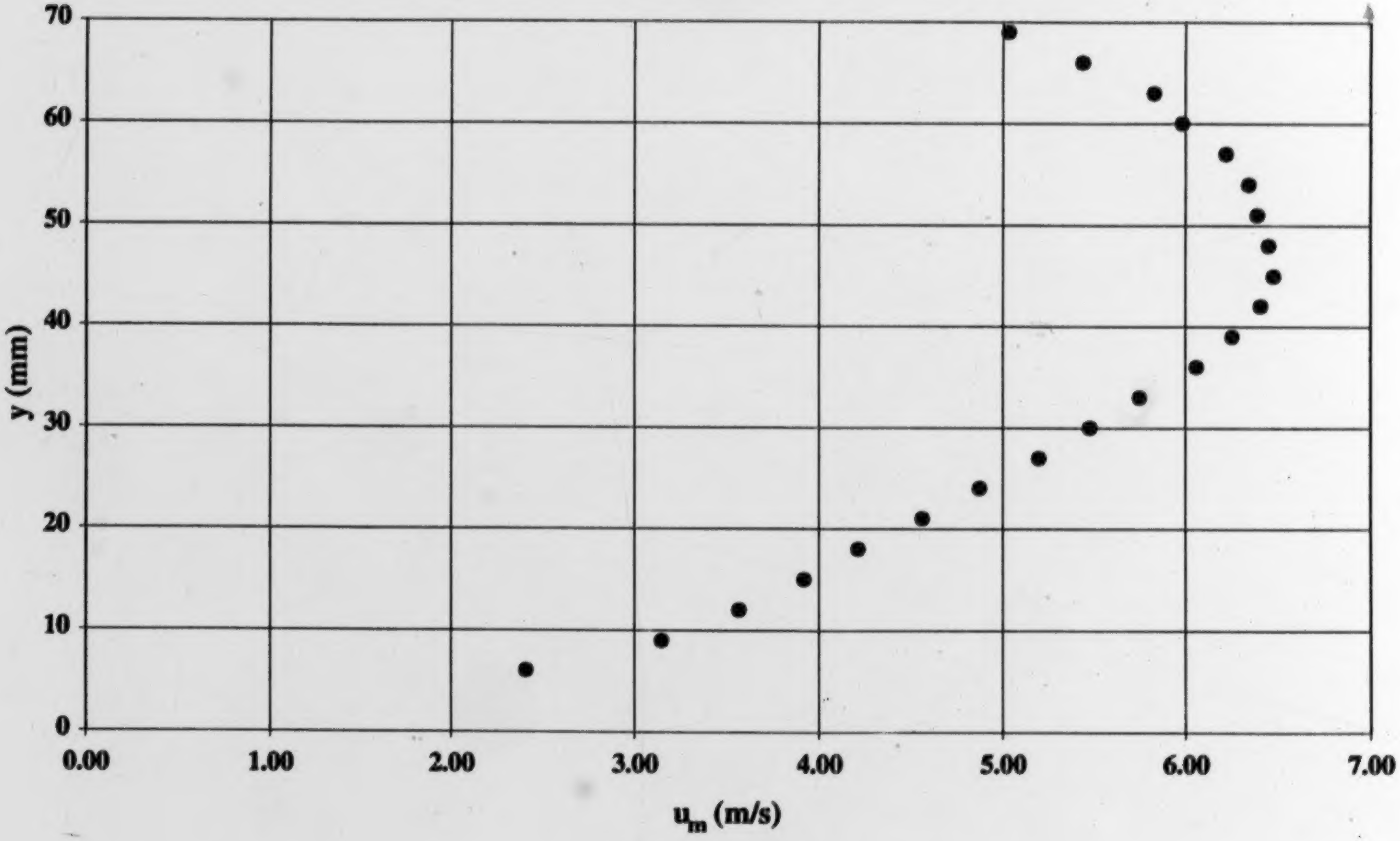

Figure B.41 Velocity profile at step tip #60 in a stepped spillway with l/h=0.8, h= 31.25 mm (yc/h=3.4)

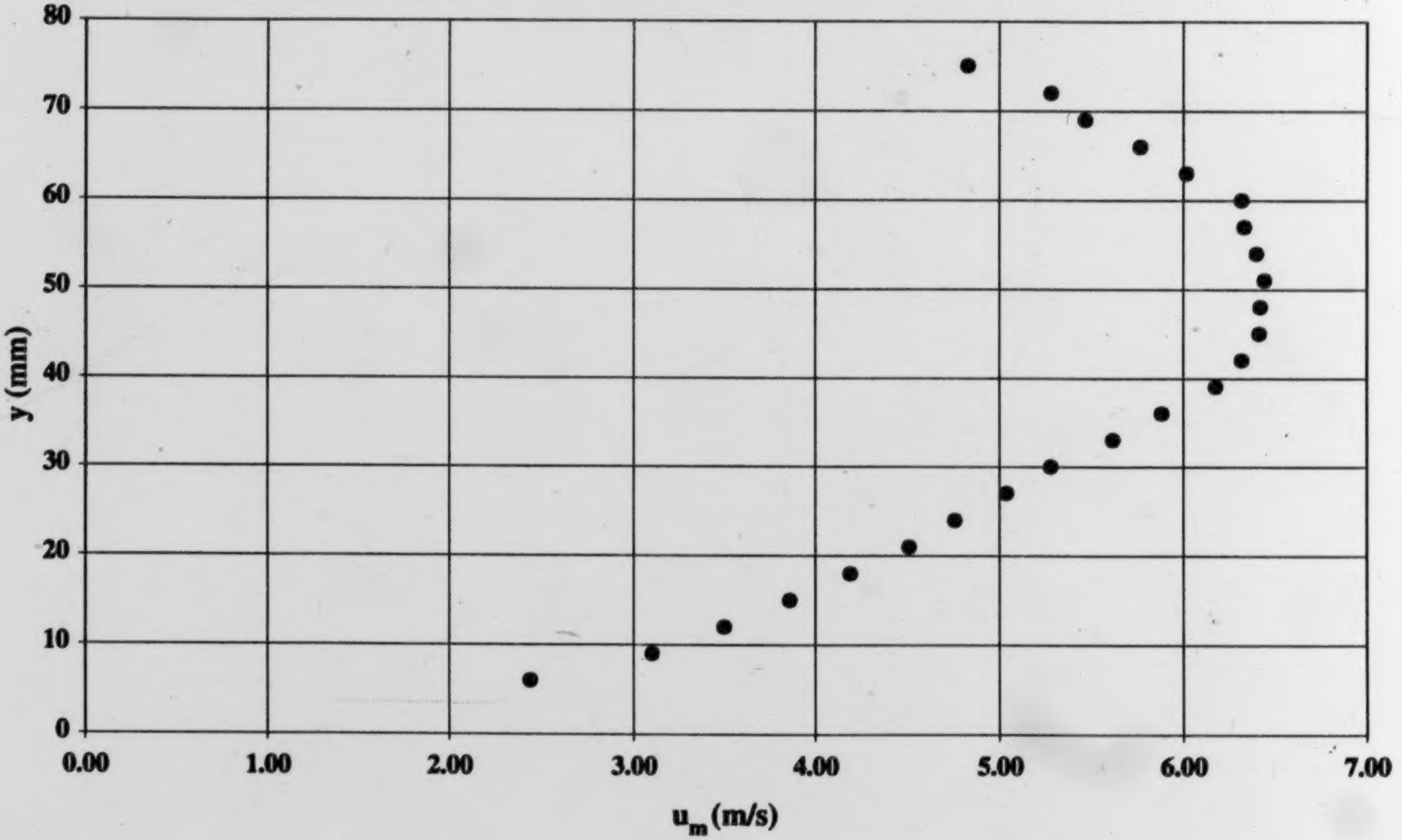

Figure B.42 Velocity profile at step tip #60 in a stepped spillway with l/h=0.8, h= 31.25 mm (yc/h=3.6)

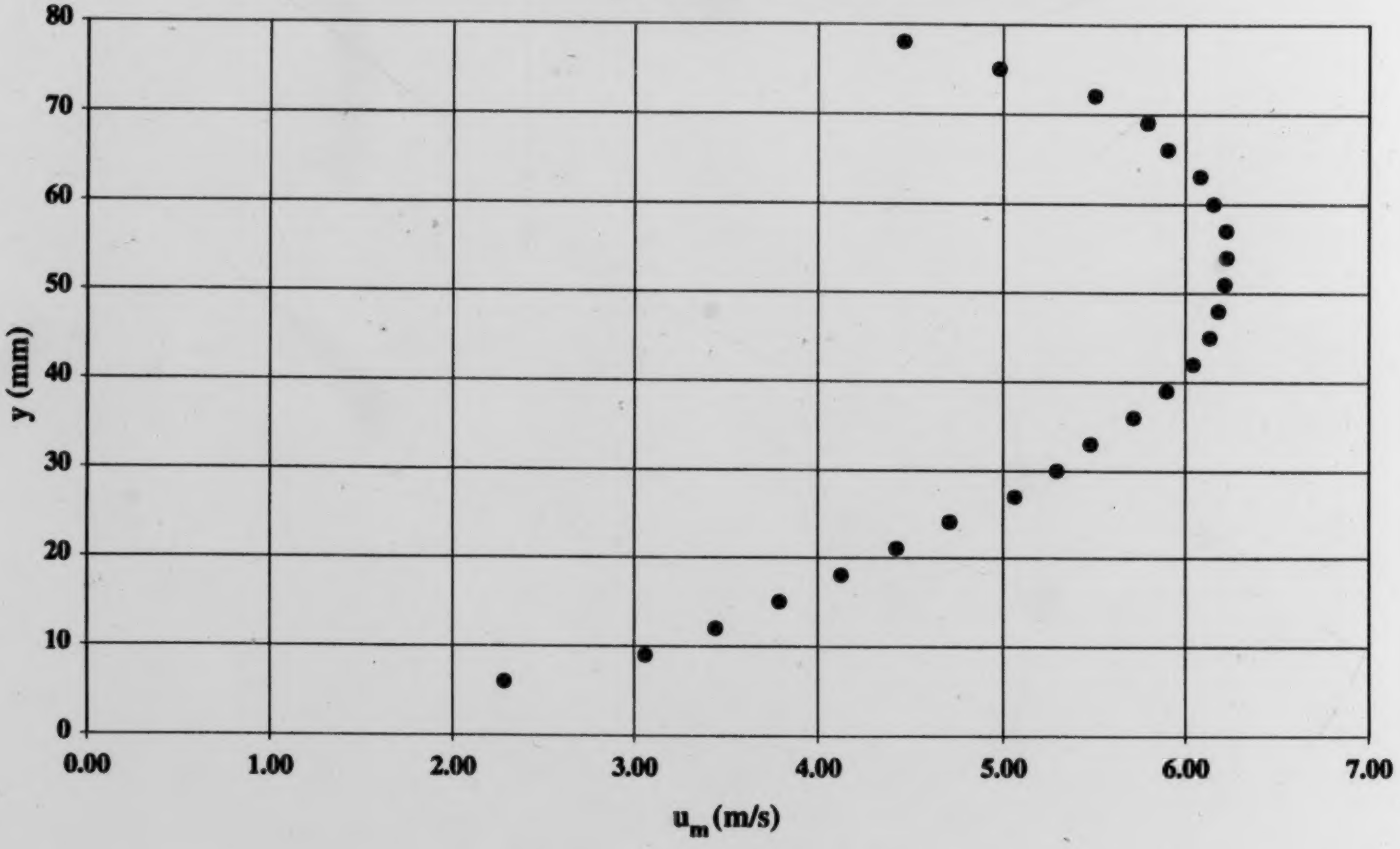

Figure B.43 Velocity profile at step tip #60 in a stepped spillway with l/h=0.8, h= 31.25 mm (yc/h=3.8)

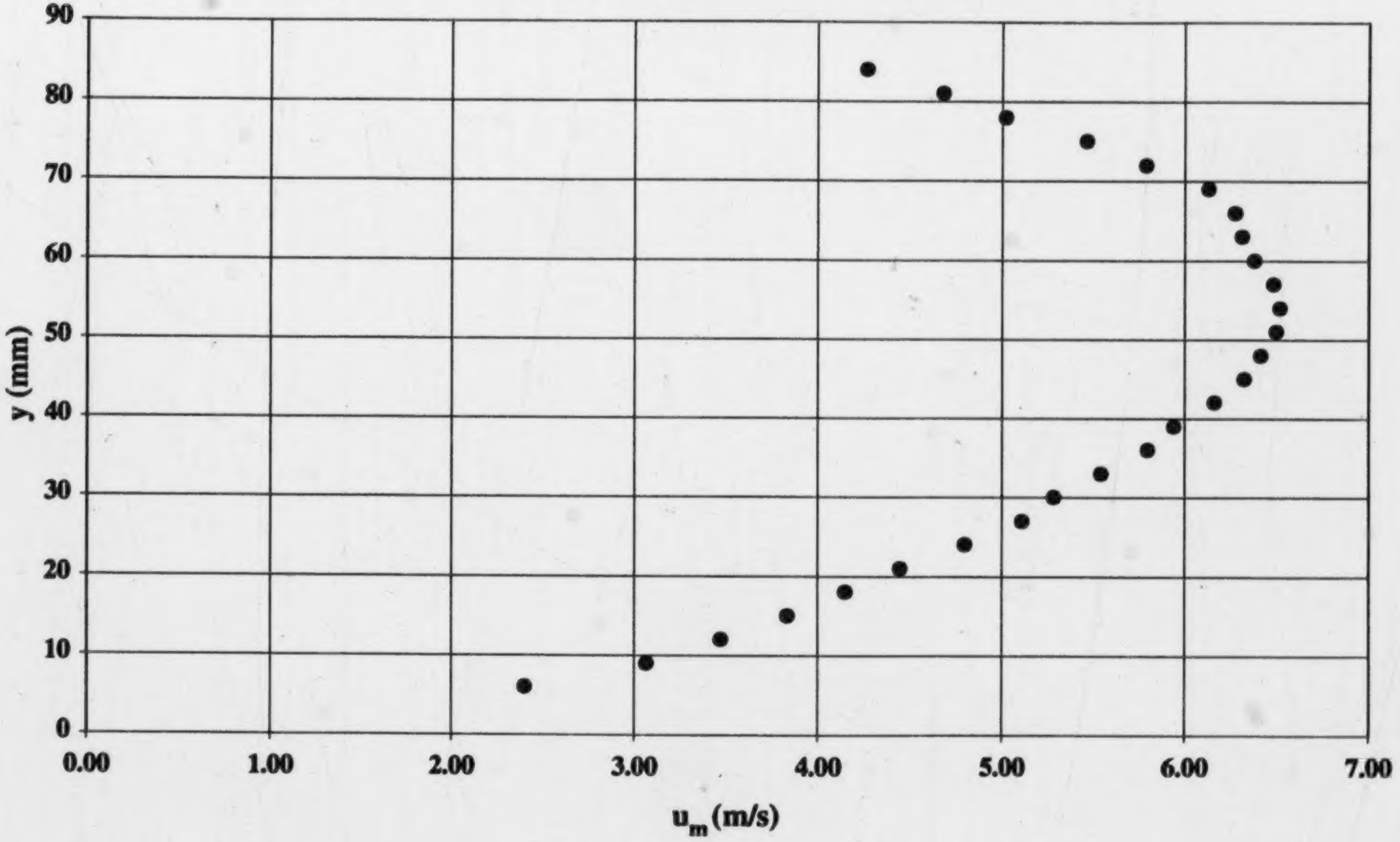

Figure B.44 Velocity profile at step tip #60 in a stepped spillway with l/h=0.8, h= 31.25 mm (yc/h=4.0)

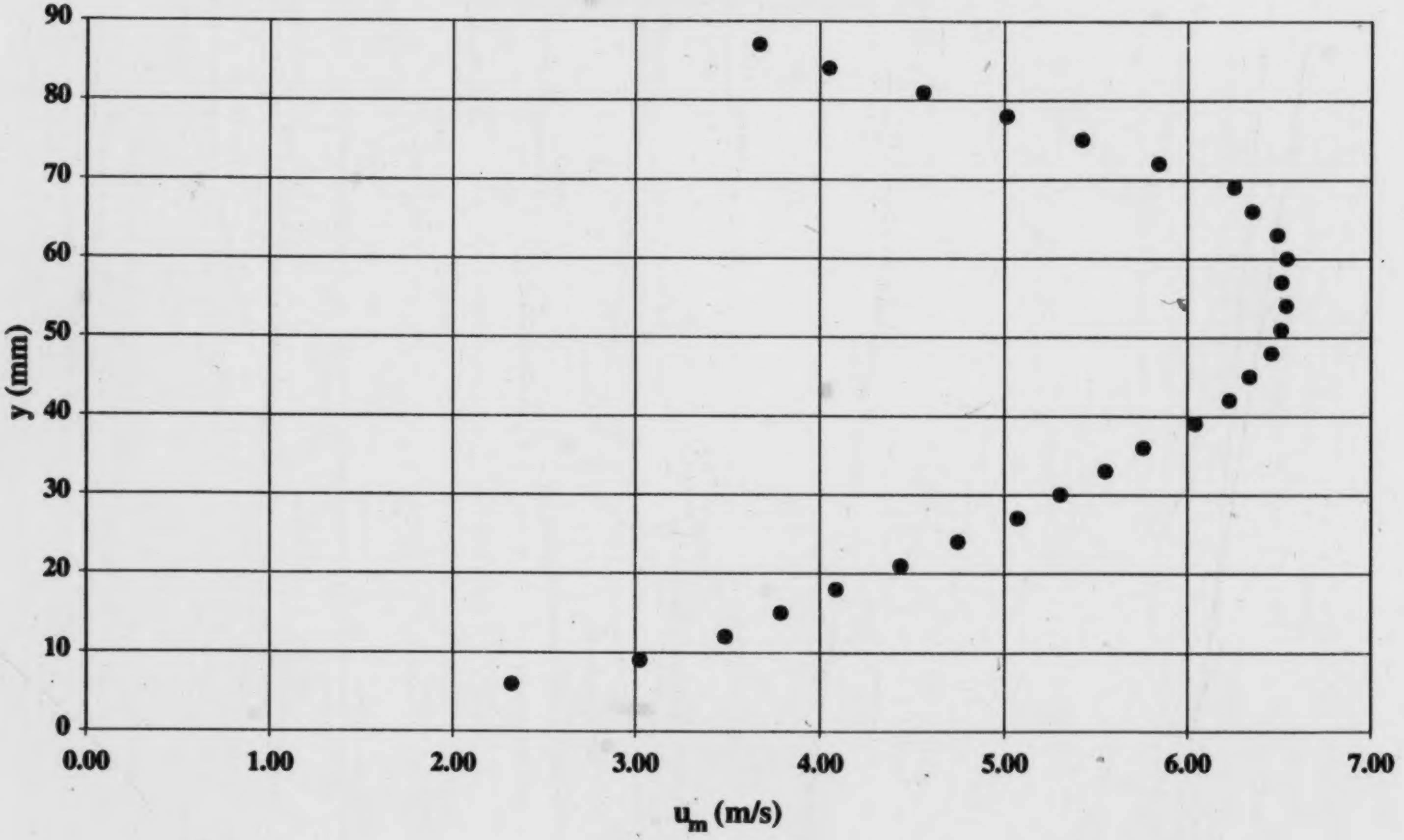

Figure B.45 Velocity profile at step tip #60 in a stepped spillway with l/h=0.8, h= 31.25 mm (yc/h=4.2)

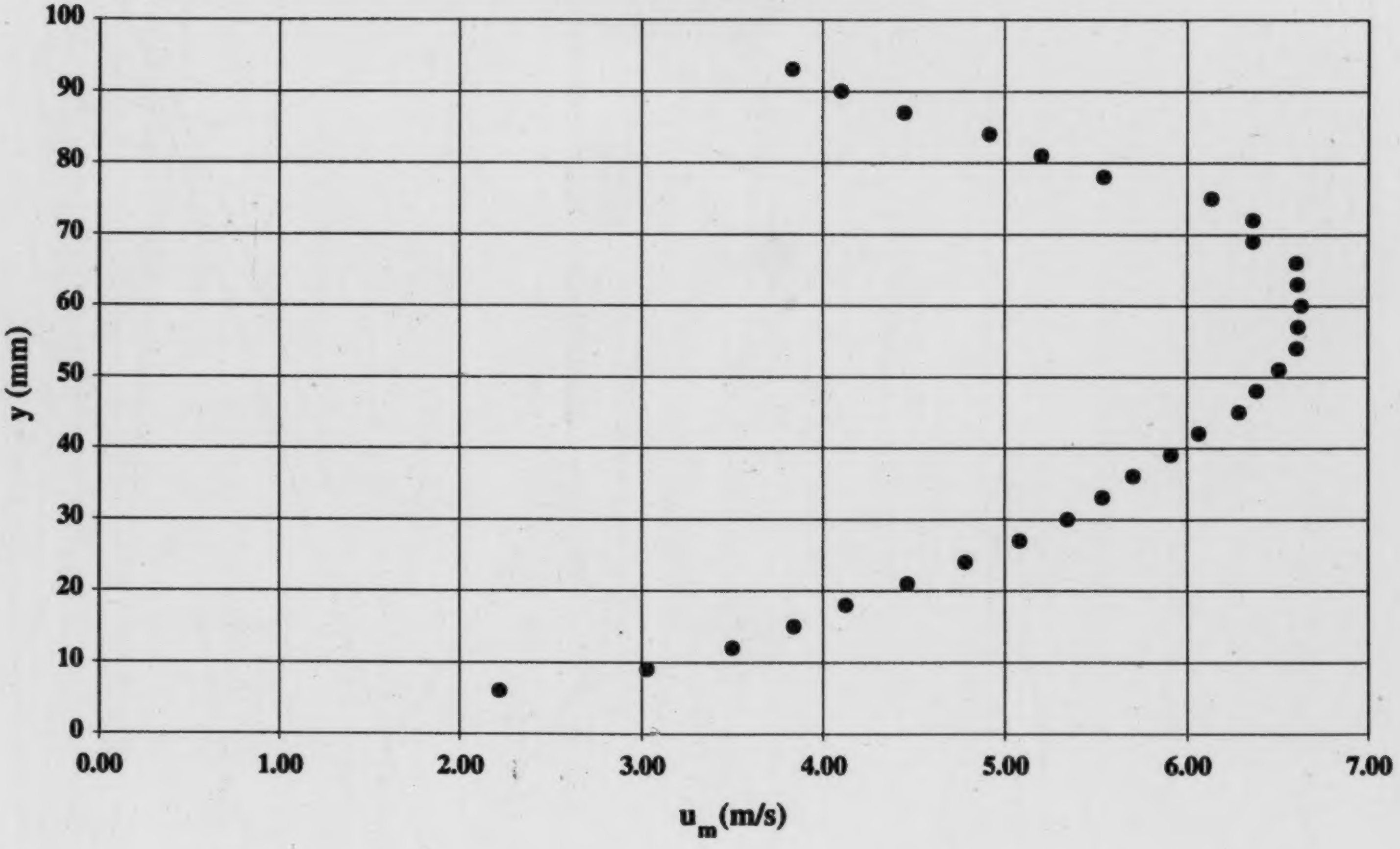

Figure B.46 Velocity profile at step tip #60 in a stepped spillway with l/h=0.8, h= 31.25 mm (yc/h=4.4)

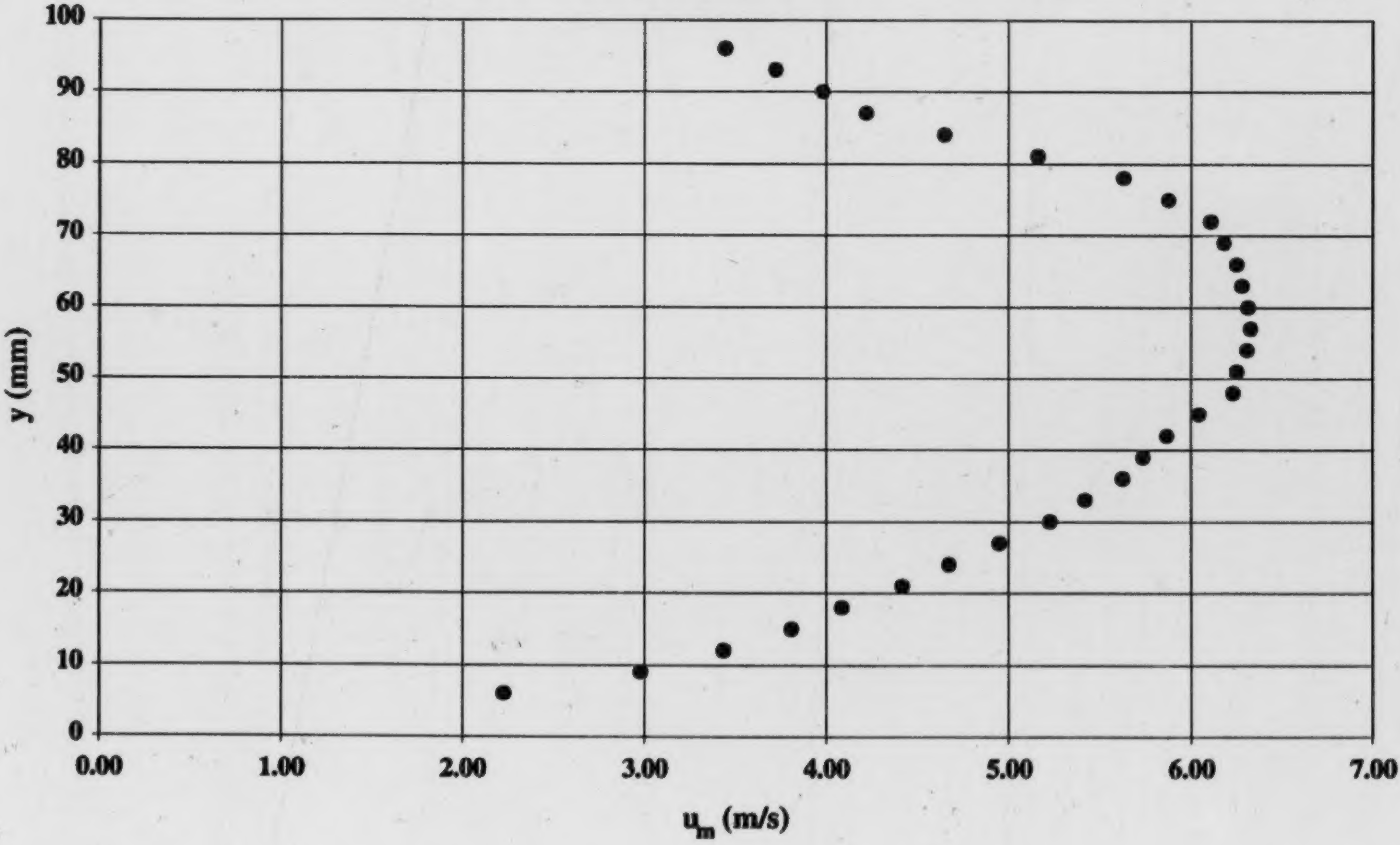

APPENDIX C

LOGARITHMIC VELOCITY PROFILES AT DIFFERENT ORIGINS FOR VARIOUS VALUES OF FLOW DISCHARGE, STEP HEIGHT, AND CHANNEL SLOPE

Figure C.1 Logarithmic velocity profiles at different origins at step #13 in a stepped spillway with l/h=0.6, h= 125. mm, k= 76.6 mm (yc/h=0.7)

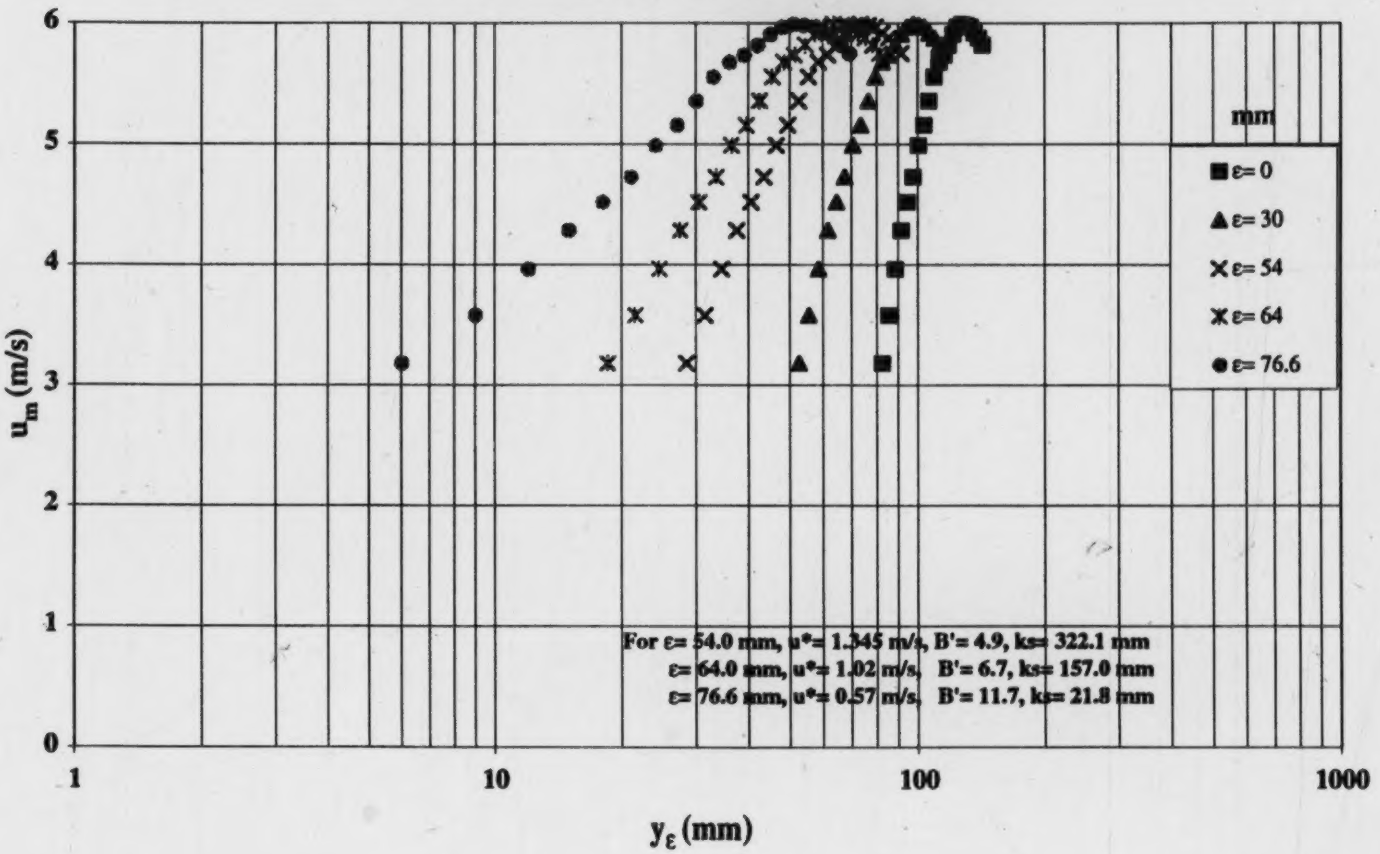

Figure C.2 Logarithmic velocity profiles at different origins at step #13 in a stepped spillway with l/h=0.6, h= 125. mm, k= 76.6 mm (yc/h=0.8)

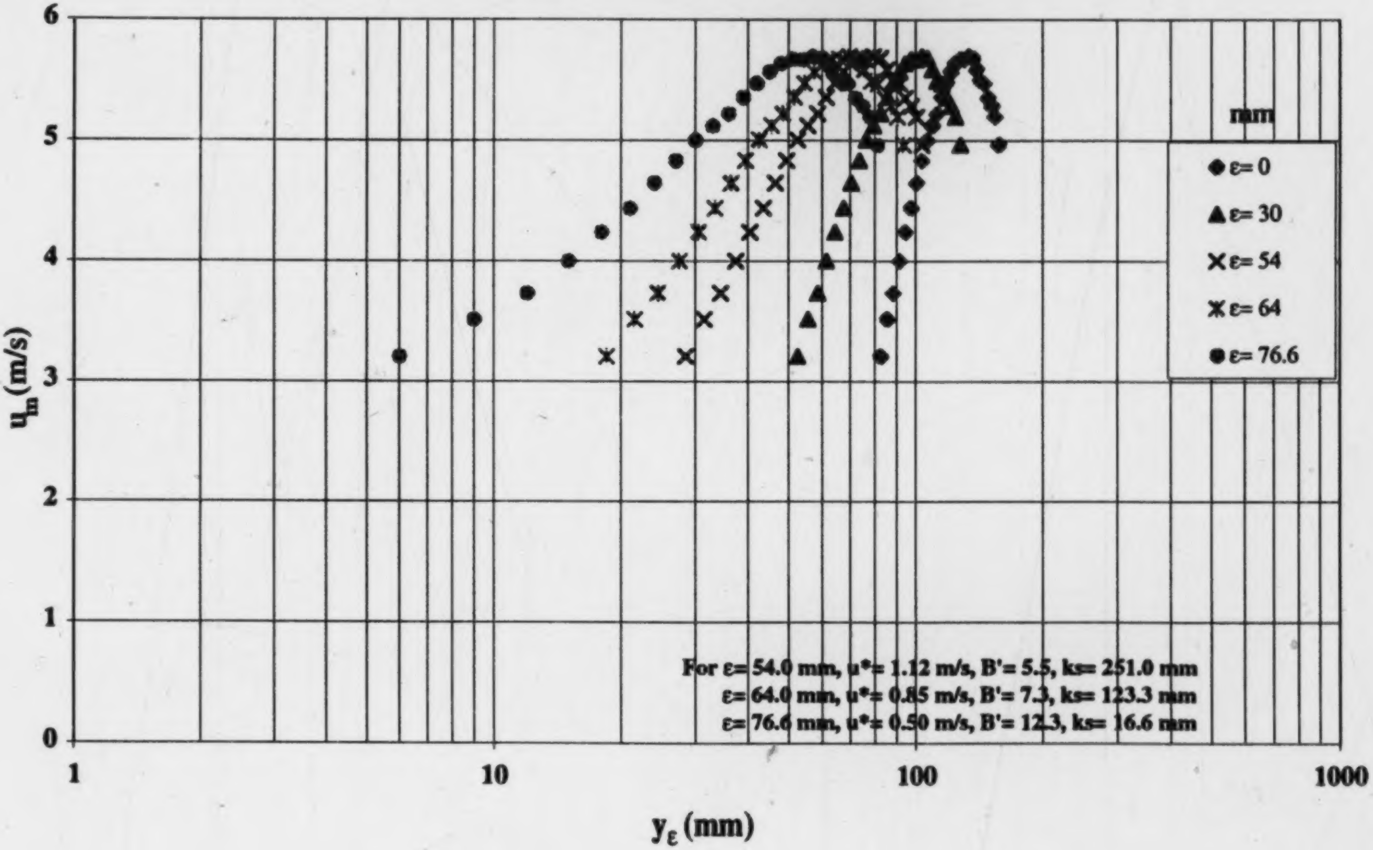

Figure C.3 Logarithmic velocity profiles at different origins at step #13 in a stepped spillway with l/h=0.6, h= 125. mm, k= 76.6 mm (yc/h=1.0)

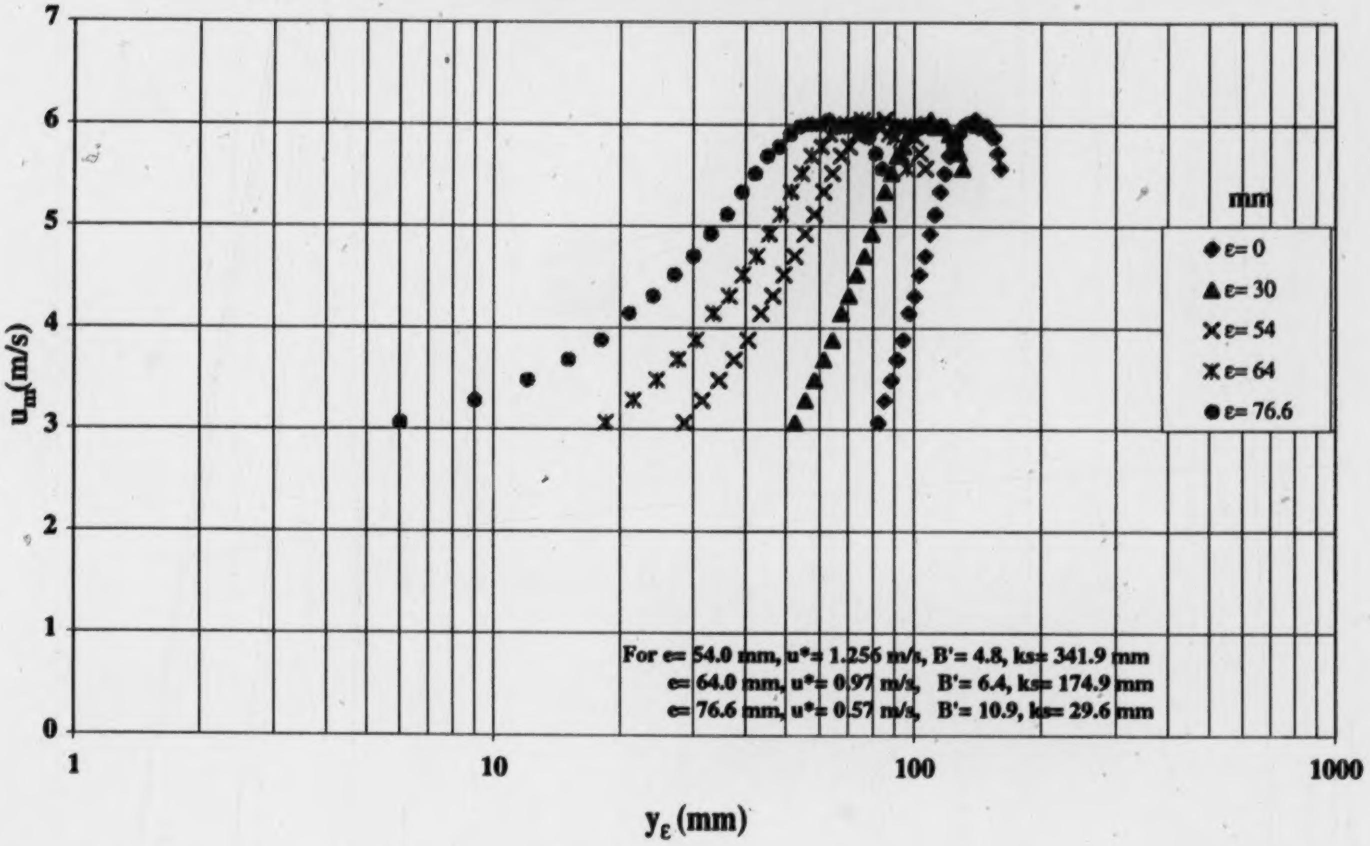

Figure C.4 Logarithmic velocity profiles at different origins at step #13 in a stepped spillway with l/h=0.6, h= 125. mm, k= 76.6 mm (yc/h=1.1)

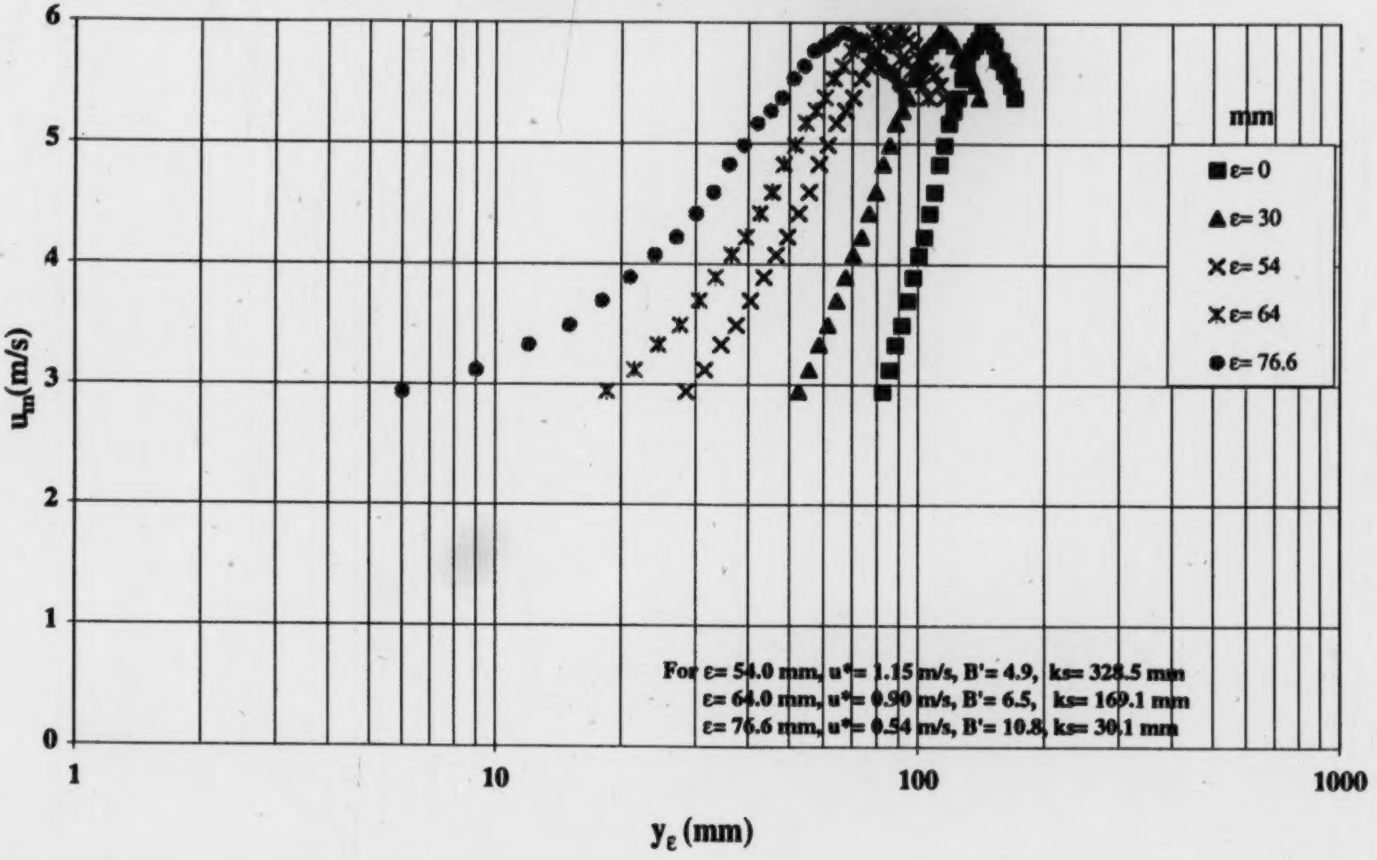

Figure C.5 Logarithmic velocity profiles at different origins at step #13 in a stepped spillway with l/h=0.6, h= 125. mm, k= 76.6 mm (yc/h=1.2)

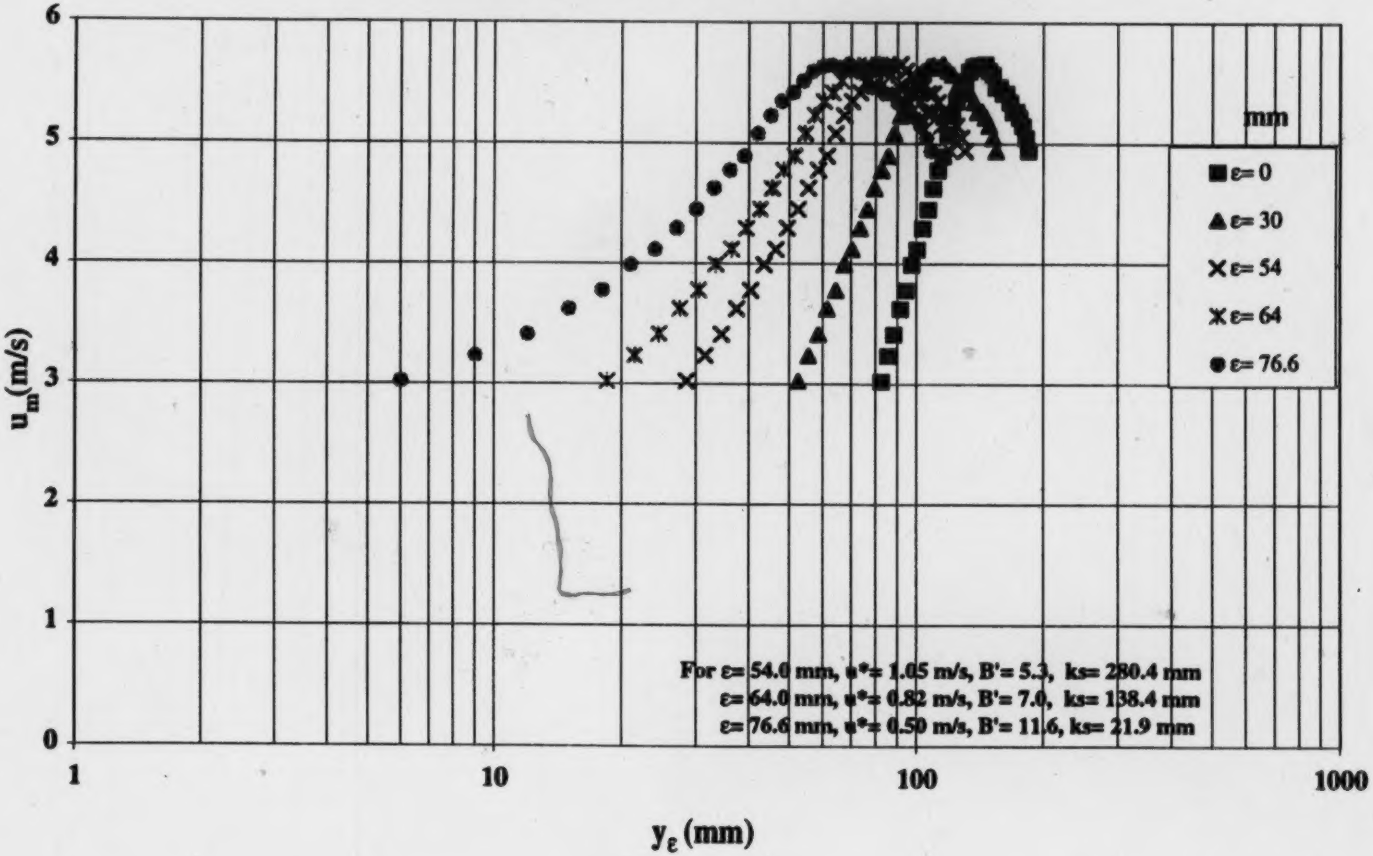

Figure C.6 Logarithmic velocity profiles at different origins at step #13 in a stepped spillway with l/h=0.6, h= 125. mm, k= 76.6 mm (yc/h=1.3)

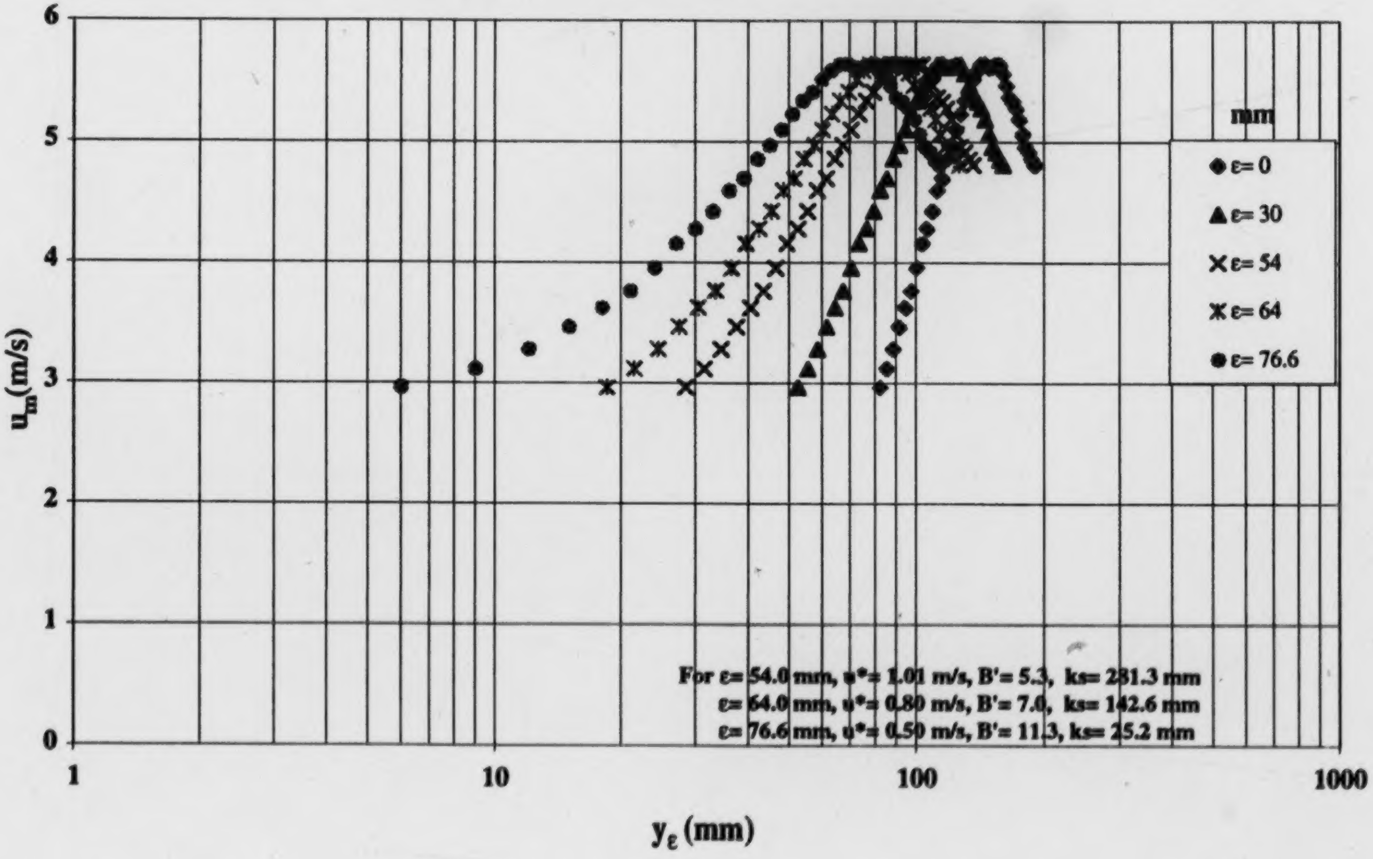

Figure C.7 Logarithmic velocity profiles at different origins at step #26 in a stepped spillway with l/h=0.6, h= 62.5 mm, k= 38.3 mm (yc/h=1.3)

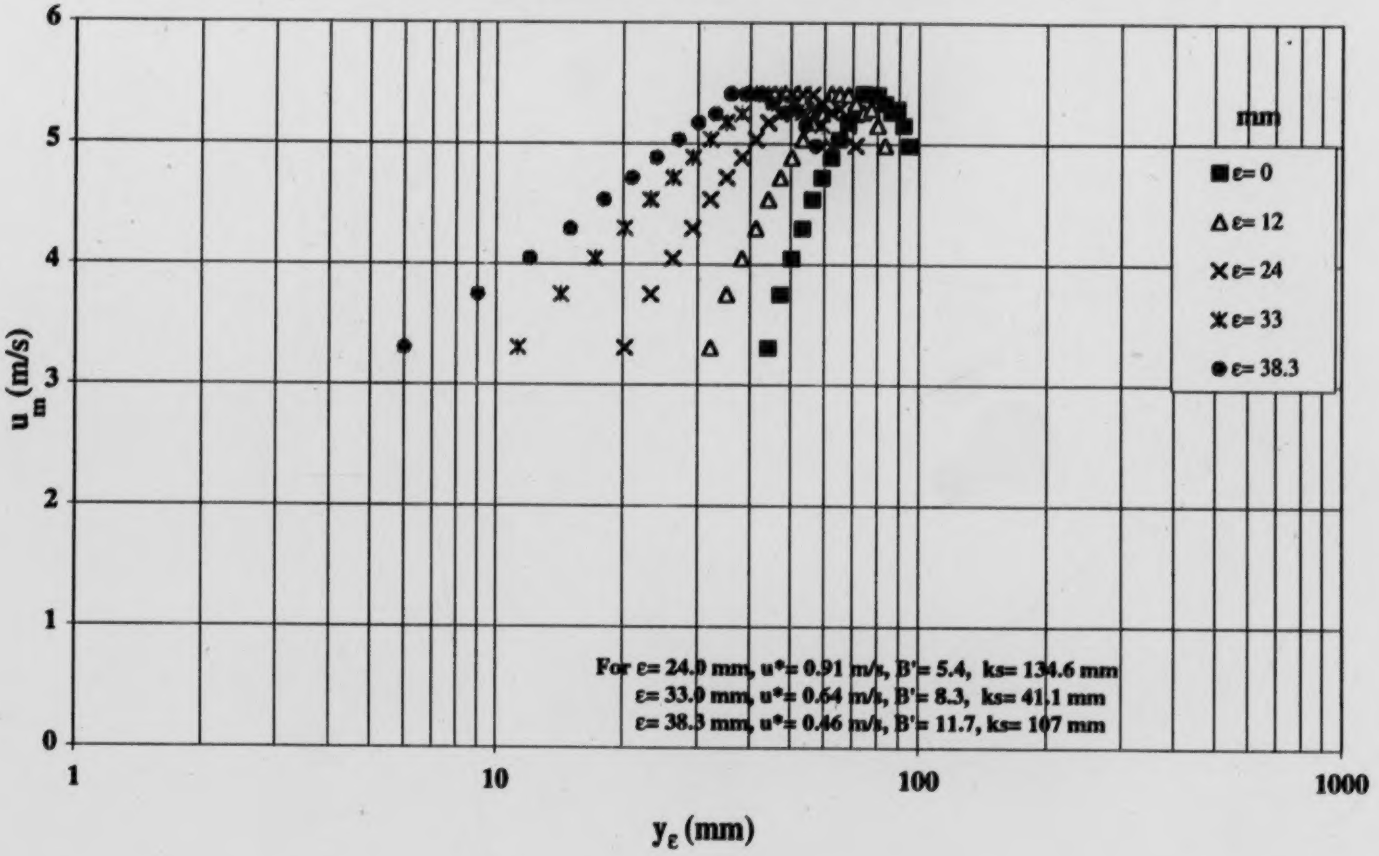

Figure C.8 Logarithmic velocity profiles at different origins at step #26 in a stepped spillway with l/h=0.6, h= 62.5 mm, k= 38.3 mm (yc/h=1.4)

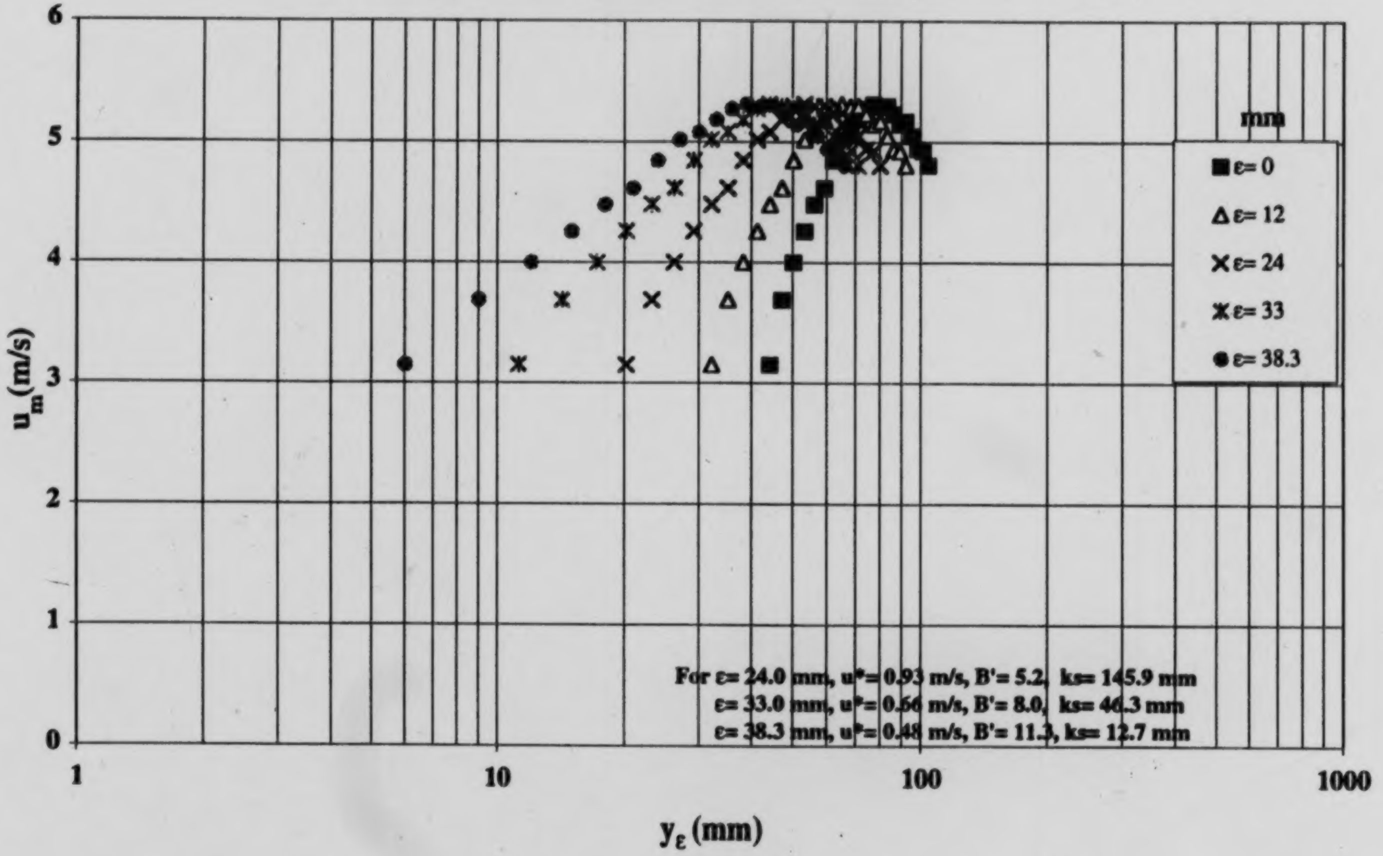

Figure C.9 Logarithmic velocity profiles at different origins at step #26 in a stepped spillway with l/h=0.6, h= 62.5 mm, k= 38.3 mm (yc/h=1.5)

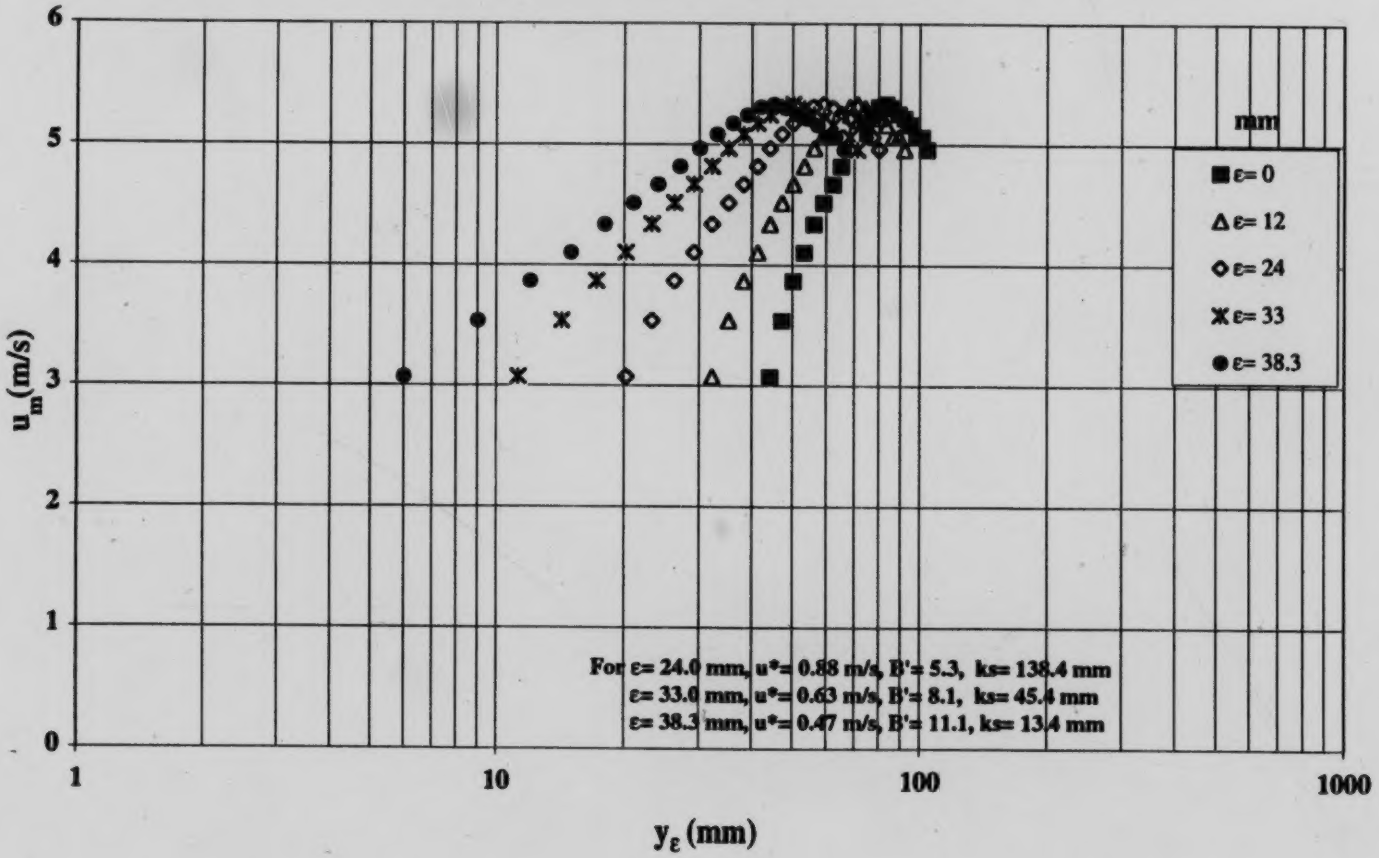

Figure C.10 Logarithmic velocity profiles at different origins at step #26 in a stepped spillway with l/h=0.6, h= 62.5 mm, k= 38.3 mm (yc/h=1.6)

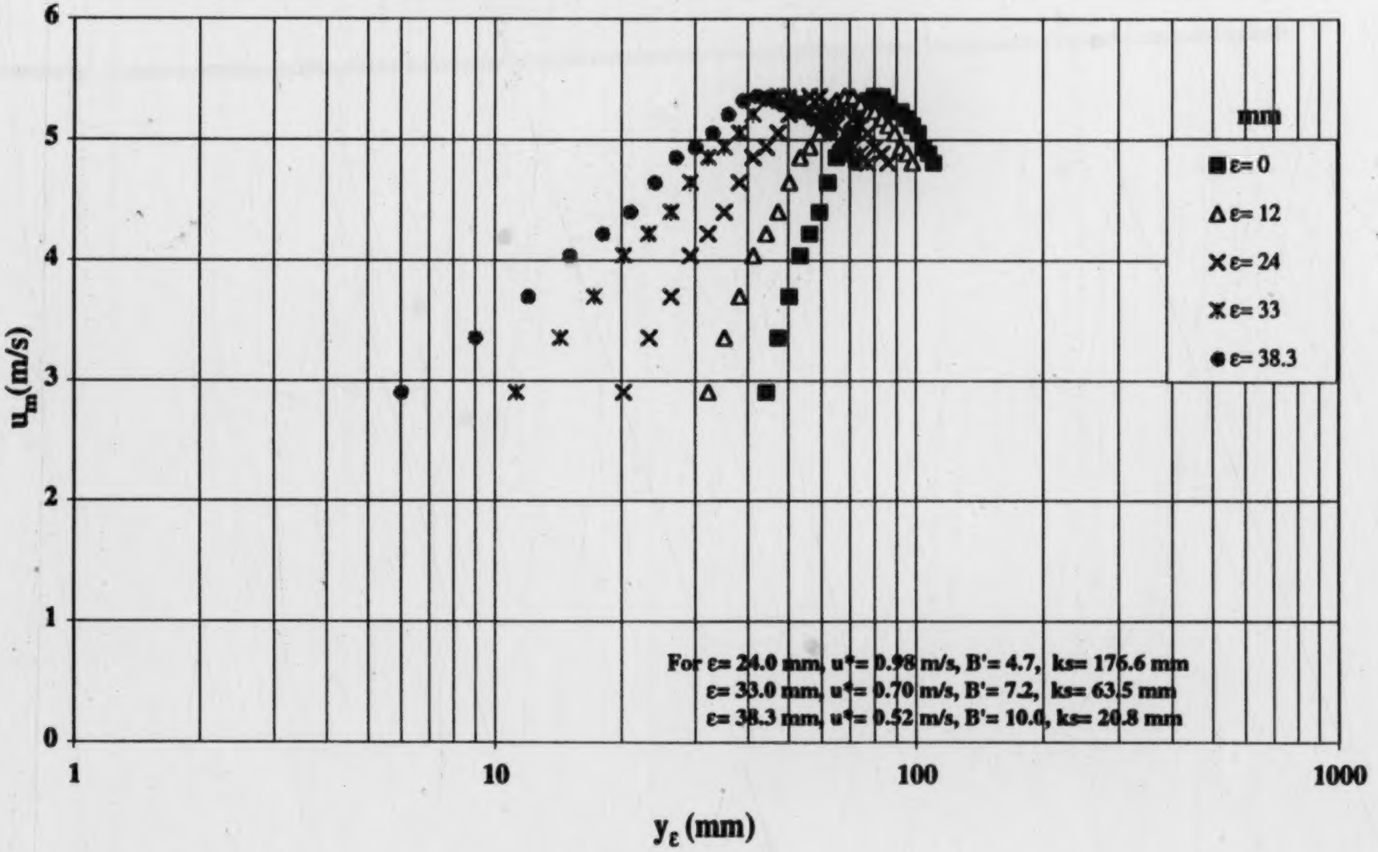

Figure C.11 Logarithmic velocity profiles at different origins at step #26 in a stepped spillway with l/h=0.6, h= 62.5 mm, k= 38.3 mm (yc/h=1.7)

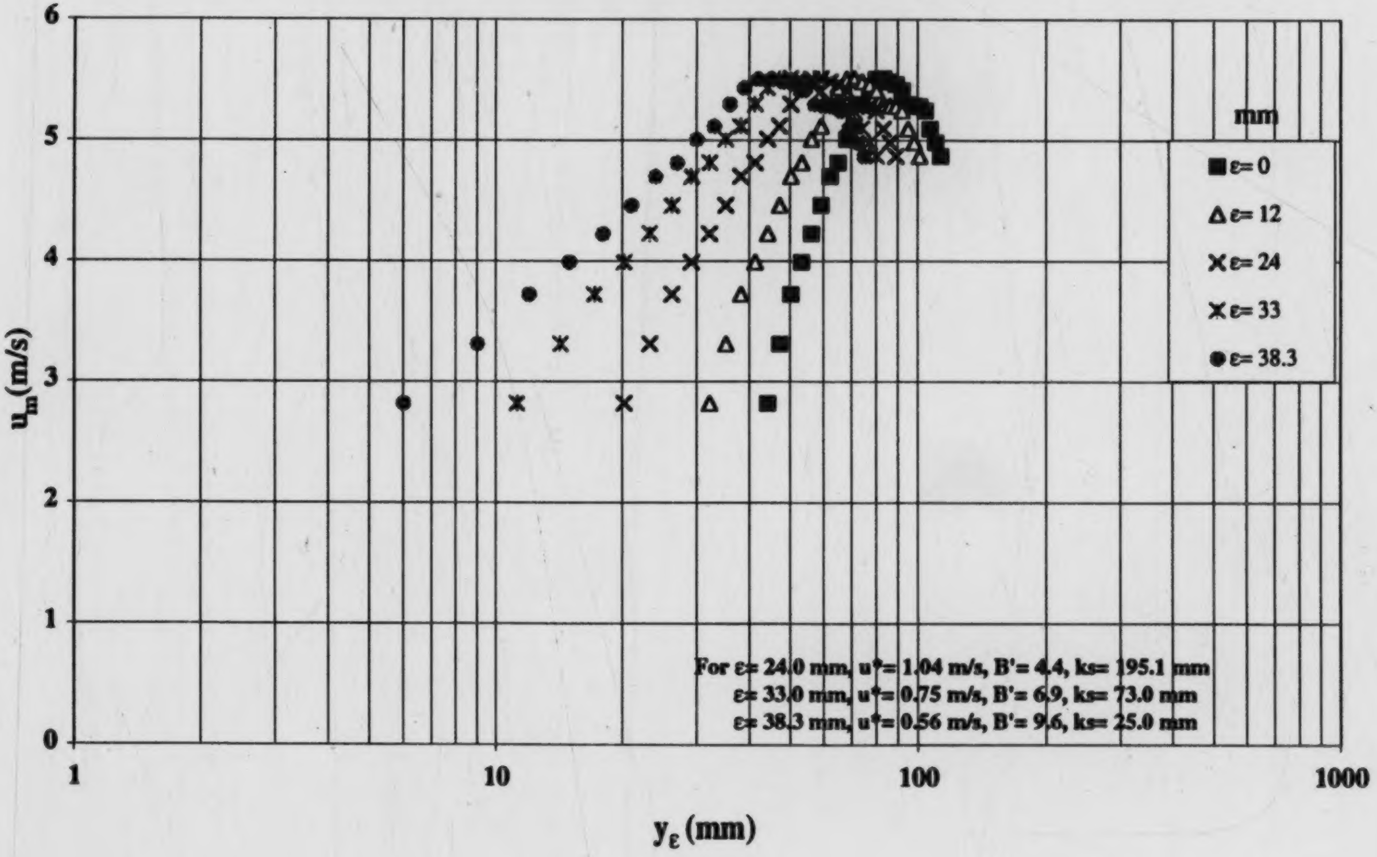

Figure C.12 Logarithmic velocity profiles at different origins at step #26 in a stepped spillway with l/h=0.6, h= 62.5 mm, k= 38.3 mm (yc/h=1.8)

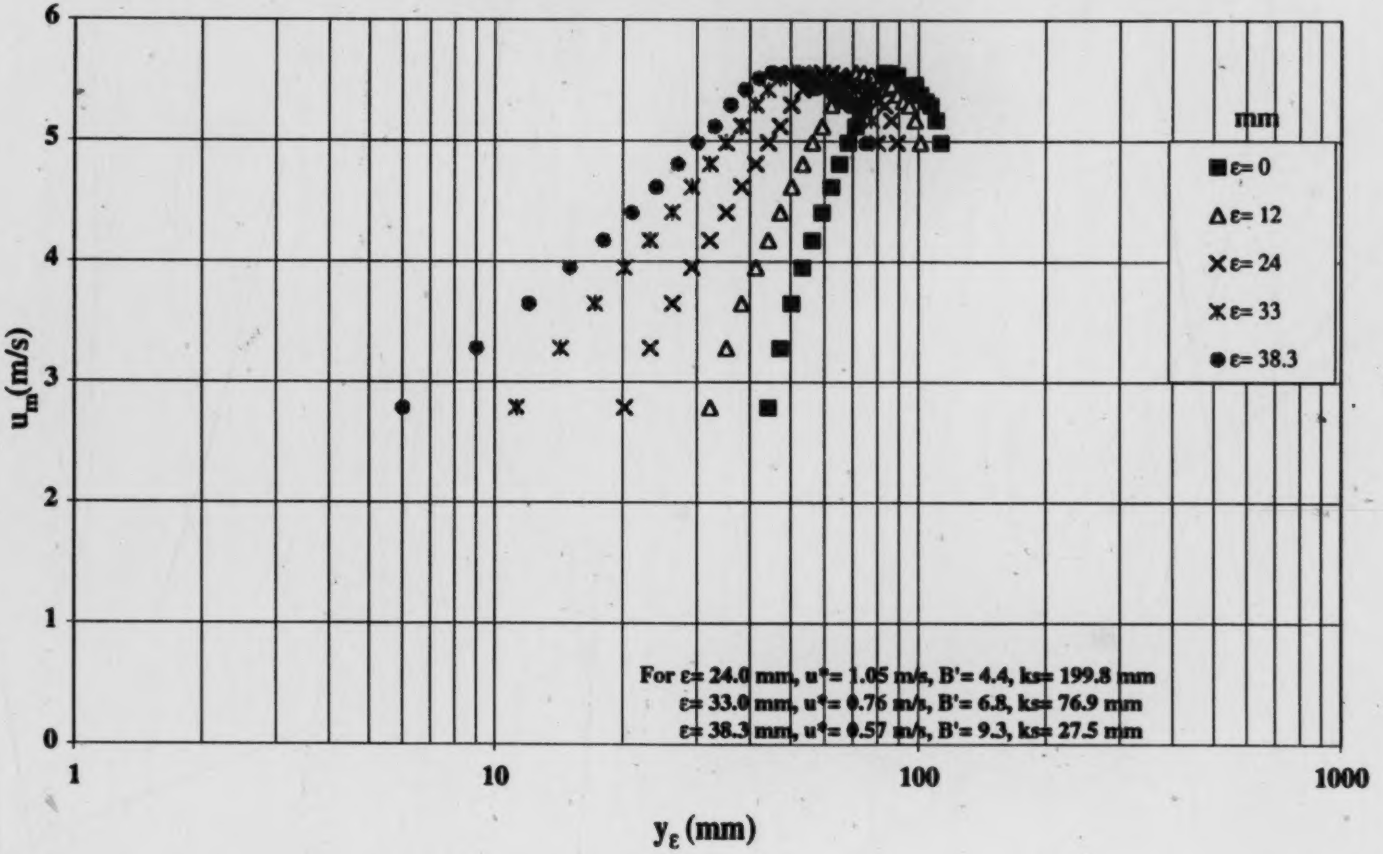

Figure C.13 Logarithmic velocity profiles at different origins at step #26 in a stepped spillway with l/h=0.6, h= 62.5 mm, k= 38.3 mm (yc/h=2.0)

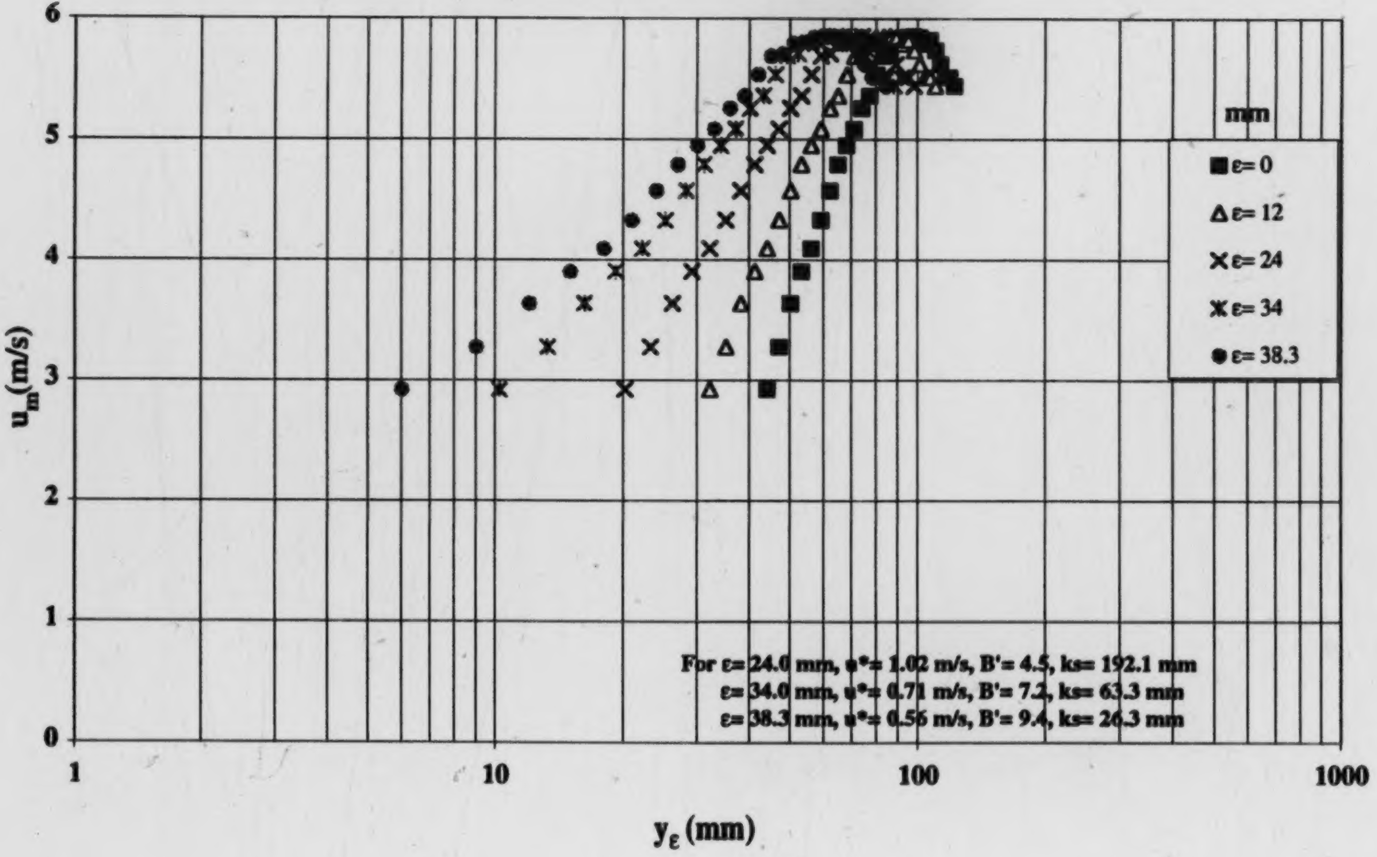

Figure C.14 Logarithmic velocity profiles at different origins at step #26 in a stepped spillway with l/h=0.6, h= 62.5 mm, k= 38.3 mm (yc/h=2.1)

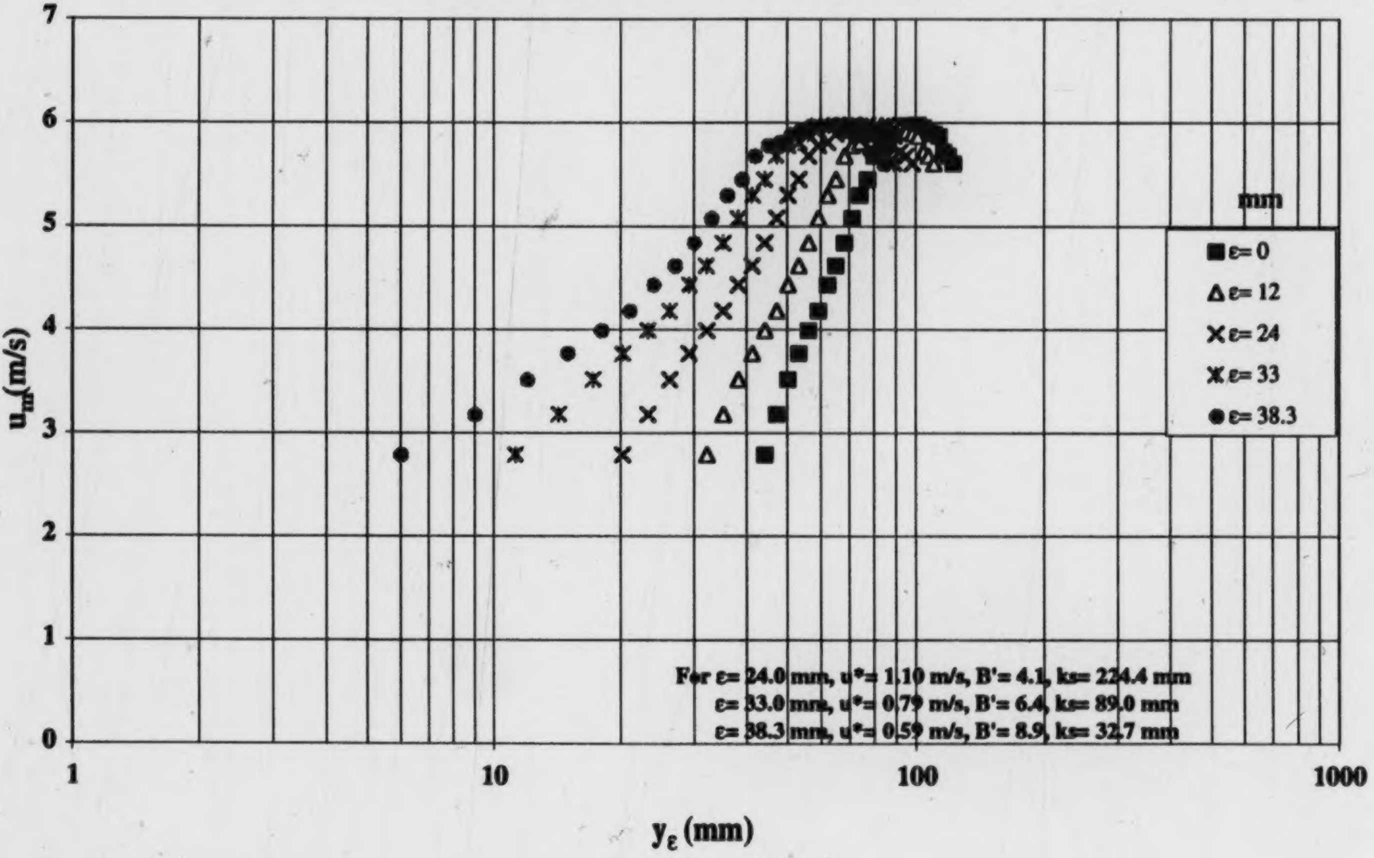

Figure C.15 Logarithmic velocity profiles at different origins at step #26 in a stepped spillway with l/h=0.6, h= 62.5 mm, k= 38.3 mm (yc/h=2.2)

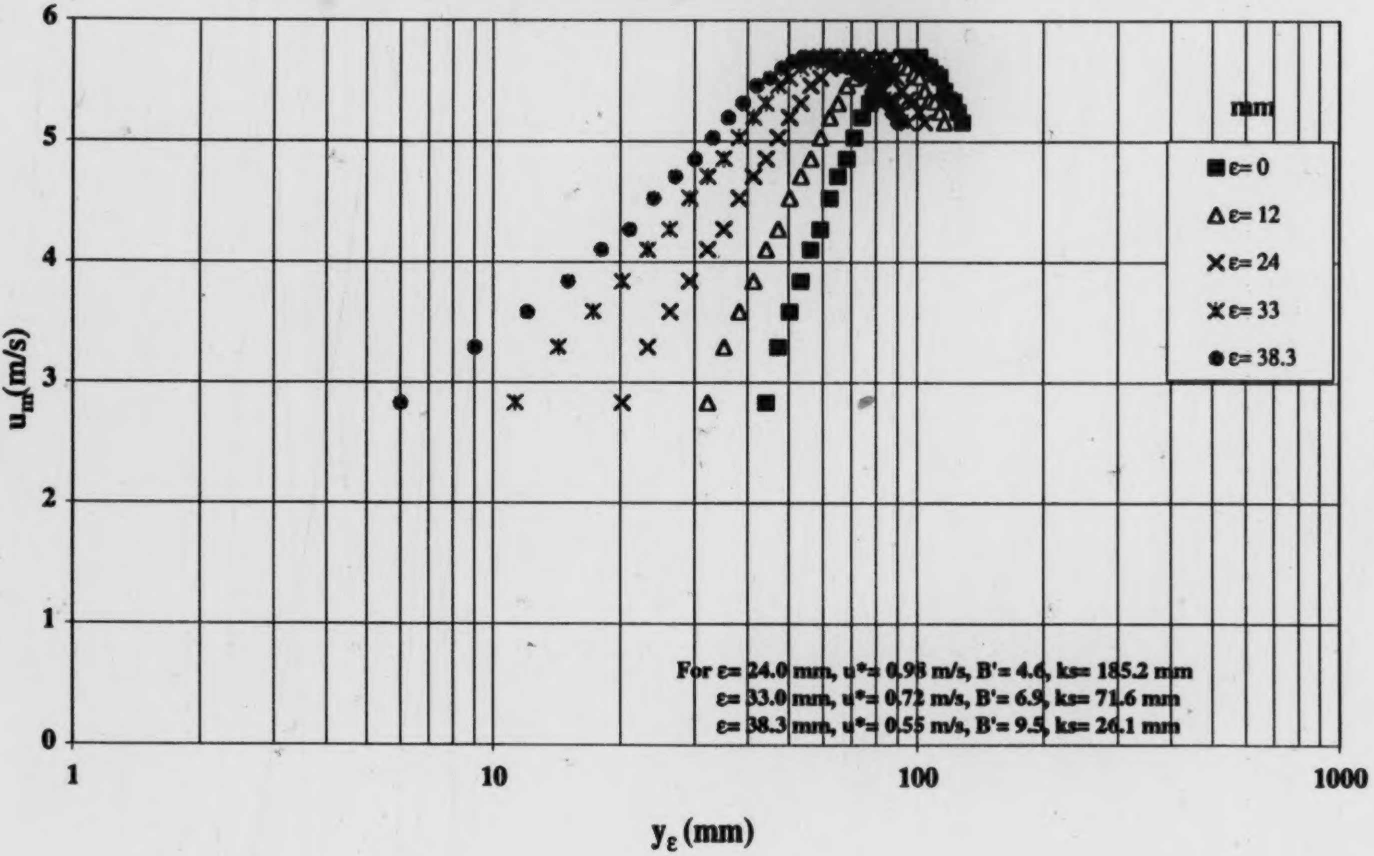

For ε= 24.0 mm, u*= 0.98 m/s, B'= 4.6, ks= 185.2 mm
ε= 33.0 mm, u*= 0.72 m/s, B'= 6.9, ks= 71.6 mm
ε= 38.3 mm, u*= 0.55 m/s, B'= 9.5, ks= 26.1 mm

Figure C.16 Logarithmic velocity profiles at different origins at step #26 in a stepped spillway with l/h=0.6, h= 62.5 mm, k= 38.3 mm (yc/h=2.3)

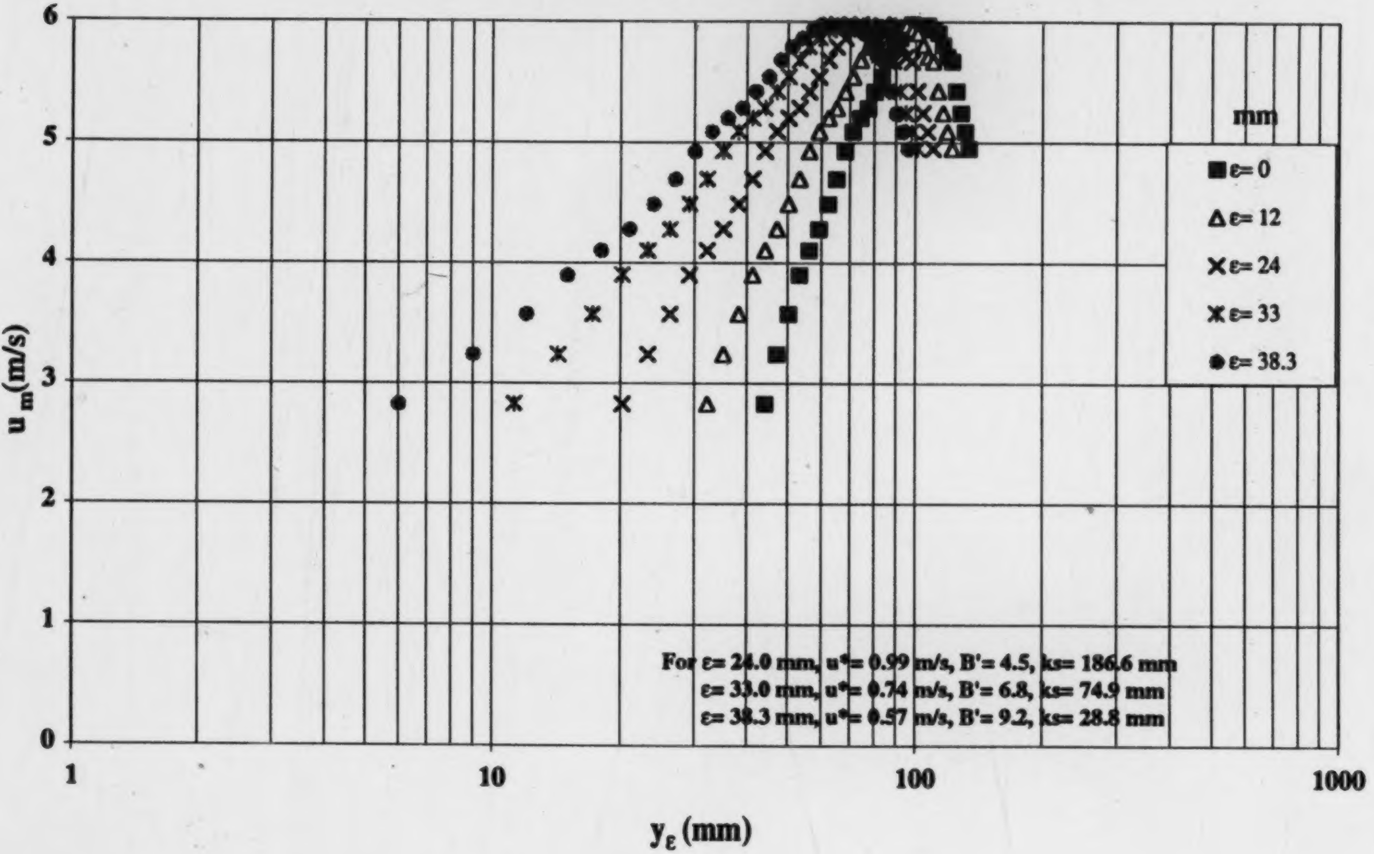

Figure C.17 Logarithmic velocity profiles at different origins at step #26 in a stepped spillway with l/h=0.6, h= 62.5 mm, k= 38.3 mm (yc/h=2.4)

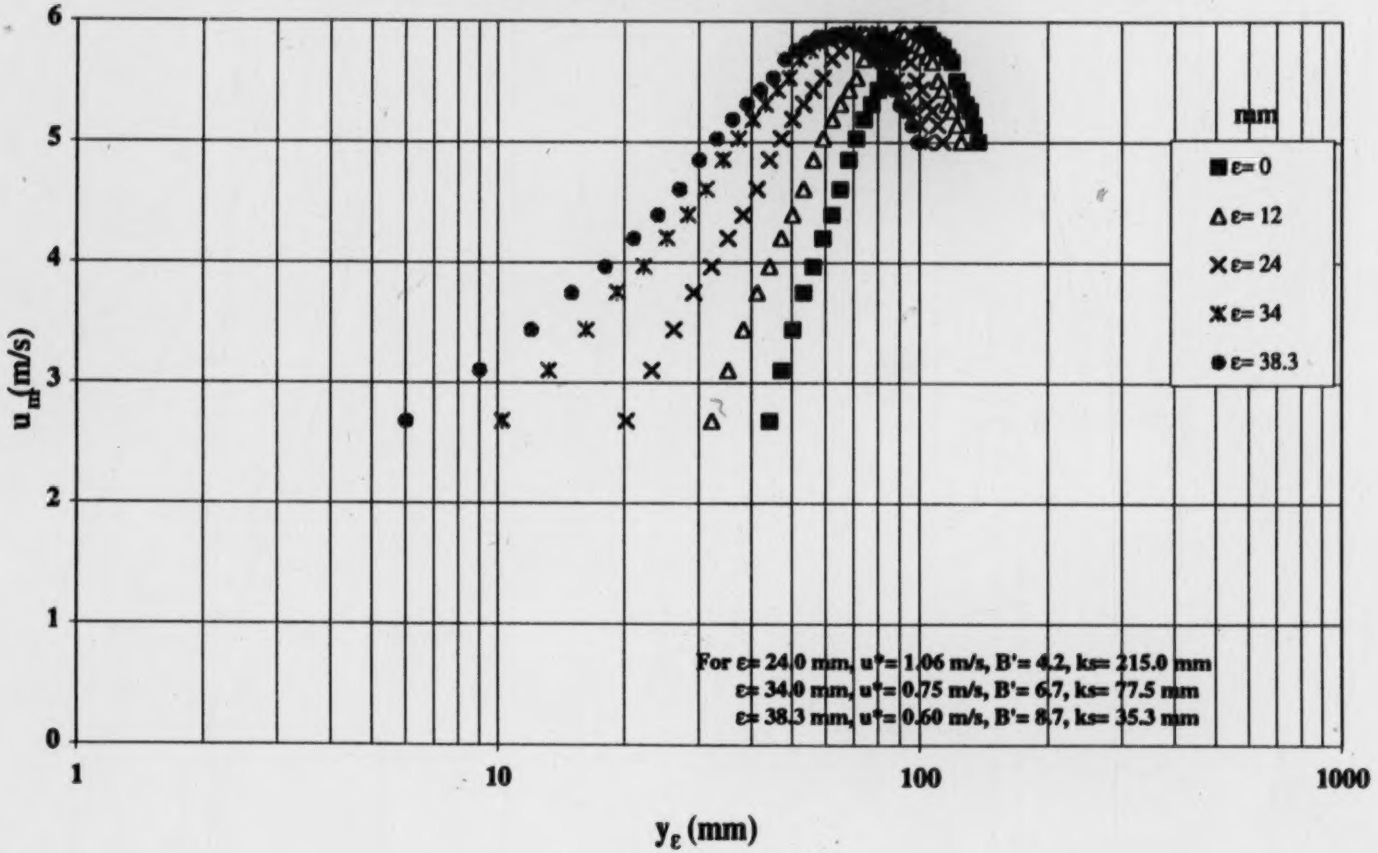

Figure C.18 Logarithmic velocity profiles at different origins at step #26 in a stepped spillway with l/h=0.6, h= 62.5 mm, k= 38.3 mm (yc/h=2.5)

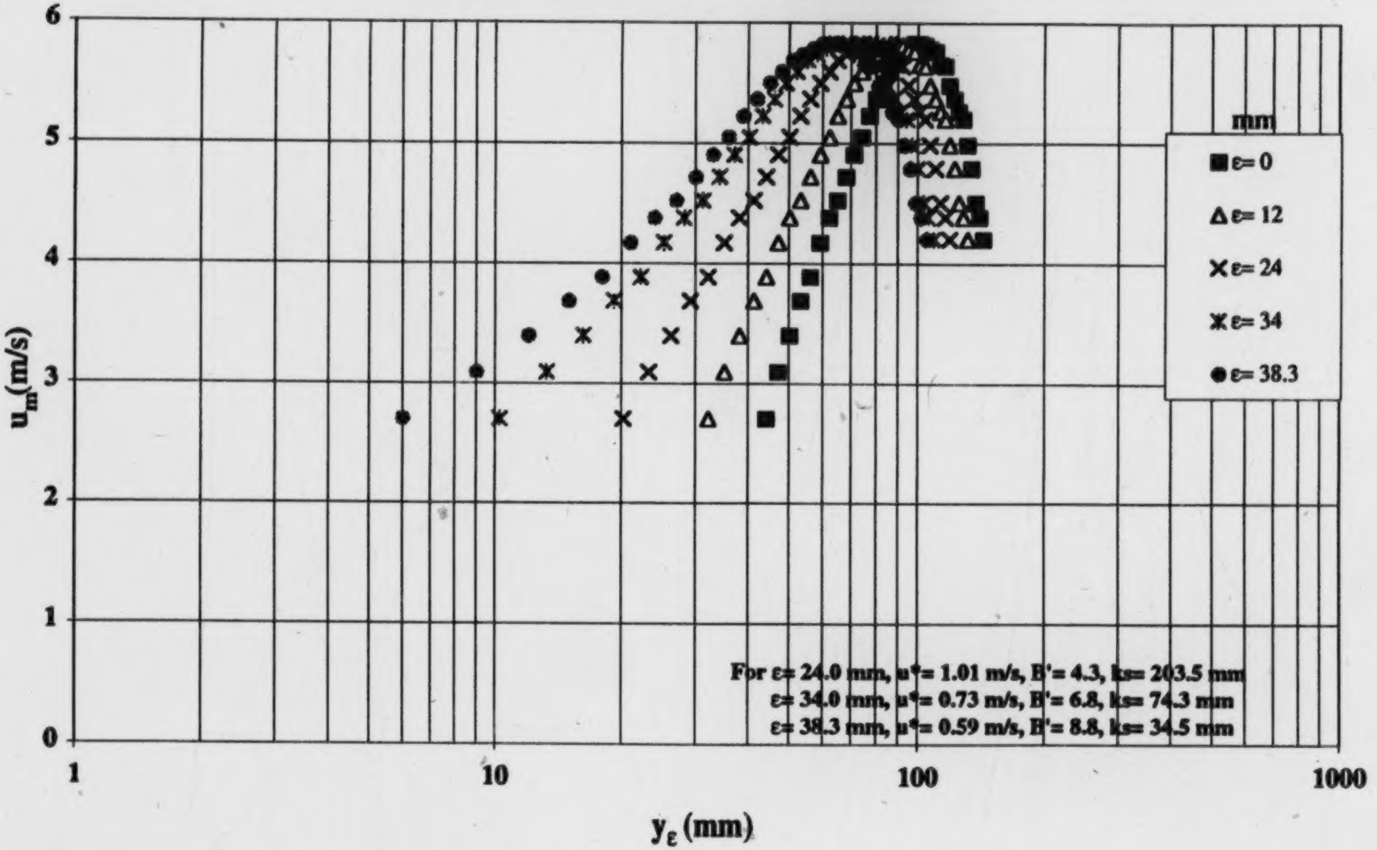

Figure C.19 Logarithmic velocity profiles at different origins at step #26 in a stepped spillway with l/h=0.6, h= 62.5 mm, k= 38.3 mm (yc/h=2.6)

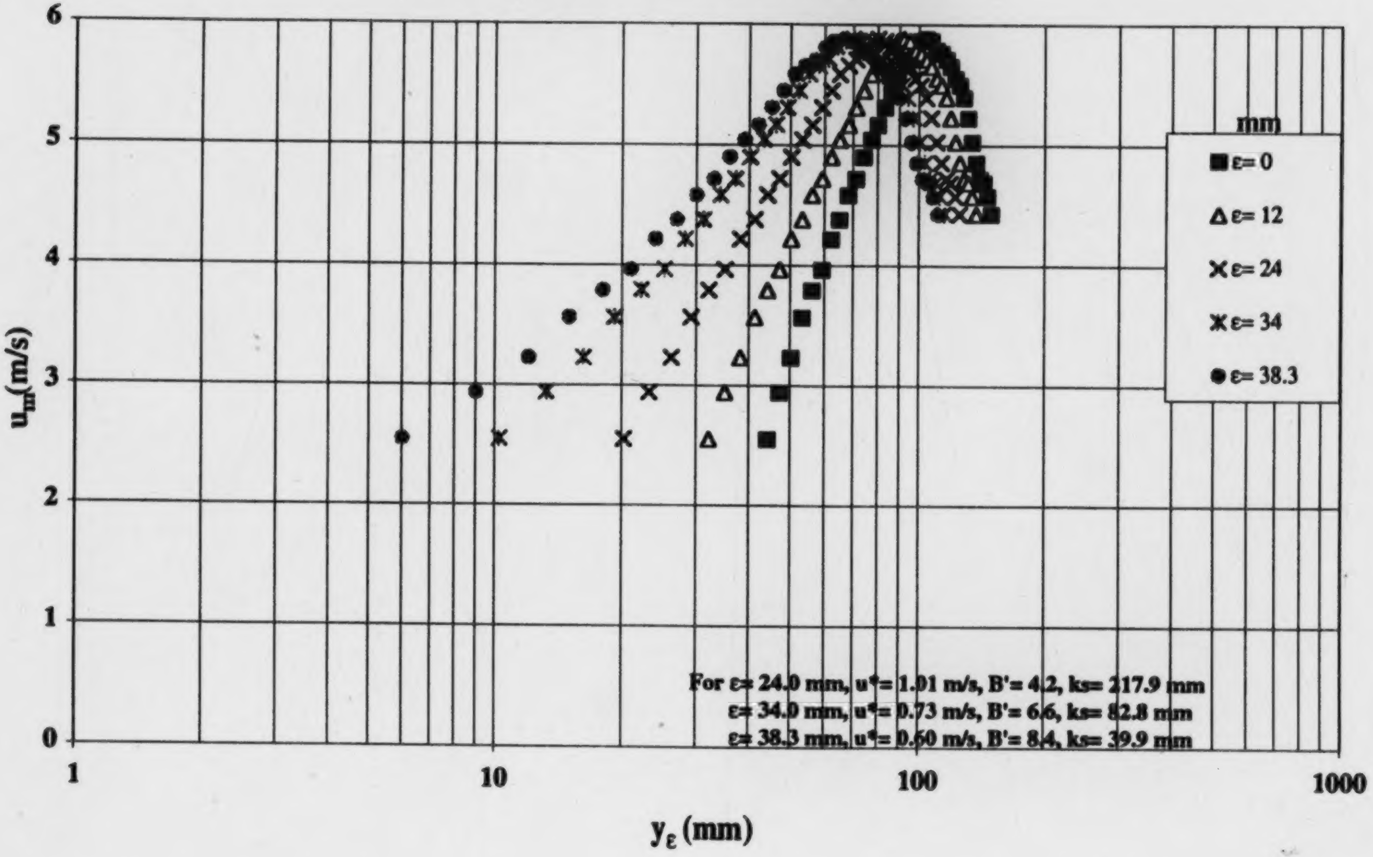

Figure C.20 Logarithmic velocity profiles at different origins at step #64 in a stepped spillway with l/h=0.6, h= 31.25 mm, k= 19.14 mm (yc/h=2.6)

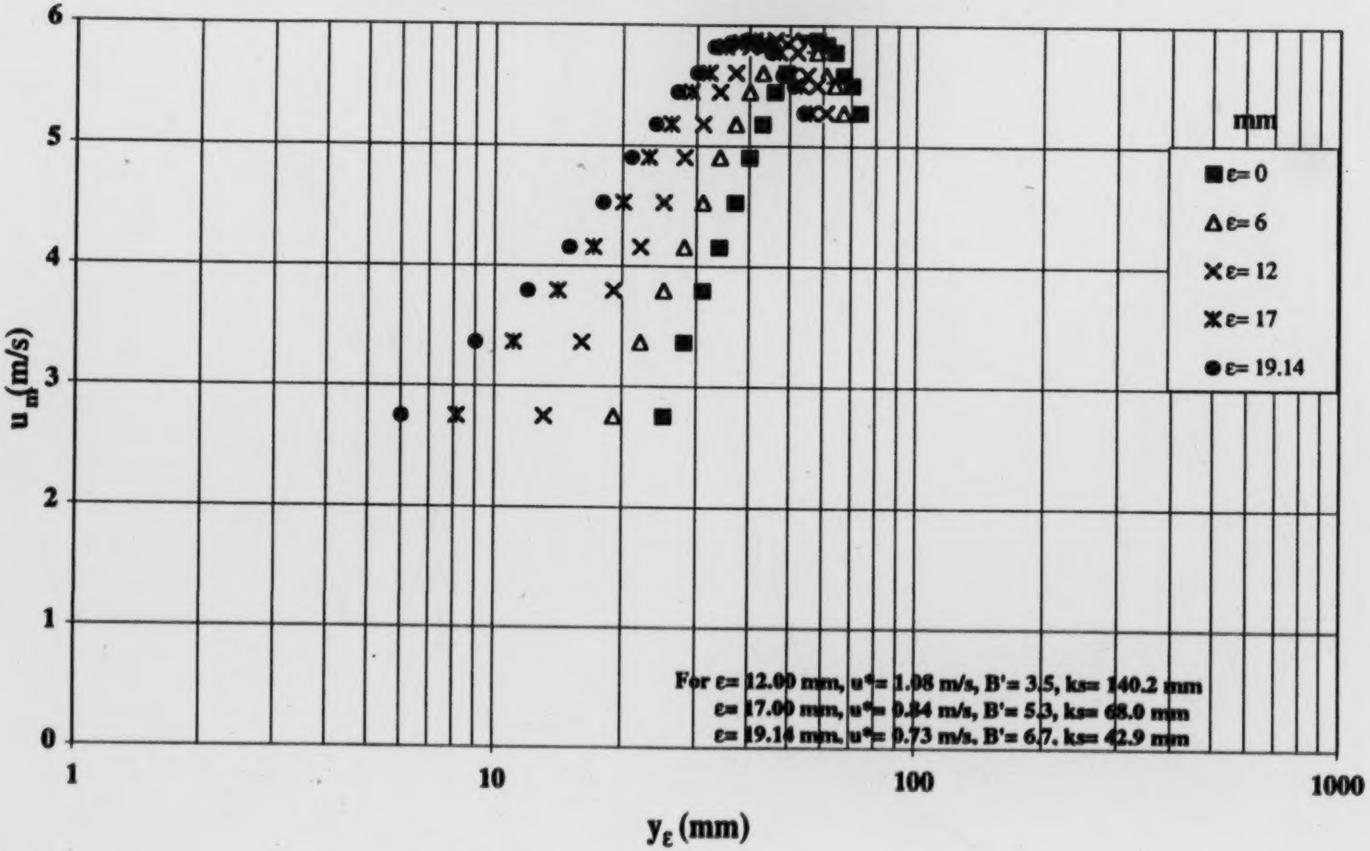

Figure C.21 Logarithmic velocity profiles at different origins at step #64 in a stepped spillway with l/h=0.6, h= 31.25 mm, k= 19.14 mm (yc/h=2.8)

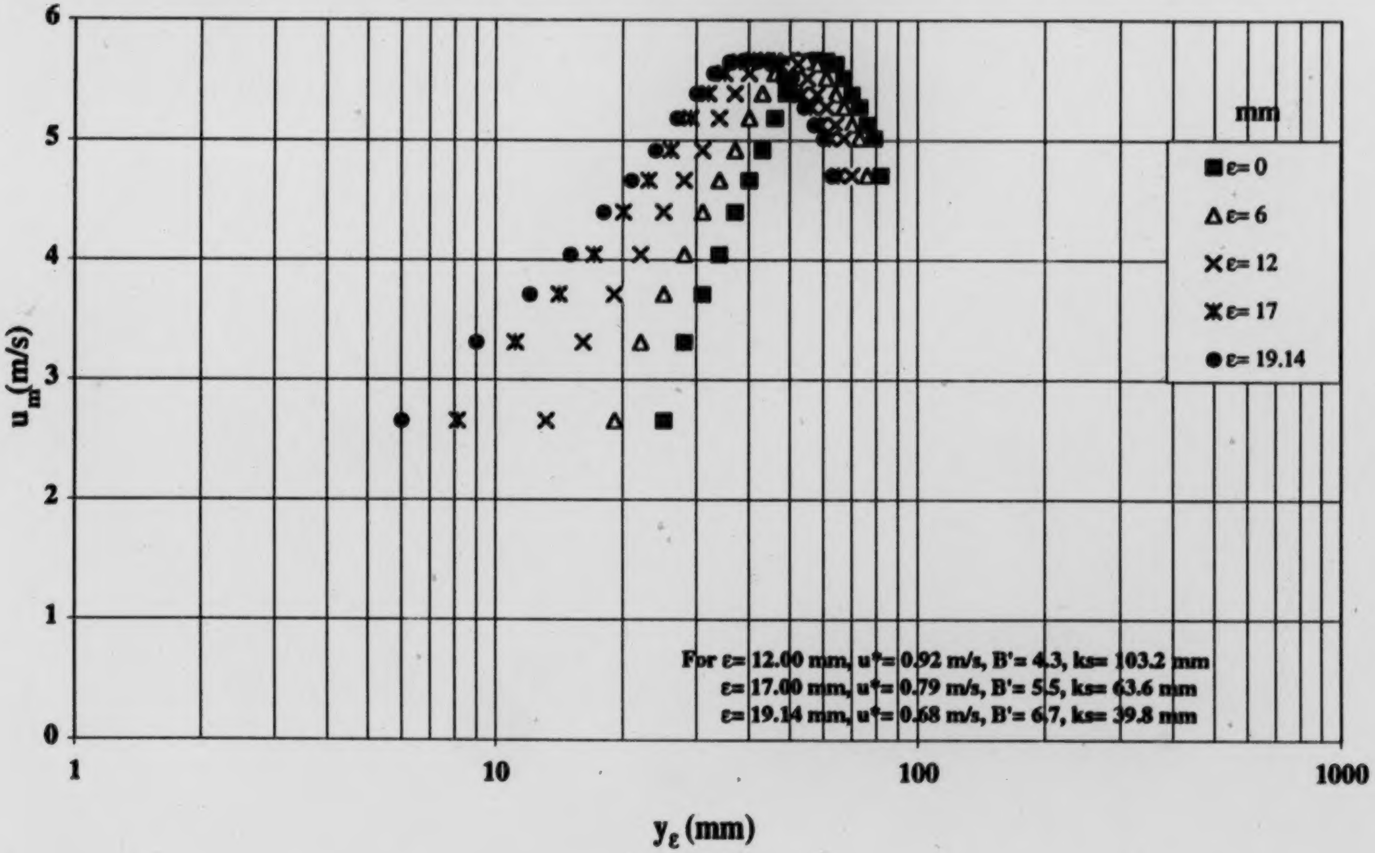

Figure C.22 Logarithmic velocity profiles at different origins at step #64 in a stepped spillway with l/h=0.6, h= 31.25 mm, k= 19.14 mm (yc/h=3.0)

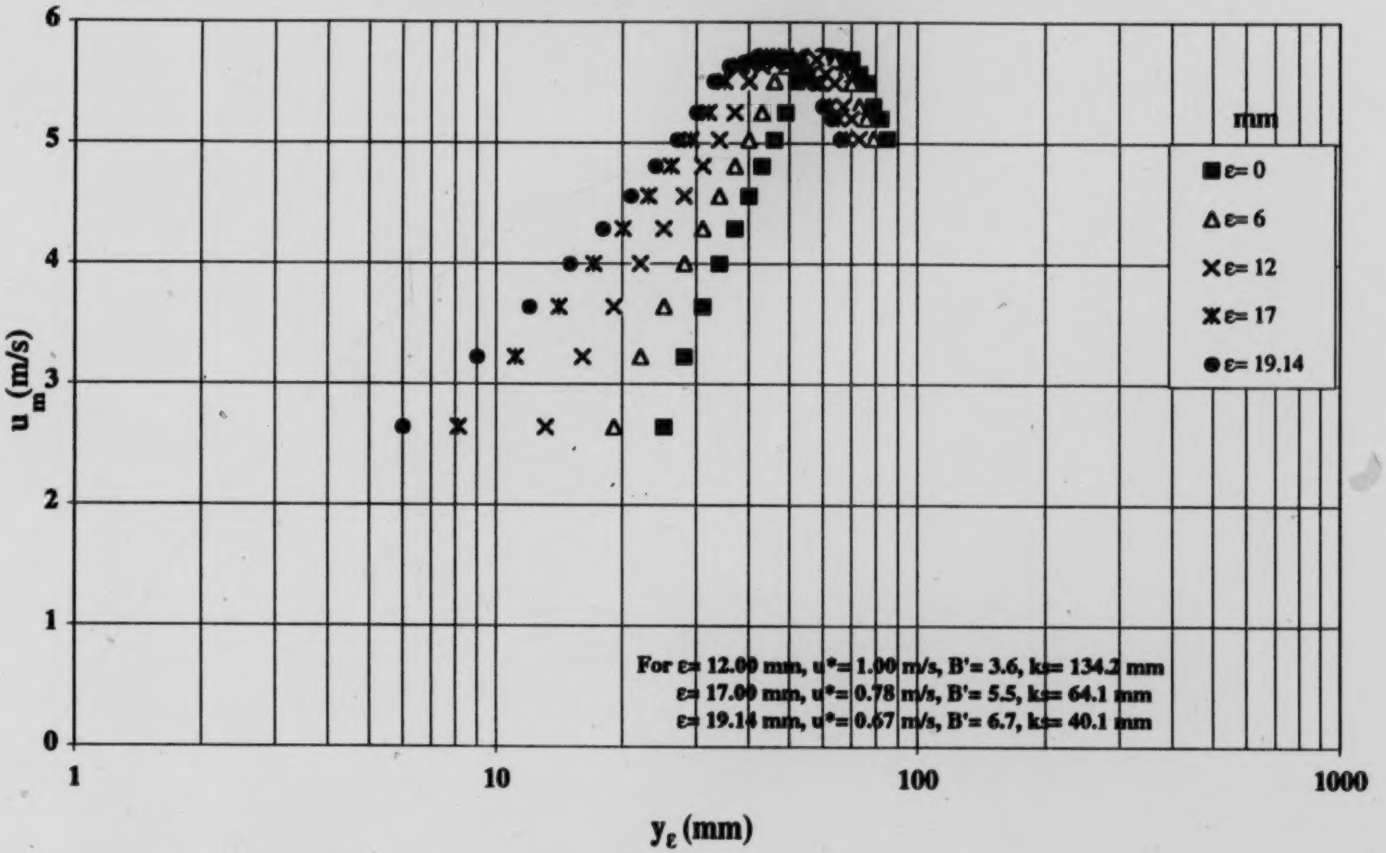

Figure C.23 Logarithmic velocity profiles at different origins at step #64 in a stepped spillway with l/h=0.6, h= 31.25 mm, k= 19.14 mm (yc/h=3.2)

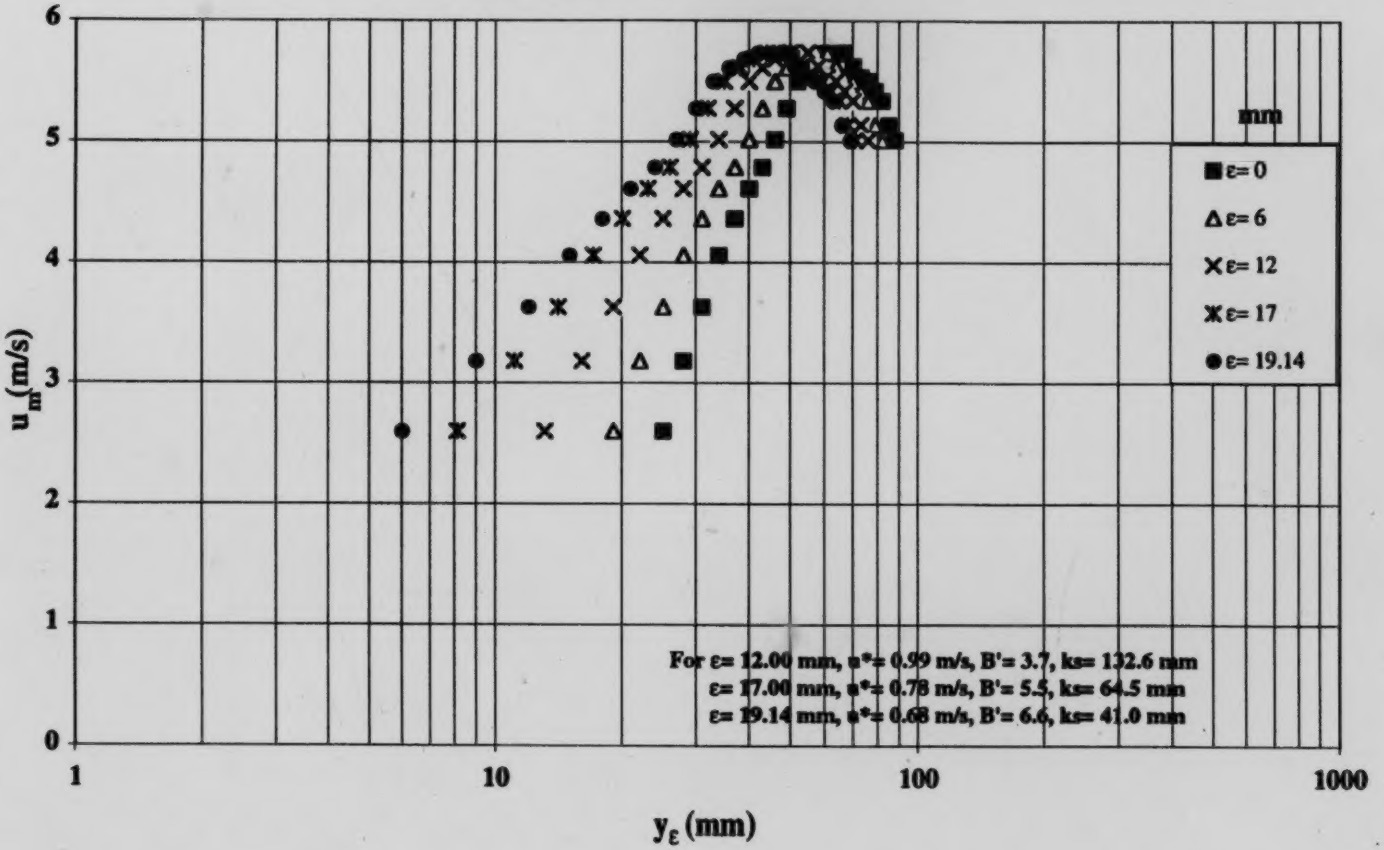

Figure C.24 Logarithmic velocity profiles at different origins at step #64 in a stepped spillway with l/h=0.6, h= 31.25 mm, k= 19.14 mm (yc/h=3.4)

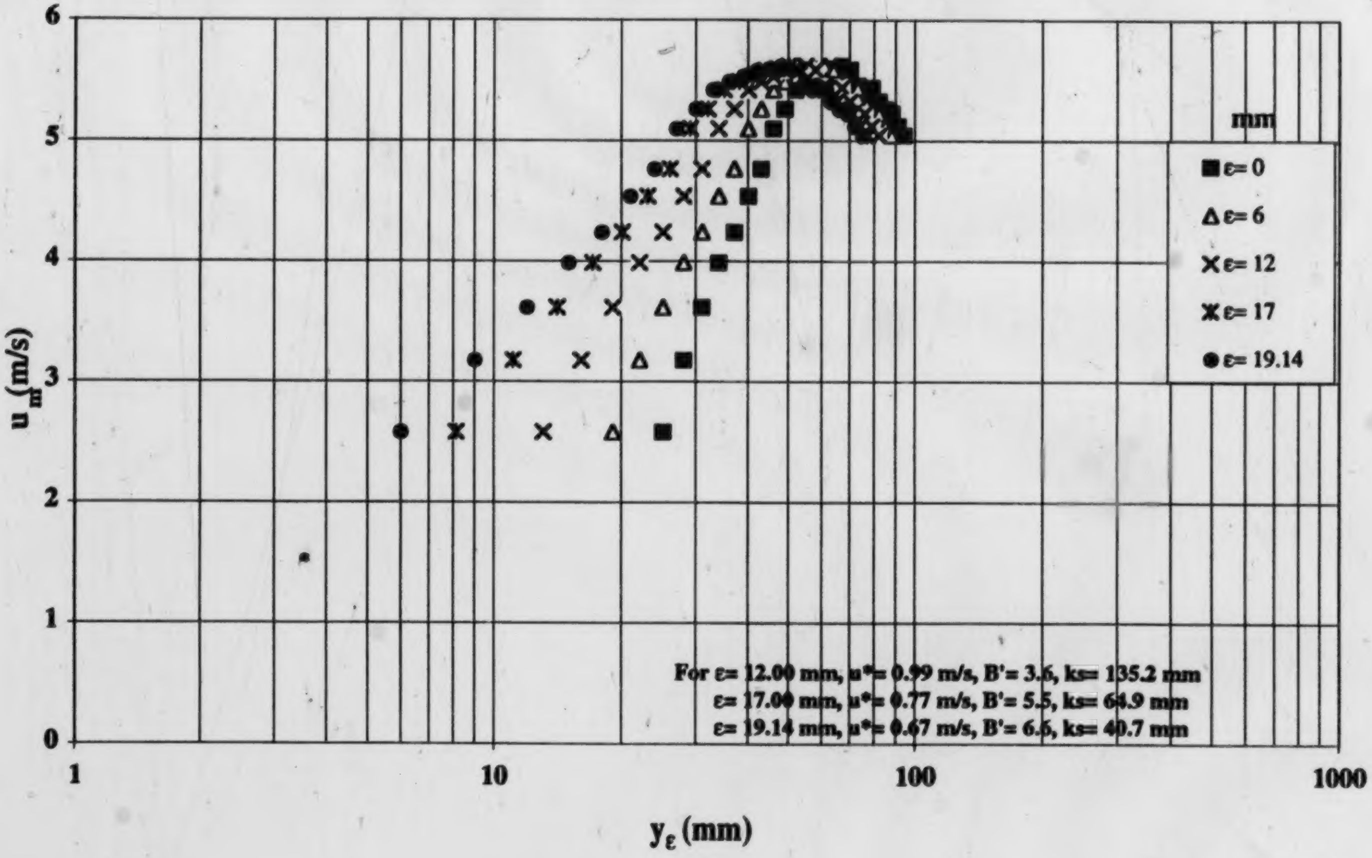

Figure C.25 Logarithmic velocity profiles at different origins at step #64 in a stepped spillway with l/h=0.6, h= 31.25 mm, k= 19.14 mm (yc/h=3.6)

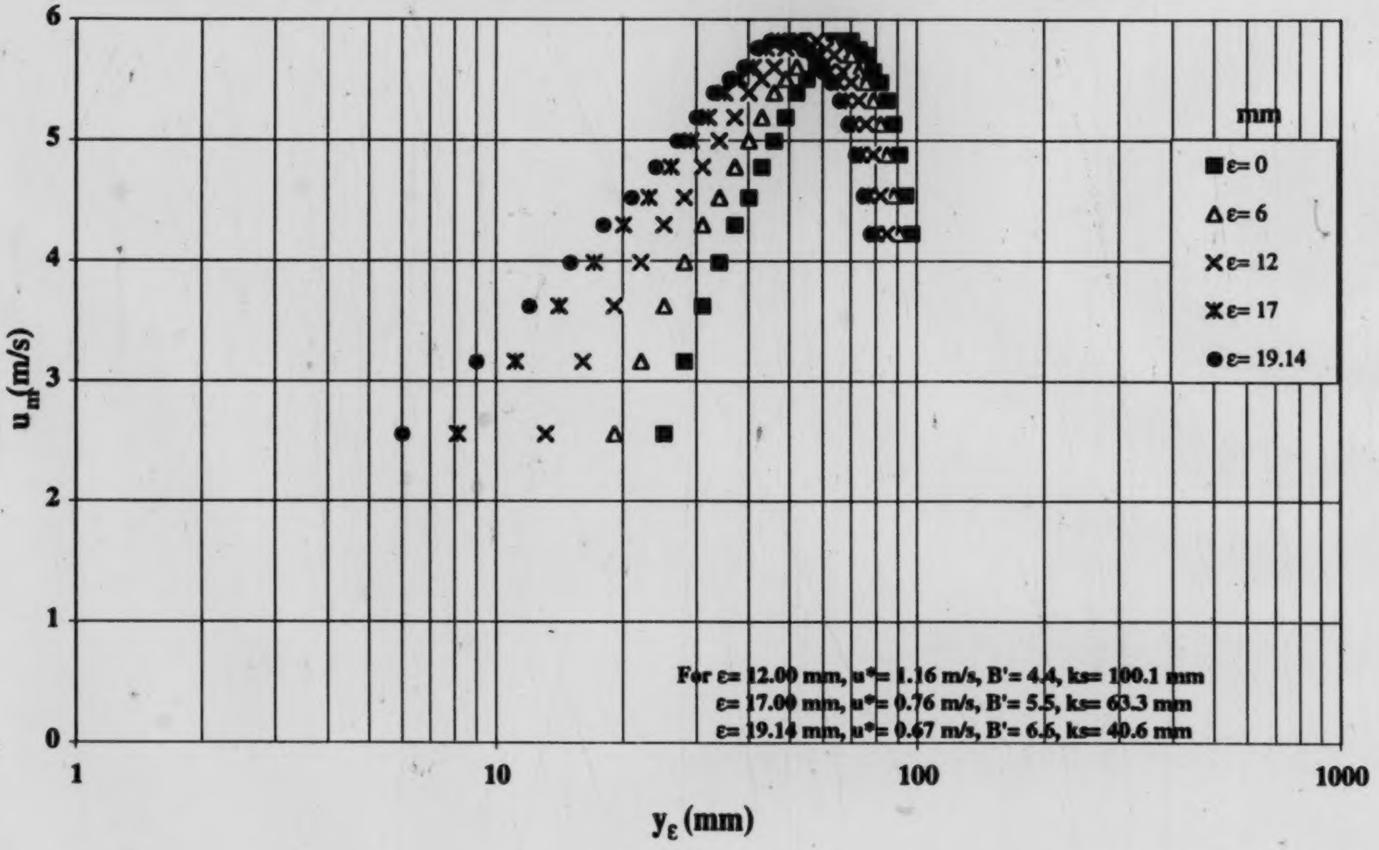

Figure C.26 Logarithmic velocity profiles at different origins at step #64 in a stepped spillway with l/h=0.6, h= 31.25 mm, k= 19.14 mm (yc/h=3.8)

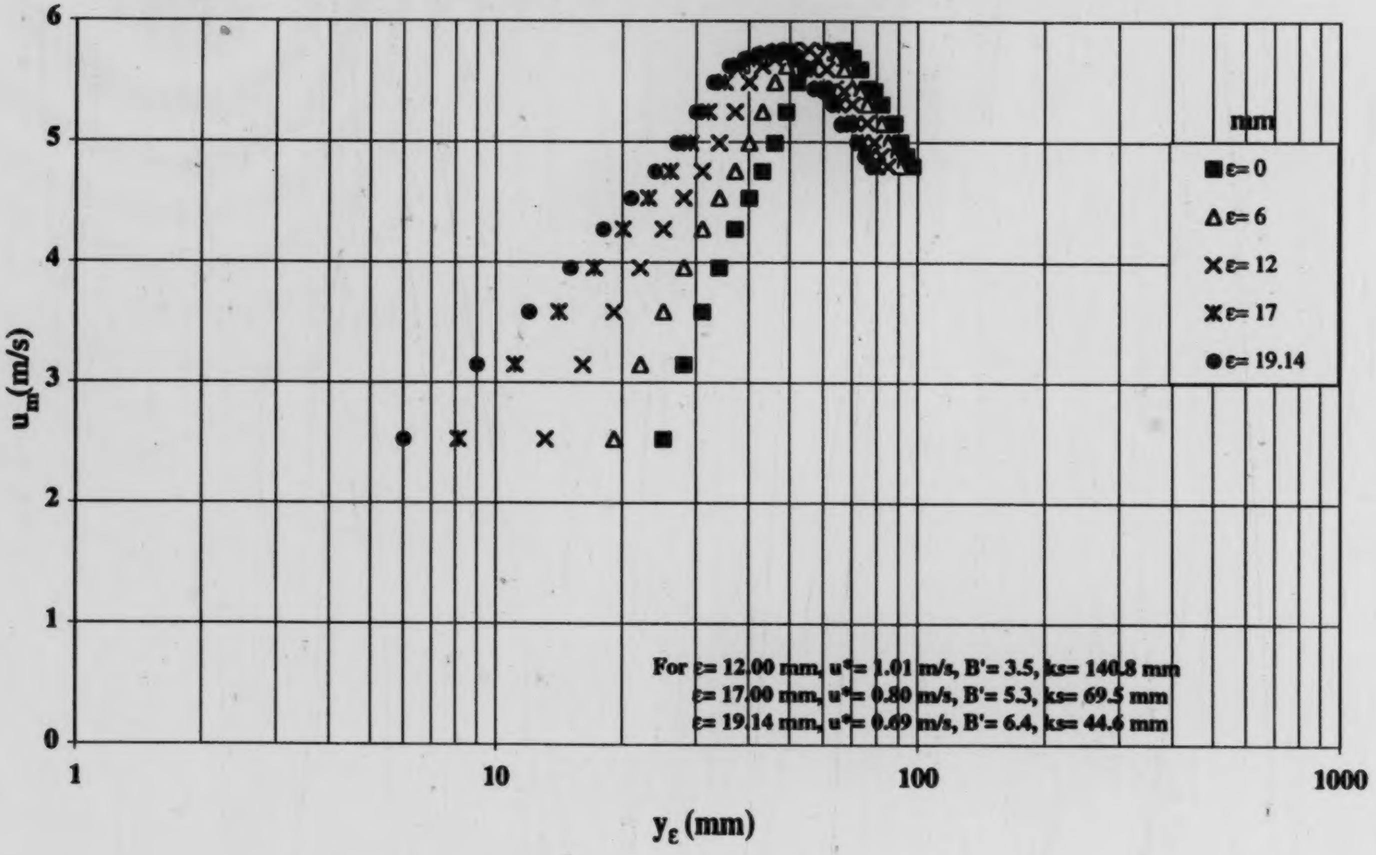

Figure C.27 Logarithmic velocity profiles at different origins at step #64 in a stepped spillway with l/h=0.6, h= 31.25 mm, k= 19.14 mm (yc/h=4.0)

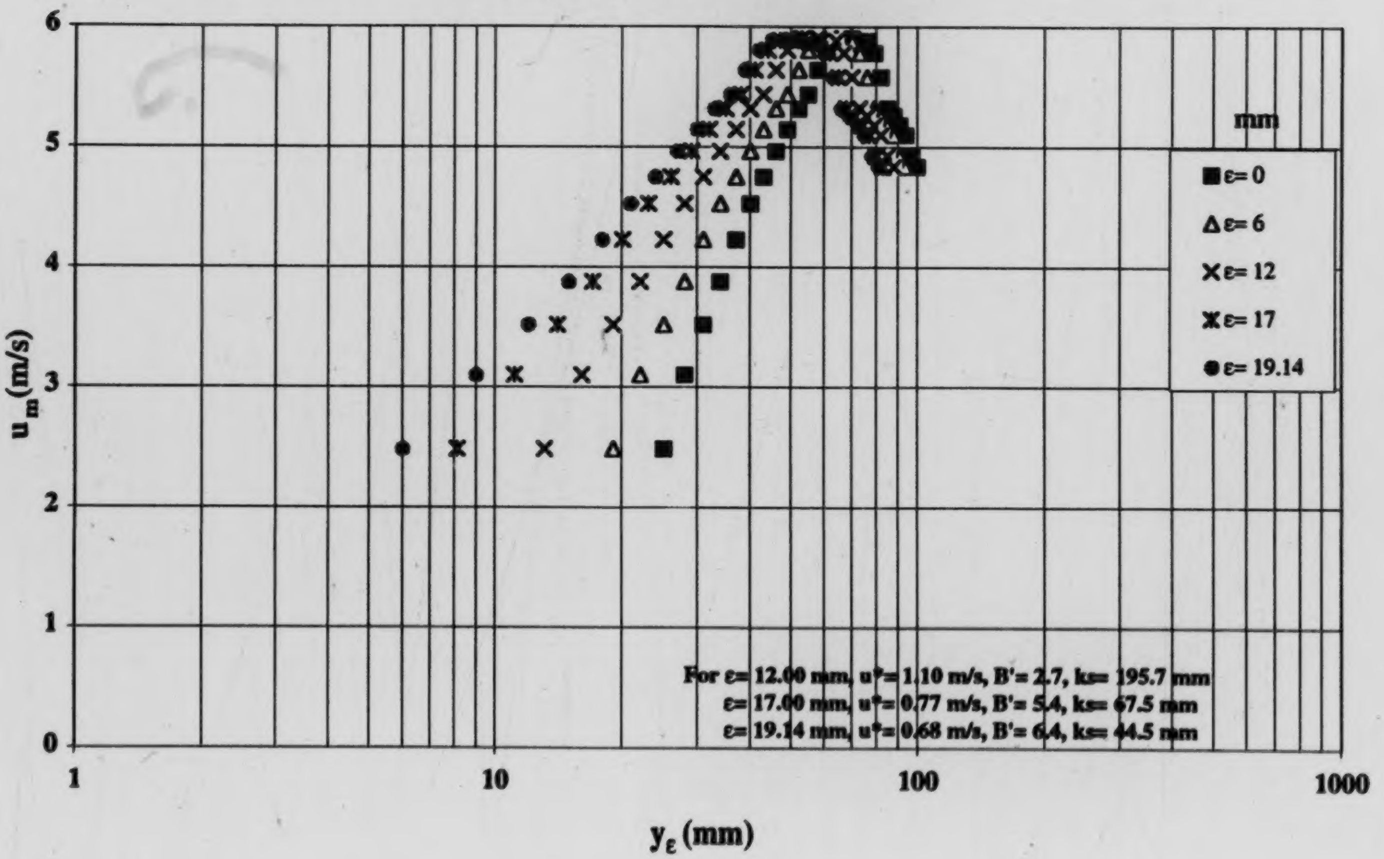

Figure C.28 Logarithmic velocity profiles at different origins at step #64 in a stepped spillway with l/h=0.6, h= 31.25 mm, k= 19.14 mm (yc/h=4.2)

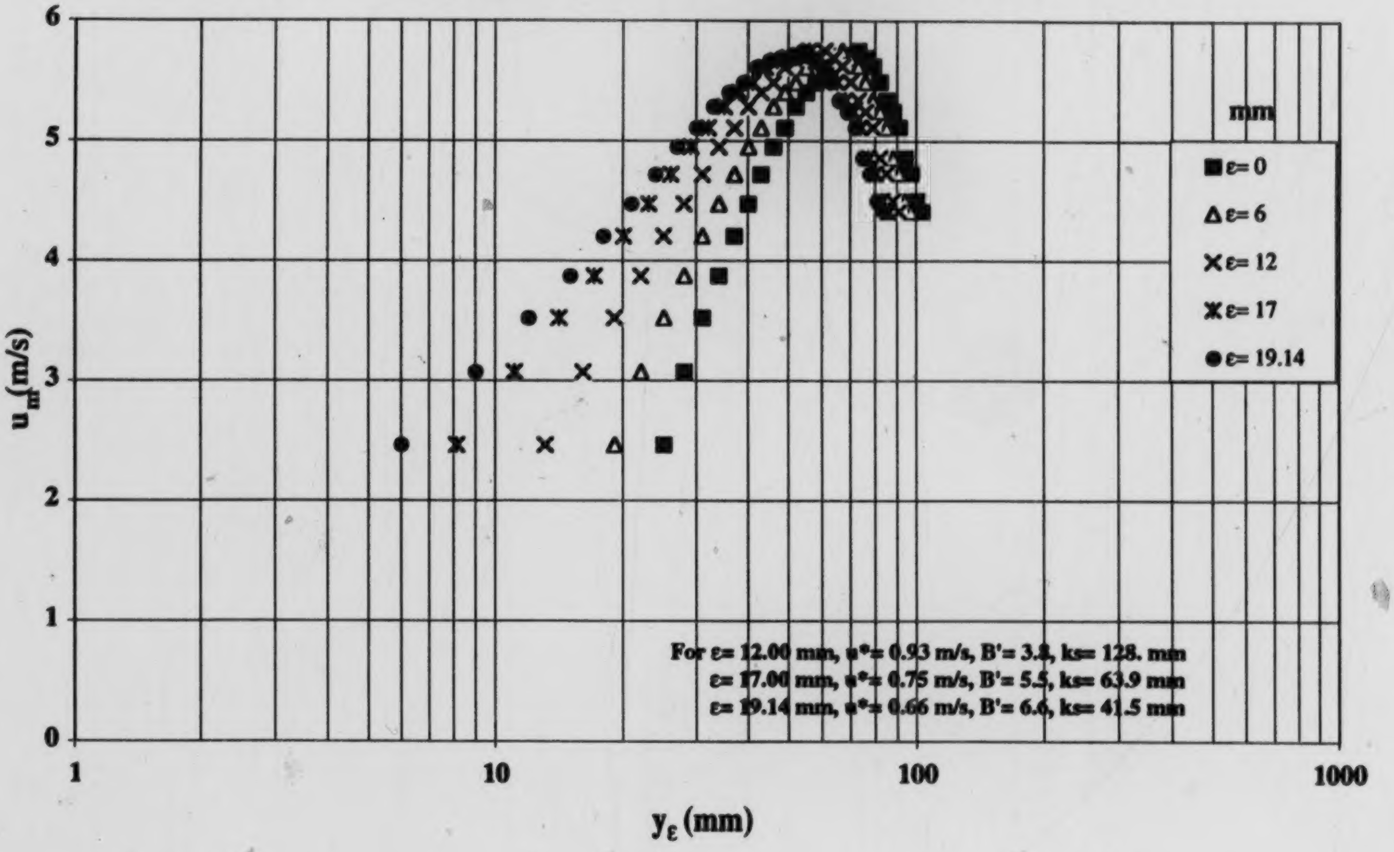

Figure C.29 Logarithmic velocity profiles at different origins at step #64 in a stepped spillway with l/h=0.6, h= 31.25 mm, k= 19.14 mm (yc/h=4.4)

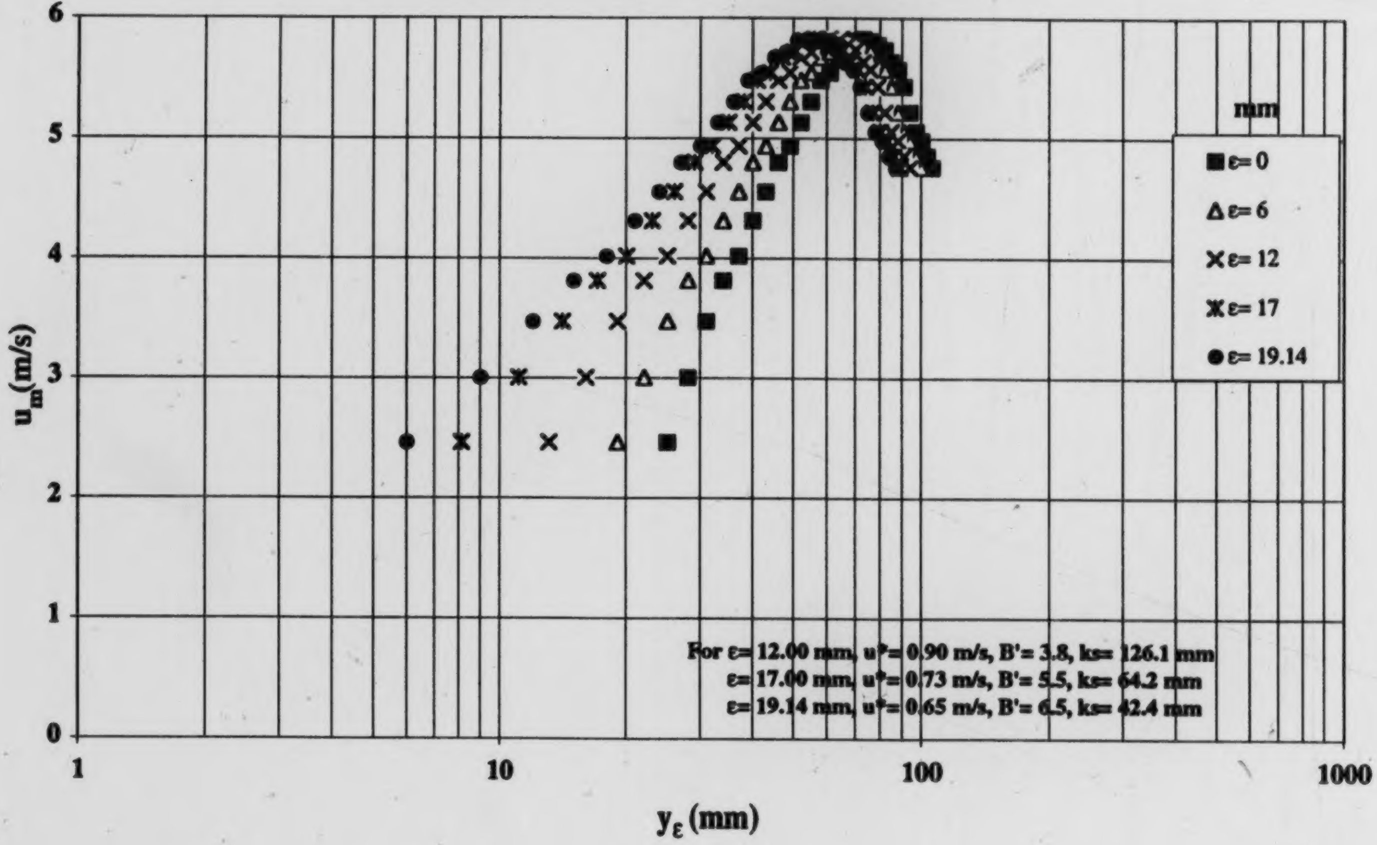

Figure C.30 Logarithmic velocity profiles at different origins at step #15 in a stepped spillway with l/h=0.8, h= 125. mm, k= 83.3 mm (yc/h=0.7)

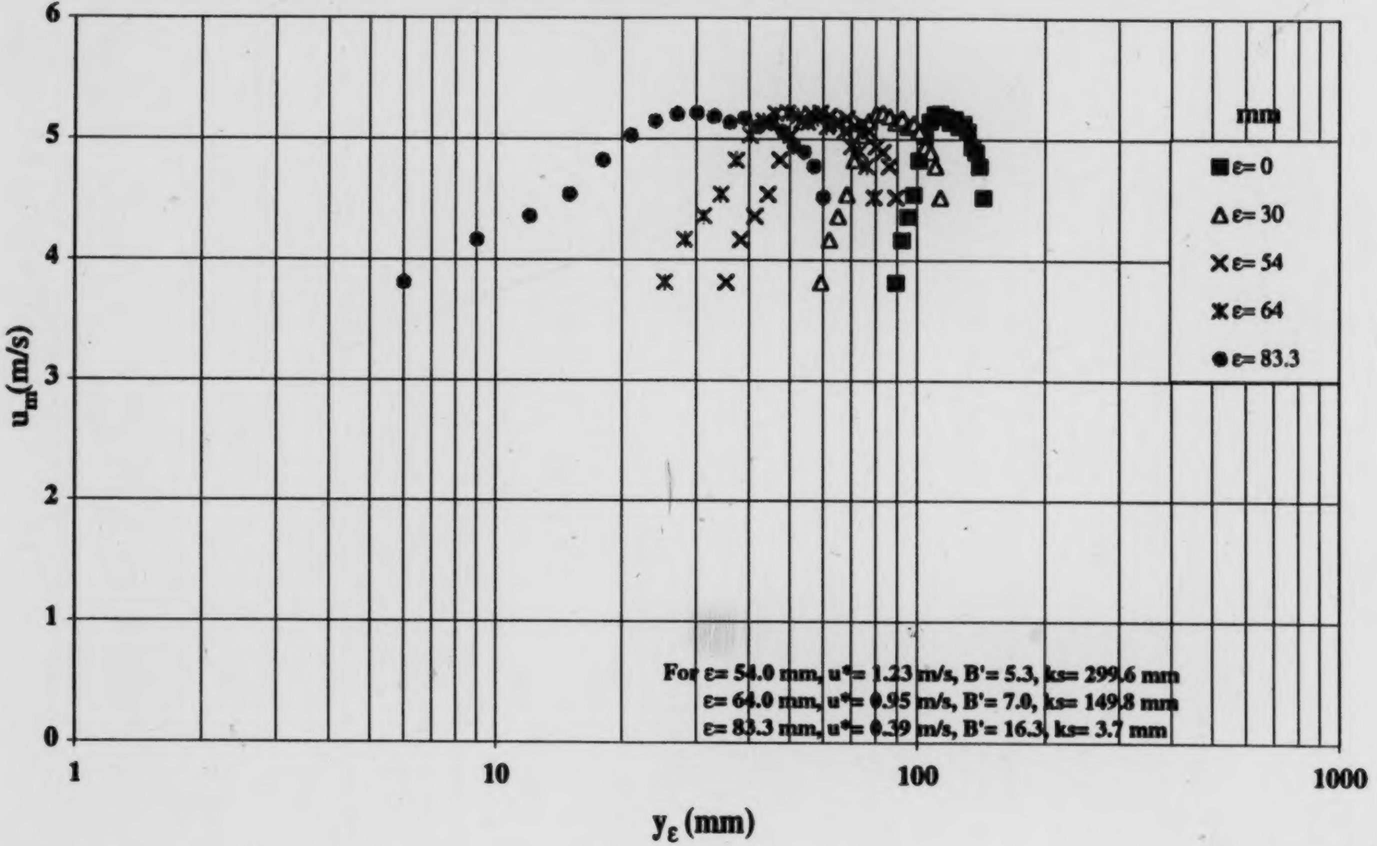

Figure C.31 Logarithmic velocity profiles at different origins at step #15 in a stepped spillway with l/h=0.8, h= 125. mm, k= 83.3 mm (yc/h=0.8)

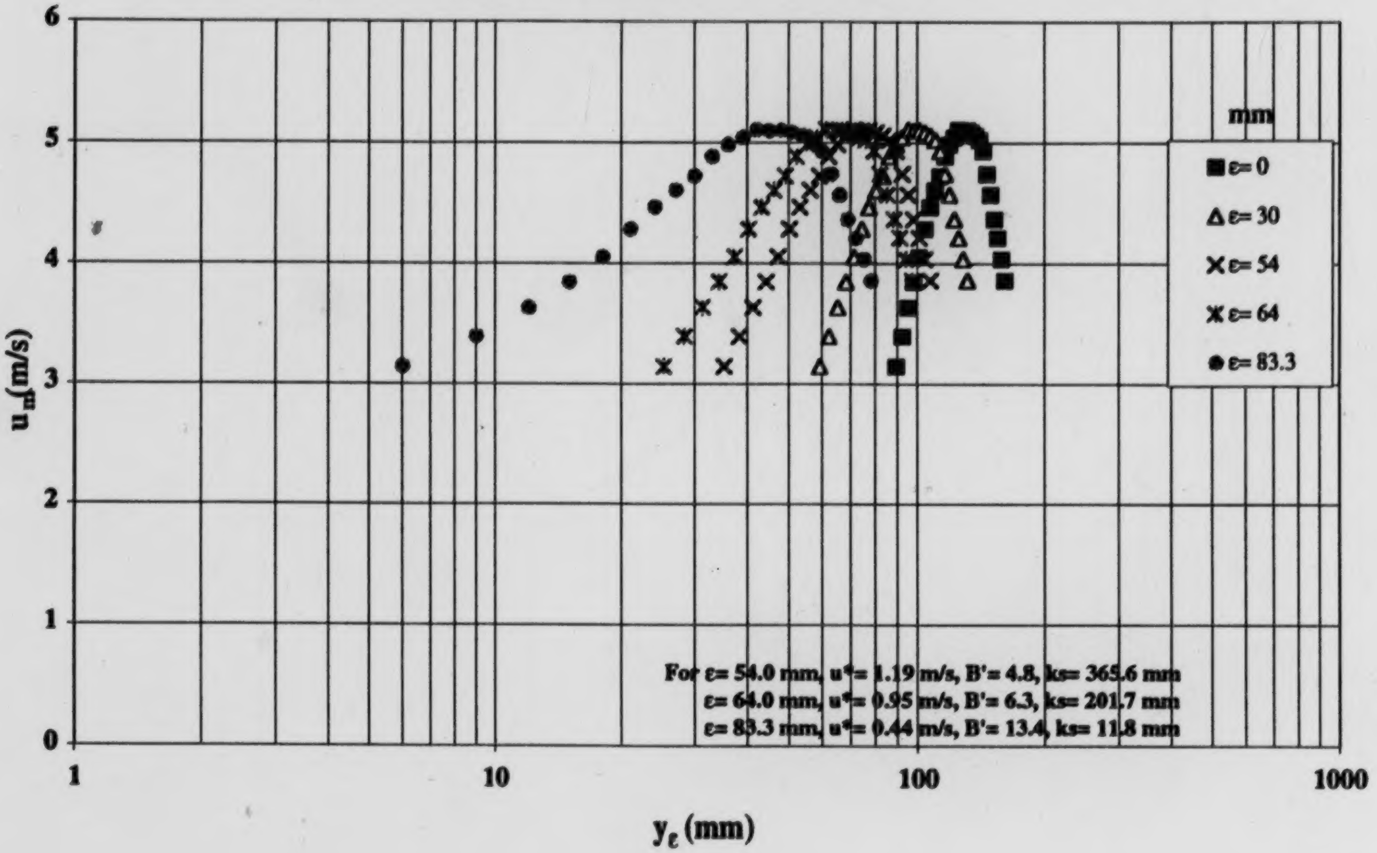

Figure C.32 Logarithmic velocity profiles at different origins at step #15 in a stepped spillway with l/h=0.8, h= 125. mm, k= 83.3 mm (yc/h=0.9)

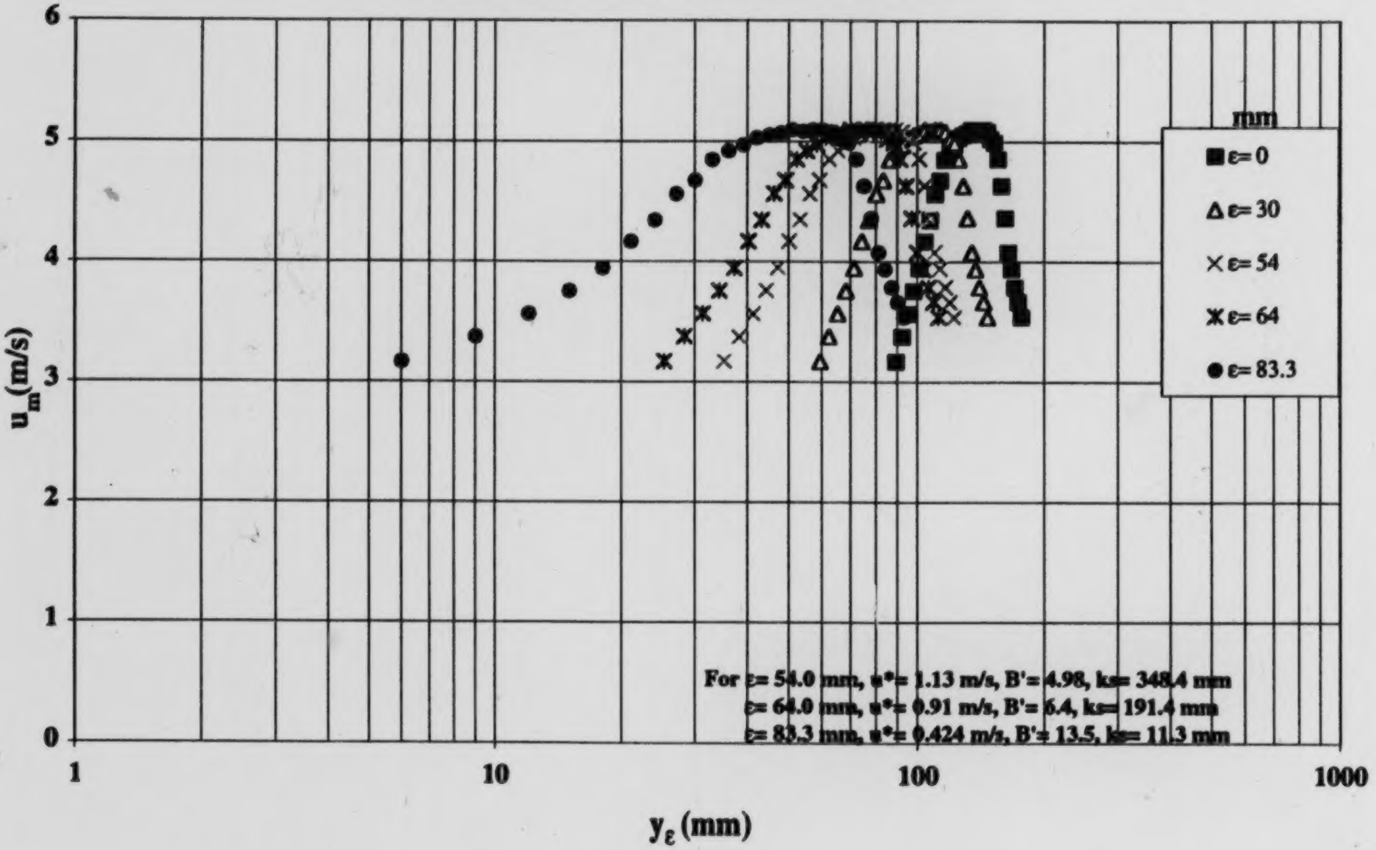

Figure C.33 Logarithmic velocity profiles at different origins at step #15 in a stepped spillway with l/h=0.8, h= 125. mm, k= 83.3 mm (yc/h=1.0)

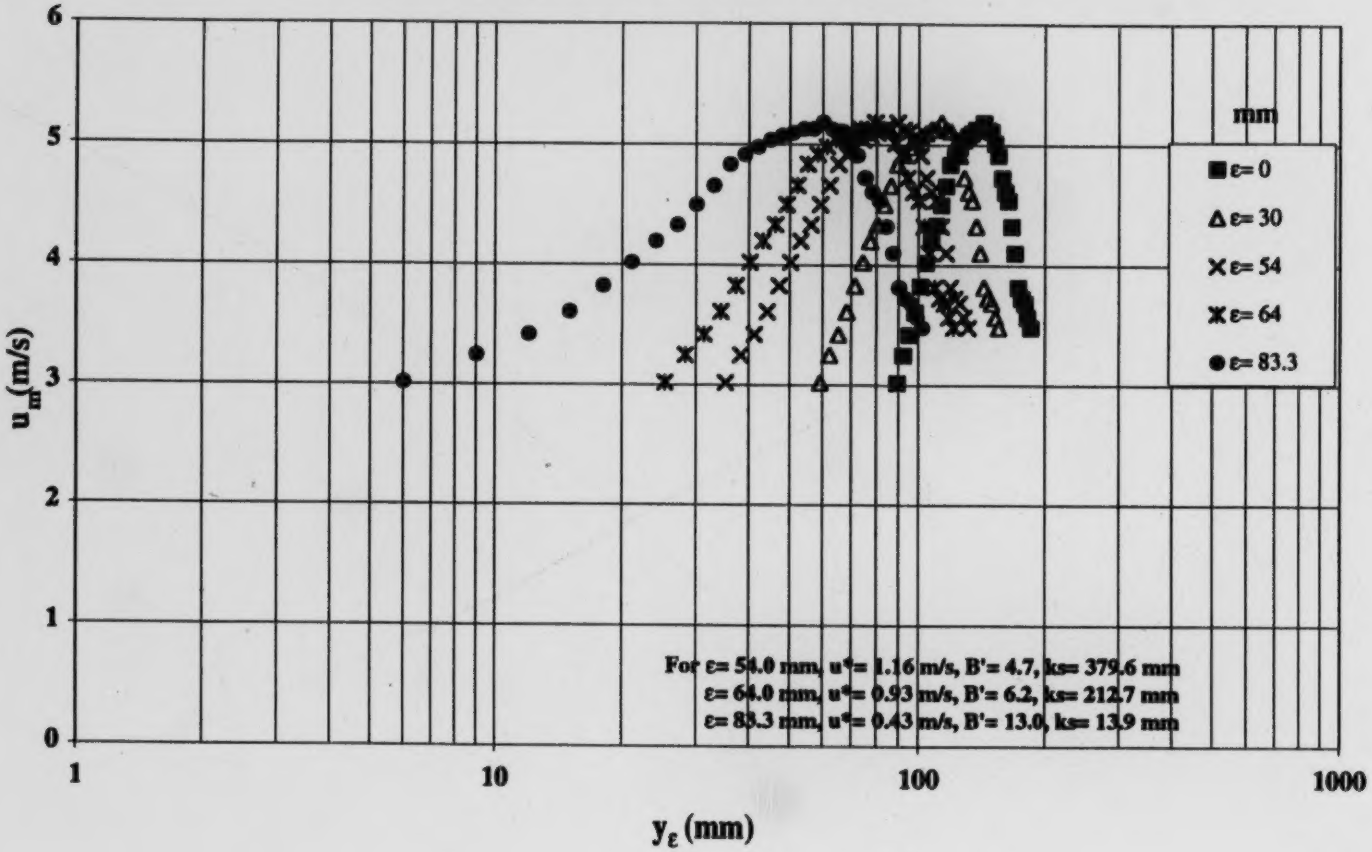

Figure C.34 Logarithmic velocity profiles at different origins at step #15 in a stepped spillway with l/h=0.8, h= 125. mm, k= 83.3 mm (yc/h=1.1)

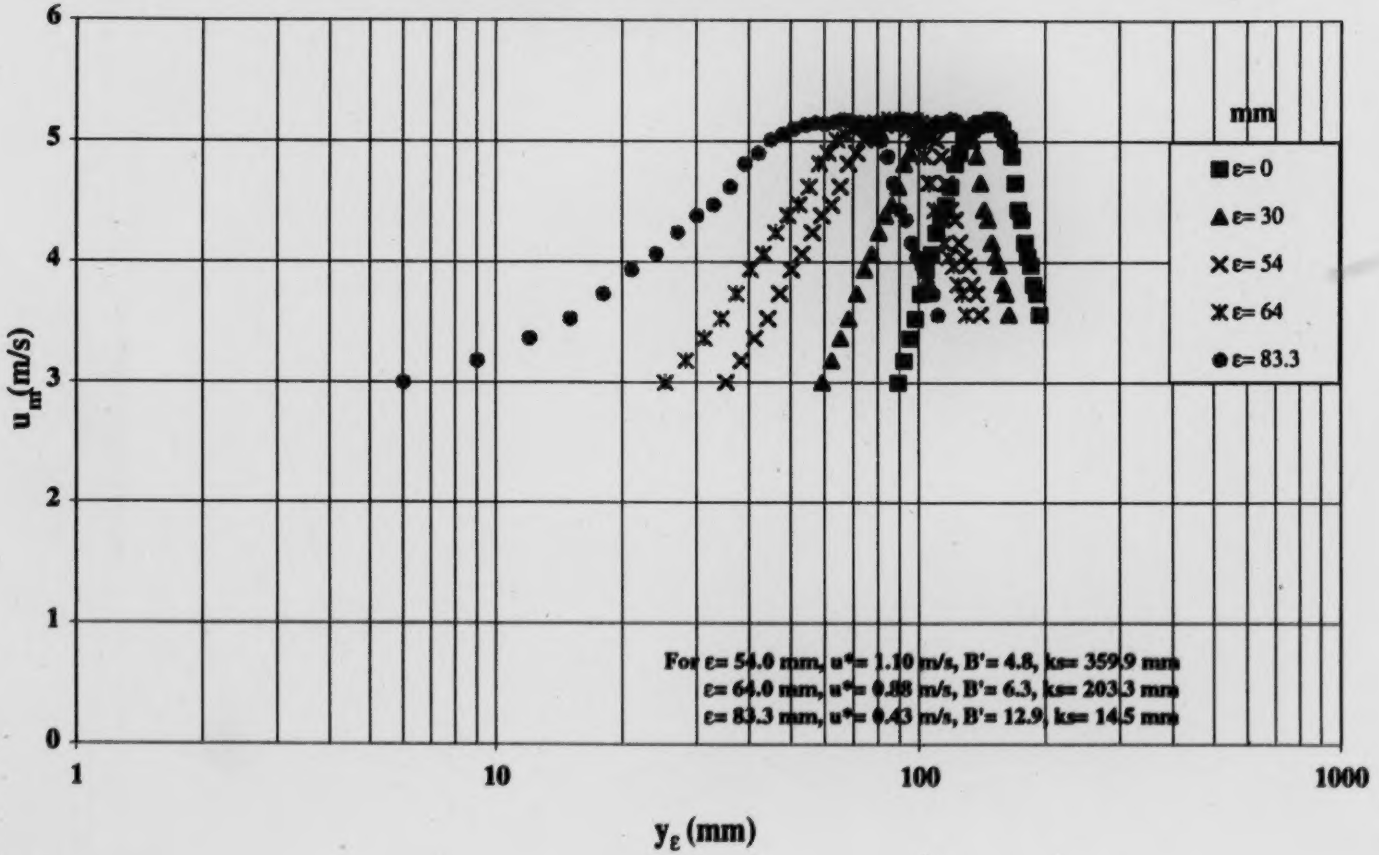

Figure C.35 Logarithmic velocity profiles at different origins at step #15 in a stepped spillway with l/h=0.8, h= 125. mm, k= 83.3 mm (yc/h=1.2)

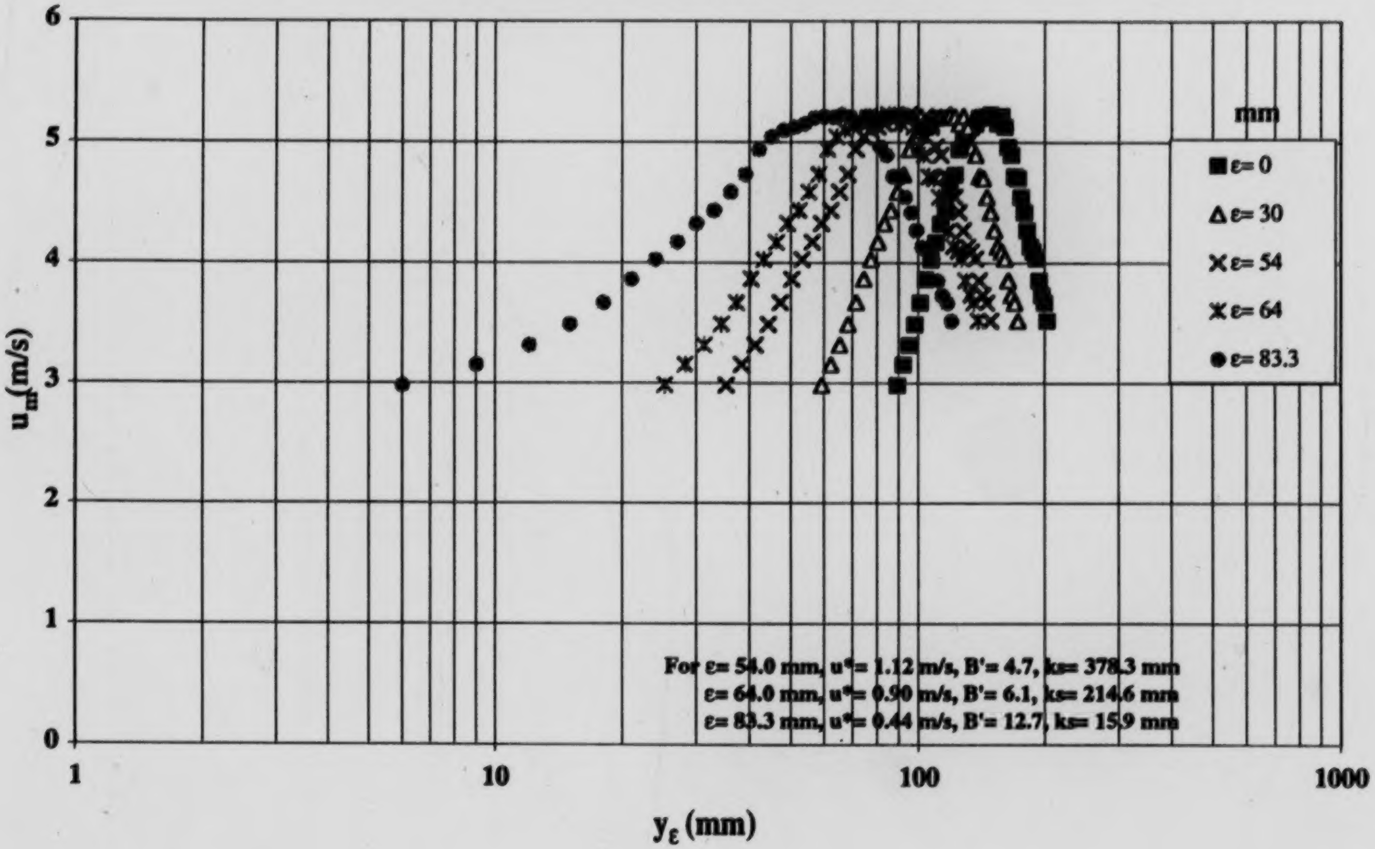

For ε= 54.0 mm, u*= 1.12 m/s, B'= 4.7, ks= 378.3 mm
ε= 64.0 mm, u*= 0.90 m/s, B'= 6.1, ks= 214.6 mm
ε= 83.3 mm, u*= 0.44 m/s, B'= 12.7, ks= 15.9 mm

Figure C.36 Logarithmic velocity profiles at different origins at step #15 in a stepped spillway with l/h=0.8, h= 125. mm, k= 83.3 mm (yc/h=1.3)

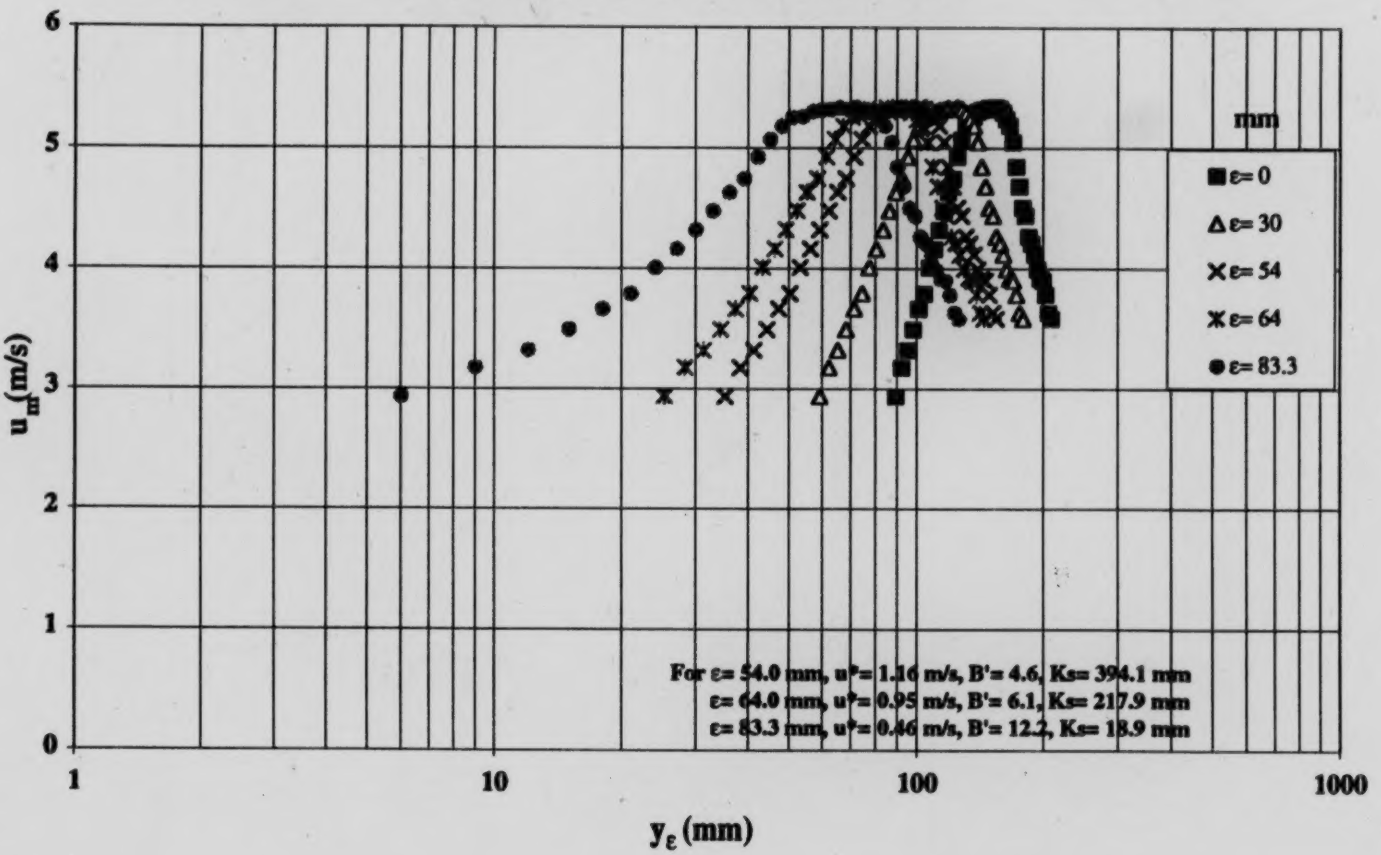

Figure C.37 Logarithmic velocity profiles at different origins at step #60 in a stepped spillway with l/h=0.8, h= 31.25 mm, k= 20.8 mm (yc/h=2.6)

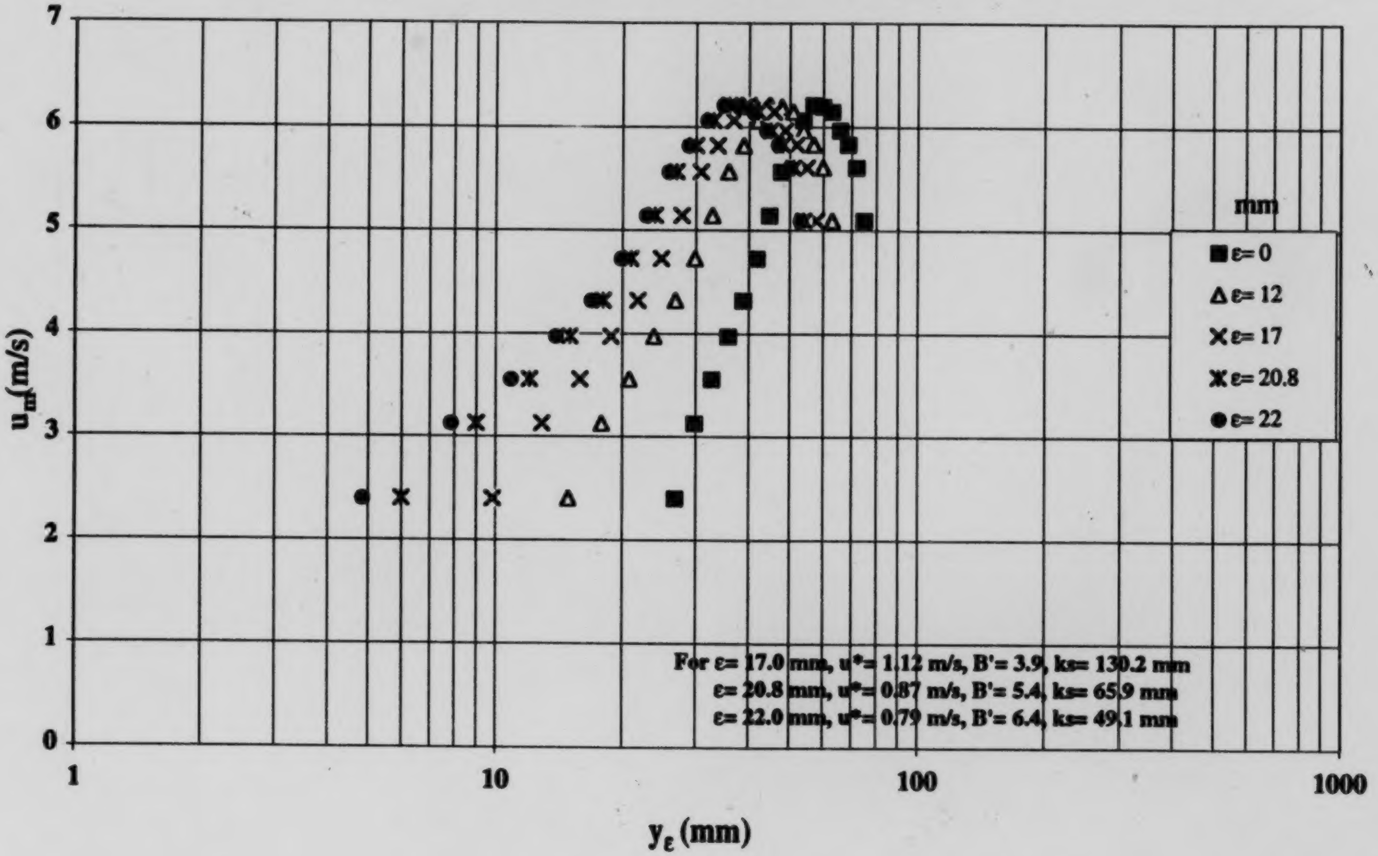

Figure C.38 Logarithmic velocity profiles at different origins at step #60 in a stepped spillway with l/h=0.8, h= 31.25 mm, k= 20.8 mm (yc/h=2.8)

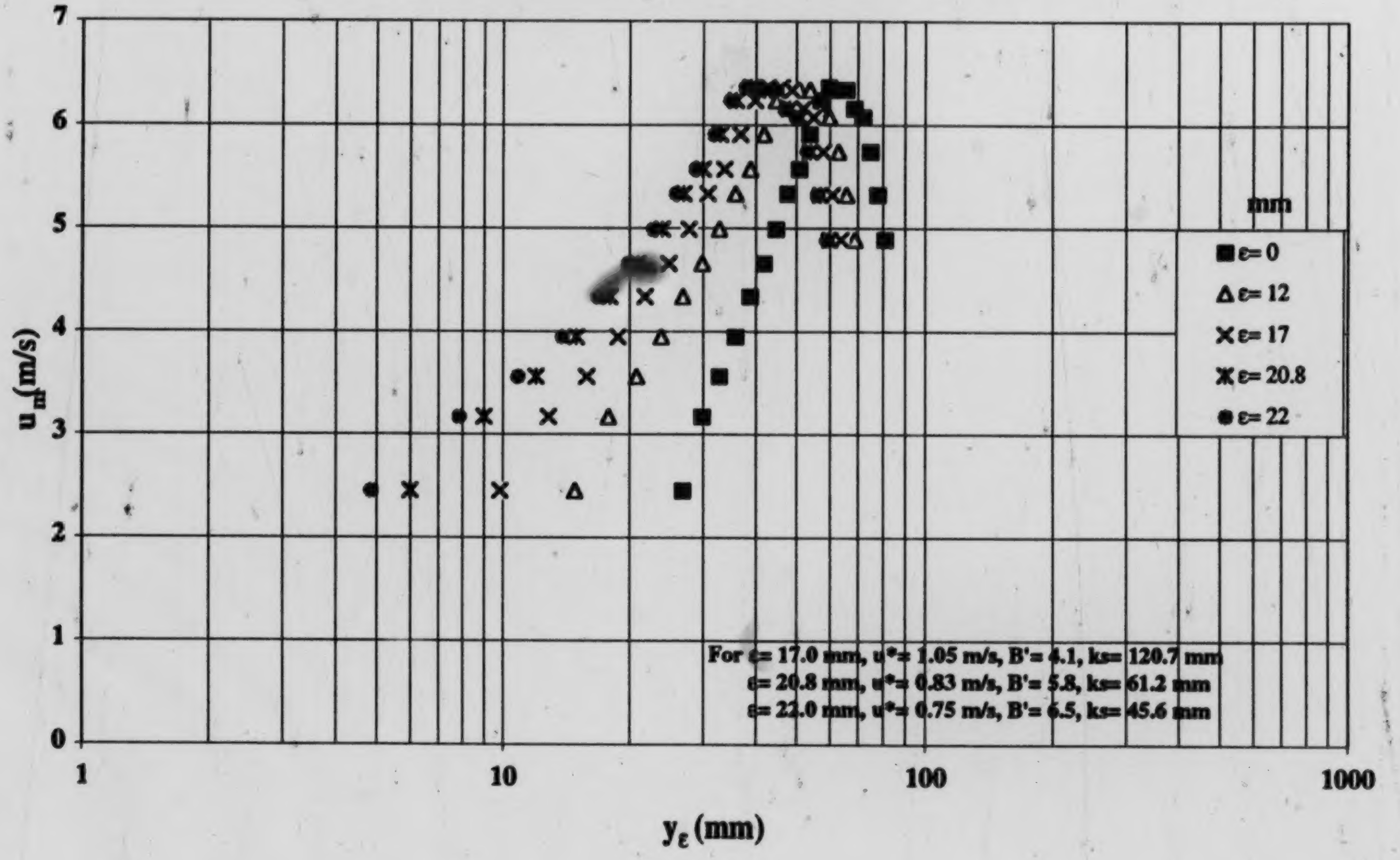

Figure C.39 Logarithmic velocity profiles at different origins at step #60 in a stepped spillway with l/h=0.8, h= 31.25 mm, k= 20.8 mm (yc/h=3.0)

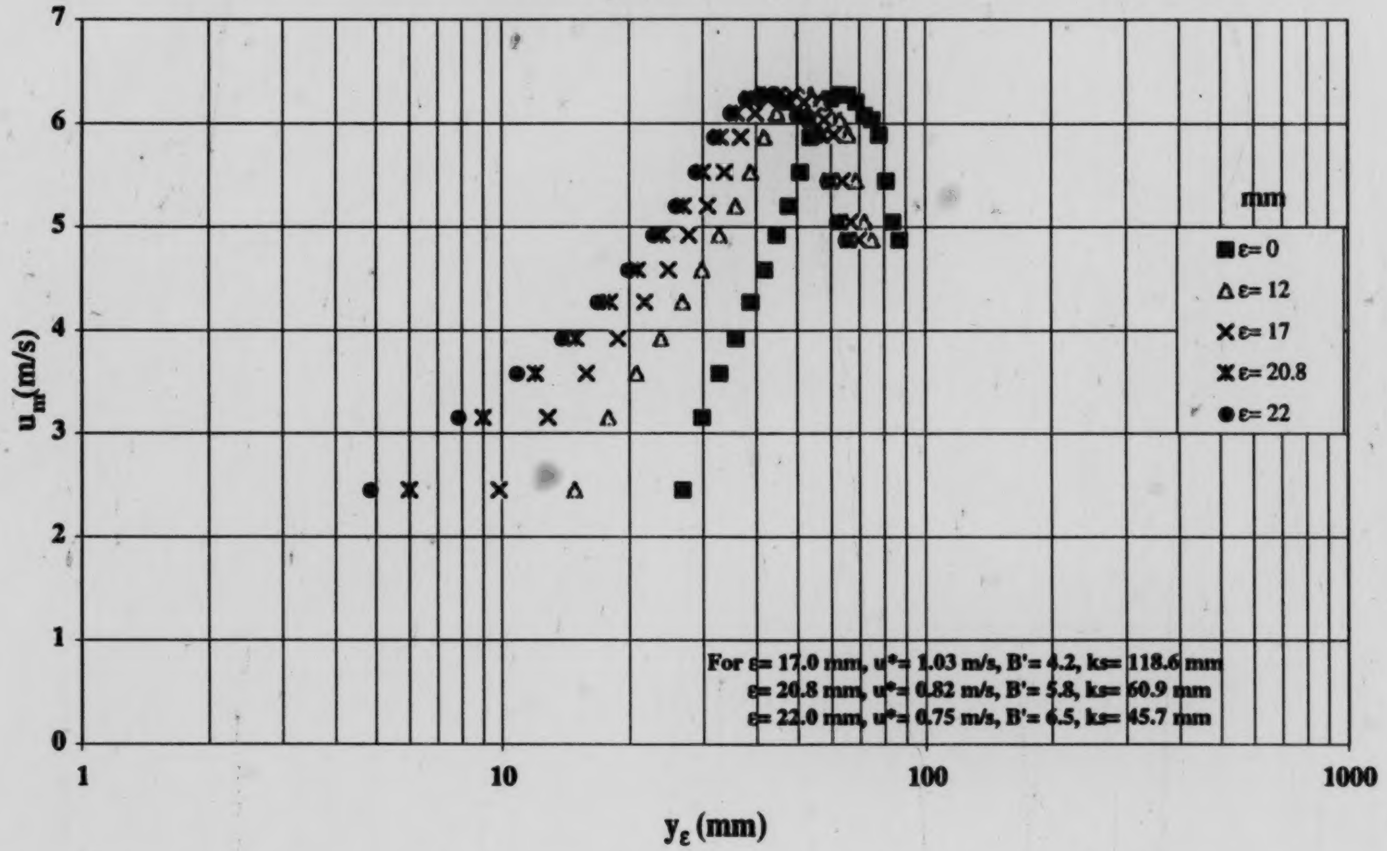

Figure C.40 Logarithmic velocity profiles at different origins at step #60 in a stepped spillway with l/h=0.8, h= 31.25 mm, k= 20.8 mm (yc/h=3.2)

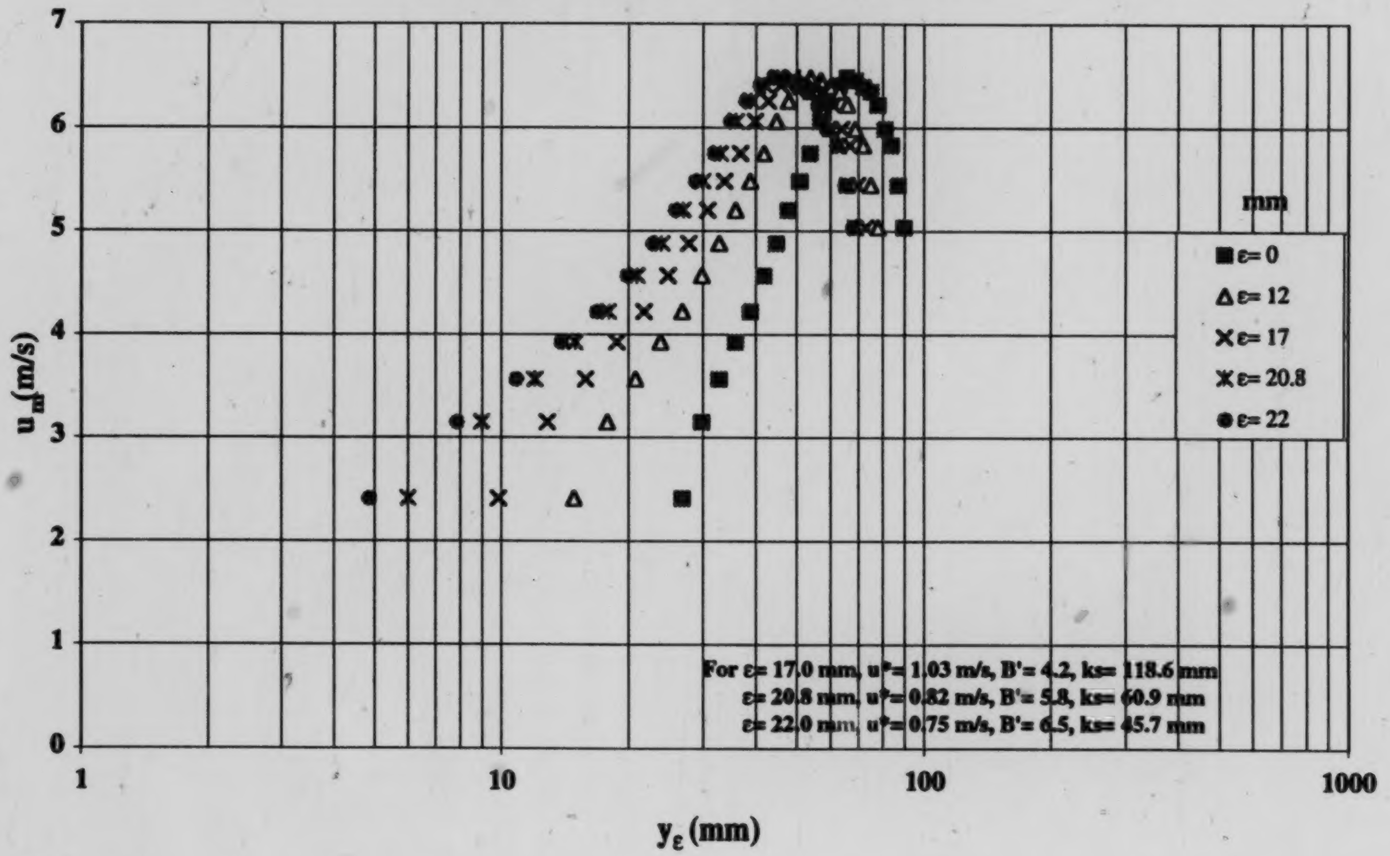

Figure C.41 Logarithmic velocity profiles at different origins at step #60 in a stepped spillway with l/h=0.8, h= 31.25 mm, k= 20.8 mm (yc/h=3.4)

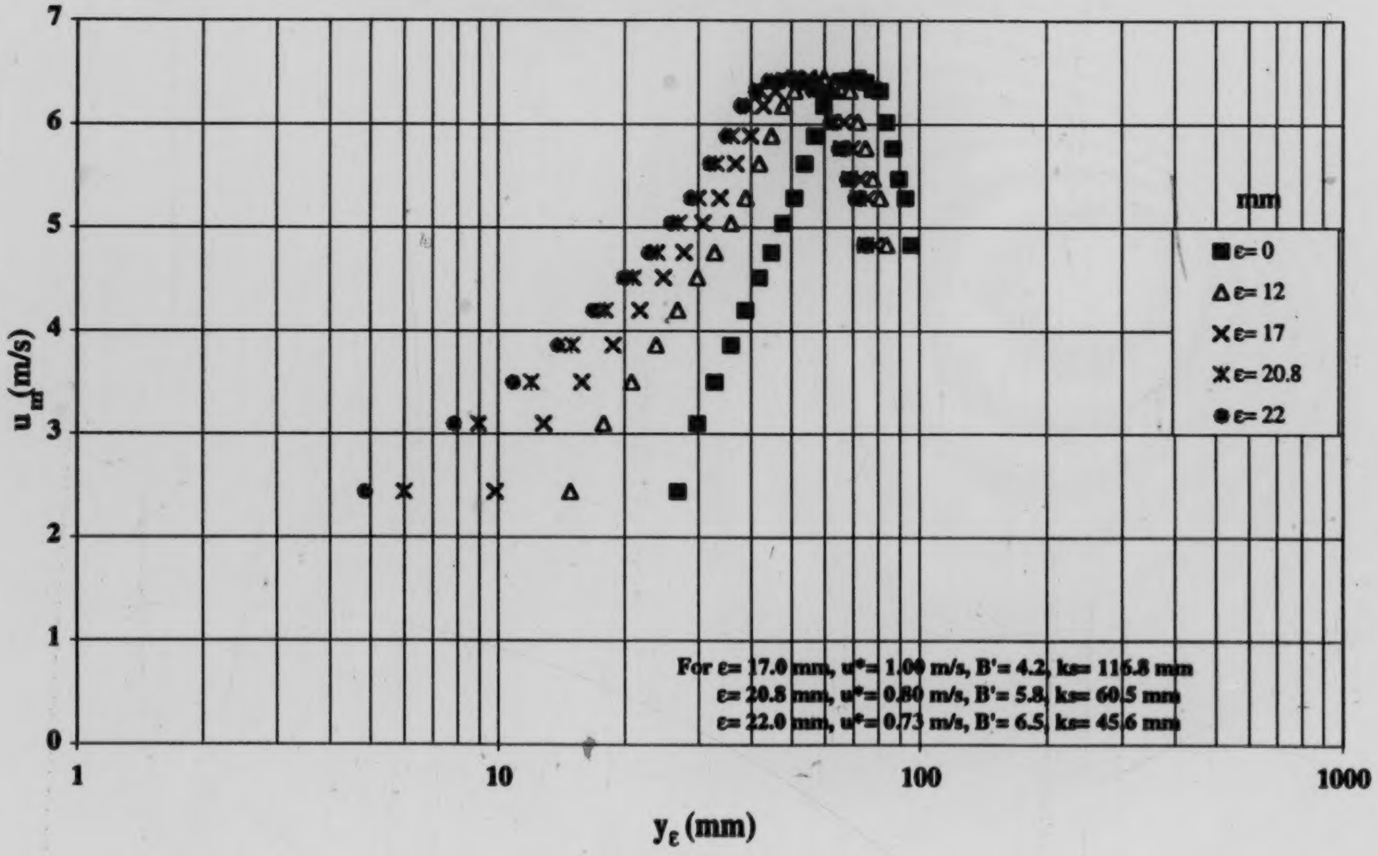

Figure C.42 Logarithmic velocity profiles at different origins at step #60 in a stepped spillway with l/h=0.8, h= 31.25 mm, k= 20.8 mm (yc/h=3.6)

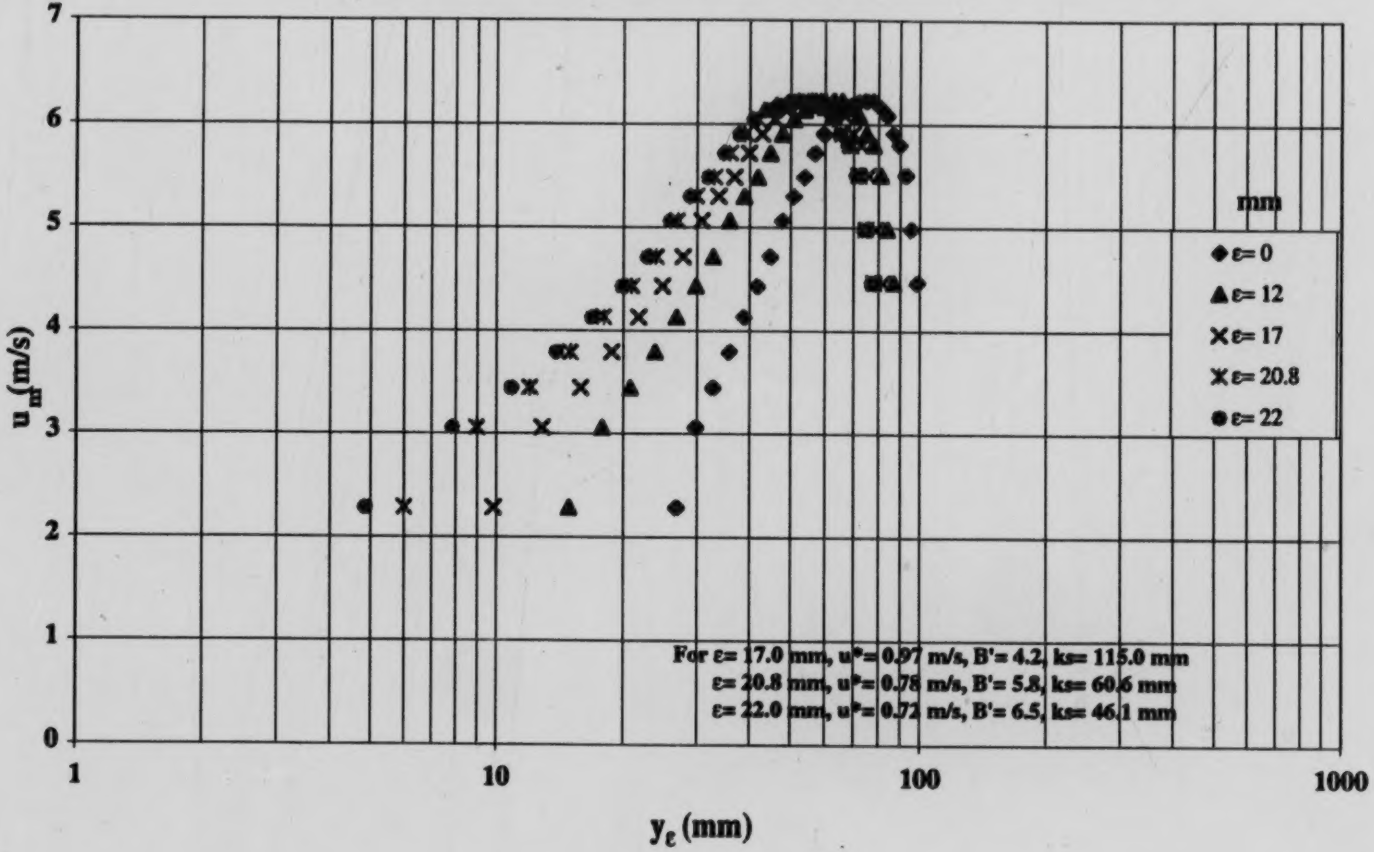

Figure C.43 Logarithmic velocity profiles at different origins at step #60 in a stepped spillway with l/h=0.8, h= 31.25 mm, k= 20.8 mm (yc/h=3.8)

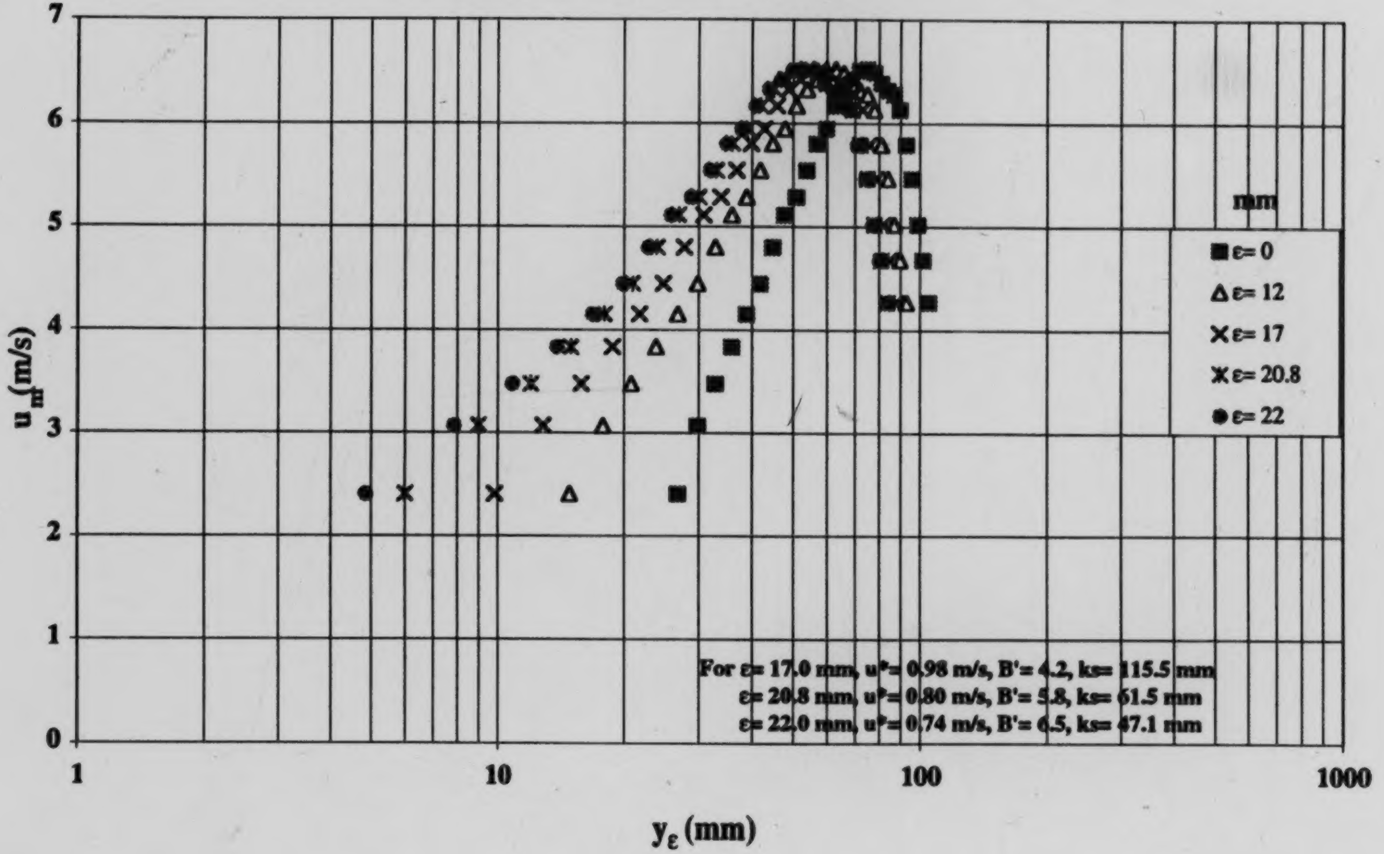

Figure C.44 Logarithmic velocity profiles at different origins at step #60 in a stepped spillway with l/h=0.8, h= 31.25 mm, k= 20.8 mm (yc/h=4.0)

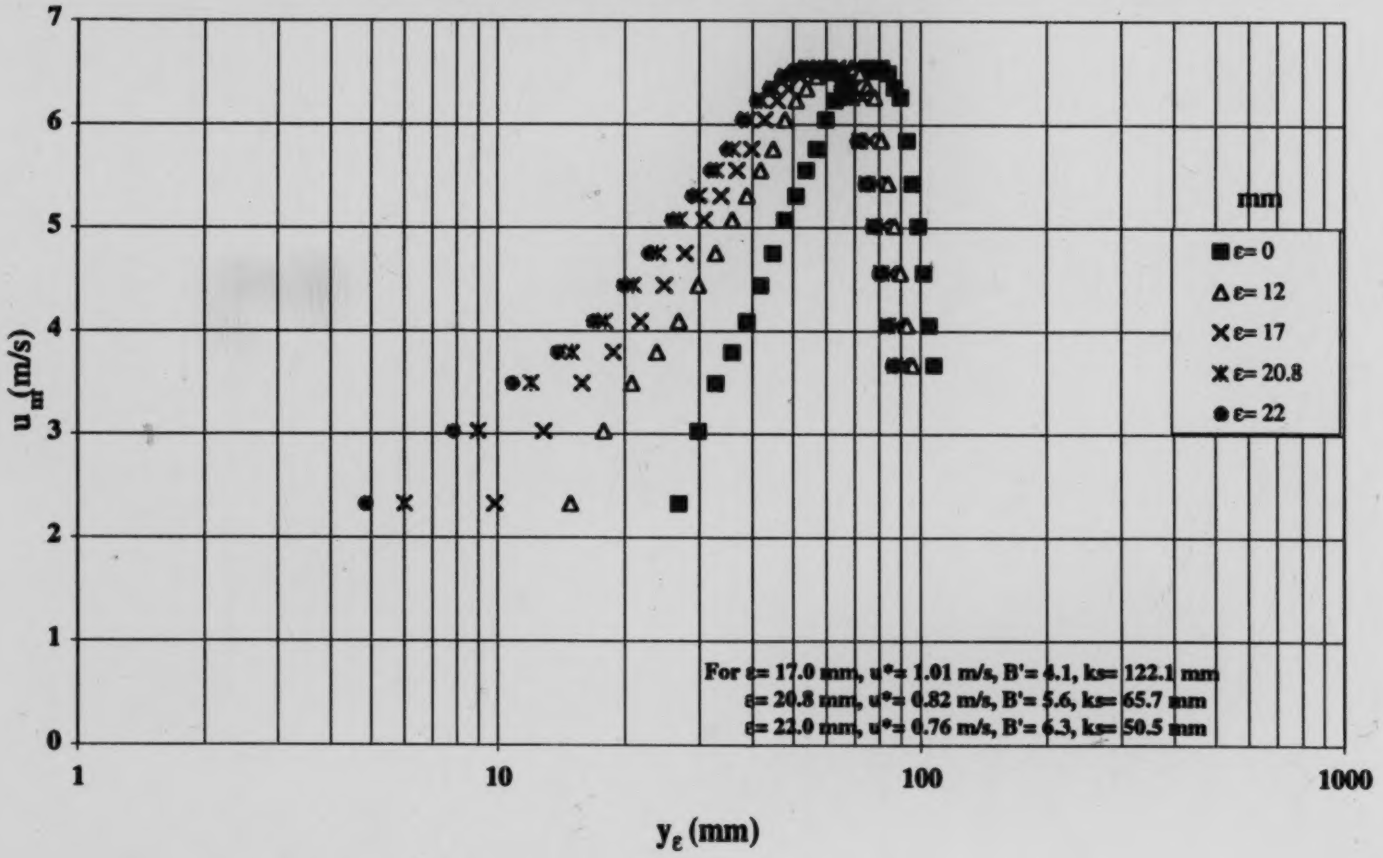

Figure C.45 Logarithmic velocity profiles at different origins at step #60 in a stepped spillway with l/h=0.8, h= 31.25 mm, k= 20.8 mm (yc/h=4.2)

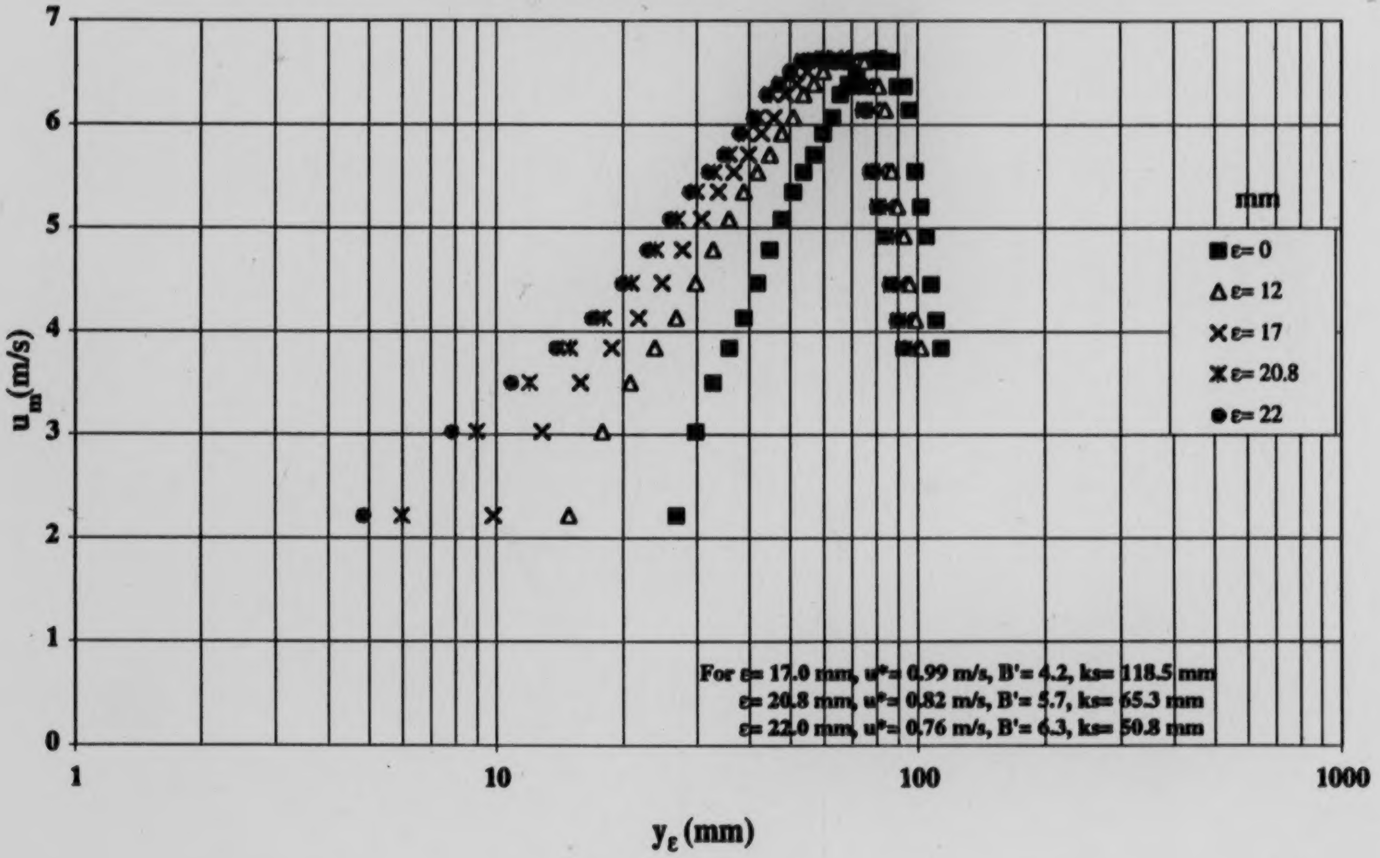

Figure C.46 Logarithmic velocity profiles at different origins at step #60 in a stepped spillway with l/h=0.8, h= 31.25 mm, k= 20.8 mm (yc/h=4.4)

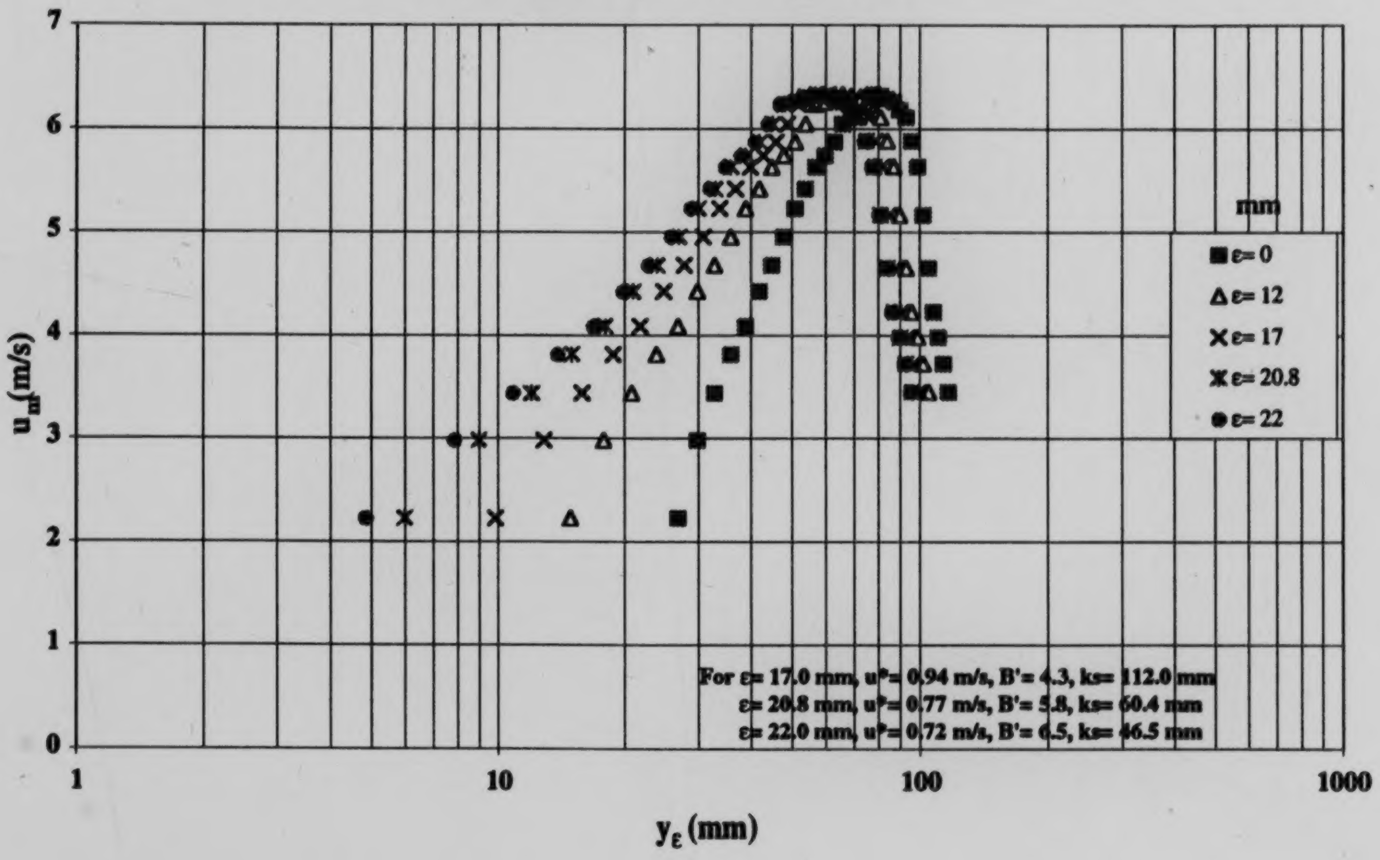
7
6
5
4
3
2
1
0
u_m(m/s)
1
10
100
1000
y_ε (mm)
mm
■ ε= 0
Δ ε= 12
X ε= 17
Ж ε= 20.8
● ε= 22
For ε= 17.0 mm, u*= 0.94 m/s, B'= 4.3, ks= 112.0 mm
ε= 20.8 mm, u*= 0.77 m/s, B'= 5.8, ks= 60.4 mm
ε= 22.0 mm, u*= 0.72 m/s, B'= 6.5, ks= 46.5 mm